frontiers | Research Topics

Multi-omics application in exploring potential biomarkers targeting resistance of anti-cancer drugs

Edited by
Hailin Tang, Diane S. Allen-Gipson and Zhi Tian

Coordinated by
Jindong Xie

Published in
Frontiers in Pharmacology
Frontiers in Oncology

FRONTIERS EBOOK COPYRIGHT STATEMENT

The copyright in the text of individual articles in this ebook is the property of their respective authors or their respective institutions or funders. The copyright in graphics and images within each article may be subject to copyright of other parties. In both cases this is subject to a license granted to Frontiers.

The compilation of articles constituting this ebook is the property of Frontiers.

Each article within this ebook, and the ebook itself, are published under the most recent version of the Creative Commons CC-BY licence. The version current at the date of publication of this ebook is CC-BY 4.0. If the CC-BY licence is updated, the licence granted by Frontiers is automatically updated to the new version.

When exercising any right under the CC-BY licence, Frontiers must be attributed as the original publisher of the article or ebook, as applicable.

Authors have the responsibility of ensuring that any graphics or other materials which are the property of others may be included in the CC-BY licence, but this should be checked before relying on the CC-BY licence to reproduce those materials. Any copyright notices relating to those materials must be complied with.

Copyright and source acknowledgement notices may not be removed and must be displayed in any copy, derivative work or partial copy which includes the elements in question.

All copyright, and all rights therein, are protected by national and international copyright laws. The above represents a summary only. For further information please read Frontiers' Conditions for Website Use and Copyright Statement, and the applicable CC-BY licence.

ISSN 1664-8714
ISBN 978-2-8325-6288-8
DOI 10.3389/978-2-8325-6288-8

About Frontiers

Frontiers is more than just an open access publisher of scholarly articles: it is a pioneering approach to the world of academia, radically improving the way scholarly research is managed. The grand vision of Frontiers is a world where all people have an equal opportunity to seek, share and generate knowledge. Frontiers provides immediate and permanent online open access to all its publications, but this alone is not enough to realize our grand goals.

Frontiers journal series

The Frontiers journal series is a multi-tier and interdisciplinary set of open-access, online journals, promising a paradigm shift from the current review, selection and dissemination processes in academic publishing. All Frontiers journals are driven by researchers for researchers; therefore, they constitute a service to the scholarly community. At the same time, the *Frontiers journal series* operates on a revolutionary invention, the tiered publishing system, initially addressing specific communities of scholars, and gradually climbing up to broader public understanding, thus serving the interests of the lay society, too.

Dedication to quality

Each Frontiers article is a landmark of the highest quality, thanks to genuinely collaborative interactions between authors and review editors, who include some of the world's best academicians. Research must be certified by peers before entering a stream of knowledge that may eventually reach the public - and shape society; therefore, Frontiers only applies the most rigorous and unbiased reviews. Frontiers revolutionizes research publishing by freely delivering the most outstanding research, evaluated with no bias from both the academic and social point of view. By applying the most advanced information technologies, Frontiers is catapulting scholarly publishing into a new generation.

What are Frontiers Research Topics?

Frontiers Research Topics are very popular trademarks of the *Frontiers journals series*: they are collections of at least ten articles, all centered on a particular subject. With their unique mix of varied contributions from Original Research to Review Articles, Frontiers Research Topics unify the most influential researchers, the latest key findings and historical advances in a hot research area.

Find out more on how to host your own Frontiers Research Topic or contribute to one as an author by contacting the Frontiers editorial office: frontiersin.org/about/contact

Multi-omics application in exploring potential biomarkers targeting resistance of anti-cancer drugs

Topic editors
Hailin Tang — Sun Yat-sen University Cancer Center (SYSUCC), China
Diane S. Allen-Gipson — University of South Florida, United States
Zhi Tian — University of South Florida, United States

Topic coordinator
Jindong Xie — Sun Yat-sen University Cancer Center (SYSUCC), China

Citation
Tang, H., Allen-Gipson, D. S., Tian, Z., Xie, J., eds. (2025). *Multi-omics application in exploring potential biomarkers targeting resistance of anti-cancer drugs*. Lausanne: Frontiers Media SA. doi: 10.3389/978-2-8325-6288-8

Table of contents

05 Editorial: Multi-omics application in exploring potential biomarkers targeting resistance of anti-cancer drugs
Huan Wang, Jindong Xie, Zhi Tian, Diane S. Allen-Gipson and Hailin Tang

08 The prognostic and immunological role of MCM3 in pan-cancer and validation of prognosis in a clinical lower-grade glioma cohort
Qian-Rong Huang, Qian Jiang, Ju-Yuan Tan, Ren-Bao Nong, Jun Yan, Xia-Wei Yang, Li-Gen Mo, Guo-Yuan Ling, Teng Deng and Yi-Zhen Gong

26 Application of immune checkpoint inhibitors for resectable gastric/gastroesophageal cancer
Feizhi Lin, Yongming Chen, Bowen Huang, Shenghang Ruan, Jun Lin, Zewei Chen, Chunyu Huang and Baiwei Zhao

39 Protein and metabolic profiles of tyrosine kinase inhibitors co-resistant liver cancer cells
Zengbin Wang, Linqing Wu, Yu Zhou, Zhong Chen, Tao Zhang, Hong Wei and Zhihong Wang

52 Dorsomorphin attenuates ABCG2-mediated multidrug resistance in colorectal cancer
Xiao-Peng Li, Liang-Qi Cao, Ze-Zhong Yu, Ke He, Peng-Bo Ding, Ji-Sheng Li, Yi-Yao Shan, Yu-Bin Su, Zhong-Min Yuan and Zhi Shi

59 Clinical significance and biological function of interferon regulatory factor 1 in non-small cell lung cancer
Jialin Su, Shuhua Tan, Yuning Li, Xinglong Chen, Jiasi Liu, Yongzhong Luo, Changqie Pan and Lemeng Zhang

73 Combined aqupla, paclitaxel liposome, and docetaxel treatment: survival and biomarker outcomes in recurrent ovarian cancer patients
Jie Yang, Mengyu Zhang, Yilei Zhang, Lanfen Zhu and Qiming Wang

85 Prediction of immunotherapy response of bladder cancer with a pyroptosis-related signature indicating tumor immune microenvironment
Zihan Xu, Yujie Zhao, Yong Zhang, Xiaowei Liu, Linlin Song, Meixu Chen, Guixiu Xiao, Xuelei Ma and Hubing Shi

103 EMT-related gene classifications predict the prognosis, immune infiltration, and therapeutic response of osteosarcoma
Meng-Pan Li, Si-Ping Long, Wen-Cai Liu, Kun Long and Xing-Hua Gao

118 Phosphoenolpyruvate carboxykinase 2-mediated metabolism promotes lung tumorigenesis by inhibiting mitochondrial-associated apoptotic cell death
Jing Zhang, Wenjuan He, Dongmei Liu, Wenyu Zhang, Huan Qin, Song Zhang, Ailan Cheng, Qiang Li and Feilong Wang

134 Efficacy of different medications in the treatment of gynaecological tumours: a clinical meta-analysis
Qiaoying Chen

143 Integrated analyses reveal IDO1 as a prognostic biomarker coexpressed with PD-1 on tumor-associated macrophages in esophageal squamous cell carcinoma
Yaojun Peng, Lingxiong Wang, Juan Yang, Qiyan Wu, Xiaoxuan Sun, Jinying Zhang, Yanju Yu, Liping Zhang, Jie Gao, Qing Zhou, Haiyan Zhu and Fan Yin

157 Extrachromosomal circular DNAs in prostate adenocarcinoma: global characterizations and a novel prediction model
Qingliu He, Qingfu Su, Chengcheng Wei, Pu Zhang, Weihui Liu, Junyi Chen, Xiaoping Su and Wei Zhuang

169 The role of SIRT1 in autophagy and drug resistance: unveiling new targets and potential biomarkers in cancer therapy
Yujing Tang, Wantao Ju, Yanjun Liu and Qin Deng

197 *Sorbaria sorbifolia* flavonoid derivative induces mitochondrial apoptosis in human hepatoma cells through Bclaf1
Jiaxin Chen, Haoyi Cheng, Chunhua Bai, Dandan Wang, Jinghao Fu, Jinge Hao, Yixuan Wang and Zhang Xuewu

209 Cell cycle checkpoint revolution: targeted therapies in the fight against malignant tumors
Guangming Song, Jue Liu, Xing Tang, Jie Zhong, Yuhuan Zeng, Xiaodi Zhang, Jianbin Zhou, Jie Zhou, Lu Cao, Qunfeng Zhang and Yukun Li

222 Long non-coding RNAs: regulators of autophagy and potential biomarkers in therapy resistance and urological cancers
Shizong Wang, Yang Bai, Jie Ma, Liang Qiao and Mingqing Zhang

250 Enhanced tumor suppression in colorectal cancer via berberine-loaded PEG-PLGA nanoparticles
Fei Shen, Yun-Sheng Zheng, Lan Dong, Ziyang Cao and Jie Cao

262 Pan-cancer analysis of CLDN18.2 shed new insights on the targeted therapy of upper gastrointestinal tract cancers
Jun Wu, Jinghua Lu, Qiuyue Chen, Haojie Chen, Yongqiang Zheng and Minggang Cheng

frontiers | Frontiers in Pharmacology

TYPE Editorial
PUBLISHED 16 April 2025
DOI 10.3389/fphar.2025.1594064

Check for updates

OPEN ACCESS

EDITED AND REVIEWED BY
Andrea Lapucci,
University of Florence, Italy

*CORRESPONDENCE
Hailin Tang,
tanghl@sysucc.org.cn

†These authors have contributed equally to this work

RECEIVED 15 March 2025
ACCEPTED 09 April 2025
PUBLISHED 16 April 2025

CITATION
Wang H, Xie J, Tian Z, Allen-Gipson DS and Tang H (2025) Editorial: Multi-omics application in exploring potential biomarkers targeting resistance of anti-cancer drugs.
Front. Pharmacol. 16:1594064.
doi: 10.3389/fphar.2025.1594064

COPYRIGHT
© 2025 Wang, Xie, Tian, Allen-Gipson and Tang. This is an open-access article distributed under the terms of the Creative Commons Attribution License (CC BY). The use, distribution or reproduction in other forums is permitted, provided the original author(s) and the copyright owner(s) are credited and that the original publication in this journal is cited, in accordance with accepted academic practice. No use, distribution or reproduction is permitted which does not comply with these terms.

Editorial: Multi-omics application in exploring potential biomarkers targeting resistance of anti-cancer drugs

Huan Wang[1†], Jindong Xie[1†], Zhi Tian[2], Diane S. Allen-Gipson[3] and Hailin Tang[1*]

[1]State Key Laboratory of Oncology in South China, Guangdong Provincial Clinical Research Center for Cancer, Sun Yat-sen University Cancer Center, Guangzhou, China, [2]Department of Molecular Pharmacology and Physiology, Morsani College of Medicine, Unversity of South Florida, Tampa, FL, United States, [3]USF Health Taneja College of Pharmacy, Department of Pharmaceutical Sciences, University of South Florida, Tampa, FL, United States

KEYWORDS

multi-omics, biomarker, drug resistance, oncology, tumor microenvironment

Editorial on the Research Topic
Multi-omics application in exploring potential biomarkers targeting resistance of anti-cancer drugs

Anti-cancer drug resistance denotes the capacity of cancer cells to withstand the effects of therapeutic agents. This phenomenon is both highly prevalent and complex within the context of cancer treatment, and it constitutes a major factor contributing to diminished therapeutic efficacy and adverse patient outcomes (Gao et al., 2024). Cancer drug resistance constitutes a fundamental challenge in contemporary oncology, stemming from the intricate regulation of complex biological networks by tumor cells to circumvent drug-induced cytotoxic effects (Lei et al., 2020). To systematically elucidate this complex mechanism, multi-omics technologies have emerged as a pivotal advancement in contemporary research. Through the integration of multidimensional data derived from genomics, transcriptomics, proteomics, metabolomics, and additional omics layers, multi-omics studies develop a comprehensive atlas of tumor biological systems (Kreitmaier et al., 2023). In comparison to traditional single-omics analyses, this integrative approach effectively captures cascade regulatory relationships across molecular hierarchies, thereby elucidating the network-based mechanisms that underlie drug resistance. In the field of biomarker discovery, multi-omics approaches offer distinct advantages. In the realm of biomarker discovery, multi-omics technologies demonstrate distinct advantages. For instance, through the integration of transcriptomic and proteomic approaches, researchers can elucidate how neoplastic cells evade pharmacological interventions by modifying gene expression profiles and altering protein functional states (Xie et al., 2020). Regarding the investigation of drug resistance mechanisms, multi-omics methodologies equip researchers with robust analytical tools. The systematic integration of metabolomic datasets with systems biology modeling enables comprehensive delineation of molecular pathways underlying therapeutic resistance (Eicher et al., 2020). The current Research Topic, "Multi-omics Application in Exploring Potential Biomarkers Targeting Resistance of Anti-Cancer Drugs", convenes leading researchers in this highly anticipated field to

present a Research Topic of authoritative reviews and compelling original articles. These articles provide an in-depth understanding and an innovative, comprehensive perspective on drug resistance mechanisms, multi-omics methodologies, and potential strategies for overcoming drug resistance.

Advancements in multi-omics technologies, particularly those achieving single-cell resolution and spatiotemporal dynamic analysis, are increasingly elucidating the complex regulatory mechanisms underlying cancer drug resistance. These developments present new opportunities for the formulation of innovative therapeutic strategies. Pharmaco-omics has emerged as a prominent research frontier. Wu et al. conducted integrative analyses combining pharmaco-omics with genomic and transcriptomic datasets, that elevated expression of CLDN18.2 is significantly associated with poor prognosis in bladder cancer (BLCA), esophageal carcinoma (ESCA), and pancreatic adenocarcinoma (PAAD). This study comprehensively elucidates the biological functions and clinical relevance of CLDN18.2 in cancer, thereby offering novel insights for the development of targeted therapies. Similarly, He et al. employed multidimensional integration of pharmaco-omics, genomics, and immunomics to characterize the landscape of extrachromosomal circular DNA (eccDNA) in prostate adenocarcinoma (PRAD). Their research identified eccDNA-derived ZNF330 and PITPNM3 as potential biomarkers. Their risk stratification model provides novel insights for prognostic assessment and the development of immunotherapy strategies. Expanding methodological approaches, Huang et al. further integrated pharmaco-omics with epigenetic profiling and single-cell omics to investigate the pan-cancer expression patterns, prognostic significance, and associations of MCM3 with tumor immune microenvironments, subsequently validating its prognostic utility in a clinical cohort of lower-grade glioma (LGG).

In addition to pharmaco-omics, proteomic investigations remain a prominent focus in oncology research. Peng et al. employed proteomics, genomics, and bioinformatics tools to explore the function of indoleamine 2,3-dioxygenase 1 (IDO1) within the tumor microenvironment (TME) of esophageal squamous cell carcinoma (ESCC). Their findings indicate that tumor-associated macrophages (TAMs) with elevated IDO1 expression contribute to an immunosuppressive TME, thereby reducing the effectiveness of immunotherapy. Through an analysis of RNA-seq data from The Cancer Genome Atlas (TCGA) involving 95 patients, supplemented by clinical validation in 77 patients, they found that targeting IDO1 in TAMs could serve as a viable strategy to counteract immune resistance. This underscores the potential of IDO1 inhibitors as adjunctive agents to improve the efficacy of immunotherapeutic interventions. In parallel, Huang et al. conducted a multidimensional analysis by integrating proteomics, transcriptomics, and clinical omics to explore the expression patterns, prognostic value, immune signatures, and clinical relevance of the minichromosomal maintenance complex component 3 (MCM3) gene across pan-cancer cohorts, with specific validation in lower-grade glioma (LGG). Their work comprehensively elucidated the molecular mechanisms and clinical potential of MCM3 in oncology.

Zhang et al. combined transcriptomic and proteomic data to explore the role of mitochondrial PCK2 in NSCLC. They found that PCK2-driven gluconeogenesis helps cancer cells evade mitochondrial apoptosis, indicating that targeting metabolic pathways like gluconeogenesis could be a strategy to combat drug resistance in nutrient-poor tumor environments. Wang et al. further advanced this field by combining proteomics and metabolomics to study hepatocellular carcinoma (HCC) resistance mechanisms to tyrosine kinase inhibitors (TKIs) sorafenib and lenvatinib, providing a global perspective on HCC drug resistance and facilitating the discovery of novel therapeutic targets.

The integration of genomics and transcriptomics remains a prominent research direction. Su et al. combined genomics (IRF1 mutation analysis, target gene prediction), transcriptomics (GSEA pathway enrichment, correlations between gene expression and immune factors), and single-cell omics (single-cell transcriptomic profiling of IRF1 distribution) to investigate the clinical significance and biological functions of interferon regulatory factor 1 (IRF1) in NSCLC patients undergoing chemoimmunotherapy. Similarly, Xu et al. integrated multidimensional data (gene expression, mutations, immune cell infiltration, clinical outcomes) to analyze associations between pyroptosis-related genes (PRGs) and the tumor immune microenvironment (TME), constructing a predictive model for immunotherapy response and prognosis. Li et al. leveraged transcriptomics (RNA sequencing), genomics (somatic mutation profiling), and single-cell RNA sequencing (scRNA-seq) to evaluate the predictive value of epithelial-mesenchymal transition (EMT)-related genes in osteosarcoma (OS) prognosis, immune infiltration, and therapeutic response.

Additional exploratory studies, while not employing multi-omics technologies, have innovatively proposed novel strategies to address anti-cancer drug resistance. Shen et al. investigated the use of PEG-PLGA nanoparticles loaded with berberine (Ber) to enhance inhibitory effects on colorectal cancer (CRC). Utilizing transcriptomics (RNA-Seq), they analyzed gene expression changes in HCT116 cells treated with free Ber *versus* nanoparticle-encapsulated Ber (NPBer), clarifying its regulatory effects on critical signaling pathways and biological processes. Chen et al. conducted targeted mechanistic studies on flavonoid derivatives (DMF: 4′,5-dihydroxy-7-piperazinylmethoxy-8-methoxyflavone) extracted and chemically modified from the traditional Chinese herb Sorbaria sorbifolia, elucidating their antitumor effects on hepatocellular carcinoma (HCC) cells and underlying molecular mechanisms. Li et al. explored the role of dorsomorphin in suppressing ABCG2-mediated multidrug resistance (MDR) in CRC. They demonstrated that dorsomorphin reverses MDR by directly inhibiting ATP-binding cassette transporters2 (ABCG2) transporter activity, identifying it as a potential multi-target inhibitor, though further validation of its *in vivo* efficacy is required. Yang et al. compared the efficacy and safety of two chemotherapy regimens (NP group: nedaplatin + liposomal paclitaxel vs. ND group: nedaplatin + docetaxel) in platinum-sensitive recurrent ovarian cancer (ROC) patients. By retrospectively analyzing clinical data (e.g., FIGO staging, number of recurrent lesions) from 121 patients, they found that the ND regimen conferred superior survival benefits with manageable toxicity, supporting personalized therapeutic strategies.

The thematic scope also includes review articles focusing on high-impact research directions. For instance, Song et al.

systematically summarized the molecular mechanisms of cell cycle regulation, the principles of targeted therapies, and preclinical/clinical trial data, highlighting the application of cell cycle checkpoints and their inhibitors in cancer treatment. Wang et al. comprehensively reviewed the roles of long non-coding RNAs (lncRNAs) in urological cancers (prostate, bladder, renal cancers), emphasizing their regulation of autophagy in cancer progression, therapy resistance, and biomarker potential, with partial integration of transcriptomic and epigenetic omics technologies. Chen's article focused on statistical meta-analyses of clinical data, systematically evaluating the survival impacts of various drugs (e.g., metformin, statins, β-blockers, aspirin) in gynecologic malignancies (ovarian, endometrial cancers). Tang et al. reviewed the central role of SIRT1 (Sirtuin 1) in cancer autophagy and drug resistance, emphasizing molecular mechanisms, signaling pathways, and preclinical models (e.g., gene knockout, inhibitor treatment, cell/animal studies).

In summary, therapeutic resistance to antineoplastic agents remains a formidable challenge in oncology. Addressing cancer drug resistance necessitates the development of innovative therapeutic strategies, including immunotherapy, gene editing, and precision medicine paradigms, as well as collaborative efforts across multiple disciplines spanning basic research, clinical investigations, and public health initiatives. Chemoresistance represents a central obstacle in cancer management, and its investigation not only facilitates improved patient prognostication but also establishes critical directions for future therapeutic innovation. Key research priorities include mechanistic investigations of resistance, novel drug development, combination therapeutic regimens, and individualized treatment approaches. The integrative application of multi-omics technologies provides transformative conceptual frameworks for these endeavors, enabling the identification of novel biomarkers and therapeutic targets. Such advancements hold potential to enhance therapeutic efficacy, circumvent resistance mechanisms, and generate promising pathways for translational research and clinical implementation. It is our expectation that discoveries in this field will catalyze further innovation, with anticipation of groundbreaking progress in the evolving landscape of oncology therapeutics.

Author contributions

HW: Writing – original draft. JX: Writing – original draft. ZT: Writing – review and editing. DA-G: Writing – review and editing. HT: Writing – review and editing.

Funding

The author(s) declare that no financial support was received for the research and/or publication of this article.

Acknowledgments

We would like to thank all authors and reviewers for their contributions to this Research Topic. Their efforts help us to communicate current knowledge under this Research Topic to a worldwide audience.

Conflict of interest

The authors declare that the research was conducted in the absence of any commercial or financial relationships that could be construed as a potential conflict of interest.

Generative AI statement

The author(s) declare that no Generative AI was used in the creation of this manuscript.

Publisher's note

All claims expressed in this article are solely those of the authors and do not necessarily represent those of their affiliated organizations, or those of the publisher, the editors and the reviewers. Any product that may be evaluated in this article, or claim that may be made by its manufacturer, is not guaranteed or endorsed by the publisher.

References

Eicher, T., Kinnebrew, G., Patt, A., Spencer, K., Ying, K., Ma, Q., et al. (2020). Metabolomics and multi-omics integration: a survey of computational methods and resources. *Metabolites* 10 (5), 202. doi:10.3390/metabo10050202

Gao, H., Xi, Z., Dai, J., Xue, J., Guan, X., Zhao, L., et al. (2024). Drug resistance mechanisms and treatment strategies mediated by Ubiquitin-Specific Proteases (USPs) in cancers: new directions and therapeutic options. *Mol. Cancer* 23 (1), 88. doi:10.1186/s12943-024-02005-y

Kreitmaier, P., Katsoula, G., and Zeggini, E. (2023). Insights from multi-omics integration in complex disease primary tissues. *Trends Genet.* 39 (1), 46–58. doi:10.1016/j.tig.2022.08.005

Lei, Z. N., Tian, Q., Teng, Q. X., Wurpel, J. N. D., Zeng, L., Pan, Y., et al. (2020). Understanding and targeting resistance mechanisms in cancer. *MedComm* 4 (3). doi:10.1002/mco2.265

Xie, J., Deng, X., Xie, Y., Zhu, H., Liu, P., Deng, W., et al. (2020). Multi-omics analysis of disulfidptosis regulators and therapeutic potential reveals glycogen synthase 1 as a disulfidptosis triggering target for triple-negative breast cancer. *MedComm* 5 (3). doi:10.1002/mco2.502

frontiers | Frontiers in Pharmacology

TYPE Original Research
PUBLISHED 18 April 2024
DOI 10.3389/fphar.2024.1390615

Check for updates

OPEN ACCESS

EDITED BY
Zhi Tian,
University of South Florida, United States

REVIEWED BY
Minghua Wu,
Central South University, China
Bo Chen,
Guangdong Provincial People's Hospital, China
Manbo Cai,
Nanhua University, China

*CORRESPONDENCE
Yi-Zhen Gong,
gongyizhen@gxmu.edu.cn
Teng Deng,
dengtengmd@163.com

†These authors have contributed equally to this work and share first authorship

RECEIVED 23 February 2024
ACCEPTED 05 April 2024
PUBLISHED 18 April 2024

CITATION
Huang Q-R, Jiang Q, Tan J-Y, Nong R-B, Yan J, Yang X-W, Mo L-G, Ling G-Y, Deng T and Gong Y-Z (2024), The prognostic and immunological role of MCM3 in pan-cancer and validation of prognosis in a clinical lower-grade glioma cohort.
Front. Pharmacol. 15:1390615.
doi: 10.3389/fphar.2024.1390615

COPYRIGHT
© 2024 Huang, Jiang, Tan, Nong, Yan, Yang, Mo, Ling, Deng and Gong. This is an open-access article distributed under the terms of the Creative Commons Attribution License (CC BY). The use, distribution or reproduction in other forums is permitted, provided the original author(s) and the copyright owner(s) are credited and that the original publication in this journal is cited, in accordance with accepted academic practice. No use, distribution or reproduction is permitted which does not comply with these terms.

The prognostic and immunological role of MCM3 in pan-cancer and validation of prognosis in a clinical lower-grade glioma cohort

Qian-Rong Huang[1†], Qian Jiang[1†], Ju-Yuan Tan[1], Ren-Bao Nong[1], Jun Yan[1], Xia-Wei Yang[2], Li-Gen Mo[1], Guo-Yuan Ling[1], Teng Deng[1]* and Yi-Zhen Gong[3]*

[1]Department of Neurosurgery, Guangxi Medical University Cancer Hospital, Nanning, China, [2]Guangxi Medical University, Nanning, China, [3]Department of Clinical Research, Guangxi Medical University Cancer Hospital, Nanning, China

Background: Previous studies have shown that MCM3 plays a key role in initiating DNA replication. However, the mechanism of MCM3 function in most cancers is still unknown. The aim of our study was to explore the expression, prognostic role, and immunological characteristics of MCM3 across cancers.

Methods: We explored the expression pattern of MCM3 across cancers. We subsequently explored the prognostic value of MCM3 expression by using univariate Cox regression analysis. Spearman correlation analysis was performed to determine the correlations between MCM3 and immune-related characteristics, mismatching repair (MMR) signatures, RNA modulator genes, cancer stemness, programmed cell death (PCD) gene expression, tumour mutation burden (TMB), microsatellite instability (MSI), and neoantigen levels. The role of MCM3 in predicting the response to immune checkpoint blockade (ICB) therapy was further evaluated in four immunotherapy cohorts. Single-cell data from CancerSEA were analysed to assess the biological functions associated with MCM3 in 14 cancers. The clinical correlation and independent prognostic significance of MCM3 were further analysed in the TCGA and CGGA lower-grade glioma (LGG) cohorts, and a prognostic nomogram was constructed. Immunohistochemistry in a clinical cohort was utilized to validate the prognostic utility of MCM3 expression in LGG.

Results: MCM3 expression was upregulated in most tumours and strongly associated with patient outcomes in many cancers. Correlation analyses demonstrated that MCM3 expression was closely linked to immune cell infiltration, immune checkpoints, MMR genes, RNA modulator genes, cancer stemness, PCD genes and the TMB in most tumours. There was an obvious difference in outcomes between patients with high MCM3 expression and those with low MCM3 expression in the 4 ICB treatment cohorts. Single-cell analysis indicated that MCM3 was mainly linked to the cell cycle, DNA damage and DNA repair. The expression of MCM3 was associated with the

clinical features of LGG patients and was an independent prognostic indicator. Finally, the prognostic significance of MCM3 in LGG was validated in a clinical cohort.

Conclusion: Our study suggested that MCM3 can be used as a potential prognostic marker for cancers and may be associated with tumour immunity. In addition, MCM3 is a promising predictor of immunotherapy responses.

KEYWORDS

pan-cancer, minichromosome maintenance complex component 3 (MCM3), immunotherapy, prognosis, lower-grade glioma

Introduction

In recent decades, the incidence of cancer has been increasing, which has been fuelled by population growth, population ageing, and the implementation of advanced early detection and treatment modalities. This scenario has led to an ever-growing population of cancer survivors, thus contributing to an alarming global burden of cancer that now represents a significant threat to the health of humanity (Sung et al., 2021). Despite the rapid development of early prevention and treatment techniques for cancer, the mortality rate of cancer remains a concern (Torre et al., 2015; Miller et al., 2022). As research continues to advance, an increasing number of researchers are focusing on the common features of cancer. Pan-cancer analysis, which compares data such as gene mutation, gene expression, and protein expression data across different types of cancer, employs sophisticated bioinformatics techniques to identify shared and distinct characteristics among cancers (Cancer Genome Atlas Research et al., 2013). Previous research has demonstrated that a number of genes are crucial for the immune microenvironment, prognosis, and drug resistance in pan-cancer (Fu et al., 2022; Pan et al., 2022; Xie et al., 2022; Zhou et al., 2023). Consequently, this analytical approach has proven to be a powerful tool for investigating the genetic and molecular basis of numerous cancer types (Xu et al., 2020; Chen et al., 2021).

Minichromosome maintenance complex component 3 (MCM3) is a crucial member of the MCM protein family that interacts with other members (MCM2 and MCM4-7) to form a durable heterohexameric complex, which plays a pivotal role in initiating DNA replication (Madine et al., 2000; Evrin et al., 2014; Deegan and Diffley, 2016; Sedlackova et al., 2020). MCM3 is highly expressed in diverse types of malignancies, including breast cancer (Lokkegaard et al., 2021), ovarian cancer (Li et al., 2021), colorectal cancer (Zhou et al., 2020), and prostate cancer (Hsu et al., 2021). Notably, multiple studies have demonstrated that elevated MCM3 expression is strongly linked to tumour progression, metastasis, and prognosis (Li et al., 2021; Lokkegaard et al., 2021; Yang et al., 2019; Zhou et al., 2020). In addition, phosphorylated MCM3 has been shown to promote cell proliferation and inhibit cell apoptosis in renal cell carcinoma cells (Gao et al., 2022). Another study suggested that the MCM3 proliferation index was more clinically relevant than Ki-67 in the characterization of salivary gland tumours (Raja et al., 2021). Indeed, MCM3 not only plays a crucial role in DNA replication but is also involved in the DNA damage response and DNA repair (Drissi et al., 2018). Cancers rely on the activation of DNA repair pathways to maintain genomic stability, stemness, and chemotherapy resistance (Abad et al., 2020; Wang et al., 2021); therefore, further evaluation of the relationship of MCM3 with DNA repair genes and cancer stemness across cancers is warranted. Overall, investigations of MCM3 have been largely limited to a small number of cancer types, and the role of MCM3 in various malignancies and the underlying mechanisms remain incompletely understood.

Herein, we comprehensively assessed the expression and prognostic role of MCM3 across cancers. We then systematically evaluated the associations of MCM3 with immune signatures, mismatching repair (MMR) genes, RNA modulator genes, cancer stemness, programmed cell death (PCD) genes, the TMB, MSI, and neoantigen levels. In our study, the ability of MCM3 to predict immunotherapy response was also evaluated, and its association with 14 biological functions was evaluated at the single-cell level. In addition, based on data from The Cancer Genome Atlas (TCGA) and Chinese Glioma Genome Atlas (CGGA) databases, further clinical correlation analysis, independent prognostic analysis, nomogram construction, and biological function exploration were conducted in LGG cohorts. Finally, the clinical correlation and prognostic significance of MCM3 in LGG were verified in a clinical cohort from Guangxi Medical University Cancer Hospital.

Materials and methods

Data collection and expression analysis

The mRNA data (TPM) for the TCGA pan-cancer cohort and corresponding normal tissues from the GTEx were downloaded from UCSC database. Survival data for each type of cancer were also downloaded from UCSC. The mRNA data were log2 (TPM+1) transformed. We first compared MCM3 mRNA expression in tumour and normal tissues and evaluated the differences between groups by using the Wilcoxon test. We further evaluated MCM3 protein levels across cancers by utilizing the CPTAC portal in the UALCAN database. By employing the GEPIA online database, we preliminarily investigated the relationship between MCM3 expression and clinical stage. In this study, we also explored the genomic alterations of MCM3 across cancers by using the cBioPortal database. Immunofluorescence (IF) images from the HPA database were used to identify the subcellular localization of MCM3 in tumours. In addition, immunohistochemistry (IHC) was used to compare MCM3 protein expression in LGG and normal brain tissue.

Prognosis evaluation

We analysed the association between MCM3 expression and patient outcomes for each cancer type. In this study, we evaluated four prognostic indicators, including overall survival (OS), progression-free interval (PFI), disease-specific survival (DSS), and disease-free interval (DFI). MCM3 expression was included as a continuous variable in univariate Cox regression analysis according to the "survival" package in R. In addition, a heatmap was generated to display the survival analysis results associated with MCM3 across cancers.

Assessment of relevant characteristics

The tumour microenvironment (TME) plays a key role in tumour formation and progression (Xiao 2021; Zou et al., 2023). We assessed the relationships between MCM3 and TME-related parameters (immune, stromal and ESTIMATE scores) across cancers by using the "estimate" package (Yoshihara et al., 2013). By using the "IOBR" package, we applied the TIMER algorithm to measure the relationship between MCM3 expression and the infiltration levels of six immune cell types across cancers (Li et al., 2017). We extracted expression data for immune checkpoint components (inhibitory and stimulatory) and several PCD (pyroptosis, cuproptosis, anoikis, necroptosis, disulfdptosis and autophagy) markers and evaluated the association of MCM3 expression with these markers. The correlation of MCM3 with 5 MMR signatures and 44 RNA modification genes (m1A, m5C and m6A) in pan-cancer was analysed (Liang et al., 2022). In addition, we obtained pan-cancer differentially methylated probe-based stemness index (DMPsi) from the study by Malta et al. to determine the relationship between MCM3 expression and cancer stemness (Malta et al., 2018).

Immunotherapy prediction and drug sensitivity analysis

TMB, MSI, and neoantigens have been reported to influence cancer prognosis and immunotherapy response (Ettinger et al., 2019; Picard et al., 2020). We also investigated the association of MCM3 with these markers. In addition, we selected four cohorts of tumour patients who were receiving ICB therapy to further evaluate the ability of MCM3 to predict the response to immunotherapy. By using the "survminer" package in R, we determined the optimal cut-off value and divided the IMvigor210 (urinary tumours), GSE176307 (urothelial cancer), GSE135222 (non-small cell lung cancer, NSCLC) and GSE91061 (melanoma) cohorts into high-MCM3 and low-MCM3 groups. We then compared the outcomes and treatment responses between the high-MCM3 and low-MCM3 subgroups. The data for these immunotherapy cohorts were obtained from the http://research-pub.gene.com/IMvigor210CoreBiologies/packageVersions/, TIGER (http://tiger.canceromics.org/#/download) and GEO (https://www.ncbi.nlm.nih.gov/geo/) websites. Finally, we explored the correlation between MCM3 expression and drug sensitivity by using CTRP and GDSC data from the GSCA database (http://bioinfo.life.hust.edu.cn/GSCA/#/drug) to help identify potential drugs targeting MCM3.

Single-cell analysis

CancerSEA is a single-cell sequencing database for assessing the status and function of single cells in a variety of tumours (Yuan et al., 2019). Herein, we analysed the correlation between MCM3 expression and 14 functions based on single-cell data from the CancerSEA database via Spearman analysis. In addition, by using single-cell data from the TISCH database (http://tisch.comp-genomics.org/) (Sun et al., 2021), we further evaluated the expression of MCM3 in different cancer cell subtypes.

Clinical correlation analysis of MCM3 in LGG

For in-depth analysis of LGG, mRNA data (FPKM) and clinical information from LGG cohorts were obtained from the TCGA and CGGA databases. We transformed the expression data *via* log2(FPKM+1) transformation. We then analysed the relationships between MCM3 mRNA expression and five clinical parameters, and the differences between the two groups were evaluated by using the Wilcoxon test. Based on the median expression value, we compared the OS of the high-MCM3 and low-MCM3 expression groups by using the Kaplan–Meier (KM) method. A time-dependent receiver operating characteristic (timeROC) curve was used to evaluate the efficacy of MCM3 in predicting survival. These analyses were performed by using the "timeROC" package in R. By using three glioma single-cell datasets (GSE139448, GSE163108 and GSE162631) in the TISCH database, MCM3 expression in different immune cells of glioma was evaluated.

Nomogram construction, enrichment analysis and TMB analysis in LGG

The prognostic role of MCM3 was further assessed via multivariate analysis in the TCGA training cohort. With the "rms" package, independent prognostic features were selected to construct a prediction nomogram. The CGGA cohort served as the validation cohort. We used timeROC curves, calibration curves, decision curve analysis (DCA) and Kaplan–Meier (KM) curves to systematically evaluate the predictive ability of the model. To explore more potential biological mechanisms of MCM3 activity in LGG, differentially expressed genes (DEGs) between the two subgroups of the TCGA cohort were identified, and enrichment analyses, including GO, KEGG, and GSEA, were performed by using the "clusterProfiler" and "enrichplot" packages. P. adjust <0.05 was used as the significance threshold for enrichment analysis in GO and KEGG analyses, while $p < 0.05$ was defined as statistically significant in GESA. We also analysed the mutation frequency and TMB of the two subgroups in the TCGA cohort. The mutation data were evaluated and visualized by using the "maftools" software package. The TIDE algorithm is a novel tool for evaluating immunotherapy responses (Cao et al., 2020). We calculated TIDE

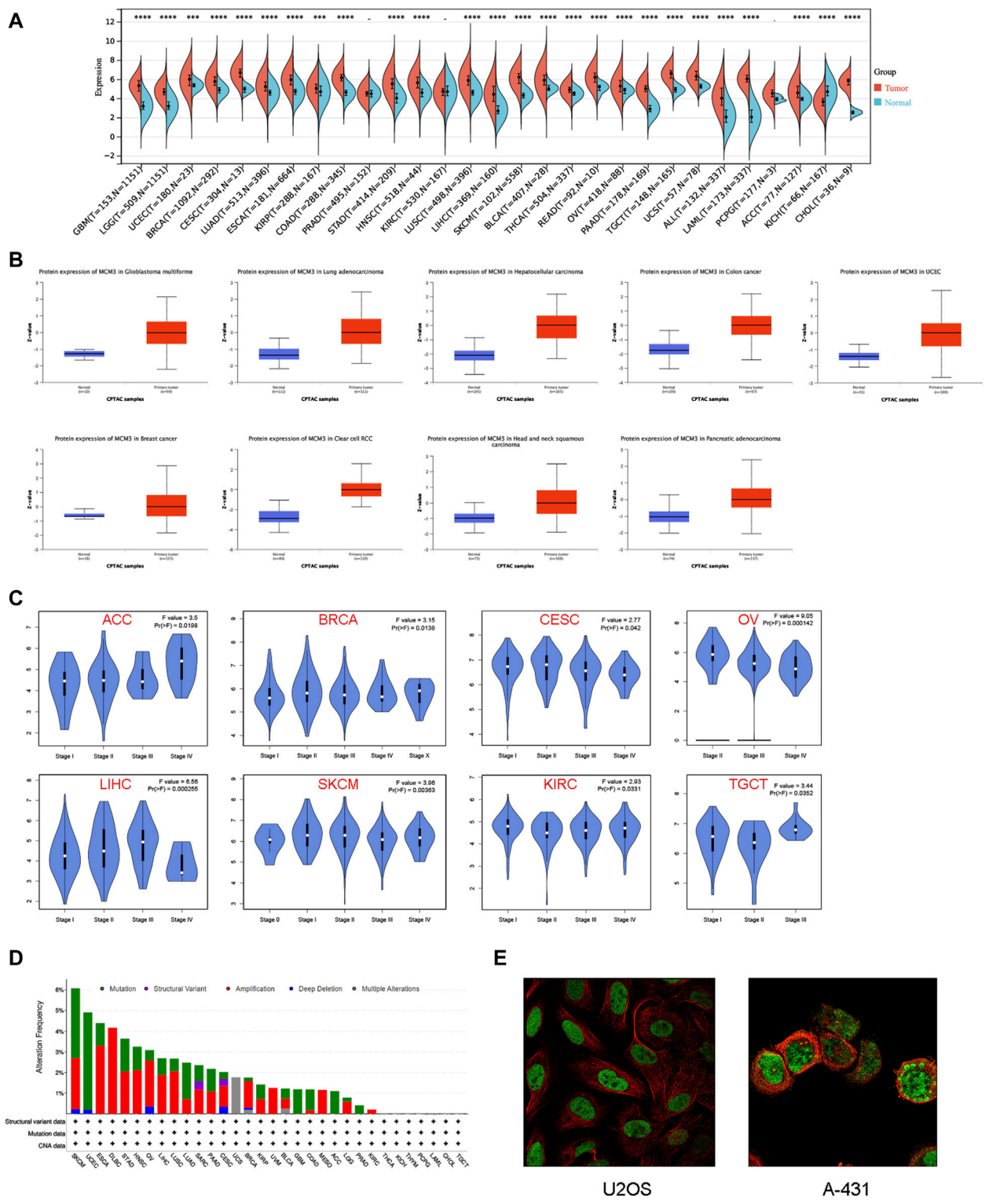

FIGURE 1
Expression patterns of MCM3 in pan-cancer. **(A)** Differences in MCM3 between tumor and normal tissues based on TCGA and GETx data. **(B)** Comparison of protein levels based on CPTAC data. **(C)** Clinical correlation analysis based on GEPIA database. **(D)** The genomic alteration of MCM3 in pan-cancer. **(E)** Immunofluorescence results showed the localization of MCM3 in cell lines. ****$p < 0.0001$.

scores for the TCGA-LGG cohort by using the TIDE database and compared the scores between the two subgroups.

Validation of the prognostic significance of MCM3 in LGG

We first compared MCM3 protein levels in LGG and normal brain tissue by using the HPA database. We then validated the prognostic value of MCM3 in LGG in a clinical cohort. Tumour specimens and clinicopathological parameters were collected from patients with newly diagnosed LGG who underwent surgical treatment at Guangxi Medical University Cancer Hospital between May 2013 and December 2018. Tumour specimens were embedded in paraffin immediately after collection, and clinicopathological information was collected for all of the patients. This clinical cohort was followed up until July 2019, with death or progression as the end events, and both OS and progression-free survival (PFS) were calculated. IHC staining for MCM3 was then performed on paraffin-embedded LGG tissue. The MCM3 antibody was purchased from Boster Biological Technology Company (article number: BA2186). The percentage of positively stained cells was scored as follows: 0 (0%), 1 (1%–25%), 2 (26%–50%), 3 (51%–75%), and 4 (76%–100%). The intensity of staining was scored as follows: 0 (no staining), 1 (weak), 2 (moderate), and 3 (strong). The expression of MCM3 was determined as the product of these two scores. Ultimately, a score of 0–2 was defined as indicating negative MCM3 expression, and a score of 3–12 was defined as indicating positive MCM3 expression (Zhang et al., 2016).

Statistical analysis

In this study, comparisons of MCM3 expression in normal and tumour tissues and analyses of the correlation of MCM3 levels with clinical features in LGG were performed via the Wilcoxon test. The prognostic significance of MCM3 was assessed by using univariate, multivariate Cox and Kaplan–Meier (KM) (log-rank test) analyses. The relationships between MCM3 expression and immunological characteristics, PCD gene expression, TMB, MSI, neoantigen levels, and biological functions at the single-cell level were evaluated via Spearman analysis. Chi-square tests were utilized to compare the proportions between two groups. The remaining methods are described in the Methods section. A P-value <0.05 was considered to indicate statistical significance. The analysis and graphing in this study were performed in R (v 3.6.3). A portion of the pan-cancer analysis and graphing of MCM3 was performed through two online websites (Home for researchers [https://www.home-for-researchers.com/static/index.html#/] and Xiantaoxueshu [https://www.xiantaozi.com/]).

Results

Expression patterns of MCM3 across cancers

We first investigated the differences in MCM3 mRNA levels between normal and tumour tissues. The results showed that the expression of MCM3 was upregulated in most tumours but significantly lower in KICH tissues than in normal tissues. In PRAD, KIRC, and PCPG, the differences were not significant (Figure 1A). Data from the CPTAC portal confirmed elevated MCM3 protein expression in a variety of cancers, including GBM, LUAD, LIHC, COAD, UCEC, BRCA, KIRC, HNSC, and PAAD (Figure 1B). By using the GEPIA database, we analysed the association between MCM3 and clinical stage across cancers. We found that MCM3 expression was significantly associated with the clinical stages of eight cancers, including ACC, BRCA, CESC, KIRC, LIHC, OV, SKCM and TGCT (Figure 1C). We further explored the genomic alteration status of MCM3 across cancers via the cBioPortal website. Overall, genetic variations in MCM3 occur in less than 5% of most cancers. The highest frequency of MCM3 variants (>6%) was found in SKCM, with "mutation" and "amplification" being the main types. UCEC had the highest incidence (>4%) of "mutations", whereas DLBC had the highest incidence (>4%) of "amplification" (Figure 1D). IF of tumour cells from the HPA database showed that MCM3 protein was localized in the nuclei of U2OS (osteosarcoma) and A-431 (cutaneous squamous cell) cell lines (Figure 1E).

Prognostic significance of MCM3 across cancers

We subsequently used univariate Cox analysis to explore the prognostic significance of MCM3 in multiple aspects, including OS, the PFI, DSS and the DFI. The results showed that MCM3 expression levels were closely linked to different outcomes in many cancers (Figure 2A). For OS, MCM3 was a risk index for LGG, ACC, LIHC, KICH, SARC and MESO but a protective factor for OV and THYM (Figure 2B). The upregulation of MCM3 suggested that LGG, ACC, LIHC, KICH, PRAD and SARC had shorter PFIs, whereas OV and GBM had longer PFIs (Figure 2C). For DSS, MCM3 expression was a risk factor in LGG, KICH, ACC, LIHC, SARC, LUAD, KIRP and PRAD and a protective factor in OV (Figure 2D). In addition, high MCM3 expression was associated with a shorter DFI in LIHC, CESC, COAD, KIRP and LUSC (Figure 2E).

Association between MCM3 expression and tumour immunity

We investigated the relationship between MCM3 and tumour immunity in three aspects, including the TME profile, immune cell infiltration and immune checkpoint factor expression. The results showed that MCM3 expression was negatively correlated with the stromal score, immune score, and ESTIMATE score in most tumours, whereas significant positive correlations with these scores were observed in LGG, KIRC and PRAD (Figure 3A). By using the TIMER algorithm, we evaluated the infiltration levels of six immune cell types across cancers. MCM3 expression was positively correlated with immune cell infiltration in most tumours, especially in KIRC, LGG, LIHC, PCPG, PRAD and THCA (Figure 3B). Similarly, MCM3 expression was positively correlated with immune checkpoint factor expression in most tumours, especially in HNSC, KIRC, LIHC, LGG, UVM, KICH, and PRAD (Figure 3C).

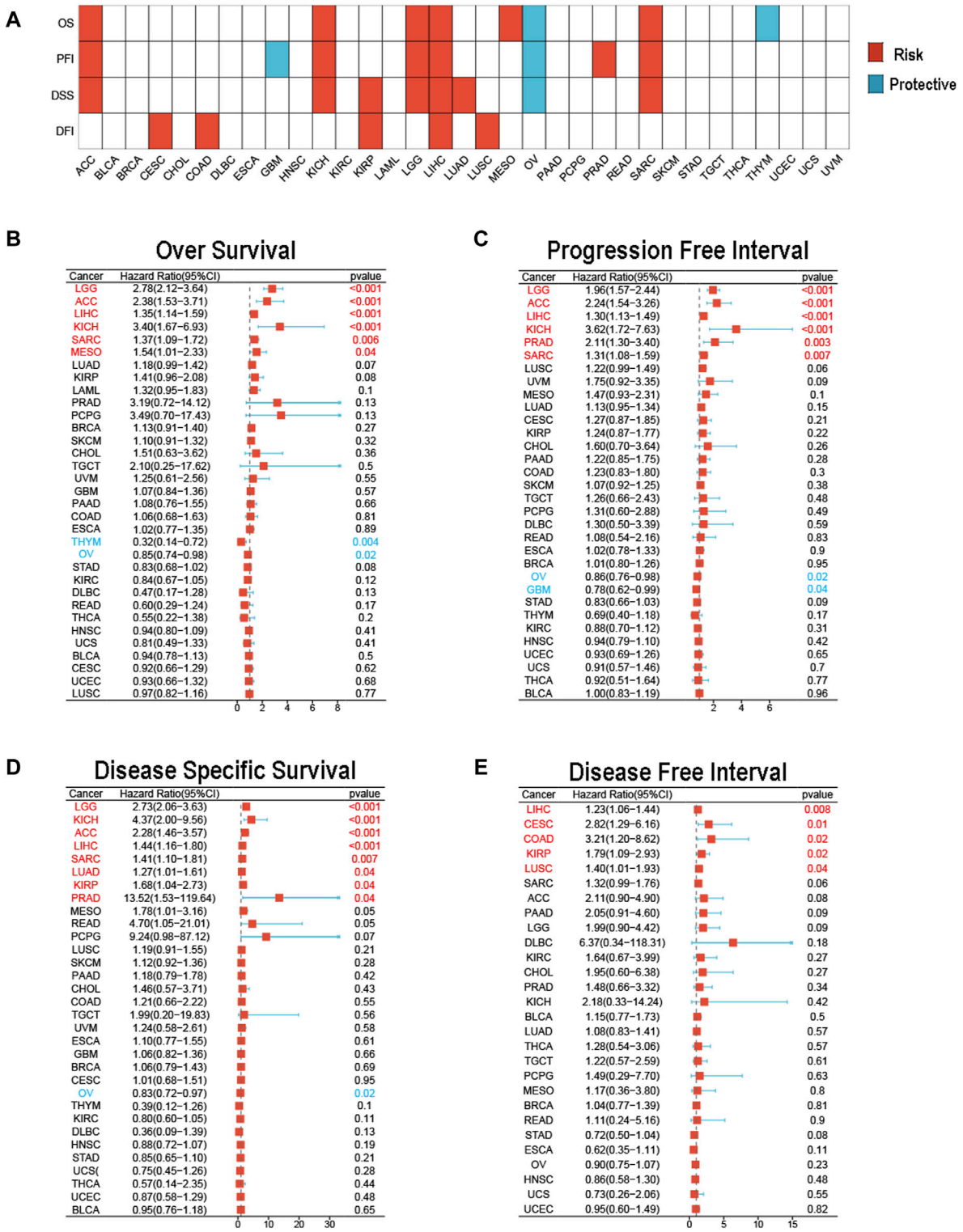

FIGURE 2
Prognostic value of MCM3 in pan-cancer. **(A)** The heatmap shows results of univariate Cox regression analysis. **(B)** Forest plot of MCM3 expression and OS across cancers. **(C)** Forest plot of MCM3 expression and PFI across cancers. **(D)** Forest plot of MCM3 expression and DSS across cancers. **(E)** Forest plot of MCM3 expression and DFI across cancers.

Surprisingly, MCM3 was positively correlated with the expression of several immune checkpoint molecules, such as HMGB1, BTN3A2, CD276, and VEGFA, in almost all of the tumours.

For the MMR signatures, we found a significant positive correlation between them and MCM3 broadly in pan-cancer, and a negative correlation between EPCAM and

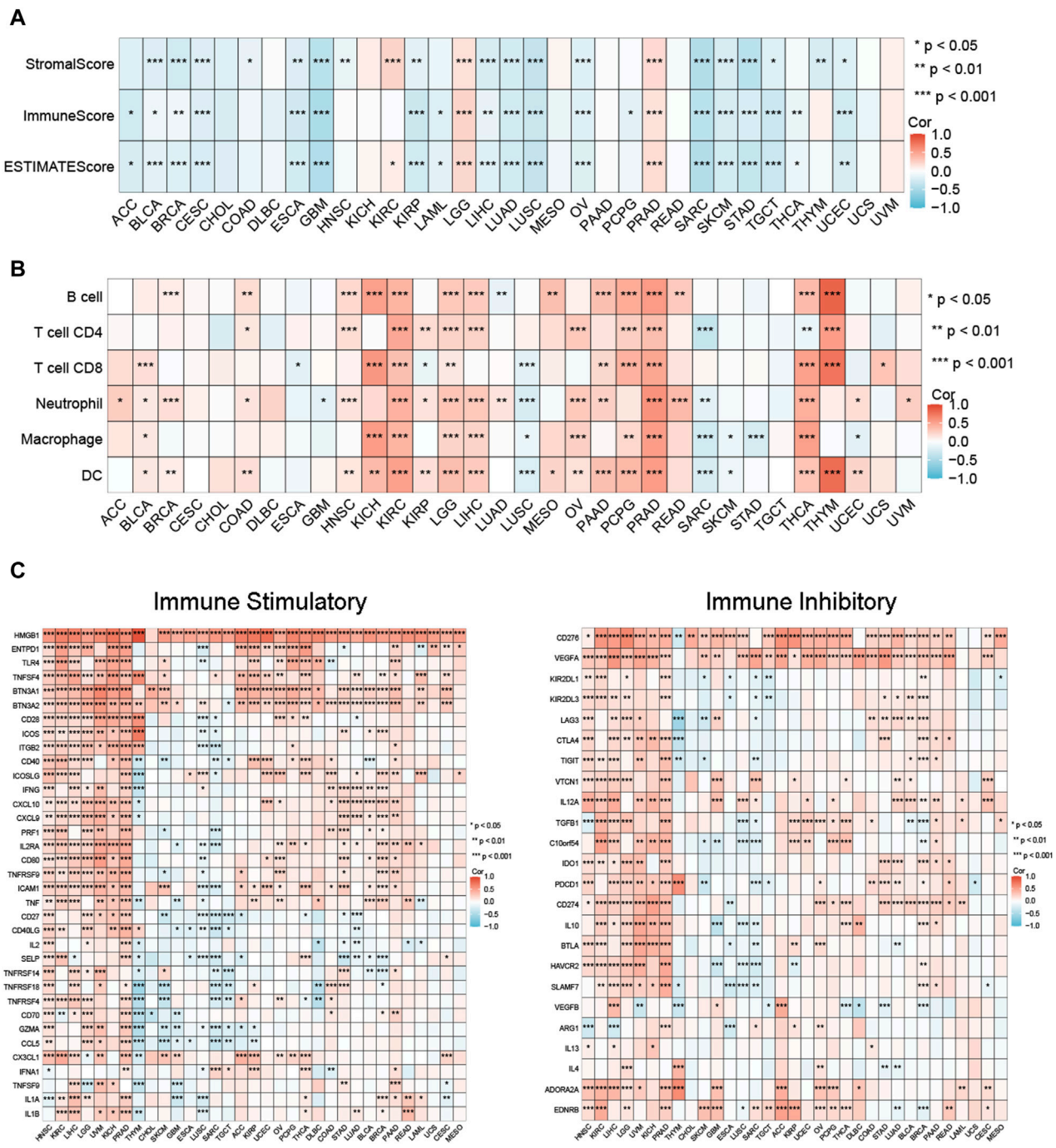

FIGURE 3
Relationship between MCM expression and immune-related features in pan-cancer. **(A)** MCM3 expression and tumor microenvironment relate parameters. **(B)** MCM3 expression and immune cell infiltration. **(C)** MCM3 expression and immune checkpoints. *$p < 0.05$, **$p < 0.01$, ***$p < 0.001$.

MCM3 expression in LGG and THYM (Supplementary Figure S1A). Moreover, we observed a positive correlation between MCM3 expression and DMPsi in DLBC, LGG and STAD and a negative correlation between MCM3 expression and THYM, KIRP and THCA (Supplementary Figure S1B), thus suggesting that MCM3 may be involved in DNA repair-mediated cancer stemness. Interestingly, we also found that MCM3 was positively correlated with most RNA modulator genes across cancers (Supplementary Figure S1C).

Recently, PCD modalities, such as pyroptosis, cuproptosis, anoikis, necroptosis, disulfdptosis and autophagy, have been reported to play important roles in the development and progression of cancer. Therefore, we further explored the relationship between MCM3 and markers of PCD. The results indicated a general correlation between

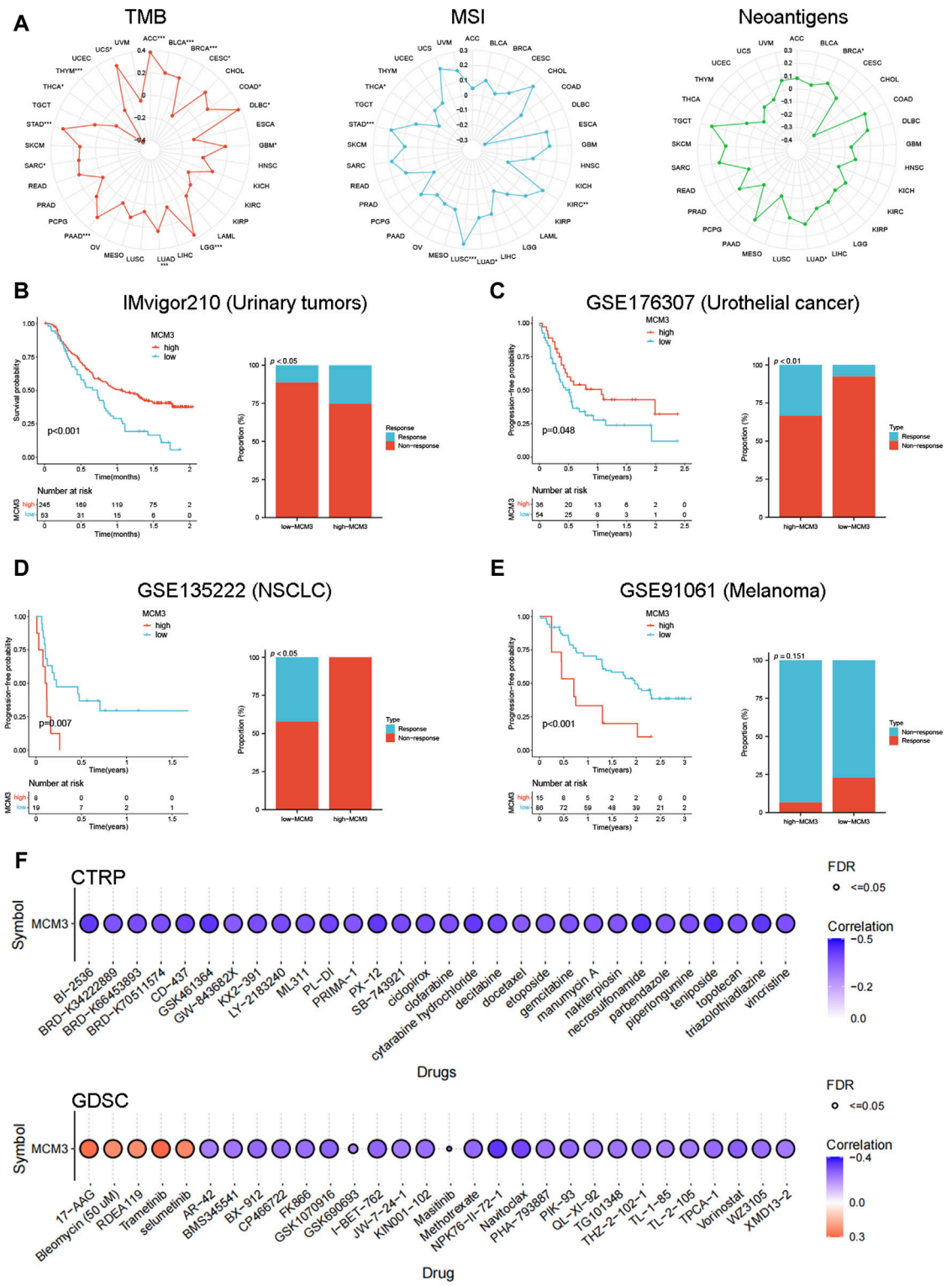

FIGURE 4
Immunotherapy and drug sensitivity analysis. **(A)** Relationship between MCM3 expression and TMB, MSI, and neoantigens. **(B–E)** Prognostic significance of MCM3 and proportion of immunotherapy response between high- and low-MCM3 groups in four cohorts receiving ICB therapy. **(F)** Drug sensitivity analysis of MCM3 based on CTPR and GDSC data. *$p < 0.05$, **$p < 0.01$, ***$p < 0.001$.

MCM3 and PCD markers. Among these genes, MCM3 was significantly correlated with most pyroptosis genes across cancers, except for CHOL, MESO and UCS (Supplementary Figure S2A). Similarly, MCM3 was generally associated with markers of cuproptosis, anoikis, necroptosis, disulfdptosis and autophagy in most tumours (Supplementary Figure S2B–F).

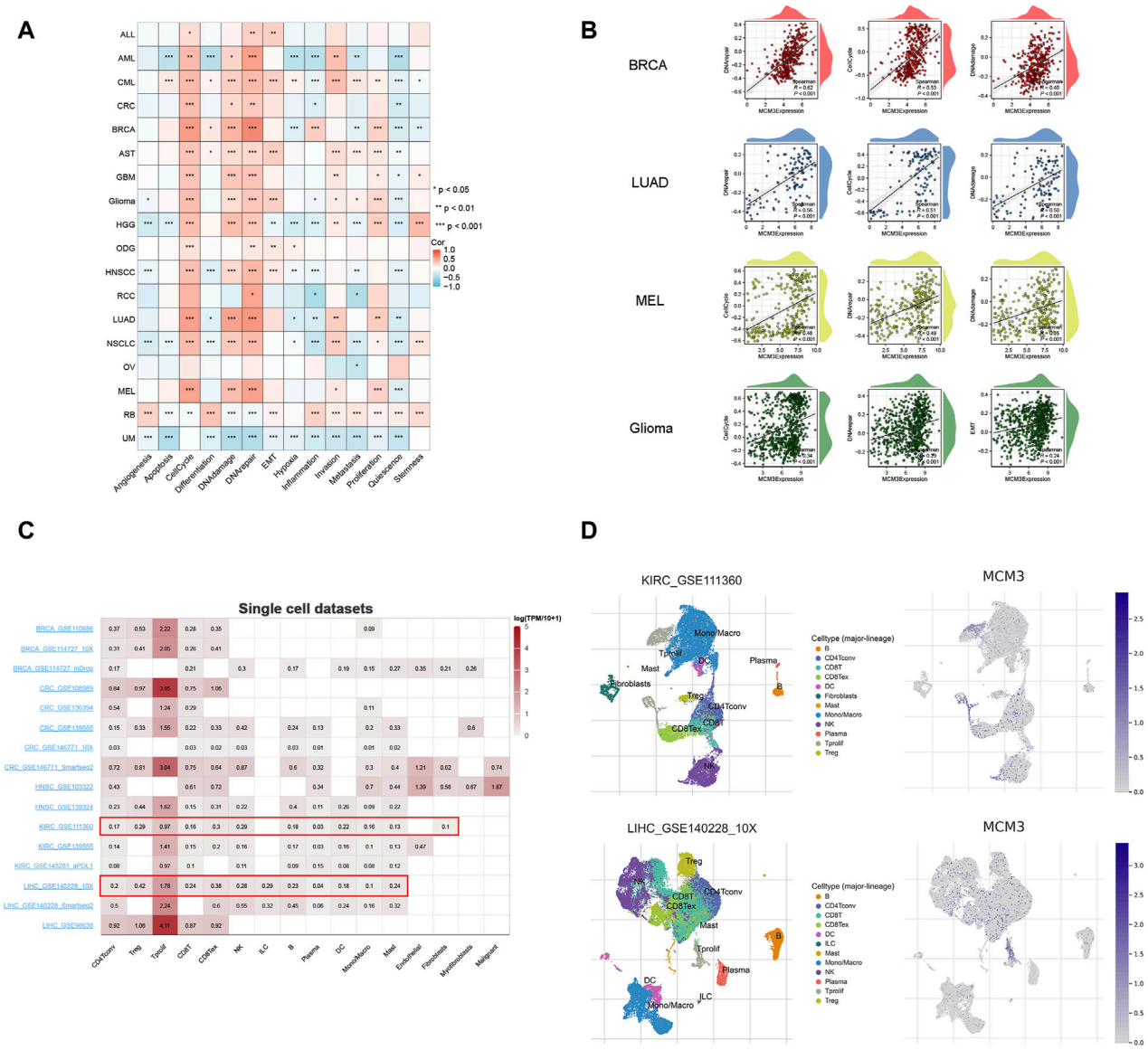

FIGURE 5
Single-cell analysis of MCM3. **(A)** Correlation between MCM3 and 14 biological functions. **(B)** The top three functions in BRCA, LUAD, MEL and glioma. **(C)** Datasets of single-cell expression of MCM3 from TISCH website. **(D)** Distribution of MCM3 among cell types in the GSE111360 and GSE140228 datasets. *$p < 0.05$, **$p < 0.01$, ***$p < 0.001$.

Associations of MCM3 with immunotherapy response and drug sensitivity

Considering that TMB, MSI, and neoantigen expression are common genomic alterations that are closely associated with cancer prognosis and immunotherapeutic responses (Ettinger et al., 2019; Ben-David and Amon, 2020; Picard et al., 2020), we measured the association between MCM3 and these alterations across cancers. As shown in Figure 4A, MCM3 and TMB were positively correlated in 12 cancers and negatively correlated in three cancers. There was a positive correlation between MCM3 expression and MSI in KIRC, LUAD, LUSC and STAD but a negative correlation in THCA. In contrast, the correlation of neoantigen expression with MCM3 was generally not significant; additionally, a positive correlation was shown only in BRCA and LUAD (Figure 4A). We subsequently evaluated the ability of MCM3 to predict the response to immunotherapy in four clinical cohorts receiving ICB therapy. Survival analysis demonstrated an obvious difference in prognosis between the two subgroups in all of the cohorts (Figures 4B–E). In addition to the GSE91061 cohort, there were significant differences in the proportion of patients who experienced treatment benefits between the two subgroups (Figures 4B–E). These data indicated that MCM3 expression could effectively distinguish patients who had different responses to ICB treatment and further suggested that MCM3 could be used as a potential marker to assess immunotherapy responses. Finally, based on data from the CTRP and GDSC databases, we investigated the association of MCM3 with drug sensitivity to explore potential targeted drugs. The CTRP results demonstrated that the MCM3 level was negatively correlated with sensitivity to most drugs. The GDSC results

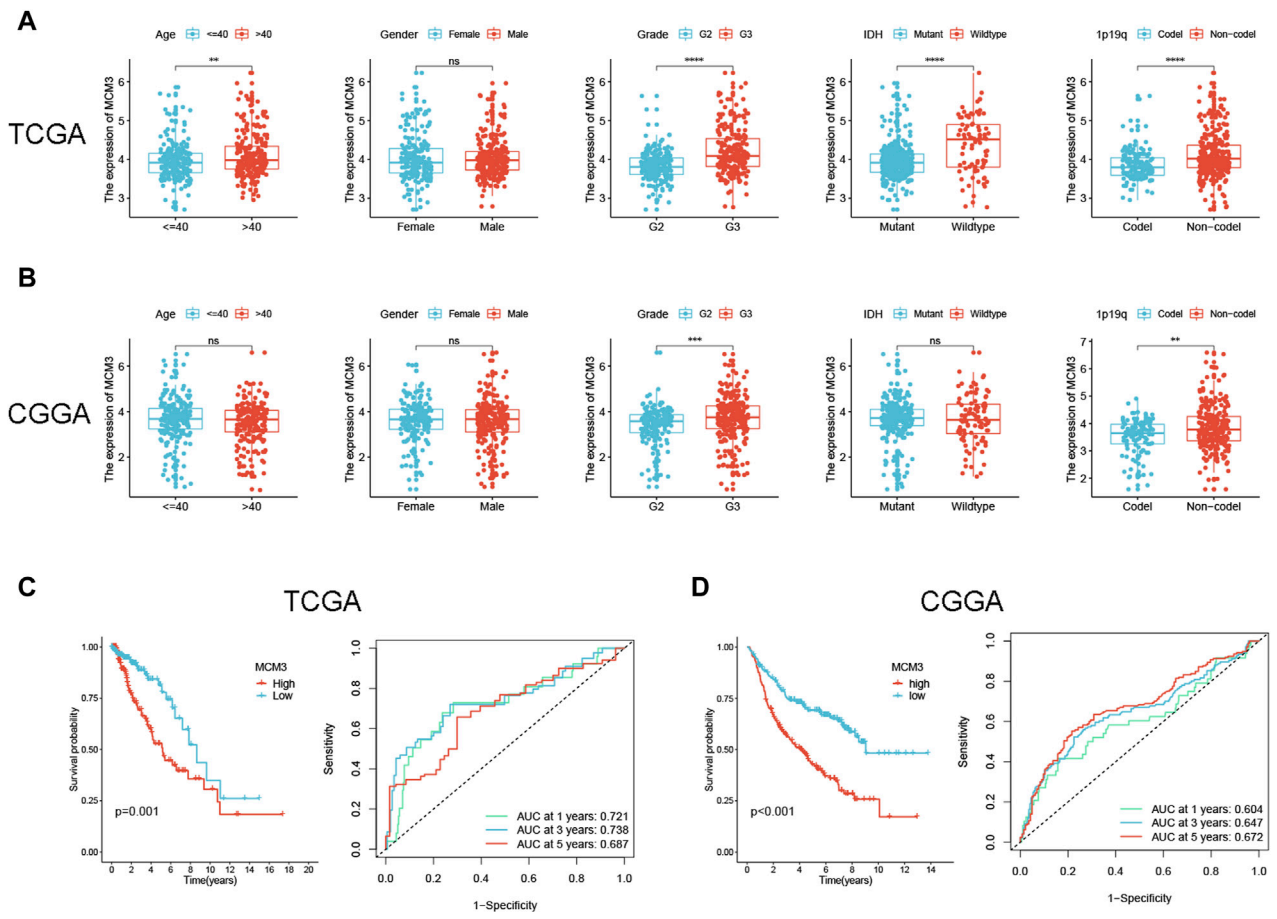

FIGURE 6
Correlation between MCM3 expression and clinical features and prognosis of LGG. **(A, B)** Relationship between MCM3 and clinical features in TCGA and CGGA cohorts. **(C, D)** Evaluation of the ability of MCM3 expression to predict prognosis in TCGA and CGGA cohorts. ns: no significance, $^{**}p < 0.01$, $^{***}p < 0.001$, $^{****}p < 0.0001$.

showed that sensitivity to five drugs, including 17-AAG, bleomycin (50 μM), RDEA119, trametinib and selumetinib, was positively correlated with MCM3 expression, whereas sensitivity to other drugs was negatively correlated with MCM3 expression (Figure 4F). These results may provide a basis for developing therapies targeting MCM3.

Single-cell analysis

We evaluated the relationship between MCM3 and 14 biological functions in multiple cancers at the single-cell level by using the CancerSEA database. As the heatmap shows, MCM3 is closely linked to these biological functions in most cancers. Among them, the cell cycle, DNA damage and DNA repair had the most significant correlations with MCM3 expression (Figure 5A). In addition, we generated correlation plots of the top three functions in BRCA, LUAD, MEL, and glioma (Figure 5B). The TISCH data showed that MCM3 was widely expressed in most immune cells, with major concentrations in CD4Tconv, Treg, Tprolif, CD8T, CD8Tex and NK cells (Figure 5C). Figure 5D shows the expression of MCM3 in the GSE111360 and GSE140228 single-cell datasets collected.

Clinical correlation analysis of MCM3 in LGG

Preliminary results indicated that MCM3 was dysregulated in LGG and could be used as a prognostic predictor of LGG (including OS, PFI and DSS). In addition, MCM3 expression was closely related to various immune features of LGG. We further investigated the correlation between MCM3 and clinical parameters and verified its prognostic value in LGG. The clinical data of the two publicly available cohorts are shown in Supplementary Table S1. In the TCGA cohort, MCM3 expression was closely correlated with age, grade, IDH expression, and 1p19q deletion status (Figure 6A). In CGGA cohort, MCM3 expression was closely linked to the grade and 1p19q deletion status (Figure 6B). KM analysis also showed that MCM3 has good predictive value. In the TCGA cohort, patients with low MCM3 expression had longer OS than those with high MCM3 expression, and the AUC values of MCM3 expression for predicting 1-, 3- and 5-year survival in LGG patients were 0.721,

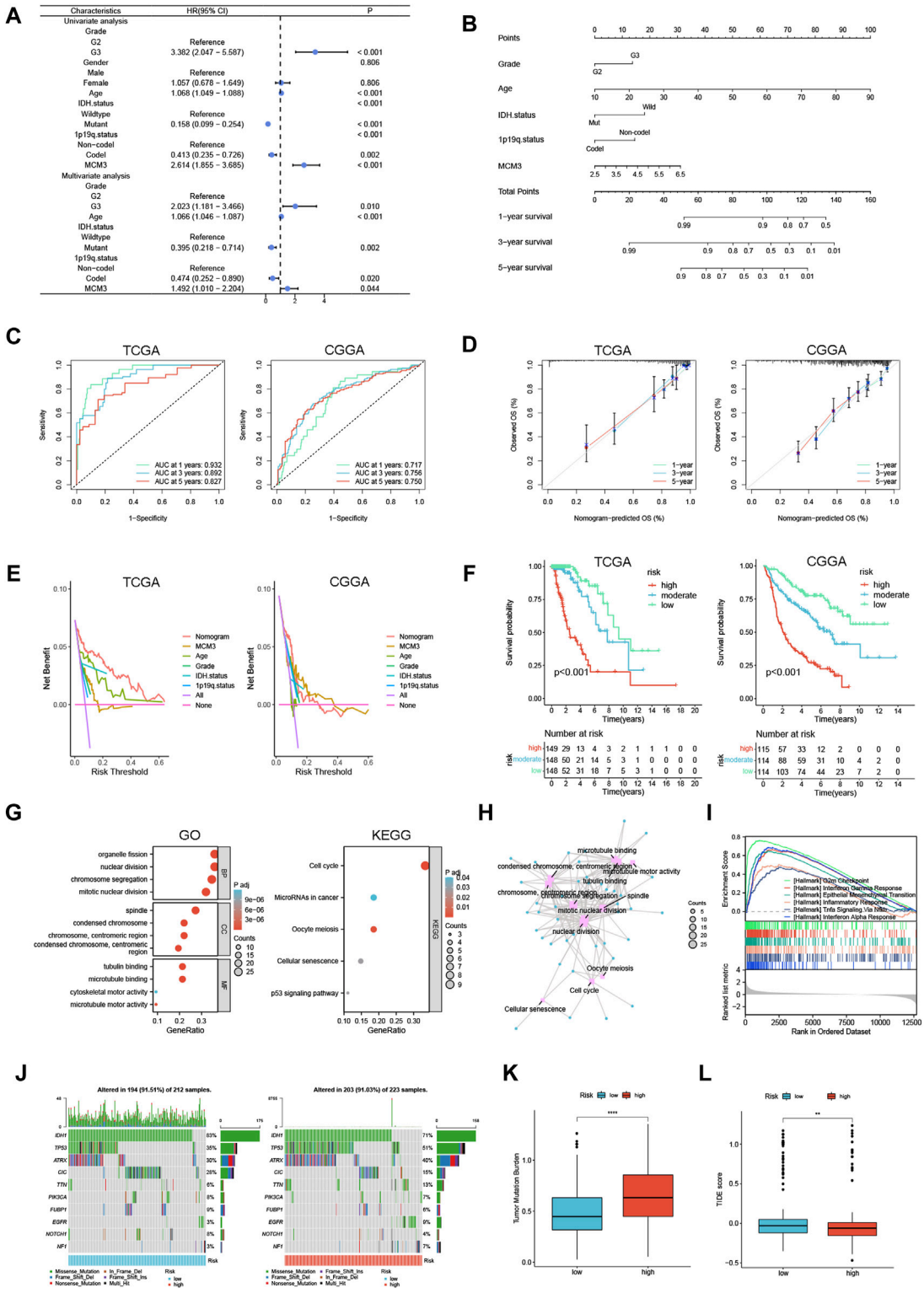

FIGURE 7
Construction of a prognostic nomogram and analysis of MCM3 related functions in LGG. **(A)** Univariate/multivariate Cox analysis was performed based on TCGA cohort. **(B)** Establishment of a prognostic nomogram based on multivariate analysis results. **(C–F)** Nomogram model evaluation, including timeROC, calibration, DCA and KM curves. **(G)** GO and KEGG analyses based on differentially expressed genes in TCGA. **(H)** An interaction network between GO and KEGG. **(I)** The GSEA analysis in TCGA cohort. **(J)** The waterfall map shows the top 10 genes with the highest mutation probability. **(K, L)** TMB and TIDE score were compared between the two groups. $^{**}p < 0.01$, $^{****}p < 0.0001$.

0.738 and 0.687, respectively. (Figure 6C). The KM curve of the CGGA cohort showed similar results, with AUC values of 0.604, 0.647 and 0.672, respectively (Figure 6D). We evaluated MCM3 expression in immune cells by using three datasets from the TISCH database. In the GSE139448 dataset, MCM3 expression was highest in malignant cells, whereas in the GSE163108 and GSE162631 datasets, MCM3 expression was highest in Tprolif and Mono/Macro cells, respectively (Supplementary Figure S3). Our findings demonstrated that the expression of MCM3 differed in different cell types and that there were differences in cell components among samples, which may be related to the heterogeneity of the glioma microenvironment.

Nomogram construction, enrichment analysis and TMB analysis in LGG

Furthermore, univariate/multivariate Cox analysis indicated that MCM3 had independent prognostic significance in the TCGA cohort (Figure 7A). To improve the clinical application value of MCM3, our study incorporated independent prognostic parameters from the TCGA cohort to construct a nomogram, and the CGGA cohort served as the validation cohort (Figure 7B). The model AUC values were significantly improved in both cohorts (Figure 7C). The calibration curves showed that the results predicted by the model were close to the actual observed results (Figure 7D). The DCA curves showed that the model was more beneficial for predicting the outcome of LGG patients than any single prognostic factor (Figure 7E). Based on the risk scores calculated by the model, the two cohorts were evenly divided into three subgroups, and the survival analysis indicated obvious differences in OS among the subgroups (Figure 7F), which further suggested that the MCM3-based prognostic nomogram could be an effective risk assessment tool for LGG patients. A total of 77 DEGs between the high-MCM3 and low-MCM3 groups in the TCGA training cohort were identified. GO results indicated that the DEGs were closely linked to organelle fission, nuclear division, chromosome segregation, mitotic nuclear division, chromosomes, centromeric region and microtubule binding. According to the KEGG analysis, these DEGs were mainly enriched in the terms “cell cycle”, “microRNAs in cancer”, “cellular senescence” and “p53 signalling pathway” (Figure 7G). An interactive network plot was constructed to show the relationships between the GO and KEGG terms (Figure 7H). We also performed GSEA, and several common functions and pathways, such as the G2M checkpoint, epithelial mesenchymal transition (EMT), inflammatory response, Tnfa signalling *via* Nfkb, and interferon alpha response, were obviously enriched in the TCGA high-MCM3 group (NES>1.5, p-value <0.001) (Figure 7I). The waterfall map shows the top 10 genes with the highest mutation probability shared by the two subgroups (Figure 7J). Notably, IDH1 has been identified as being an important prognostic marker for LGG, and the likelihood of IDH mutation is greater in the low-MCM3 subgroup, which to some extent explains the better prognosis in this subgroup. In addition, we investigated the relationships of MCM3 with TMB and TIDE, and our data demonstrated that the high-MCM3 group had higher TMB levels and lower TIDE scores (Figures 7K, L).

Validation of the prognostic significance of MCM3 in LGG

IHC results from the HPA showed that MCM3 expression was elevated in LGG tissue (Figure 8A). The clinical features of our validation cohort are shown in Supplementary Table S2. Figure 8B shows a typical representation of negative and positive MCM3 expression in our cohort. By using chi-square tests, we found that the rate of MCM3 positivity was significantly greater in patients with tumours ≥ 5 cm in size and grade III tumours (Figures 8C, D). KM methods showed that MCM3-positive patients had shorter OS and PFS than MCM3-negative patients (Figures 8E, F). In addition, univariate analysis demonstrated that MCM3 expression was correlated with OS and PFS, thus further confirming its prognostic significance in LGG. However, MCM3 did not have independent prognostic significance in our cohort, which may be related to the small sample size (Figures 8G, H).

Discussion

MCM3, which is a component of the hexameric protein complex, has diagnostic and prognostic value in some cancers (Hsu et al., 2021; Li et al., 2020; Li et al., 2021; Lokkegaard et al., 2021; Zhou et al., 2020). However, the role of MCM3 in other cancer types is unclear. In our study, a pan-cancer analysis and a single-cell analysis were performed to explore the prognostic role, immunological value, and associated biological mechanisms of MCM3. Furthermore, given that MCM3 is closely related to LGG in many ways, we further analysed the relationships between the clinical features, prognosis, and potential biological functions of MCM3 and LGG and validated its prognostic value in a clinical LGG cohort.

Our pan-cancer analysis demonstrated that MCM3, which may have significant prognostic value, was upregulated in 25 tumours, including GBM, LGG, and UCEC. High MCM3 expression was related to poor prognosis in LGG, ACC, LIHC, KICH and SARC patients. Cao et al. suggested that MCM3 may serve as a potential prognostic biomarker for medulloblastoma; this was the first study to elucidate the correlation between MCM3 and central nervous system tumours (L. Cao et al., 2022). Previous studies have shown that MCM2, MCM3 and MCM7 levels are closely linked to glioma prognosis (Söling et al., 2005). Moreover, MCM3 was an independent predictor of prognosis in anaplastic astrocytoma patients (Söling et al., 2005). However, the role of MCM3 in LGG remains unknown. This study was the first to show that high MCM3 expression was linked to shorter OS, DSS, and PFI in LGG patients. Aporowicz’s research suggested that MCM3 could serve as a diagnostic and proliferative marker of ACC (Aporowicz et al., 2019). Our data showed that high MCM3 expression was associated with shorter OS, PFI, and DSS in ACC patients and may be an effective complement for identifying potential markers of ACC. Previous studies have shown that MCM3 is a potential marker for the diagnosis, treatment, and prognosis of LIHC (Zhuang, Yang and Meng, 2018; Yang et al., 2019; Mohamed et al., 2022). Our study showed that high MCM3 expression was associated with shorter OS, PFI, DFI, and DSS in LIHC patients, which was consistent with previous results. A previous study suggested that MCM3 phosphorylation is a new

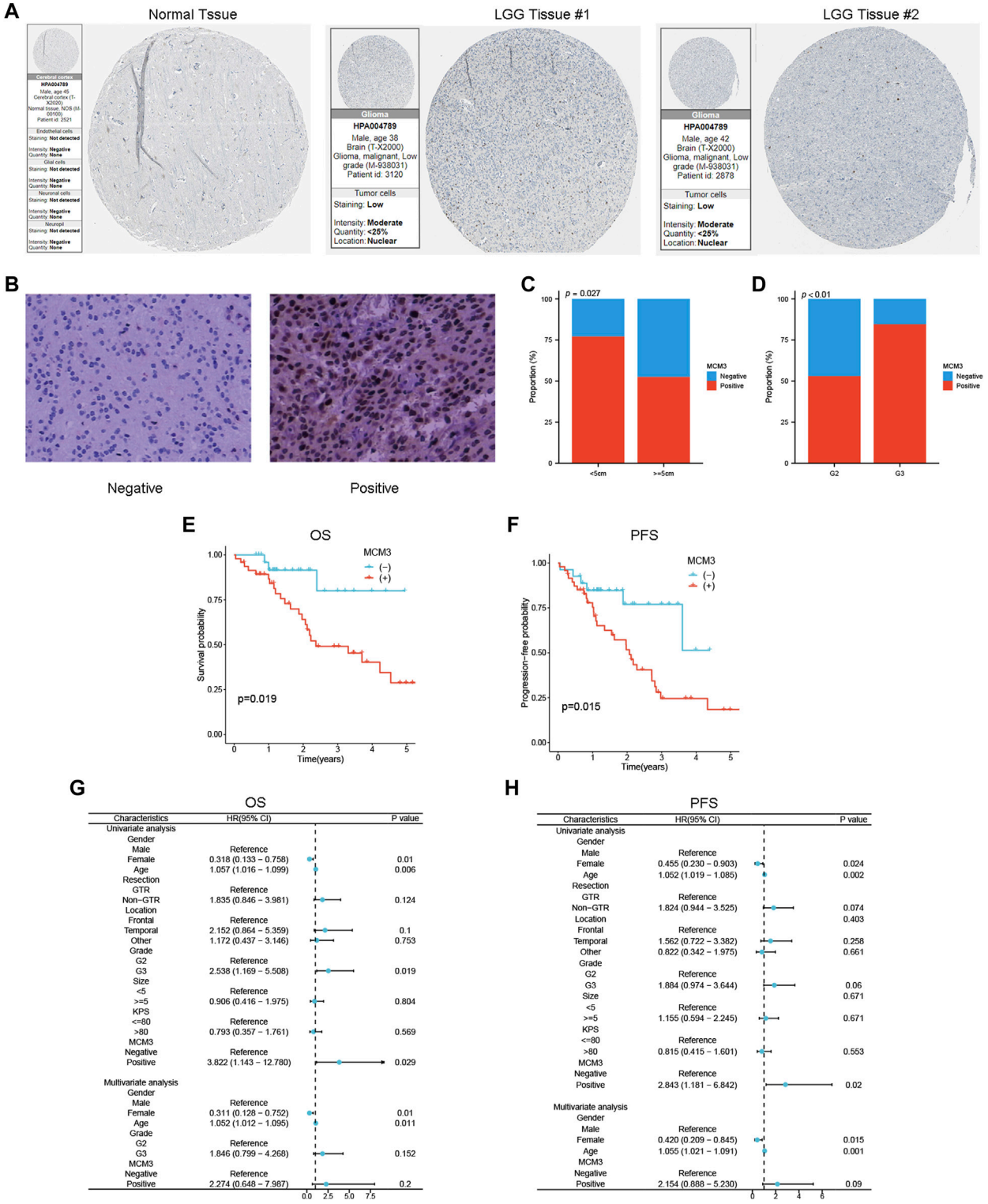

FIGURE 8
Validation of the association between MCM3 and clinical features and prognosis of LGG. **(A)** MCM3 protein expression in normal and tumor tissues from HPA database. **(B)** Representative plots of negative and positive immunohistochemical results. **(C, D)** Relationship between MCM3 expression and tumor size and grade. **(E, F)** Survival curves for OS and PFS in clinical cohort. **(G, H)** Univariate and multivariate Cox regression analysis for OS and PFS.

mechanism for regulating the proliferation and apoptosis of renal cell carcinoma cells (Gao et al., 2020). KICH is a type of renal cell carcinoma. Our study showed that high MCM3 levels were associated with shorter OS, PFI, and DSS in KICH patients. Moreover, MCM3 was also closely linked to OS, PFI, and DSS in SARC patients, and this was the first study to show the relationship

between MCM3 and SARC patients. Kang et al. reported that high MCM3 expression at both the mRNA and protein levels was associated with longer survival in tubo-ovarian high-grade serous carcinoma patients (Kang et al., 2022). Another study reported that MCM3 is a marker of proliferation in ovarian malignancies (Kobierzycki et al., 2013). In this study, we found that high MCM3 expression in OV was associated with longer PFI, DSS and OS. Therefore, the role of MCM3 in OV should be further evaluated.

We found that in most cancers, MCM3 was closely related to the immune score, stromal score, and ESTIMATE score. In addition, MCM3 was closely associated with tumour-infiltrating immune cells in most cancers. By secreting immunosuppressive cytokines, Tregs downregulate the expression of stimulatory molecules, thus inhibiting the activation of effector T cells and reducing T-cell infiltration in LGG (Lim et al., 2018; Haddad et al., 2022). Ahmadzadeh's study demonstrated that $CD8^+$ T cells stimulate granulocytes to produce granulocyte colony-stimulating factor and perforin to kill tumour cells (Ahmadzadeh et al., 2009). Previous studies have shown that $CD4^+$ T cells play an important role in directly eliminating tumours or indirectly providing support for the tumour-killing function of $CD8^+$ T cells (Kennedy and Celis, 2008; Melssen and Slingluff, 2017; Borst et al., 2018). In our study, MCM3 was closely associated with $CD4^+$ T cells and $CD8^+$ T cells in KIRC, LGG, LIHC, PCPG, PRAD and THCA. However, the effect of MCM3 on the immune microenvironment of these cancers and its prognostic value require further study. With the development of high-throughput sequencing technologies, many targets and methods for screening potential beneficiaries of immunotherapy have been identified (Giustini and Bazhenova, 2021; Zhang et al., 2021). In this study, we investigated the potential of MCM3 as a novel predictor of immunotherapy efficacy. The expression of MCM3 was strongly associated with the expression of immune checkpoint molecules and the TMB in most cancers. An earlier study suggested that TMB can be used as a marker of ICB response, with patients with higher TMB levels benefiting more from ICB (Newman et al., 2020). However, McGrail et al. argued that a high TMB does not predict ICB responses in all cancers (McGrail et al., 2021). Overall, MCM3 expression was positively related to TMB in 12 cancers, especially ACC, DLBC, LGG, PAAD and STAD, thus suggesting that patients with high MCM3 expression in these cancers may be more sensitive to immunotherapy. Furthermore, there was a significant difference in the response to immunotherapy between patients with high and low MCM3 in the four clinical cohorts receiving ICB, thus suggesting that MCM3 is a good predictor of immunotherapy response. The TIDE score is another predictor of ICB therapy response, and a low TIDE score is associated with increased sensitivity to ICB therapy (Jiang et al., 2021). In LGG, we found that patients with high MCM3 expression had a greater TMB and a lower TIDE score; therefore, this group of patients could benefit from ICB therapy. Yang et al. identified MCM3 as being a potential therapeutic target for HCC (Yang et al., 2019). Kang et al. showed that MCM3 was associated with immunotherapy in patients with tubo-ovarian high-grade serous carcinoma (Kang et al., 2022). The results of these studies were consistent with our study. The study by Jonathan demonstrated that MSI may be associated with the presence of new immunogenic epitopes to more precisely guide immunotherapy (Dudley et al., 2016). A previous study showed that LUSC patients with high MSI tend to have improved OS (Hu et al., 2023). In our study, MCM3 expression was positively related to MSI level in STAD, KIRC, LUAD and LUSC. Taken together, these findings highlight the potential of MCM3 as being a predictor for immunotherapy efficacy. Drug sensitivity analysis suggested that the expression of MCM3 was positively correlated with sensitivity to 17-AAG, bleomycin (50 μM), RDEA119, trametinib and selumetinib. These data may provide some basis for therapies targeting MCM3.

Tumours are diseases in which cells undergo continual excessive division. Cell cycle checkpoints serve to prevent genetic errors during cell division (Matthews et al., 2022). In our research, single-cell analysis demonstrated that MCM3 was associated with the cell cycle, DNA damage and DNA repair across cancers. In previous studies, MCM3 was shown to act as a proliferation marker and regulate programmed cell death in tumour cells, such as hepatocellular carcinoma, tubo-ovarian high-grade serous carcinoma, oral squamous cell carcinoma, odontogenic cysts and ameloblastoma (Valverde et al., 2018; Jaafari-Ashkavandi et al., 2019). Our study is consistent with the abovementioned findings, thus suggesting that MCM3 may function as a cell cycle checkpoint. Taken together, these results suggest that MCM3 could be not only an immunotherapy target but also a cell cycle checkpoint, thus indicating that MCM3 may be a promising therapeutic target in cancer.

We found that MCM3 expression is correlated with clinical features and prognosis in LGG and is an independent prognostic parameter of LGG. The MCM3-based model can accurately predict the prognosis of LGG, exhibiting good potential for clinical application. GO and KEGG results indicated that MCM3 was mainly involved in cell cycle-related processes and cancer-related pathways. Stewart et al. suggested that MCM3 is involved in the EMT process, thus promoting the invasion and metastasis of prostate cancer (Stewart et al., 2017). Another study demonstrated that MCM3 is overexpressed in medulloblastoma and is involved in tumour cell invasion and metastasis (Lau et al., 2010). Our single-cell and GSEA analyses showed that MCM3 was closely linked to EMT, which to some extent explained the poor prognosis of LGG patients caused by MCM3 overexpression. In addition, previous studies have demonstrated that essential nodes in crucial pathways may be specifically blocked to slow glioma progression, which further suggests that MCM3 may be a promising therapeutic target for LGG (Tang et al., 2014; Liu et al., 2023). In our clinical cohort, MCM3 expression was correlated with the clinical features and prognosis of patients with LGG. However, some limitations of our study should be considered. The MCM3 expression results and prognostic value in most cancers were mainly determined based on publicly available data and need to be validated in clinical cohorts. Moreover, the mechanism by which MCM3 affects the occurrence and development of LGG needs to be clarified by further experiments. Whether MCM3 can predict immunotherapy responses or serve as a novel immunotherapy target needs to be confirmed by additional experimental and clinical trial data.

Conclusion

Our study suggested that MCM3 can be used as a potential prognostic marker for tumours and may be associated with tumour immunity. In addition, MCM3 is a promising predictor of immunotherapy responses.

Data availability statement

The datasets presented in this study can be found in online repositories. The names of the repository/repositories and accession number(s) can be found in the article/Supplementary Material.

Ethics statement

The studies involving humans were approved by the Ethics Committee of the Guangxi Medical University Cancer Hospital. The studies were conducted in accordance with the local legislation and institutional requirements. The participants provided their written informed consent to participate in this study.

Author contributions

Q-RH: Conceptualization, Funding acquisition, Methodology, Writing–original draft. QJ: Data curation, Software, Visualization, Writing–original draft. J-YT: Data curation, Validation, Writing–original draft. R-BN: Data curation, Investigation, Supervision, Writing–original draft. JY: Formal Analysis, Investigation, Project administration, Writing–original draft. X-WY: Formal Analysis, Investigation, Resources, Writing–original draft. L-GM: Formal Analysis, Investigation, Project administration, Writing–original draft. G-YL: Data curation, Project administration, Writing–original draft. TD: Conceptualization, Funding acquisition, Methodology, Project administration, Writing–review and editing. Y-ZG: Conceptualization, Investigation, Methodology, Writing–review and editing.

Funding

The author(s) declare that financial support was received for the research, authorship, and/or publication of this article. This research was supported by the Youth Program of the Scientific Research Foundation of Guangxi Medical University Cancer Hospital (YQJ2022-10) and the Opening Project of Guangxi Medical and Health Appropriate Technology Development and Promotion Project (Nos. S2022114 and S2020097).

Conflict of interest

The authors declare that the research was conducted in the absence of any commercial or financial relationships that could be construed as a potential conflict of interest.

Publisher's note

All claims expressed in this article are solely those of the authors and do not necessarily represent those of their affiliated organizations, or those of the publisher, the editors and the reviewers. Any product that may be evaluated in this article, or claim that may be made by its manufacturer, is not guaranteed or endorsed by the publisher.

Supplementary material

The Supplementary Material for this article can be found online at: https://www.frontiersin.org/articles/10.3389/fphar.2024.1390615/full#supplementary-material

References

Abad, E., Graifer, D., and Lyakhovich, A. (2020). DNA damage response and resistance of cancer stem cells. *Cancer Lett.* 474, 106–117. doi:10.1016/j.canlet.2020.01.008

Ahmadzadeh, M., Johnson, L., Heemskerk, B., Wunderlich, J., Dudley, M., White, D., et al. (2009). Tumor antigen-specific CD8 T cells infiltrating the tumor express high levels of PD-1 and are functionally impaired. *Blood* 114 (8), 1537–1544. doi:10.1182/blood-2008-12-195792

Aporowicz, M., Czopnik, P., Kubicka, E., Piotrowska, A., Dziegiel, P., Bolanowski, M., et al. (2019). Minichromosome maintenance proteins MCM-3, MCM-5, MCM-7, and ki-67 as proliferative markers in adrenocortical tumors. *Anticancer Res.* 39 (3), 1151–1159. doi:10.21873/anticanres.13224

Ben-David, U., and Amon, A. (2020). Context is everything: aneuploidy in cancer. *Nat. Rev. Genet.* 21 (1), 44–62. doi:10.1038/s41576-019-0171-x

Borst, J., Ahrends, T., Bąbała, N., Melief, C., and Kastenmüller, W. J. N. r. I. (2018). CD4+ T cell help in cancer immunology and immunotherapy. *Nat. Rev. Immunol.* 18 (10), 635–647. doi:10.1038/s41577-018-0044-0

Cancer Genome Atlas Research, N., Weinstein, J. N., Collisson, E. A., Mills, G. B., Shaw, K. R., Ozenberger, B. A., et al. (2013). The cancer Genome atlas pan-cancer analysis project. *Nat. Genet.* 45 (10), 1113–1120. doi:10.1038/ng.2764

Cao, L., Zhao, Y., Liang, Z., Yang, J., Wang, J., Tian, S., et al. (2022). Corrigendum: systematic analysis of MCM3 in pediatric medulloblastoma *via* multi-omics analysis. *Front. Mol. Biosci.* 9, 1076243. doi:10.3389/fmolb.2022.1076243

Cao, R., Yuan, L., Ma, B., Wang, G., and Tian, Y. (2020). Immune-related long non-coding RNA signature identified prognosis and immunotherapeutic efficiency in bladder cancer (BLCA). *Cancer Cell Int.* 20, 276. doi:10.1186/s12935-020-01362-0

Chen, F., Fan, Y., Cao, P., Liu, B., Hou, J., Zhang, B., et al. (2021). Pan-cancer analysis of the prognostic and immunological role of HSF1: a potential target for survival and immunotherapy. *Oxid. Med. Cell Longev.* 2021, 5551036. doi:10.1155/2021/5551036

Deegan, T. D., and Diffley, J. F. (2016). MCM: one ring to rule them all. *Curr. Opin. Struct. Biol.* 37, 145–151. doi:10.1016/j.sbi.2016.01.014

Drissi, R., Anais, C., Alyson, M., Dominique, L., Blais-Brochu, S., Jean, D., et al. (2018). Destabilization of the MiniChromosome Maintenance (MCM) complex modulates the cellular response to DNA double strand breaks. *Cell Cycle* 17, 2593–2609. doi:10.1080/15384101.2018.1553336

Dudley, J., Lin, M., Le, D., and Eshleman, J. (2016). Microsatellite instability as a biomarker for PD-1 blockade. *Clin. Cancer Res.* 22 (4), 813–820. doi:10.1158/1078-0432.Ccr-15-1678

Ettinger, D., Wood, D., Aggarwal, C., Aisner, D., Akerley, W., Bauman, J., et al. (2019). NCCN guidelines insights: non-small cell lung cancer, version 1.2020. *J. Natl. Compr. Canc Netw.* 17 (12), 1464–1472. doi:10.6004/jnccn.2019.0059

Evrin, C., Fernandez-Cid, A., Riera, A., Zech, J., Clarke, P., Herrera, M. C., et al. (2014). The ORC/Cdc6/MCM2-7 complex facilitates MCM2-7 dimerization during

prereplicative complex formation. *Nucleic Acids Res.* 42 (4), 2257–2269. doi:10.1093/nar/gkt1148

Fu, L., Bao, J., Li, J., Li, Q., Lin, H., Zhou, Y., et al. (2022). Crosstalk of necroptosis and pyroptosis defines tumor microenvironment characterization and predicts prognosis in clear cell renal carcinoma. *Front. Immunol.* 13, 1021935. doi:10.3389/fimmu.2022.1021935

Gao, Z., Man, X., Li, Z., Bi, J., Liu, X., and Li, Z. (2022). PLK1 promotes proliferation and suppresses apoptosis of renal cell carcinoma cells by phosphorylating MCM3. *Cancer Gene Ther.* 29, 627. doi:10.1038/s41417-022-00458-1

Gao, Z., Man, X., Li, Z., Bi, J., Liu, X., Li, Z., et al. (2020). PLK1 promotes proliferation and suppresses apoptosis of renal cell carcinoma cells by phosphorylating MCM3. *Cancer Gene Ther.* 27 (6), 412–423. doi:10.1038/s41417-019-0094-x

Giustini, N., and Bazhenova, L. J. L. C. (2021). Recognizing prognostic and predictive biomarkers in the treatment of non-small cell lung cancer (NSCLC) with immune checkpoint inhibitors (ICIs). *Lung Cancer (Auckl)* 12, 21–34. doi:10.2147/lctt.S235102

Haddad, A., Young, J., Oh, J., Okada, H., and Aghi, M. (2022). The immunology of low-grade gliomas. *Neurosurg. Focus* 52 (2), E2. doi:10.3171/2021.11.Focus21587

Hsu, E. C., Shen, M., Aslan, M., Liu, S., Kumar, M., Garcia-Marques, F., et al. (2021). MCM2-7 complex is a novel druggable target for neuroendocrine prostate cancer. *Sci. Rep.* 11 (1), 13305. doi:10.1038/s41598-021-92552-x

Hu, Z., Liu, Z., Zheng, J., Peng, Y., Lu, X., Li, J., et al. (2023). Microsatellite instability-related prognostic risk score (MSI-pRS) defines a subset of lung squamous cell carcinoma (LUSC) patients with genomic instability and poor clinical outcome. *Front. Genet.* 14, 1061002. doi:10.3389/fgene.2023.1061002

Jaafari-Ashkavandi, Z., Mehranmehr, F., Roosta, E., and Research, C. (2019). MCM3 and Ki67 proliferation markers in odontogenic cysts and ameloblastoma. *J. Oral Biol. Craniofac Res.* 9 (1), 47–50. doi:10.1016/j.jobcr.2018.09.003

Jiang, P., Li, Y., Xu, Z., and He, S. (2021). A signature of 17 immune-related gene pairs predicts prognosis and immune status in HNSCC patients. *Transl. Oncol.* 14 (1), 100924. doi:10.1016/j.tranon.2020.100924

Kang, E., Millstein, J., Popovic, G., Meagher, N., Bolithon, A., Talhouk, A., et al. (2022). MCM3 is a novel proliferation marker associated with longer survival for patients with tubo-ovarian high-grade serous carcinoma. *Virchows Arch.* 480 (4), 855–871. doi:10.1007/s00428-021-03232-0

Kennedy, R., and Celis, E. (2008). Multiple roles for CD4+ T cells in anti-tumor immune responses. *Immunol. Rev.* 222, 129–144. doi:10.1111/j.1600-065X.2008.00616.x

Kobierzycki, C., Pula, B., Skiba, M., Jablonska, K., Latkowski, K., Zabel, M., et al. (2013). Comparison of minichromosome maintenance proteins (MCM-3, MCM-7) and metallothioneins (MT-I/II, MT-III) expression in relation to clinicopathological data in ovarian cancer. *Anticancer Res.* 33 (12), 5375–5383.

Lau, K., Chan, Q., Pang, J., Li, K., Yeung, W., Chung, N., et al. (2010). Minichromosome maintenance proteins 2, 3 and 7 in medulloblastoma: overexpression and involvement in regulation of cell migration and invasion. *Oncogene* 29 (40), 5475–5489. doi:10.1038/onc.2010.287

Li, H., Wei, B., Li, Z., Wang, X., Jia, W., Xu, Y., et al. (2020). Diagnostic and prognostic value of MCM3 and its interacting proteins in hepatocellular carcinoma. *Oncol. Lett.* 20 (6), 308. doi:10.3892/ol.2020.12171

Li, T., Fan, J., Wang, B., Traugh, N., Chen, Q., Liu, J., et al. (2017). TIMER: a web server for comprehensive analysis of tumor-infiltrating immune cells. *Cancer Res.* 77 (21), e108–e110. doi:10.1158/0008-5472.Can-17-0307

Li, Y., Zou, J., Zhang, Q., Quan, F., Cao, L., Zhang, X., et al. (2021). Systemic analysis of the DNA replication regulator MCM complex in ovarian cancer and its prognostic value. *Front. Oncol.* 11, 681261. doi:10.3389/fonc.2021.681261

Liang, X., Zhang, H., Wang, Z., Zhang, X., Dai, Z., Zhang, J., et al. (2022). JMJD8 is an M2 macrophage biomarker, and it associates with DNA damage repair to facilitate stemness maintenance, chemoresistance, and immunosuppression in pan-cancer. *Front. Immunol.* 13, 875786. doi:10.3389/fimmu.2022.875786

Lim, M., Xia, Y., Bettegowda, C., and Weller, M. (2018). Current state of immunotherapy for glioblastoma. *World Neurosurg.* 15 (7), 422–442. doi:10.1038/s41571-018-0003-5

Liu, A., Jiang, B., Song, C., Zhong, Q., Mo, Y., Yang, R., et al. (2023). Isoliquiritigenin inhibits circ0030018 to suppress glioma tumorigenesis via the miR-1236/HER2 signaling pathway. *MedComm* 4 (3), e282. doi:10.1002/mco2.282

Lokkegaard, S., Elias, D., Alves, C. L., Bennetzen, M. V., Laenkholm, A. V., Bak, M., et al. (2021). MCM3 upregulation confers endocrine resistance in breast cancer and is a predictive marker of diminished tamoxifen benefit. *NPJ Breast Cancer* 7 (1), 2. doi:10.1038/s41523-020-00210-8

Madine, M. A., Swietlik, M., Pelizon, C., Romanowski, P., Mills, A. D., and Laskey, R. A. (2000). The roles of the MCM, ORC, and Cdc6 proteins in determining the replication competence of chromatin in quiescent cells. *J. Struct. Biol.* 129 (2-3), 198–210. doi:10.1006/jsbi.2000.4218

Malta, T., Sokolov, A., Gentles, A., Burzykowski, T., Poisson, L., Weinstein, J., et al. (2018). Machine learning identifies stemness features associated with oncogenic dedifferentiation. *Cell* 173 (2), 338–354.e15. doi:10.1016/j.cell.2018.03.034

Matthews, H., Bertoli, C., and de Bruin, R. (2022). Cell cycle control in cancer. *Nat. Rev. Mol. Cell Biol.* 23 (1), 74–88. doi:10.1038/s41580-021-00404-3

McGrail, D., Pilié, P., Rashid, N., Voorwerk, L., Slagter, M., Kok, M., et al. (2021). High tumor mutation burden fails to predict immune checkpoint blockade response across all cancer types. *Ann. Oncol.* 32 (5), 661–672. doi:10.1016/j.annonc.2021.02.006

Melssen, M., and Slingluff, C. (2017). Vaccines targeting helper T cells for cancer immunotherapy. *Curr. Opin. Immunol.* 47, 85–92. doi:10.1016/j.coi.2017.07.004

Miller, K. D., Nogueira, L., Devasia, T., Mariotto, A. B., Yabroff, K. R., Jemal, A., et al. (2022). Cancer treatment and survivorship statistics, 2022. *CA Cancer J. Clin.* 72 (5), 409–436. doi:10.3322/caac.21731

Mohamed, A., Abd El Hafez, A., Eltantawy, A., Mahfouz, M., and Aimm, M. (2022). Diagnostic and prognostic value of isolated and combined MCM3 and glypican-3 expression in hepatocellular carcinoma: a novel immunosubtyping prognostic model. *Appl. Immunohistochem. Mol. Morphol.* 30 (10), 694–702. doi:10.1097/pai.0000000000001080

Newman, J., Seetharamu, N., and Saif, M. (2020). Burden of proof: evaluating the efficacy of tumor mutational burden (TMB) in predicting response to immune checkpoint inhibitors. *Cancer Med. J.* 3, 17–21.

Pan, S., Sun, S., Liu, B., and Hou, Y. (2022). Pan-cancer landscape of the RUNX protein family reveals their potential as carcinogenic biomarkers and the mechanisms underlying their action. *J. Transl. Intern. Med.* 10 (2), 156–174. doi:10.2478/jtim-2022-0013

Picard, E., Verschoor, C., Ma, G., and Pawelec, G. (2020). Relationships between immune landscapes, genetic subtypes and responses to immunotherapy in colorectal cancer. *Front. Immunol.* 11, 369. doi:10.3389/fimmu.2020.00369

Raja, R., Shetty, D., Juneja, S., Tandon, A., and Gulati, N. (2021). MCM3 proliferative index is worthier over Ki-67 in the characterization of salivary gland tumors. *Indian J. Pathol. Microbiol.* 64 (1), 22–27. doi:10.4103/ijpm.Ijpm_63_20

Sedlackova, H., Rask, M. B., Gupta, R., Choudhary, C., Somyajit, K., and Lukas, J. (2020). Equilibrium between nascent and parental MCM proteins protects replicating genomes. *Nature* 587 (7833), 297–302. doi:10.1038/s41586-020-2842-3

Söling, A., Sackewitz, M., Volkmar, M., Schaarschmidt, D., Jacob, R., Holzhausen, H., et al. (2005). Minichromosome maintenance protein 3 elicits a cancer-restricted immune response in patients with brain malignancies and is a strong independent predictor of survival in patients with anaplastic astrocytoma. *Clin. Cancer Res.* 11 (1), 249–258. doi:10.1158/1078-0432.249.11.1

Stewart, P., Khamis, Z., Zhau, H., Duan, P., Li, Q., Chung, L., et al. (2017). Upregulation of minichromosome maintenance complex component 3 during epithelial-to-mesenchymal transition in human prostate cancer. *Oncotarget* 8 (24), 39209–39217. doi:10.18632/oncotarget.16835

Sun, D., Wang, J., Han, Y., Dong, X., Ge, J., Zheng, R., et al. (2021). TISCH: a comprehensive web resource enabling interactive single-cell transcriptome visualization of tumor microenvironment. *Nucleic Acids Res.* 49, D1420–D1430. doi:10.1093/nar/gkaa1020

Sung, H., Ferlay, J., Siegel, R. L., Laversanne, M., Soerjomataram, I., Jemal, A., et al. (2021). Global cancer statistics 2020: GLOBOCAN estimates of incidence and mortality worldwide for 36 cancers in 185 countries. *CA Cancer J. Clin.* 71 (3), 209–249. doi:10.3322/caac.21660

Tang, H., Wang, Z., Liu, Q., Liu, X., Wu, M., and Li, G. (2014). Disturbing miR-182 and -381 inhibits BRD7 transcription and glioma growth by directly targeting LRRC4. *PLoS One* 9 (1), e84146. doi:10.1371/journal.pone.0084146

Torre, L. A., Bray, F., Siegel, R. L., Ferlay, J., Lortet-Tieulent, J., and Jemal, A. (2015). Global cancer statistics, 2012. *CA Cancer J. Clin.* 65 (2), 87–108. doi:10.3322/caac.21262

Valverde, L., de Freitas, R., Pereira, T., de Resende, M., Agra, I., Dos Santos, J., et al. (2018). MCM3: a novel proliferation marker in oral squamous cell carcinoma. *Appl. Immunohistochem. Mol. Morphol.* 26 (2), 120–125. doi:10.1097/pai.0000000000000397

Wang, X., Qiu, W., Liu, H., Li, T., Ye, H., Li, Y., et al. (2021). The prognostic value of combining CD133 and mismatch repair proteins in patients with colorectal cancer. *Clin. Exp. Pharmacol. Physiol.* 48 (1), 54–63. doi:10.1111/1440-1681.13408

Xiao, Y. Y. D., and Yu, D. (2021). Tumor microenvironment as a therapeutic target in cancer. *Pharmacol. Ther.* 221, 107753. doi:10.1016/j.pharmthera.2020.107753

Xie, J., Zhang, J., Tian, W., Zou, Y., Tang, Y., Zheng, S., et al. (2022). The pan-cancer multi-omics landscape of FOXO family relevant to clinical outcome and drug resistance. *Int. J. Mol. Sci.* 23 (24), 15647. doi:10.3390/ijms232415647

Xu, W. X., Zhang, J., Hua, Y. T., Yang, S. J., Wang, D. D., and Tang, J. H. (2020). An integrative pan-cancer analysis revealing LCN2 as an oncogenic immune protein in tumor microenvironment. *Front. Oncol.* 10, 605097. doi:10.3389/fonc.2020.605097

Yang, W., Pan, Y., and You, C. (2019). CDK1, CCNB1, CDC20, BUB1, MAD2L1, MCM3, BUB1B, MCM2, and RFC4 may Be potential therapeutic targets for hepatocellular carcinoma using integrated bioinformatic analysis. *Biomed. Res. Int.* 2019, 1245072. doi:10.1155/2019/1245072

Yoshihara, K., Shahmoradgoli, M., Martínez, E., Vegesna, R., Kim, H., Torres-Garcia, W., et al. (2013). Inferring tumour purity and stromal and immune cell admixture from expression data. *Nat. Commun.* 4, 2612. doi:10.1038/ncomms3612

Yuan, H., Yan, M., Zhang, G., Liu, W., Deng, C., Liao, G., et al. (2019). CancerSEA: a cancer single-cell state atlas. *Nucleic Acids Res.* 47, D900–D908. doi:10.1093/nar/gky939

Zhang, H., Wang, Z., Dai, Z., Wu, W., Cao, H., Li, S., et al. (2021). Novel immune infiltrating cell signature based on cell pair algorithm is a prognostic marker in cancer. *Front. Immunol.* 12, 694490. doi:10.3389/fimmu.2021.694490

Zhang, Y., Luo, J., He, R., Huang, W., Li, Z., Li, P., et al. (2016). Expression and clinicopathological implication of DcR3 in lung cancer tissues: a tissue microarray study with 365 cases. *Onco Targets Ther.* 9, 4959–4968. doi:10.2147/ott.S105225

Zhou, H., Xiong, Y., Zhang, G., Liu, Z., Li, L., Hou, S., et al. (2020). Elevated expression of minichromosome maintenance 3 indicates poor outcomes and promotes G1/S cell cycle progression, proliferation, migration and invasion in colorectal cancer. *Biosci. Rep.* 40 (7). doi:10.1042/BSR20201503

Zhou, X., Lin, K., Fu, L., Liu, F., Lin, H., Chen, Y., et al. (2023). Overexpression of TREM1 is associated with the immune-suppressive microenvironment and unfavorable prognosis in pan-cancer. *J. Inflamm. Res.* 16, 1375–1391. doi:10.2147/jir.S398284

Zhuang, L., Yang, Z., and Meng, Z. (2018). Upregulation of BUB1B, CCNB1, CDC7, CDC20, and MCM3 in tumor tissues predicted worse overall survival and disease-free survival in hepatocellular carcinoma patients. *Biomed. Res. Int.* 2018, 7897346. doi:10.1155/2018/7897346

Zou, Y., Ye, F., Kong, Y., Hu, X., Deng, X., Xie, J., et al. (2023). The single-cell landscape of intratumoral heterogeneity and the immunosuppressive microenvironment in liver and brain metastases of breast cancer. *Adv. Sci.* 10 (5), e2203699. doi:10.1002/advs.202203699

Glossary

Pan-cancer

ACC	Adrenocortical carcinoma
BLCA	Bladder Urothelial Carcinoma
BRCA	Breast invasive carcinoma
CESC	Cervical squamous cell carcinoma and endocervical adenocarcinoma
CHOL	Cholangiocarcinoma
COAD	Colon adenocarcinoma
DLBC	Lymphoid Neoplasm Diffuse Large B-cell Lymphoma
ESCA	Esophageal carcinoma
GBM	Glioblastoma multiforme
HNSC	Head and Neck squamous cell carcinoma
KICH	Kidney Chromophobe
KIRC	Kidney renal clear cell carcinoma
KIRP	Kidney renal papillary cell carcinoma
LAML	Acute Myeloid Leukemia
LGG	Lower-Grade Glioma
LIHC	Liver hepatocellular carcinoma
LUAD	Lung adenocarcinoma
LUSC	Lung squamous cell carcinoma
MESO	Mesothelioma
OV	Ovarian serous cystadenocarcinoma
PAAD	Pancreatic adenocarcinoma
PCPG	Pheochromocytoma and Paraganglioma
PRAD	Prostate adenocarcinoma
READ	Rectum adenocarcinoma
SARC	Sarcoma
SKCM	Skin Cutaneous Melanoma
STAD	Stomach adenocarcinoma
TGCT	Testicular Germ Cell Tumors
THCA	Thyroid carcinoma
THYM	Thymoma
UCEC	Uterine Corpus Endometrial Carcinoma
UCS	Uterine Carcinosarcoma
UVM	Uveal Melanoma

frontiers | Frontiers in Pharmacology

TYPE Review
PUBLISHED 09 May 2024
DOI 10.3389/fphar.2024.1391562

Check for updates

OPEN ACCESS

EDITED BY
Zhi Tian,
University of South Florida, United States

REVIEWED BY
Wenliang Su,
Peking University First Hospital, China
Zibo Li,
Changsha Medical University, China

*CORRESPONDENCE
Baiwei Zhao,
zhaobw@sysucc.org.cn
Chunyu Huang,
huangchy@sysucc.org.cn

†These authors have contributed equally to this work and share first authorship

RECEIVED 26 February 2024
ACCEPTED 18 April 2024
PUBLISHED 09 May 2024

CITATION
Lin F, Chen Y, Huang B, Ruan S, Lin J, Chen Z, Huang C and Zhao B (2024), Application of immune checkpoint inhibitors for resectable gastric/gastroesophageal cancer.
Front. Pharmacol. 15:1391562.
doi: 10.3389/fphar.2024.1391562

COPYRIGHT
© 2024 Lin, Chen, Huang, Ruan, Lin, Chen, Huang and Zhao. This is an open-access article distributed under the terms of the Creative Commons Attribution License (CC BY). The use, distribution or reproduction in other forums is permitted, provided the original author(s) and the copyright owner(s) are credited and that the original publication in this journal is cited, in accordance with accepted academic practice. No use, distribution or reproduction is permitted which does not comply with these terms.

Application of immune checkpoint inhibitors for resectable gastric/gastroesophageal cancer

Feizhi Lin†, Yongming Chen†, Bowen Huang†, Shenghang Ruan, Jun Lin, Zewei Chen, Chunyu Huang* and Baiwei Zhao*

State Key Laboratory of Oncology in South China, Guangdong Provincial Clinical Research Center for Cancer, Sun Yat-Sen University Cancer Center, Guangzhou, China

Gastric/gastroesophageal junction (G/GEJ) cancer represents a significant global health challenge. Radical surgery remains the cornerstone of treatment for resectable G/GEJ cancer. Supported by robust evidence from multiple clinical studies, therapeutic approaches, including adjuvant chemotherapy or chemoradiation, and perioperative chemotherapy, are generally recommended to reduce the risk of recurrence and enhance long-term survival outcomes post-surgery. In recent years, immune checkpoint inhibitors (ICIs) have altered the landscape of systemic treatment for advanced or metastatic G/GEJ cancer, becoming the standard first-line therapy for specific patients. Consequently, exploring the efficacy of ICIs in the adjuvant or neoadjuvant setting for resectable G/GEJ cancer is worthwhile. This review summarizes the current advances in the application of ICIs for resectable G/GEJ cancer.

KEYWORDS

perioperative treatment, gastric cancer, immunotherapy, neoadjuvant therapy, adjuvant therapy, chemotherapy

Introduction

Gastric/gastroesophageal junction (G/GEJ) cancer represents a significant global cancer burden. In 2020, G/GEJ cancer accounted for over one million new cases and roughly 769,000 deaths, ranking as the fifth most frequently diagnosed cancer and the fourth leading cause of cancer-related mortality (Siegel et al., 2021; Sung et al., 2021). There is a geographical variation in incidence rates, with Eastern Asia and Eastern Europe reporting the highest, while Northern America, Northern Europe, and African regions report relatively low rates (Sung et al., 2021). Notably, an upward trend in the incidence among young adults is observed globally, transcending traditional high- and low-risk regions (Sung et al., 2021). Owing to the subtle symptoms of early-stage G/GEJ cancer, a considerable proportion of patients receive diagnoses at advanced stages, resulting in a poor prognosis (Guan et al., 2023).

Distal, subtotal or total gastrectomy along with D2 lymphadenectomy is defined as standard surgery for resectable G/GEJ cancer (Wang et al., 2021; Ajani et al., 2022; Lordick et al., 2022). Various clinical trials have confirmed the superiority of adjuvant and neoadjuvant-adjuvant therapy compared to surgery alone for resectable cases (Guan et al., 2023). In East Asian countries like Japan and Korea, where screening program is

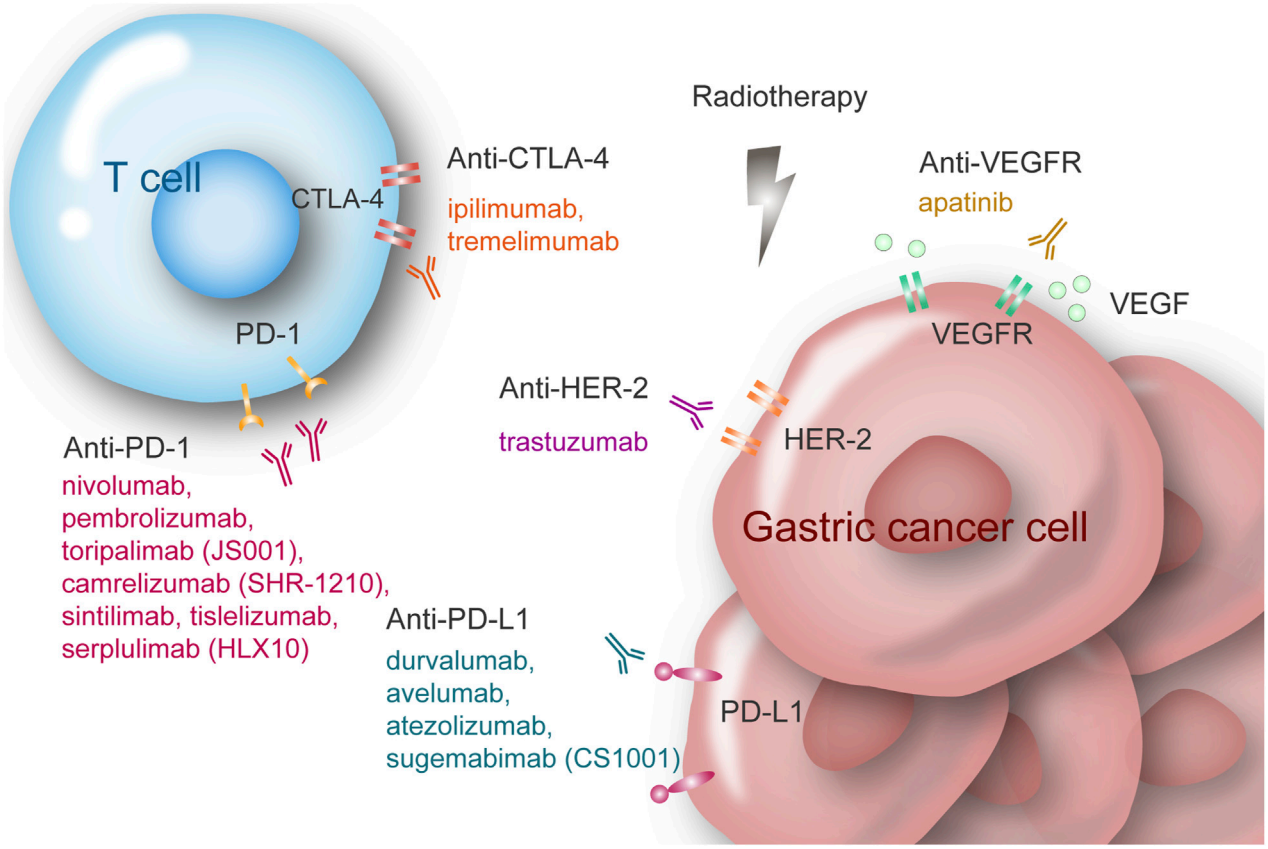

FIGURE 1
Multiple modalities for locally advanced gastric/gastroesophageal cancer.

widely conducted, treatment typically involves D2 gastrectomy followed by adjuvant chemotherapy, even though neoadjuvant therapy is becoming more common. Conversely, western countries put more focus on neoadjuvant-adjuvant therapy in combination with surgery (Suh and Yang, 2015; Allemani et al., 2018; Yanagimoto et al., 2023). Despite the significant progress in the therapeutic strategies and surgical techniques, there remains a rather high risk of recurrence and metastasis in resectable cases, with the 5-year survival rates showing a substantial decline in patients beyond stage II (Li et al., 2018).

The emergence of immune checkpoint inhibitors (ICIs) has revolutionized the management of various solid malignancies. Key inhibitory immune checkpoints, including cytotoxic T-lymphocyte-associated protein 4 (CTLA-4 or CD152), programmed cell death protein 1 (PD-1 or CD279), and programmed death-ligand 1 (PD-L1 or CD274), serve as crucial modulators of the immune system by downregulating T cell activity. Cancer cells exploit this mechanism to evade immune detection, often leading to worse outcomes (Bagchi et al., 2021). Immune checkpoint inhibitors (ICIs), specifically designed monoclonal antibodies, counteract these checkpoints, potentiating T cell-mediated tumor destruction (Marin-Acevedo et al., 2021). Common ICIs are categorized based on their specific targets: anti-PD-1 antibodies (e.g., nivolumab and pembrolizumab), anti-PD-L1 antibodies (e.g., durvalumab and avelumab), and anti-CTLA-4 antibodies (e.g., ipilimumab and tremelimumab) (Figure 1).

For advanced G/GEJ cancer, ATTRACTION-2 validated the efficacy of ICIs in the later-line treatment (Kang et al., 2017). Furthermore, results from CHECKMATE-649, ORIENT-16 indicated that the combination of ICIs and chemotherapy offers survival benefits as a first-line treatment (Janjigian et al., 2021a; Xu et al., 2021). Immunotherapy has become the standard first-line treatment for advanced G/GEJ cancer patients with PD-L1 CPS ≥5 (4–6). Given this, various clinical trials are investigating its efficacy in the postoperative and perioperative setting in resectable cases (Guan et al., 2023). Current research is focused on exploring the synergetic effects of combining immunotherapy with other modalities such as chemotherapy, radiotherapy, and targeted therapy (Figure 1). In this review, we summarize the clinical trials concerning the application of ICIs in resectable G/GEJ cancer.

Application of ICIS in the adjuvant setting

Surgery alone for locally advanced GC yields unsatisfied outcomes, with a postoperative 5-year overall survival (OS) rate below 50% even after D2 gastrectomy (Smith et al., 2005). Adjuvant therapy aims to reduce microscopic disease and prevent recurrence. Stage II or III cancer patients undergoing radical surgery are advised to receive adjuvant chemotherapy, especially in Asian populations, as supported by multiple clinical trials. The Japanese ACTS-GC trial

showed that adjuvant S-1 monotherapy for 1 year after surgery provides a survival advantage over surgery alone in stage II/III GC patients (Sasako et al., 2011). The CLASSIC trial, conducted in South Korea, China, and Taiwan, confirmed the advantages of adjuvant capecitabine and oxaliplatin (CAPOX) for stage II-IIIB G/GEJ cancer patients undergoing D2 gastrectomy *versus* surgery only (Bang et al., 2012). The Korean ARTIST two trial compared surgery followed by 1 year of S-1 monotherapy, 6 months of S-1 combined with oxaliplatin (SOX), or a combination of radiotherapy plus SOX (SOXRT) for lymph node-positive stage II/III GC patients. The study revealed that adjuvant SOX extended disease-free survival (DFS) compared to S-1 alone (Park et al., 2021). In the Chinese RESOLVE trial, patients with cT4aN + or cT4bNany G/GEJ cancer were compared across three treatment arms: surgery followed by adjuvant CAPOX, adjuvant SOX, or perioperative SOX. Result showed that adjuvant SOX was noninferior to adjuvant CAPOX in patients with cT4aN + or cT4bNany G/EGJ cancer in DFS(20). The JACCRO GC-07 trial in Japan verified the superiority of docetaxel plus S-1 (DS) over S-1 monotherapy as postoperative treatment in pathological stage III GC patients (Yoshida et al., 2019; Kakeji et al., 2022). These findings provide insights into the selection of adjuvant therapies for stage II-III gastric cancer. S-1 alone may be preferred for patients with stage II cancer or those with a poor performance status, while combination therapies like CAPOX, SOX, or DS are recommended for patients with pathological stage III disease (Wang et al., 2021; Japanese Gastric Cancer Association, 2023). The integration of ICIs into adjuvant therapy for operable G/GEJ cancer is currently being investigated to assess potential survival benefits (Table 1).

The ATTRACTION-5 (NCT03006705) trial, presented at ASCO 2023, was a phase 3, Asian, double-blind, randomized study to evaluate the efficacy of nivolumab combined with adjuvant chemotherapy (either S-1 monotherapy or CAPOX) in patients with pathological stage III G/GEJ cancer who had undergone D2 (or more extensive) gastrectomy. 755 patients were randomly assigned to the Nivolumab plus chemotherapy (N + C) arm and the placebo plus chemotherapy (P + C) arm. The primary endpoint, centrally-assessed relapse-free survival (RFS), was not met (HR 0.90; 95% CI 0.69–1.18; p = 0.4363). The centrally-assessed 3-year RFS rates were 68.4% (95% CI 63.0–73.2) in the N + C group and 65.3% (95% CI 59.9–70.2) in the P + C group. Incidences of grade≥3 treatment-related adverse events (TRAEs), serious TRAEs, and TRAEs leading to treatment discontinuation were 54.4%, 25.3%, and 9.2% in the N + C group *versus* 46.8%, 10.7%, and 3.5% in the P + C group, respectively. Subgroup analysis showed that patients with PD-L1 expression ≥1% might benefit from N + C treatment. A majority of patients had low PD-L1 expression in the study cohorts may represent an important factor for the negative outcomes (Terashima et al., 2023). The subgroup analysis from CheckMate-649, along with a meta-analysis, have consistently found that in patients with low PD-L1 combined positive score (CPS), the therapeutic benefits of ICIs combined with chemotherapy may diminish (Janjigian et al., 2021a; Shitara et al., 2022; Yoon et al., 2022). This observation could be particularly relevant in the postoperative adjuvant setting, where significant changes in the tumor microenvironment (TME), including the near elimination of PD-L1 positive tumor cells, might impede the ability of ICIs to activate the immune system effectively.

JUPITER-15 (NCT05180734) is an ongoing, phase 3, global, double-blind study assessing the efficacy and safety of combining toripalimab with adjuvant chemotherapy (XELOX or SOX) in comparison to placebo with adjuvant chemotherapy. It includes patients who have undergone radical gastrectomy (R0, D2 or higher lymphadenectomy) and have a postoperative pathological stage II or III G/GEJ adenocarcinoma, regardless of PD-L1 expression. Another ongoing phase 2 randomized study NCT05184946 is exploring the efficacy and safety of camrelizumab plus SOX for adjuvant therapy of pathologic stage III G/GEJ adenocarcinoma compared to the standard SOX regimen. Given their similarity to the ATTRACTION-5 trial in design, these trials may not yield positive results.

According to a meta-analysis of MAGIC, CLASSIC, ARTIST, and ITACA-S, resectable mismatch repair deficiency (dMMR) or microsatellite instability-high (MSI-H) GC patients tend to have better outcomes with surgery alone than with postoperative adjuvant chemotherapy (Pietrantonio et al., 2019). However, these patients respond well to immunotherapy (Kang and Chau, 2020). The ongoing, phase 2, three-arm, randomized NCT05468138 trial aims to demonstrate that dMMR/MSI-H G/GEJ cancer patients who receive sintilimab or nivolumab monotherapy after D2 radical gastrectomy will have a more favorable prognosis than those receiving standard postoperative adjuvant chemotherapy (SOX/XELOX) or undergoing follow-up observation. Additionally, the phase 2 NCT05769725 trial is evaluating serplulimab in combination with DS *versus* DS alone as adjuvant treatment therapy in pathologic stage IIIc GC with PD-L1 CPS≥5/EBV+ (Epstein-Barr virus positive)/dMMR/MSI-H. These investigations will contribute to elucidating whether adjuvant immunotherapy can benefit specific patient populations.

Based on the results of ARTIST 2, adjuvant radiotherapy is not routinely recommended after D2 gastrectomy for GC due to its limited impact on reducing recurrence rates when added to SOX (19). However, in clinical practice, patients with advanced postoperative staging and a high risk of local recurrence (defined as inadequate safety margins, vascular tumor emboli, perineural invasion, advanced N-stage, or a high lymph node metastasis ratio) may consider adjuvant radiotherapy after comprehensive systemic treatment (Wang et al., 2021). NCT04997837 is a multicenter, randomized controlled, phase 3 study designed to assess the efficacy and safety of postoperative adjuvant chemotherapy CAPOX/SOX/FOLFOX (folinic acid, fluorouracil and oxaliplatin) with PD-1 inhibitors (nivolumab/toripalimab/pembrolizumab/tilelizumab/sintilimab/carrelizumab) and chemoradiotherapy (CRT) in comparison with adjuvant chemotherapy alone for patients with D2/R0 resected pN3 G/GEJ adenocarcinoma. Patients in the PD-1+CRT cohort will receive PD-1 inhibitors and chemotherapy for 6 weeks, followed by concurrent chemoradiotherapy (cCRT), another 6 weeks of PD-1 inhibitors and chemotherapy, and maintenance PD-1 inhibitors for up to 1 year after radiotherapy. While patients in the CT cohort will receive chemotherapy only for 6 months. The study aims to assess the 3-year DFS (primary endpoint), OS, RFS and adverse effects to identify the most effective treatment approach.

TABLE 1 Clinical trials of ICIs in adjuvant setting.

Trial	Patients	Agent (target)	Phase, arm	Study design	Size	Primary endpoint	
ATTRACTION-5 (NCT03006705)	-	Nivolumab (PD-1)	III, two-arm	Nivolumab + S-1/CAPOX	377	3-year RFS	68.4%
				Placebo + S-1/CAPOX	378		65.3%
JUPITER-15 (NCT05180734)	-	Toripalimab (PD-1)	III, two-arm	Toripalimab + SOX/XELOX	340	DFS	
				Placebo + SOX/XELOX	340		
NCT05184946	-	Camrelizumab (PD-1)	II, two-arm	Camrelizumab + SOX	36	3-year DFS	
				SOX only	36		
NCT05468138	dMMR/MSI-H	Sintilimab/Nivolumab (PD-1)	II/III, three-arm	Sintilimab/Nivolumab only	141	3-year DFS	
				SOX/XELOX only			
				observation			
NCT05769725	PD-L1CPS≥5/EBV+/dMMR/MSI-H	Serplulimab (PD-1)	II, two-arm	Serplulimab + DS	35	1-year DFS	
				DS only	35		
NCT04997837	D2/R0 resected with pN3	multiple PD-1 inhibitors	III, two-arm	PD-1+CRT	433	3-year DFS	
				Chemotherapy			

CAPOX: Capecitabine + Oxaliplatin; XELOX: Xeloda + Oxaliplatin; SOX: S-1 + Oxaliplatin; DS: Docetaxel + S-1; CRT: chemoradiotherapy; RFS: recurrence free survival; DFS: disease free survival.

10.3389/fphar.2024.1391562

Application of ICIS in the perioperative setting

Perioperative (neoadjuvant and adjuvant) therapy is a standard of care for resectable G/GEJ cancer. Conventional neoadjuvant chemotherapy and radiotherapy aims to reduce tumor size and improve surgical resectability, while neoadjuvant immunotherapy can boost tumor-specific T cells to enhance both intratumoral and systemic anti-tumor immunity (Lin et al., 2023; Topalian et al., 2023).

ICIs in combination with chemotherapy

The MAGIC trial established the survival benefit of perioperative ECF (epirubicin, cisplatin, and fluorouracil) regimen plus surgery *versus* surgery alone in patients with operable G/GEJ, or lower esophageal adenocarcinoma (Cunningham et al., 2006). The French FNCLCC/FFCD trial revealed the similar efficacy of FP regimen (fluorouracil and cisplatin) to ECF (Ychou et al., 2011). The FLOT4-AIO trial has led to the replacement of ECF with the FLOT regimen (fluorouracil, leucovorin, oxaliplatin, and docetaxel) as the favored perioperative treatment in Europe (Al-Batran et al., 2019). The Korean PRODIGY trial showed that neoadjuvant DOS (docetaxel, oxaliplatin, and S-1) followed by surgery and adjuvant S-1 is superior to surgery plus adjuvant S-1 for resectable GC, despite some criticism regarding the postoperative S-1 monotherapy (Tougeron et al., 2022). In the Chinese RESOLVE trial, perioperative SOX therapy showed an improvement over adjuvant CAPOX therapy (Zhang et al., 2021). Based on these evidences, the treatment of neoadjuvant therapy followed by surgery and adjuvant therapy is recommended for resectable locally advanced GC in different countries (Wang et al., 2021; Ajani et al., 2022; Lordick et al., 2022). The FLOT regimen is most frequently used in western countries, while SOX is preferred in China. Ongoing research, including phase II and III trials, is investigating whether adding ICIs to perioperative treatment can improve survival outcomes for resectable G/GEJ cancer patients (Table 2).

The result of the single-arm, phase 2 NCT03939962 study was reported at ASCO 2020. All 16 patients with resectable G/GEJ adenocarcinoma completed neoadjuvant therapy with camrelizumab plus FOLFOX without confirmed progressive disease. Of 13 evaluable patients, 1 (8%) achieved pathological complete response (pCR), 3 (23%) had tumor regression grade (TRG) 1, and 10 (77%) showed stage reduction, and eight experienced lymphonodus pCR. The most common grade 3–4 TRAEs included neutropenia (19%), leukopenia (13%), and anorexia (6%) (Liu et al., 2020). The single-arm, phase 2 PANDA (NCT03448835) study, presented at ASCO 2022, demonstrated a 45% pCR and 70.0% major pathologic response (MPR) rate with neoadjuvant atezolizumab plus DOC (docetaxel, oxaliplatin, and capecitabine) treatment in 20 patients. Notably, intestinal-type Lauren classification patients had a 60% (9/15) pCR and 80% (12/15) MPR rate. The median follow-up of 29 months revealed a DFS rate of 75%. Two patients (10%) experienced grade 3 immune-related adverse events (IRAEs) (Verschoor et al., 2022). Another single-arm, phase 2 trial (NCT03488667), also reported at ASCO 2022, showed 19% ypCR (tumor regression score, TRS = 0) and 92% pathological response (TRS ≤2) in 26 of 35 patients treated with neoadjuvant mFOLFOX plus pembrolizumab, with grade 3/4 toxicities reported in 21 patients (Sun et al., 2022). These findings showed a promising pathological response rate with acceptable toxicity profiles when combining chemotherapy with ICIs as neoadjuvant therapy for locally advanced G/GEJ cancer.

The DANTE trial (NCT03421288) was a phase 2b study comparing atezolizumab plus FLOT against FLOT alone in operable G/GEJ adenocarcinoma patients. Patients in Arm A received atezolizumab with FLOT for four neoadjuvant and four adjuvant cycles followed by eight cycles of atezolizumab monotherapy, while patients in Arm B received FLOT alone for 4 + 4 cycles. Presented at ASCO 2022, the combination therapy showed improved tumor downstaging and a higher pCR rate (24% vs. 15%), especially in patients with higher PD-L1 expression (33% vs. 12% in CPS ≥10) and MSI-H tumors (63% vs. 27%). This led to the trial's advancement to phase 3, focusing on patients with high immune responsiveness (MSI-H, PD-L1 CPS≥1, TMB≥10/MB, or EBV+) (Al-Batran et al., 2022; Al-Batran et al., 2023). The single-arm, phase 2 ICONIC trial (NCT03399071), presented at ASCO-GI 2023, evaluated FLOT-A (FLOT with avelumab) in early-stage operable esophagogastric adenocarcinoma patients with ≥cT2-4 or N+. The trial closed early with a 15% pCR rate in 34 patients, below the 25% target. However, higher PD-L1 CPS was associated with improved TRG3 and reduced TRG4/5 rates, even after excluding patients with dMMR/MSI-H tumors. With a 15.8-month median follow-up, the 12-month PFS was 93.1%, showing promise compared to historical perioperative FLOT results (Gordon et al., 2023).

The phase 2, open-label, randomized NCT04250948 trial evaluated the efficacy of combining toripalimab to perioperative SOX/XELOX in resectable cT3-4 aN + M0 G/GEJ cancer. 108 patients were randomized evenly into either receiving three preoperative and five postoperative cycles of SOX/XELOX (C arm) or receiving toripalimab with SOX/XELOX followed by 6 months of toripalimab maintenance therapy (C + T arm). Results presented at ASCO 2023 revealed a significant increase in the TRG0/1 rate in the C + T arm by 24.0% ($p = 0.009$), with a rate of 44.4% (24/54; 95% CI 30.9%–58.6%) compared to 20.4% (11/54; 95% CI 10.6%–33.5%) in the C arm. Moreover, the C + T arm showed a higher pCR rate of 24.1% (13/54; 95% CI 13.5%–37.6%), which was significantly higher ($p = 0.039$) compared to 9.3% (5/54; 95% CI 3.1%–20.3%) in the C arm. Surgical morbidity (11.8% in the C + T arm vs. 13.5% in the C arm) and mortality (1.9% vs. 0%) and grade 3–4 TRAEs (27.8% vs. 25.9%) were similar between two arms (Yuan et al., 2023). This study provides compelling evidence supporting the combination therapy in the perioperative setting and long-term survival data are anticipated to confirm its survival benefit.

Impressive results were reported in the perioperative and advanced-stage treatment of gastric cancer (GC) with the use of FOLFIRINOX (fluorouracil, leucovorin, oxaliplatin, and irinotecan) (Catenacci et al., 2020; Park et al., 2020). The phase 2 NCT04908566 trial compared toripalimab with FOLFIRINOX (Group A) and toripalimab with SOX (Group B) in the perioperative setting for operable G/GEJ adenocarcinoma. As shown at ASCO 2023, the study enrolled 54 eligible patients (A group 21, B group 33) and achieved R0 resection in all 32 patients who underwent surgery. While the

TABLE 2 Clinical trials of ICIs plus chemotherapy in perioperative setting.

Trial	Patients	Agent (target)	Phase, arm	Study design	Size	pCR (%)	MPR (%)
NCT03939962	-	Camrelizumab (PD-1)	II, single-arm	Camrelizumab + FOLFOX	16	7.7	30.8
PANDA (NCT03448835)	-	Atezolizumab (PD-L1)	II, single-arm	Atezolizumab + DOC	20	45.0	70.0
NCT03488667	-	Pembrolizumab (PD-1)	II, single-arm	Pembrolizumab + mFOLFOX	35	19.2	-
DANTE (NCT03421288)	MSI-H,PD-L1 CPS≥1, TMB10/MB, or EBV+	Atezolizumab (PD-L1)	II/III, two-arm	Atezolizumab + FLOT	146	24	-
				FLOT only	149	15	-
ICONIC (NCT03399071)	-	Avelumab (PD-L1)	II, single-arm	Avelumab + FLOT	34	15	-
NCT04250948	-	Toripalimab (PD-1)	II, two-arm	Toripalimab + SOX/XELOX	54	24.1	44.4
				SOX/XELOX only	54	9.3	20.4
NCT04908566	-	Toripalimab (PD-1)	II, two-arm	Toripalimab + FOLFIRINOX	21	15.4	31.6
				Toripalimab + SOX	33	10.5	23.1
KEYNOTE-585 (NCT03221426)	-	Pembrolizumab (PD-1)	III, two-arm	Pembrolizumab + XP/FP/FLOT	502	13.0	-
				Placebo + XP/FP/FLOT	505	2.4	-
MATTERHORN (NCT04592913)	-	Durvalumab (PD-L1)	III, two-arm	Durvalumab + FLOT	474	19	27
				Placebo + FLOT	474	7	14
NCT04139135	PD-L1 CPS≥5	Serplulimab (PD-1)	III, two-arm	Serplulimab + SOX	321	-	-
				Placebo + SOX	321	-	-
NICE (NCT04744649)	PD-L1 CPS≥5 or dMMR/MSI-H, EBV+	Toripalimab (PD-1)	II, two-arm	Toripalimab + SOX/XELOX	55	-	-
				SOX/XELOX only	55	-	-
NCT04367025	PD-L1 CPS≥1	Camrelizumab (PD-1)	II, single-arm	Camrelizumab + SOX	70	-	-
MONEO (NCT03979131)	-	Avelumab (PD-L1)	II, single-arm	Avelumab + FLOT	40	-	-
NCT05101616	-	Camrelizumab (PD-1)	I/II, two-arm	Camrelizumab + nab-PTX + SOX	50	-	-
				nab-PTX + S-1+ oxaliplatin	50	-	-
TACTIC (NCT05593458)	-	Sintilimab (PD-1)	II, two-arm	Artery-infused oxaliplatin + S-1+ Sintilimab	95	-	-
				SOX + Sintilimab	95	-	-
NCT05994456	dMMR/MSI-H	Toripalimab (PD-1)	II, single-arm	Toripalimab only	24	-	-
NCT05836584	dMMR/MSI-H	Atezolizumab (PD-L1)	II, two-arm	Atezolizumab only	120	-	-
				Atezolizumab + FLOT/ mFOLFOX/CAPOX	120	-	-

FOLFOX: Folinic acid + Fluorouracil + Oxaliplatin; mFOLFOX: modified FOLFOX; DOC: Docetaxel + Oxaliplatin + S-1; FLOT: Fluorouracil + Leucovorin + Oxaliplatin + Docetaxel; SOX: S-1 + Oxaliplatin; XELOX: Xeloda + Oxaliplatin; CAPOX: Capecitabine + Oxaliplatin; FOLFIRINOX: Fluorouracil + Leucovorin + Oxaliplatin + Irinotecan; XP: Xeloda + Cisplatin; FP: Fluorouracil + Cisplatin; nab-PTX: nab-paclitaxel; pCR: pathologic Complete Response; MPR: major pathologic response.

TRG 0-1 rate was higher in Group B, but the difference was not statistically significantly (31.58% vs. 23.08%, p = 0.703). PCR was achieved by 15.4% in A and 10.5% in B (2 patients each), with tumor downstaging observed in 71.9% patients (8 in A and 15 in B). TRAEs occurred in 46.3% (25/54) of patients, with 18.5% (10/54) experiencing grade ≥3 TRAEs, including neutropenia, thrombocytopenia, and myelosuppression (Liu et al., 2023). The trial suggests a potential treatment option, yet further investigation is needed to determine the suitability of intensive *versus* simplified treatment for neoadjuvant therapy.

The global phase 3 KEYNOTE-585 trial (NCT03221426) enrolled patients with stage II, III, or IVa G/GEJ cancer. Participants were randomly assigned to either pembrolizumab plus FP/XP (Xeloda and cisplatin) or placebo plus chemotherapy (1:1 ratio, the main cohort).

After three cycles of neoadjuvant therapy and subsequent curative surgery, those achieving R0 resection received 14 cycles of adjuvant therapy (3 cycles of combination therapy followed by 11 cycles of pembrolizumab or placebo monotherapy). Additionally, a safety FLOT cohort was introduced based on the AIO-FLOT4 study results, assigning patients randomly to either pembrolizumab or placebo plus FLOT. The primary endpoints were OS, EFS, and pCR. The results, presented at the ESMO Congress 2023, highlighted a notable increase in pCR rates within the main cohort, with a 10.9% improvement (95% CI 7.5–14.8; $p < 0.00001$) observed (12.9% with pembrolizumab vs. 2.0% with placebo). Additionally, the main plus FLOT cohort exhibited a 10.6% increase (95% CI 7.4–14.0; $p < 0.0001$) in pCR rates (13.0% vs. 2.4%). However, the improvement in pCR did not translate into a substantial extension in EFS for either the main cohort (median: 44.4 months vs. 25.3 months; HR 0.81; 95% CI 0.67–0.99; $p = 0.0198$) or the main plus FLOT cohort (median: 45.8 months vs. 25.7 months; HR 0.81; 95% CI 0.68–0.97). Moreover, there was also no significant improvement in OS in the main cohort (median: 60.7 months vs. 58.0 months; HR 0.90; 95% CI: 0.73–1.12). Rates of grade ≥3 drug-related adverse events (AEs) were comparable between the two groups in the main cohort (65% vs. 63%) (Shitara et al., 2023).

The preliminary results of the phase 3, double-blind, randomized MATTERHORN trial (NCT04592913) was also presented at the ESMO 2023. 948 patients with resectable G/GEJ cancer were randomized in a 1:1 ratio to receive durvalumab or placebo plus FLOT for two cycles of neoadjuvant and two cycles of adjuvant therapy, followed by 10 additional cycles of durvalumab or placebo. There was a significant 12% increase (OR 3.08, 95% CI 2.03–4.67; $p < 0.00001$) in the pCR rate, a secondary endpoint, among durvalumab group (19%) compared with placebo group (7%). Additionally, TRG 0/1 rates were higher in the durvalumab group (27% vs. 14%). Surgery completion rate (87% vs. 84%) and R0 resection rate (86% in each arm) were similar between two groups. Treatment with durvalumab resulted in greater surgical downstaging (23% pT0 and 52% pN0) *versus* placebo (11% pT0 and 36% pN0). The rates of grade 3–4 AEs (69% with durvalumab vs. 68% with placebo), TRAEs (95% vs. 94%) and grade 3–4 TRAEs (58% vs. 56%) were comparable (Janjigian et al., 2023). The primary endpoint of EFS is under investigation. While promising, recommending ICIs in perioperative therapy requires further follow-up data.

As to the lack of prolonged survival in KEYNOTE-585 despite improved pCR, it was pointed out at the meeting that immunotherapy was most effective in PD-L1-positive GC, but the patients in this trial were not selected based on biomarkers. In patients with CPS ≥10, pembrolizumab did exhibit a trend toward improved EFS (HR 0.69, 95% CI 0.48–1.01). Additionally, the majority of patients received cisplatin-based chemotherapy instead of the ESMO-recommended FLOT regimen. Notably, MATTERHORN, which has a similar design to KEYNOTE-585 but uses FLOT as the only chemotherapy regimen, achieved higher pCR rates, even in the control arm. Oxaliplatin may be more effective than cisplatin in the perioperative setting.

HLX10-006-GCneo (NCT04139135) is a phase 3 clinical trial comparing serplulimab plus SOX to placebo plus SOX in the perioperative setting for PD-L1 CPS ≥5 GC patients. Patients receive three cycles of neoadjuvant SOX treatment with serplulimab or placebo. After surgery, the serplulimab plus SOX group continues serplulimab monotherapy for 17 cycles, while the control group uses SOX alone for five cycles. The NICE trial (NCT04744649) is a phase 2, open-label, randomized study that compares toripalimab plus SOX/XELOX to SOX/XELOX alone in the perioperative treatment of resectable G/GEJ cancer (cT3-4aNxM0 or cT2N + M0) with PD-L1 CPS ≥5. Additionally, there are two exploratory groups investigating toripalimab plus SOX/XELOX in EBV + or dMMR/MSI-H patients. Each group receives 4 + 4 cycles of perioperative therapy. The phase 2 study NCT04367025 evaluates the perioperative SOX plus camrelizumab in G/GEJ cancer patients with PD-L1 CPS ≥1. The treatment involves 2-4 cycles of neoadjuvant and 2-4 cycles of adjuvant therapy. The phase 2, open-label MONEO (NCT03979131) trial investigates whether adding avelumab to FLOT chemotherapy improves pCR rate in G/GEJ adenocarcinoma compared to the historical data of chemotherapy alone in the perioperative setting. Patients will receive four cycles of neoadjuvant FLOT plus avelumab and four cycles of adjuvant therapy of the same schema, followed by avelumab maintenance therapy up to 1 year. NCT05101616 is a phase 1/2 randomized controlled trial examining neoadjuvant chemotherapy with/without camrelizumab for locally advanced GC (T3-4aN1-3M0). The chemotherapy regimen includes nab-paclitaxel (nab-PTX), S-1, and oxaliplatin. These trials will offer valuable insights into different combinations of chemotherapy and immunotherapy, contributing valuable data to expand the spectrum of treatment options.

Conventional SOX regimen consists of oral S-1 and intravenous oxaliplatin. The phase 3 TACTIC (NCT05593458) study evaluates whether replacing intravenous oxaliplatin with arterially infused oxaliplatin, combined with oral S-1 and sintilimab, can be a better neoadjuvant option for locally advanced G/GEJ cancer. Patients receive either three cycles of conventional SOX chemotherapy plus sintilimab or arterially infused oxaliplatin plus S-1 and sintilimab. Following radical surgery, they undergo three cycles of adjuvant chemotherapy using conventional SOX regimen plus sintilimab, with S-1 administered until 1 year after surgery.

As previously mentioned, dMMR/MSI-H GC patients exhibit a high sensitivity to immunotherapy but a limited response to chemotherapy (Pietrantonio et al., 2019). The DANTE study revealed a remarkable 63% increase of pCR rate in MSI-H patients with the combination of immunotherapy and chemotherapy (Al-Batran et al., 2022). It represents a key predictive biomarker for ICIs. NCT05994456 is an ongoing single-arm phase 2 trial evaluating toripalimab monotherapy in the perioperative management of locally advanced dMMR/MSI-H G/GEJ adenocarcinoma. Another ongoing randomized phase 2 study, NCT05836584, compares perioperative atezolizumab combined with chemotherapy (FLOT or mFOLFOX or CAPOX) to atezolizumab monotherapy. Their results are awaited and more investigations are required to advance our understanding and optimize the perioperative treatment options for these specific patient populations.

ICIs in combination with chemoradiation therapy

Neoadjuvant chemoradiotherapy is recommended for locally advanced esophagogastric cancer due to its efficacy in reducing the

TABLE 3 Clinical trials of ICIs plus CRT/targeted therapy or dual ICIs in perioperative setting.

Trial	Patients	Agent (target)	Phase, arm	Study design	Size	pCR (%)	MPR (%)
Neo-PLANET (NCT03631615)	-	Camrelizumab (PD-1)	II, single-arm	Camrelizumab + XELOX + cCRT	36	33.3	44.4
SHARED (ChiCTR1900024428)	-	Sintilimab (PD-1)	II, single-arm	Sintilimab + S-1+nab-PTX + cCRT	34	38.2	79.4
RARE (NCT05941481)	-	Tislelizumab (PD-1)	II, single-arm	Tislelizumab + XELOX + cCRT	21	-	-
GERCOR NEONIPIGA (NCT04006262)	dMMR/MSI-H	Nivolumab + Ipilimumab (PD-1, CTLA-4)	II, single-arm	Nivolumab + Ipilimumab	29	58.6	-
INFINITY (NCT04817826)	dMMR/MSI-H and EBV-	Durvalumab + Tremelimumab (PD-L1, CTLA-4)	II, single-arm, multi-cohort	Durvalumab + Tremelimumab	18	60	80
NCT03950271	HER2+	Camrelizumab (PD-1)	II, single-arm	Camrelizuma + Trastuzumab + CAPOX	16	31.3	56.3
NCT04819971	HER2+	Tislelizumab (PD-1)	II, single-arm	Tislelizumab + Trastuzumab + DOS	7	42.9	57.1
NCT05504720	HER2+	Pembrolizumab (PD-1)	II, single-arm	Pembrolizumab + Trastuzumab + FLOT	30	-	-
NCT05218148	HER2+	Sintilimab (PD-1)	II, two-arm	Sintilimab + Trastuzumab + SOX	22	-	-
				SOX only	22	-	-
NCT03878472	-	Camrelizumab (PD-1)	II, single-arm	Camrelizumab + Apatinib + S-1 ± oxaliplatin	19	15.8	26.3
DRAGON-IV/AHEAD-G208 (NCT04208347)	-	Camrelizumab (PD-1)	III, two-arm	SOXRC	256	18.3	51.5
				SOX only	256	5.0	37.8
TAOS-3B-Trial (NCT05223088)	-	Tislelizumab (PD-1)	II, single-arm	Tislelizumab + Apatinib + SOX	25	24	36
TAOS-3B-Trial-2 (NCT05699655)	-	Tislelizumab (PD-1)	II/III, two-arm	Tislelizumab + Apatinib + SOX	65	-	-
				SOX only	65	-	-

XELOX: Xeloda + Oxaliplatin; CAPOX: Capecitabine + Oxaliplatin; DOS: Docetaxel + Oxaliplatin + S-1; FLOT: Fluorouracil + Leucovorin + Oxaliplatin + Docetaxel; SOX: S-1 + Oxaliplatin; SOXRC: SOX + Apatinib + Camrelizumab; nab-PTX: nab-paclitaxel; cCRT: concurrent Chemoradiotherapy; pCR: pathologic Complete Response; MPR: major pathologic response.

risk of postoperative recurrence by more comprehensively eradicating micrometastases (Wang et al., 2021; Ajani et al., 2022). Radiotherapy at one site may lead to reduction or disappearance of non-irradiated distant tumors or metastatic lesions, which is known as the abscopal effect (Mole, 1953), as it can activate the host immune response (Postow et al., 2012; Ngwa et al., 2018). In addition, radiotherapy has been shown to alter the tumor immune microenvironment including upregulating the expression levels immune checkpoints (Theelen et al., 2019; McLaughlin et al., 2020). The combination of radiotherapy and immunotherapy can synergistically enhance treatment outcomes (Ngwa et al., 2018; Sato et al., 2020), providing benefits in the perioperative management of locally advanced GC patients (Table 3).

The single-arm, phase 2 Neo-PLANET trial (NCT03631615) explored camrelizumab combined with cCRT in locally advanced G/GEJ adenocarcinoma. 36 patients received preoperative sequential treatment with XELOX, cCRT (capecitabine, 45Gy/25f), XELOX, and concurrent camrelizumab since initiating chemotherapy. Of these, 33 patients (91.7%) underwent surgery with all achieving R0 resection. The pCR (ypT0, primary endpoint) rate reached 33.3% (95% CI: 18.6–51.0), meeting the pre-specified endpoint. Other rates included total pCR (ypT0N0, 33.3%), MPR (44.4%), and R0 resection (91.7%). Additionally, 77.8% (28/36) of patients reached ypN0 status. After a 2-year follow-up, PFS and OS rates were 66.9% and 76.1%, respectively. However, grade 3–4 AEs were observed in 86.1% (31/36) of patients, with the most common being decreased lymphocyte count (75.0%, 27/36) (Tang et al., 2022).

In another phase 2, single-arm trial (SHARED, ChiCTR1900024428), 34 patients with locally advanced G/GEJ cancers received neoadjuvant therapy involving one cycle of sintilimab and chemotherapy (S-1 and nab-PTX), followed by 5 weeks of cCRT (45Gy/25F, nab-PTX) and sintilimab, along with an additional cycle of sintilimab and chemotherapy (Jia et al., 2023). After surgery, three cycles of adjuvant sintilimab and chemotherapy were administered. All patients underwent neoadjuvant therapy and achieved R0 resection. The study met

its predefined primary endpoint, with 38.2% (13/34) patients achieving pCR (95% CI 22.2–56.4). In addition, 27 patients (79.4%) had MPR. The median DFS and EFS were 17.0 (95%CI 11.1–20.9) and 21.1 (95%CI 14.7–26.1) months, respectively. The median OS was not reached, with 1-year OS rate observed at 92.6% (95%CI 50.1%–99.5%). During preoperative therapy, 17 (50.0%) patients experienced grade ≥3 AEs, primarily myelosuppression.

The findings of Neo-PLANET and ChiCTR1900024428 highlight the promising efficacy of ICIs combined with cCRT for the perioperative management of locally advanced esophagogastric adenocarcinoma. Furthermore, the ongoing randomized phase 2 NeoRacing (NCT05161572) study is investigating the efficacy and safety of perioperative SOX with the addition of sintilimab, with or without preoperative chemoradiation (S-1 orally, 45Gy/25f), for cT3-4 aN + M0 or cT4bNanyM0 G/GEJ cancer (Zhou et al., 2022). Another ongoing single-arm phase 2 RARE (NCT05941481) study is evaluating neoadjuvant chemo-hypofractionated radiotherapy (XELOX, 30Gy/12f) combined with tislelizumab in cases staged as cT1-2N + M0 or T3-T4aNanyM0.

Dual ICIs strategy

CTLA-4 signaling is crucial in inhibiting the initiation of T-cell responses, while PD-1 plays a significant role later, dampening T-cell activity within the TME (Ye et al., 2023). Theoretically, combining CTLA-4 and PD-1 inhibitors offers synergistic effects (Buchbinder and Desai, 2016). However, the CHECKMATE-649 trial's nivolumab plus ipilimumab cohort revealed that this dual ICI approach did not offer survival benefits for advanced GC patients and was halted due to severe AEs. Notably, in MSI-H tumors, the combination therapy did result in longer median OS (HR 0.28; 95% CI 0.08–0.92) and a higher objective response rate (ORR, 70%; 95% CI 35–93) compared to chemotherapy (Shitara et al., 2022). The dual ICIs strategy has been explored in several perioperative setting studies (Table 3).

The single-arm phase 2 GERCOR NEONIPIGA (NCT04006262) study included 32 patients with resectable dMMR/MSI-H G/GEJ adenocarcinoma, comprising nine with cT2-T3N0, 22 with cT2-T3N1, and one incorrectly included with cT3N1M1. Neoadjuvant therapy with nivolumab and ipilimumab was administered, followed by surgery and adjuvant nivolumab therapy. Six patients (19%) experienced grade 3/4 neoadjuvant TRAEs. Three patients (one was M1 at inclusion) did not undergo surgery and achieved a full endoscopic remission evidenced by tumor-absent biopsies and had normal computed tomography scans. All 29 surgical patients achieved R0 resection, with 17 (58.6%; 90% CI 41.8–74.1) reaching pCR (ypT0N0, the primary endpoint) (André et al., 2023). These results suggest that MSI-H patients may avoid surgical treatment through dual ICIs strategy.

At ASCO-GI 2023, the phase 2, multicenter, single-arm, multi-cohort trial INFINITY (NCT04817826) was presented, which investigated the combination of tremelimumab plus durvalumab as neoadjuvant (Cohort 1) or definitive (Cohort 2) treatment for dMMR/MSI-H and EBV- (EBV negative) resectable G/GEJ adenocarcinoma. Cohort one started with $18^{-\Delta\Delta CT}$2-4Nany patients; however, one patient withdrew consent, and two opted out of surgery after achieving a complete clinical-pathological response. Out of the 15 patients assessed, the pCR and MPR rates were 60% and 80%, respectively. Grade ≥3 immune-related adverse events (IRAEs) were observed in three patients, involving colitis, pneumonitis, and liver toxicity. There were two post-operative deaths not related to the cancer or treatment adverse effects, and no recurrences were reported (Pietrantonio et al., 2023). These outcomes encourage further investigation into the non-surgical management using dual immune checkpoint inhibitors, with results from Cohort two anticipated.

In the phase 2 VESTIGE trial (NCT03443856), researchers investigated the efficacy of adjuvant nivolumab and low-dose ipilimumab therapy (nivo/ipi arm) compared to chemotherapy (chemo arm) in 189 stage Ib-IVa G/GEJ adenocarcinoma patients identified as high risk for recurrence (ypN1-3 and/or R1 status) following neoadjuvant chemotherapy (a fluoropyrimidine-platinum regimen) and D2 lymphadenectomy. Presented at ESMO-WCGIC 2023, the findings at a median follow-up of 11.1 months revealed a median DFS of 11.9 months (95% CI 8.4–16.8) for the nivo/ipi arm, significantly shorter than the 23.3 months (95% CI 11.8-not reached) observed in the chemo arm (HR 1.80, 95% CI 1.09–2.98, $p = 0.02$). Additionally, the median OS for the nivo/ipi arm was 25.1 months (95% CI 18.6– not reached), *versus* not reached for the chemo arm (HR 1.79, 95% CI 0.89–3.59, $p = 0.1$) These results led to a halt in further trial enrollment (Smyth et al., 2023). These outcomes suggest that adjuvant chemotherapy might be the preferable option in the adjuvant setting.

ICIs in combination with targeted therapy

Approximately 15%–20% of G/GEJ cancers exhibit positivity for human epidermal growth factor receptor 2 (HER2+) (Guan et al., 2023). The pivotal ToGA study highlighted the benefits of adding trastuzumab, an anti-HER2 drug, to chemotherapy, extending OS and increasing ORR from 35% to 47% (Bang et al., 2010). This finding established trastuzumab combined with chemotherapy as the primary treatment approach for patients with HER2+ status. Further advancement came with the KEYNOTE-811 trial, which showed that incorporating pembrolizumab into this first-line regimen for advanced HER2+ GC significantly raised the ORR from 51.9% to 74.4% (Janjigian et al., 2021b). Consequently, the combination of pembrolizumab, trastuzumab, and chemotherapy for first-line treatment received accelerated approval from the Food and Drug Administration granted. The potential of this triplet therapy in neoadjuvant therapy for HER2+ G/GEJ cancer deserves further exploration (Table 3).

In the single-arm, phase 2 NCT03950271 study, 22 patients with resectable HER2+ G/GEJ adenocarcinoma received camrelizumab combined with trastuzumab and CAPOX for neoadjuvant therapy. Of these, 16 patients underwent D2 resection, with 9 (56.3%) achieved MPR, including 5 (31.3%) with pCR (ypT0N0M0), and the ORR was 77.3% (Li et al., 2022). Another similar single-arm, phase 2 trial (NCT04819971) demonstrated a pCR rate of 42.9% (3/7) and an MPR rate of 57.1% (4/7) with the perioperative treatment of tislelizumab, trastuzumab and DOS (Zhao et al., 2023). These trials

suggest that the triple combination therapy is promising, with encouraging pCR and an acceptable toxicity profile. The single-arm, phase 2 NCT05504720 study is currently investigating the combination of pembrolizumab, trastuzumab and FLOT in this setting and the phase 2 NCT05218148 study is evaluating SOX with sintilimab and trastuzumab *versus* SOX only.

Tumor angiogenesis is pivotal in cancer development. Anti-angiogenic drugs, which inhibit the pro-angiogenic effects of vascular endothelial growth factor (VEGF) on its receptor (VEGFR-2), not only normalize tumor blood vessels but also alter the tumor's immune environment, promoting the infiltration of $CD8^+$ and $CD4^+$ lymphocytes, reversing immune suppression to an inflammatory state (Shrimali et al., 2010; Tian et al., 2017; Ciciola et al., 2020). The addition of anti-angiogenic agents to ICIs and chemotherapy regimens may enhance neoadjuvant therapy efficacy. Apatinib, a highly selective VEGFR-2 inhibitor, has shown to extend OS and is approved for third- or later-line treatment of advanced or metastatic G/GEJ adenocarcinoma (Li et al., 2016; Wang et al., 2021).

The phase 2, single-arm NCT03878472 study evaluated the combination of camrelizumab, apatinib, and S-1 with or without oxaliplatin as neoadjuvant/conversion therapy for cT4a/bN + GC. Tumor downstaging was achieved in 76.0% (19/25) of cases. The pCR and MPR rates were 15.8% (3/19; 95% CI 3.4%–39.6%) and 26.3% (5/19; 95% CI 9.1%–51.2%), respectively. Specifically, among cT4aN + patients, 18.2% (2/11) achieved pCR, and 36.4% (4/11) achieved MPR. Following a median observation period of 26.7 months, 55.6% (5/9) of the patients undergoing radical resection were free of recurrence. Notably, there were no reported complications of grade 3 or higher (Li et al., 2021).

The preliminary findings of the phase 3 DRAGON-IV/AHEAD-G208 trial (NCT04208347) were reported at ESMO 2023. 360 patients with cT3-4N + M0 G/GEJ adenocarcinoma were randomized to receive three cycles of either SOXRC (SOX, apatinib and camrelizumab) or SOX monotherapy as neoadjuvant therapy. After radical surgery, the SOXRC group continued with three cycles of triple combination therapy, as well as maintenance therapy with carrelizumab and apatinib, while the SOX group received three cycles of SOX followed by S-1 maintenance therapy. In the ITT population, the SOXRC group showed a significantly higher pCR rate of 18.3% (95% CI 13.0–24.8) compared to 5.0% (95% CI 2.3–9.3) in the SOX group. The ypT0N0 rate in the SOXRC group was 16.7%, and the MPR rate was 51.1%, higher than the SOX group's 4.4% and 37.8%, respectively. The pCR rates among patients who underwent surgery were 21.3% for SOXRC and 5.8% for SOX, with R0 resection rates of 98.7% and 94.2%, respectively. Toxicities were manageable and did not affect the feasibility of surgery. The study provides a feasible and safe option for resectable G/GEJ cancer patients (Li et al., 2023). Subsequent follow-up data are anticipated.

At ESMO-IO 2022, the single-arm, phase 2 TAOS-3B-Trial (NCT05223088) reported that SOX combined with tislelizumab and apatinib as neoadjuvant therapy for locally advanced G/GEJ cancer led to a 92% ORR and 100% disease control rate in 25 patients. The R0 resection rate was 100%, with pCR and MPR rates of 24% (6/25) and 36% (9/25), respectively. All patients experienced manageable TRAEs (Chen et al., 2022). Furthermore, the ongoing TAOS-3B-Trial-2 (NCT05699655) is comparing this regimen to SOX alone for neoadjuvant treatment in the same population.

Conclusion and future perspective

Incorporating immunotherapy into adjuvant treatment has yielded disappointing outcomes for unselected patients, potentially due to the near elimination of immunotherapy-sensitive tumor cells post-surgery. However, its effectiveness in specific populations warrants further exploration. The addition of immunotherapy to neoadjuvant chemotherapy has demonstrated superior pCR rates compared to traditional treatments in multiple studies for resectable locally advanced G/GEJ cancer. Moreover, combining targeted therapy or radiation therapy with immunotherapy in neoadjuvant treatments has shown promising outcomes. Optimizing treatment sequences, dose intensity and schedule of these combinations for better efficacy and less toxicity remains a key focus for future research. However, the direct correlation of pCR to long-term survival benefits is not always clear, as seen in the KEYNOTE-585 trial (Shitara et al., 2023). Many studies are still in the preliminary or phase II stages, highlighting the need for long-term follow-up and larger phase 3 randomized controlled trials. Moreover, the choice of chemotherapy agents, particularly the potential superiority of oxaliplatin-based regimens over cisplatin, is crucial when used with ICIs. In addition, neoadjuvant immunotherapy leverages higher levels of endogenous tumor antigen present in the primary tumor to enhance T cell priming while the primary tumor is in place (Topalian et al., 2020). Whether neoadjuvant immunotherapy is sufficient to be a definitive treatment for certain patients, allowing them to avoid surgery, is worth further investigation.

Future research should also focus on identifying effective predictive biomarkers. The 2023 NCCN guideline version two recommends neoadjuvant or perioperative ICIs for dMMR/MSI-H cT2+Nany GC patients. Research shows that GC with high PD-L1 expression, EBV+, and TMB-high responds better to immunotherapy, while *H. pylori* infection may impair its efficacy (Lin et al., 2020; Oster et al., 2022). Circulating tumor DNA, monitored by liquid biopsies, shows potential in predicting ICI responses (Jin et al., 2020; Ma et al., 2023). These biomarkers are worth further investigation and combinatorial biomarker strategies are more reasonable than traditional single immune-specific markers. Additionally, components of the TME such as the extracellular matrix, immune cells, stromal cells, aberrant blood vessels, cytokines, and growth factors play critical roles in tumor growth, development, progression, and treatment response (Mou et al., 2023; Roy and George, 2023; Wong et al., 2023). Multi-omics tools not only facilitate new biomarker discovery but also allow in-depth exploration within TME, including immune cell types, quantities, spatial distribution and various molecules, which could drive advancements of precision immunotherapy (Han and Zhan, 2022).

In conclusion, immunotherapy shows great promise in the management of resectable locally advanced G/GEJ cancer. Effective ICI combinations and further high-quality evidence are needed to firmly establish its role in clinical guidelines. And in-depth research is required to refine patient selection through biomarker optimization.

Author contributions

FL: Writing–original draft. YC: Writing–original draft. BH: Writing–original draft, Visualization. SR: Investigation, Writing–original draft. JL: Writing–original draft, Investigation. ZC: Visualization, Writing–original draft. CH: Writing–review and editing. BZ: Conceptualization, Writing–review and editing.

Funding

The author(s) declare that no financial support was received for the research, authorship, and/or publication of this article.

Conflict of interest

The authors declare that the research was conducted in the absence of any commercial or financial relationships that could be construed as a potential conflict of interest.

Publisher's note

All claims expressed in this article are solely those of the authors and do not necessarily represent those of their affiliated organizations, or those of the publisher, the editors and the reviewers. Any product that may be evaluated in this article, or claim that may be made by its manufacturer, is not guaranteed or endorsed by the publisher.

References

Ajani, J. A., D'Amico, T. A., Bentrem, D. J., Chao, J., Cooke, D., Corvera, C., et al. (2022). Gastric cancer, version 2.2022, NCCN clinical practice guidelines in oncology. *J. Natl. Compr. Canc Netw.* 20 (2), 167–192. doi:10.6004/jnccn.2022.0008

Al-Batran, S.-E., Homann, N., Pauligk, C., Goetze, T. O., Meiler, J., Kasper, S., et al. (2019). Perioperative chemotherapy with fluorouracil plus leucovorin, oxaliplatin, and docetaxel versus fluorouracil or capecitabine plus cisplatin and epirubicin for locally advanced, resectable gastric or gastro-oesophageal junction adenocarcinoma (FLOT4): a randomised, phase 2/3 trial. *Lancet London, Engl.* 393 (10184), 1948–1957. doi:10.1016/S0140-6736(18)32557-1

Al-Batran, S.-E., Lorenzen, S., Thuss-Patience, P. C., Homann, N., Schenk, M., Lindig, U., et al. (2022). Surgical and pathological outcome, and pathological regression, in patients receiving perioperative atezolizumab in combination with FLOT chemotherapy versus FLOT alone for resectable esophagogastric adenocarcinoma: interim results from DANTE, a randomized, multicenter, phase IIb trial of the FLOT-AIO German Gastric Cancer Group and Swiss SAKK. *J. Clin. Oncol.* 40 (16_Suppl. l), 4003. doi:10.1200/jco.2022.40.16_suppl.4003

Al-Batran, S.-E., Lorenzen, S., Thuss-Patience, P. C., Homann, N., Schenk, M., Lindig, U., et al. (2023). A randomized, open-label, phase II/III efficacy and safety study of atezolizumab in combination with FLOT versus FLOT alone in patients with gastric cancer and adenocarcinoma of the oesophagogastric junction and high immune responsiveness: the IKF-S633/DANTE trial, a trial of AIO in collaboration with SAKK. *J. Clin. Oncol.* 41 (16_Suppl. l), TPS4177–TPS. doi:10.1200/jco.2023.41.16_suppl.tps4177

Allemani, C., Matsuda, T., Di Carlo, V., Harewood, R., Matz, M., Nikšić, M., et al. (2018). Global surveillance of trends in cancer survival 2000-14 (CONCORD-3): analysis of individual records for 37 513 025 patients diagnosed with one of 18 cancers from 322 population-based registries in 71 countries. *Lancet* 391 (10125), 1023–1075. doi:10.1016/S0140-6736(17)33326-3

André, T., Tougeron, D., Piessen, G., de la Fouchardière, C., Louvet, C., Adenis, A., et al. (2023). Neoadjuvant nivolumab plus ipilimumab and adjuvant nivolumab in localized deficient mismatch repair/microsatellite instability-high gastric or esophagogastric junction adenocarcinoma: the GERCOR NEONIPIGA phase II study. *J. Clin. Oncol. Official J. Am. Soc. Clin. Oncol.* 41 (2), 255–265. doi:10.1200/JCO.22.00686

Bagchi, S., Yuan, R., and Engleman, E. G. (2021). Immune checkpoint inhibitors for the treatment of cancer: clinical impact and mechanisms of response and resistance. *Annu. Rev. Pathol.* 16, 223–249. doi:10.1146/annurev-pathol-042020-042741

Bang, Y. J., Kim, Y. W., Yang, H. K., Chung, H. C., Park, Y. K., Lee, K. H., et al. (2012). Adjuvant capecitabine and oxaliplatin for gastric cancer after D2 gastrectomy (CLASSIC): a phase 3 open-label, randomised controlled trial. *Lancet* 379 (9813), 315–321. doi:10.1016/S0140-6736(11)61873-4

Bang, Y. J., Van Cutsem, E., Feyereislova, A., Chung, H. C., Shen, L., Sawaki, A., et al. (2010). Trastuzumab in combination with chemotherapy versus chemotherapy alone for treatment of HER2-positive advanced gastric or gastro-oesophageal junction cancer (ToGA): a phase 3, open-label, randomised controlled trial. *Lancet* 376 (9742), 687–697. doi:10.1016/S0140-6736(10)61121-X

Buchbinder, E. I., and Desai, A. (2016). CTLA-4 and PD-1 pathways: similarities, differences, and implications of their inhibition. *Am. J. Clin. Oncol.* 39 (1), 98–106. doi:10.1097/COC.0000000000000239

Catenacci, D. V. T., Chase, L., Lomnicki, S., Karrison, T., de Wilton Marsh, R., Rampurwala, M. M., et al. (2020). Evaluation of the association of perioperative UGT1A1 genotype-dosed gFOLFIRINOX with margin-negative resection rates and pathologic response grades among patients with locally advanced gastroesophageal adenocarcinoma: a phase 2 clinical trial. *JAMA Netw. Open* 3 (2), e1921290. doi:10.1001/jamanetworkopen.2019.21290

Chen, L., Ye, Z., Liu, G., Lin, Q., Chi, Y., Wang, J., et al. (2022). 85P Tislelizumab combined with apatinib and oxaliplatin plus S1 as neoadjuvant therapy for Borrmann IV large Borrmann III type and bulky N positive advanced gastric cancer: a single-arm multicenter trial (TAOS-3B-Trial). *Immuno-Oncology Technol.* 16, 100189. doi:10.1016/j.iotech.2022.100189

Ciciola, P., Cascetta, P., Bianco, C., Formisano, L., and Bianco, R. (2020). Combining immune checkpoint inhibitors with anti-angiogenic agents. *J. Clin. Med.* 9 (3), 675. doi:10.3390/jcm9030675

Cunningham, D., Allum, W. H., Stenning, S. P., Thompson, J. N., Van de Velde, C. J. H., Nicolson, M., et al. (2006). Perioperative chemotherapy versus surgery alone for resectable gastroesophageal cancer. *N. Engl. J. Med.* 355 (1), 11–20. doi:10.1056/NEJMoa055531

Gordon, A., Challoner, B., Athauda, A., Woolston, A., Mansukhani, S., Dunstan, M., et al. (2023). Primary results of the ICONIC phase 2 trial of perioperative FLOT plus avelumab (FLOT-A) in operable oesophagogastric adenocarcinoma (OGA). *J. Clin. Oncol.* 41 (4_Suppl. l), 446. doi:10.1200/jco.2023.41.4_suppl.446

Guan, W. L., He, Y., and Xu, R. H. (2023). Gastric cancer treatment: recent progress and future perspectives. *J. Hematol. Oncol.* 16 (1), 57. doi:10.1186/s13045-023-01451-3

Han, C., and Zhan, Q. (2022). Precision medicine revolutionizes cancer diagnosis and treatment. *Med. Rev.* 2 (6), 541–543. doi:10.1515/mr-2022-0041

Janjigian, Y. Y., Al-Batran, S. E., Wainberg, Z. A., Van Cutsem, E., Molena, D., Muro, K., et al. (2023). LBA73 Pathological complete response (pCR) to durvalumab plus 5-fluorouracil, leucovorin, oxaliplatin and docetaxel (FLOT) in resectable gastric and gastroesophageal junction cancer (GC/GEJC): interim results of the global, phase III MATTERHORN study. *Ann. Oncol.* 34, S1315–S1316. doi:10.1016/j.annonc.2023.10.074

Janjigian, Y. Y., Kawazoe, A., Yañez, P., Li, N., Lonardi, S., Kolesnik, O., et al. (2021b). The KEYNOTE-811 trial of dual PD-1 and HER2 blockade in HER2-positive gastric cancer. *Nature* 600 (7890), 727–730. doi:10.1038/s41586-021-04161-3

Janjigian, Y. Y., Shitara, K., Moehler, M., Garrido, M., Salman, P., Shen, L., et al. (2021a). First-line nivolumab plus chemotherapy versus chemotherapy alone for advanced gastric, gastro-oesophageal junction, and oesophageal adenocarcinoma (CheckMate 649): a randomised, open-label, phase 3 trial. *Lancet* 398 (10294), 27–40. doi:10.1016/S0140-6736(21)00797-2

Japanese Gastric Cancer Association (2023). Japanese Gastric Cancer Treatment Guidelines 2021 (6th edition). *Gastric Cancer* 26 (1), 1–25. doi:10.1007/s10120-022-01331-8

Jia, W., Xiaofeng, L., Qin, L., Yao, F., Song, L., Yang, Z., et al. (2023). Neoadjuvant sintilimab in combination with concurrent chemoradiotherapy for locally advanced gastric or gastroesophageal junction adenocarcinoma: a single-arm phase 2 trial. *Nat. Commun.* 14 (1), 4904. doi:10.1038/s41467-023-40480-x

Jin, Y., Chen, D. L., Wang, F., Yang, C. P., Chen, X. X., You, J. Q., et al. (2020). The predicting role of circulating tumor DNA landscape in gastric cancer patients treated with immune checkpoint inhibitors. *Mol. Cancer* 19 (1), 154. doi:10.1186/s12943-020-01274-7

Kakeji, Y., Yoshida, K., Kodera, Y., Kochi, M., Sano, T., Ichikawa, W., et al. (2022). Three-year outcomes of a randomized phase III trial comparing adjuvant chemotherapy with S-1 plus docetaxel versus S-1 alone in stage III gastric cancer: JACCRO GC-07. *Gastric Cancer* 25 (1), 188–196. doi:10.1007/s10120-021-01224-2

Kang, B. W., and Chau, I. (2020). Current status and future potential of predictive biomarkers for immune checkpoint inhibitors in gastric cancer. *ESMO Open* 5 (4), e000791. doi:10.1136/esmoopen-2020-000791

Kang, Y. K., Boku, N., Satoh, T., Ryu, M. H., Chao, Y., Kato, K., et al. (2017). Nivolumab in patients with advanced gastric or gastro-oesophageal junction cancer refractory to, or intolerant of, at least two previous chemotherapy regimens (ONO-4538-12, ATTRACTION-2): a randomised, double-blind, placebo-controlled, phase 3 trial. *Lancet* 390 (10111), 2461–2471. doi:10.1016/S0140-6736(17)31827-5

Li, C., Zheng, Y., Shi, Z., Yang, L., Zhang, B., Wang, Z., et al. (2023). 1512MO Perioperative camrelizumab (C) combined with rivoceranib (R) and chemotherapy (chemo) versus chemo for locally advanced resectable gastric or gastroesophageal junction (G/GEJ) adenocarcinoma: the first interim analysis of a randomized, phase III trial (DRAGON IV). *Ann. Oncol.* 34, S852. doi:10.1016/j.annonc.2023.09.1425

Li, J., Qin, S., Xu, J., Xiong, J., Wu, C., Bai, Y., et al. (2016). Randomized, double-blind, placebo-controlled phase III trial of apatinib in patients with chemotherapy-refractory advanced or metastatic adenocarcinoma of the stomach or gastroesophageal junction. *J. Clin. Oncol.* 34 (13), 1448–1454. doi:10.1200/JCO.2015.63.5995

Li, N., Li, Z., Fu, Q., Zhang, B., Zhang, J., Wan, X., et al. (2022). Phase II study of SHR1210 and trastuzumab in combination with CAPOX for neoadjuvant treatment of HER2-positive gastric or gastroesophageal junction (GEJ) adenocarcinoma. *J. Clin. Oncol.* 40 (4_Suppl. l), 296. doi:10.1200/jco.2022.40.4_suppl.296

Li, P., Huang, C. M., Zheng, C. H., Russo, A., Kasbekar, P., Brennan, M. F., et al. (2018). Comparison of gastric cancer survival after R0 resection in the US and China. *J. Surg. Oncol.* 118 (6), 975–982. doi:10.1002/jso.25220

Li, S., Yu, W., Xie, F., Liu, Z., Lv, W., Shi, D., et al. (2021). A prospective, phase II, single-arm study of neoadjuvant/conversion therapy with camrelizumab, apatinib, S-1 ± oxaliplatin for locally advanced cT4a/bN+ gastric cancer. *J. Clin. Oncol.* 39 (15_Suppl. l), 4061. doi:10.1200/jco.2021.39.15_suppl.4061

Lin, Q., Wang, X., and Hu, Y. (2023). The opportunities and challenges in immunotherapy: insights from the regulation of PD-L1 in cancer cells. *Cancer Lett.* 569, 216318. doi:10.1016/j.canlet.2023.216318

Lin, X., Zong, C., Zhang, Z., Fang, W., and Xu, P. (2020)2023). Progresses in biomarkers for cancer immunotherapy. *MedComm* 4 (5), e387. doi:10.1002/mco2.387

Liu, R., Ji, Z., Wang, X., Zhang, L., Yang, Y., Ning, T., et al. (2023). Toripalimab combined with fluorouracil, leucovorin calcium, oxaliplatin and irinotecan (FOLFIRINOX) regimen or combined with oxaliplatin and tegafur (SOX) regimen in perioperative treatment of locally advanced resectable gastric or gastroesophageal junction adenocarcinoma (G/GEJ): an open-label, randomized, phase II study. *J. Clin. Oncol.* 41 (16_Suppl. l), e16090–e. doi:10.1200/jco.2023.41.16_suppl.e16090

Liu, Y., Han, G., Li, H., Zhao, Y., Zhuang, J., Wang, G., et al. (2020). Camrelizumab combined with FOLFOX as neoadjuvant therapy for resectable locally advanced gastric and gastroesophageal junction adenocarcinoma. *J. Clin. Oncol.* 38 (15_Suppl. l), 4536. doi:10.1200/jco.2020.38.15_suppl.4536

Lordick, F., Carneiro, F., Cascinu, S., Fleitas, T., Haustermans, K., Piessen, G., et al. (2022). Gastric cancer: ESMO Clinical Practice Guideline for diagnosis, treatment and follow-up. *Ann. Oncol.* 33 (10), 1005–1020. doi:10.1016/j.annonc.2022.07.004

Ma, S., Zhou, M., Xu, Y., Gu, X., Zou, M., Abudushalamu, G., et al. (2023). Clinical application and detection techniques of liquid biopsy in gastric cancer. *Mol. Cancer* 22 (1), 7. doi:10.1186/s12943-023-01715-z

Marin-Acevedo, J. A., Kimbrough, E. O., and Lou, Y. (2021). Next generation of immune checkpoint inhibitors and beyond. *J. Hematol. Oncol.* 14 (1), 45. doi:10.1186/s13045-021-01056-8

McLaughlin, M., Patin, E. C., Pedersen, M., Wilkins, A., Dillon, M. T., Melcher, A. A., et al. (2020). Inflammatory microenvironment remodelling by tumour cells after radiotherapy. *Nat. Rev. Cancer* 20 (4), 203–217. doi:10.1038/s41568-020-0246-1

Mole, R. H. (1953). Whole body irradiation; radiobiology or medicine? *Br. J. Radiol.* 26 (305), 234–241. doi:10.1259/0007-1285-26-305-234

Mou, P., Ge, Q. H., Sheng, R., Zhu, T. F., Liu, Y., and Ding, K. (2023). Research progress on the immune microenvironment and immunotherapy in gastric cancer. *Front. Immunol.* 14, 1291117. doi:10.3389/fimmu.2023.1291117

Ngwa, W., Irabor, O. C., Schoenfeld, J. D., Hesser, J., Demaria, S., and Formenti, S. C. (2018). Using immunotherapy to boost the abscopal effect. *Nat. Rev. Cancer* 18 (5), 313–322. doi:10.1038/nrc.2018.6

Oster, P., Vaillant, L., Riva, E., McMillan, B., Begka, C., Truntzer, C., et al. (2022). *Helicobacter pylori* infection has a detrimental impact on the efficacy of cancer immunotherapies. *Gut* 71 (3), 457–466. doi:10.1136/gutjnl-2020-323392

Park, H., Jin, R. U., Wang-Gillam, A., Suresh, R., Rigden, C., Amin, M., et al. (2020). FOLFIRINOX for the treatment of advanced gastroesophageal cancers: a phase 2 nonrandomized clinical trial. *JAMA Oncol.* 6 (8), 1231–1240. doi:10.1001/jamaoncol.2020.2020

Park, S. H., Lim, D. H., Sohn, T. S., Lee, J., Zang, D. Y., Kim, S. T., et al. (2021). A randomized phase III trial comparing adjuvant single-agent S1, S-1 with oxaliplatin, and postoperative chemoradiation with S-1 and oxaliplatin in patients with node-positive gastric cancer after D2 resection: the ARTIST 2 trial. *Ann. Oncol. Official J. Eur. Soc. Med. Oncol.* 32 (3), 368–374. doi:10.1016/j.annonc.2020.11.017

Pietrantonio, F., Miceli, R., Raimondi, A., Kim, Y. W., Kang, W. K., Langley, R. E., et al. (2019). Individual patient data meta-analysis of the value of microsatellite instability as a biomarker in gastric cancer. *J. Clin. Oncol.* 37 (35), 3392–3400. doi:10.1200/JCO.19.01124

Pietrantonio, F., Raimondi, A., Lonardi, S., Murgioni, S., Cardellino, G. G., Tamberi, S., et al. (2023). INFINITY: a multicentre, single-arm, multi-cohort, phase II trial of tremelimumab and durvalumab as neoadjuvant treatment of patients with microsatellite instability-high (MSI) resectable gastric or gastroesophageal junction adenocarcinoma (GAC/GEJAC). *J. Clin. Oncol.* 41 (4_Suppl. l), 358. doi:10.1200/jco.2023.41.4_suppl.358

Postow, M. A., Callahan, M. K., Barker, C. A., Yamada, Y., Yuan, J., Kitano, S., et al. (2012). Immunologic correlates of the abscopal effect in a patient with melanoma. *N. Engl. J. Med.* 366 (10), 925–931. doi:10.1056/NEJMoa1112824

Roy, A. M., and George, S. (2023). Emerging resistance vs. losing response to immune check point inhibitors in renal cell carcinoma: two differing phenomena. *Cancer Drug Resist* 6 (3), 642–655. doi:10.20517/cdr.2023.47

Sasako, M., Sakuramoto, S., Katai, H., Kinoshita, T., Furukawa, H., Yamaguchi, T., et al. (2011). Five-year outcomes of a randomized phase III trial comparing adjuvant chemotherapy with S-1 versus surgery alone in stage II or III gastric cancer. *J. Clin. Oncol.* 29 (33), 4387–4393. doi:10.1200/JCO.2011.36.5908

Sato, H., Okonogi, N., and Nakano, T. (2020). Rationale of combination of anti-PD-1/PD-L1 antibody therapy and radiotherapy for cancer treatment. *Int. J. Clin. Oncol.* 25 (5), 801–809. doi:10.1007/s10147-020-01666-1

Shitara, K., Ajani, J. A., Moehler, M., Garrido, M., Gallardo, C., Shen, L., et al. (2022). Nivolumab plus chemotherapy or ipilimumab in gastro-oesophageal cancer. *Nature* 603 (7903), 942–948. doi:10.1038/s41586-022-04508-4

Shitara, K., Rha, S. Y., Wyrwicz, L. S., Oshima, T., Karaseva, N., Osipov, M., et al. (2023). LBA74 Pembrolizumab plus chemotherapy vs chemotherapy as neoadjuvant and adjuvant therapy in locally-advanced gastric and gastroesophageal junction cancer: the phase III KEYNOTE-585 study. *Ann. Oncol.* 34, S1316. doi:10.1016/j.annonc.2023.10.075

Shrimali, R. K., Yu, Z., Theoret, M. R., Chinnasamy, D., Restifo, N. P., and Rosenberg, S. A. (2010). Antiangiogenic agents can increase lymphocyte infiltration into tumor and enhance the effectiveness of adoptive immunotherapy of cancer. *Cancer Res.* 70 (15), 6171–6180. doi:10.1158/0008-5472.CAN-10-0153

Siegel, R. L., Miller, K. D., Fuchs, H. E., and Jemal, A. (2021). Cancer statistics. *CA Cancer J. Clin.* 71 (1), 7–30. doi:10.3322/caac.21387

Smith, D. D., Schwarz, R. R., and Schwarz, R. E. (2005). Impact of total lymph node count on staging and survival after gastrectomy for gastric cancer: data from a large US-population database. *J. Clin. Oncol.* 23 (28), 7114–7124. doi:10.1200/JCO.2005.14.621

Smyth, E., Mauer, M., Cella, C., Ben-Aharon, I., Piessen, G., Wyrwicz, L., et al. (2023). O-6 EORTC 1707 VESTIGE: adjuvant immunotherapy in patients (pts) with resected gastroesophageal adenocarcinoma (GEA) following preoperative chemotherapy with high risk for recurrence (ypN+ and/or R1)—an open-label randomized controlled phase II study. *Ann. Oncol.* 34, S182–S183. doi:10.1016/j.annonc.2023.04.021

Suh, Y. S., and Yang, H. K. (2015). Screening and early detection of gastric cancer: east versus west. *Surg. Clin. North Am.* 95 (5), 1053–1066. doi:10.1016/j.suc.2015.05.012

Sun, W., Saeed, A., Al-Rajabi, R. M. T., Kasi, A., Veeramachaneni, N. K., Al-Kasspooles, M. F., et al. (2022). A phase II study of perioperative mFOLFOX plus pembrolizumab combination in patients with potentially resectable adenocarcinoma of the esophageal, gastroesophageal junction (GEJ) and stomach. *J. Clin. Oncol.* 40 (16_Suppl. l), 4047. doi:10.1200/jco.2022.40.16_suppl.4047

Sung, H., Ferlay, J., Siegel, R. L., Laversanne, M., Soerjomataram, I., Jemal, A., et al. (2021). Global cancer statistics 2020: GLOBOCAN estimates of incidence and mortality worldwide for 36 cancers in 185 countries. *CA a cancer J. Clin.* 71 (3), 209–249. doi:10.3322/caac.21660

Tang, Z., Wang, Y., Liu, D., Wang, X., Xu, C., Yu, Y., et al. (2022). The Neo-PLANET phase II trial of neoadjuvant camrelizumab plus concurrent chemoradiotherapy in locally advanced adenocarcinoma of stomach or gastroesophageal junction. *Nat. Commun.* 13 (1), 6807. doi:10.1038/s41467-022-34403-5

Terashima, M., Kang, Y.-K., Kim, Y.-W., Boku, N., Chung, H. C. C., Chen, J.-S., et al. (2023). ATTRACTION-5: a phase 3 study of nivolumab plus chemotherapy as postoperative adjuvant treatment for pathological stage III (pStage III) gastric or gastroesophageal junction (G/GEJ) cancer. *J. Clin. Oncol.* 41 (16_Suppl. l), 4000. doi:10.1200/jco.2023.41.16_suppl.4000

Theelen, W., Peulen, H. M. U., Lalezari, F., van der Noort, V., de Vries, J. F., Aerts, J., et al. (2019). Effect of pembrolizumab after stereotactic body radiotherapy vs pembrolizumab alone on tumor response in patients with advanced non-small cell lung cancer: results of the PEMBRO-RT phase 2 randomized clinical trial. *JAMA Oncol.* 5 (9), 1276–1282. doi:10.1001/jamaoncol.2019.1478

Tian, L., Goldstein, A., Wang, H., Ching Lo, H., Sun Kim, I., Welte, T., et al. (2017). Mutual regulation of tumour vessel normalization and immunostimulatory reprogramming. *Nature* 544 (7649), 250–254. doi:10.1038/nature21724

Topalian, S. L., Forde, P. M., Emens, L. A., Yarchoan, M., Smith, K. N., and Pardoll, D. M. (2023). Neoadjuvant immune checkpoint blockade: a window of opportunity to advance cancer immunotherapy. *Cancer Cell* 41 (9), 1551–1566. doi:10.1016/j.ccell.2023.07.011

Topalian, S. L., Taube, J. M., and Pardoll, D. M. (2020). Neoadjuvant checkpoint blockade for cancer immunotherapy. *Science.* 367 (6477), eaax0182. doi:10.1126/science.aax0182

Tougeron, D., Dahan, L., El Hajbi, F., Le Malicot, K., Evesque, L., Aparicio, T., et al. (2022). The PRODIGE 59-DURIGAST trial: a randomized phase II study evaluating

FOLFIRI plus durvalumab and FOLFIRI plus durvalumab plus tremelimumab in second-line treatment of patients with advanced gastric or gastro-esophageal junction adenocarcinoma. *J. Clin. Oncol.* 40 (16_Suppl. l), 4036. doi:10.1200/jco.2022.40.16_suppl.4036

Verschoor, Y. L., Kodach, L., Berg, J., Sandick, J., Dieren, J. V., Balduzzi, S., et al. (2022). Neoadjuvant atezolizumab plus docetaxel/oxaliplatin/capecitabine in non-metastatic gastric and gastroesophageal junction adenocarcinoma: the PANDA trial. *J. Clin. Oncol.* 40 (16_Suppl. l), 4059. doi:10.1200/jco.2022.40.16_suppl.4059

Wang, F. H., Zhang, X. T., Li, Y. F., Tang, L., Qu, X. J., Ying, J. E., et al. (2021). The Chinese Society of Clinical Oncology (CSCO): clinical guidelines for the diagnosis and treatment of gastric cancer. *Cancer Commun. (Lond).* 41 (8), 747–795. doi:10.1002/cac2.12193

Wong, R. S., Ong, R. J., and Lim, J. S. (2023). Immune checkpoint inhibitors in breast cancer: development, mechanisms of resistance and potential management strategies. *Cancer Drug Resist* 6 (4), 768–787. doi:10.20517/cdr.2023.58

Xu, J., Jiang, H., Pan, Y., Gu, K., Cang, S., Han, L., et al. (2021). LBA53 Sintilimab plus chemotherapy (chemo) versus chemo as first-line treatment for advanced gastric or gastroesophageal junction (G/GEJ) adenocarcinoma (ORIENT-16): first results of a randomized, double-blind, phase III study. *Ann. Oncol.* 32, S1331. doi:10.1016/j.annonc.2021.08.2133

Yanagimoto, Y., Kurokawa, Y., and Doki, Y. (2023). Essential updates 2021/2022: perioperative and surgical treatments for gastric and esophagogastric junction cancer. *Ann. Gastroenterol. Surg.* 7 (5), 698–708. doi:10.1002/ags3.12711

Ychou, M., Boige, V., Pignon, J.-P., Conroy, T., Bouché, O., Lebreton, G., et al. (2011). Perioperative chemotherapy compared with surgery alone for resectable gastroesophageal adenocarcinoma: an FNCLCC and FFCD multicenter phase III trial. *J. Clin. Oncol. Official J. Am. Soc. Clin. Oncol.* 29 (13), 1715–1721. doi:10.1200/JCO.2010.33.0597

Ye, F., Dewanjee, S., Li, Y., Jha, N. K., Chen, Z. S., Kumar, A., et al. (2023). Advancements in clinical aspects of targeted therapy and immunotherapy in breast cancer. *Mol. Cancer* 22 (1), 105. doi:10.1186/s12943-023-01805-y

Yoon, H. H., Jin, Z., Kour, O., Kankeu Fonkoua, L. A., Shitara, K., Gibson, M. K., et al. (2022). Association of PD-L1 expression and other variables with benefit from immune checkpoint inhibition in advanced gastroesophageal cancer: systematic review and meta-analysis of 17 phase 3 randomized clinical trials. *JAMA Oncol.* 8 (10), 1456–1465. doi:10.1001/jamaoncol.2022.3707

Yoshida, K., Kodera, Y., Kochi, M., Ichikawa, W., Kakeji, Y., Sano, T., et al. (2019). Addition of docetaxel to oral fluoropyrimidine improves efficacy in patients with stage III gastric cancer: interim analysis of JACCRO GC-07, a randomized controlled trial. *J. Clin. Oncol.* 37 (15), 1296–1304. doi:10.1200/JCO.18.01138

Yuan, S., Nie, R.-C., Jin, Y., Liang, C.-C., Jian, R., Li, Y.-F., et al. (2023). Perioperative PD-1 antibody toripalimab plus SOX or XELOX chemotherapy versus SOX or XELOX alone for locally advanced gastric or gastro-oesophageal junction cancer: results from a prospective, randomized, open-label, phase II trial. *J. Clin. Oncol.* 41 (16_Suppl. l), 4001. doi:10.1200/jco.2023.41.16_suppl.4001

Zhang, X., Liang, H., Li, Z., Xue, Y., Wang, Y., Zhou, Z., et al. (2021). Perioperative or postoperative adjuvant oxaliplatin with S-1 versus adjuvant oxaliplatin with capecitabine in patients with locally advanced gastric or gastro-oesophageal junction adenocarcinoma undergoing D2 gastrectomy (RESOLVE): an open-label, superiority and non-inferiority, phase 3 randomised controlled trial. *Lancet Oncol.* 22 (8), 1081–1092. doi:10.1016/S1470-2045(21)00297-7

Zhao, C., Meng, X., Shan, Z., Jiang, J., Liu, X., Li, H., et al. (2023). Efficacy and safety of perioperative chemotherapy combined with tislelizumab and trastuzumab for HER2-positive resectable gastric/gastroesophageal junction cancer (GC/EGJC): preliminary results of a phase 2, single-arm trial. *J. Clin. Oncol.* 41 (16_Suppl. l), e16084–e. doi:10.1200/jco.2023.41.16_suppl.e16084

Zhou, M., Yang, W., Xuan, Y., Zou, W., Wang, Y., Zhang, Z., et al. (2022). A study protocol of a randomized phase II trial of perioperative chemoimmunotherapy verses perioperative chemoimmunotherapy plus preoperative chemoradiation for locally advanced gastric (G) or gastroesophageal junction (GEJ) adenocarcinoma: the NeoRacing study. *BMC Cancer* 22 (1), 710. doi:10.1186/s12885-022-09786-9

frontiers | Frontiers in Pharmacology

TYPE Original Research
PUBLISHED 21 May 2024
DOI 10.3389/fphar.2024.1394241

Check for updates

OPEN ACCESS

EDITED BY
Hailin Tang,
Sun Yat-sen University Cancer Center (SYSUCC), China

REVIEWED BY
Xinhua Li,
Third Affiliated Hospital of Sun Yat-sen University, China
Baharan Fekry,
University of Texas Health Science Center at Houston, United States

*CORRESPONDENCE
Zhihong Wang,
zhihongwang1980@126.com
Hong Wei,
weihong2023@126.com

†These authors have contributed equally to this work

RECEIVED 01 March 2024
ACCEPTED 05 April 2024
PUBLISHED 21 May 2024

CITATION
Wang Z, Wu L, Zhou Y, Chen Z, Zhang T, Wei H and Wang Z (2024), Protein and metabolic profiles of tyrosine kinase inhibitors co-resistant liver cancer cells.
Front. Pharmacol. 15:1394241.
doi: 10.3389/fphar.2024.1394241

COPYRIGHT
© 2024 Wang, Wu, Zhou, Chen, Zhang, Wei and Wang. This is an open-access article distributed under the terms of the Creative Commons Attribution License (CC BY). The use, distribution or reproduction in other forums is permitted, provided the original author(s) and the copyright owner(s) are credited and that the original publication in this journal is cited, in accordance with accepted academic practice. No use, distribution or reproduction is permitted which does not comply with these terms.

Protein and metabolic profiles of tyrosine kinase inhibitors co-resistant liver cancer cells

Zengbin Wang[1†], Linqing Wu[1†], Yu Zhou[2†], Zhong Chen[3†], Tao Zhang[1], Hong Wei[4,5]* and Zhihong Wang[4,6]*

[1]Department of Immunology, School of Basic Medical Sciences, Fujian Medical University, Fuzhou, China, [2]Department of Clinical Pharmacy and Pharmacy Administration, School of Pharmacy, Fujian Medical University, Fuzhou, China, [3]Department of Hepatobiliary Surgery, Fujian Provincial Hospital, Fuzhou, China, [4]Shengli Clinical Medical College of Fujian Medical University, Fuzhou, China, [5]Department of Cadres's Healthcare Office, Fujian Provincial Hospital, Fuzhou, China, [6]Department of Hematology, Fujian Provincial Hospital, Fuzhou, China

Hepatocellular Carcinoma (HCC) patients often develop resistance to tyrosine kinase inhibitors (TKIs) like sorafenib (SR) and lenvatinib (RR). We established HCC cell lines resistant to these drugs and analyzed the correlation between protein and metabolite profiles using bioinformatics. Our analysis revealed overexpression of MISP, CHMP2B, IL-18, TMSB4X, and EFEMP1, and downregulation of IFITM3, CA4, AGR2, and SLC51B in drug-resistant cells. Differential signals are mainly enriched in steroid hormone biosynthesis, cell adhesion, and immune synapses, with metabolic pathways including cytochrome P450 drug metabolism, amino acid metabolism, and glycolysis. Proteomics and metabolomics analysis showed co-enrichment signals in drug metabolism, amino acids, glucose metabolism, ferroptosis, and other biological processes. Knocking down MISP, CHMP2B, IL-18, TMSB4X, and EFEMP1 significantly reduced drug resistance, indicating their potential as therapeutic response biomarkers. This study characterizes protein and metabolic profiles of drug-resistant HCC cells, exploring metabolite-protein relationships to enhance understanding of drug resistance mechanisms and clinical treatment.

KEYWORDS

sorafenib, lenvatinib, drug resistance, proteomics, metabolomics, hepatocellular carcinoma

Introduction

Sorafenib and lenvatinib, both belonging to the class of tyrosine kinase inhibitors (TKIs), serve as molecularly targeted drugs for the treatment of HCC. Their primary focus is on suppressing multiple crucial targets involved in tumor angiogenesis, signal transduction pathways, and immune regulation (Chan and Chan, 2023; Villarruel-Melquiades et al., 2023). Sorafenib and lenvatinib effectively restrain the advancement of HCC by impeding an assortment of receptor tyrosine kinases (RTKs) (Faivre et al., 2020). Sorafenib primarily suppresses the growth and angiogenesis of HCC cells by targeting and inhibiting vascular endothelial growth factor receptors (VEGFR) as well as the Raf/MEK/ERK signaling pathway (Jiang et al., 2023). In addition, sorafenib can also affect the regulation of tumor related immune cells and their factors, promoting the body's immune response. Lenvatinib mainly inhibits various receptors and pathways within cells, such as VEGFR, platelet-derived growth factor receptors (PDGF),

fibroblast growth factor receptors (FGFR) and hepatocyte factor receptor (c-KIT), to inhibit cell proliferation, promote cell apoptosis, and block angiogenesis, thereby achieving the effect of treating HCC (Laface et al., 2022). Despite the availability of TKIs, the reality is that most patients with advanced HCC eventually develop either innate or acquired resistance to these therapies (De Mattia et al., 2019). It is imperative to develop novel treatment strategies to address TKI resistance in advanced HCC patients.

Recent studies have shown that epigenetics, transport processes, regulated cell death, tumor microenvironment, hypoxia and viral reactivation play a role in the production and development of sorafenib resistance in HCC (Tang et al., 2020; Ladd et al., 2024). Lenvatinib resistance also has a similar mechanism to sorafenib resistance, including noncoding RNA regulation, tumor immune microenvironment and expansion of cancer stem cells (Tao et al., 2023). In addition, the combination of immune checkpoint inhibitors (ICI) and TKIs has important therapeutic significance in the treatment of HCC (Starzer et al., 2024). However, understanding the mechanism of TKIs resistance from a global perspective is still unclear.

The aim of this study is to investigate the mechanism of TKIs resistance and identify new therapeutic targets. In addition, this study attempts to determine the protein and metabolic profiles of TKIs resistance, providing insights for overall treatment rather than targeted therapy alone.

Materials and methods

Reagents and kits

Reagents and antibodies are as follows: sorafenib (MedChemExpress, Cat# HY-10201); lenvatinib (MedChemExpress, Cat# HY-10981); fetal bovine serum (Gemini Bio, Sacramento, CA); Lipofectamine 3,000 (Invitrogen); Dulbecco's Modified Eagle Medium (DMEM) (Gibco, Grand Island, NY); Fluoromount with 4′, 6- diamidino-2-phenylindole (DAPI) (Sigma-Aldrich, St. Louis, MO); Puromycin (Solarbio Life Science, Beijing, China); GAPDH (Proteintech, Cat# 60004-1-Ig); MISP (Proteintech, Cat# 26338-1-AP); CHMP2B (Proteintech, Cat# 12527-1-AP); TMSB4X (Proteintech, Cat# 19850-1-AP); IL-18 (ABclonal, Cat# A1115); EFEMP1 (Abcam, Cat# ab256457).

Clinical specimens

Retrospective collection of tissue paraffin embedded samples from HCC patients admitted to Fujian Provincial Hospital from January 2023 to December 2023. This research protocol has been approved by the Ethics Committee of Fujian Provincial Hospital (K2023-05-016).

Cell lines

The Huh7 cell lines (RRID: CVCL_0336, JCRB0403, Japan) were cultured in DMEM, supplemented with 10% FBS and 100 U/mL Penicillin/Streptomycin, and maintained at 37°C in a 5% CO_2 atmosphere. The cells underwent routine testing for *mycoplasma* contamination, which confirmed their freedom from contamination.

Establishment of sorafenib-resistant and lenvatinib-resistant HCC cells

The Huh7/SR and Huh7/RR cell lines, which are resistant to sorafenib or lenvatinib, were created in a previous study (Wang et al., 2023b; Leung et al., 2023). Briefly, Huh7 cells were cultured with gradually increasing doses of sorafenib or lenvatinib. Both Huh7/SR and Huh7/RR cells were cultured at a constant concentration of 10 μM.

siRNA transfection

si *MISP* (target sequence: TTCCGTTTCTATCTTCCTTTAGA), si *CHMP2B* (target sequence: AAGAAAACCGTGGATGGAATTAG), si *IL-18* (target sequence: AACTATTTGTCGCAGGAATAAAG), si *TMSB4X* (target sequence: TAGCTGTTTAACTTTGTAAGATG), si *EFEMP1* (target sequence: CGCACAGATTCACAATGTTGAAA) and scrambled control si RNA (si Control), were purchased from Tsingke Biotechnology Co., Ltd. All siRNA transfections were performed using Lipofectamine 3,000 according to the manufacturer's protocol.

Cell viability assay

The CCK-8 reagent was used to test cell viability in accordance with the manufacturer's instructions. In brief, the 96 well plate had 5,000 cells per well. Next, 10 μL of CCK-8 reagent was added to each well. The absorbance of every well was measured at 450 nm with a microplate reader (BioTek, Winooski, VT).

Immunoblotting

Immunoblotting was based on our previous research (Wang et al., 2023a). The total protein samples (25 μg) were separated through SDS-PAGE were separated via SDS-PAGE and transferred onto PVDF membranes (Biosharp, Hefei, China). Following this, the membranes were blocked with 5% bovine serum albumin (BSA) at room temperature for 1 h. The primary antibodies were applied to the membranes and incubated overnight at 4°C. After this step, secondary antibodies were added and incubated at room temperature for 1 h. The resulting bands were detected and visualized using a Hypersensitive ECL Chemiluminescence Kit (NcmECL Ultra, ABP Biosciences, Beltsville, MD, USA). The study utilized several primary antibodies: anti-MISP (1:1,000), anti-CHMP2B (1:1,000), anti-IL-18 (1:1,000), anti-TMSB4X (1:1,000), and anti-EFEMP1 (1:1,000), anti-GAPDH (1:5,000).

Cell proliferation assay

The EdU Cell Proliferation Kit (Solarbio, China) was utilized to quantify cell proliferation as per the guidelines furnished by the manufacturer. Upon combining with a fluorescent azide, proliferating cells emitted a vibrant red fluorescence that was visualized under a fluorescent microscope.

4D-DIA quantitative proteomics

4D-DIA quantitative proteomics was detected and analyzed by Novogen Co., Ltd. The software used for integrating metabolomics and proteomics data were presented in Supplementary Table S1. The steps are as follows.

Protein extraction

The sample was treated with lysis buffer (8 M urea supplemented with 1 mM PMSF and 2 mM EDTA) and subjected to ultrasonic waves to break down the cells. Following this, the residual debris was eliminated by centrifuging the mixture at 15000 g and at a temperature of 4°C for a duration of 10 min. BCA protein quantitation assay was employed to deduce the total protein concentration.

Digestion and cleanup

For tryptic digestion, an identical quantity of proteins from each sample was employed. The supernatants were supplemented with 8 M urea (200 μL) and reduced using 10 mM DTT at 37°C for a period of 45 min, following which they were alkylated using 50 mM iodoacetamide (IAM) at room temperature for 15 min in a darkroom. The resulting mixture was precipitated by adding 4× volume of chilled acetone and incubating at −20°C for 2 h. After centrifuging, the protein precipitate was air-dried, and then resuspended in a solution of 200 μL of 25 mM ammonium bicarbonate along with 3 μL of trypsin (Promega). The mixture was allowed to undergo overnight digestion at 37°C. Next, the resulting peptides were purified using a C18 Cartridge. Afterward, the peptides were dried using a Vacuum Concentration Meter, concentrated by vacuum centrifugation and eventually redissolved in a solution of 0.1% (v/V) formic acid.

LC-MS/MS analysis

A nanoElute UHPLC (Bruker Daltonics, Germany) was utilized to perform liquid chromatography (LC). The reverse-phase C18 column, which was commercially available with an integrated CaptiveSpray Emitter, allowed for the separation of approximately 200 ng peptides at a flow rate of 0.3 μL/min for 40 min. The integrated Toaster column oven maintained the separation temperature at 50°C. The mobile phases used were A and B, with 0.1 vol.-% formic acid in water and 0.1% formic acid in ACN respectively. Over the initial 25 min, mobile phase B was increased from 2% to 22%, and then, over the subsequent 5 min, it was augmented to 35%, further progressing to 80% over a period of subsequent 5 min while being held at 80% for a further 5 min. The LC was linked online to a hybrid timsTOF Pro2 (Bruker Daltonics, Germany) via a CaptiveSpray nano-electrospray ion source. In order to identify the suitable acquisition windows for diaPASEF mode, the timsTOF Pro2 was initially managed in Data-Dependent Parallel Accumulation-Serial Fragmentation (PASEF) mode with 4 PASEF MS/MS frames in 1 complete frame. The capillary voltage of 1500 V was set, while the MS and MS/MS spectra were gathered from 100 to 1700 m/z. As for the ion mobility range (1/*K*0), 0.85–1.3 Vs/cm2 was employed.

Database search and quantification

DIA-NN (v1.8.1) was utilized to analyze the MS raw data using a library-free approach. The uniprot_proteomeUP000005640_human_20230504.fasta database (which amounted to 82492 sequences) was employed to develop a spectra library via deep learning algorithms of neural networks. The MBR option was employed to produce a spectral library from DIA data, which was then reanalyzed utilizing this library. The search results were subjected to FDR adjustments to less than 1% at both protein and precursor ion levels; the remaining identifications were implemented for further quantification analysis.

Untargeted metabolomics

Untargeted metabolomics was detected and analyzed by Novogen Co., Ltd. The steps are as follows.

Cell samples class I

A 500 μL solution, containing the internal standard, was added to the cell sample, vortexed for 3 min, and subsequently subjected to a single freeze-thaw cycle consisting of placement in liquid nitrogen for 5 min followed by dry ice for 5 min, after which it was thawed on ice and vortexed for 2 min. A 300 μL supernatant was collected and stored at −20°C for 30 min. Afterward, it was centrifuged once again at 12000 rpm for 3 min, at 4°C. Following which, 200 μL aliquots of the supernatant were transferred for LC-MS analysis.

HPLC conditions

All of the samples were subjected to two LC/MS assays. One aliquot was analyzed using positive ion conditions, and was eluted from the T3 column (Waters ACQUITY Premier HSS T3 Column 1.8 μm, 2.1 mm * 100 mm), utilizing 0.1% formic acid in water as solvent A and 0.1% formic acid in acetonitrile as solvent B across the following gradient: 5%–20% within 2 min, followed by an increase to 60% in the subsequent 3 min, then an increase to 99% within 1 min, followed by a retention time of 1.5 min, thereafter returning to the initial 5% mobile phase B within 0.1 min, and a retention time of 2.4 min. The second aliquot was analyzed using negative ion conditions, utilizing the same elution gradient as the positive mode.

MS conditions (AB)

Data acquisition was performed using the information-dependent acquisition (IDA) mode, and the Analyst TF 1.7.1 Software (Sciex, Concord, ON, Canada) was used for this purpose. The TOF MS scan parameters were set at a mass range of 50–1,000 Da, with an accumulation time of 200 ms, and a dynamic background subtract was enabled. The product ion scan parameters were set at a mass range of 25–1,000 Da, with an accumulation time of 40 ms.

Statistical analysis

The results are expressed as mean ± SD and conducted using GraphPad Prism V.8. For normally distributed data with homogeneous variance, use unpaired t-tests to compare two samples. The comparison between multiple groups was conducted using one-way analysis of variance. A p-value <0.05 is considered statistically significant.

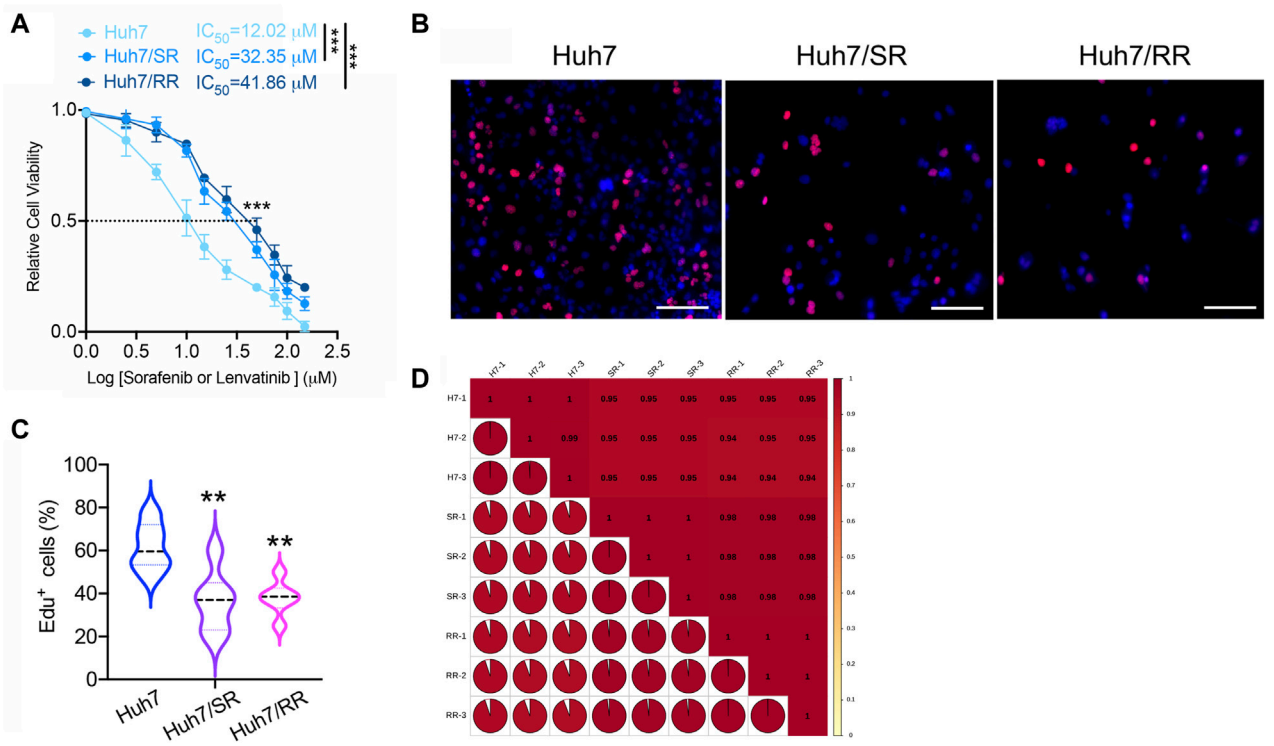

FIGURE 1
Quality evaluation of quantitative results between proteomic samples. **(A)** The IC_{50} values of Huh7, Huh7/SR, and Huh7/RR cells were detected. n = 3. Data were analyzed by unpaired t-test: ***$p < 0.001$. **(B,C)** The Edu proliferation detection kit was used to detect the number of Edu positive cells, n = 6. Bar = 50 μm. Data were analyzed using One-Way ANOVA analysis: **$p < 0.01$. **(D)** Pearson's Correlation Coefficient. The value of |R| indicates the strength of the correlation between two samples, with values approaching 1 indicating a strong correlation.

Results

Quality evaluation of quantitative results between proteomic samples

We produced Huh7 sorafenib resistant and lenvatinib resistant cell lines (Huh7/SR, Huh7/RR), respectively. Compared to the parental Huh7 cells, both Huh7/SR and Huh7/RR cells have higher IC_{50} values (Figure 1A). We next used the EdU proliferation detection kit to compare the number of EdU positive cells between parental cells and drug-resistant cells. It was found that compared to parental cells, both sorafenib and lenvatinib resistant cells had fewer Edu positive cells (Figures 1B, C). This indicates a decrease in the proliferation ability of drug-resistant cells. To evaluate the co-resistance mechanism of these two types of drug-resistant cells, we used 4D-DIA quantitative proteomics technology to explore the differences in protein expression. Both Huh7 and Huh7/RR, as well as Huh7 and Huh7/SR, have correlation coefficients greater than or equal to 0.94 (Figure 1D).

Protein differential expression analysis

Cluster heatmaps display differences in protein expression patterns between two drug-resistant cells and parental cells (Figure 2A). In comparison to Huh7 cells, Huh7/SR cells displayed an increase in 972 protein expressions and a decrease in 1,051 protein expressions. Similarly, Huh7/RR cells showed an increase in 1,071 protein expressions and a decrease in 1,072 protein expressions (Figures 2B, C). Compared to Huh7/SR cells, Huh7/RR cells upregulated 504 proteins and downregulated 389 proteins (Supplementary Figure S1). Notably, we identified the top 10 upregulated and downregulated proteins. Co-upregulated proteins included MISP, CHMP2B, IL-18, TMSB4X and EFEMP1, while co-downregulated proteins comprised of IFITM3, CA4, AGR2 and SLC51B (Figures 2B, C). Subcellular localization analysis of proteins found that they are mainly concentrated in the nucleus, cytoplasm, mitochondrion and plasma membrane (Figures 2D, E). Venn diagram showed that there are 1,315 common differentially expressed proteins in both groups (Figure 2F). These data indicate that many proteins in drug-resistant cells have undergone changes, indicating that the protein profile has been reconstructed.

Functional enrichment of differentially expressed proteins

The gene ontology (GO) enrichment analysis revealed that, in comparison to Huh7 cells, both Huh7/SR and Huh7/RR cells exhibited shared differential enrichment signals. These signals were primarily associated with integral components of the plasma membrane, extracellular space, extracellular region, basolateral plasma membrane, apical plasma membrane, chaperonin-containing T-complex, calcium-dependent phospholipid binding, and immunological synapse (Figures 3A, B). KEGG pathway

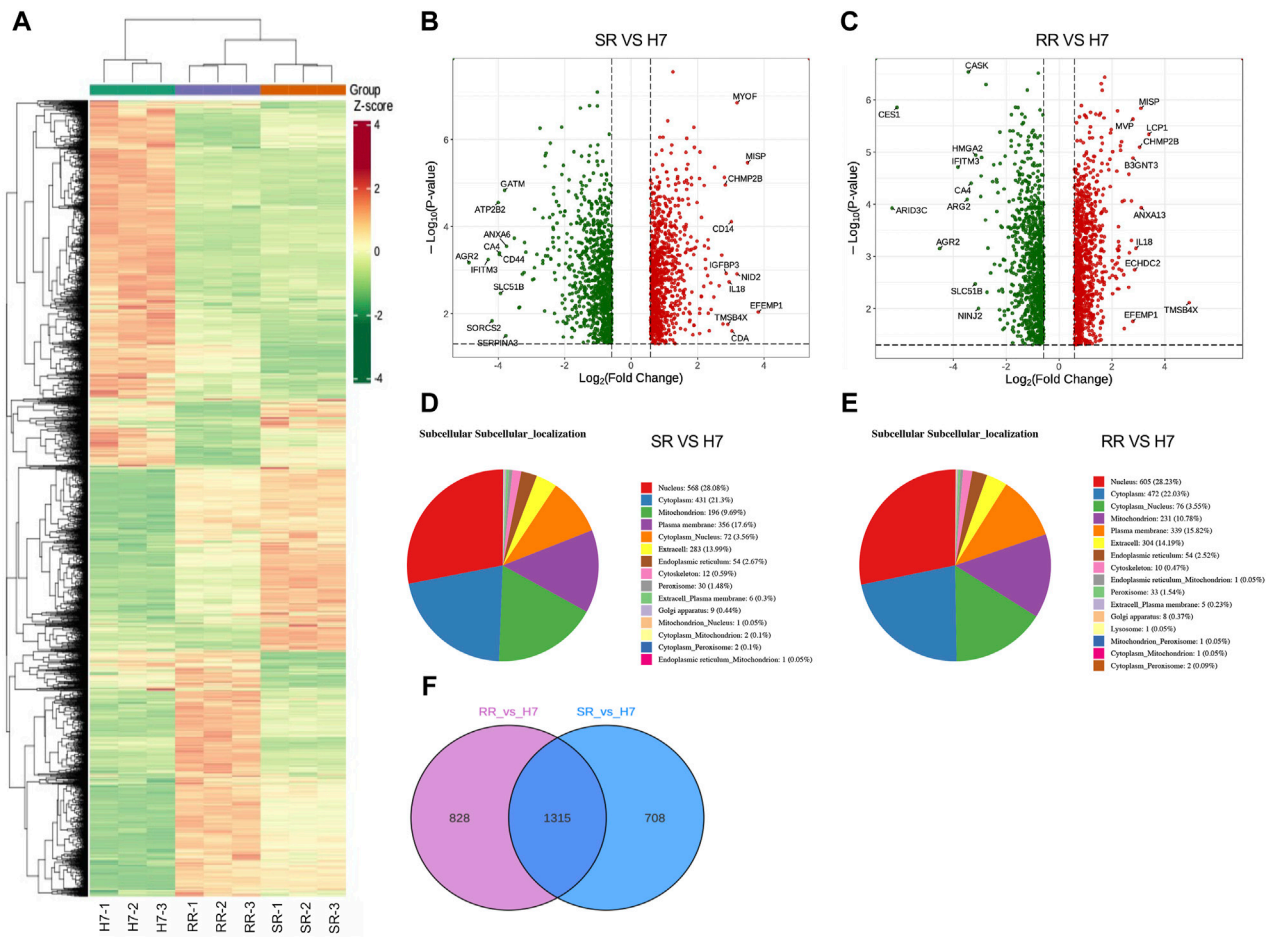

FIGURE 2
Protein differential expression analysis. **(A)** Differential protein clustering heatmap. Rows represent clustering of differentially expressed proteins, while columns represent clustering of samples. **(B,C)** Differential protein volcano plot. The horizontal axis represents log2 of the differential multiple, the vertical axis represents -$\log_{10}$ p-value, and the red and green scatter dots represent the up and downregulated differential proteins. **(D,E)** Subcellular localization of proteins that were differentially expressed is depicted with each subcellular compartment represented by a distinct color. The number of proteins that were annotated for each subcellular compartment is noted outside the parentheses, while the proportion of differentially expressed proteins annotated for each subcellular compartment is noted within the parentheses as compared to the total subcellular annotation. **(F)** Differential protein Venn diagram. n = 3.

analysis showed that the common differential enrichment signals in Huh7/SR and Huh7/RR cells primarily involved steroid hormone biosynthesis, cell adhesion molecules, mucin type O-glycan biosynthesis, and glycosphingolipid biosynthesis—lacto and neolacto series (Figures 3C, D). Furthermore, the structural domain enrichment analysis revealed that the common differential structural domains in Huh7/SR and Huh7/RR cells were primarily associated with immunoglobulin-like folds and subtypes, immunoglobulin-like domains and their superfamily, immunoglobulin subtype 2, chaperone tailless complex polypeptide 1 (TCP-1), chaperonin TCP-1, conserved sites, groEL-like equatorial domain superfamily, and fibronectin type III (Figures 3E, F). Protein protein interaction analysis (PPI) showed that both Huh7/SR vs. Huh7 and Huh7/RR vs. Huh7 exhibited highly complex differentially expressed protein interactions, while the interaction of Huh7/RR vs. Huh7/SR was relatively reduced (Figure 3G). These results indicate that the Huh7/SR and Huh7/RR cell populations exhibit unique molecular characteristics, revealing rich pathways and structural domains involved in cellular signaling, biosynthesis, and immune responses, which can provide valuable insights for drug resistance in HCC treatment.

Quality evaluation of quantitative results between metabolomic samples

Because both proteins and metabolites are closely related to cellular function. We have constructed a proteomic profile of drug-resistant cells, and we next continue to construct a metabolomic profile of drug-resistant cells. PCA results showed differences in metabolomic separation trends among groups (Figure 4A). PC1 Scores suggested that the test samples were within the range of 3 standard deviations (SD) (Figure 4B). The clustering heatmap provided the differences in metabolites between two types of drug-resistant cells and parental cells (Figures 4C, D). The differential metabolite volcano plots displayed a visual representation of the statistical significance and magnitude of differences in metabolite

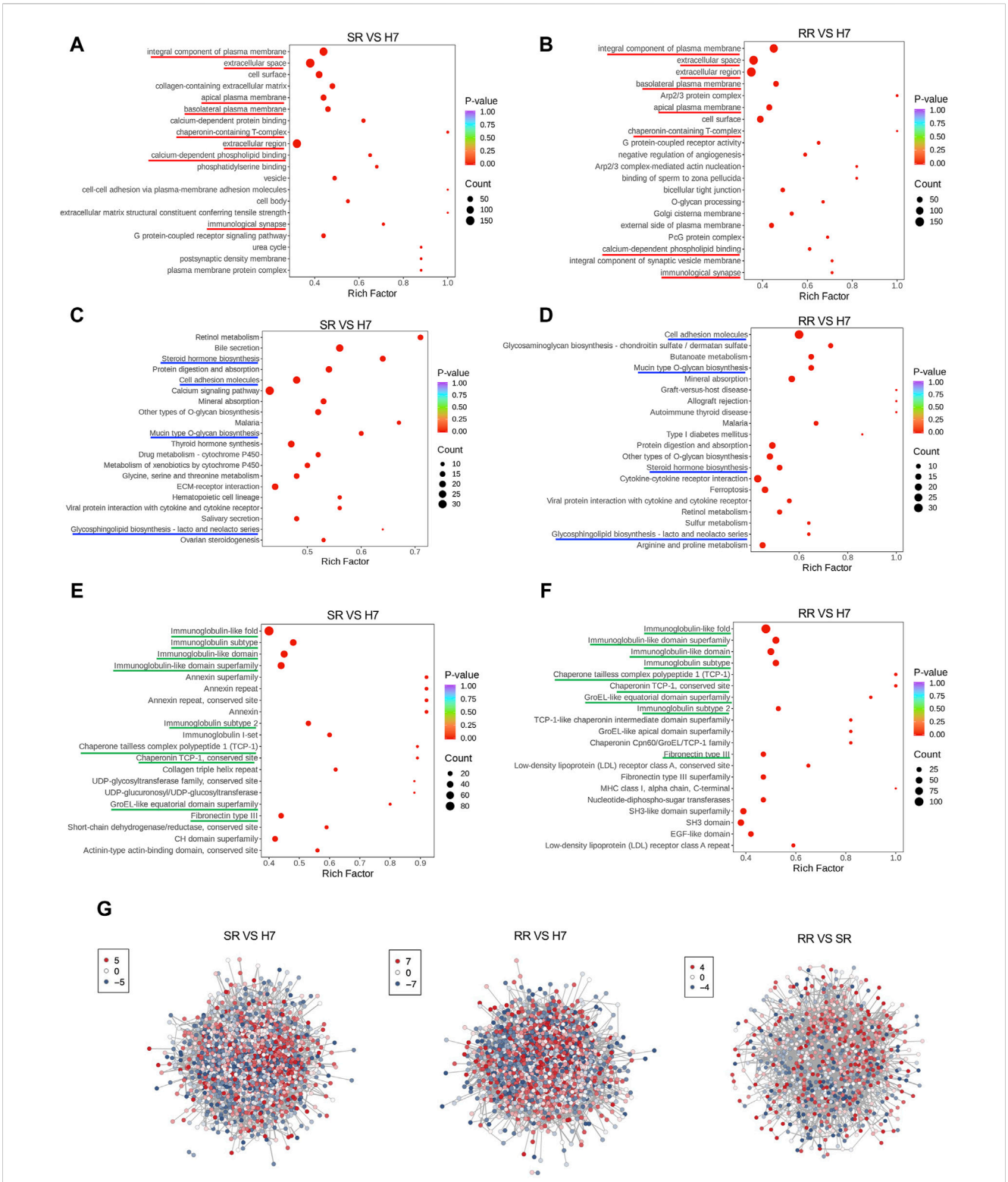

FIGURE 3
Functional enrichment of differentially expressed proteins. **(A,B)** Bubble charts depicted the GO enrichment analysis results. The horizontal axis showed the enrichment factor (DiffRatio/BgRatio ratio), reflecting the degree of enrichment, while the vertical axis displayed the name of the GO entry. **(C,D)** Bubble charts illustrated the KEGG enrichment analysis results. The horizontal axis showed the enrichment factor, reflecting the level of enrichment, while the vertical axis showed the KEGG pathway. **(E,F)** Bubble diagrams suggested the results of the structural domain enrichment analysis. The horizontal axis exhibited the enrichment factor, reflecting the level of enrichment, while the vertical axis showed the description of the IPR entry. **(G)** Differential expression protein interaction network. The differential expression protein interaction network diagram demonstrated the differentially expressed proteins. Each node represented a protein, with color change from red to blue indicating the expression level change from up to down. $n = 3$.

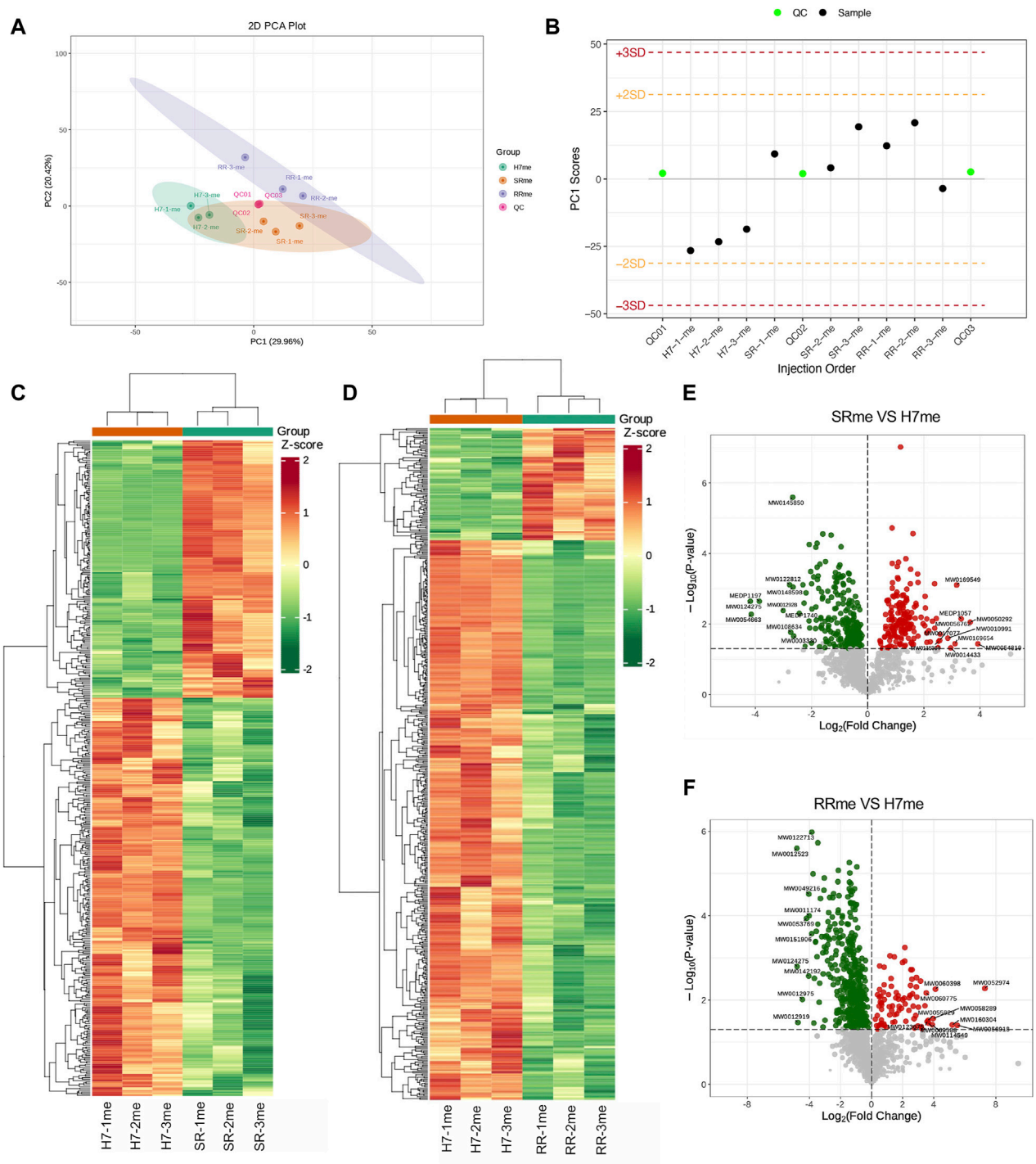

FIGURE 4
Quality evaluation of quantitative results between metabolomic samples. **(A)** PCA was performed to analyze the variance in the data. **(B)** The Sample PC1 control chart showed the PC1 value of the experimental and quality control samples plotted against the order of detection. The yellow and red lines depicted positive and negative 2 and 3 standard deviation ranges, respectively. **(C,D)** The cluster diagrams exhibited sample and metabolite information grouped according to the standardized relative content values. The horizontal axis represented sample information, the vertical axis represented metabolite information, and different colors indicated the degree of variation in the content (red represents high, green represents low). **(E,F)** Differential metabolite volcano map. $n = 3$.

abundance between groups. Compared to the Huh7 cells, the Huh7/SR cells had 176 metabolites elevated and 272 metabolites decreased (Figure 4E), while the Huh7/RR cell group had 89 metabolites elevated and 444 metabolites decreased (Figure 4F). These results can aid in understanding the metabolic pathways and regulatory mechanisms underlying cellular function and disease, providing a basis for potential biomarker discovery and therapeutic intervention.

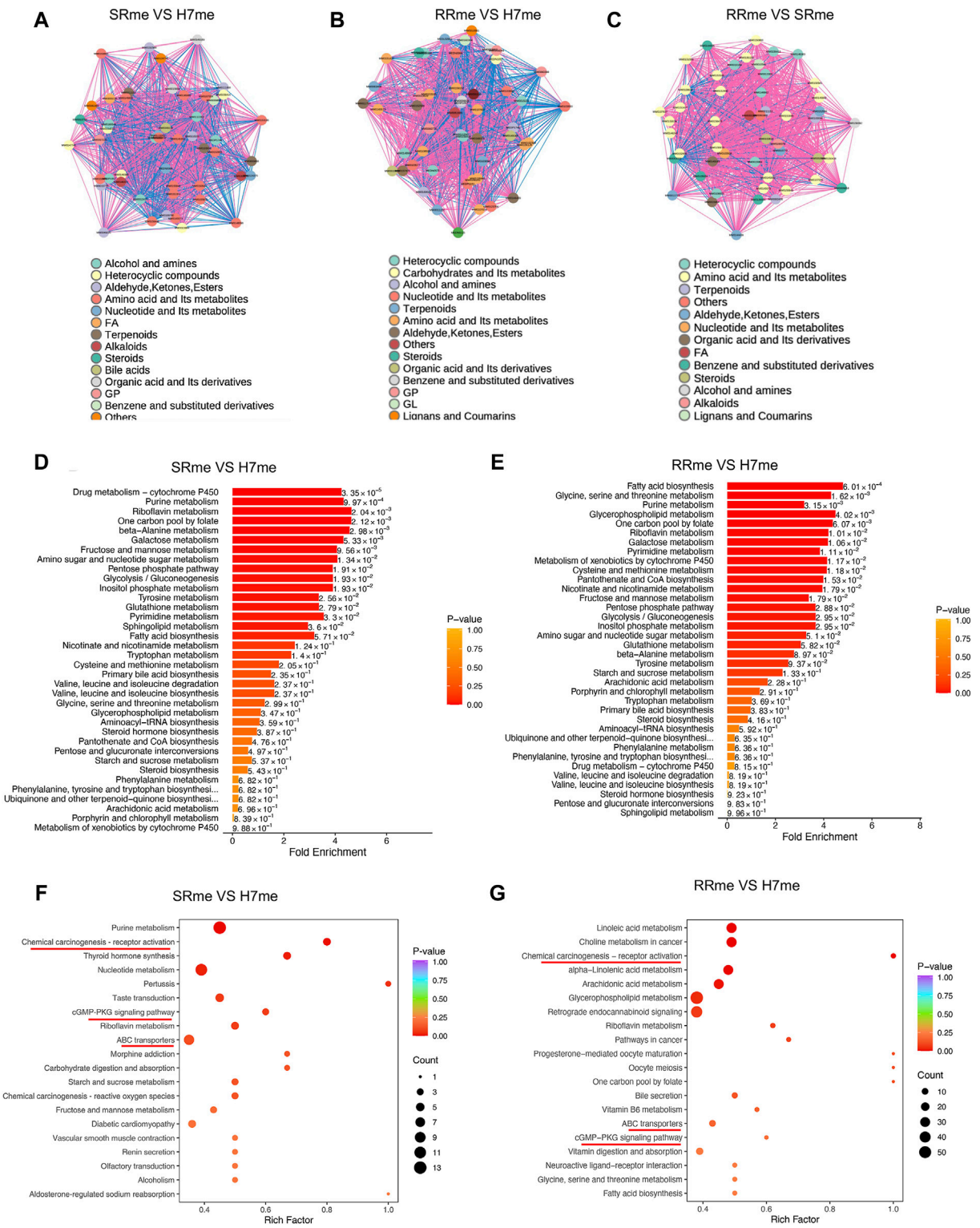

FIGURE 5
Functional enrichment analysis of differential metabolites. **(A–C)** Diagram portraying the correlation network of differential metabolites. The pink lines denoted positive correlation, while the blue lines indicated negative correlation. The line thickness was indicative of the absolute value of the correlation coefficient, with thicker lines denoting greater correlation strength. **(D,E)** Analysis of Metabolic Enrichment (MSEA). **(F,G)** Differential metabolite KEGG enrichment map. The horizontal axis corresponds to the Rich Factor associated with each pathway. The color of the point reflected the *p*-value, with redder points indicating greater significance of enrichment. The point size was proportional to the number of enriched differential metabolites. $n = 3$.

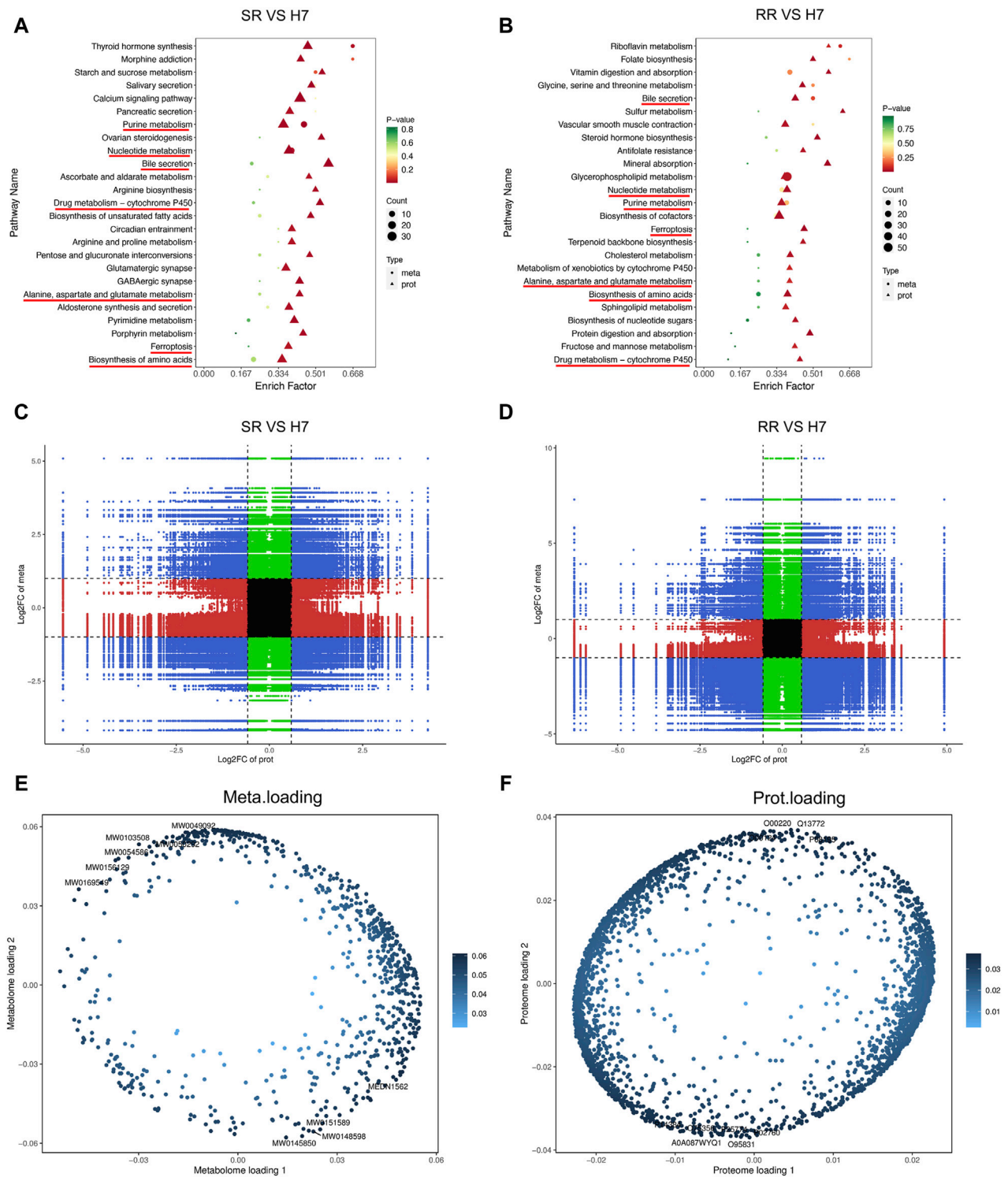

FIGURE 6
Combination analysis of proteomic and metabolomic profiles. **(A,B)** KEGG enrichment analysis bubble chart. The horizontal axis represented the enrichment factor (Diff/Background) of the pathway in different omics, while the vertical axis represents the name of the KEGG pathway. The gradient of red, yellow, and green showed a significant change in the degree of enrichment from high to medium to low, with *p*-value as the representative. The bubble shapes represented different omics, while the bubble sizes demonstrated the number of differential metabolites or proteins. The dots became larger as the numbers increase. **(C,D)** Correlation analysis nine quadrant chart. The horizontal axis represents the $\log_2$ FC of proteins, and the vertical axis represents the $\log_2$ FC of metabolites. **(E,F)** O2PLS analysis. $n = 3$.

Functional enrichment analysis of differential metabolites

To conduct in-depth analysis of differential metabolites, we conducted correlation analysis and enrichment analysis on differential metabolites. The correlation between differential metabolites indicated that amino acid and its metabolites were most significant among the three groups compared (Figures 5A–C). Metabolic Enrichment Analysis (MSEA) found that a large number of metabolic pathways were enriched, including: drug metabolism cytochrome P450, amino acid metabolism, fatty acid biosynthesis, pure metabolism, and glycolis/gluconeogenesis (Figures 5D, E). KEGG analysis of differential metabolites uncovered that the signal pathways jointly enriched in Huh7/SR and Huh7/RR cells involve the activation of chemical carcinogenesis receptors, the CGMP-PKG signaling pathway, and ABC transporters (Figures 5F, G).

Combination analysis of proteomic and metabolomic profiles

By combining the proteomics and metabolomics analysis, it can be seen from the KEGG analysis results that the co-enriched signals of metabolism and proteomics in the two resistant cells are mainly reflected in: drug metabolism cytochrome P450, alanine, aspartate and glucose metabolism, ferroptosis, biosynthesis of amino acids, bill secretion, nucleotide metabolism, and pure metabolism (Figures 6A, B). The correlation analysis between proteins and metabolites revealed a intricate relationship within drug-resistant cells. Specifically, the third and seventh quadrants exhibited proteins and metabolites displaying a positive correlation, whereas the first and ninth quadrants indicated proteins and metabolites with discordant regulatory patterns (Figures 6C, D). Subsequently, we selected all proteins and metabolites that exhibited differential expression and utilized them to construct an O2PLS model. We then conducted a preliminary variable screening process where we identified variables that possessed a high correlation and weight in different data groups through load plots (Figures 6E, F). Through these analyses, we established a connection between differential metabolites and proteins, allowing for a comprehensive understanding of the underlying mechanisms of drug resistance.

MISP, CHMP2B, IL-18, TMSB4X, and EFEMP1 are associated with drug resistance recurrence

To validate the protein family spectrum findings in drug-resistant cells, we selected HCC tissues from patients who underwent lenvatinib treatment and those with recurrence after such treatment. HE staining revealed necrosis in HCC tissue from patients treated with lenvatinib, along with an enhanced presence of immune infiltrating cells in para-carcinoma tissues and a notable increase in cancer cells in recurrent carcinoma tissue. These observations corroborate our understanding of the proteomic profiles in drug-resistant HCC cells (Figure 7A). The expression of MISP, CHMP2B, IL-18, TMSB4X, and EFEMP1 proteins in carcinoma tissue was higher than that in para-carcinoma tissues (Figure 7B). Survival analysis showed that high expression of MISP, CHMP2B, IL-18, TMSB4X, and EFEMP1 is not associated with poor prognosis in HCC (Figure 7C). Therefore, we speculated that these 5 proteins may not be related to tumor growth, but rather to drug resistance. We found that the expression levels of these 5 proteins in drug-resistant cells were significantly higher than those in parental cells, both in sorafenib resistant cells and lenvatinib resistant cells (Figure 7D). In addition, we used siRNA technology to knock down the expression of these 5 proteins one by one, and after being knocked down, the IC50 values of drug-resistant cells significantly decreased (Figures 7E, F). These results suggest that targeting these proteins will reduce drug resistance.

Discussion

Many HCC patients may develop drug resistance or relapse shortly after receiving first-line drug treatment, leading to poor treatment outcomes (Wang et al., 2024). The heterogeneity of HCC cells, their escape mechanisms, the existence of single nucleotide polymorphisms in drug metabolism, and the inadequate resilience of the patient's immune system can all potentially contribute to the resistance of HCC patients to TKIs (Chen et al., 2022; Salani et al., 2022). Therefore, in-depth research on drug resistance mechanisms is essential for understanding the emergence of drug resistance in HCC cells. In our previous study, we discovered that knocking out XPO1 can effectively reduce the resistance of HCC cells to sorafenib (Wang et al., 2023b). The combination of XPO1 inhibitor KPT-8602 and sorafenib has a better tumor treatment effect than sorafenib alone. In this study, we established a comprehensive resistance spectrum, encompassing both metabolites and proteins. Notably, the co-enrichment signals observed in drug-resistant cells are primarily reflected in drug metabolism, specifically involving cytochrome P450 (Wei et al., 2022; McGill et al., 2023), amino acids and glucose metabolism (Guo et al., 2023b), ferroptosis (Guo et al., 2023a; Li et al., 2023), biosynthesis of amino acids, bill secretion, nucleotide metabolism, and pure metabolism. This also suggests that for the resistance mechanism of TKIs, we should not only focus on a single resistance target, but more research needs to be mapped to the overall resistance spectrum.

The protein and metabolic profile of drug-resistant cells is reshaped. We found that common differentially enriched signals in drug-resistant cells involve cell adhesion molecules. Previous studies have also shown that highly enriched in the processes of cell-cell adhesion response to sorafenib resistance (Chai et al., 2021). We also found that cell adhesion molecules are highly expressed in drug-resistant cells. Focal adhesion kinase (FAK) is a key factor in the resistance of lenvatinib in HCC (Hou et al., 2024). FAK inhibitor TAE226 combined with sorafenib reduces HCC growth *in vitro* and *in vivo* (Romito et al., 2021). In addition, we suggest that MISP, CHMP2B, IL-18, TMSB4X and EFEMP1 may serve as predictive biomarkers for TKIs treatment. Cultivating NK cells by activating IL-12 and IL-18 can promote the therapeutic effect of sorafenib (Eresen et al., 2024). Combined with the GEPIA database analysis, it was confirmed that the expression of these genes is not significantly correlated with the prognosis of HCC patients, which also suggests their potential important relationship with TKIs resistance.

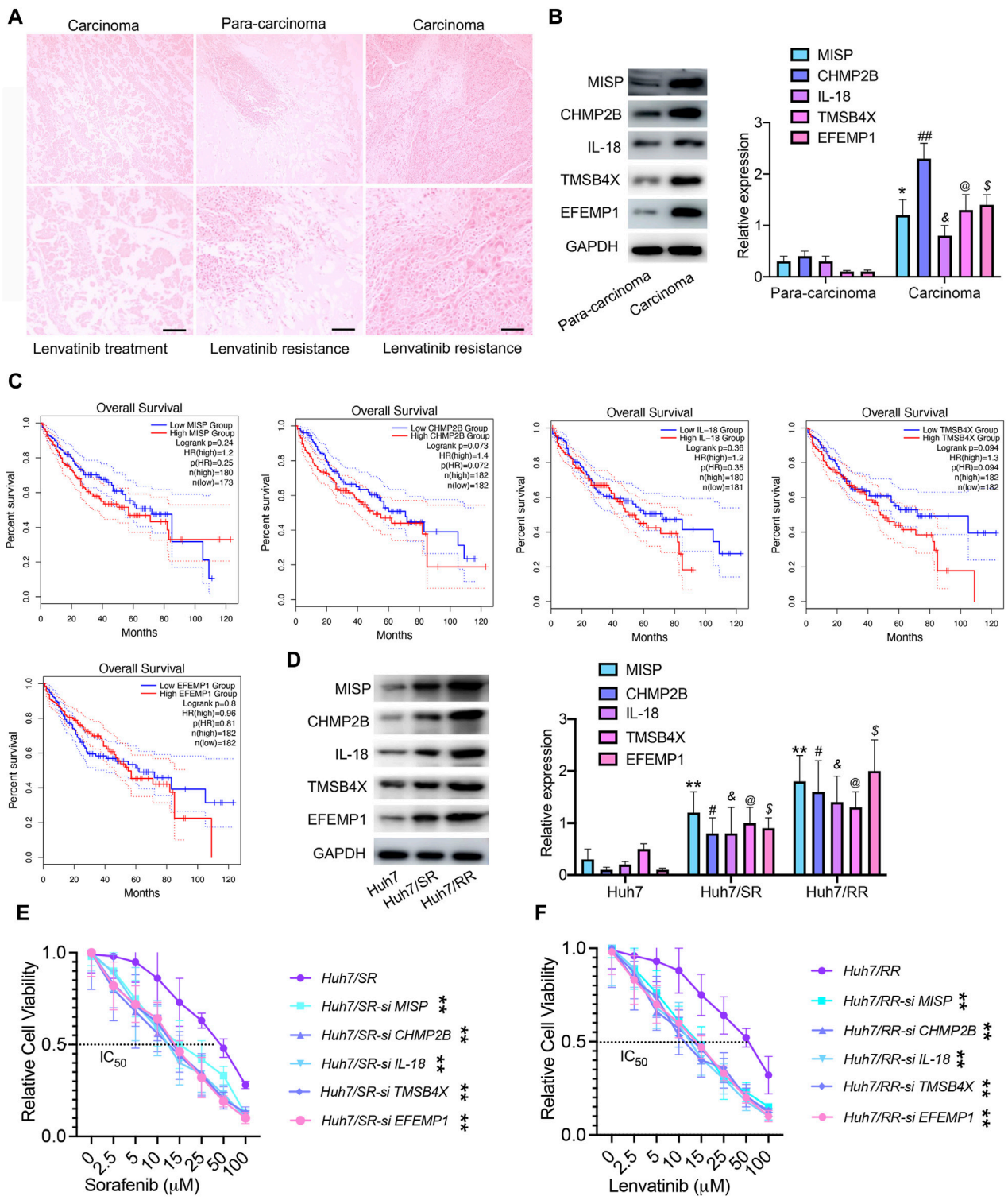

FIGURE 7
MISP, CHMP2B, IL-18, TMSB4X, and EFEMP1 are associated with drug resistance recurrence. **(A)** HE staining, Bar = 100 μm. **(B)** Immunoblotting was used to detect the expression levels of MISP, CHMP2B, IL-18, TMSB4X, and EFEMP1 proteins. Data are means ± SD from three experiments, analyzed by unpaired *t*-test: $^{*}p < 0.05$; $^{\#}p < 0.05$; $^{@}p < 0.05$; $^{\$}p < 0.05$; $^{\&}p < 0.05$, $n = 3$. **(C)** Overall survival of patients, grouped by high/low expression status of MISP, CHMP2B, IL-18, TMSB4X, and EFEMP1, plotted as Kaplan-Meier curve using the Gene Expression Profiling Interactive Analysis module (GEPIA). **(D)** Immunoblotting was used to detect the expression levels of MISP, CHMP2B, IL-18, TMSB4X, and EFEMP1 proteins. Data are means ± SD from three experiments, analyzed by One-Way ANOVA analysis: $^{**}p < 0.01$; $^{\#}p < 0.05$; $^{@}p < 0.05$; $^{\$}p < 0.05$; $^{\&}p < 0.05$, $n = 3$. **(E,F)** IC_{50} values of drug-resistant cells and drug-resistant cells transfected with si RNA. Data were analyzed by unpaired *t*-test: $^{**}p < 0.01$, $n = 3$.

Drug-resistant cells exhibit reduced expression of IFITM3, CA4, AGR2, and SLC51B. Notably, SLC51B, a gene linked to liver metabolism and immune microenvironment (Cheng et al., 2021), suggests a pivotal role in the intricate relationship between TKIs resistance and liver metabolic immunity. Paradoxically, AGR2 is highly expressed in sorafenib resistant cells, supporting endoplasmic reticulum homeostasis and cell survival (Guo et al., 2016). This may be due to inconsistent drug concentrations used to establish drug-resistant cells. Additionally, we propose an important relationship between cellular metabolites and TKIs resistance. Drug metabolism cytochrome P450 (Naveed et al., 2021), amino acid metabolism, fatty acid biosynthesis, pure metabolism, and glycolis/gluconeogenesis are significantly enriched in drug-resistant cells. Sorafenib enhances cytochrome P450 lipid metabolites in patient with HCC (Leineweber et al., 2023), further underscoring the intricate link between cellular metabolism and drug resistance.

This study is not without limitations. While we detect the expression of MISP, CHMP2B, IL-18, TMSB4X, and EFEMP1 proteins in liver tissue samples from HCC patients receiving lenvatinib treatment, the same proteins were not detected in those receiving sorafenib treatment. This may be due, in part, to the fact that lenvatinib is currently the preferred drug in clinical practice. Nonetheless, we have further validated these results using drug-resistant cells and siRNA. In addition, the mechanisms of action between metabolic and protein profiles, as well as their relationship with drug resistance, require in-depth research.

In summary, targeting a single drug resistance mechanism is insufficient. A comprehensive approach combining protein and metabolomics interventions is crucial for reducing drug resistance in HCC from a holistic perspective.

Data availability statement

The original contributions presented in the study are publicly available. This data can be found here: https://www.ebi.ac.uk/pride/archive/projects/PXD052321, with identifier PXD052321.

Ethics statement

The studies involving humans were approved by this research protocol has been approved by the Ethics Committee of Fujian Provincial Hospital (K2023-05-016). The studies were conducted in accordance with the local legislation and institutional requirements. The participants provided their written informed consent to participate in this study.

Author contributions

ZeW: Funding acquisition, Investigation, Methodology, Project administration, Supervision, Validation, Writing–original draft, Writing–review and editing. LW: Data curation, Writing–original draft, Writing–review and editing. YZ: Investigation, Validation, Writing–original draft. ZC: Investigation, Validation, Writing–original draft. TZ: Methodology, Supervision, Writing–original draft. HW: Conceptualization, Supervision, Writing–original draft. ZhW: Conceptualization, Funding acquisition, Project administration, Supervision, Writing–original draft.

Funding

The author(s) declare that financial support was received for the research, authorship, and/or publication of this article. This work was supported by the startup grant for High-level Talents of Fujian Medical University (XRCZX2023024), the Scientific Research Project of Fujian Education Department (JZ230018), the Natural Science Foundation of Fujian Province (2021J01664), and the joint funds for the innovation of science and technology, Fujian province (2020Y9027).

Conflict of interest

The authors declare that the research was conducted in the absence of any commercial or financial relationships that could be construed as a potential conflict of interest.

Publisher's note

All claims expressed in this article are solely those of the authors and do not necessarily represent those of their affiliated organizations, or those of the publisher, the editors and the reviewers. Any product that may be evaluated in this article, or claim that may be made by its manufacturer, is not guaranteed or endorsed by the publisher.

Supplementary material

The Supplementary Material for this article can be found online at: https://www.frontiersin.org/articles/10.3389/fphar.2024.1394241/full#supplementary-material

References

Chai, X., Guo, J., Dong, R., Yang, X., Deng, C., Wei, C., et al. (2021). Quantitative acetylome analysis reveals histone modifications that may predict prognosis in hepatitis B-related hepatocellular carcinoma. *Clin. Transl. Med.* 11, e313. doi:10.1002/ctm2.313

Chan, L. L., and Chan, S. L. (2023). The evolving role of lenvatinib at the new era of first-line hepatocellular carcinoma treatment. *Clin. Mol. Hepatol.* 29, 909–923. doi:10.3350/cmh.2023.0114

Cheng, J., Li, Y., Wang, X., Dong, Z., Chen, Y., Zhang, R., et al. (2021). Response stratification in the first-line combined immunotherapy of hepatocellular carcinoma at genomic, transcriptional and immune repertoire levels. *J. Hepatocell. Carcinoma* 8, 1281–1295. doi:10.2147/JHC.S326356

Chen, R., Li, Q., Xu, S., Ye, C., Tian, T., Jiang, Q., et al. (2022). Modulation of the tumour microenvironment in hepatocellular carcinoma by tyrosine kinase inhibitors: from modulation to combination therapy targeting the microenvironment. *Cancer Cell Int.* 22, 73. doi:10.1186/s12935-021-02435-4

De Mattia, E., Cecchin, E., Guardascione, M., Foltran, L., Di Raimo, T., Angelini, F., et al. (2019). Pharmacogenetics of the systemic treatment in advanced

hepatocellular carcinoma. *World J. Gastroenterol.* 25, 3870–3896. doi:10.3748/wjg.v25.i29.3870

Eresen, A., Pang, Y., Zhang, Z., Hou, Q., Chen, Z., Yu, G., et al. (2024). Sorafenib plus memory like natural killer cell combination therapy in hepatocellular carcinoma. *Am. J. Cancer Res.* 14, 344–354.

Faivre, S., Rimassa, L., and Finn, R. S. (2020). Molecular therapies for HCC: looking outside the box. *J. Hepatol.* 72, 342–352. doi:10.1016/j.jhep.2019.09.010

Guo, J. J., Ma, L. L., Shi, H. T., Zhu, J. B., Wu, J., Ding, Z. W., et al. (2016). Alginate oligosaccharide prevents acute doxorubicin cardiotoxicity by suppressing oxidative stress and endoplasmic reticulum-mediated apoptosis. *Mar. Drugs* 14, 231. doi:10.3390/md14120231

Guo, L., Hu, C., Yao, M., and Han, G. (2023a). Mechanism of sorafenib resistance associated with ferroptosis in HCC. *Front. Pharmacol.* 14, 1207496. doi:10.3389/fphar.2023.1207496

Guo, S., Zhang, C., Zeng, H., Xia, Y., Weng, C., Deng, Y., et al. (2023b). Glycolysis maintains AMPK activation in sorafenib-induced Warburg effect. *Mol. Metab.* 77, 101796. doi:10.1016/j.molmet.2023.101796

Hou, W., Gad, S. A., Ding, X., Dhanarajan, A., and Qiu, W. (2024). Focal adhesion kinase confers lenvatinib resistance in hepatocellular carcinoma via the regulation of lysine-deficient kinase 1. *Mol. Carcinog.* 63, 173–189. doi:10.1002/mc.23644

Jiang, H., Liao, J., Wang, L., Jin, C., Mo, J., and Xiang, S. (2023). The multikinase inhibitor axitinib in the treatment of advanced hepatocellular carcinoma: the current clinical applications and the molecular mechanisms. *Front. Immunol.* 14, 1163967. doi:10.3389/fimmu.2023.1163967

Ladd, A. D., Duarte, S., Sahin, I., and Zarrinpar, A. (2024). Mechanisms of drug resistance in HCC. *Hepatology* 79, 926–940. doi:10.1097/HEP.0000000000000237

Laface, C., Fedele, P., Maselli, F. M., Ambrogio, F., Foti, C., Molinari, P., et al. (2022). Targeted therapy for hepatocellular carcinoma: old and new opportunities. *Cancers (Basel)* 14, 4028. doi:10.3390/cancers14164028

Leineweber, C. G., Rabehl, M., Pietzner, A., Rohwer, N., Rothe, M., Pech, M., et al. (2023). Sorafenib increases cytochrome P450 lipid metabolites in patient with hepatocellular carcinoma. *Front. Pharmacol.* 14, 1124214. doi:10.3389/fphar.2023.1124214

Leung, C. O. N., Yang, Y., Leung, R. W. H., So, K. K. H., Guo, H. J., Lei, M. M. L., et al. (2023). Broad-spectrum kinome profiling identifies CDK6 upregulation as a driver of lenvatinib resistance in hepatocellular carcinoma. *Nat. Commun.* 14, 6699. doi:10.1038/s41467-023-42360-w

Li, Q., Chen, K., Zhang, T., Jiang, D., Chen, L., Jiang, J., et al. (2023). Understanding sorafenib-induced ferroptosis and resistance mechanisms: implications for cancer therapy. *Eur. J. Pharmacol.* 955, 175913. doi:10.1016/j.ejphar.2023.175913

Mcgill, M. R., Kaufman, Y. J., Lobianco, F. V., Schleiff, M. A., Aykin-Burns, N., and Miller, G. P. (2023). The role of cytochrome P450 3A4-mediated metabolism in sorafenib and lapatinib hepatotoxicity. *Livers* 3, 310–321. doi:10.3390/livers3020022

Naveed, H., Reglin, C., Schubert, T., Gao, X., Arold, S. T., and Maitland, M. L. (2021). Identifying novel drug targets by iDTPnd: a case study of kinase inhibitors. *Genomics Proteomics Bioinforma.* 19, 986–997. doi:10.1016/j.gpb.2020.05.006

Romito, I., Porru, M., Braghini, M. R., Pompili, L., Panera, N., Crudele, A., et al. (2021). Focal adhesion kinase inhibitor TAE226 combined with Sorafenib slows down hepatocellular carcinoma by multiple epigenetic effects. *J. Exp. Clin. Cancer Res.* 40, 364. doi:10.1186/s13046-021-02154-8

Salani, F., Genovesi, V., Vivaldi, C., Massa, V., Cesario, S., Bernardini, L., et al. (2022). Primary resistance to immunotherapy-based regimens in first line hepatocellular carcinoma: perspectives on jumping the hurdle. *Cancers (Basel)* 14, 4896. doi:10.3390/cancers14194896

Starzer, A. M., Wolff, L., Popov, P., Kiesewetter, B., Preusser, M., and Berghoff, A. S. (2024). The more the merrier? Evidence and efficacy of immune checkpoint- and tyrosine kinase inhibitor combinations in advanced solid cancers. *Cancer Treat. Rev.* 125, 102718. doi:10.1016/j.ctrv.2024.102718

Tang, W., Chen, Z., Zhang, W., Cheng, Y., Zhang, B., Wu, F., et al. (2020). The mechanisms of sorafenib resistance in hepatocellular carcinoma: theoretical basis and therapeutic aspects. *Signal Transduct. Target Ther.* 5, 87. doi:10.1038/s41392-020-0187-x

Tao, M., Han, J., Shi, J., Liao, H., Wen, K., Wang, W., et al. (2023). Application and resistance mechanisms of lenvatinib in patients with advanced hepatocellular carcinoma. *J. Hepatocell. Carcinoma* 10, 1069–1083. doi:10.2147/JHC.S411806

Villarruel-Melquiades, F., Mendoza-Garrido, M. E., García-Cuellar, C. M., Sánchez-Pérez, Y., Pérez-Carreón, J. I., and Camacho, J. (2023). Current and novel approaches in the pharmacological treatment of hepatocellular carcinoma. *World J. Gastroenterol.* 29, 2571–2599. doi:10.3748/wjg.v29.i17.2571

Wang, Z., Pan, B., Qiu, J., Zhang, X., Ke, X., Shen, S., et al. (2023a). SUMOylated IL-33 in the nucleus stabilizes the transcription factor IRF1 in hepatocellular carcinoma cells to promote immune escape. *Sci. Signal* 16, eabq3362. doi:10.1126/scisignal.abq3362

Wang, Z., Pan, B., Yao, Y., Qiu, J., Zhang, X., Wu, X., et al. (2023b). XPO1 intensifies sorafenib resistance by stabilizing acetylation of NPM1 and enhancing epithelial-mesenchymal transition in hepatocellular carcinoma. *Biomed. Pharmacother.* 160, 114402. doi:10.1016/j.biopha.2023.114402

Wang, Z., Zhou, C., Zhang, Y., Tian, X., Wang, H., Wu, J., et al. (2024). From synergy to resistance: navigating the complex relationship between sorafenib and ferroptosis in hepatocellular carcinoma. *Biomed. Pharmacother.* 170, 116074. doi:10.1016/j.biopha.2023.116074

Wei, K. L., Gao, G. L., Chou, Y. T., Lin, C. Y., Chen, S. C., Chen, Y. L., et al. (2022). Sorafenib is an antagonist of the aryl hydrocarbon receptor. *Toxicology* 470, 153118. doi:10.1016/j.tox.2022.153118

frontiers | Frontiers in Pharmacology

TYPE Brief Research Report
PUBLISHED 24 May 2024
DOI 10.3389/fphar.2024.1393693

Check for updates

OPEN ACCESS

EDITED BY
Hailin Tang,
Sun Yat-sen University Cancer Center (SYSUCC), China

REVIEWED BY
Changliang Shan,
Nankai University, China
Xiaofang Guo,
University of South Florida, United States

*CORRESPONDENCE
Zhi Shi,
tshizhi@jnu.edu.cn

†These authors have contributed equally to this work

RECEIVED 29 February 2024
ACCEPTED 25 April 2024
PUBLISHED 24 May 2024

CITATION
Li X-P, Cao L-Q, Yu Z-Z, He K, Ding P-B, Li J-S, Shan Y-Y, Su Y-B, Yuan Z-M and Shi Z (2024), Dorsomorphin attenuates ABCG2-mediated multidrug resistance in colorectal cancer. *Front. Pharmacol.* 15:1393693. doi: 10.3389/fphar.2024.1393693

COPYRIGHT
© 2024 Li, Cao, Yu, He, Ding, Li, Shan, Su, Yuan and Shi. This is an open-access article distributed under the terms of the Creative Commons Attribution License (CC BY). The use, distribution or reproduction in other forums is permitted, provided the original author(s) and the copyright owner(s) are credited and that the original publication in this journal is cited, in accordance with accepted academic practice. No use, distribution or reproduction is permitted which does not comply with these terms.

Dorsomorphin attenuates ABCG2-mediated multidrug resistance in colorectal cancer

Xiao-Peng Li[1,2†], Liang-Qi Cao[3†], Ze-Zhong Yu[1,2†], Ke He[1], Peng-Bo Ding[2], Ji-Sheng Li[2], Yi-Yao Shan[2], Yu-Bin Su[2], Zhong-Min Yuan[4] and Zhi Shi[1,2]*

[1]Cancer Minimally Invasive Therapies Centre, Guangdong Second Provincial General Hospital, Jinan University, Guangzhou, China, [2]Department of Cell Biology and Institute of Biomedicine, Guangdong Provincial Biotechnology and Engineering Technology Research Center, Guangdong Provincial Key Laboratory of Bioengineering Medicine, Genomic Medicine Engineering Research Center of Ministry of Education, MOE Key Laboratory of Tumor Molecular Biology, National Engineering Research Center of Genetic Medicine, State Key Laboratory of Bioactive Molecules and Druggability Assessment, College of Life Science and Technology, Jinan University, Guangzhou, China, [3]Key Laboratory of Neurogenetics and Channelopathies of Guangdong Province and the Ministry of Education of China, The Second Affiliated Hospital, Institute of Neuroscience, Guangzhou Medical University, Guangzhou, China, [4]Department of Hepatobiliary Surgery, The Second Affiliated Hospital of Guangzhou Medical University, Guangzhou, China

Colorectal cancer is a common malignant tumor with high mortality, for which chemotherapy resistance is one of the main reasons. The high expression of ABCG2 in the cancer cells and expulsion of anticancer drugs directly cause multidrug resistance (MDR). Therefore, the development of new ABCG2 inhibitors that block the active causes of MDR may provide a strategy for the treatment of colorectal cancer. In this study, we find that dorsomorphin (also known as compound C or BML-275) potently inhibits the transporter activity of ABCG2, thereby preserving the chemotherapeutic agents mitoxantrone and doxorubicin to antagonize MDR in ABCG2-overexpressing colorectal cancer cells. Additionally, dorsomorphin does not alter ABCG2 protein expression. The results of molecular docking studies show that dorsomorphin is bound stably to the ABCG2-binding pocket, suggesting that dorsomorphin is a potent ABCG2 inhibitor that attenuates ABCG2-mediated MDR in colorectal cancer.

KEYWORDS

dorsomorphin, chemosensitivity, ABCG2, multidrug resistance, colorectal cancer

1 Introduction

Cancer multidrug resistance (MDR) refers to the resistance of cancer cells to various anticancer agents that are unrelated to structure and function, which reduces the effects of chemotherapy and is not conducive to the survival of cancer patients (Fan et al., 2023). An important reason for the development of MDR is ABCG2 overexpression in the cancer cells, which can excrete the anticancer drugs against the concentration gradient (Li et al., 2016). As one of the ATP-binding cassette transporters, ABCG2 is a transmembrane protein on the cell membrane that can obtain energy to expel substrates out of the cell through ATP hydrolysis (Eckenstaler and Benndorf, 2020). ABCG2 directly supports many anticancer drugs, such as mitoxantrone (Sugimoto et al., 2003), doxorubicin (Stacy et al., 2013), irinotecan (Nielsen et al., 2017), imatinib (Noguchi et al., 2009), dasatinib (Eadie et al., 2014), and erlotinib (Shi

et al., 2007). Given the important role of ABCG2 in mediating MDR, effective ABCG2 inhibitors can help reverse MDR. Several research groups have discovered a series of ABCG2 inhibitors, such as AZ32 (Liu et al., 2021), AZ-628 (Wang J. Q. et al., 2020), febuxostat (Miyata et al., 2016), fumitremorgin C (Toyoda et al., 2019), GSK2606414 (Yu et al., 2023), KU55933 (Liu et al., 2022), MK-2206 (Gao et al., 2023), NVP-TAE684 (Wang J. et al., 2020), OTS964 (Yang et al., 2021), and VKIN-1 (Narayanan et al., 2021). However, there is no ABCG2 inhibitor that has been used successfully in clinical settings to reverse cancer MDR. Therefore, there is an urgent need to develop novel ABCG2 inhibitors.

In this study, we investigate the effects of dorsomorphin (also known as compound C or BML-275) on ABCG2 activity and ABCG2-mediated MDR in colorectal cancer. Colorectal cancer is one of the main types of fatal cancers (Ghasemian et al., 2023), and ABCG2 expression has been associated with tumor responses to irinotecan-based or FOLFOX therapy in metastatic colorectal cancer patients (Lin et al., 2013; Palshof et al., 2020). Our findings demonstrate that dorsomorphin is a potent ABCG2 inhibitor that attenuates ABCG2-mediated MDR in colorectal cancer.

2 Materials and methods

2.1 Reagents and cell culture

Dorsomorphin (#1219188-18-9), KU55933 (#587871-26-9), mitoxantrone (#70476-82-3), doxorubicin (#A603456-0025), cisplatin (#AA1A8019B), rhodamine 123 (#62669-70-9), and 3-(4,5-dimethylthiazol-yl)-2,5-diphenyl-tetrazolium bromide (MTT; #298-93-1) were procured from MREDA Technology Inc. (Beijing, China), TargetMol Chemicals Inc. (Shanghai, China), D&B Biotech Inc. (Shanghai, China), Sangon Biotech Inc. (Shanghai, China), Qilu Pharmaceutical Co. (Jinan, China), Sigma-Aldrich Trading Co. (Shanghai, China), and Yuanye Biotech Co. (Shanghai, China), respectively. Anti-ABCG2 antibody (#RLT0053) and anti-β-actin antibody (#SC-47778) were purchased from Ruiying Biotech (Wuxi, China) and Santa Cruz Biotech (Santa Cruz, California, United States), respectively. Human colorectal cancer cells S1-M1-80 vector with ABCG2 overexpression and S1-M1-80 sgABCG2 with ABCG2-knockout were established as reported previously (Liu et al., 2021) and cultured in Dulbecco's modified Eagle's medium (#C11995500BT) with 10% fetal bovine serum (#10270-106) from Thermo Fisher Scientific Inc. (Waltham, Massachusetts, United States) at 37°C in a humid atmosphere of 5% CO_2.

2.2 Cytotoxicity assay

The cells were cultured in 96-well plates at 7×10^3 cells/well and treated with the indicated agents for 72 h. After incubating with 500 mg/mL MTT for another 4 h and discarding the solution in the wells, approximately 50 μL of dimethylsulfoxide (DMSO) was added to each well. The absorbance was then detected at 570 nm with a BioTek Synergy H1 microplate reader from Agilent Technologies Inc. (Santa Clara, California, United States). The Bliss method was used to calculate the 50% inhibitive concentration (IC_{50}), as reported previously (Zhang et al., 2017).

2.3 Drug accumulation assay

The cells were cultured in 12-well plates at 5×10^4 cells/well and incubated with the indicated concentration of dorsomorphin or KU55933 for 1 h. After incubating with mitoxantrone, doxorubicin, or rhodamine 123 at a concentration of 10 μM for another 2 h, the images of the cells were acquired using the LSM900 confocal microscope from Carl Zeiss Inc. (Oberkohen, Germany). Next, the cells were collected and analyzed with a CytoFLEX flow cytometer from Beckman Coulter Inc. (Brea, California, United States), as reported previously (Liu et al., 2022).

2.4 Western blot

The cells were lysed with a lysis buffer (containing 1% NP-40, 0.5% sodium deoxycholate, 0.1% SDS, 10 ng/mL phenylmethanesulfonyl fluoride, 0.03% aprotinin, and 1 μM sodium orthovanadate) at 4°C for 30 min. After centrifuging for 10 min at 1.4×10^4 *g*, the protein supernatants were collected and separated using 10% SDS-PAGE gels and transferred to polyvinylidene difluoride membranes. After blocking with 5% bovine serum albumin, the membranes were incubated with the specified primary antibodies and the corresponding horseradish-peroxidase-conjugated secondary antibodies. The signals were then acquired and examined using a ChemiDoc XRS chemiluminescent gel imaging system from Analytik Jena AG (Thuringia, Germany).

2.5 Docking analysis

The human ABCG2 protein crystal structure was archived from the Protein Data Bank (PDB ID: 6vxi). The molecular dockings of dorsomorphin and ABCG2 were analyzed using AutoDock Vina, and the data were visualized using PyMOL.

2.6 Statistical analysis

The significant differences were determined using Student's t-test in GraphPad prism 8.3.0, and a p-value <0.05 was considered to be statistically significant.

3 Results

3.1 Dorsomorphin restores the chemosensitivity of colorectal cancer cells with ABCG2 overexpression

To investigate the effects of dorsomorphin (whose chemical structure is shown in Figure 1A) on colorectal cancer cells with ABCG2 overexpression, we first performed the MTT assay to assess the cytotoxicity of dorsomorphin in both the S1-M1-80 vector and S1-M1-80 sgABCG2 cells. Dorsomorphin at 1 μM did not show cytotoxicity in both types of cells (Figure 1B). Therefore, dorsomorphin was applied at concentrations of 0.3 μM and 1 μM to examine its sensitizing effects. As presented in Figures 1C, D and Table 1, compared with the known

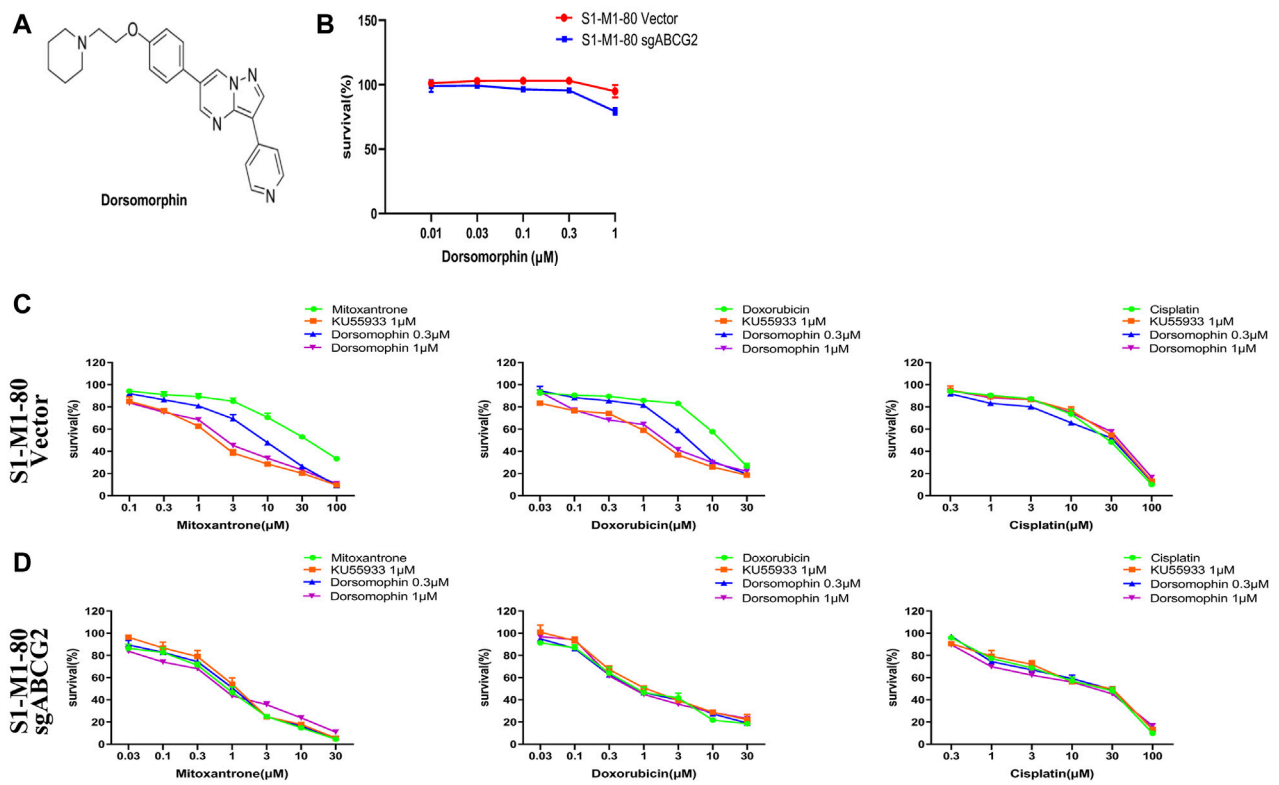

FIGURE 1
Dorsomorphin restores the chemosensitivity of colorectal cancer cells with ABCG2 overexpression. **(A)** Chemical structure of dorsomorphin. The cells were treated with the indicated agents for 72 h and examined via MTT assay. The representative cell survival curves are shown in **(B–D)**.

ABCG2 inhibitor KU55933, dorsomorphin relatively restores the chemosensitivity of the ABCG2 substrate mitoxantrone and doxorubicin in a dose-dependent manner only in the S1-M1-80 vector cells and not in the S1-M1-80 sgABCG2 cells. Both KU55933 and dorsomorphin are unable to restore the chemosensitivity of the non-ABCG2 substrate cisplatin in both types of cells. These results suggest that dorsomorphin can restore the chemosensitivity of colorectal cancer cells with ABCG2 overexpression.

3.2 Dorsomorphin increases the ABCG2 substrate levels in colorectal cancer cells with ABCG2 overexpression

To further explore whether dorsomorphin could directly suppress the transporter activity of ABCG2, we conducted drug accumulation experiments on the ABCG2 substrates mitoxantrone, doxorubicin, and rhodamine 123 with both the S1-M1-80 vector and S1-M1-80 sgABCG2 cells. As presented in Figure 2A–C, the levels of mitoxantrone, doxorubicin, and rhodamine 123 in the S1-M1-80 sgABCG2 cells are higher than those in the S1-M1-80 vector cells. Moreover, compared with KU55933, dorsomorphin relatively increases the levels of mitoxantrone, doxorubicin, and rhodamine 123 in a dose-dependent manner only in the S1-M1-80 vector cells and not in the S1-M1-80 sgABCG2 cells. These data indicate that dorsomorphin can increase the ABCG2 substrate levels in colorectal cancer cells with ABCG2 overexpression.

3.3 Dorsomorphin does not alter the protein level of ABCG2 or the mode of binding with ABCG2

To test the effects of dorsomorphin on the protein level of ABCG2, we treated the S1-M1-80 vector cells with 1 μM dorsomorphin for 24, 48, and 72 h. The results of Western blotting show that dorsomorphin has no effect on the protein level of ABCG2 in the S1-M1-80 vector cells (Figure 3A). Next, we carried out a structure-based docking analysis to explore the binding of dorsomorphin with ABCG2. As shown in Figures 3B, C, dorsomorphin is located in the ABCG2-binding pocket, and the hydrophobic amino acid sites, such as Val-401, Asn-436, Phe-439, Ile-543, and Val-546, on ABCG2 engage in hydrophobic interactions to stabilize the binding conformation of dorsomorphin. Dorsomorphin is also observed to form intermolecular hydrogen bonds with Asn-436 of TM2 on ABCG2 and π-π bonds with Ph-439 of TM2 on ABCG2 to further stabilize its binding conformation.

4 Discussion

Dorsomorphin, initially named as compound C, was earlier identified as an AMP-activated protein kinase (AMPK; Ki = 109 nM) inhibitor but did not obviously suppress the activities of structurally related kinases, including JAK3, PKA, PKCθ, SYK, and ZAPK (Zhou et al., 2001). Dorsomorphin was also observed to inhibit

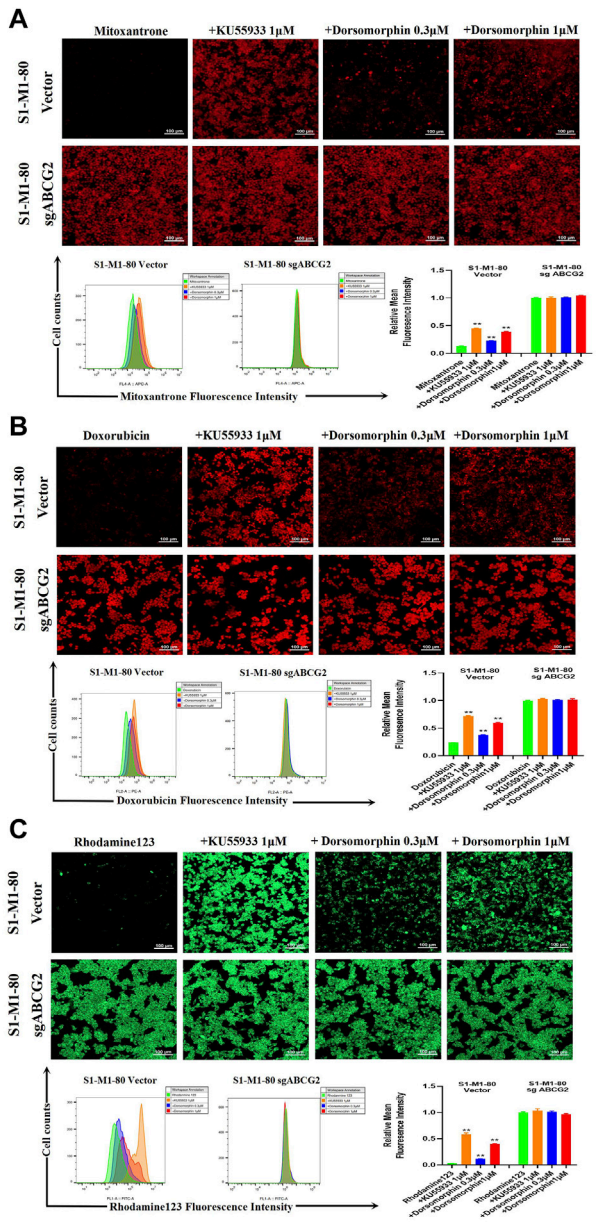

FIGURE 2
Dorsomorphin increases the ABCG2 substrate levels in colorectal cancer cells with ABCG2 overexpression. The cells were incubated with 10 μM **(A)** mitoxantrone, **(B)** doxorubicin, and **(C)** rhodamine 123 for 2 h after preincubation with dorsomorphin or KU55933 for 1 h and imaged with a confocal microscope, followed by quantification with a flow cytometer. $^{**}p < 0.01$ compared with the corresponding group.

the bone morphogenetic protein (BMP) type I receptors activin receptor-like kinase (ALK) 2, ALK3, and ALK6, thereby suppressing BMP-induced SMAD1/5/8 phosphorylation and transcription of the target genes in zebrafish (Yu et al., 2008). This compound was named dorsomorphin owing to its ability to induce dorsoventral patterning defects that usually occur in BMP-pathway-mutant zebrafish embryos (Yu et al., 2008). In a profiling study of dorsomorphin against 70 human kinases, dorsomorphin at 1 μM suppressed the activities of 10 out of 70 kinases more powerfully than it suppressed 73% of the AMPK activity, including (from the strongest to weakest) MELK1, PHK,

TABLE 1 Summary of the IC_{50} values. The fold-reversal value was computed by dividing the IC_{50} of each drug in the S1-M1-80 vector or S1-M1-80 sgABCG2 cells in the absence and presence of inhibitors. $^{*}p < 0.05$ and $^{**}p < 0.01$ compared with the corresponding group.

Compound	IC_{50} (μM) ± SD (fold reversal)	
	S1-M1-80 vector	S1-M1-80 sgABCG2
Mitoxantrone	31.407 ± 2.119 (1.00)	0.911 ± 0.087 (34.47)
+KU55933 1 μM	2.012 ± 0.067 (15.61)**	1.106 ± 0.113 (30.91)
+Dorsomorphin 0.3 μM	7.180 ± 0.778 (4.37)**	0.849 ± 0.116 (37.01)
+Dorsomorphin 1 μM	2.870 ± 0.243 (10.94)**	0.882 ± 0.177 (35.60)
Doxorubicin	11.920 ± 0.605 (1.00)	0.776 ± 0.128 (15.37)
+KU55933 1 μM	1.562 ± 0.069 (7.63)**	0.919 ± 0.084 (12.97)
+Dorsomorphin 0.3 μM	4.783 ± 0.352 (2.49)*	0.749 ± 0.098 (15.91)
+Dorsomorphin 1 μM	2.063 ± 0.194 (5.78)**	0.667 ± 0.049 (17.87)
Cisplatin	28.933 ± 0.472 (1.00)	27.830 ± 1.682 (1.04)
+KU55933 1 μM	28.813 ± 1.259 (1.00)	28.000 ± 0.616 (1.03)
+Dorsomorphin 0.3 μM	28.093 ± 1.715 (1.03)	25.820 ± 2.586 (1.12)
+Dorsomorphin 1 μM	27.797 ± 4.721 (1.04)	23.943 ± 0.777 (1.21)

DYRK3, ERK8, DYRK1A, MNK1, Lck, DYRK2, Src, and HIPK2 (Bain et al., 2007). In another profiling study of dorsomorphin against 123 human kinases, dorsomorphin at 1 μM suppressed the activities of 31 out of 123 kinases more powerfully than it suppressed 50% of the AMPK activity, including (from the strongest to weakest) VEGFR, RIPK2, ERK8, GCK, CLK2, DYRK1A, PHK, ABL, CAMKKβ, CK1, NUAK1, MELK, PRK2, YES1, Lck, EPHB2, IRAK4, TrkA, HIPK2, MINK1, IRR, EPHB4, Src, EPHA2, MLK3, FGFR1, DYRK3, EPHB3, CK2, ALK3, and MARK3 (Vogt et al., 2011). In the present study, we found that dorsomorphin at 0.3 μM can inhibit the ABCG2 transporter activity, thereby preserving the chemotherapeutic agents mitoxantrone and doxorubicin to antagonize MDR in ABCG2-overexpressing colorectal cancer cells. Additionally, dorsomorphin does not alter ABCG2 protein expression. The results of molecular docking show that dorsomorphin is bound stably to the ABCG2-binding pockets; therefore, dorsomorphin is a multitarget agent.

The anticancer effects of dorsomorphin have been explored extensively. Dorsomorphin causes cell-cycle arrest at the G2/M phase and apoptosis in glioma cells through AMPK-dependent and -independent mechanisms (Vucicevic et al., 2009). Another study has shown that the dorsomorphin AMPK-independent mode induces G2/M cell-cycle arrest, autophagy, and necroptosis through activation of the calpain/cathepsin pathway and inhibition of AKT/mTORC1/C2 in glioma cells (Liu et al., 2014). Additionally, the dorsomorphin AMPK-independent mode induces apoptosis through increased ceramide production in breast cancer cells (Jin et al., 2009). Dorsomorphin also causes G2/M cell-cycle arrest and growth inhibition by inducing autophagy and apoptosis in human colorectal cancer cells (Yang et al., 2012). Moreover, dorsomorphin inhibits cell

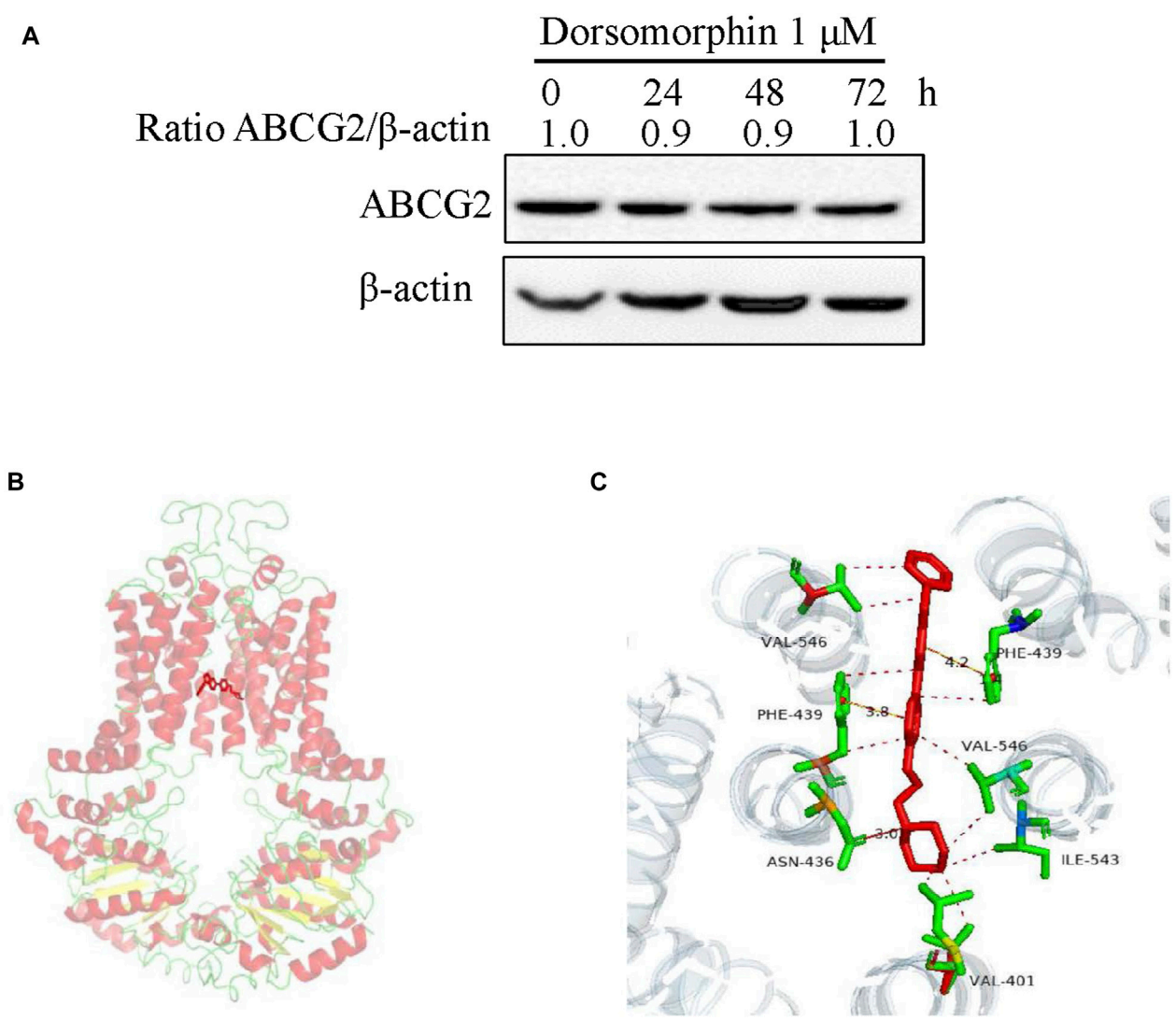

FIGURE 3
Dorsomorphin does not alter the protein level of ABCG2 or mode of binding with ABCG2. **(A)** ABCG2 expression levels in S1-M1-80 vector cells treated with 1 μM dorsomorphin for the indicated time points were measured via Western blot assay. **(B)** Optimal docked positions of dorsomorphin (red lines) within the binding pocket of human ABCG2 generated using AutoDock Vina. **(C)** Magnification of the highlighted area showing GSK2606414 interactions with the residues Val-401, Asn-436, Phe-439, Ile-543, and Val-546 of ABCG2.

growth and migration by interfering with the Akt/mTOR/Wnt pathways in colon cancer cells (Ghanaatgar-Kasbi et al., 2019). The dorsomorphin AMPK-independent mode enhances TRAIL-induced apoptosis through reactive-oxygen-species-mediated decreases of c-FLIPL and Mcl-1 in human renal cancer cells (Jang et al., 2010). Dorsomorphin also AMPK-independently causes cancer cell apoptosis and enhances the sensitivity of cancer cells to both HSP90 and proteasome inhibitors through downregulation of the nuclear heat shock factor 1 (Li et al., 2019). Dorsomorphin sensitizes multiple acute leukemia cells to BH3 mimetic-induced cell death by decreasing the phosphorylation of BAD at Ser75 and Ser99 to enhance BAD translocation to the mitochondria and inhibit $BCLX_L$ (Jia et al., 2024). In the present work, our data show that dorsomorphin can restore the sensitivity of mitoxantrone and doxorubicin in colorectal cancer cells with ABCG2 overexpression *in vitro*. However, the effects of dorsomorphin *in vivo* need to be explored in the future. In conclusion, dorsomorphin is a potent ABCG2 inhibitor that can attenuate ABCG2-mediated MDR in colorectal cancer.

Data availability statement

The original contributions presented in the study are included in the article/supplementary material; further inquiries can be directed to the corresponding author.

Ethics statement

Ethical approval was not required for the studies on humans in accordance with the local legislation and institutional requirements because only commercially available established cell lines were used.

Author contributions

X-PL: investigation, methodology, project administration, writing–original draft, and writing–review and editing. L-QC: investigation, project administration, validation, writing–original draft, and writing–review and editing. Z-ZY: methodology, project administration, software, writing–original draft, and writing–review and editing. KH: formal analysis, resources, and writing–review and editing. P-BD: investigation, validation, and writing–review and editing. J-SL: data curation, formal analysis, and writing–review and editing. Y-YS: methodology, validation, and writing–review and editing. Z-BS: formal analysis, software, and writing–review and editing. Z-MY: funding acquisition, resources, and writing–review and editing. ZS: conceptualization, funding acquisition, resources, supervision, writing–original draft, and writing–review and editing.

Funding

The author(s) declare that financial support was received for the research, authorship, and/or publication of this article.

Acknowledgments

The authors thank the financial support from the National Natural Science Foundation of China (No. 82272996 to ZS), the Science and Technology Program of Guangzhou (No. 202206010081 to ZS), and the Foundation of Guangzhou Municipal Science and Technology Bureau (No. 202002020088 to Z-MY).

Conflict of interest

The authors declare that the research was conducted in the absence of any commercial or financial relationships that could be construed as a potential conflict of interest.

Publisher's note

All claims expressed in this article are solely those of the authors and do not necessarily represent those of their affiliated organizations, or those of the publisher, the editors, and the reviewers. Any product that may be evaluated in this article, or claim that may be made by its manufacturer, is not guaranteed or endorsed by the publisher.

Supplementary material

The Supplementary Material for this article can be found online at: https://www.frontiersin.org/articles/10.3389/fphar.2024.1393693/full#supplementary-material

References

Bain, J., Plater, L., Elliott, M., Shpiro, N., Hastie, C. J., McLauchlan, H., et al. (2007). The selectivity of protein kinase inhibitors: a further update. *Biochem. J.* 408 (3), 297–315. doi:10.1042/bj20070797

Eadie, L. N., Hughes, T. P., and White, D. L. (2014). Interaction of the efflux transporters ABCB1 and ABCG2 with imatinib, nilotinib, and dasatinib. *Clin. Pharmacol. Ther.* 95 (3), 294–306. doi:10.1038/clpt.2013.208

Eckenstaler, R., and Benndorf, R. A. (2020). 3D structure of the transporter ABCG2-What's new? *Br. J. Pharmacol.* 177 (7), 1485–1496. doi:10.1111/bph.14991

Fan, J., To, K. K. W., Chen, Z. S., and Fu, L. (2023). ABC transporters affects tumor immune microenvironment to regulate cancer immunotherapy and multidrug resistance. *Drug Resist Updat* 66, 100905. doi:10.1016/j.drup.2022.100905

Gao, H. L., Cui, Q., Wang, J. Q., Ashby, C. R., Jr., Chen, Y., Shen, Z. X., et al. (2023). The AKT inhibitor, MK-2206, attenuates ABCG2-mediated drug resistance in lung and colon cancer cells. *Front. Pharmacol.* 14, 1235285. doi:10.3389/fphar.2023.1235285

Ghanaatgar-Kasbi, S., Amerizadeh, F., Rahmani, F., Hassanian, S. M., Khazaei, M., Ferns, G. A., et al. (2019). AMP-kinase inhibitor dorsomorphin reduces the proliferation and migration behavior of colorectal cancer cells by targeting the AKT/mTOR pathway. *IUBMB Life* 71 (12), 1929–1936. doi:10.1002/iub.2136

Ghasemian, A., Omear, H. A., Mansoori, Y., Mansouri, P., Deng, X., Darbeheshti, F., et al. (2023). Long non-coding RNAs and JAK/STAT signaling pathway regulation in colorectal cancer development. *Front. Genet.* 14, 1297093. doi:10.3389/fgene.2023.1297093

Jang, J. H., Lee, T. J., Yang, E. S., Min do, S., Kim, Y. H., Kim, S. H., et al. (2010). Compound C sensitizes Caki renal cancer cells to TRAIL-induced apoptosis through reactive oxygen species-mediated down-regulation of c-FLIPL and Mcl-1. *Exp. Cell Res.* 316 (13), 2194–2203. doi:10.1016/j.yexcr.2010.04.028

Jia, J., Ji, W., Saliba, A. N., Csizmar, C. M., Ye, K., Hu, L., et al. (2024). AMPK inhibition sensitizes acute leukemia cells to BH3 mimetic-induced cell death. *Cell Death Differ.* 31, 405–416. doi:10.1038/s41418-024-01283-9

Jin, J., Mullen, T. D., Hou, Q., Bielawski, J., Bielawska, A., Zhang, X., et al. (2009). AMPK inhibitor Compound C stimulates ceramide production and promotes Bax redistribution and apoptosis in MCF7 breast carcinoma cells. *J. Lipid Res.* 50 (12), 2389–2397. doi:10.1194/jlr.M900119-JLR200

Li, N., Wang, T., Li, Z., Ye, X., Deng, B., Zhuo, S., et al. (2019). Dorsomorphin induces cancer cell apoptosis and sensitizes cancer cells to HSP90 and proteasome inhibitors by reducing nuclear heat shock factor 1 levels. *Cancer Biol. Med.* 16 (2), 220–233. doi:10.20892/j.issn.2095-3941.2018.0235

Li, W., Zhang, H., Assaraf, Y. G., Zhao, K., Xu, X., Xie, J., et al. (2016). Overcoming ABC transporter-mediated multidrug resistance: molecular mechanisms and novel therapeutic drug strategies. *Drug Resist Updat* 27, 14–29. doi:10.1016/j.drup.2016.05.001

Lin, P. C., Lin, H. H., Lin, J. K., Lin, C. C., Yang, S. H., Li, A. F., et al. (2013). Expression of ABCG2 associated with tumor response in metastatic colorectal cancer patients receiving first-line FOLFOX therapy--preliminary evidence. *Int. J. Biol. Markers* 28 (2), 182–186. doi:10.5301/jbm.5000004

Liu, K., Chen, Y., Shi, X. B., Xing, Z. H., He, Z. J., Wang, S. T., et al. (2022). Inhibiting the activity of ABCG2 by KU55933 in colorectal cancer. *Recent Pat. Anticancer Drug Discov.* 17 (4), 387–395. doi:10.2174/1574892817666220112100036

Liu, K., Li, Y. C., Chen, Y., Shi, X. B., Xing, Z. H., He, Z. J., et al. (2021). AZ32 reverses ABCG2-mediated multidrug resistance in colorectal cancer. *Front. Oncol.* 11, 680663. doi:10.3389/fonc.2021.680663

Liu, X., Chhipa, R. R., Nakano, I., and Dasgupta, B. (2014). The AMPK inhibitor compound C is a potent AMPK-independent antiglioma agent. *Mol. Cancer Ther.* 13 (3), 596–605. doi:10.1158/1535-7163.Mct-13-0579

Miyata, H., Takada, T., Toyoda, Y., Matsuo, H., Ichida, K., and Suzuki, H. (2016). Identification of febuxostat as a new strong ABCG2 inhibitor: potential applications and risks in clinical situations. *Front. Pharmacol.* 7, 518. doi:10.3389/fphar.2016.00518

Narayanan, S., Fan, Y. F., Gujarati, N. A., Teng, Q. X., Wang, J. Q., Cai, C. Y., et al. (2021). VKNG-1 antagonizes ABCG2-mediated multidrug resistance via p-AKT and bcl-2 pathway in colon cancer: *in vitro* and *in vivo* study. *Cancers (Basel)* 13 (18), 4675. doi:10.3390/cancers13184675

Nielsen, D. L., Palshof, J. A., Brunner, N., Stenvang, J., and Viuff, B. M. (2017). Implications of ABCG2 expression on irinotecan treatment of colorectal cancer patients: a review. *Int. J. Mol. Sci.* 18 (9), 1926. doi:10.3390/ijms18091926

Noguchi, K., Katayama, K., Mitsuhashi, J., and Sugimoto, Y. (2009). Functions of the breast cancer resistance protein (BCRP/ABCG2) in chemotherapy. *Adv. Drug Deliv. Rev.* 61 (1), 26–33. doi:10.1016/j.addr.2008.07.003

Palshof, J. A., Cederbye, C. N., Høgdall, E. V. S., Poulsen, T. S., Linnemann, D., Nygaard, S. B., et al. (2020). ABCG2 protein levels and association to response to first-line irinotecan-based therapy for patients with metastatic colorectal cancer. *Int. J. Mol. Sci.* 21 (14), 5027. doi:10.3390/ijms21145027

Shi, Z., Peng, X. X., Kim, I. W., Shukla, S., Si, Q. S., Robey, R. W., et al. (2007). Erlotinib (Tarceva, OSI-774) antagonizes ATP-binding cassette subfamily B member 1 and ATP-binding cassette subfamily G member 2-mediated drug resistance. *Cancer Res.* 67 (22), 11012–11020. doi:10.1158/0008-5472.Can-07-2686

Stacy, A. E., Jansson, P. J., and Richardson, D. R. (2013). Molecular pharmacology of ABCG2 and its role in chemoresistance. *Mol. Pharmacol.* 84 (5), 655–669. doi:10.1124/mol.113.088609

Sugimoto, Y., Tsukahara, S., Imai, Y., Sugimoto, Y., Ueda, K., and Tsuruo, T. (2003). Reversal of breast cancer resistance protein-mediated drug resistance by estrogen antagonists and agonists. *Mol. Cancer Ther.* 2 (1), 105–112.

Toyoda, Y., Takada, T., and Suzuki, H. (2019). Inhibitors of human ABCG2: from technical background to recent updates with clinical implications. *Front. Pharmacol.* 10, 208. doi:10.3389/fphar.2019.00208

Vogt, J., Traynor, R., and Sapkota, G. P. (2011). The specificities of small molecule inhibitors of the TGFß and BMP pathways. *Cell Signal* 23 (11), 1831–1842. doi:10.1016/j.cellsig.2011.06.019

Vucicevic, L., Misirkic, M., Janjetovic, K., Harhaji-Trajkovic, L., Prica, M., Stevanovic, D., et al. (2009). AMP-activated protein kinase-dependent and -independent mechanisms underlying *in vitro* antiglioma action of compound C. *Biochem. Pharmacol.* 77 (11), 1684–1693. doi:10.1016/j.bcp.2009.03.005

Wang, J., Wang, J. Q., Cai, C. Y., Cui, Q., Yang, Y., Wu, Z. X., et al. (2020a). Reversal effect of ALK inhibitor NVP-TAE684 on ABCG2-overexpressing cancer cells. *Front. Oncol.* 10, 228. doi:10.3389/fonc.2020.00228

Wang, J. Q., Teng, Q. X., Lei, Z. N., Ji, N., Cui, Q., Fu, H., et al. (2020b). Reversal of cancer multidrug resistance (MDR) mediated by ATP-binding cassette transporter G2 (ABCG2) by AZ-628, a RAF kinase inhibitor. *Front. Cell Dev. Biol.* 8, 601400. doi:10.3389/fcell.2020.601400

Yang, W. L., Perillo, W., Liou, D., Marambaud, P., and Wang, P. (2012). AMPK inhibitor compound C suppresses cell proliferation by induction of apoptosis and autophagy in human colorectal cancer cells. *J. Surg. Oncol.* 106 (6), 680–688. doi:10.1002/jso.23184

Yang, Y., Wu, Z. X., Wang, J. Q., Teng, Q. X., Lei, Z. N., Lusvarghi, S., et al. (2021). OTS964, a TOPK inhibitor, is susceptible to ABCG2-mediated drug resistance. *Front. Pharmacol.* 12, 620874. doi:10.3389/fphar.2021.620874

Yu, P. B., Hong, C. C., Sachidanandan, C., Babitt, J. L., Deng, D. Y., Hoyng, S. A., et al. (2008). Dorsomorphin inhibits BMP signals required for embryogenesis and iron metabolism. *Nat. Chem. Biol.* 4 (1), 33–41. doi:10.1038/nchembio.2007.54

Yu, Z. Z., Xu, B. Q., Wang, Y. Y., Zhang, P. W., Shu, Y. B., and Shi, Z. (2023). GSK2606414 sensitizes ABCG2-overexpressing multidrug-resistant colorectal cancer cells to chemotherapeutic drugs. *Biomedicines* 11 (11), 3103. doi:10.3390/biomedicines11113103

Zhang, W. J., Li, Y., Wei, M. N., Chen, Y., Qiu, J. G., Jiang, Q. W., et al. (2017). Synergistic antitumor activity of regorafenib and lapatinib in preclinical models of human colorectal cancer. *Cancer Lett.* 386, 100–109. doi:10.1016/j.canlet.2016.11.011

Zhou, G., Myers, R., Li, Y., Chen, Y., Shen, X., Fenyk-Melody, J., et al. (2001). Role of AMP-activated protein kinase in mechanism of metformin action. *J. Clin. Invest.* 108 (8), 1167–1174. doi:10.1172/jci13505

frontiers | Frontiers in Pharmacology

TYPE Original Research
PUBLISHED 10 June 2024
DOI 10.3389/fphar.2024.1413699

Check for updates

OPEN ACCESS

EDITED BY
Hailin Tang,
Sun Yat-sen University Cancer Center (SYSUCC), China

REVIEWED BY
Guanmin Jiang,
The Fifth Affiliated Hospital of Sun Yat-sen University, China
Xiaofang Guo,
University of South Florida, United States

*CORRESPONDENCE
Lemeng Zhang,
zhanglemeng@hnca.org.cn

RECEIVED 07 April 2024
ACCEPTED 17 May 2024
PUBLISHED 10 June 2024

CITATION
Su J, Tan S, Li Y, Chen X, Liu J, Luo Y, Pan C and Zhang L (2024), Clinical significance and biological function of interferon regulatory factor 1 in non-small cell lung cancer. *Front. Pharmacol.* 15:1413699. doi: 10.3389/fphar.2024.1413699

COPYRIGHT
© 2024 Su, Tan, Li, Chen, Liu, Luo, Pan and Zhang. This is an open-access article distributed under the terms of the Creative Commons Attribution License (CC BY). The use, distribution or reproduction in other forums is permitted, provided the original author(s) and the copyright owner(s) are credited and that the original publication in this journal is cited, in accordance with accepted academic practice. No use, distribution or reproduction is permitted which does not comply with these terms.

Clinical significance and biological function of interferon regulatory factor 1 in non-small cell lung cancer

Jialin Su[1,2], Shuhua Tan[1], Yuning Li[1,2], Xinglong Chen[1,2], Jiasi Liu[2], Yongzhong Luo[1], Changqie Pan[1] and Lemeng Zhang[1]*

[1]Thoracic Medicine Department, Hunan Cancer Hospital, Changsha, Hunan Province, China, [2]School of Life and Health Sciences, Hunan University of Science and Technology, Xiangtan, Hunan Province, China

The clinical application and biological function of interferon regulatory factor 1 (IRF1) in non-small cell lung cancer (NSCLC) patients undergoing chemoimmunotherapy remain elusive. The aim of this study was to investigate the predictive and prognostic significance of IRF1 in NSCLC patients. We employed the cBioPortal database to predict frequency changes in IRF1 and explore its target genes. Bioinformatic methods were utilized to analyze the relationship between IRF1 and immune regulatory factors. Retrospective analysis of clinical samples was conducted to assess the predictive and prognostic value of IRF1 in chemoimmunotherapy. Additionally, A549 cells with varying IRF1 expression levels were constructed to investigate its effects on NSCLC cells, while animal experiments were performed to study the role of IRF1 *in vivo*. Our findings revealed that the primary mutation of IRF1 is deep deletion and it exhibits a close association with immune regulatory factors. KRAS and TP53 are among the target genes of IRF1, with interferon and IL-2 being the predominantly affected pathways. Clinically, IRF1 levels significantly correlate with the efficacy of chemoimmunotherapy. Patients with high IRF1 levels exhibited a median progression-free survival (mPFS) of 9.5 months, whereas those with low IRF1 levels had a shorter mPFS of 5.8 months. IRF1 levels positively correlate with PD-L1 distribution and circulating IL-2 levels. IL-2 enhances the biological function of IRF1 and recapitulates its role *in vivo* in the knockdown group. Therefore, IRF1 may possess predictive and prognostic value for chemoimmunotherapy in NSCLC patients through the regulation of the IL-2 inflammatory pathway.

KEYWORDS

interferon regulatory Factor-1, non-small cell lung cancer, interleukin-2, chemoimmunotherapy, inflammatory pathway

Introduction

Lung cancer remains the leading cause of cancer-related deaths worldwide, with NSCLC accounting for 80%–85% of these cases. Recently, the combination of immune checkpoint inhibitors (ICIs) and chemotherapy has received a lot of attention, and this combination is recommended as an initial treatment option (Lantuejoul et al., 2020). However, the discovery of prognostic and predictive biomarkers for chemoimmunotherapy holds significant clinical importance. IRF1 is the earliest interferon regulatory factor, and its expression regulates the malignant biological behavior of tumor cells (Kirchhoff et al., 1993), IRF1 inactivation increases the risk of tumorigenesis (Nozawa et al., 1999). Previously, we report

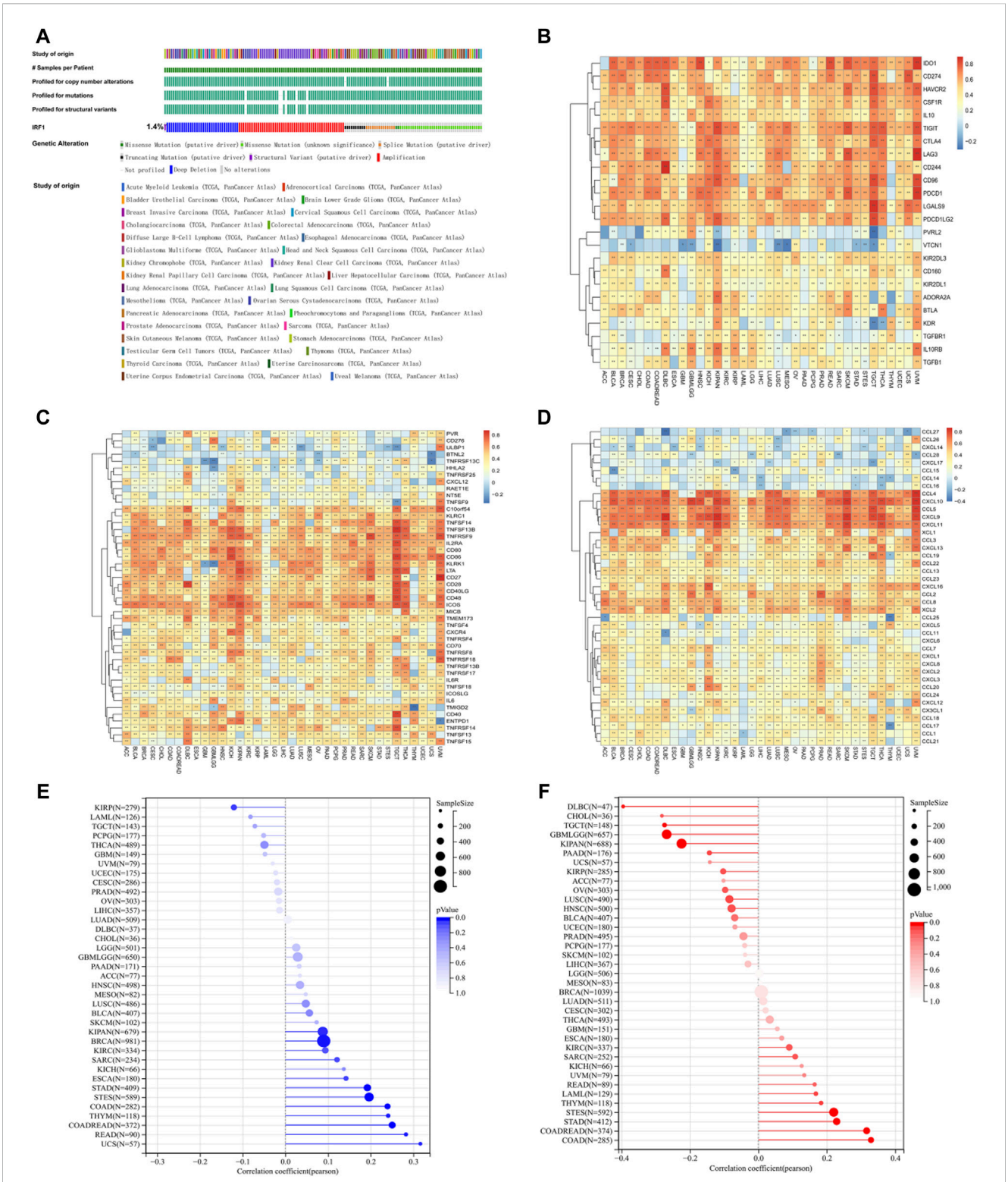

FIGURE 1
The effects of IRF1 gene in pan-cancers. **(A)**: IRF1 mutation in pan-cancer samples; The various colors in the first row of the bar graph represent various types of cancer, while the other bar graphs below represent various types of mutations. **(B)**: The correlation between IRF1 and immunosuppressive gene set in pan-cancer. The horizontal axis represents various types of cancer, the vertical axis represents the set of immunosuppressive genes, color represents the correlation coefficient, red represents a positive correlation, blue represents a negative correlation, and the darker the color represents the greater correlation; **(C)**: The correlation between IRF1 and immune stimulating gene set in pan-cancer; The horizontal axis represents various types of cancer, the vertical axis represents the set of Immune Stimulation, color represents the correlation coefficient, red represents a positive correlation, blue represents a negative correlation, and the darker the color represents the greater correlation; **(D)**: The correlation between IRF1 and chemokine gene set in pan-cancer; The horizontal axis represents various types of cancer, the vertical axis represents the set of chemokine, color represents the correlation coefficient, red represents a positive correlation, blue represents a negative correlation, and the darker the color represents the

(*Continued*)

FIGURE 1 (Continued)
greater correlation; **(E)**: Correlation between IRF1 and TMB; **(F)**: Correlation graph between IRF1 and MSI; The horizontal axis represents the correlation coefficient, the vertical axis represents the set of various cancer genes, and the color represents the *p*-value, the darker color represents the more significant correlation.

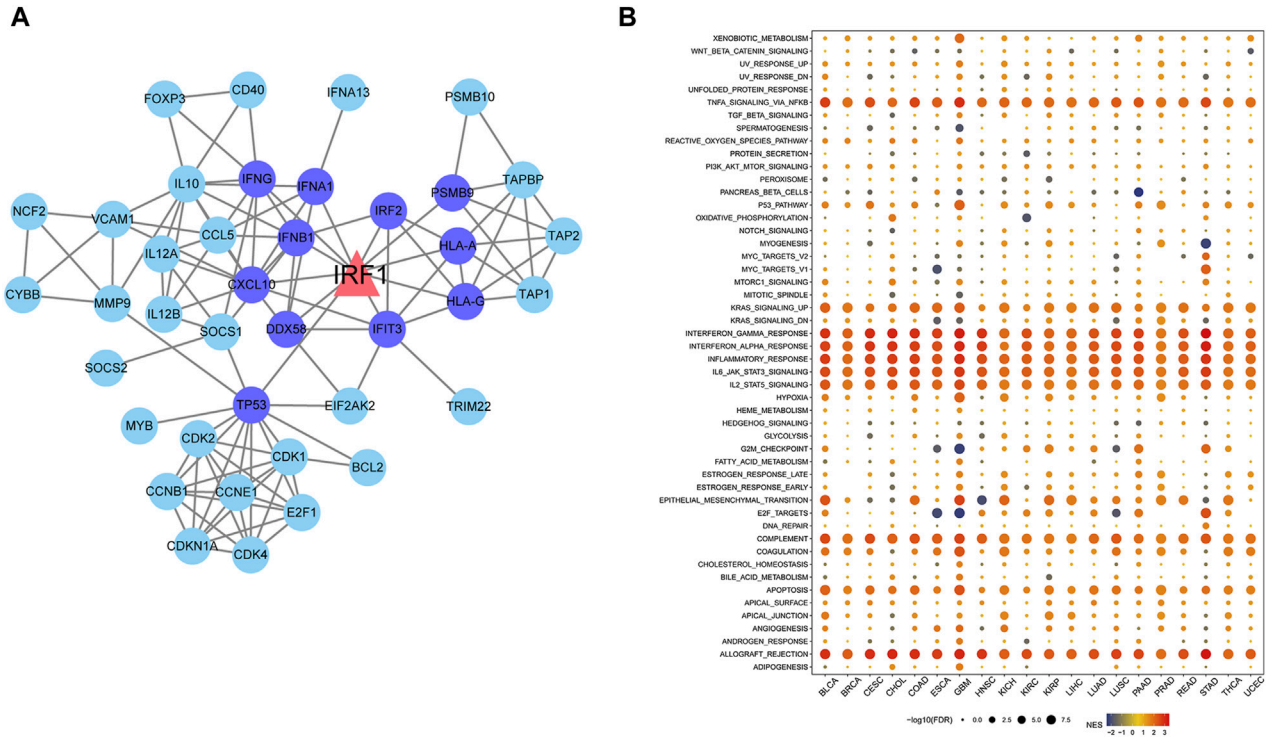

FIGURE 2
Network diagram of IRF1 target genes and pathways enriched by IRF1 based on GSEA. **(A)**: The triangle in the figure represents the target gene of IRF1, the circles are all target genes of IRF1, the dark blue represents the target gene directly related to IRF1. **(B)**: The horizontal axis represents various types of cancer, the vertical axis represents various pathways, the size of the point represents significance, the larger the point represents the more significant, and the color represents the standardized enrichment score.

that IRF1 increases chemotherapy sensitivity in NSCLC by modulating apoptosis and autophagy (Zhang et al., 2022). However, the clinical significance of IRF1 in NSCLC patients who receiving both chemotherapy and immunotherapy remains largely unknown.

IRF1 was associated with pro-inflammatory cytokines release, lymphocyte growth and differentiation, innate and acquired immunity, which might be closely related to immunotherapy efficacy (Miyamoto et al., 1988; Feng et al., 2021). Since IRF1 was closely related to efficacy of both immunotherapy and chemotherapy, its clinical significance in chemoimmunotherapy is worth studying. Therefore, we first investigated the clinical significance and biological functional role of IRF1 by bio-informatics methods. Then we analyzed the efficacy of chemoimmunotherapy based on different IRF1 levels by clinical samples retrospectively. The function of IRF1 in proliferation, migration, and invasion were analyzed *in vitro*. The effect of IRF1 on tumorigenic ability of tumor cells was analyzed *in vivo*. A comprehensive, in-depth understanding of the clinical application and biological function of IRF1 in NSCLC chemoimmunotherapy, is of great theoretical and practical significance for NSCLC treatment.

Materials and methods

Frequency changes in the IRF1 gene

The mutation status of IRF1 was analyzed using the cBioPortal database (http://www.cbioportal.org/) (Gao et al., 2013). The name of the IRF1 gene was used for the mutation-related analysis and visualization.

Genomics enrichment analysis (GSEA) of IRF1

Samples were grouped based on the expression levels of the IRF1 gene, and differential expression analysis between groups was performed using the Limma package in R software (Version 3.10.3, http://www.bioconductor.org/packages/2.9/bioc/html/limma.html) (Kerr, 2003). To analyze the pathways enriched by IRF1, GSEA analysis was performed using the R package clusterProfiler with MSigDB v7.2 (http://software.broadinstitute.org/gsea/msigdb/

10.3389/fphar.2024.1413699

TABLE 1 Clinical characteristics of enrolled NSCLC patients.

Factors	IRF1 low (n = 96)	IRF1 high (n = 72)	*p*-Value
Age, n (%)			0.891
<60 years	40 (41.7)	31 (43.1)	
≥60 years	56 (58.3)	41 (56.9)	
Gender, n (%)			0.954
Male	68 (70.8)	52 (72.2)	
Female	28 (29.2)	20 (27.8)	
Pathological type, n (%)			0.623
LUSC	55 (57.3)	45 (62.5)	
LUAD	38 (39.6)	24 (33.3)	
others	3 (3.1)	3 (4.2)	
PD-L1 (%), n (%)			0.024*
<1	34 (35.4)	12 (16.7)	
1–49	50 (52.1)	43 (59.7)	
>50	12 (12.5)	17 (23.6)	
Smoking status, n (%)			0.908
≤400	42 (43.8)	30 (41.7)	
>400	54 (56.2)	42 (58.3)	
PS score, n (%)			0.637
0	8 (8.3)	5 (6.9)	
1	86 (89.6)	66 (91.7)	
2	2 (2.1)	1 (1.4)	
T stage, n (%)			0.644
1	5 (5.2)	6 (8.3)	
2	11 (11.5)	10 (13.8)	
3	48 (50.0)	34 (47.2)	
4	32 (33.3)	28 (38.9)	
N stage, n (%)			0.081
0	4 (4.2)	1 (1.4)	
1	22 (22.9)	10 (13.9)	
2	38 (39.6)	33 (45.8)	
3	32 (33.3)	28 (38.9)	
M stage, n (%)			0.389
0	10 (10.4)	9 (12.5)	
1	86 (89.6)	63 (87.5)	
TNM stage, n (%)			0.389
IIIB/IIIC	10 (10.4)	9 (12.5)	
IV	86 (89.6)	63 (87.5)	
Metastasis site, n (%)			0.187
≤3	43 (44.8)	35 (48.6)	
>3	53 (55.2)	37 (51.4)	
IL-2 median (pg/mL), n (%)			0.014*
≤7.15	55 (57.3)	25 (34.7)	
>7.15	41 (42.7)	47 (65.3)	
IL-6 median (pg/mL), n (%)			0.131
≤62.59	54 (56.3)	32 (44.4)	
>62.59	42 (43.8)	40 (55.6)	
TNFα median (pg/mL), n (%)			0.212
≤74.01	52 (54.2)	32 (44.4)	
>74.01	44 (45.8)	40 (55.6)	

(Continued on following page)

TABLE 1 (*Continued*) Clinical characteristics of enrolled NSCLC patients.

Factors	IRF1 low (n = 96)	IRF1 high (n = 72)	*p*-Value
Interferon γ median (ng/mL), n (%)			0.533
≤0.18	50 (52.1)	34 (47.2)	
>0.18	46 (47.9)	38 (52.8)	
CD3 cell percentage, n (%)			0.891
≤66.81	37 (38.5)	27 (37.5)	
>66.81	59 (61.5)	45 (62.5)	
CD4 cell percentage, n (%)			0.727
≤35.66	18 (18.8)	12 (16.7)	
>35.66	78 (81.3)	60 (83.3)	
CD8 cell percentage, n (%)			0.588
≤23.73	29 (30.2)	19 (26.4)	
>23.73	67 (69.8)	53 (73.6)	
B cell percentage, n (%)			0.527
≤8.43	58 (60.4)	40 (55.6)	
>8.43	38 (39.6)	32 (44.4)	
NK cell percentage, n (%)			0.752
≤21.52	13 (13.5)	11 (15.3)	
>21.52	83 (86.5)	61 (84.7)	
Chemoimmunotherapy Efficacy, n (%)			0.017*
CR + PR	43 (44.8)	49 (68.1)	
SD + PD	53 (55.2)	23 (31.9)	

*p-value <0.05 was considered as a significant difference.

index.jsp) (Shannon et al., 2003) symbols. GMT served as a rich background, and the analysis was performed based on the IRF1 level combined with the sample grouping information.

Relationship between IRF1 and immune regulatory factors TMB and MSI

TMB is defined as the total number of base mutations per million cells in a tumor that can stimulate the production of tumor-specific and highly immunogenic antibodies, and has been recognized as a novel target for predicting the effectiveness of tumor immunotherapy. MSI is defined as the phenomenon wherein a new micro-satellite allele appears at a micro-satellite site in a tumor compared to normal tissue owing to the insertion or deletion of repetitive units, which leads to functional defects in DNA mismatch repair in the tumor tissue. The expression matrices of IRF1 and immune regulatory gene sets from dataset were extracted, and the Spear-man correlation coefficients between IRF1 and various genes, TMB, and MSI in the immune regulatory gene set were calculated using the cor. test function in R software.

Prediction of the IRF1 target genes

Target genes of IRF1 were predicted using the TRRUST Database (https://www.grnpedia.org/trrust/) (Han et al., 2018). To ensure that the interactions in the database were experimentally validated, the target genes were selected using MeSH vocabulary queries and continuously improving sentence-based text-mining algorithms, and carefully proofread manually after mining. Protein-protein interaction (PPI) was performed using the STRING (version 11.0, http://www.string-db.org/) database after target gene selection for IRF1 (Szklarczyk et al., 2021). Required Confidence (combined score) > 0.7 was selected as the threshold for PPI, and relevant files were downloaded in tsv format. After obtaining the PPI relationship pair file, Cytoscape software (version 3.4.0, http://chianti.ucsd.edu/cytoscape-3.4.0/) was used to construct the network (Shannon et al., 2003).

Correlation analysis between IRF1 expression and immunotherapy

The TIDE score was calculated based on the mRNA expression matrix (http://tide.dfci.harvard.edu/) to predict immune therapy response. The difference in the TIDE scores of IRF1 between the high- and low-expression groups was compared using the R package ggpubr (version 0.6.0).

Clinical sample collection and analysis

Between February 2021 and December 2022, 168 NSCLC patients with receiving first-line chemoimmunotherapy from Hunan Cancer Hospital, China, were analyzed retrospectively. NSCLC was diagnosed by pathological examination. Epidermal growth factor receptor (EGFR) and anaplastic lymphoma kinase (ALK) mutation was were excluded. Information, including age,

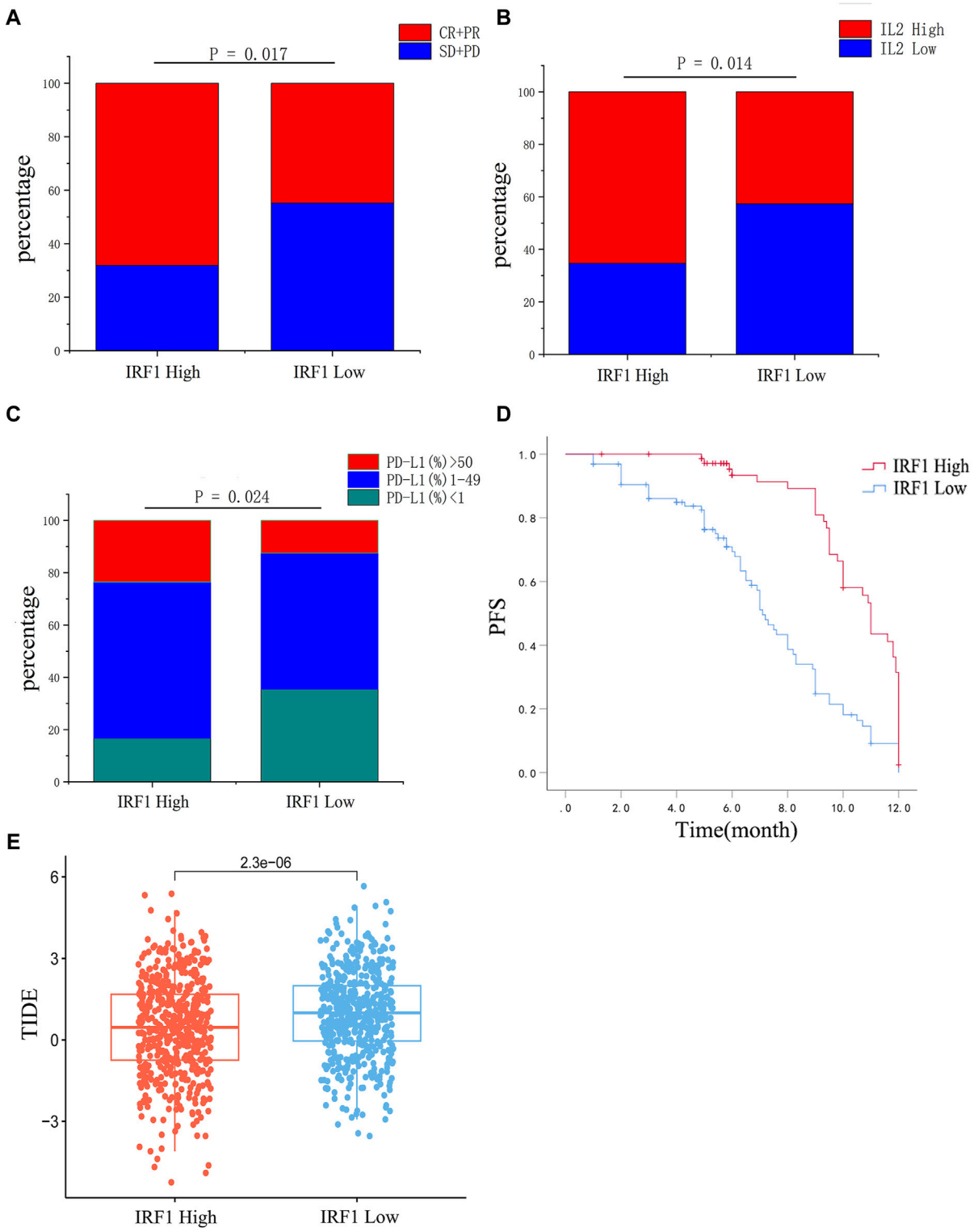

FIGURE 3
Correlation analysis between IRF1 expression and chemoimmunotherapy in NSCLC. **(A)** The efficacy of chemoimmunotherapy between the high IRF1 group and the low IRF1 group. **(B)** Expression of IL2 between high IRF1 group and low IRF1 group. **(C)** The expression of PD-L1 between the high IRF1 group and the low IRF1 group. **(D)** The expression of IRF1 is associated with PFS of first-line chemoimmunotherapy in NSCLC patients; **(E)** Box plot of IRF1 gene expression and tumor immune dysfunction and exclusion (TIDE) score. The horizontal axis represents the high and low groups distinguished by the IRF1 expression value, while the vertical axis represents the respective TIDE scores of the high and low groups. Each point in the graph represents a sample.

TABLE 2 Cox regression analysis of significant correlation factors of IRF1.

Variables	Univariate analysis		*p*-Value
	HR	Or (95%CI)	
Age	1.003	0.896-1.122	0.959
Gender	1.616	0.109-3.524	0.585
Pathological type	4.381	0.663-2.928	0.125
PD-L1 level	0.752	0.593-1.101	0.038*
Smoke Status	2.002	0.999-2.001	0.906
PS score	1.688	0.291-9.799	0.561
T stage	0.891	0.407-1.952	0.773
N stage	2.079	0.856-5.051	0.106
M stage	1.145	0.042-3.921	0.936
TNM Stage	1.145	0.042-3.921	0.936
Metastasis site	1.594	0.798-3.167	0.187
IL-2	0.437	0.227-0.843	0.024*
IL-6	0.716	0.330-1.553	0.161
TNFα	0.869	0.417-1.809	0.707
Interferon γ	0.759	0.395-1.460	0.409
Chemoimmunotherapy Efficacy	0.824	0.682-1.214	0.041*
CD3 cell percentage	1.001	0.433-2.312	0.998
CD4 cell percentage	1.247	0.466-3.340	0.663
CD8 cell percentage	1.399	0.615-3.182	0.423
B cell percentage	1.375	0.714-2.647	0.345
NK cell percentage	0.638	0.206-1.975	0.436

*p-value <0.05 was considered as a significant difference.

gender, pathological type, Lung adenocarcinoma (LUAD) and Lung squamous cell carcinoma (LUSC), PD-L1 (%), smoking status, PS score, TNM stage were collected. The TNM classification was according to National Comprehensive Cancer Network Classification Standard Eight Edition. All the patients were received first-line chemotherapy plus ICIs. Treatment regimens for LUSC was nab-paclitaxel 260 mg/m^{2}intravenously (IV) plus carboplatin AUC five IV days 1once every 3 weeks plus ICIs. Treatment regimens for LUAD was pemetrexed 500 mg/m2 IV plus carboplatin AUC five IV days 1once every 3 weeks plus ICIs. The measurable tumor was evaluated once every 6 weeks in the first 12 months and once every 9 weeks in year two and beyond using Response Evaluation Criteria in Solid Tumors (RECIST) version1.1. The efficacy of chemoimmunotherapy were classified into complete response (CR), partial response (PR), stable disease (SD), progressive disease (PD). The combination rate of CR and PR were as objective response rate (ORR). Progression-free survival (PFS) was defined as the length of time during and following primary treatment without progression, as demonstrated by radiological and clinical examinations. The study was granted by the Ethics Committee of Hunan Cancer Hospital and conducted in compliance with the principles of the Declaration of Helsinki. Written informed consent was obtained from all the enrolled patients.

Circulating biomarker analyze

Once whole blood was collected in tubes containing EDTA anticoagulant, samples were centrifuged at 400 *g* for 2 hours at 4°C. The plasma samples have been collected and then stored at −80°C before to utilization. Chemical ELISA Kit (Huamei, Wuhan, China) was used to assess TNFα, interferon γ, IL-2, and IL-6. Hunan Cancer Hospital's central laboratory examined B cells, natural killer (NK), CD3, CD4, and CD8 percentages, as well as serum tumor indicators.

Immunohistochemistry (IHC)

Fixed or fresh tumor biopsy samples were obtained from patients before treatment. PD-L1 and IRF1 expression was evaluated by IHC staining as described before (Zhou et al., 2014; Zhang et al., 2022). PD-L1 positivity was defined as TC≧1%.

IRF1 quantification by IHC

IRF1 staining was scored independently by two pathologists and was calculated using a previously defined scoring system (Zhou et al., 2014). Briefly, the proportion of positive tumor cell was scored as: 0 = <5%; 1+ = 5–20%; 2+ = 21–50%; 3+ = 50–70% and 4+ = 70–100%. The intensity was arbitrarily scored as 0 = weak (no color or light blue), 1 = moderate (light yellow), 2 = strong (yellow brown), and 3 = very strong (brown). The overall score was calculated by multiplying the two scores obtained from each sample. a score of ≥8 was defined as high IRF1 expression and scores of <8 defined low IRF1 expression. All the enrolled patients were divided into two groups according to the expression levels of IRF1: a group with high IRF1 levels and a group with low IRF1 levels (Supplementary Figure S1). The relationship between IRF1 levels and clinical characteristics was subsequently analyzed.

Reagents and antibodies

IL-2 (sigma)10 ng/mL was used for 12 h. IRF1Ab was from Santa Cruz (Santa Cruz, CA, USA) and PDL1 Ab 22C3 was from Dako Agilent. Goat anti-rabbit secondary antibodies were purchased from Thermo Fisher Scientifc Inc. (Waltham, MA, USA). CCK-8 solution was from Guangzhou Yitao Biotechnology Co, LTD (Guangzhou, China). Nude mice were from Hunan Slack Jingda Experimental Animal Co., LTD. (Hunan, China). Matrigel was purchased from Corning Life Sciences (Wujiang) Co., LTD (Jiangsu, China). Phosphate buffer salt solution (PBS), trypsin, Dulbecco's modified eagle medium (DMEM), fetal bovine serum (FBS) were purchased from Gibco Life Technologiesin (New York,USA). Crystal violet staining solution, 4% paraformaldehyde fix solution was purchased

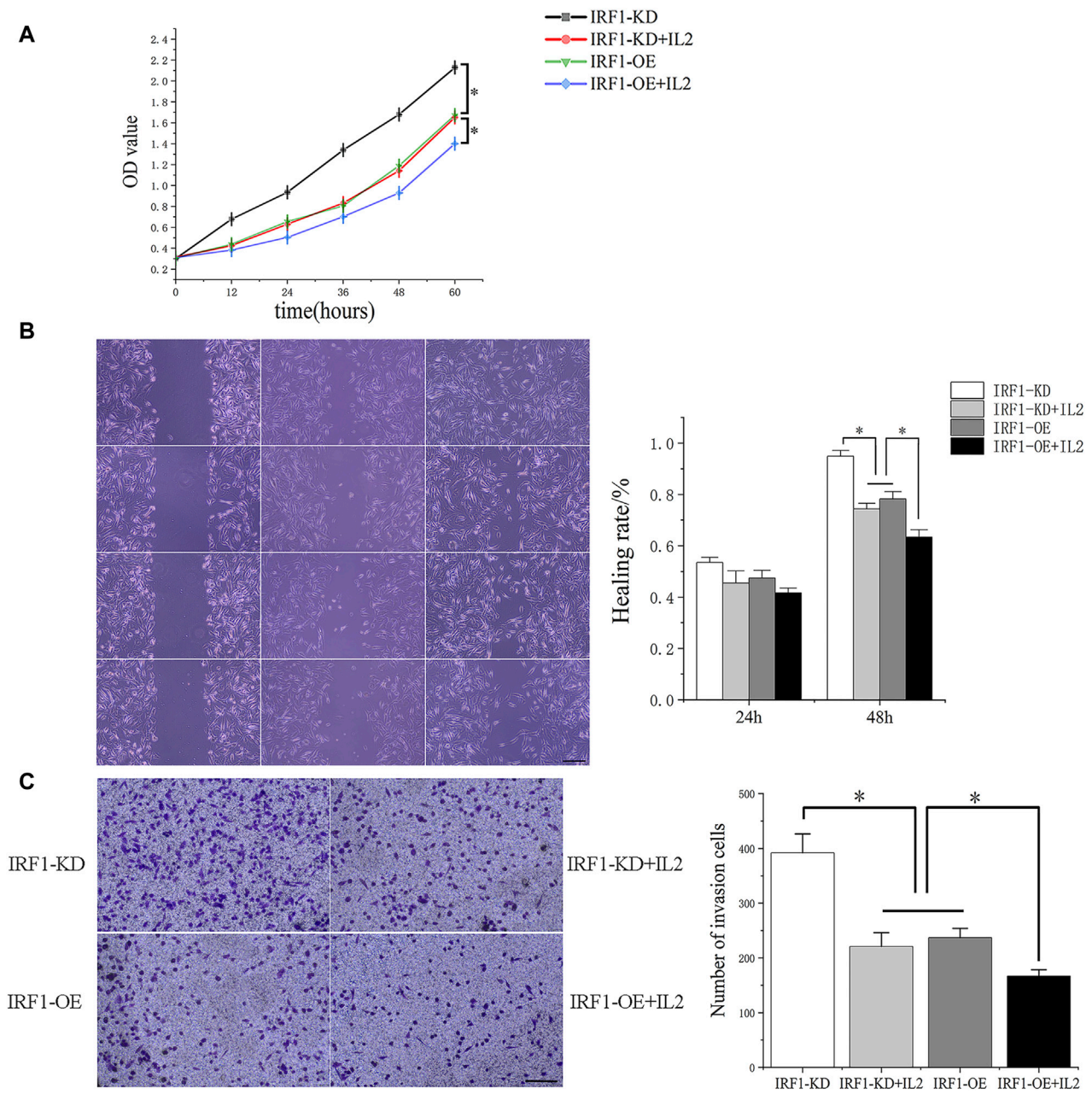

FIGURE 4
The synergistic effect of IRF1 and IL-2 in A549 lung cancer cells. **(A)** Proliferation curves of each experimental group; **(B)** The effects of IRF1 and IL2 on the healing rate of A549 cells were detected by scratch test (The scale is 100 μm); **(C)** The effects of IRF1 and IL2 on the invasion ability of A549 were detected by Transwell methodt (The scale is 100 μm). (*$p < 0.05$).

from Shanggong Bioengineering (Shanghai) Co., LTD (Shanghai, China).

Cell culture and transfection

The American Type Culture Collection (Manassas, VA, USA) provided the human lung cancer cell lines A549. A titer of 1 × 109TU/mL was generated for IRF1 shRNA and overexpression lentiviral vectors (Hanyin, Shanghai, China). Using 5 μg/mL polyamine in RMI-1640 media, these vectors were transfected into cells at a multiplicity of infection (MOI) of 20:1. The cells were grown in new culture media outlets for 48 h following a 4-h transfection. The effectiveness of IRF1 overexpression (OE) and knockdown (KD) was evaluated using flow cytometry and Western blotting.

CCK-8 cell proliferation experiment

After cell concentration was adjusted, cells were inoculated into 96-well plates with 5×10^4 cells per well. Cells in each group

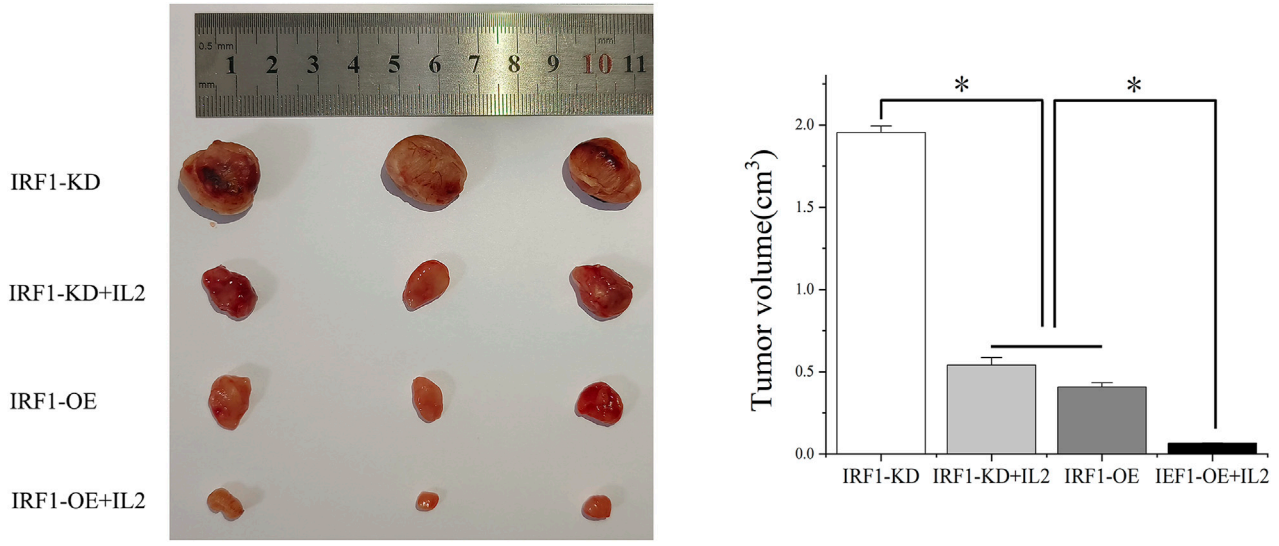

FIGURE 5
The synergistic effect of IRF1 and IL-2 *in vivo*. The synergistic effect of IRF1 and IL-2 on tumor inhibition *in vivo* was determined by subcutaneous tumor formation in nude mice. (*$p < 0.05$).

were provided with four multiple Wells and blank controls, and cultured in an incubator for 0h, 24 h and 48h, with 10 μL CCK-8 solution per well and incubated for 2 h away from light. optical density (OD) at 450 nm was measured. The experiment was repeated 3 times.

Transwell experiment

The 100 μL matrix glue was added to each Transwell chamber for coagulation. The cells were suspended and adjusted to 1×10^4 cells/mL. 100μL cells were taken and added to the upper chamber of the chamber for 48 h. The cells were removed and fixed with 4% formaldehyde for 20min. The cells were stained with 0.02% crystal violet solution for 10 min Three fields of view were randomly selected to take photos.

Scratch experiment

Cells were added into the 6-well plate at the rate of 1×10^6 cells per well, and cultured until the fusion rate reached 100%. Samples were taken and patted at 0h, 24 h and 48h, respectively, and the scratch healing rate was assessed. The experiment was repeated three times.

Animal studies

The experimental subjects consisted of nude mice (Hunan Slack Jingda Experimental Animal Co., LTD., Hunan, China) aged between 6 and 8 weeks. All animal procedures adhered to the guidelines for experimental animal care and use set forth by Hunan Cancer Hospital and received approval from the Ethics Committee of Hunan Cancer Hospital. Cells were digested and adjusted to concentration 1×10^7/mL. Each nude mouse received an inoculation of 100 μL of cell lines under the right armpit skin. Nude mouse in IRF1-OE + IL2 and IRF1-KD + IL2 groups were injected with recombinant IL-2 (1×10^5 units; Beijing Sihuan Biopharmaceutical Co., LTD., Beijing, China) once every 2 days, while the remaining groups received equivalent volumes of saline. The tumor-bearing mice were killed by cervical dislocation 4 weeks after the inoculation, and the tumors were removed. Tumor volume was calculated (tumor volume = $(\pi/6)\times\text{length}\times\text{width}^2$).

Single cell analysis of NSCLC

The distribution and expression of IRF1 in a single-cell dataset of NSCLC were analyzed using TISCH2 (http://tisch.comp-genomics.org/) (Sun et al., 2021). The pan-cancer risk value (HR) of this gene was also determined.

Statistical analyses

The information can be seen as the average ± standard deviation. The software known as SPSS was used to do statistical analysis using the *t*-test or chi-square test. We evaluated the association between IRF1 expression and clinical variables using univariate analysis. The chi-squared test was used to determine the differences between the groups with high and low IRF1 levels. The medium TNFα, interferon γ, IL-2 and IL-6 and percentage of CD3, CD4, CD8, NK, B cells were identified as optimal cut-off point. The Kaplan-Meier method was applied to estimate the median PFS. Spearman's correlation coefficient was

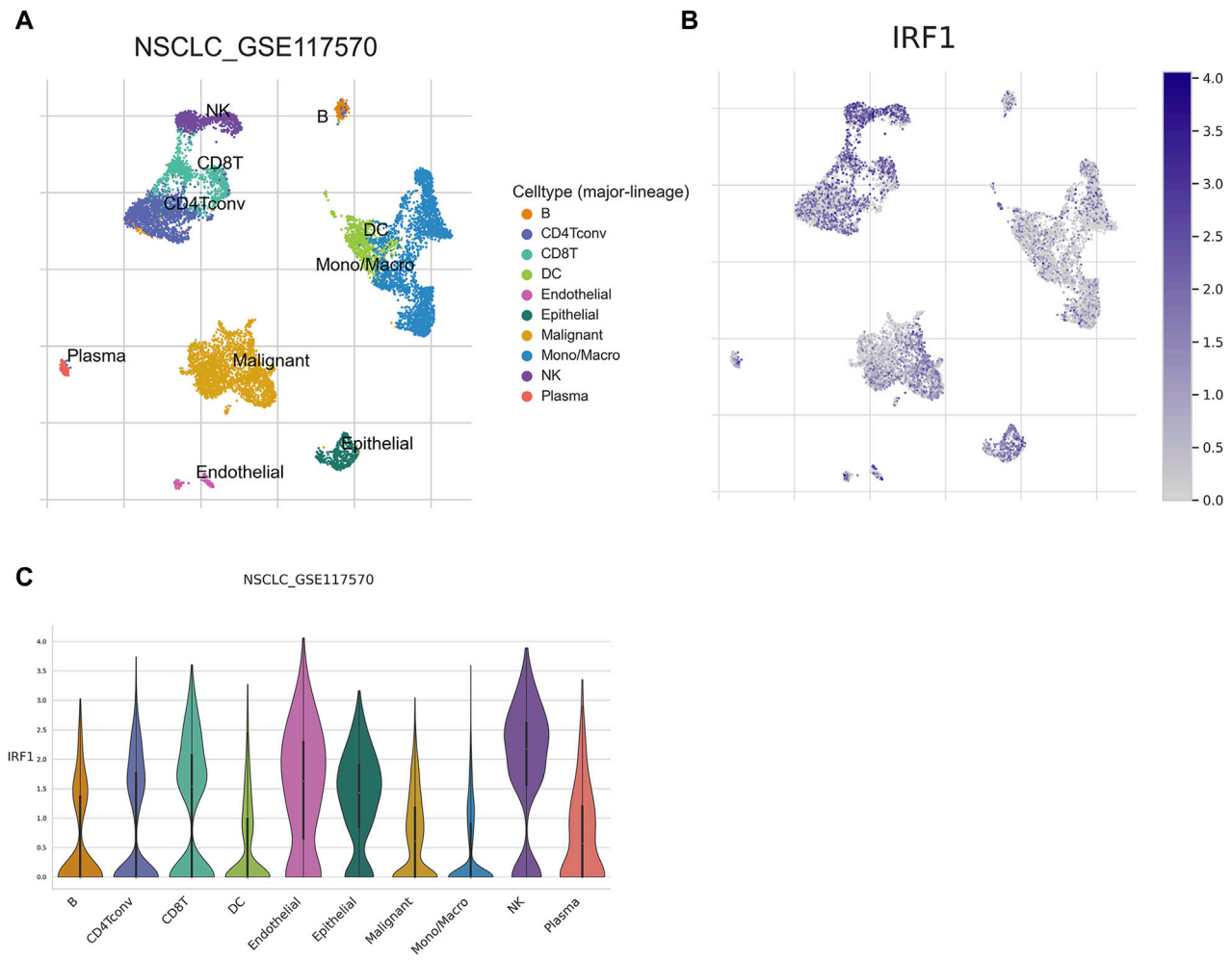

FIGURE 6
Single cell analysis of IRF1. **(A)** Single cell UMAP map; Each color represents a cell type, and each dot represents a cell. **(B)** Scatter plot of IRF1 single cell expression distribution; the darker the color represents the higher expression, and each dot represents a cell; **(C)** Violin diagram of IRF1 expression in cells; The horizontal axis represents the cell type, while the vertical axis represents the expression level of IRF1 in each cell type.

used to calculate the relationship. $p < 0.05$ was considered to indicate a statistically significant difference.

Results

Different frequency changes of IRF1 and its relationship with immune regulatory factors, TMB, and MSI

As described before (Zhang et al., 2022), IRF1 expression was downregulated in LUAD and LUSC. According to Figure 1A, the mutation frequency of IRF1 was 1.4%, and the main mutations was deep deletions. In the immunosuppressive gene set, IRF1 positively correlated with IDO, TIGIT and LAG3 (Figure 1B). In the immune stimulation gene set, IRF1 positively correlated with IL2RA and CD80 (Figure 1C). Regarding chemokines, IRF1 positively correlated with CXCL10, CCL4 and CXCL9 (Figure 1D). IRF1 levels was closely correlated with TMB (Figure 1E) and MSI (Figure 1F). Thus, IRF1 might be closely regulate the response to immunotherapy.

IRF1 targeted genes and functional roles

A total of 57 IRF1-related genes were explored (Supplementary Table S1). TF-target gene network analysis showed that 11 genes were directly related to IRF1, including TP53, IRF2, IFNG, IFNA1, IFNB1, CXCL10 and HLA, which were closely related with interferon release and immunity regulation (Figure 2A). Differences in functional pathways were evaluated using GSEA. The pathways mainly affected by IRF1 included interferon responses and IL-2 signaling, which were mainly associated with inflammatory responses (Figure 2B). Both targeted genes and functional role analyze indicated IRF1 might play a crucial role in inflammatory responses and immunity regulation.

Correlation analysis between IRF1 level and efficacy of chemoimmunotherapy

The baseline characteristics of the enrolled NSCLC patients are shown in Table 1. Significant differences were observed between patients with high IRF1 and low IRF1 levels for chemoimmunotherapy efficacy (Figure 3A). Patients with high IRF1 level were with higher ORR of 68.1%, while low IRF1 group with was lower ORR of 44.8% ($p < 0.05$) (Table 1). Patients of high IRF1 group were also with higher circulating IL-2 level ($p < 0.05$) (Table 1; Figure 3B) and PD-L1 distribution ($p < 0.05$) (Table 1; Figure 3C). Univariate analysis revealed that IRF1 levels were significantly associated with circulating IL-2 level and PD-L1 distribution (Table 2). High IRF1 level group was with longer PFS, a median PFS (mPFS) of 9.5 months. At 6 months, the PFS rate is 85% while at 12 months, the PFS rate is 39%. Conversely, low IRF1 group was with shorter mPFS of 5.8 months. At 6 months, the PFS rate is 48% while at 12 months, the PFS rate is 29% (Figure 3D). Clinical data supported the correlation between IRF1 level and chemoimmunotherapy efficacy and prognosis in NSCLC. Bio-informatics analyse was also used to further confirm the clinical application of IRF1 in chemoimmunotherapy. Based on the combined expression matrix of LUAD and LUSC in TCGA, patients were divided into high and low IRF1 expression groups. As shown in Figure 3E, significant differences of TIDE score were found between IRF1 high and low groups ($p < 0.01$), indicating a significant correlation between IRF1 expression immunotherapy response.

The synergistic effect of IRF1 and IL-2 in A549 lung cancer cells

As showed the highest levels of IRF1 transcription and expression following cisplatin treatment (Zhang et al., 2022), A549 lung cancer cells were chosen for further *in vitro* study. IRF1 overexpression and knockdown by lentiviral and shRNA were confirmed by Western blotting and flowcytometry (data not shown). The overexpression of IRF1 significantly inhibit the proliferation, invasion and migration of A549 lung cancer cells (Figures 4A–C); and IL-2 augment the function of IRF1 on A549 lung cancer cells (Figures 4A–C). While in IRF1 knockdown group, IL-2 pretreatment mimics the effects of IRF1, including inhibition of proliferation, invasion and migration (Figures 4A–C). It is suggested that the synergistic effect of IRF1 and IL-2 in A549 lung cancer cells *in vitro*.

The synergistic effect of IRF1 and IL-2 *in vivo*

To further investigate the synergistic effect of IRF1 and IL-2, we transplanted IRF1 OE and IRF1 KD A549 cell line into nude mice. After 4 weeks of inoculation, we found that overexpression of IRF1 significantly inhibits the tumor growth of A549 lung cancer cells. And IL-2 injection enhanced the function of IRF1 on A549 lung cancer cells. In the IRF1 knockdown group, IL-2 treatment simulated the effect of IRF1 and significantly inhibited the tumor growth. It shows the synergistic effect of IRF1 and IL-2 *in vivo* (Figure 5).

Single cell analysis of IRF1 in NSCLC

Given the *in vitro* synergistic anti-tumor function of IRF1 and IL-2, we further explore the potential immune cell types which might play a major role in the complex tumor microenvironment. The expression of IRF1 in NSCLC single-cell data was analyzed using the TISCH2 database, and GSE117570 was used to perform IRF1-based single-cell analysis. UMAP revealed 11 cell sub-types, including NK, endothelial, and malignant cells (Figure 6A). The expression levels of IRF1 in each cell types were further analyzed. The expression level of IRF1 was higher in NK and endothelial cells than other sub-types (Figures 6B, C). Further study should be focused on NK cells and related receptor to explore the interplay between IRF1 and IL-2 *in vivo*.

Discussion

The critical function of IRF1 in the immune systems of various cancers has been explored (Kirchhoff et al., 1993; Kim et al., 2002), the clinical application and biological function of IRF1 in NSCLC patients who receiving chemoimmunotherapy remains unknown. In our investigation, we discovered using bioinformatics analysis that IRF1 is intimately associated with the control of immunological activation, potentially impacting the outcome of immunotherapy. IRF1 also had a role in the control of other inflammatory responses, such as IL2 signaling. Clinical research has revealed a significant correlation between IRF1 and the level of circulating IL-2, which is linked to the effectiveness and prognosis of chemotherapy for non-small cell lung cancer. IRF1 and IL2 have a synergistic impact that inhibits the proliferation, migration, and invasion of A549 lung cancer cells, as demonstrated by both *in vitro* and *in vivo* tests (Figure 7).

Our data showed that IRF1 expression levels were correlated with immunosuppressive genes, such as IDO, TIGIT and LAG3, and immune stimulation genes, such as IL2RA and CD80. Meanwhile, the gene was also closely correlated with TMB and MSI. Extensive researches have confirmed that, the factors, including immunosuppressive and immune-stimulatory gene sets, TMB, and MSI, were all valuable predictive biomarkers for immunotherapy (Chang et al., 2018; Strickler et al., 2021; Turan et al., 2021). Therefore, IRF1 might be a critical biomarker for evaluating treatment efficacy for patients receiving immunotherapy. Furthermore, we have also observed that high IRF1 level group was with longer PFS, and low IRF1 group was with shorter PFS. Meanwhile, clinical data also supported the correlation between IRF1 level and prognosis in NSCLC. Therefore, patients with higher IRF1 levels might be more easily to achieve benefit from immunotherapy in clinic. Interestingly, IRF1-mediated PDL1 levels have been reported previously (Sato et al., 2017). Moreover, tumor immune microenvironment plays a role in interferon γ stimulated PD-L1 expression in tumors (Bally et al., 2016; Liu et al., 2018). In circulating tumor cells, PD-L1 and IRF1 expression levels are all associated with immunotherapy efficacy (Kennedy et al., 2019). Therefore, IRF1, along with PD-L1, might serve as a predictive biomarker for immunotherapy response.

Cancer-associated inflammation affects malignancy related events, including tumor metastasis, angiogenesis, survival, and proliferation (Gomes et al., 2014). We showed that IRF1 is mainly involved in pathways associated with inflammation

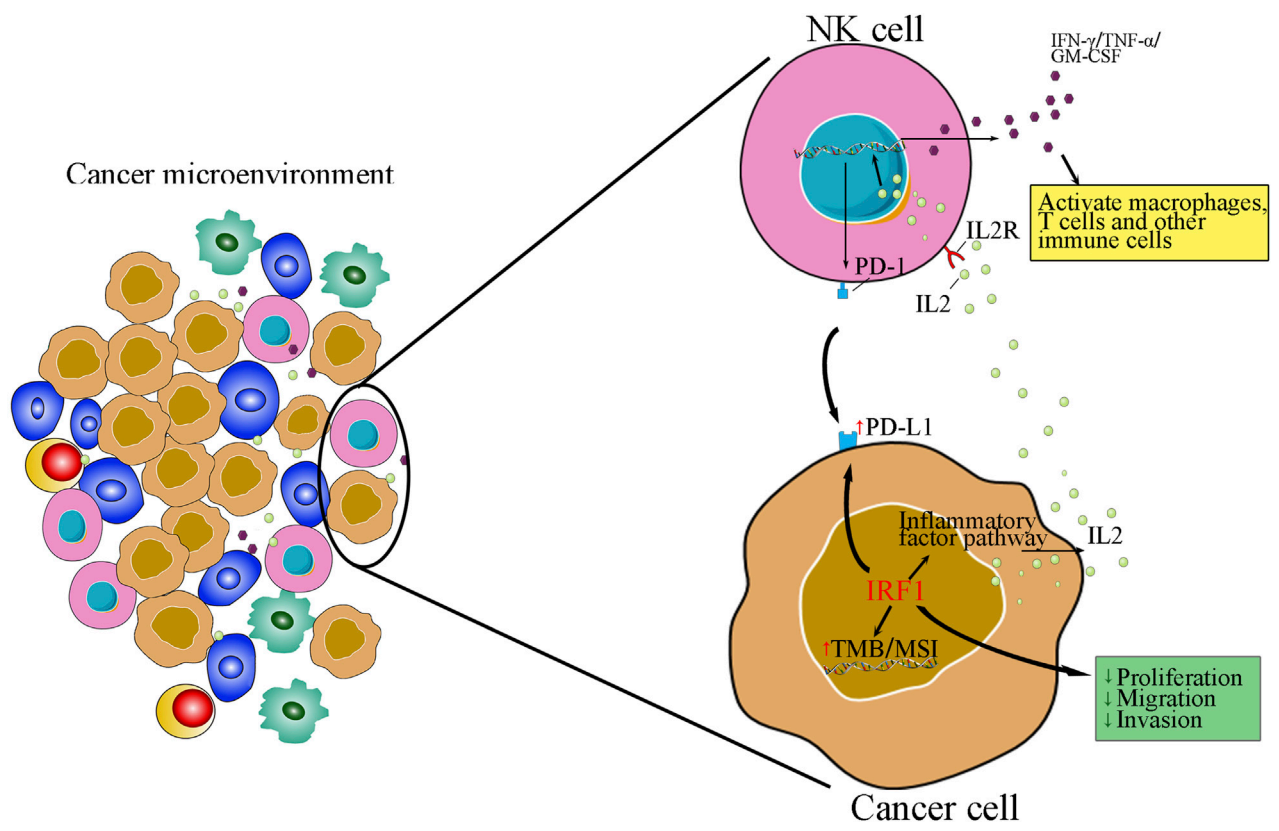

FIGURE 7
An schematic of how interplay of IRF1 and IL-2 in tumour micro-environment in NSCLC.

and interferon, such as interferon γ and IL-2 signaling. The critical role of the IL-2 signaling pathway in various cancers has been extensively studied (Alvarez et al., 2006). IRF1 and IL-2 are both involved in immune response while IRF1 may influence the expression of genes involved in immune responses, including those related to IL-2 (Konjevic et al., 2010; Perazzio et al., 2017). Utilizing IL-2 successfully counteracts the inhibitory impact of elevated IRF1 expression on the proliferation, migration, and invasion of lung adenocarcinoma cells. It is worth noting that the specific regulation between IRF1 and IL-2 may vary depending on the context of immune response. The intricate interplay between various transcription factors and cytokines ensures a coordinated and effective immune response (Devenish et al., 2021). In our study, the synergistic effect of IRF1 and IL2 has been found in chemotherapy combined with immunotherapy in NSCLC. Therefore, these results indicate that both IRF1 and IL2 are key components of antitumor immunity.

We also found that IRF1 levels were higher in NK cells, suggesting that IRF1 might mediate NK cell induced immunity regulation. Previously, Gungabeesoonv et al. revealed that loss of IRF1 in neutrophils would lead to failure of immunotherapy (Gungabeesoon et al., 2023). Meanwhile, neutrophils have been shown to suppress the NK cell infiltration, by downregulating CCR1 and to impair anti-tumor capabilities by cell-to-cell interactions, through the PD-L1/PD-1 axis (Sun et al., 2020). IRF1 was previously demonstrated to be tumor suppressor gene mediated by increasing the secretion of activated NK cells migration (Yan et al., 2021). NK cells are valuable in generating an antitumor effect, and immunotherapy targeting NK cells are recognized as promising therapeutic strategies for treating tumors (Wang et al., 2022). Additionally, IL2 might enhance NK cytotoxicity (Hernandez et al., 2022). Single cell sequencing suggests that NK cells with IRF1 overexpression in NSCLC (Figure 7). Thus, targeting IRF1/IL2 axis may be used to modulate immunotherapy-elicited NK cells and neutrophil responses via cell-to-cell interactions. However, the function of NK cells and detailed mechanisms of correlation between IRF1 and IL2 in immunotherapy responses requires further validation by observing NK cell proliferation, invasion and migration mediated by IRF1 and IL2 levels. Meanwhile, the secretion of immune related cytokines, such as IFN-γ, TNF-β, should also be recorded. Furthermore, our previous data have shown that IRF-1 levels could regulate mitochondrial depolarization, oxidative stress, and autophagy in A549 cells (Zhang et al., 2022). These processes might also occur among subjects underwent chemoimmunotherapy. Therefore, further *in vitro* and *in vivo* study should be designed to observe cellular processes such as autophagy, apoptosis, and mitochondrial homeostasis in cell models with overexpression or downregulation IRF1 via flow cytometry and corresponding assay kits.

In summary, IRF1 might be with predictive and prognostic value for chemoimmunotherapy in NSCLC patients through regulation of inflammatory pathway, including IL-2. However, further research is needed to explore the underlying mechanisms.

Data availability statement

The original contributions presented in the study are included in the article/Supplementary Material, further inquiries can be directed to the corresponding author.

Ethics statement

The studies involving humans were approved by the Ethics Committee of Hunan Cancer Hospital, affiliated with Hunan Cancer Hospital. The studies were conducted in accordance with the local legislation and institutional requirements. The participants provided their written informed consent to participate in this study. The animal study was approved by Ethics Committee of Hunan Cancer Hospital, affiliated with Hunan Cancer Hospital. The study was conducted in accordance with the local legislation and institutional requirements.

Author contributions

ST: Writing–original draft, Writing–review and editing, Investigation, Software, Validation. JS: Data curation, Formal Analysis, Methodology, Writing–original draft, Writing–review and editing. YuL: Data curation, Formal Analysis, Conceptualization, Writing–original draft, Writing–review and editing. XC: Conceptualization, Resources, Visualization, Writing–original draft, Writing–review and editing. JL: Data curation, Software, Supervision, Writing–original draft, Writing–review and editing. YoL: Formal Analysis, Project administration, Resources, Writing–original draft, Writing–review and editing. CP: Data curation, Methodology, Visualization, Writing–original draft, Writing–review and editing. LZ: Methodology, Project administration, Writing–original draft, Writing–review and editing.

Funding

The author(s) declare that financial support was received for the research, authorship, and/or publication of this article. This study was supported by grants from the National Natural Science Foundation of Hunan Province (2023JJ60039); Natural Science Foundation of Hunan Province National Health Commission (B202303027655), Natural Science Foundation of Changsha Science and Technology Bureau (Kq2208150), and Wu Jieping Foundation of China (320.6750.2022-22-59, 320.6750.2022-17-41); Guangdong Association of Clinical Trials (GACT)/Chinese Thoracic Oncology Group (CTONG) and Guangdong Provincial Key Lab of Translational Medicine in Lung Cancer (Grant No. 2017B030314120); the science and technology innovation Program of Hunan Province (2023SK4024).

Conflict of interest

The authors declare that the research was conducted in the absence of any commercial or financial relationships that could be construed as a potential conflict of interest.

Publisher's note

All claims expressed in this article are solely those of the authors and do not necessarily represent those of their affiliated organizations, or those of the publisher, the editors and the reviewers. Any product that may be evaluated in this article, or claim that may be made by its manufacturer, is not guaranteed or endorsed by the publisher.

Supplementary material

The Supplementary Material for this article can be found online at: https://www.frontiersin.org/articles/10.3389/fphar.2024.1413699/full#supplementary-material

SUPPLEMENTARY FIGURE S1
Representative images of IRF1 immunohistochemical staining in non-small-cell lung carcinomas. A High IRF1 expression in squamous cell carcinoma; B low IRF1 expression in squamous cell carcinoma; C High IRF1 expression in adenocarcinoma; D low IRF1 expression in adenocarcinoma.

SUPPLEMENTARY TABLE S1
Clinical characteristics of enrolled NSCLC patients.

References

Alvarez, J. V., Greulich, H., Sellers, W. R., Meyerson, M., and Frank, D. A. (2006). Signal transducer and activator of transcription 3 is required for the oncogenic effects of non-small-cell lung cancer-associated mutations of the epidermal growth factor receptor. *Cancer Res.* 66 (6), 3162–3168. doi:10.1158/0008-5472.CAN-05-3757

Bally, A. P., Austin, J. W., and Boss, J. M. (2016). Genetic and epigenetic regulation of PD-1 expression. *J. Immunol.* 196 (6), 2431–2437. doi:10.4049/jimmunol.1502643

Chang, L., Chang, M., Chang, H. M., and Chang, F. (2018). Microsatellite instability: a predictive biomarker for cancer immunotherapy. *Appl. Immunohistochem. Mol. Morphol.* 26 (2), e15–e21. doi:10.1097/PAI.0000000000000575

Devenish, L. P., Mhlanga, M. M., and Negishi, Y. (2021). Immune regulation in time and space: the role of local- and long-range genomic interactions in regulating immune responses. *Front. Immunol.* 12, 662565. doi:10.3389/fimmu.2021.662565

Feng, H., Zhang, Y. B., Gui, J. F., Lemon, S. M., and Yamane, D. (2021). Interferon regulatory factor 1 (IRF1) and anti-pathogen innate immune responses. *PLoS Pathog.* 17 (1), e1009220. doi:10.1371/journal.ppat.1009220

Gao, J., Aksoy, B. A., Dogrusoz, U., Dresdner, G., Gross, B., Sumer, S. O., et al. (2013). Integrative analysis of complex cancer genomics and clinical profiles using the cBioPortal. *Sci. Signal* 6 (269), pl1. doi:10.1126/scisignal.2004088

Gomes, M., Teixeira, A. L., Coelho, A., Araújo, A., and Medeiros, R. (2014). The role of inflammation in lung cancer. *Adv. Exp. Med. Biol.* 816, 1–23. doi:10.1007/978-3-0348-0837-8_1

Gungabeesoon, J., Gort-Freitas, N. A., Kiss, M., Bolli, E., Messemaker, M., Siwicki, M., et al. (2023). A neutrophil response linked to tumor control in immunotherapy. *Cell* 186 (7), 1448–1464.e20. doi:10.1016/j.cell.2023.02.032

Han, H., Cho, J. W., Lee, S., Yun, A., Kim, H., Bae, D., et al. (2018). TRRUST v2: an expanded reference database of human and mouse transcriptional regulatory interactions. *Nucleic Acids Res.* 46 (D1), D380–D386. doi:10.1093/nar/gkx1013

Hernandez, R., Põder, J., LaPorte, K. M., and Malek, T. R. (2022). Engineering IL-2 for immunotherapy of autoimmunity and cancer. *Nat. Rev. Immunol.* 22 (10), 614–628. doi:10.1038/s41577-022-00680-w

Kennedy, L., Ramirez, A. B., U'Ren, L., Sun, Y., Durenberger, G., Chow, L. Q. M., et al. (2019). Circulating tumor cell (CTC) PD-L1 and interferon regulatory factor-1 (IRF-1) expression as biomarkers of anti-PD-(L)1 response. *J. Clin. Oncol.* 37 (15_Suppl. 1), e14032. doi:10.1200/jco.2019.37.15_suppl.e14032

Kerr, M. K. (2003). Linear models for microarray data analysis: hidden similarities and differences. *J. Comput. Biol.* 10 (6), 891–901. doi:10.1089/106652703322756131

Kim, E. J., Lee, J. M., Namkoong, S. E., Um, S. J., and Park, J. S. (2002). Interferon regulatory factor-1 mediates interferon-gamma-induced apoptosis in ovarian carcinoma cells. *J. Cell Biochem.* 85 (2), 369–380. doi:10.1002/jcb.10142

Kirchhoff, S., Schaper, F., and Hauser, H. (1993). Interferon regulatory factor 1 (IRF-1) mediates cell growth inhibition by transactivation of downstream target genes. *Nucleic Acids Res.* 21 (12), 2881–2889. doi:10.1093/nar/21.12.2881

Konjevic, G., Mirjačić Martinović, K., Vuletić, A., and Radenković, S. (2010). Novel aspects of *in vitro* IL-2 or IFN-α enhanced NK cytotoxicity of healthy individuals based on NKG2D and CD161 NK cell receptor induction. *Biomed. Pharmacother.* 64 (10), 663–671. doi:10.1016/j.biopha.2010.06.013

Lantuejoul, S., Sound-Tsao, M., Cooper, W. A., Girard, N., Hirsch, F. R., Roden, A. C., et al. (2020). PD-L1 testing for lung cancer in 2019: perspective from the IASLC pathology committee. *J. Thorac. Oncol.* 15 (4), 499–519. doi:10.1016/j.jtho.2019.12.107

Liu, Y., Li, Y., Liu, S., Adeegbe, D. O., Christensen, C. L., Quinn, M. M., et al. (2018). NK cells mediate synergistic antitumor effects of combined inhibition of HDAC6 and BET in a SCLC preclinical model. *Cancer Res.* 78 (13), 3709–3717. doi:10.1158/0008-5472.CAN-18-0161

Miyamoto, M., Fujita, T., Kimura, Y., Maruyama, M., Harada, H., Sudo, Y., et al. (1988). Regulated expression of a gene encoding a nuclear factor, IRF-1, that specifically binds to IFN-beta gene regulatory elements. *Cell* 54 (6), 903–913. doi:10.1016/s0092-8674(88)91307-4

Nozawa, H., Oda, E., Nakao, K., Ishihara, M., Ueda, S., Yokochi, T., et al. (1999). Loss of transcription factor IRF-1 affects tumor susceptibility in mice carrying the Ha-ras transgene or nullizygosity for p53. *Genes Dev.* 13 (10), 1240–1245. doi:10.1101/gad.13.10.1240

Perazzio, A. S., Oliveira, J. S. R., Figueiredo, V. L. P., and Chauffaille, M. d. L. L. F. (2017). Increase of IRF-1 gene expression and impairment of T regulatory cells suppression activity on patients with myelodysplastic syndrome: a longitudinal one-year study. *Leuk. Res.* 55, 6–17. doi:10.1016/j.leukres.2017.01.008

Sato, H., Niimi, A., Yasuhara, T., Permata, T. B. M., Hagiwara, Y., Isono, M., et al. (2017). DNA double-strand break repair pathway regulates PD-L1 expression in cancer cells. *Nat. Commun.* 8 (1), 1751. doi:10.1038/s41467-017-01883-9

Shannon, P., Markiel, A., Ozier, O., Baliga, N. S., Wang, J. T., Ramage, D., et al. (2003). Cytoscape: a software environment for integrated models of biomolecular interaction networks. *Genome Res.* 13 (11), 2498–2504. doi:10.1101/gr.1239303

Strickler, J. H., Hanks, B. A., and Khasraw, M. (2021). Tumor mutational burden as a predictor of immunotherapy response: is more always better? *Clin. Cancer Res.* 27 (5), 1236–1241. doi:10.1158/1078-0432.CCR-20-3054

Sun, D., Wang, J., Han, Y., Dong, X., Ge, J., Zheng, R., et al. (2021). TISCH: a comprehensive web resource enabling interactive single-cell transcriptome visualization of tumor microenvironment. *Nucleic Acids Res.* 49 (D1), D1420–D1430. doi:10.1093/nar/gkaa1020

Sun, R., Xiong, Y., Liu, H., Gao, C., and Weng, J. (2020). Tumor-associated neutrophils suppress antitumor immunity of NK cells through the PD-L1/PD-1 axis. *Transl. Oncol.* 13 (10), 100825. doi:10.1016/j.tranon.2020.100825

Szklarczyk, D., Gable, A. L., Nastou, K. C., Lyon, D., Kirsch, R., Pyysalo, S., et al. (2021). The STRING database in 2021: customizable protein-protein networks, and functional characterization of user-uploaded gene/measurement sets. *Nucleic Acids Res.* 49 (D1), D605–D612. doi:10.1093/nar/gkaa1074

Turan, T., Kongpachith, S., Halliwill, K., Roelands, J., Hendrickx, W., Marincola, F. M., et al. (2021). A balance score between immune stimulatory and suppressive microenvironments identifies mediators of tumour immunity and predicts pan-cancer survival. *Br. J. Cancer* 124 (4), 760–769. doi:10.1038/s41416-020-01145-4

Wang, W., Zhao, J., Hao, C., Hu, S., Chen, C., Cao, Y., et al. (2022). The development of chiral nanoparticles to target NK cells and CD8(+) T cells for cancer immunotherapy. *Adv. Mater* 34 (16), e2109354. doi:10.1002/adma.202109354

Yan, Y., Zheng, L., Du, Q., Yazdani, H., Dong, K., Guo, Y., et al. (2021). Interferon regulatory factor 1(IRF-1) activates anti-tumor immunity via CXCL10/CXCR3 axis in hepatocellular carcinoma (HCC). *Cancer Lett.* 506, 95–106. doi:10.1016/j.canlet.2021.03.002

Zhang, L., Cheng, T., Yang, H., Chen, J., Wen, X., Jiang, Z., et al. (2022). Interferon regulatory factor-1 regulates cisplatin-induced apoptosis and autophagy in A549 lung cancer cells. *Med. Oncol.* 39 (4), 38. doi:10.1007/s12032-021-01638-z

Zhou, H., Chen, J. h., Hu, J., Luo, Y. z., Li, F., Xiao, L., et al. (2014). High expression of Toll-like receptor 5 correlates with better prognosis in non-small-cell lung cancer: an anti-tumor effect of TLR5 signaling in non-small cell lung cancer. *J. Cancer Res. Clin. Oncol.* 140 (4), 633–643. doi:10.1007/s00432-014-1616-4

frontiers | Frontiers in Oncology

TYPE Original Research
PUBLISHED 17 June 2024
DOI 10.3389/fonc.2024.1422117

Check for updates

OPEN ACCESS

EDITED BY
Hailin Tang,
Sun Yat-sen University Cancer Center (SYSUCC), China

REVIEWED BY
Yuan Cheng,
Chongqing Medical University, China
Yulai Zhou,
The University of Texas Health Science Center at San Antonio, United States

*CORRESPONDENCE
Qiming Wang
m13957885162_1@163.com

RECEIVED 23 April 2024
ACCEPTED 27 May 2024
PUBLISHED 17 June 2024

CITATION
Yang J, Zhang M, Zhang Y, Zhu L and Wang Q (2024) Combined aqupla, paclitaxel liposome, and docetaxel treatment: survival and biomarker outcomes in recurrent ovarian cancer patients.
Front. Oncol. 14:1422117.
doi: 10.3389/fonc.2024.1422117

COPYRIGHT
© 2024 Yang, Zhang, Zhang, Zhu and Wang. This is an open-access article distributed under the terms of the Creative Commons Attribution License (CC BY). The use, distribution or reproduction in other forums is permitted, provided the original author(s) and the copyright owner(s) are credited and that the original publication in this journal is cited, in accordance with accepted academic practice. No use, distribution or reproduction is permitted which does not comply with these terms.

Combined aqupla, paclitaxel liposome, and docetaxel treatment: survival and biomarker outcomes in recurrent ovarian cancer patients

Jie Yang, Mengyu Zhang, Yilei Zhang, Lanfen Zhu and Qiming Wang*

Department of Gynecology, Women's and Children's Hospital of Ningbo University, Ningbo, Zhejiang, China

As one lethal malignancy in women's reproductive systems, ovarian cancer (OC) is frequently detected at an advanced phase during diagnosis. when the disease has spread widely. The absence of obvious symptoms and powerful screening tools in the early stages makes treatment difficult and the prognosis poor. Despite the clinical remission that can be achieved in some patients after initial treatment, the recurrence rate is conspicuous, posing a considerable challenge in treating recurrent OC (ROC). In the retrospective analysis, we compared the effects of two treatment regimens, aqupla combined with paclitaxel liposome (NP group) versus aqupla combined with docetaxel (ND group), on survival and biomarkers in patients with ROC. The study included 121 OC patients, and clinical data were collected through an electronic medical record system, outpatient review records, and a follow-up record system. The results revealed a notably higher overall remission rate in the ND group than the NP group, but revealed no notable inter-group discrepancy in toxicities, implying that the aqupla combined with docetaxel regimen may be more effective in platinum-sensitive ROC patients. Additionally, post-treatment CA125 levels were lower in patients in the ND group, suggesting that the regimen may be more effective in reducing tumour load. Survival analysis further revealed that treatment regimen, FIGO stage, number of recurrent lesions, and pretreatment CA125 level were independent prognostic factors affecting patients' 5-year OS and PFS. Overall for ROC patients, especially platinum-sensitive patients, the aqupla in combination with docetaxel regimen provided an improved survival benefit with a comparable safety profile, highlighting the importance of individualised treatment strategies.

KEYWORDS

aqupla, paclitaxel liposome, docetaxel, recurrent ovarian cancer, survival, biomarkers

1 Introduction

Ovarian cancer (OC) is one prevalent malignancy among gynaecological tumours, but also one of the most lethal (1). OC usually occurs in hard-to-detect areas, the early signs are atypical and variable, and there is a lack of efficient early detection methods (2). As a result, more than 70 per cent of patients have advanced cancer when diagnosed (3). For patients with advanced disease, whose long-term survival is not promising, tumour cytoreduction is the most common treatment option, supplemented by a combination of platinum and paclitaxel chemotherapy after surgery (4). Unfortunately, about 70–80 per cent of patients with moderate to advanced disease experience disease recurrence (5, 6). In the management of relapses, there is no consistent pattern of treatment, and chemotherapy is at the centre of treatment.

However, not all patients have the opportunity to undergo secondary tumour cytoreduction. For some patients, the risks and burdens of a second surgery may be beyond their reach for a variety of personal reasons, including family and financial constraints, as well as medical considerations (7, 8). This means that these patients can only choose chemotherapy as their primary treatment. Platinum-based chemotherapy is the mainstay in treating recurrent OC (ROC) and involves a large number of patients. In preparing a treatment plan for these patients, due consideration needs to be given to the possible side effects and complications arising from the different treatment options, as well as to the impact on the survival of the patients (9) Aqupla is a second-generation platinum-based chemotherapeutic agent. Compared with cisplatin and carboplatin, aqupla reduces nephrotoxicity and gastrointestinal side effects to a certain extent while maintaining similar anti-tumour activity (10). Inhibits the proliferation and growth of cancer cells through forming crosslinks with DNA and blocking DNA replication and transcription. Paclitaxel liposome is a liposomal formulation of paclitaxel which, by encapsulating paclitaxel in liposomes, improves its pharmacokinetic properties and increases its concentration in tumour tissues while reducing its toxicity to normal tissues (11). Docetaxel is another microtubule stabiliser with a mechanism similar to paclitaxel but with a different chemical structure (12). Docetaxel inhibits cell division by preventing the depolymerisation of microtubules, leading to cancer cell death (13). The combination of aqupla with paclitaxel liposome and docetaxel is common in treating ROC, but the advantages and disadvantages of the two regimens remain controversial.

In this study, a comparative analysis of the effects of two therapeutic regimens, aqupla combined with paclitaxel liposome and aqupla and combined with cetaxel, was conducted in ROC, aiming to investigate the differences between the two regimens in terms of therapeutic effect, patient survival and The study is to investigate the discrepancies between these two regimens regarding therapeutic efficacy, patient survival, and adverse effects, as well as the primary factors impacting the survival of ROC patients.

2 Materials and methods

2.1 Clinical data collection

Retrospective analysis of clinical data of OC patients treated at our hospital from Jan. 2015 to Jan. 2019. The research was conducted with permission of Women's and Children's Hospital of Ningbo University Medical Ethics Committee (Approval No. EC2024–030).

The research is based on the electronic medical record system, outpatient review record and follow-up record system to obtain the relevant information of patients. Clinical information included: International Federation of Gynecology and Obstetrics Staging (FIGO) staging (14), age, Pathology Type, Initial Surgical Treatment, Eastern Cooperative Oncology Group Performance Status (ECOG) Score (15), Maximum diameter of recurrent lesions, number of recurrent lesions, response to platinum drugs, history of diabetes mellitus, history of hypertension, clinical outcome of the patient, incidence of adverse events. Laboratory parameters include: pre- and post-treatment Carcinoembryonic Antigen (CEA), Cancer Antigen 19–9 (CA19–9), Cancer Antigen 125 (CA125), Cluster of Differentiation 4 (CD4), Cluster of Differentiation 3 (CD3), as well as Cluster of Differentiation 8 (CD8).

2.2 Inclusion and exclusion criteria

Inclusion criteria: (1) confirmed diagnosis of OC, fallopian tube cancer, primary peritoneal cancer after pathological examination; (2) recurrence after achieving complete remission level in primary treatment, first recurrence, platinum-free interval >6 months; (3) tumour markers and imaging tests suggesting recurrence, no contraindication to surgery or chemotherapy; (4) complete case data; (5) follow up to the survival outcome.

Exclusion criteria: (1) previous history of other malignant tumours; (2) history of severe allergy to platinum and other drugs; (3) bone marrow dysfunction. (4) Combined liver and kidney function abnormalities. (5) Undergoing secondary tumour cytoreduction after recurrence. (6) Expected survival time of the patient is less than 6 months.

2.3 Patient grouping

Based on the inclusion and exclusion criteria, we obtained 121 eligible cases. A query of the electronic medical record system revealed that 64 patients received aqupla combined with paclitaxel liposome treatment (NP group), while 57 patients received aqupla combined with docetaxel treatment (ND group).

2.4 Treatment regimen

NP group: On the first day, patients were treated with paclitaxel liposome (product code H20030357, 30 mg, manufacturer: Nanjing Green Leaf Pharmaceutical Co., Ltd.) at a dose of 130–170 mg/m², mixed with 500 ml of dextrose solution (5%) and administered through intravenous drip over 3 h. On the second day, aqupla (Product No. H20143133, 20 mg, Manufacturer: Jiangsu Oseikang Pharmaceutical Co., Ltd.) was used at 85–105 mg/m², mixed with 500 ml of 0.9% saline, by intravenous drip over 1 hour. After completion of the drip, the intravenous drip was continued with 1500 ml to 2000 ml of 0.9% saline.

ND group: On the first day, patients were treated with docetaxel (Product No. H20093092, 20 mg, Manufacturer: Zhejiang Haizheng Pharmaceutical Co., Ltd.) at 60–100 mg/m², mixed with 500 ml of dextrose solution (5%), and used intravenously for more than 30 min. The second day of aqupla treatment was comparable to the NP group.

Both groups will be treated in three-week cycles. At each cycle, the patient's systemic status and treatment efficacy will be assessed. If the patient deteriorates or cannot tolerate the treatment, the chemotherapy regimen will be discontinued. Patients in both groups will receive two to six cycles of chemotherapy.

2.5 Follow-up

The follow-up duration in the study was five years. We used medical record searches as well as outpatient and telephone visits to follow up the patients. During the five-year duration, we kept detailed records of the patients' outpatient visits. We also looked at the patient's overall health status, including but not limited to whether the disease had recurred or metastasised, as well as whether the patient had survived or died. Five-year over survival (OS): This is calculated from the time the patient was first diagnosed with a relapse until the patient's death within five years. Progression-Free Survival (PFS): The duration from the end of the patient's first relapse therapy to the point of disease progression, relapse, or patient death, with the first of these three conditions as the endpoint.

2.6 Clinical outcome assessment

At the end of chemotherapy, the overall clinical outcomes of patients in the NP and ND groups were compared and analysed between drug-resistant and susceptible patients in the two groups, judged in the light of the World Health Organization (WHO) criteria for assessing the effectiveness on solid tumours (16). Changes in tumour markers and CD cells prior and post therapy were compared between the NP and ND groups, as assessed according to the WTO classification criteria for acute and subacute toxic reactions to anticancer drugs (17). Cox regression was conducted for analysing the prognostic factors affecting patients' 5-year OS as well as PFS, and survival curves were plotted for the prognostic factors. The flow chart of this study is as follows (Figure 1).

2.7 Statistical analyses

This present study was conducted using GraphPad 8 software package to draw the required pictures. The distribution of the measured data was tested using the K-S test, and when the data were normally distributed data were tested using the t-test, intergroup comparisons were made using the independent samples t-test (for comparison of testing indicators between the pre-treatment and post-treatment NP and ND groups), and intragroup comparisons were made using the paired t-test (for comparison of testing indicators between the pre-treatment and post-treatment NP, ND groups), and were expressed in t. Non-normally distributed data were analysed by the rank sum test, and were expressed as Z. Count data were described through rate (%), using chi-square test, described by $\chi 2$, K-M survival curves were used to plot patients' 2-year survival, and multifactorial Cox regression was performed for analysing the independent prognostic factors affecting 5-year OS and PFS in ROC patients. A variance inflation factor (VIF) was used to assess collinearity between each predictor variable in the model. According to conventional statistical criteria, VIF values greater than 10 are considered to indicate significant collinearity, while VIF values for all variables in our analysis are below 5, indicating that there is no significant collinearity problem in our model (Supplementary Tables S1, S2). $P<0.05$ implies a notable difference.

3 Results

3.1 Inter-group comparison of general clinical data

Inter-group comparison of the clinical characteristics revealed no statistically significant differences in age, FIGO staging, pathological type, initial surgical treatment, ECOG score, maximum diameter of recurrent lesions, number of recurrent lesions, response to platinum drugs, history of diabetes mellitus, and history of hypertension between the NP and ND groups ($P>0.05$, Table 1). The age, FIGO staging, pathological type, initial surgical treatment, ECOG score, maximum diameter of recurrent lesions, number of recurrent lesions, response to platinum drugs, history of diabetes mellitus and history of hypertension were not statistically different between the NP and ND groups ($P>0.05$, Table 1).

Comparison of treatment efficacy between patients with resistance and sensitivity.

Firstly, the remission of NP group patients was compared, and no notable difference was observed between the overall number of remissions of resistance patients and sensitivity patients ($\chi 2$ = 2.848,0.091), while a conspicuous difference was found between the overall number of remission of ND group resistance patients and sensitivity patients ($\chi 2$ = 5.760,0.016). Whereas there existed no

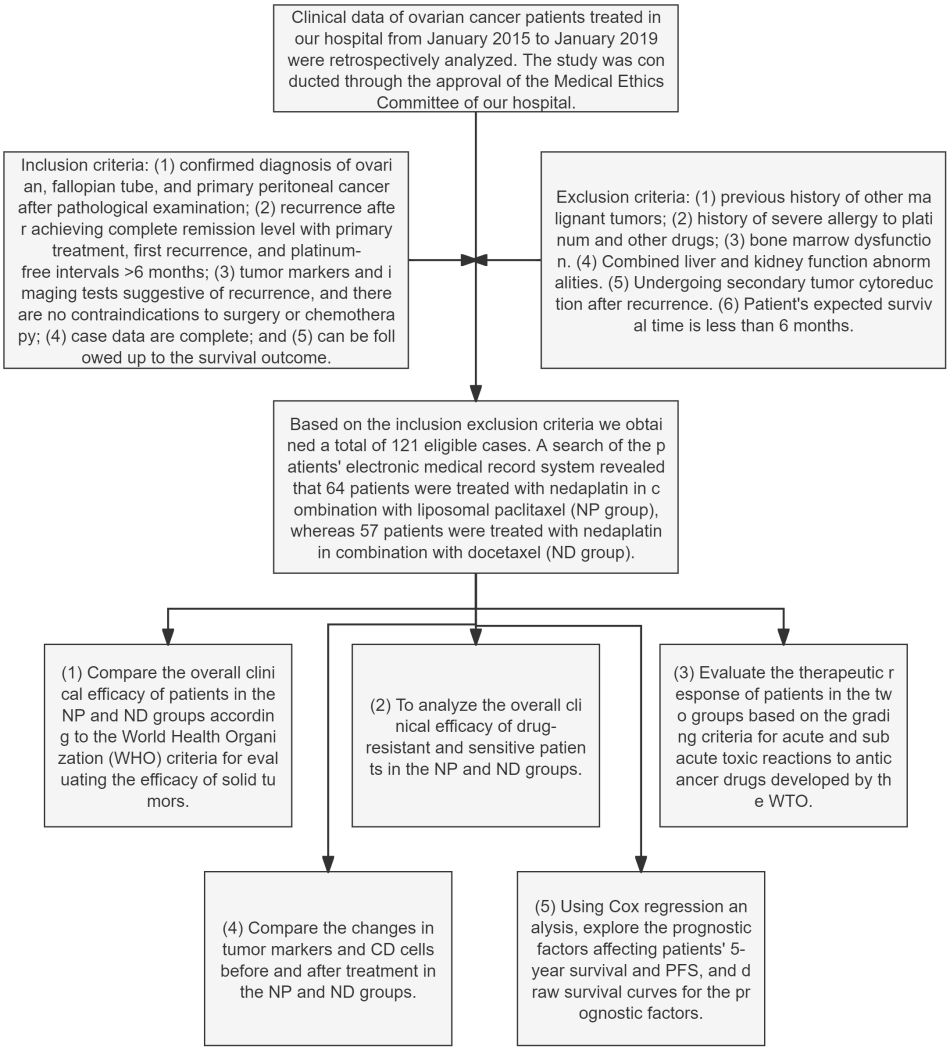

FIGURE 1
Flowchart for the research Paclitaxel liposome treatment (NP group), and Docetaxel treatment (ND group).

notable inter-group difference regarding the overall remission rate ($\chi 2$ = 0.005,0.940, Figure 2).

3.2 Changes in tumour markers before and after treatment

The CEA, CA125 and CA19–9 levels were compared between the two groups prior and post treatment, and no conspicuous difference was found between the two groups in terms of CEA, CA125 and CA19–9 before treatment (P>0.05, Figure 3). The serum CEA, CA125 and CA19–9 in both groups decreased notably after therapy (P<0.05, Figure 3), but further comparison showed notably higher serum CA125 in NP group patients in contrast to ND group patients (P<0.05), whereas no notable difference existed between the two groups in CEA and CA19–9 (P>0.05, Figure 3). No notable inter-group difference was observed regarding CEA and CA19–9 after treatment (P>0.05, Figure 3).

3.3 Changes in immune function before and after treatment

Inter-group comparison of CD3, CD4 and CD8 levels before and after treatment revealed no notable difference in CD3, CD4 and CD8 between the two groups before therapy (P>0.05, Figure 4). After therapy, the serum levels of CD3 and CD4 increased significantly, while CD8 decreased significantly (P<0.05, Figure 4), and further comparison showed no notable inter-group difference in the CD3, CD4 and CD8 levels between after treatment (P>0.05, Figure 4).

3.4 Statistical analysis of adverse reactions in two patient groups

The adverse reactions of the two groups revelled no notable differences between the two groups regarding leukopenia,

10.3389/fonc.2024.1422117

TABLE 1 Comparison of general clinical data between two patient groups.

Clinical characteristic		NP group (n=64)	ND group (n=57)	χ2/t	P
Age		54.00 [44.75,66.00]	51.00 [47.00,62.00]	0.719	0.473
FIGO staging					
	I-II	16	18	0.646	0.422
	III-IV	48	39		
Pathological type					
	Serous	38	30	0.557	0.455
	Other	26	27		
Initial surgical treatment					
	Yes	60	50	1.327	0.249
	No	4	7		
ECOG score					
	0–1	48	44	0.08	0.778
	≥2	16	13		
Maximum diameter of recurrent lesions					
	<4cm	42	29	2.704	0.1
	≥4cm	22	28		
Number of recurrent lesions					
	1	29	22	0.558	0.455
	>1	35	35		
Response to platinum drugs					
	Sensitivity	22	23	0.461	0.497
	Resistance	42	34		
History of diabetes mellitus					
	Present	14	16	0.621	0.431
	Absent	50	41		
History of hypertension					
	Present	16	11	0.565	0.452
	Absent	48	46		

International Federation of Gynecology and Obstetrics Staging (FIGO) staging, Eastern Cooperative Oncology Group Performance Status (ECOG) score.

thrombocytopenia, haemoglobin reduction, gastrointestinal reactions, muscle pain, hepatic impairment and renal impairment (P>0.05, Table 2).

3.5 Survival analysis

In order to determine the survival factors affecting ROC patients, we analysed patients' five-year OS and PFS separately by Cox regression. Cox regression analysis of five-year survival identified FIGO staging (P=0.033, HR=0.456, 95%CI=0.222–0.938), number of recurrent lesions (P<0.001, HR=0.268, 95% CI=0.140–0.513) and pre-treatment CA125 (P=0.005, HR=1.001, 95%CI=1.000–1.002) as independent prognostic factors for 5-year OS in ROC patients (Table 3, Figure 5). While PFS Cox regression analysis identified treatment regimen (P=0.004, HR=1.759, 95% CI=1.196),FIGO staging (P=0.007, HR=0.568, 95%CI=0.376–0.858), number of recurrent lesions (P<0.001, HR=0.416, 95% CI=0.285–0.608) and pre-treatment CA125 (P=0.002, HR=1.001, 95%CI=1.000–1.002) as the independent prognostic factors for PFS of ROC patients (Table 4, Figure 6).

4 Discussion

Even after standardised treatment, the overall survival of OC patients is still unsatisfactory, mainly due to the high recurrence rate of OC (18, 19). For ROC patients, the main goals of treatment include prolonging survival and lifting quality of life. Therefore, an in-depth study of the factors affecting ROC and a comparison of the effects of different treatments are of great clinical significance to increase the PFS from the first recurrence to the next progression of the disease and to improve the overall survival after recurrence.

In the study, we found no notable difference in the number of overall remissions between patients with resistance and sensitivity in the NP group, while the number of overall remissions in patients with sensitivity in the ND group was higher in contrast to patients with resistance, and there was no inter-group difference in the statistics of toxic side effects. It is suggested that aqupla in combination with docetaxel is more suitable for the therapy of platinum-sensitive ROC and does not increase the side effects in patients. We believe that this is due to the fact that docetaxel, as a microtubule stabiliser, inhibits cell division by preventing the depolymerisation of microtubules, leading to cancer cell death (20). Although its mechanism is similar to that of paclitaxel, docetaxel has a different chemical structure and exhibits stronger inhibitory effects on resistant tumour cells. This is particularly true in patients exhibiting resistance to platinum-based drugs or paclitaxel, and is the reason why docetaxel is more effective in the therapy of patients with aqupla-sensitive ROC.

CA125, as one membrane-associated protein, is extensively adopted in the diagnosis, therapy monitoring and recurrence monitoring of OC. Although it is not a marker specific to OC, it plays an important role in diagnostic assistance, assessment of treatment efficacy, monitoring of disease recurrence, and prognostic assessment (21, 22). For example, Liu et al. (23) suggested that increased serum levels of CA125 are one biomarker that can be adopted for modifying the prognosis of OC as determined by BRCA mutations and family history. Additionally, Gong et al. (24) implied that elevated expression of CA125 is strongly bound up with the condition of OC, and when its expression exceeds 175.243 kU/L, it suggests that patients with OC have a high risk of unfavourable prognosis, and should be intervened in early stage to prevent the recurrence or metastasis of OC. We found that the changes of tumour markers and CD cells were positive in both groups through treatment, but interestingly, except for CA125, the rest of the indicators were not notably

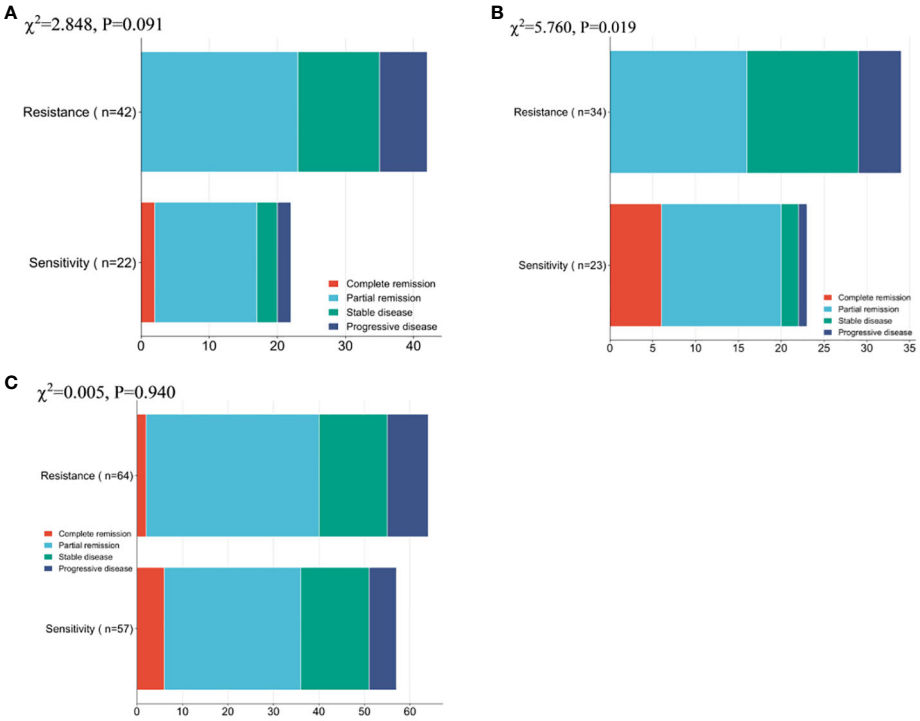

FIGURE 2
Patient Clinical Efficacy Assessment **(A)** Comparison of the overall number of remissions between drug-resistant and sensitive patients in the NP group. **(B)** Comparison of the overall number of remissions between drug-resistant patients and sensitive patients in the ND group. **(C)** Comparison of the overall number of patients in remission between patients in the NP group and patients in the ND group. Paclitaxel liposome treatment (NP group), and Docetaxel treatment (ND group).

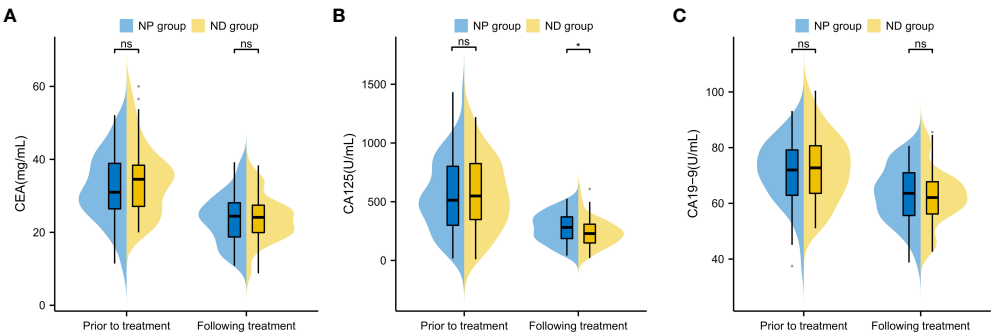

FIGURE 3
Comparison of Tumour Marker Changes Before and After Treatment in Patients **(A)** Inter-group Comparison of CEA Levels Before and After Treatment **(B)** Inter-group Comparison of CA125 Levels Before and After Treatment **(C)** Inter-group Comparison of CA19–9 Levels Before and After Treatment Note: Carcinoembryonic Antigen (CEA), Cancer Antigen 125 (CA125), Cancer Antigen 19–9 (CA19–9), Paclitaxel liposome treatment (NP group), and Docetaxel treatment (ND group).

different between the two groups after treatment. In the ND group, CA125 was lower than that of NP patients after treatment, suggesting that the aqupla combined with docetaxel regimen may be more effective in reducing the tumour load. Therefore, in the treatment and management of OC, changes in the CA125 level can reflect the response to treatment, in which a decrease in the level usually indicates that the treatment is effective, while an increase in the level can indicate progression or recurrence of the disease, which should be intervened and prevented at an early stage.

Screening for prognostic factors in ROC patients is essential for identifying key variables, and by analysing these factors, physicians are able to optimise treatment strategies, improve treatment outcomes and patients' quality of life (25, 26), and provide important guidance in the development of novel therapeutic approaches and the formulation of effective follow-up plans.

At the end of the study we used Cox regression to screen the factors affecting 5-year OS and PFS of patients. Our results showed that FIGO staging, number of recurrent lesions and pretreatment

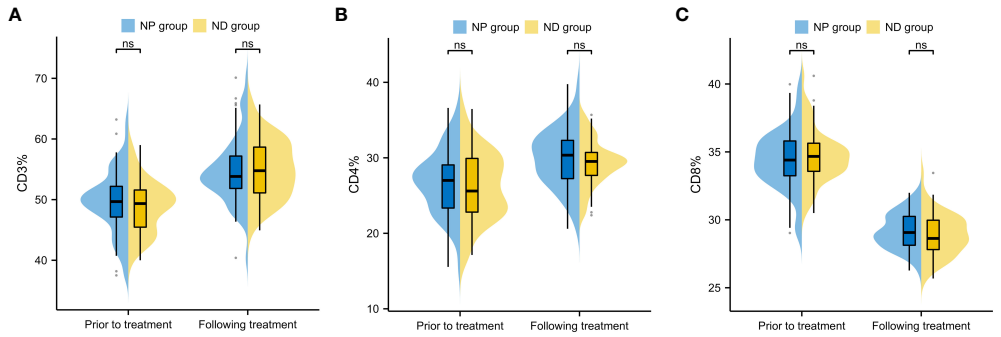

FIGURE 4
Comparison of changes in immune function indexes before and after treatment of patients **(A)** Inter-group comparison of CD3 level changes before and after treatment **(B)** Inter-group comparison of CD4 level changes before and after treatment. **(C)** Inter-group comparison of CD8 level changes before and after treatment. Cluster of Differentiation 3 (CD3), Cluster of Differentiation 4 (CD4), Cluster of Differentiation 8 (CD8), Paclitaxel liposome treatment (NP group), and Docetaxel treatment (ND group).

CA125 were independent prognostic factors for 5-year OS and PFS in ROC patients. And interestingly we found that ND regimen prolonged PFS in ROC patients. FIGO staging ≥ III-IV means that the cancer is more advanced and has spread to the peritoneum or lymph nodes. In this case, the cancer is not only more difficult to treat, but also increases the chance of recurrence. Table 1 also shows a higher number of patients with stage III-IV in contrast to that of stage I-II, which means that the higher the staging, the worse the

TABLE 2 Account of adverse drug reactions.

Adverse reactions	NP group (n=64)			ND group (n=57)			χ2	P
	Grade 0	Grade I-II	Grade III-IV	Grade 0	Grade I-II	Grade III-IV		
Leukopenia	5	43	16	6	31	20	2.083	0.353
Thrombocytopenia	56	8	1	46	9	3	1.646	0.439
Anaemia	58	6	0	48	9	1	2.254	0.324
Gastrointestinal reactions	29	33	2	31	26	0	2.501	0.286
Myalgia	45	19	0	35	22	0	1.068	0.301
Hepatic impairment	35	29	0	33	23	1	1.351	0.509
Renal impairment	32	32	0	26	31	0	0.232	0.630

TABLE 3 Five-year OS in patients with recurrent ovarian cancer Cox regression analysis.

	Univariate Cox regression				Multivariate Cox regression			
	P	HR	Lower	Upper	P	HR	Lower	Upper
Treatment regimen	0.932	0.977	0.570	1.675				
Age	0.196	1.434	0.830	2.476				
FIGO staging	0.020	0.427	0.208	0.875	0.033	0.456	0.222	0.938
Pathological type	0.673	1.126	0.649	1.953				
Initial surgical treatment	0.740	1.189	0.429	3.294				
ECOG score	0.390	1.339	0.689	2.601				
Maximum diameter of recurrent lesions	0.860	0.952	0.553	1.640				
Number of recurrent lesions	0.000	0.285	0.149	0.543	<0.001	0.268	0.140	0.513

(Continued)

TABLE 3 Continued

	Univariate Cox regression				Multivariate Cox regression			
	P	HR	Lower	Upper	P	HR	Lower	Upper
Response to platinum drugs	0.731	1.101	0.635	1.910				
History of diabetes mellitus	0.622	1.166	0.633	2.147				
History of hypertension	0.082	0.513	0.242	1.088				
Pre-treatment CA125	0.007	1.001	1.000	1.002	0.005	1.001	1.000	1.002
Pre-treatment CA19–9	0.890	1.002	0.979	1.025				
Pre-treatment CEA	0.380	0.987	0.958	1.016				
Pre-treatment CD3	0.686	1.013	0.953	1.076				
Pre-treatment CD4	0.816	1.007	0.948	1.070				
Pre-treatment CD8	0.762	0.980	0.861	1.116				

International Federation of Gynecology and Obstetrics Staging(FIGO) staging, Eastern Cooperative Oncology Group Performance Status (ECOG) score, Carcinoembryonic Antigen (CEA), Cancer Antigen 125 (CA125), and Cancer Antigen 19–9 (CA19–9), Cluster of Differentiation 3 (CD3), Cluster of Differentiation 4 (CD4), and Cluster of Differentiation 8 (CD8).

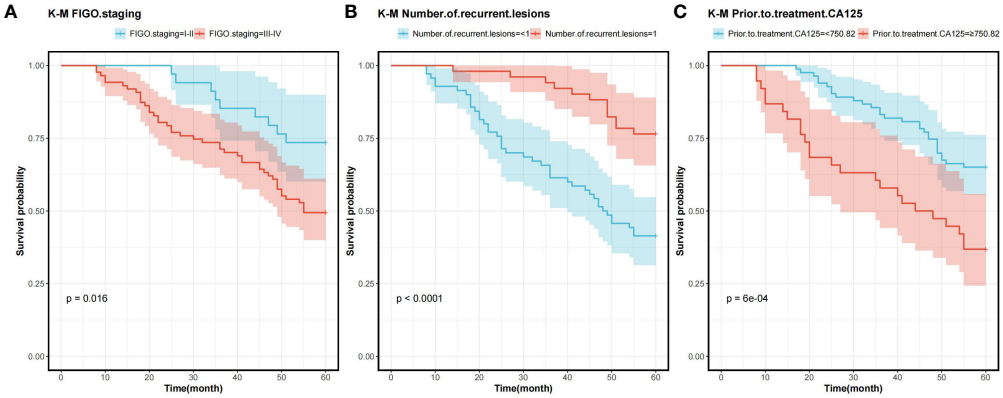

FIGURE 5
Survival curves for 5-year OS prognostic factors **(A)** 5-year OS curves comparing patients with different FIGO staging **(B)** 5-year OS curves comparing patients with different number of recurrent lesions **(C)** 5-year OS curves comparing patients with high and low CA125 expression. Overall survival rate (OS), International Federation of Gynecology and Obstetrics Staging(FIGO), and Cancer Antigen 125 (CA125).

TABLE 4 Five-year PFS in patients with recurrent ovarian cancer Cox regression analysis.

	Univariate Cox regression				Multivariate Cox regression			
	P	HR	Lower	Upper	P	HR	Lower	Upper
Treatment regimen	0.009	1.660	1.136	2.425	0.004	1.759	1.196	2.588
Age	0.689	1.081	0.738	1.584				
FIGO staging	0.006	0.569	0.380	0.852	0.007	0.568	0.376	0.858
Pathological type	0.531	1.123	0.781	1.614				
Initial surgical treatment	0.451	1.271	0.681	2.373				
ECOG score	0.660	1.101	0.718	1.687				
Maximum diameter of recurrent lesions	0.171	1.294	0.895	1.871				

(Continued)

TABLE 4 Continued

	Univariate Cox regression				Multivariate Cox regression			
	P	HR	Lower	Upper	P	HR	Lower	Upper
Number of recurrent lesions	0.000	0.477	0.329	0.690	0.000	0.416	0.285	0.608
Response to platinum drugs	0.894	0.975	0.670	1.418				
History of diabetes mellitus	0.617	1.112	0.733	1.686				
History of hypertension	0.203	0.756	0.491	1.163				
Pre-treatment CA125	0.005	1.001	1.000	1.001	0.002	1.001	1.000	1.002
Pre-treatment CA19–9	0.197	0.990	0.975	1.005				
Pre-treatment CEA	0.298	0.989	0.970	1.009				
Pre-treatment CD3	0.723	1.008	0.966	1.051				
Pre-treatment CD4	0.793	1.005	0.967	1.045				
Pre-treatment CD8	0.829	1.010	0.922	1.106				

International Federation of Gynecology and Obstetrics Staging (FIGO) staging, Eastern Cooperative Oncology Group Performance Status (ECOG) score, Carcinoembryonic Antigen (CEA), Cancer Antigen 125 (CA125), and Cancer Antigen 19–9 (CA19–9), Cluster of Differentiation 3 (CD3), Cluster of Differentiation 4 (CD4), and Cluster of Differentiation 8 (CD8).

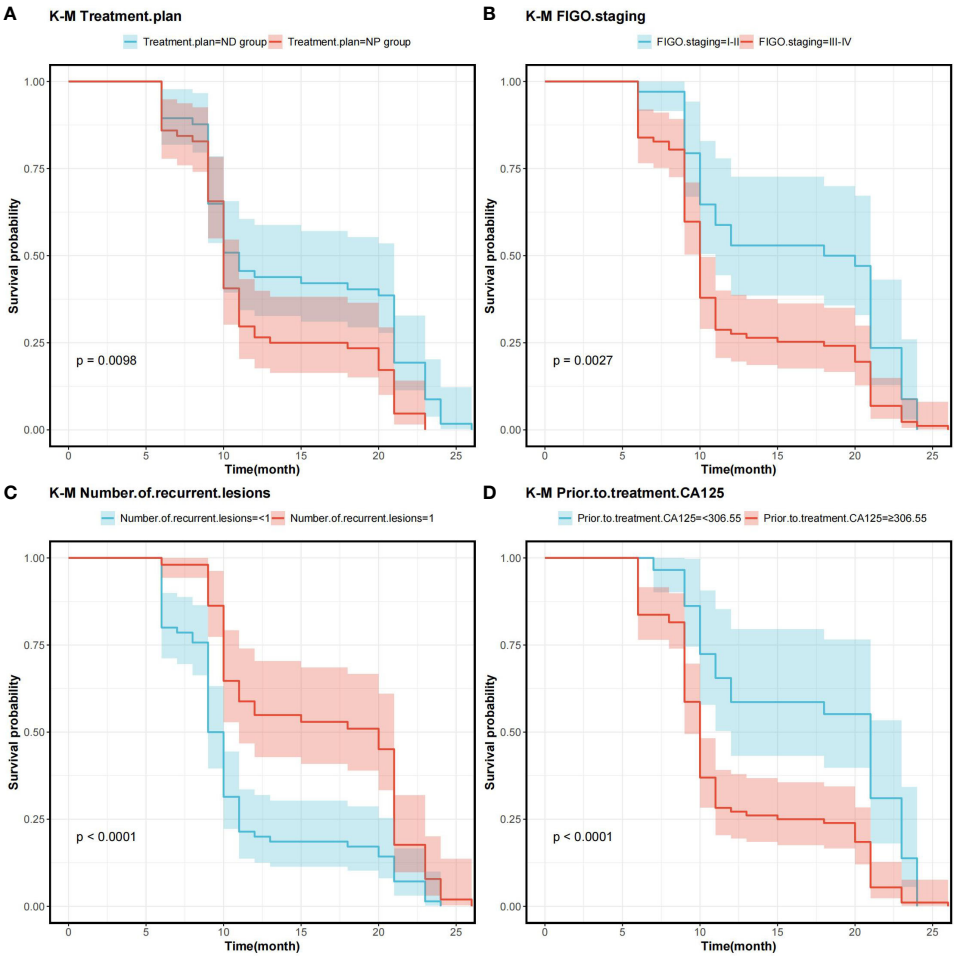

FIGURE 6
Survival curves on prognostic factors for PFS **(A)** PFS curves for comparing various treatment regimens in patients. **(B)** PFS curves based on different FIGO staging in patients. **(C)** PFS curves of patients with varying numbers of recurrent lesions. **(D)** PFS curves comparing patients with high and low CA125 expression Note: Progression-Free Survival (PFS), International Federation of Gynecology and Obstetrics Staging(FIGO), and Cancer Antigen 125 (CA125).

prognosis of the patients usually is. For example, FIGO III-IV was identified as one independent prognostic factor for OS and PFS in OC patients in research by Bai et al. (27). In addition, a SEER database –based study proposed FIGO staging as an independent prognostic factor for malignant germ cell tumours of the ovary (28). In addition, a study by Shibuya (29) et al. similarly suggested that an increase in clinical stage leads to a poorer postoperative prognosis in patients with OC, resulting in a decrease in the overall survival of the patients. An increase in the number of recurrent lesions reflects the extensive and heterogeneous nature of the tumour and is indicative of a greater capacity for tumour survival and spread. Multiple recurrent lesions imply that the tumour is resistant to prior treatment and more difficult to control with local therapy, leading to a poorer prognosis. In a multicentre study, an analysis of prognostic factors in 670 patients with recurrent epithelial OC revealed a notably worse prognosis in patients with ≥3 recurrent sites (30). Also in a study by Fan et al. (31), it was found that patients with 1 recurrent lesion had significantly longer median survival and OS compared to patients with recurrent epithelial OC with more than 1 lesion.

Additionally, research by Zang et al. (32) suggested that the extent of recurrent disease (single or multiple) is critical in determining the prognosis of patients with ovarian tumours of malignant potential. CA125 is one crucial biomarker for OC, and its high level is often linked to high tumour load and disease activity. The association of CA125 with OC prognosis has been reported in several articles. For example, Fleming et al. (33) suggested that continuous CA125 monitoring for early detection of recurrence might improve the optimal rate of secondary cytoreduction and potentially impact the overall survival of ROC patients. Another report showed (34) that the therapy effect of platinum-refractory/resistance ROC could be predicted by the reduction of CA125 levels after 2 courses of treatment. The ND regimen prolongs PFS in ROC patients, mainly because of the unique mechanism of action of docetaxel and its synergistic effect with aqupla. Docetaxel, as a microtubule stabiliser, is able to inhibit cancer cell division by hindering microtubule depolymerisation, a mechanism that may show enhanced activity in cancer cells resistant to conventional therapy (35–37). When combined with aqupla, a platinum drug capable of forming DNA cross-links, the two drugs act at different phases of the cell cycle, generating a powerful synergistic effect that enhances anti-tumour activity and thus prolongs PFS more effectively.

5 Study limitations

In the present study, we faced several key limitations in examining the effects of NP versus ND regimens on survival and biomarkers in ROC patients. First, the study in retrospective design probably has been affected by selection bias and information bias. Additionally, the number of samples in the study was limited, comprising only 121 patients, and this small sample size may have affected the efficacy of the statistical analyses. Finally, as a single-centre study, extrapolation of the results may be limited because the population and treatment setting covered by the study might not be reflective of other regions or countries. We hope future research will need to validate and extend our findings using a larger, multicentre and randomised controlled design to verify the conclusions.

6 Future research directions

Given these limitations, future studies should aim to validate and expand upon our results. A larger, multicentre approach is crucial to increase sample size and variability, providing a more comprehensive analysis. Additionally, adopting a randomized controlled design can offer more robust evidence by reducing biases and confounding factors. Such research would be invaluable in verifying our conclusions and enhancing the external validity of these findings, thereby enabling better-informed clinical decisions regarding NP and ND regimens in ROC patients.

7 Conclusion

In ROC patients, particularly platinum-sensitive patients, the aqupla in combination with docetaxel regimen provided an improved survival benefit with a comparable safety profile, underscoring the importance of individualised treatment strategies.

Data availability statement

The original contributions presented in the study are included in the article/Supplementary Material. Further inquiries can be directed to the corresponding author.

Ethics statement

The studies involving humans were approved by ethics committee of Women's and Children's Hospital of Ningbo University. The studies were conducted in accordance with the local legislation and institutional requirements. The participants provided their written informed consent to participate in this study.

Author contributions

JY: Conceptualization, Data curation, Methodology, Writing – original draft. MZ: Formal analysis, Software, Validation, Writing – original draft. YZ: Formal analysis, Methodology, Writing – original draft. LZ: Formal analysis, Investigation, Writing – original draft. QW: Formal analysis, Supervision, Writing – review & editing.

Funding

The author(s) declare that no financial support was received for the research, authorship, and/or publication of this article.

Conflict of interest

The authors declare that the research was conducted in the absence of any commercial or financial relationships that could be construed as a potential conflict of interest.

Publisher's note

All claims expressed in this article are solely those of the authors and do not necessarily represent those of their affiliated organizations, or those of the publisher, the editors and the reviewers. Any product that may be evaluated in this article, or claim that may be made by its manufacturer, is not guaranteed or endorsed by the publisher.

Supplementary material

The Supplementary Material for this article can be found online at: https://www.frontiersin.org/articles/10.3389/fonc.2024.1422117/full#supplementary-material

References

1. Torre LA, Trabert B, DeSantis CE, Miller KD, Samimi G, Runowicz CD, et al. Ovarian cancer statistics, 2018. *CA Cancer J Clin*. (2018) 68:284–96. doi: 10.3322/caac.21456

2. Stone R, Sakran JV, Long Roche K. Salpingectomy in ovarian cancer prevention. *Jama*. (2023) 329:2015–6. doi: 10.1001/jama.2023.6979

3. Stewart C, Ralyea C, Lockwood S. Ovarian cancer: an integrated review. *Semin Oncol Nurs*. (2019) 35:151–6. doi: 10.1016/j.soncn.2019.02.001

4. Harter P, Sehouli J, Vergote I, Ferron G, Reuss A, Meier W, et al. Randomized trial of cytoreductive surgery for relapsed ovarian cancer. *N Engl J Med*. (2021) 385:2123–31. doi: 10.1056/NEJMoa2103294

5. Mutlu Sütcüoğlu B, Sütcüoğlu O. Cytoreductive surgery with or without hyperthermic intraperitoneal chemotherapy in advanced ovarian cancer. *Lancet Oncol*. (2023) 24:e457. doi: 10.1016/S1470-2045(23)00471-0

6. Osann K, Wenzel L, McKinney C, Wagner L, Cella D, Fulci G, et al. Fear of recurrence, emotional well-being and quality of life among long-term advanced ovarian cancer survivors. *Gynecol Oncol*. (2023) 171:151–8. doi: 10.1016/j.ygyno.2023.02.015

7. Pignata S, CC S, Du Bois A, Harter P, Heitz F. Treatment of recurrent ovarian cancer. *Ann Oncol*. (2017) 28:viii51–viii6. doi: 10.1093/annonc/mdx441

8. Francis KE, Kim SI, Friedlander M, Gebski V, Ray-Coquard I, Clamp A, et al. The impact of olaparib dose reduction and treatment interruption on treatment outcome in the SOLO2/ENGOT-ov21 platinum-sensitive recurrent ovarian cancer. *Ann Oncol*. (2022) 33:593–601. doi: 10.1016/j.annonc.2022.02.222

9. Buechel M, Herzog TJ, Westin SN, Coleman RL, Monk BJ, Moore KN. Treatment of patients with recurrent epithelial ovarian cancer for whom platinum is still an option. *Ann Oncol*. (2019) 30:721–32. doi: 10.1093/annonc/mdz104

10. Lheureux S, Cristea MC, Bruce JP, Garg S, Cabanero M, Mantia-Smaldone G, et al. Adavosertib plus gemcitabine for platinum-resistant or platinum-refractory recurrent ovarian cancer: a double-blind, randomised, placebo-controlled, phase 2 trial. *Lancet*. (2021) 397:281–92. doi: 10.1016/S0140-6736(20)32554-X

11. Kase AM, Azzouqa AG, Kochuveettil S, Colon-Otero G. Efficacy of gemcitabine in combination with nanoparticle albumin-bound paclitaxel in the treatment of recurrent ovarian cancer: A retrospective single institution review. *Cancer Med*. (2023) 12:9434–8. doi: 10.1002/cam4.5705

12. Wang J, Han N, Wang HL, Zhang ZM, Fan QX. [Therapeutic effect of docetaxel combined with oxaliplatin for treatment of recurrent epithelial ovarian cancer]. *Nan Fang Yi Ke Da Xue Xue Bao*. (2009) 29:2319–20.

13. Boere I, Vergote I, Hanssen R, Jalving M, Gennigens C, Ottevanger P, et al. CINOVA: a phase II study of CPC634 (nanoparticulate docetaxel) in patients with platinum resistant recurrent ovarian cancer. *Int J Gynecol Cancer*. (2023) 33:1247–52. doi: 10.1136/ijgc-2023-004308

14. Berek JS, Renz M, Kehoe S, Kumar L, Friedlander M. Cancer of the ovary, fallopian tube, and peritoneum: 2021 update. *Int J Gynaecol Obstet*. (2021) 155 Suppl 1:61–85. doi: 10.1002/ijgo.13878

15. Mischel AM, Rosielle DA. Eastern cooperative oncology group performance status 434. *J palliative Med*. (2022) 25:508–10. doi: 10.1089/jpm.2021.0599

16. Moore KN, Oza AM, Colombo N, Oaknin A, Scambia G, Lorusso D, et al. randomized trial of mirvetuximab soravtansine versus chemotherapy in patients with platinum-resistant ovarian cancer: primary analysis of FORWARD I. *Ann Oncol*. (2021) 32:757–65. doi: 10.1016/j.annonc.2021.02.017

17. Wu MF, Liang JX, Li H, Ye YF, Liang WF, Wang LJ, et al. Effects of neoadjuvant hyperthermic intraperitoneal chemotherapy on chemotherapy response score and recurrence in high-grade serous ovarian cancer patients with advanced disease: A multicentre retrospective cohort study. *BJOG: an Int J obstetrics gynaecology*. (2022) 129 Suppl 2:5–13. doi: 10.1111/1471-0528.17323

18. Baek MH, Park EY, Ha HI, Park SY, Lim MC, Fotopoulou C, et al. Secondary cytoreductive surgery in platinum-sensitive recurrent ovarian cancer: A meta-analysis. *J Clin Oncol*. (2022) 40:1659–70. doi: 10.1200/JCO.21.02085

19. Pujade-Lauraine E, Combe P. Recurrent ovarian cancer. *Ann Oncol*. (2016) 27 Suppl 1:i63–i5. doi: 10.1093/annonc/mdw079

20. Zhou HH, Chen X, Cai LY, Nan XW, Chen JH, Chen XX, et al. Erastin reverses ABCB1-mediated docetaxel resistance in ovarian cancer. *Front Oncol*. (2019) 9:1398. doi: 10.3389/fonc.2019.01398

21. Zhao H, Wu L, Dai J, Sun K, Zi Z, Guan J, et al. Ligand-based adoptive T cell targeting CA125 in ovarian cancer. *J Transl Med*. (2023) 21:596. doi: 10.1186/s12967-023-04271-8

22. Charkhchi P, Cybulski C, Gronwald J, Wong FO, Narod SA, Akbari MR. CA125 and ovarian cancer: A comprehensive review. *Cancers (Basel)*. (2020) 12:3730. doi: 10.3390/cancers12123730

23. Liu W, Wang Z, Ma J, Hou Y, Zhao J, Dong B, et al. Elevated serum level of CA125 is a biomarker that can be used to alter prognosis determined by BRCA mutation and family history in ovarian cancer. *Genet Test Mol Biomarkers*. (2017) 21:547–54. doi: 10.1089/gtmb.2017.0104

24. Gong Z, Han S, Zhang C, Zhao H, Xu J, Sun X. Value of serum miR-21, HE4 and CA125 in surveillance for postoperative recurrent or metastatic ovarian cancer. *Pak J Med Sci*. (2022) 38:939–45. doi: 10.12669/pjms.38.4.5158

25. Li H, Li M, Tang C, Xu L. Screening and prognostic value of potential biomarkers for ovarian cancer. *Ann Transl Med*. (2021) 9:1007. doi: 10.21037/atm

26. Faaborg L, Andersen RF, Waldstrøm M, Henriksen JR, Adimi P, Jakobsen A, et al. Prognostic impact of circulating methylated homeobox A9 DNA in patients undergoing treatment for recurrent ovarian cancer. *Cancers (Basel)*. (2022) 14:1766. doi: 10.3390/cancers14071766

27. Bai G, Zhou Y, Rong Q, Qiao S, Mao H, Liu P. Development of nomogram models based on peripheral blood score and clinicopathological parameters to predict preoperative advanced stage and prognosis for epithelial ovarian cancer patients. *J Inflammation Res*. (2023) 16:1227–41. doi: 10.2147/JIR.S401451

28. Shao C, Guo H, Chen L, Chen J, Wang L, Wang H. Prognostic factors and clinic-pathologic characteristics of ovarian tumor with different histologic subtypes-a SEER database population study of 41,376 cases. *Transl Cancer Res*. (2023) 12:1937–50. doi: 10.21037/tcr

29. Shibuya Y, Shimada M, Tsuji K, Shigeta S, Tanase Y, Matsuo K, et al. Prognostic factors of 2018 FIGO stage IB-IIA cervical cancer with absence of high/intermediate surgical-pathological risk factors. *Jpn J Clin Oncol*. (2022) 52:1289–96. doi: 10.1093/jjco/hyac125

30. Son JH, Kong TW, Park SJ, Lee EJ, Kim HS, Kim NK, et al. Optimum selection criteria for secondary cytoreductive surgery in patients with recurrent epithelial ovarian cancer: A multicenter study from the Gynecologic Oncology Research Investigators coLLaborAtion group (GORILLA-3001). *J Surg Oncol*. (2023) 128:645–52. doi: 10.1002/jso.27303

31. Fan XM, Zhang J, Niu SH, Li KX, Song CZ. Secondary cytoreductive surgery in recurrent epithelial ovarian cancer: A prognostic analysis with 103 cases. *Int J Surg*. (2017) 38:61–6. doi: 10.1016/j.ijsu.2016.12.031

32. Zang RY, Yang WT, Shi DR, Xing Y, Cai SM. Recurrent ovarian carcinoma of low Malignant potential: the role of secondary surgical cytoreduction and the prognosis in Chinese patients. *J Surg Oncol*. (2005) 91:67–72. doi: 10.1002/jso.20280

33. Fleming ND, Cass I, Walsh CS, Karlan BY, Li AJ. CA125 surveillance increases optimal resectability at secondary cytoreductive surgery for recurrent epithelial ovarian cancer. *Gynecol Oncol*. (2011) 121:249–52. doi: 10.1016/j.ygyno.2011.01.014

34. Ooyama T, Shimoji Y, Nakasone T, Arakaki Y, Taira Y, Nakamoto T, et al. Effects of pegylated liposomal doxorubicin and CA125 level variability analysis in platinum-refractory/resistant recurrent ovarian cancer. *Anticancer Res*. (2022) 42:3017–22. doi: 10.21873/anticanres.15786

35. Taylor SE, Petschauer JS, Donovan H, Schorzman A, Razo J, Zamboni WC, et al. Phase I study of intravenous oxaliplatin and intraperitoneal docetaxel in recurrent ovarian cancer. *Int J Gynecol Cancer*. (2019) 29:147–52. doi: 10.1136/ijgc-2018-000055

36. Bruchim I, Weeg N, Alpert Y, Sade D, Piura E, Fishman A. High efficacy and low toxicity of the modified docetaxel and carboplatin protocol in patients with recurrent ovarian cancer-A phase 2 cohort study. *Int J Gynecol Cancer*. (2016) 26:640–7. doi: 10.1097/IGC.0000000000000666

37. Coleman RL, Duska LR, Ramirez PT, Heymach JV, Kamat AA, Modesitt SC, et al. Phase 1–2 study of docetaxel plus aflibercept in patients with recurrent ovarian, primary peritoneal, or fallopian tube cancer. *Lancet Oncol*. (2011) 12:1109–17. doi: 10.1016/S1470-2045(11)70244-3

frontiers | Frontiers in Pharmacology

TYPE Original Research
PUBLISHED 25 June 2024
DOI 10.3389/fphar.2024.1387647

Check for updates

OPEN ACCESS

EDITED BY
Hailin Tang,
Sun Yat-Sen University Cancer Center (SYSUCC), China

REVIEWED BY
Xiangmei Zhang,
Fourth Hospital of Hebei Medical University, China
Qianrong Huang,
Guangxi Medical University Cancer Hospital, China

*CORRESPONDENCE
Xuelei Ma,
drmaxuelei@gmail.com
Hubing Shi,
shihb@scu.edu.cn

†These authors have contributed equally to this work and share first authorship

RECEIVED 18 February 2024
ACCEPTED 04 June 2024
PUBLISHED 25 June 2024

CITATION
Xu Z, Zhao Y, Zhang Y, Liu X, Song L, Chen M, Xiao G, Ma X and Shi H (2024), Prediction of immunotherapy response of bladder cancer with a pyroptosis-related signature indicating tumor immune microenvironment. *Front. Pharmacol.* 15:1387647. doi: 10.3389/fphar.2024.1387647

COPYRIGHT
© 2024 Xu, Zhao, Zhang, Liu, Song, Chen, Xiao, Ma and Shi. This is an open-access article distributed under the terms of the Creative Commons Attribution License (CC BY). The use, distribution or reproduction in other forums is permitted, provided the original author(s) and the copyright owner(s) are credited and that the original publication in this journal is cited, in accordance with accepted academic practice. No use, distribution or reproduction is permitted which does not comply with these terms.

Prediction of immunotherapy response of bladder cancer with a pyroptosis-related signature indicating tumor immune microenvironment

Zihan Xu[1†], Yujie Zhao[1†], Yong Zhang[2†], Xiaowei Liu[1], Linlin Song[1], Meixu Chen[1], Guixiu Xiao[1], Xuelei Ma[3]* and Hubing Shi[1]*

[1]Institute for Breast Health Medicine, State Key Laboratory of Biotherapy, West China Hospital, Sichuan University and Collaborative Innovation Center, Chengdu, Sichuan, China, [2]Department of Medical Oncology, Cancer Center, West China Hospital, Sichuan University, Chengdu, Sichuan, China, [3]Department of Biotherapy, West China Hospital and State Key Laboratory of Biotherapy, Sichuan University, Chengdu, Sichuan, China

Background: Although prognostic models based on pyroptosis-related genes (PRGs) have been constructed in bladder cancer (BLCA), the comprehensive impact of these genes on tumor microenvironment (TME) and immunotherapeutic response has yet to be investigated.

Methods: Based on expression profiles of 52 PRGs, we utilized the unsupervised clustering algorithm to identify PRGs subtypes and ssGSEA to quantify immune cells and hallmark pathways. Moreover, we screened feature genes of distinct PRGs subtypes and validated the associations with immune infiltrations in tissue using the multiplex immunofluorescence. Univariate, LASSO, and multivariate Cox regression analyses were employed to construct the scoring scheme.

Results: Four PRGs clusters were identified, samples in cluster C1 were infiltrated with more immune cells than those in others, implying a favorable response to immunotherapy. While the cluster C2, which shows an extremely low level of most immune cells, do not respond to immunotherapy. CXCL9/CXCL10 and SPINK1/DHSR2 were identified as feature genes of cluster C1 and C2, and the specimen with high CXCL9/CXCL10 was characterized by more CD8 + T cells, macrophages and less Tregs. Based on differentially expressed genes (DEGs) among PRGs subtypes, a predictive model (termed as PRGs score) including five genes (CACNA1D, PTK2B, APOL6, CDK6, ANXA2) was built. Survival probability of patients with low-PRGs score was significantly higher than those with high-PRGs score. Moreover, patients with low-PRGs score were more likely to benefit from anti-PD1/PD-L1 regimens.

Conclusion: PRGs are closely associated with TME and oncogenic pathways. PRGs score is a promising indicator for predicting clinical outcome and immunotherapy response.

KEYWORDS

pyroptosis, bladder cancer, tumor microenvironment, immunotherapy, predictive model

1 Introduction

Bladder cancer (BLCA) has been reported as the 11th most prevalent cancer globally, with about 550,000 new cases per annum (Lenis et al., 2020; Teoh et al., 2020). According to epidemiological investigations, smoking is the most crucial risk factor for BLCA. Furthermore, strategies to inhibit smoking have indicated improved survival of patients with lung cancer; however, it has not indicated successful outcomes in BLCA patients (Cumberbatch et al., 2016). These observations suggest that BLCA has unique genetic/epigenetic alterations, and immune responses (Cao et al., 2020). Based on the pathological characteristics, BLCA can be divided into non-muscular invasive and muscular invasive types (Wang et al., 2023). However, different BLCA has different challenges, for instance, non-muscular invasive BLCA has a high recurrence rate after surgery, while muscular invasive BLCA indicates a very poor prognosis, with only few patients surviving more than 5 years. (Chou et al., 2016; Ghandour et al., 2019). In recent years, immunotherapy has made great progress. Anti-programmed cell death protein ligand-1 antibody (αPD-L1) has been approved by the US Food and Drug Administration (FDA) for BLCA treatment since 2016, with its usage spanning from non-muscle invasive to metastatic disease (Schneider et al., 2019). However, a significant number of BLCA patients do not respond to these treatments (Galsky et al., 2020; Powles et al., 2021). On the one hand, numerous tumors exhibit an "immune-cold" phenotype, characterized by an immunosuppressive tumor microenvironment (TME), rendering them unresponsive to current immunotherapeutic agents (Lee et al., 2022; Zhang et al., 2023). On the other hand, αPD-L1 is a viable choice only for programmed cell death protein-ligand 1 (PD-L1) positive BLCA patients, while PD-L1 expression varies between individuals (Afonso et al., 2020). Therefore, it is essential to identify driving factors in genetic/epigenetic and immune level and construct a new predictive model for immunotherapy response and survival in BLCA (He et al., 2021).

Pyroptosis is a kind of programmed cell death, with inflammation triggered by detrimental signals or pathogenic microbial infection (Frank and Vince, 2019). Furthermore, it is manifested with cell swelling, lysis, and cytoplasmic content secretion. It is an essential host resistance mechanism against infection by pathogenic microbes. However, increased or uncontrolled pyroptosis is harmful and even fatal for the host. Previous studies indicated that pyroptosis was linked with the initiation and progression of various cancers, as well as affecting the TME. Much literature has revealed that pyroptosis is critically involved in tumor development (Fang et al., 2020). Additionally, crosstalk between TME and pyroptosis has also been indicated (Orning et al., 2019; Erkes et al., 2020). TME primarily comprises endothelial cells, fibroblasts, extracellular matrix, immune and inflammatory cells, and diffuse chemokines and cytokines, which are notably associated with tumor initiation and progression (Runa et al., 2017). Currently, because of technical limitations, most research only investigated 1 or 2 pyroptosis-related genes (PRGs) in cell and animal models. However, antitumor effects require highly coordinated interactions among many genes. Therefore, comprehensive research on the characteristics of various PRGs-mediated TME cell infiltration is essential and may furnish crucial data on mechanisms of BLCA oncogenesis and progression, as well as predict the immunotherapy response.

This study aims to classify subtypes of different immune infiltrates by analyzing the PRGs in BLCA patients and construct a scoring model, for prognosis prediction and clinical treatment guidance. TCGA-BLCA patients were used to identify and validate four pyroptosis-linked subtypes that were related to immune infiltration and prognosis. Based on differentially expressed genes (DEGs) assessed by the 4 pyroptosis subtypes, the patients were categorized into two geneClusters. Moreover, the LASSO-Cox method was employed to establish the pyroptosis correlation model and elucidate the risk score. Overall, the four pyroptosis-related subtypes and scoring systems constructed in this study could predict immune infiltration, prognosis, and immunotherapy response. Additionally, the acquired data indicated a potential link between TME, pyroptosis, immunotherapy response, and prognosis in BLCA patients.

2 Materials and methods

2.1 Data sources

Figure 1 indicates the study's flowchart. BLCA sample's clinicopathological and gene expression (fragments per kilobase million, FPKM) data were acquired from The Cancer Genome Atlas (TCGA; 406 BLCA patients) (https://portal.gdc.cancer.gov/) and the Gene Expression Omnibus (GEO; 165 BLCA patients) (https://www.ncbi.nlm.nih.gov/geo/). Detailed information on the selected BLCA patients is given in Supplementary Table S1. Clinical information included tumor grade, age, TNM stage, follow-up time, sex, and survival status. Data in this research were downloaded from publicly available datasets, therefore ethics committee approval was not required.

2.2 Consensus clustering for pyroptosis-related genes in BLCA

Using the "REACTOME_PYROPTOSIS" item of MSigDB (http://www.broad.mit.edu/gsea/msigdb/) and previous literature (Ye et al., 2021), 52 PRGs were identified (details in Supplementary Table S2). Furthermore, based on the expression profiles of these PRGs, unsupervised clustering was conducted by using the "ConsensusClusterPlus" package to categorize participants into distinct molecular subtypes (termed: PRGs clusters). To ensure the cluster's reliability, clustering was repeated 1,000 times. DEGs between the different PRGs clusters were identified using the "limma" package in R with a fold-change of 1.5 and an adjusted p-value of <0.001. Finally, we screened and identified 240 DEGs. Additionally, based on expression of DEGs, unsupervised clustering was carried out to classify patients into distinct clusters (termed: geneClusters).

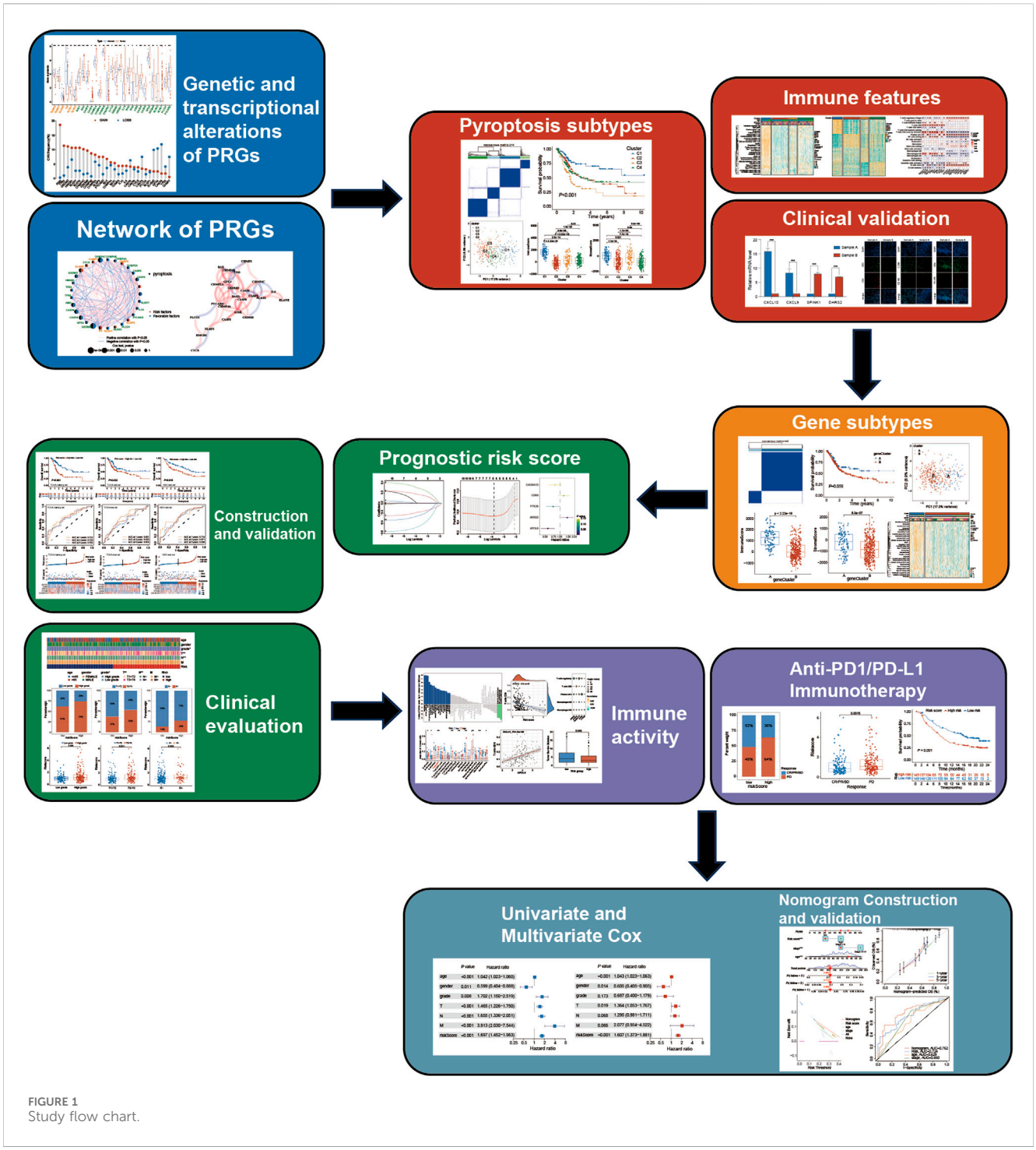

FIGURE 1
Study flow chart.

2.3 Construction and validation of the PRGs-DEGs risk score system

Using the "caret" package, TCGA acquired 406 BLCA patients who were randomly categorized in a 1:1 ratio into the train and test cohorts. Then the risk scoring system was constructed in the TCGA-train cohort. Briefly, survival-related genes were assessed via the univariate Cox regression using PRGs-DEGs, and then LASSO regression was carried out to exclude overfitting genes. To build the predictive model, the filtered genes were subjected to multivariate Cox regression using the forward/backward method.

The PRGs-DEGs risk score was calculated as follows:

$$\text{PRGs} - \text{DEGs risk score} = \Sigma\ (\text{Expi} * \text{coefi})$$

Where Expi and Coefi indicated the expression of each gene and risk coefficient, respectively. According to the median risk score value from the TCGA-train cohort, other patients from the TCGA-test and GEO cohorts were categorized into high-risk (HR) and low-risk

(LR) subgroups. The log-rank test and the Kaplan-Meier curve were applied to determine the survival differences between LR and HR subgroups. Moreover, the area under the curve (AUC) value of the receiver operating characteristic (ROC) curve was assessed to elucidate the reliability of the predictive model.

2.4 Clinical correlation and stratification analyses

The PRGs cluster's clinical value was identified via consensus clustering. Moreover, the association of PRGs clusters with clinicopathological features (including tumor grade, age, TNM stage, and sex) was compared. Furthermore, Kaplan-Meier curves were drawn by the "survival," whereas using the "survminer" R packages, the differences between overall survival (OS) and progression-free survival (PFS) among different PRGs clusters were assessed. Additionally, Chi-square tests were utilized to elucidate the relationship between PRGs-DEGs risk score and clinical features. Furthermore, univariate and multivariate analyses were conducted to evaluate if the risk score was independent of other clinicopathological parameters using the BLCA cohort. A stratified analysis was also carried out to assess if the risk score maintained its predictive ability across subgroups based on the aforementioned clinicopathological parameters.

2.5 Tumor purity analysis and single sample gene set enrichment analysis (ssGSEA)

According to the gene expression profiles, the ESTIMATE algorithm in R was employed to calculate the tumor purity of each patient including immune and stromal scores. Furthermore, the expression profiles were converted into the scoring matrix of hallmark pathways/phenotypes or immune infiltrations via the R "GSVA" package (method = "ssGSEA"). The reference hallmark gene set was acquired from GSEA (https://www.gsea-msigdb.org/gsea). Then, differential analyses of ssGSEA scores were carried out for distinct PRGs clusters, geneClusters, or HR/LR score clusters. As a continuous variable, the PRGs-DEGs risk score was evaluated for the correlation with ssGSEA scores related to hallmark pathways/phenotypes and immune infiltrations. Additionally, the association of the risk signature gene levels with ssGSEA scores of substantially altered pathways/phenotypes and immune infiltrations was assessed, respectively.

2.6 Quantitative real-time PCR (qRT-PCR)

The BLCA and para-carcinoma tissues used in this study were gifted from another research group. This research was authorized by the Institutional Research Ethics Committee of West China Hospital. For the detection of the mRNA levels of marker genes and prognostic genes, qRT-PCR was employed. Briefly, whole RNA was acquired using Trizol (Thermo Fisher Scientific), reverse transcribed to single-strand cDNA. For qRT-PCR amplification, qRT-PCR was conducted using SYBR® Green Real-time PCR Master Mix (TOYOBO). GAPDH was utilized for normalizing the relative mRNA levels. Supplementary Table S3 enlists the sequences of primers employed.

2.7 Immunofluorescence (IF)

The tissues of BLCA and para-carcinoma obtained above were paraffin-embedded. CD163, CD8, and FoxP3 were used as specific markers for tumor-associated macrophages (TAMs), CD8 + T cells, and regulatory T cells (Tregs), respectively. The samples were dewaxed in xylene, rehydrated using alcohol, blocked with the help of endogenous peroxidase, treated overnight with specific antibodies at 4°C in a humidified box, and then tagged with secondary antibodies. Lastly, the samples were counterstained with hematoxylin and visualized by diaminobenzidine.

2.8 Immunotherapy susceptibility analysis

Tumor mutational burden (TMB) was compared between the LR and HR score groups. The clinical and transcriptome data of the IMvigor210 cohort were acquired from a freely available software and data package (http://research-pub.gene.com/IMvigor210CoreBiologies). The anti-PD-L1 treated advanced urothelial carcinoma patient's dataset was utilized to assess the predictive capability of the PRGs-DEGs scoring system for immunotherapy response. The proportions of various immunotherapy responses, including the stable disease (SD), partial response (PR), complete response (CR), and progressive disease (PD). Moreover, the survival differences between the LR and HR subgroups were compared.

2.9 Establishment and validation of a nomogram for overall survival

According to the independent predictive factors such as the PRGs-DEGs scoring system ($p < 0.05$), a nomogram risk score for OS was constructed using the R "rms" package. Then, the calibration curve analysis, ROC, and decision curves analysis were carried out to elucidate the performance of the nomogram scoring system. Furthermore, calibration curves were plotted for the survival probability at 1-, 3-, and 5-year to elucidate the precision of the combined model. The clinical utility of each predictive variable was assessed via decision curve analysis. Additionally, AUC values of ROC curves were utilized to assess the reliability of each single predictive variable and the combined nomogram model.

2.10 Statistical analyses

For statistical measurement, the R software (version 4.2.5) was employed. Correlations among variables were analyzed by Pearson or Spearman coefficient. The intergroup differences in continuous variables were compared via the *t*-test. Based on the Kaplan-Meier method, the survival curves were drawn. Furthermore, the ROC curves were employed to assess the accuracy of PRGs-DEGs risk score for predicting survival and PRGs clusters. All the statistical

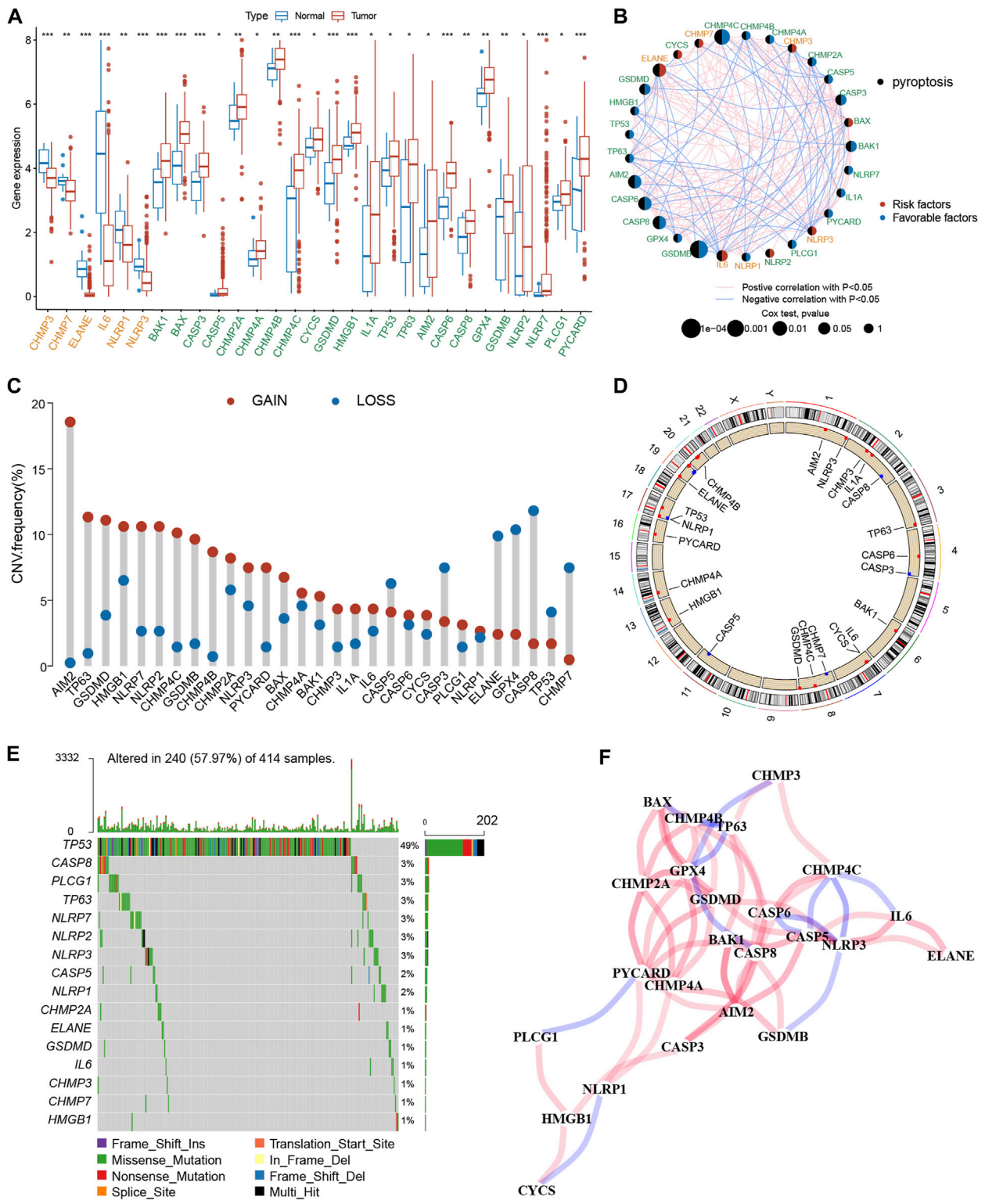

FIGURE 2
Genetic and transcriptional alterations of PRGs in BLCA. **(A)** The expression difference of 29 PRGs between normal tissue and BLCA tissue. **(B)** Interactions among PRGs in BLCA. **(C)** The CNV variation frequency of PRGs. Red circle: amplified frequency; blue circle: missing frequency. **(D)** Locations of CNV alterations in PRGs on 23 chromosomes. **(E)** Mutation frequencies of PRGs in the patients with BLCA from the TCGA cohort. **(F)** The correlation network of the PRGs. The asterisk represents the statistical p value (*$p < 0.05$; **$p < 0.01$; ***$p < 0.001$). PRGs, pyroptosis-related genes; BLCA, bladder cancer; TCGA, The Cancer Genome Atlas; CNV, copy number variant.

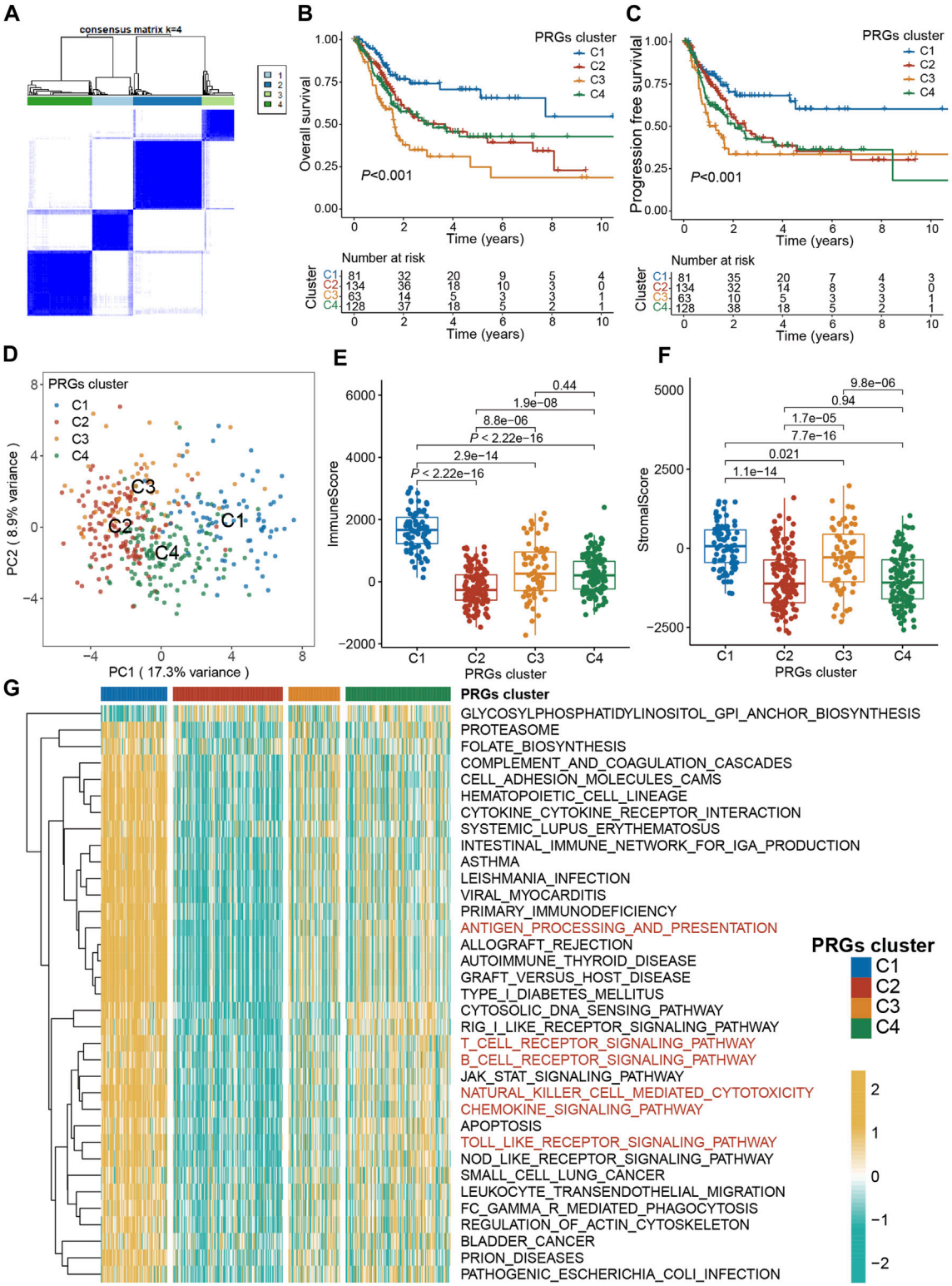

FIGURE 3
Pyroptosis subtypes and clinicopathological and biological characteristics of four distinct subtypes of samples divided by consistent clustering. **(A)** Consensus matrix heatmap defining four clusters (k = 4) and their correlation area. **(B)** The OS Kaplan-Meier curve of different clusters in BLCA patients. **(C)** The PFS Kaplan-Meier curve of different clusters in BLCA patients. **(D)** PCA analysis showing a remarkable difference in transcriptomes between the four subtypes. **(E)** The distribution of immune score, and **(F)** stromal score inferred by ESTIMATE algorithm between the four clusters in the TCGA BLCA cohort. **(G)** The heatmap showing the results of GSVA enrichment analysis among different pyroptosis clusters. The asterisk represents the statistical p value (*p < 0.05; **p < 0.01; ***p < 0.001). PRG, pyroptosis-related gene; BLCA, bladder cancer; OS, overall survival; PFS, progression-free survival; GSVA, gene set variation analysis.

measurements were two-sided, and $p < 0.05$ was set as the significance level. The Wilcoxon and Kruskal–Wallis analyses were conducted to compare two or more clusters, respectively. The log-rank method was employed for Kaplan-Meier survival analysis to assess the statistical significance. Moreover, for Lasso Cox regression analysis, the R "glmnet" package was utilized. AUC values of ROC curves in different cohorts were calculated using the R "timeROC" package.

3 Results

3.1 Genetic and transcriptional landscape of PRGs in BLCA

The expression profiles of 52 PRGs were compared in the TCGA-BLCA cohort, and 29 DEGs were assessed between the tumor and adjacent tissues (Figure 2A). Furthermore, a pyroptosis network was constructed to illustrate the comprehensive profile of PRGs interactions, modulator associations, and their prognostic value for BLCA (Figure 2B). The gain or loss copy number variation (CNV) was very common in DEGs. For example, the frequency of gain CNV in AIM2 was up to 18.5%, and that of loss CNV in CASP8 was up to 11.1% (Figure 2C). Figure 2D demonstrates CNV alterations of the PRGs on the chromosome. Moreover, the somatic mutation of these DEGs in the TCGA-BLCA cohort was also described. It was revealed that TP53 had the highest mutation frequency (49%); however, the mutation frequencies of other DEGs were all <3% (Figure 2E). The correlation network between PRGs is shown in Figure 2F. Additionally, a notable difference was observed between the expression levels and genetic profile of PRGs of BLCA and control samples, suggesting the potential role of PRGs in BLCA oncogenesis and development.

3.2 PRGs-based identification of molecular subtypes

To explore the association between expression profiles of DEGs and BLCA subtypes, consensus cluster analysis was performed on TCGA-BLCA patients. The increase of clustering variable (k) from 2 to 10, indicated that at $k = 4$, the intra-group associations were the highest, while the intergroup associations were lowest, suggesting that the TCGA-BLCA patients could be grouped into four clusters according to the expression of PRGs (Figure 3A). The expressions of PRGs in the four clusters were shown in Supplementary Figures S1A, B. Kaplan-Meier curve for PFS and OS among the four clusters indicated that patients in cluster C1 had the best prognosis, while those in C3 had the worst prognosis ($p < 0.001$, Figures 3B, C). Based on the expression profiles of DEGs, patients in four subtypes were easily distinguished (Figure 3D). Moreover, the "ESTIMATE" algorithm was employed to elucidate the stromal and immune scores of patients, which revealed that cluster C1 had the highest immune and stromal scores, proving that tumor tissues from cluster C1 patients were infiltrated by more immune cells (Figure 3E) and by more fibro-blasts/endothelial cells (Figure 3F). Additionally, the transcriptomic matrix was transformed into a pathway matrix via the GSVA algorithm, and then the correlation of PRGs clusters with KEGG pathways was assessed. Different immune-related pathways were observed to be activated in cluster C1 (Figure 3G), including the T cell receptor signaling pathway, antigen processing-presentation, B cell receptor signaling pathway, Chemokine signaling pathway, Natural killer cell-mediated cytotoxicity, and Toll-like receptor signaling pathway.

3.3 Infiltrating immune cells and identification of feature genes related to PRGs clusters

First, the transcriptomic data of all genes were transformed into scores of 28 infiltrating immune cells using the ssGSEA algorithm from the R "gsva" package, and then the differential analysis of these scores among four PRGs clusters was performed. Surprisingly, ssGSEA scores of almost all immune cells in cluster C1 were substantially increased than the cluster C2 (Figure 4A; Supplementary Figure S1C). Therefore, C1 was defined as an "immune-hot" tumor and C2 as an "immune-cold" tumor. Moreover, the differential expression assessment genes linked with immune checkpoints among four clusters showed that CD274, PDCD1, CTLA4, LAG3, and TIGIT were expressed at the highest level in cluster C1 (Supplementary Figure S1D).

To promote the clinical application of novel prognostic biomarkers, key PRGs characteristic of each cluster were identified. First, using a heatmap of differentially expressed genes was employed to characterize four subtypes (Figure 4B). Then, the correlation of feature genes of C1 and C2 with ssGSEA scores of 28 immune cells was assessed. It was revealed that feature genes of the C1 subtype (immune-hot) were predominantly positively correlated with activated CD4 T cells, M1 macrophages, and CD8 T cells, while those of the C2 subtype (immune-cold) were mainly positively correlated with Tregs (Figure 4C). Among features genes, CXCL9/CXCL10 were upregulated in C1 and downregulated in C2, while SPINK1/DHES9 were upregulated in C2 and downregulated in C1 (Figure 4D). Furthermore, the expression levels of these features genes of C1 (CXCL9/CXCL10) and C2 (SPINK1/DHES9) in tumor tissues were validated and one C1 (sample A, CXCL9/CXCL10 high + SPINK1/DHES9 low) and one C2 (sample B, SPINK1/DHES9 high + CXCL9/CXCL10 low) sample were screened for subsequent immunofluorescence assay (Figure 4E). The detailed clinical features of the two BLCA patients are shown in Supplementary Table S4. Consistent with bioinformatics analysis, sample A had abundant infiltration of CD8 + T cells and CD68 + macrophages, which corresponded to C1 features, while sample B with high SPINK1 and DHRS2 expression had notably more M2 macrophages and Treg infiltration, which corresponded to C2 subtype features (Figure 4F).

3.4 Differentially expressed genes-based identification of molecular subtypes

To assess the underlying genetic alterations, first, 240 DEGs (PRGs-DEGs) among four clusters were identified. Then, based on these genes, unsupervised clustering was carried out to categorize TCGA-BLCA patients into geneClusters A ($n = 98$) and B ($n = 308$)

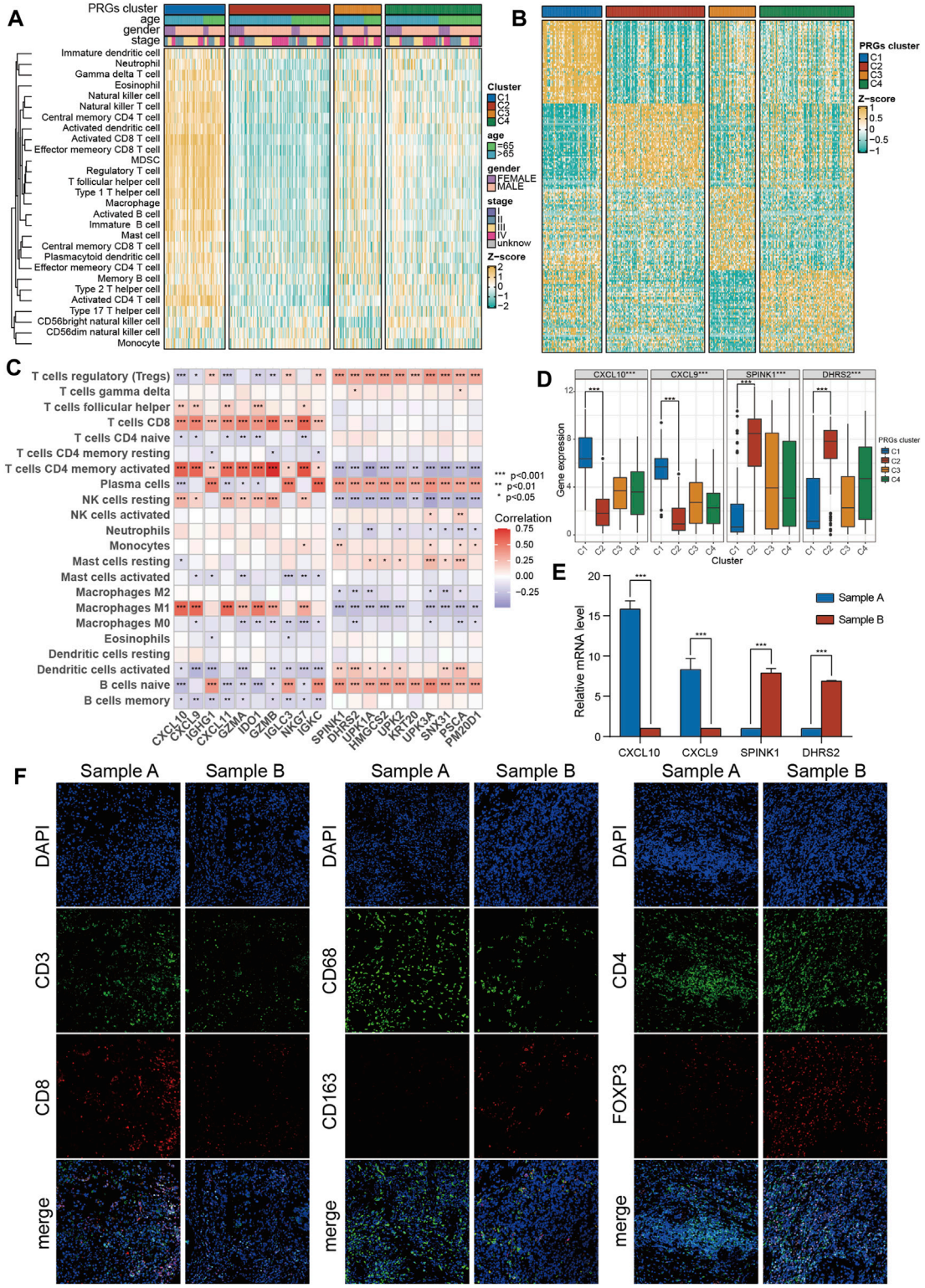

FIGURE 4
The immune features and marker genes of the four molecular clusters. **(A)** The infiltration abundance of 28 immune cell subsets evaluated by ssGSEA for four clusters. **(B)** Heatmap of differentially expressed genes for four clusters. **(C)** The association between the abundance of immune cells and the most significantly differentially expressed genes in the four clusters. **(D)** Expression of C1 and C2 cluster marker genes in the four clusters. **(E)** The expression of C1 and C2 subtype marker genes in tumor samples was detected by PCR. **(F)** The infiltration of CD8 + T cells, macrophages and Tregs in tumor samples was detected by immunofluorescence. The asterisk represents the statistical p value (*$p < 0.05$; **$p < 0.01$; ***$p < 0.001$). ssGSEA, single sample gene set enrichment analysis.

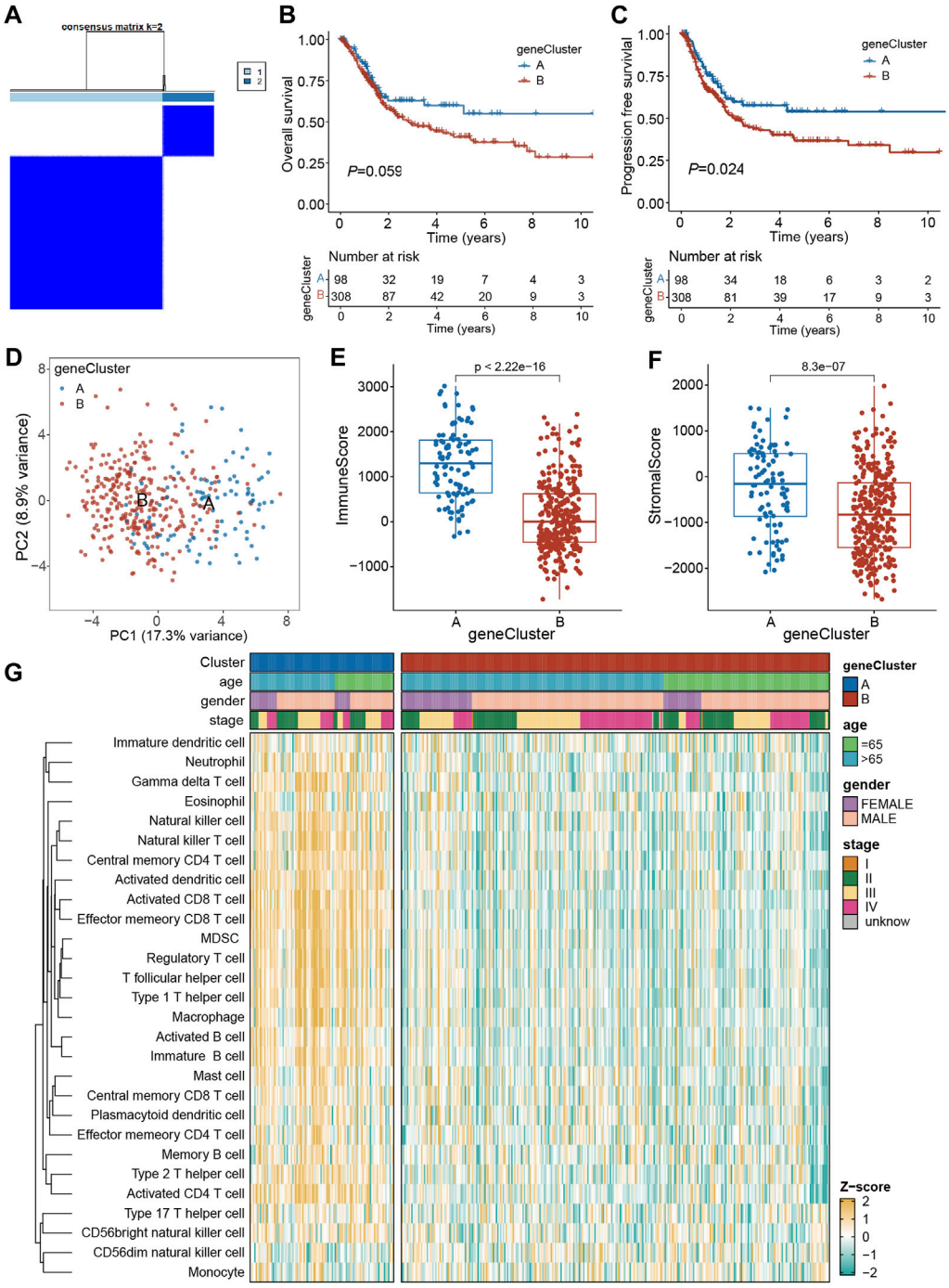

FIGURE 5
Identification of geneClusters based on PRGs-DEGs. **(A)** Consensus matrix heatmap defining two clusters (k = 2) and their correlation area. **(B)** Kaplan-Meier curves for OS of the two geneClusters. **(C)** Kaplan-Meier curves for PFS of the two geneClusters. **(D)** PCA analysis showing a remarkable difference in transcriptomes between the two geneClusters. **(E)** The distribution of immune score, and **(F)** stromal score inferred by ESTIMATE algorithm between the two geneClusters in the TCGA BLCA cohort. **(G)** The infiltration abundance of 28 immune cell subsets evaluated by ssGSEA for the two geneClusters. The asterisk represents the statistical p value (*$p < 0.05$; **$p < 0.01$; ***$p < 0.001$). DEGs, differentially expressed genes; OS, overall survival; PFS, progression-free survival; PRGs, pyroptosis-related genes.

(Figure 5A). Kaplan-Meier curve revealed that geneCluster A patients had longer OS and PFS than geneCluster B patients, although the difference in OS was not significant ($p = 0.059$) (Figures 5B, C). Moreover, PCA analysis also validated that both geneClusters were well distinguishable by PRGs-DEGs (Figure 5D). Additionally, the immune and stromal scores between the two geneClusters were assessed, which indicated that immune and stromal scores in geneCluster A were both markedly increased than geneCluster B ($p < 0.001$) (Figures 5E, F). This might be why geneCluster A patients had longer OS and PFS than geneCluster

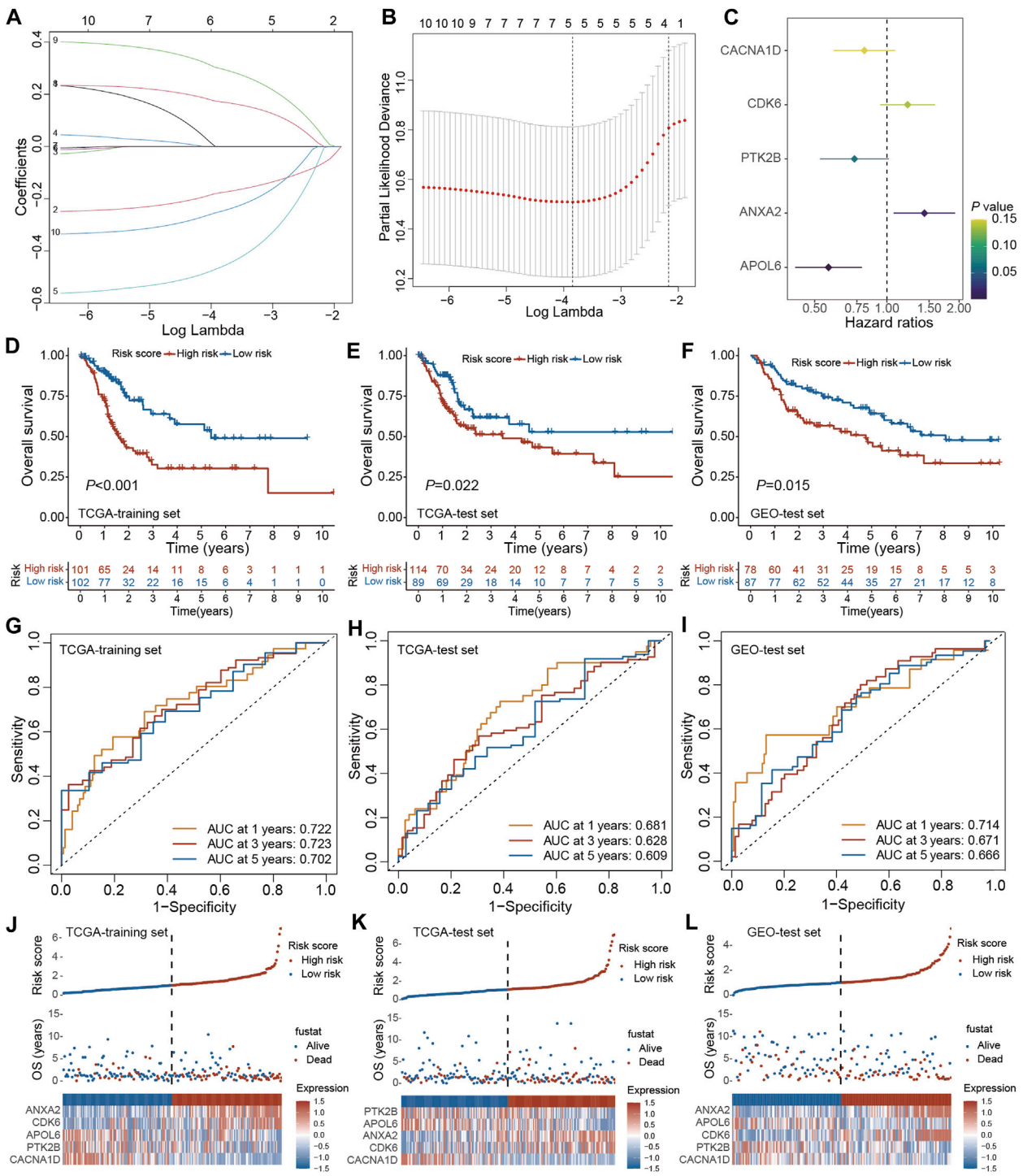

FIGURE 6
Construction and validation of the PRGs-DEGs risk score in the training and test set. **(A,B)** The LASSO method of PRGs associated with prognosis. **(C)** Forrest plot of the multivariate Cox regression analysis of five genes. **(D)** Kaplan–Meier curves of survival in TCGA training set. **(E)** Kaplan–Meier curves of survival in TCGA test set. **(F)** Kaplan–Meier curves of survival in GEO test set. **(G)** Time-dependent ROC curve of the risk score model for predicting 1, 3, 5 years in TCGA training set. **(H)** Time-dependent ROC curve of the risk score model for predicting 1, 3, 5 years in TCGA test set. **(I)** Time-dependent ROC curve of the risk score model for predicting 1, 3, 5 years in GEO test set. **(J)** The distribution, survival status, and heat map of risk scores in the TCGA training set. **(K)** The distribution, survival status, and heat map of risk scores in the TCGA test set. **(L)** The distribution, survival status, and heat map of risk scores in the GEO test set. The asterisk represents the statistical *p* value (**p* < 0.05; ***p* < 0.01; ****p* < 0.001). PRGs, pyroptosis-related genes; LASSO, least absolute shrinkage and selection operator; PCA, principal component analysis; OS, overall survival; ROC, receiver operating characteristic.

B patients. Furthermore, ssGSEA scores of almost all infiltrating immune cells in geneCluster A were remarkably higher than those in geneCluster B (Figure 5G).

3.5 Construction and validation of PRGs-DEGs risk scoring system

The prognostic model was established using the TCGA training set and its performance was evaluated through internal testing with the TCGA test set and external testing with the GEO test set. Based on 240 PRGs-DEGs, the risk scoring system was generated using the TCGA-BLCA train cohort. The univariate Cox regression analysis identified 46 survival-related genes, which were further screened to 10 by LASSO regression analysis (Figures 6A, B). Subsequently, the predictive model was generated using the multivariate Cox regression analysis, and 5 genes were identified. According to the hazard ratio in the model, CACNA1D, PTK2B, and APOL6 were tumor suppressor genes, while CDK6 and ANXA2 were oncogenes (Figure 6C). The PRGs score was calculated as follows: PRGs score = (−0.216021228 × CACNA1D) + (0.199209604 × CDK6) + (−0.310925889 × PTK2B) + (0.360364278 × ANXA2) + (−0.56043276 × APOL6).

The patients were then categorized as LR and HR cohorts based on the median PRGs score. PCA analysis confirmed that the PRGs score based on the above five genes could well distinguish the two risk groups (Supplementary Figure S2A). Moreover, the correlation analysis also validated that PRGs score was negatively linked with tumor suppressor genes (CACNA1D, PTK2B, and APOL6) and positively linked with oncogenes (CDK6 and ANXA2) (Supplementary Figures S2B–F). The expression of PRGs between the HR and LR groups is illustrated in Supplementary Figure S2G. It was observed that BLCA patients' prognosis in the LR cohort was better than the HR cohort in both the training and internal test sets (Figures 6D, E). ROC analysis revealed that AUC for 1/3/5 years OS was 0.722/0.723/0.702 for the training set and 0.681/0.628/0.609 for the internal test set, respectively (Figures 6G, H). Additionally, with the help of the heatmap, the expression levels of the 5 PRGs of the prognostic model in the LR and HR cohorts were visualized (Figures 6J, K). It was validated that the constructed model could help predict the outcomes of BLCA patients.

For validating the prognostic model in the external test set, each patient's PRGs score was assessed based on the aforementioned PRGs score formula. The external test set patients were categorized into the LR and HR cohorts based on the training set's median PRGs score value. In line with the data acquired for the training set, the HR group patients in the external test set indicated a poorer prognosis than the LR group patients (Figure 6F). Additionally, the ROC analysis revealed an AUC of 0.714/0.671/0.666 for 1/3/5 years OS (Figure 6I). Figure 6L demonstrates the survival status and the heatmap of these 5 prognostic genes in the external test set. Overall, these results indicated that the constructed prognostic model could accurately predict a BLCA patient's prognosis from the external test set.

To validate the expression of the five genes involved in the risk signature in BLCA patients, we collected clinical BLCA samples and paired normal tissues, and analyzed them using qPCR. As demonstrated in Figure 7, CDK6 and ANXA2 exhibited elevated expression levels in tumors, whereas CACNA1D, PTK2B, and APOL6 exhibited significantly reduced expression levels in tumors. These distinctions align with our bioinformatic findings, suggesting that these genes may serve as innovative biomarkers for prognostic prediction of BLCA.

3.6 The association of PRGs-DEGs risk score with clinicopathologic characteristics

The clinical relevance of the PRGs-DEGs risk model was assessed. The chi-square test was carried out to elucidate the differences in clinicopathological features between LR and HR subgroups. The heatmap indicates that the pathologic T stage, tumor grade, and pathologic N stage were closely linked with the PRGs score ($p < 0.001$) (Figure 8A). Furthermore, the proportions of high tumor grade, pathologic T3 + T4 stage and lymph node (+) in the HR subgroup were substantially greater than in the LR subgroup, whereas proportions of low tumor grade, pathologic T1 + T2 stage, and lymph node (−) in the HR subgroup were markedly reduced than in LR subgroup (Figures 8B–D). Additionally, the difference in PRGs score among distinct sub-groups was assessed based on clinicopathological characteristics. It was revealed that the PRGs score in high-grade, T3 + T4, and lymph node (+) subgroups were remarkably higher than those in low-grade, T1 + T2, and lymph node (−) subgroups (Figures 8E–G). To explore whether the PRGs score applies to different clinical subgroups, Kaplan-Meier curves curves were used to assess the presence of prognosis differences between LR and HR groups among diverse clinical groups. Markedly significant differences were observed between the HR and LR cohorts in the age ≤ 65, age > 65, female, male, low grade, high grade, T1-2, T3-4, N0, N1-3, and M0 groups. Overall, compared with HR, the LR cohort had a significant survival advantage (Supplementary Figure S3).

3.7 Correlation analysis of PRGs-DEGs risk score with oncogenic pathways and immune cells

To elucidate the mechanism by which the risk signature affects BLCA initiation and progression, the relation of PRGs score with the hallmark oncogenic pathways and infiltrating immune cells was assessed. The differential analysis of the ssGSEA score of hallmark pathways revealed 20 of 50 items, which were remarkably altered between LR and HR subgroups. Specifically, epithelial-mesenchymal transition, KRAS signaling, mtorc1 signaling, and TNFα signaling via NF-κB were greatly enriched in the HR subgroup (Figure 9A; Supplementary Figure S4A). Additionally, the proportions of intratumoral immune cells were quantified via the CIBERSORT algorithm. The proportions of NK and CD8 + T cells were substantially increased in the LR subgroup than in the HR subgroup, while opposite data was acquired for M2-type macrophages (type of suppressive immune cells) (Figure 9B; Supplementary Figure S4B). In particular, the PRGs score was markedly negatively linked with CD8 + T cells (Figure 9C; Supplementary Figure S5). Moreover, the relationship between these 5 signature genes and immune cell abundance was also

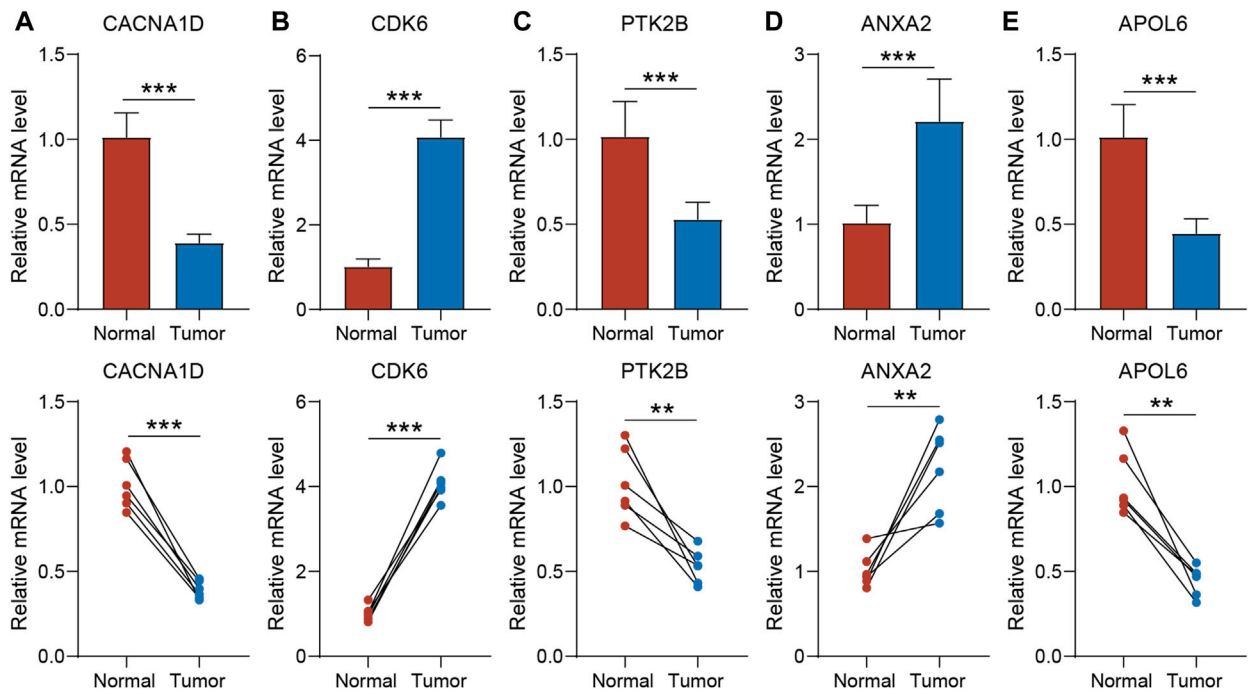

FIGURE 7
The expression of CACNA1D **(A)**, CDK6 **(B)**, PTK2B **(C)** ANXA2 **(D)** and APOL6 **(E)** in normal bladder tissue and BLCA tissue of patients. *t*-test was used to compare the expression of genes between normal and tumor. The asterisk represents the statistical *p* value (*$p < 0.05$; **$p < 0.01$; ***$p < 0.001$). BLCA, bladder cancer.

elucidated, which indicated Tregs, plasma cells, CD8 + T cells, as well as M2- and M0-type macrophages were notably correlated with these genes (Figure 9D). Particularly, the APOL6 gene was markedly positively linked with CD8 T cell infiltration (Figure 9E).

3.8 The role of the PRGs-DEGs risk score in predicting immunotherapy response

Accumulating evidence has shown that high TMB patients benefit from immunotherapy because of enhanced neoantigens. Our genomic data analysis of the TCGA-BLCA cohort indicated a lower TMB in the HR subgroup than in the LR subgroup ($p = 0.043$; Figure 9F), implying that LR subgroup patients are more likely to benefit from anti-PD-1/PD-L1 immunotherapy. Moreover, a public dataset IMvigor210 cohort was also analyzed to ensure the predictive significance of PRGs score in immunotherapy. Individuals were classified into LR and HR subgroups based on the median score. It was noticed that the proportion of responders (CR/PR/SD) in the LR subgroup was notably increased than in the HR subgroup, whereas the proportion of non-responders (PD) was substantially reduced in the LR subgroup than in the HR subgroup (Figure 9G; Supplementary Figures S4C, E). The PRGs score in the HR subgroups was markedly higher than that in the LR subgroup ($p = 0.0015$, Figure 9H; Supplementary Figures S4D, F). In addition, the Kaplan-Meier survival curve indicated that HR patients had a shorter OS than the LR patients ($p < 0.001$, Figure 9I).

3.9 The nomogram based on clinical characteristics and PRGs-DEGs risk score

Univariate and multivariable Cox regression analyses were carried out to elucidate independent prognostic factors in BLCA patients. The univariate Cox regression analysis revealed that PRGs score and most clinical parameters were prognostic factors (Figure 10A); however, multivariate Cox regression indicated that only PRGs score, pathologic T stage, and age were independent prognostic factors for OS (Figure 10B). Therefore, according to the PRGs score, tumor stage, and age, a nomogram was generated to predict BLCA patients' 1-, 3-, and 5-year survival probability (Figure 10C). One point was given to each patient for each prognostic parameter, and higher total points depicted a worse outcome. Moreover, calibration plots revealed that the nomogram had a similar performance to an ideal model (Figure 10D). Additionally, ROC and DCA data also illustrated that the nomogram had a high efficiency for clinical implementation (Figures 10E–H).

4 Discussion

Much literature has indicated the essential activity of pyroptosis in antitumor mechanisms and innate immunity (Wang et al., 2020; Tsuchiya, 2021). However, most of these researches were focused on a single TME cell or PRG; therefore, the overall influence and TME infiltration characteristics regulated by the simultaneous influence of different PRGs remain undetermined. This investigation indicated

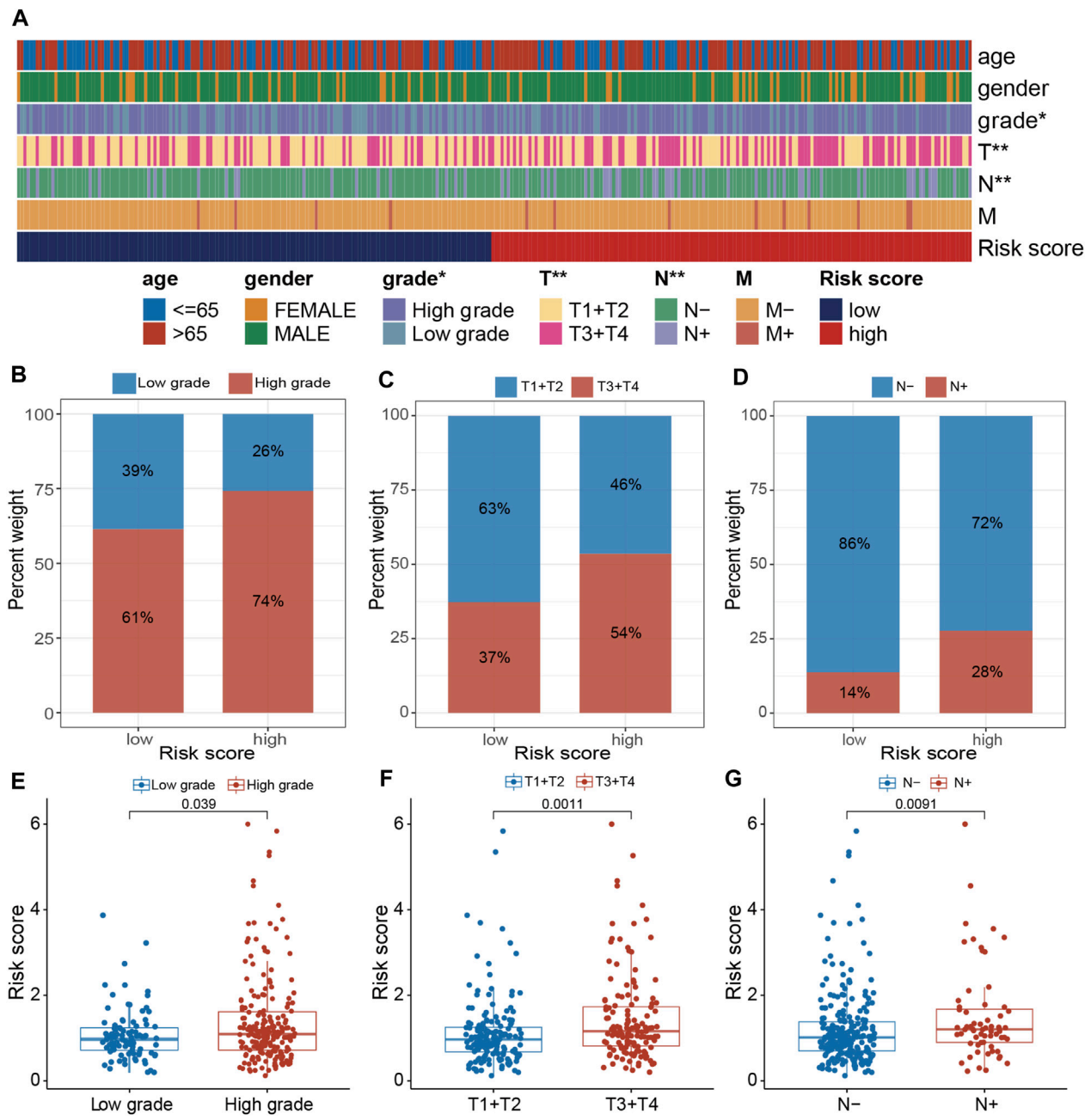

FIGURE 8
Clinical evaluation of the panel by PRGs-DEGs risk score. **(A)** A band chart of risk score and clinical features of BLCA patients. **(B)** The proportion of patients with different grade category in high- and low-risk groups. **(C)** Comparison of the risk score between the patients with different grade category ($p = 0.039$, Wilcoxon test). **(D)** The proportion of patients with different T category in high- and low-risk groups. **(E)** Comparison of the risk score between the patients with different T category ($p = 0.0011$, Wilcoxon test). **(F)** The proportion of patients with different N category in high- and low-risk groups. **(G)** Comparison of the risk score between the patients with different N category ($p = 0.0091$, Wilcoxon test). The asterisk represents the statistical p value (*$p < 0.05$; **$p < 0.01$; ***$p < 0.001$). BLCA, bladder cancer.

global transcriptional and genetic level changes of PRGs in BLCA. Here, four distinct PRGs clusters were identified based on 52 PRGs. Subtype C1 patients had the highest OS and PFS than other subtypes. Furthermore, by analyzing the differences in the TME between four clusters, we found that PRGs subtype C1 and C2 showed distinct and typical characteristics. Specifically, PRGs subtype C1 showed an "immune-hot" phenotype, which was characterized by substantial immune activation, such as antigen presentation and processing, natural killer cell-induced cytotoxicity, the B and T-cell receptor signaling pathways, the JAK-STAT signaling pathway, and the NOD-like, Toll-like, and RIG-I-like receptor signaling pathways; however, PRGs subtype C2 showed "immune-cold" characteristics. Additionally, two geneClusters were also identified according to the DEGs between the PRGs clusters. Therefore, the results of this study revealed that PRGs are a potential predictor for elucidating BLCA's clinical

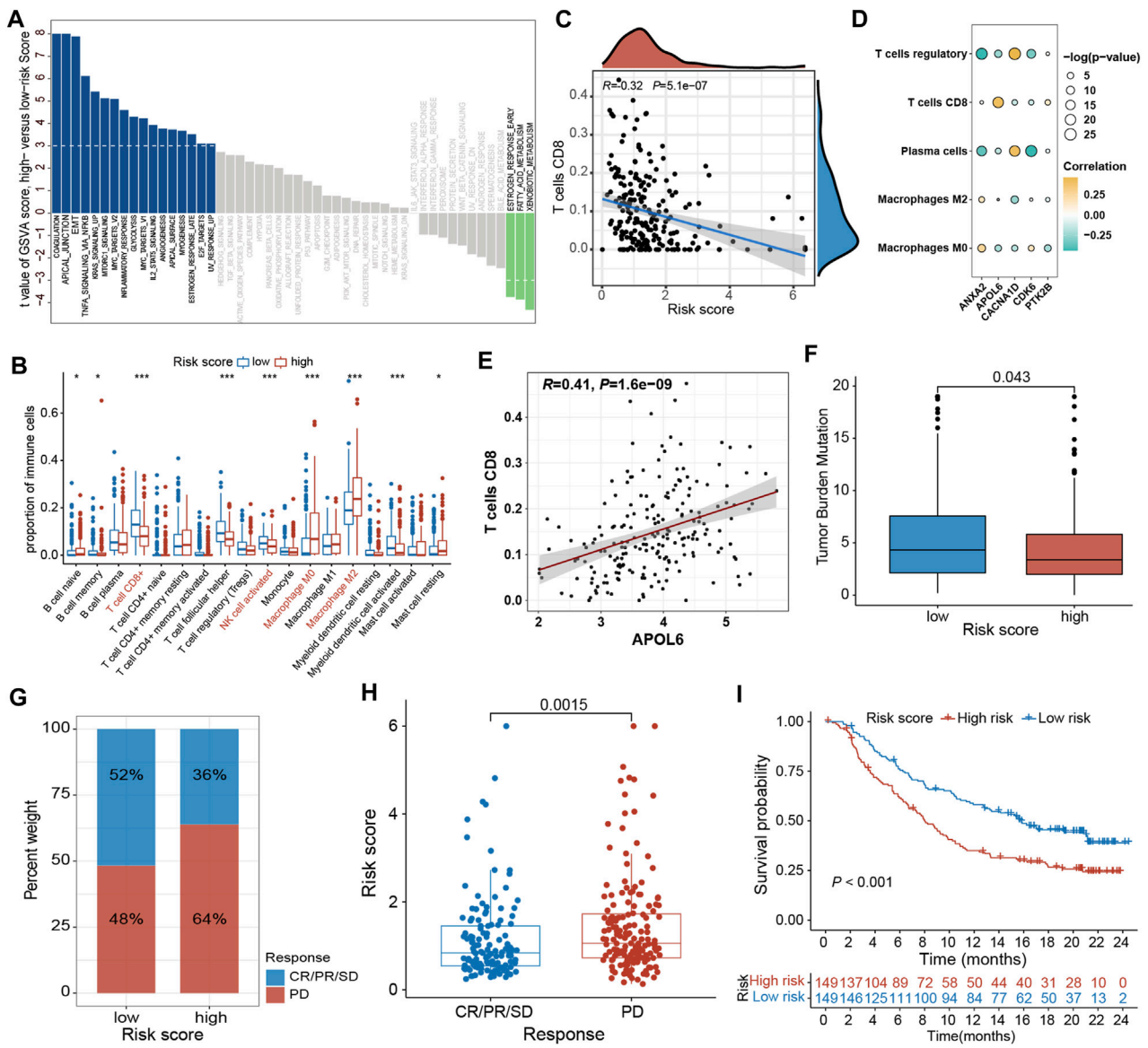

FIGURE 9
Comprehensive analysis of the PRGs-DEGs risk score in BLCA. **(A)** Differences in biological function between high- and low-risk groups. **(B)** The differences of immune cells between high- and low-risk groups based on ssGSEA. **(C)** Correlations between risk score and CD8 + T cells. **(D)** Correlations between the abundance of immune cells and 5 genes in the proposed model. **(E)** Correlations between APOL6 gene and CD8 + T cells. **(F)** Differences in TMB between high- and low-risk groups. **(G)** The proportion of patients with (CR/PR/SD) or without (PD) response to PD-L1 blockade therapy in the high- and low-risk groups in the IMvigor210 cohort. **(H)** Different risk score in CR/PR/SD group and PD group in IMvigor210 cohort ($p < 0.05$). **(I)** OS curves for the high- and low-risk groups in IMvigor210 cohort ($p = 0.002$). The asterisk represents the statistical p value (*$p < 0.05$; **$p < 0.01$; ***$p < 0.001$). BLCA, bladder cancer; ssGSEA, single sample gene set enrichment analysis; TMB, tumor mutation burden; OS, overall survival; SD, stable disease; PD, progressive disease; CR, complete response; PR, partial response.

outcomes and immunotherapy response. Thus, a robust and efficient prognostic PRGs-DEGs risk score model was established and its predictive ability was assessed. The pyroptosis patterns characterized by immune suppression and stimulation indicated HR and LR scores, respectively. The LR and HR patients indicated markedly different clinicopathological features, mutation, prognosis, immune checkpoints, TME, and anti-PD1/PD-L1 immunotherapy susceptibilities. Lastly, by integrating risk score, stage, and age, a quantitative nomogram was established, further improving the model's performance and facilitating the application of the risk score. After construction and validation, our prediction model, compared to previous models, can not only predict the prognosis of BLCA but also assess the tumor immune microenvironment and the efficacy of immunotherapy. This provides valuable diagnostic and therapeutic assistance to clinicians. The prognostic model can be employed for prognostic stratification of BLCA patients, assists in better identification of BLCA molecular pathways, and provides novel strategies for targeted therapies.

Pyroptosis is observed in pathogen-infected cells as a programmed mechanism of death and thus stimulates the body's inflammatory response (Bedoui et al., 2020). Under pathogenic

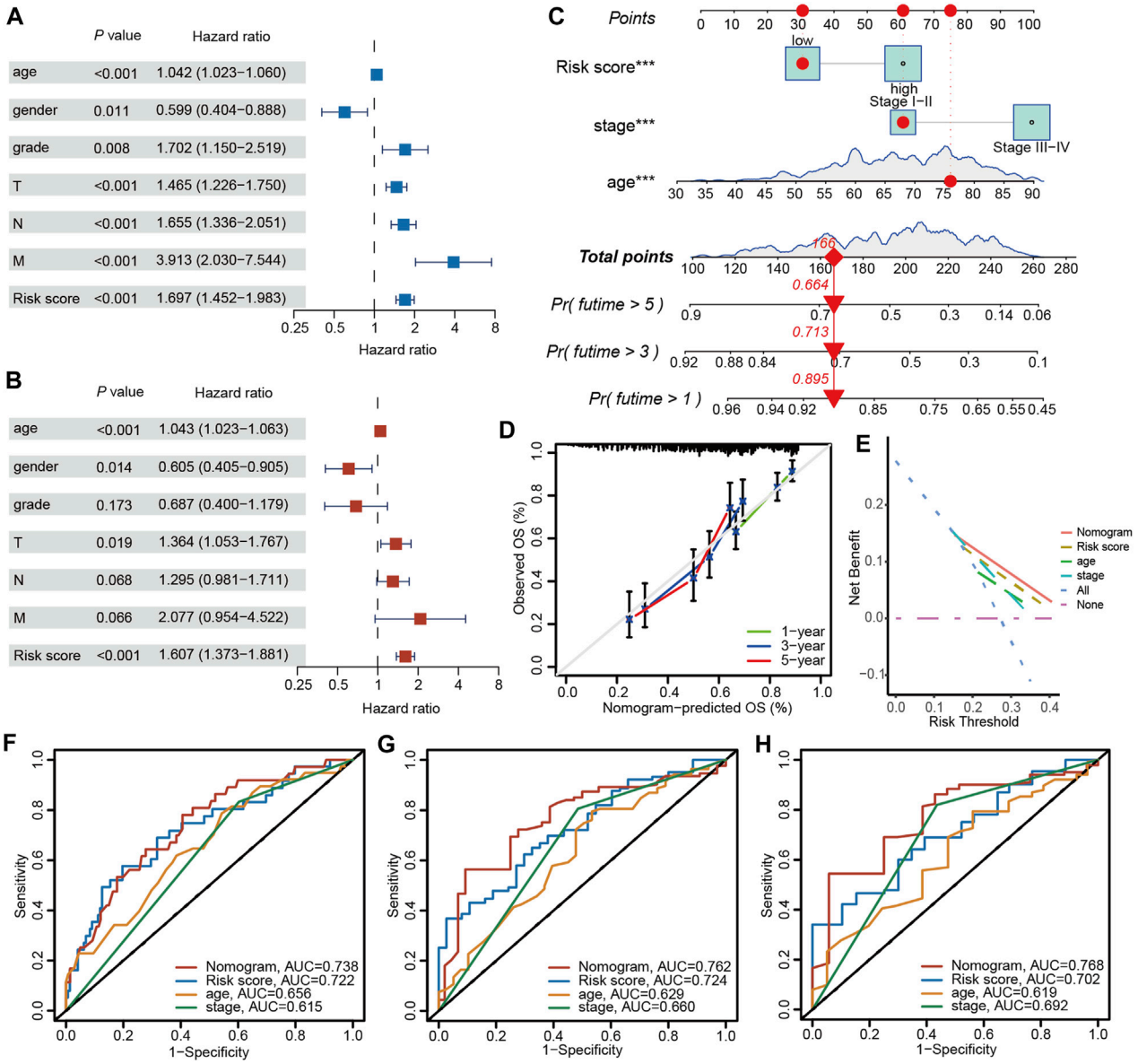

FIGURE 10
Nomogram construction and prognostic value of the signature. **(A)** Univariate and **(B)** Multivariate Cox regression analysis of clinical factors and risk score. **(C)** The nomogram for predicting the survival rate of 1-, 3-, and 5-years in BLCA patients. **(D)** Calibration plots of the nomogram. **(E)** Decision curve analysis of the nomogram of the panel. The time-dependent ROC analysis of nomogram predicting the survival rate of 1-years **(F)**, 3-years **(G)**, and 5-years **(H)** in BLCA patients. The asterisk represents the statistical *p* value (**p* < 0.05; ***p* < 0.01; ****p* < 0.001). BLCA, bladder cancer; ROC, receiver operating characteristic.

stimulation, apoptosis can transform into pyroptosis. Furthermore, pyroptosis has been associated with different pathways in various cancers. Moreover, it has been indicated to inhibit tumor growth in liver, colorectal, and skin cancers (Zaki et al., 2010; Ellis et al., 2011; Ma et al., 2016); however, it has a two-way impact on breast cancer (Chen et al., 2012). Therefore, assessing the prognostic value based on the levels of different gasdermins alone is controversial. In BLCA patients, the association between PRGs and that between PRGs and TME remains unclear. This research investigated all the direct pathways linked with pyroptosis and elucidated a prognostic signature by assessing the impact of these pathways on TME. Currently, pyroptosis has been utilized in anti-tumor therapy, and this research suggests that it is closely linked with immunotherapy efficacy and could be employed as a biomarker for efficacy prediction.

The inhibition of immunoinhibitory molecules such as PD-1 and PD-L1 can lead to tumor regression by restoring the cytotoxicity of immune cells (Bellmunt et al., 2017). To date, several immune checkpoint inhibitors (ICIs), such as atezolizumab (PD-L1 inhibitor) and nivolumab (PD-1 inhibitor), have been approved by the FDA for the treatment of advanced BLCA (Aggen and Drake, 2017; Lobo et al., 2017). However, patient responses to ICI therapy vary greatly, with some patients achieving complete remission while others experience continuous

disease progression (Jiang et al., 2020). Here, we demonstrated that PRGs can enhance anti-tumor immune responses by regulating inflammatory responses and the immune microenvironment, thereby affecting immune cell infiltration and activation in tumors. Additionally, the PRGs-DEGs risk score was significantly associated with the response of BLCA to ICI therapy, with a low-risk score indicating increased sensitivity to ICIs. This suggests that the application of the PRGs-DEGs risk score could assist in decision-making for the treatment of BLCA.

After conventional chemotherapy, BLCA prognosis is substandard, with increased levels of tumor-infiltrating lymphocytes, tumor neoantigens, and checkpoints. Although immunotherapy has undergone many advances, BLCA patients' prognosis remains heterogeneous, suggesting that TME may play an important role. The TME comprises tumor-infiltrating immune cells (TIICs), fibroblasts, bone marrow-derived inflammatory cells, lymphocytes, blood vessels, and extracellular matrix (ECM) (Turley et al., 2015). It has been indicated that TME is essentially involved in tumor development, progression, and drug resistance (Hinshaw and Shevde, 2019). Here, the pyroptosis pattern manifested by immune inhibition (subtype C2) was linked with an HR score, while those characterized by immune activation (subtype C1) were related to an LR score. Furthermore, it was discovered that the TME characteristics and the relative abundance of 22 TIICs were substantially different between different PRGs clusters and PRGs score. These results indicated the essential role of PRGs in BLCA's TME. Much research has indicated that effector memory T cells, T cells, and T-cell differentiation are crucially linked with immune defense in BLCA (Yang et al., 2022). The γδ-T cells can efficiently identify and kill BLCA cells, thereby inhibiting tumor progression (Nguyen et al., 2022). In addition, the density of T cells infiltrating BLCA tissue was positively correlated with prognosis (Poch et al., 2018; Bunch et al., 2020). Subtype C1 and the LR group had a better prognosis and indicated increased infiltration of activated memory CD4 + and CD8 + T cells, as well as γδ-T cells, indicating their positive involvement in BLCA prognosis. Tregs infiltration inhibits the anti-cancer immune response and has been linked with substandard prognosis (Tanaka and Sakaguchi, 2017). This is consistent with the results of the current study, where more Tregs were observed in the TME of C2 patients and the HR group.

Recent literature has indicated that B cells are also associated with the immune response (Cabrita et al., 2020; Helmink et al., 2020). Petitprez et al. (2020) suggested that B-cell enrichment was a significant prognostic factor for long-term survival and was positively linked with PD-1 blockade response in soft-tissue sarcomas. Furthermore, Helmink et al. (2020) suggested that the expression of B-cell-associated genes JCHAIN, MZB1, and IGLL5 was notably increased in patients who responded to immune checkpoint inhibitors than in non-responders. Moreover, tumor-infiltrating B cells were linked with a favorable prognosis in BLCA (Jiang et al., 2019; Zhou et al., 2021). Overall, these data suggest that B cells are not just bystanders in anti-tumor immunotherapy, instead, they offer new directions for immunotherapy and are powerful weapons against tumors. Here, a marked difference was observed in B-cell infiltration between the risk score groups and PRGs subtypes. Furthermore, naive B cell abundance in the C2 and HR groups with worse OS was notably lower than that in the C1 and the LR cohort. Therefore, B cell infiltration suppressed BLCA progression, consistent with previous literature (Jiang et al., 2019; Zhou et al., 2021).

With the development of molecular biology and tumor immunology, immunotherapy has opened new directions for treating tumors. Such therapies mainly include ICIs, cell therapy, and therapeutic antibodies. Currently, much research on ICIs for PD-1, CTLA-4, and PD-L1 is underway, and clinical trials have revealed their efficacy and safety in BLCA (Carosella et al., 2015; Farina et al., 2017; Hussain et al., 2018). This investigation identified increased levels of PD-1 and PD-L1 in the LR cohort, which showed a better response to anti-PD1/PD-L1 immunotherapy. In addition, TMB is a new essential characteristic of cancer and is related to microsatellite instability (Hatakeyama et al., 2018; Steuer and Ramalingam, 2018). In the human cancer genome, enhanced TMB is caused by a combination of endogenous factors and environmental damage (Roberts and Gordenin, 2014). It has been indicated that high TMB patients benefit better from immunotherapy (Carbone et al., 2017). Therefore, TMB has become another emerging biomarker for the prediction of the response to immunotherapy (Klebanov et al., 2019). Here, higher TMB was identified in the LR group, and the correlation analysis suggested that TMB was negatively correlated with the risk score. In addition, tremelimumab (anti-CTLA-4) has indicated good tolerance in BLCA patients who have not responded well to other immunotherapies (Chung et al., 2010). Overall, it was concluded that patients with LR scores; higher PD-1, CTLA-4, and PD-L1, expression; and increased TMB might respond well to ICIs.

5 Limitations

This research has certain limitations. 1) This investigation utilized data from a public database and was validated with a small clinical sample, therefore, additional *in vivo* and *in vitro* analyses and large-scale prospective research are required to validate the acquired data. 2) Some essential clinical information, including the data on neoadjuvant chemotherapy, surgery, and chemoradiotherapy, was not assessed in this study, which may affect the outcome of pyroptosis state and immune response.

6 Conclusion

In summary, this comprehensive investigation indicated the regulatory mechanism of PRGs, which affects the clinicopathological features, tumor's immune-stromal microenvironment, and prognosis of BLCA patients. Furthermore, the therapeutic liability of PRGs in immunotherapy was also indicated. This research highlights the essential evidence for the clinical implications of PRGs and furnishes a novel strategy for guiding personalized immunotherapy for BLCA patients.

Data availability statement

The original contributions presented in the study are included in the article/Supplementary Material, further inquiries can be directed to the corresponding authors.

Ethics statement

The studies involving humans were approved by the Institutional Research Ethics Committee of West China Hospital. The studies were conducted in accordance with the local legislation and institutional requirements. Written informed consent for participation was not required from the participants or the participants' legal guardians/next of kin in accordance with the national legislation and institutional requirements.

Author contributions

ZX: Conceptualization, Data curation, Formal Analysis, Methodology, Writing–original draft, Funding acquisition, Project administration, Software, Visualization. YuZ: Methodology, Project administration, Writing–original draft, Formal Analysis, Software. YoZ: Conceptualization, Formal Analysis, Software, Writing–original draft, Methodology, Visualization. XL: Investigation, Writing–original draft, Methodology, Supervision. LS: Methodology, Writing–original draft, Software, Visualization. MC: Formal Analysis, Software, Writing–original draft, Methodology. GX: Formal Analysis, Software, Writing–original draft, Methodology, Visualization. XM: Conceptualization, Supervision, Writing–review and editing, Methodology, Resources. HS: Conceptualization, Resources, Supervision, Visualization, Writing–review and editing, Methodology.

Funding

The author(s) declare that financial support was received for the research, authorship, and/or publication of this article. This work was supported by 1) the National Key Research and Development Program of China [2022YFA1207300 (2022YFA1207303)]; 2) National Natural Science Foundation of China (No. 82172634); 3) Key Program of the Science and Technology Bureau of Sichuan (No. 2021YFSY0007); 4) 1.3.5 project for disciplines of excellence, West China Hospital, Sichuan University (No. ZYGD23028); 5) The China Postdoctoral Science Foundation (2023M742486).

Acknowledgments

We would like to acknowledge TCGA and the GEO (GSE13507) network for providing data.

Conflict of interest

The authors declare that the research was conducted in the absence of any commercial or financial relationships that could be construed as a potential conflict of interest.

Publisher's note

All claims expressed in this article are solely those of the authors and do not necessarily represent those of their affiliated organizations, or those of the publisher, the editors and the reviewers. Any product that may be evaluated in this article, or claim that may be made by its manufacturer, is not guaranteed or endorsed by the publisher.

Supplementary material

The Supplementary Material for this article can be found online at: https://www.frontiersin.org/articles/10.3389/fphar.2024.1387647/full#supplementary-material

References

Afonso, J., Santos, L. L., Longatto-Filho, A., and Baltazar, F. (2020). Competitive glucose metabolism as a target to boost bladder cancer immunotherapy. *Nat. Rev. Urol.* 17 (2), 77–106. doi:10.1038/s41585-019-0263-6

Aggen, D. H., and Drake, C. G. (2017). Biomarkers for immunotherapy in bladder cancer: a moving target. *J. Immunother. Cancer* 5 (1), 94. doi:10.1186/s40425-017-0299-1

Bedoui, S., Herold, M. J., and Strasser, A. (2020). Emerging connectivity of programmed cell death pathways and its physiological implications. *Nat. Rev. Mol. Cell Biol.* 21 (11), 678–695. doi:10.1038/s41580-020-0270-8

Bellmunt, J., Powles, T., and Vogelzang, N. J. (2017). A review on the evolution of PD-1/PD-L1 immunotherapy for bladder cancer: the future is now. *Cancer Treat. Rev.* 54, 58–67. doi:10.1016/j.ctrv.2017.01.007

Bunch, B. L., Morse, J., Asby, S., Blauvelt, J., Aydin, A. M., Innamarato, P., et al. (2020). Systemic and intravesical adoptive cell therapy of tumor-reactive T cells can decrease bladder tumor growth *in vivo*. *J. Immunother. Cancer* 8 (2), e001673. doi:10.1136/jitc-2020-001673

Cabrita, R., Lauss, M., Sanna, A., Donia, M., Skaarup Larsen, M., Mitra, S., et al. (2020). Tertiary lymphoid structures improve immunotherapy and survival in melanoma. *Nature* 577 (7791), 561–565. doi:10.1038/s41586-019-1914-8

Cao, R., Yuan, L., Ma, B., Wang, G., Qiu, W., and Tian, Y. (2020). An EMT-related gene signature for the prognosis of human bladder cancer. *J. Cell. Mol. Med.* 24 (1), 605–617. doi:10.1111/jcmm.14767

Carbone, D. P., Reck, M., Paz-Ares, L., Creelan, B., Horn, L., Steins, M., et al. (2017). First-line nivolumab in stage IV or recurrent non-small-cell lung cancer. *N. Engl. J. Med.* 376, 2415–2426. doi:10.1056/nejmoa1613493

Carosella, E. D., Ploussard, G., Lemaoult, J., and Desgrandchamps, F. (2015). A systematic review of immunotherapy in urologic cancer: evolving roles for targeting of CTLA-4, PD-1/PD-L1, and HLA-G. *Eur. Urol.* 68 (2), 267–279. doi:10.1016/j.eururo.2015.02.032

Chen, L., Wang, L., Tsang, N., Ojcius, D. M., Chen, C., Ouyang, C., et al. (2012). Tumour inflammasome-derived IL-1β recruits neutrophils and improves local recurrence-free survival in EBV-induced nasopharyngeal carcinoma. *EMBO Mol. Med.* 4 (12), 1276–1293. doi:10.1002/emmm.201201569

Chou, R., Selph, S. S., Buckley, D. I., Gustafson, K. S., Griffin, J. C., Grusing, S. E., et al. (2016). Treatment of muscle-invasive bladder cancer: a systematic review. *Cancer* 122 (6), 842–851. doi:10.1002/cncr.29843

Chung, K. Y., Gore, I., Fong, L., Venook, A., Beck, S. B., Dorazio, P., et al. (2010). Phase II study of the anti-cytotoxic T-lymphocyte-associated antigen 4 monoclonal antibody, tremelimumab, in patients with refractory metastatic colorectal cancer. *J. Clin. Oncol.* 28, 3485–3490. doi:10.1200/JCO.2010.28.3994

Cumberbatch, M. G., Rota, M., Catto, J. W., and La Vecchia, C. (2016). The role of tobacco smoke in bladder and kidney carcinogenesis: a Comparison of exposures and meta-analysis of incidence and mortality risks. *Eur. Urol.* 70 (3), 458–466. doi:10.1016/j.eururo.2015.06.042

Ellis, L. Z., Liu, W., Luo, Y., Okamoto, M., Qu, D., Dunn, J. H., et al. (2011). Green tea polyphenol epigallocatechin-3-gallate suppresses melanoma growth by inhibiting inflammasome and IL-1β secretion. *Biochem. Biophys. Res. Commun.* 414 (3), 551–556. doi:10.1016/j.bbrc.2011.09.115

Erkes, D. A., Cai, W., Sanchez, I. M., Purwin, T. J., Rogers, C., Field, C. O., et al. (2020). Mutant BRAF and MEK inhibitors regulate the tumor immune microenvironment via pyroptosis. *Cancer Discov.* 10 (2), 254–269. doi:10.1158/2159-8290.CD-19-0672

Fang, Y., Tian, S., Pan, Y., Li, W., Wang, Q., Tang, Y., et al. (2020). Pyroptosis: a new frontier in cancer. *Biomed. Pharmacother. = Biomedecine Pharmacother.* 121, 109595. doi:10.1016/j.biopha.2019.109595

Farina, M. S., Lundgren, K. T., and Bellmunt, J. (2017). Immunotherapy in urothelial cancer: recent results and future perspectives. *Drugs* 77 (10), 1077–1089. doi:10.1007/s40265-017-0748-7

Frank, D., and Vince, J. E. (2019). Pyroptosis versus necroptosis: similarities, differences, and crosstalk. *Cell Death Differ.* 26 (1), 99–114. doi:10.1038/s41418-018-0212-6

Galsky, M. D., Arija, J., Bamias, A., Davis, I. D., De Santis, M., Kikuchi, E., et al. (2020). Atezolizumab with or without chemotherapy in metastatic urothelial cancer (IMvigor130): a multicentre, randomised, placebo-controlled phase 3 trial. *Lancet* 395 (10236), 1547–1557. doi:10.1016/S0140-6736(20)30230-0

Ghandour, R., Singla, N., and Lotan, Y. (2019). Treatment options and outcomes in nonmetastatic muscle invasive bladder cancer. *Trends Cancer* 5 (7), 426–439. doi:10.1016/j.trecan.2019.05.011

Hatakeyama, K., Nagashima, T., Urakami, K., Ohshima, K., Serizawa, M., Ohnami, S., et al. (2018). Tumor mutational burden analysis of 2,000 Japanese cancer genomes using whole exome and targeted gene panel sequencing. *Biomed. Res. Tokyo, Jpn.* 39 (3), 159–167. doi:10.2220/biomedres.39.159

He, H., Yi, L., Zhang, B., Yan, B., Xiao, M., Ren, J., et al. (2021). USP24-GSDMB complex promotes bladder cancer proliferation via activation of the STAT3 pathway. *Int. J. Biol. Sci.* 17 (10), 2417–2429. doi:10.7150/ijbs.54442

Helmink, B. A., Reddy, S. M., Gao, J., Zhang, S., Basar, R., Thakur, R., et al. (2020). B cells and tertiary lymphoid structures promote immunotherapy response. *Nature* 577 (7791), 549–555. doi:10.1038/s41586-019-1922-8

Hinshaw, D. C., and Shevde, L. A. (2019). The tumor microenvironment innately modulates cancer progression. *Cancer Res.* 79 (18), 4557–4566. doi:10.1158/0008-5472.CAN-18-3962

Hussain, S. A., Birtle, A., Crabb, S., Huddart, R., Small, D., Summerhayes, M., et al. (2018). From clinical trials to real-life clinical practice: the role of immunotherapy with PD-1/PD-L1 inhibitors in advanced urothelial carcinoma. *Eur. Urol. Oncol.* 1 (6), 486–500. doi:10.1016/j.euo.2018.05.011

Jiang, Q., Fu, Q., Chang, Y., Liu, Z., Zhang, J., Xu, L., et al. (2019). CD19(+) tumor-infiltrating B-cells prime CD4(+) T-cell immunity and predict platinum-based chemotherapy efficacy in muscle-invasive bladder cancer. *Cancer. Immunol. Immunother.* 68 (1), 45–56. doi:10.1007/s00262-018-2250-9

Jiang, W., Zhu, D., Wang, C., and Zhu, Y. (2020). An immune relevant signature for predicting prognoses and immunotherapeutic responses in patients with muscle-invasive bladder cancer (MIBC). *Cancer Med.* 9 (8), 2774–2790. doi:10.1002/cam4.2942

Klebanov, N., Artomov, M., Goggins, W. B., Daly, E., Daly, M. J., and Tsao, H. (2019). Burden of unique and low prevalence somatic mutations correlates with cancer survival. *Sci. Rep.* 9 (1), 4848. doi:10.1038/s41598-019-41015-5

Lee, Y. C., Lam, H. M., Rosser, C., Theodorescu, D., Parks, W. C., and Chan, K. S. (2022). The dynamic roles of the bladder tumour microenvironment. *Nat. Rev. Urol.* 19 (9), 515–533. doi:10.1038/s41585-022-00608-y

Lenis, A. T., Lec, P. M., Chamie, K., and Mshs, M. D. (2020). Bladder cancer: a review. *JAMA* 324 (19), 1980–1991. doi:10.1001/jama.2020.17598

Lobo, N., Mount, C., Omar, K., Nair, R., Thurairaja, R., and Khan, M. S. (2017). Landmarks in the treatment of muscle-invasive bladder cancer. *Nat. Rev. Urol.* 14 (9), 565–574. doi:10.1038/nrurol.2017.82

Ma, X., Guo, P., Qiu, Y., Mu, K., Zhu, L., Zhao, W., et al. (2016). Loss of AIM2 expression promotes hepatocarcinoma progression through activation of mTOR-S6K1 pathway. *Oncotarget* 7 (24), 36185–36197. doi:10.18632/oncotarget.9154

Nguyen, S., Chevalier, M. F., Benmerzoug, S., Cesson, V., Schneider, A. K., Rodrigues-Dias, S. C., et al. (2022). Vδ2 T cells are associated with favorable clinical outcomes in patients with bladder cancer and their tumor reactivity can be boosted by BCG and zoledronate treatments. *J. Immunother. Cancer* 10 (8), e004880. doi:10.1136/jitc-2022-004880

Orning, P., Lien, E., and Fitzgerald, K. A. (2019). Gasdermins and their role in immunity and inflammation. *J. Exp. Med.* 216 (11), 2453–2465. doi:10.1084/jem.20190545

Petitprez, F., de Reynies, A., Keung, E. Z., Chen, T. W., Sun, C. M., Calderaro, J., et al. (2020). B cells are associated with survival and immunotherapy response in sarcoma. *Nature* 577 (7791), 556–560. doi:10.1038/s41586-019-1906-8

Poch, M., Hall, M., Joerger, A., Kodumudi, K., Beatty, M., Innamarato, P. P., et al. (2018). Expansion of tumor infiltrating lymphocytes (TIL) from bladder cancer. *OncoImmunology* 7 (9), e1476816. doi:10.1080/2162402X.2018.1476816

Powles, T., Csoszi, T., Ozguroglu, M., Matsubara, N., Geczi, L., Cheng, S. Y., et al. (2021). Pembrolizumab alone or combined with chemotherapy versus chemotherapy as first-line therapy for advanced urothelial carcinoma (KEYNOTE-361): a randomised, open-label, phase 3 trial. *Lancet Oncol.* 22 (7), 931–945. doi:10.1016/S1470-2045(21)00152-2

Roberts, S. A., and Gordenin, D. A. (2014). Hypermutation in human cancer genomes: footprints and mechanisms. *Nat. Rev. Cancer.* 14 (12), 786–800. doi:10.1038/nrc3816

Runa, F., Hamalian, S., Meade, K., Shisgal, P., Gray, P. C., and Kelber, J. A. (2017). Tumor microenvironment heterogeneity: challenges and opportunities. *Curr. Mol. Biol. Rep.* 3 (4), 218–229. doi:10.1007/s40610-017-0073-7

Schneider, A. K., Chevalier, M. F., and Derre, L. (2019). The multifaceted immune regulation of bladder cancer. *Nat. Rev. Urol.* 16 (10), 613–630. doi:10.1038/s41585-019-0226-y

Steuer, C. E., and Ramalingam, S. S. (2018). Tumor mutation burden: leading immunotherapy to the era of precision medicine? *J. Clin. Oncol.* 36, 631–632. doi:10.1200/JCO.2017.76.8770

Tanaka, A., and Sakaguchi, S. (2017). Regulatory T cells in cancer immunotherapy. *Cell Res.* 27 (1), 109–118. doi:10.1038/cr.2016.151

Teoh, J. Y., Huang, J., Ko, W. Y., Lok, V., Choi, P., Ng, C., et al. (2020). Global trends of bladder cancer incidence and mortality, and their associations with tobacco use and gross domestic product *per capita*. *Eur. Urol.* 78 (6), 893–906. doi:10.1016/j.eururo.2020.09.006

Tsuchiya, K. (2021). Switching from apoptosis to pyroptosis: gasdermin-elicited inflammation and antitumor immunity. *Int. J. Mol. Sci.* 22 (1), 426. doi:10.3390/ijms22010426

Turley, S. J., Cremasco, V., and Astarita, J. L. (2015). Immunological hallmarks of stromal cells in the tumour microenvironment. *Nat. Rev. Immunol.* 15 (11), 669–682. doi:10.1038/nri3902

Wang, Q., Wang, Y., Ding, J., Wang, C., Zhou, X., Gao, W., et al. (2020). A bioorthogonal system reveals antitumour immune function of pyroptosis. *Nature* 579 (7799), 421–426. doi:10.1038/s41586-020-2079-1

Wang, W., Zhang, X., Jiang, S., Xu, P., Chen, K., Li, K., et al. (2023). A novel signature constructed by differential genes of muscle-invasive and non-muscle-invasive bladder cancer for the prediction of prognosis in bladder cancer. *Front. Immunol.* 14, 1187286. doi:10.3389/fimmu.2023.1187286

Yang, M., Wang, B., Hou, W., Yu, H., Zhou, B., Zhong, W., et al. (2022). Negative effects of stromal neutrophils on T cells reduce survival in resectable urothelial carcinoma of the bladder. *Front. Immunol.* 13, 827457. doi:10.3389/fimmu.2022.827457

Ye, Y., Dai, Q., and Qi, H. (2021). A novel defined pyroptosis-related gene signature for predicting the prognosis of ovarian cancer. *Cell Death Discov.* 7 (1), 71. doi:10.1038/s41420-021-00451-x

Zaki, M. H., Vogel, P., Body-Malapel, M., Lamkanfi, M., and Kanneganti, T. (2010). IL-18 production downstream of the Nlrp3 inflammasome confers protection against colorectal tumor formation. *J. Immunol.* 185 (8), 4912–4920. doi:10.4049/jimmunol.1002046

Zhang, L., Zhu, L., Tang, L., Xie, J., Gao, Y., Yu, C., et al. (2023). Glutathione-responsive nanoparticles of camptothecin prodrug for cancer therapy. *Adv. Sci.* 10 (3), e2205246. doi:10.1002/advs.202205246

Zhou, M., Zhang, Z., Bao, S., Hou, P., Yan, C., Su, J., et al. (2021). Computational recognition of lncRNA signature of tumor-infiltrating B lymphocytes with potential implications in prognosis and immunotherapy of bladder cancer. *Brief. Bioinform.* 22 (3). doi:10.1093/bib/bbaa047

frontiers | Frontiers in Pharmacology

TYPE Original Research
PUBLISHED 07 August 2024
DOI 10.3389/fphar.2024.1419040

Check for updates

OPEN ACCESS

EDITED BY
Hailin Tang,
Sun Yat-sen University Cancer Center (SYSUCC), China

REVIEWED BY
Yu Min,
Sichuan University, China
Penghao Xu,
Georgia Institute of Technology, United States
Bin Yang,
University of Pittsburgh, United States

*CORRESPONDENCE
Xing-Hua Gao,
hurryman1999@sina.com

†These authors have contributed equally to this work

RECEIVED 17 April 2024
ACCEPTED 26 July 2024
PUBLISHED 07 August 2024

CITATION
Li M-P, Long S-P, Liu W-C, Long K and Gao X-H (2024) EMT-related gene classifications predict the prognosis, immune infiltration, and therapeutic response of osteosarcoma. *Front. Pharmacol.* 15:1419040. doi: 10.3389/fphar.2024.1419040

COPYRIGHT
© 2024 Li, Long, Liu, Long and Gao. This is an open-access article distributed under the terms of the Creative Commons Attribution License (CC BY). The use, distribution or reproduction in other forums is permitted, provided the original author(s) and the copyright owner(s) are credited and that the original publication in this journal is cited, in accordance with accepted academic practice. No use, distribution or reproduction is permitted which does not comply with these terms.

EMT-related gene classifications predict the prognosis, immune infiltration, and therapeutic response of osteosarcoma

Meng-Pan Li[1,2,3†], Si-Ping Long[4†], Wen-Cai Liu[5†], Kun Long[3] and Xing-Hua Gao[1*]

[1]Department of Orthopedics, Guangzhou First People's Hospital, South China University of Technology, Guangzhou, China, [2]Department of Orthopedics, Shanghai General Hospital, Shanghai Jiao Tong University School of Medicine, Shanghai, China, [3]The First Clinical Medical College of Nanchang University, Nanchang, China, [4]The Fourth Clinical Medical College of Nanchang University, Nanchang, China, [5]Department of Orthopedics, Shanghai Sixth People's Hospital Affiliated to Shanghai Jiao Tong University School of Medicine, Shanghai, China

Background: Osteosarcoma (OS), a bone tumor with high ability of invasion and metastasis, has seriously affected the health of children and adolescents. Many studies have suggested a connection between OS and the epithelial-mesenchymal transition (EMT). We aimed to integrate EMT-Related genes (EMT-RGs) to predict the prognosis, immune infiltration, and therapeutic response of patients with OS.

Methods: We used consensus clustering to identify potential EMT-Related OS molecular subtypes. Somatic mutation, tumor immune microenvironment, and functional enrichment analyses were performed for each subtype. We next constructed an EMT-Related risk signature and evaluated it by Kaplan-Meier (K-M) analysis survival and receiver operating characteristic (ROC) curves. Moreover, we constructed a nomogram to more accurately predict OS patients' clinical outcomes. Response effects of immunotherapy in OS patients was analyzed by Tumor Immune Dysfunction and Exclusion (TIDE) analysis, while sensitivity for chemotherapeutic agents was analyzed using oncoPredict. Finally, the expression patterns of hub genes were investigated by single-cell RNA sequencing (scRNA-seq) data analysis.

Results: A total of 53 EMT-RDGs related to prognosis were identified, separating OS samples into two separate subgroups. The EMT-high subgroup showed favourable overall survival and more active immune response. Significant correlations were found between EMT-Related DEGs and functions as well as pathways linked to the development of OS. Additionally, a risk signature was established and OS patients were divided into two categories based on the risk scores. The signature presented a good predictive performance and could be recognized as an independent predictive factor for OS. Furthermore, patients with higher risk scores exhibited better sensitivity for five drugs, while no significant difference

existed in immunotherapy response between the two risk subgroups. scRNA-seq data analysis displayed different expression patterns of the hub genes.

Conclusion: We developed a novel EMT-Related risk signature that can be considered as an independent predictor for OS, which may help improve clinical outcome prediction and guide personalized treatments for patients with OS.

KEYWORDS

osteosarcoma, EMT, prognostic signature, immune infiltration, therapeutic response

Introduction

Osteosarcoma (OS), growing from osteogenic mesenchymal stem cells, has long been thought to be the most dangerous tumor in teenagers (Brown et al., 2017; Yang et al., 2021). Patients suffering from localized OS have a 5-year survival rate of approximately 65%, in contrast to roughly 20% for those with recurrent and metastatic OS (Miwa et al., 2019). At present, many treatments have been applied for the therapy of patients with OS, including surgery, chemotherapy, and neoadjuvant chemotherapy, but the overall effects are still unsatisfactory due to the emergence of drug resistance and tumor progression (Kager et al., 2017; Zhou et al., 2023). Therefore, elucidating the potential molecular mechanisms in the development of this tumor and finding new therapeutic approaches are especially important for individuals with OS to get more favourable clinical outcomes.

Many studies have reported that epithelial-mesenchymal transition (EMT) is linked to embryonic growth, cancer invasion and metastasis, and drug resistance emergence (Zhang et al., 2021). During this process, epithelial cells develop into mesenchymal cells with the ability to migrate and invade other areas of the body by losing their apical-basal polarity and intercellular adhesion (Cai et al., 2024). Moreover, EMT is abnormally activated, making cancer cells have the invasive phenotype that extend from the original tumor into the circulatory system. This results in increased cell stemness and the ability of tumor cells to resist different types of therapeutics (Derynck and Weinberg, 2019; Bakir et al., 2020; Zhang et al., 2023).

As a new research approach, bioinformatics analysis could be used to further investigate the connection between diseases and cancer-associated gene sets based on polyphyletic data sources (Gong et al., 2018). In recent years, with the rapid development of genomics, a large amount of genetic data has been provided for the diagnosis and prediction of diseases (Sommer et al., 2022). Meanwhile, various bioinformatics tools and public databases have been established successively, and the cross-fusion of different disciplines also makes the research of bioinformatics analysis more in-depth in medicine. These enable researchers to make great progress in the screening and identification of tumor markers, precise molecular typing of tumors and novel targeted therapies (Wang Q. et al., 2020; Lu et al., 2021; Matsuoka and Yashiro, 2024).

Recent research has demonstrated that EMT is connected to the progression of a variety of malignant cancers, including OS (Yang et al., 2013; Shi et al., 2019). For example, a study by Shao et al. (2022) reported that activation of EMT induced by Tetraspanin 7 overexpression could promote the proliferation and metastasis of OS cells. Moreover, Ruh et al. (2021) found that the process of osteoblastic differentiation in OS cells could be blocked by EMT-transcription factor, ZEB1. These results suggest that the EMT signature might be an OS prognostic factor. In this study, we investigated the connection among EMT, immune response and prognosis in OS patients combining with clinical and gene expression information from openly available databases. We also constructed a risk signature to better predict the prognosis of OS patients. Evaluation of therapeutic response in patients with OS was then been carried out, which may provide implications for developing new treatments and making better clinical strategies.

Materials and methods

Data acquisition

Figure 1 displays the flowchart for this investigation. Information of OS samples, including RNA sequencing data and clinical characteristics, were extracted from the Therapeutically Applicable Research to Generate Effective Treatments (TARGET; https://ocg.cancer.gov/programs/target) database. Excluding samples that lacked comprehensive clinical information, 85 OS samples were included for further analysis. Gene expression in 803 normal samples was attained from the Genome Tissue Expression (GTEx; https://gtexportal.org/home/datasets) database. Additional 53 OS samples were retrieved from the GSE21257 (https://www.ncbi.nlm.nih.gov/) as the validation cohort.

The EMT-RGs were acquired from the two datasets listed below: 1184 EMT-RGs were download from the EMT gene database (https://www.dbemt.bioinfo-minzhao.org/), and 200 EMT-RGs from the HALLMARK_EPITHELIAL_MESENCHYMAL_TRANSITION gene set in the Molecular Signatures Database (MsigDB; https://www.gsea-msigdb.org/gsea/msigdb). Given that all data in this study was freely accessible online and patients were not involved in the research directly, informed permission and ethical committee approval were not essential.

Screening EMT-Related DEGs associated with prognosis

The "DESeq2" R package was utilized to compare the gene expression levels of the OS and normal samples, thus screening differentially expressed genes (DEGs). And the thresholds for significance were set to adjust $|\log2\ (FC)| > 2.5$ and adjusted P-value < 0.01. Then the selected genes were intersected with EMT-RGs to determine the EMT-Related DEGs. By univariate Cox regression analysis, EMT-Related DEGs related to prognosis were screen out for further investigation.

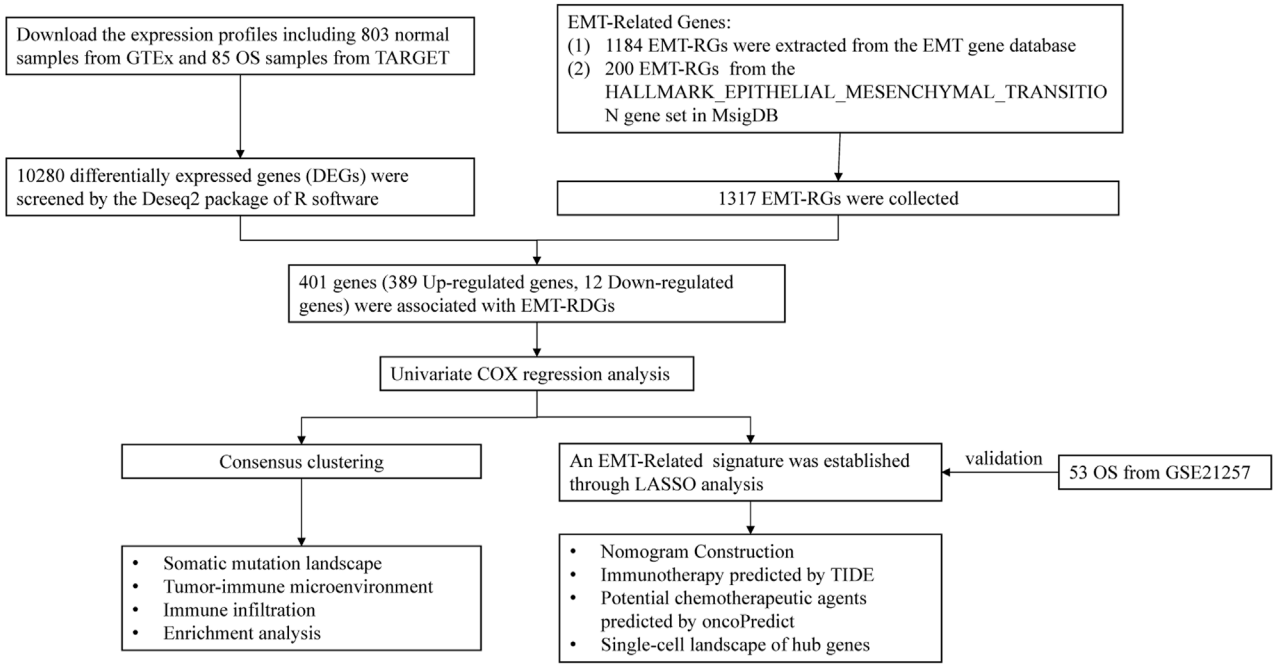

FIGURE 1
Flowchart of this study.

Consensus clustering and survival analysis

After the identification of prognostic associated EMT-Related DEGs, we identified potential molecular subtypes of the OS in terms of these genes utilizing the ConcensusClusterPlus package in R software. To identify the ideal number of clusters, the k-means clustering method was used for eight cluster numbers k, ranging from 2 to 9, and the procedure was replicated one thousand times to ensure stable outcomes. Then, the K-M survival analysis was employed in order to confirm whether the EMT-Related subtypes had a notable influence on OS patients' prognosis.

Somatic mutation landscape

In order to elucidate the notable predictive variances among subtypes from somatic mutation, we acquired data on somatic mutations of OS patients from the Cancer Genome Atlas database (https://portal.gdc.cancer.gov/). Later on, we employed the maftools R package to create waterfall plots to visualize and summarize the mutation landscape of the EMT-Related subgroups.

Tumor immune microenvironment landscape

In addition, we also attempted to explain the prognostic differences between subtypes from tumor immune microenvironment landscape. The Estimation of Stromal and Immune cells in Malignant Tumor tissues using Expression (ESTIMATE) is often used to assess the existence of stromal cells and immune cells as well as the purity of malignancies in tumor tissues (Yoshihara et al., 2013; Xie et al., 2020). Utilizing the ESTIMATE algorithm, we determined the stromal-, immune-, estimate-scores, and tumour purity of each OS sample. We analyzed the immune checkpoint (ICP) expression levels in order to assess the correlation between EMT-Related genotyping and immunological function. Furthermore, utilizing the CIBERSORT (deconvolution algorithm), 22 different kinds of human immune cells in OS were estimated, and the wilcoxon test was carried out to assess the difference of immune cell composition between EMT-Related genotyping.

Enrichment analysis landscape

To explain the prognostic differences between subtypes from the landscape of the pathway and functional landscape, we performed functional enrichment analysis in this study. Firstly, we utilized "DESeq2" R package to identify DEGs between the EMT-Related subtypes [log2 (FC) > 2.5, adjusted *P*-value < 0.01]. Then, the screened genes were employed for Gene Ontology (GO) and Kyoto Encyclopedia of Genes and Genomes (KEGG) enrichment analysis. There are three main categories contained in the GO database, including biological process (BP), cellular component (CC), and molecular function (MF). We showed the top five significant terms in BP, CC and MF. KEGG analysis showed all enriched pathways with significant differences. Furthermore, we presented the top five enriched pathways in each subtype by performing Gene Set Enrichment Analysis (GSEA) to determine which pathways were most substantially enriched in each subtype.

Construction and assessment of an EMT-Related risk signature

Before signature construction, we performed log2 (TPM + 1) on the expression data, and then used the combat function of the limma package to process the debatch effect on the training set TARGET data and the validation set GSE21257 data. In order to avoid the model overfitting, we used a combination of univariate Cox regression and LASSO Cox regression to identify suitable genes for constructing the risk signature. Each sample's risk score value was determined by the following formula:

$$Risk\ score = \sum_{i=1}^{n} coef_i \times x_i$$

where $coef_i$ denotes the LASSO Cox regression coefficient of the prognosis-related genes, x_i denotes EMT-Related gene expression level, and n indicates gene counts. Then, regarding the median risk score, patients in the training (TARGET-OS) and validation cohorts were separated into two risk subgroups (the high- and the low-risk subgroups). The differences of overall survival between the two subgroups were assessed using K-M survival analysis, with the significance of P-value < 0.05. Furthermore, we generated ROC curves and calculated the area under the curve (AUC) to assess the overall survival rate at 1-, 3-, and 5-years, thereby evaluating the predictive precision of the risk model.

Independence evaluation of the risk signature and nomogram construction

In order to ascertain whether the risk signature was independent of other clinical factors, we evaluated the risk model for OS patients using multivariate Cox regression analysis. Moreover, based on risk scores and clinical features, we constructed a nomogram to more precisely quantify the prognosis of OS patients. A score was assigned to a variable (including gender, age, tumor-site, metastatic situation and risk score) in the scoring system of the nomogram, and all the scores from each sample were added together to get the final score. Then, by the function of converting the score to its probability of the result, we could predict the probability of overall survival with each patient (Park, 2018; Liu et al., 2023). A calibration curve was generated to compare the actual and predicted 1-, 3-, and 5-year survival rates of OS patients in the training cohort in order to assess the nomogram model's predictive performance (45° dotted line represents the greatest prediction).

Immunotherapy responsiveness and potential chemotherapeutic agents analysis

We performed immunotherapy responsiveness analysis and explored chemotherapeutic agents to further explore the potential treatment measures of OS patients. In the perspective of immunotherapy, we imported the gene expression matrix into the TIDE online database (http://tide.dfci.harvard.edu/) to predict the immune checkpoint blockade (ICB) responses in OS patients, where a lower TIDE score indicated a more favorable immunotherapy response. Moreover, to identify the immune cells that had a significant association with the risk score, spearman correlation analysis was performed to examine the relationship between the risk score and the 22 immune cell scores that the CIBERSORT algorithm estimated.

OncoPredict, an R package designed by Maeser et al. (2021), is often used to predict the sensitivity of patients with cancers to drug therapies. Genomics of Drug Sensitivity in Cancer (GDSC) database (http://www.cancerrxgene.org/downloads), encompassed information of drug sensitivity (IC50) from 1,000 cell lines, facilitating the study of drug reactions and resistance in OS cell lines (Groisberg et al., 2017; Xie et al., 2022). To assess the responsiveness of TARGET-OS samples to drugs, the oncoPredict R package was employed, and the wilcoxon test (P < 0.005) was utilized to determine if chemotherapy sensitivity varied between the high and low-risk categories.

Single-cell RNA sequencing data analysis

Single-cell RNA sequencing data analysis is a ground-breaking technique in cancer research, which allows researchers to study gene expression variations at the single-cell level and determine the composition of tumor cells. Researchers will probably benefit from a thorough analysis of the immune cell composition in OS samples, which will expand their understanding of prognostic biomarkers (Su et al., 2022; Wang et al., 2022; Ji et al., 2023; Liu et al., 2024). For a deeper insight into the OS tumor immune microenvironment, we demonstrated the cellular composition in OS tumor microenvironment through Tumor Immune Single-cell Hub (TISCH; http://tisch.comp-genomics.org/gallery/) online platform. We performed multivariate Cox regression based on the genes screened by LASSO regression to find the hub genes affecting the prognosis of OS. Then, we demonstrated the expression and distribution of these hub genes in each cell of the tumor microenvironment through TISCH platform.

Results

Screening EMT-Related DEGs and identifying two EMT-Related subtypes

We identified 10,280 DEGs between 85 samples and 803 normal samples, of which 8,435 DEGs were Upregulated and 1845 DEGs were Downregulated (Figure 2A). After removing duplicate genes, 1317 EMT-RGs were collected from the two databases. And 401 genes, including 389 Upregulated genes and 12 Downregulated genes, were associated with EMT-RDGs (Figure 2B). Then, using the univariate Cox regression approach, 53 EMT-RDGs related to prognosis were identified for further investigation.

Consensus clustering analysis was carried out to investigate the potential molecular subtypes related to EMT-RDGs in OS, where the number of clusters was denoted by the letter k. When k = 2, the lowest inter-group collinearity and the highest intra-group collinearity was observed. In view of the different EMT-RG expression patterns, the OS samples in the TARGET cohort were

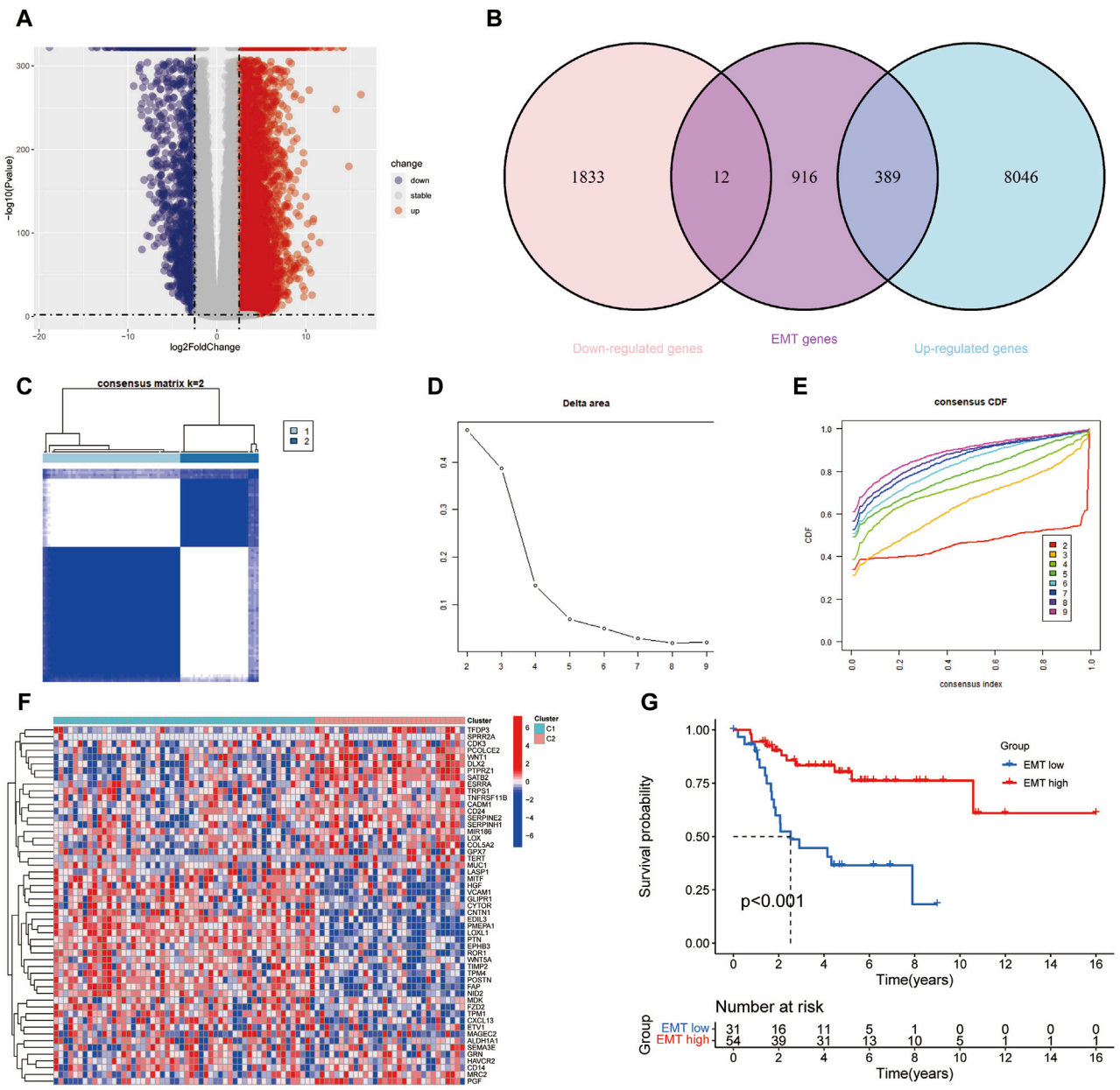

FIGURE 2
Screening differentially expressed EMT-RGs and identifying potential molecular subgroups. **(A)** Volcano plot showed the Upregulated and Downregulated DEGs between the OS and normal samples. **(B)** Venn diagram displayed the number of EMT-Related DEGs. **(C)** Heatmap showed the consensus clustering solution for 53 EMT-RDGs performed best when k = 2, and OS patients were devided into two clusters. **(D, E)** The consensus clustering delta area curve showed corresponding variations in the area under the cumulative distribution function (CDF) curve for k = 2–9. **(F)** Heatmap displayed the expression of 53 EMT-RDG in the two subtypes. High expression is denoted by red, and low expression is denoted by blue. **(G)** K-M analysis suggested that the EMT-high subgroup manifested a more extended survival period than the EMT-low group, with a notable discrepancy ($P < 0.001$).

divided into two subgroups by k-means clustering (Figures 2C–E). Comparing the gene expression levels of patients in the two cohorts of C1 and C2, they were divided into EMT-high subtype and EMT-low subtype, respectively. Figure 2F demonstrated the expression of 53 EMT-RDGs related to prognosis in the two subtypes. Additionally, K-M survival analysis revealed a noteworthy distinction between the EMT-high and EMT-low groups, with the former showing a longer survival length ($P < 0.001$, Figure 2G).

Somatic mutation landscape and tumor immune microenvironment in two EMT-Related subtypes

In the two gene subtypes, we created waterfall plots in order to visually demonstrate mutated genes (Figures 3A,B). Compared to the EMT-high group, the results presented nine decreased gene mutation frequency in the EMT-low group, including TP53, CNTNAP5, ALMS1, HECTD4, PCLO, MAPRE3, MYH7,

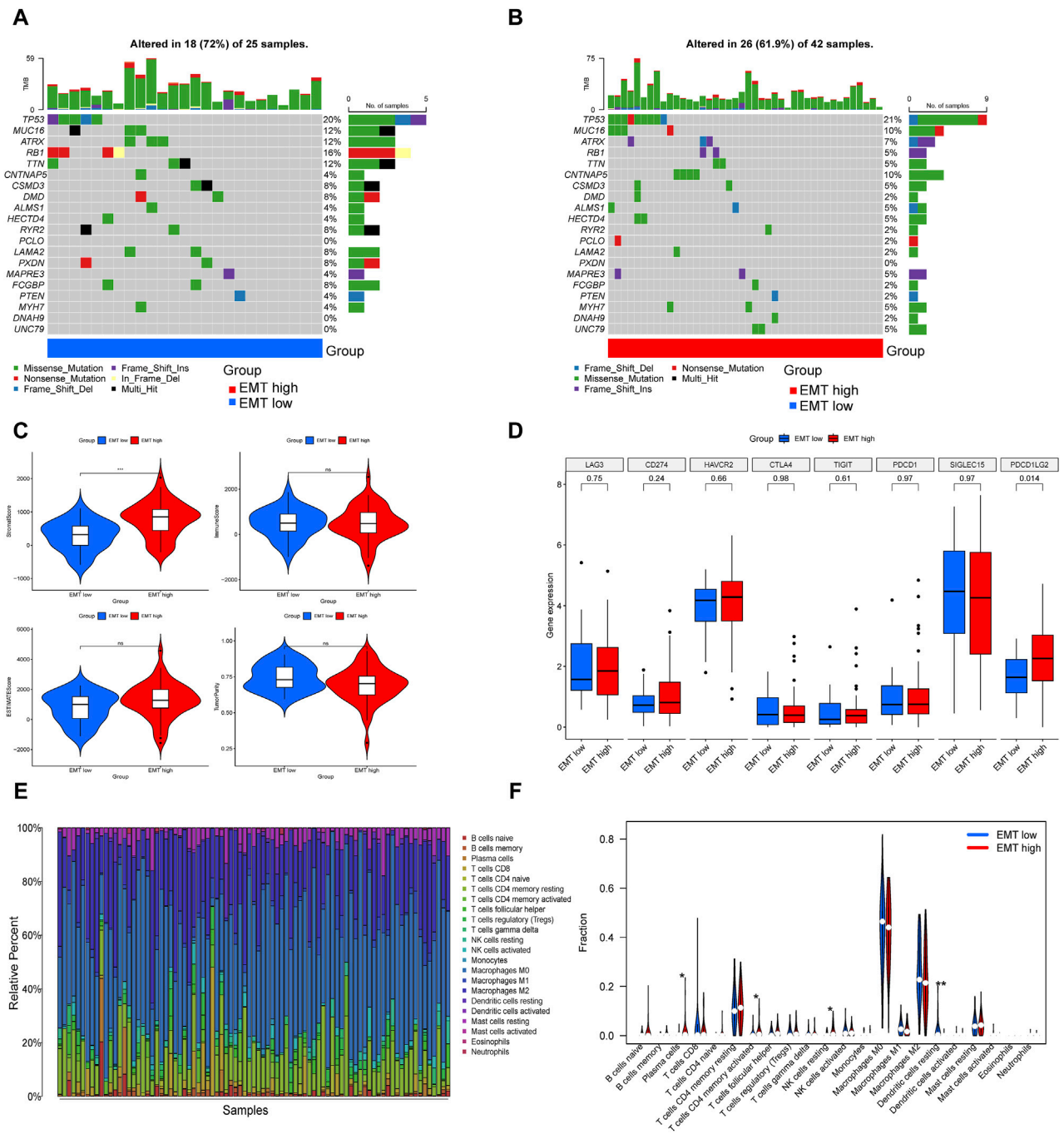

FIGURE 3
Comparison of somatic mutation landscape and immune landscape in the EMT-high and EMT-low subgroups. **(A, B)** The top 20 genes that were mutated the most often in the two subgroups were displayed in waterfall plots. **(C)** Comparisons between the two subgroups in terms of stromal score, immune score, estimate score, and tumor purity. **(D)** Box plot presented multiple immune checkpoints between the EMT-high and EMT-low subgroups. **(E)** Barplot showed 22 infiltrating immune cells' composition in each TARGET-OS sample. **(F)** Violin plot illustrated the compositional differences between the two subgroups of the 22 invading immune cells.

DNAH9 and UNC79, and the gene that showed highest frequent mutations in both groupings was TP53.

An increasing body of research indicates that immune cells in the tumor microenvironment play a crucial role in the progression of tumor (Cai et al., 2022). Utilizing the ESTIMATE, we determined the stromal-, immune-, estimate-scores, and tumor purity levels between the two subgroups, finding that the group with higher EMT-Related gene expression had a higher stromal score, while the other three showed no notable distinctions (Figure 3C). ICP expression analysis suggested that PDCD1LG2 was upregulated in the EMT-high subgroup (Figure 3D). Subsequently, we assessed the extent of immune infiltration in 22 different kinds of immune cell types of OS patients in the TARGET database by

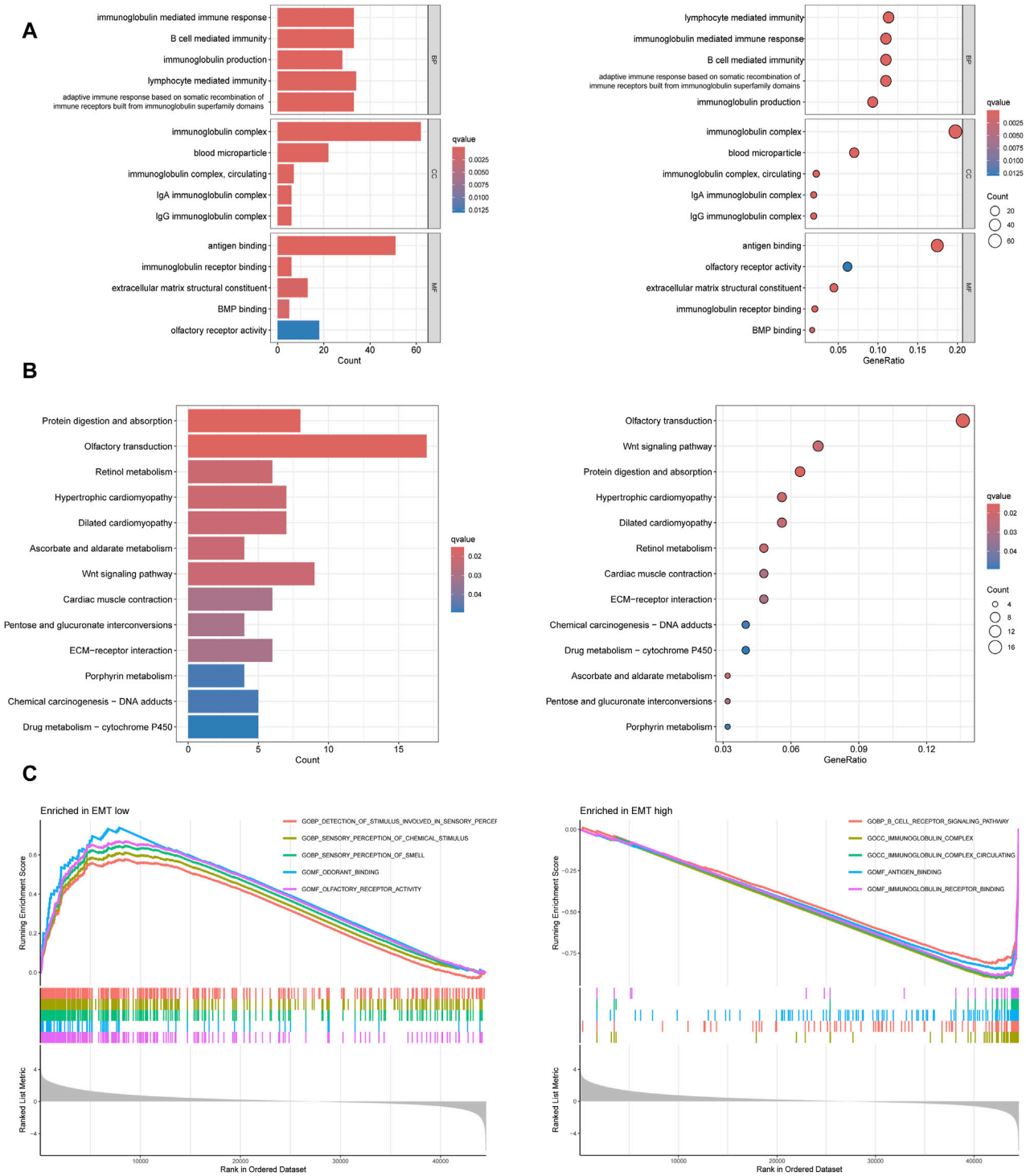

FIGURE 4
Functional enrichment analyses based on 53 prognosis-related EMT-Related DEGs. **(A)** GO enrichment analysis showed the top five significant terms in BP, CC, and MF. **(B)** KEGG enrichment analysis showed all the pathways with significant differences. **(C)** GO GESA enrichment analysis showed the top five enriched pathways in different subtypes.

the CIBERSORT (Figure 3E). In specifics, patients in the EMT-high class showed greater amounts of plasma cells, activated memory CD4 T cells and resting NK cells, whereas the fraction of resting dendritic cells was reduced in the EMT-high subgroup (Figure 3F).

GO, KEGG and GSEA enrichment analysis

GO and KEGG enrichment analysis were conducted based on 53 prognosis-related EMT-Related DEGs to clarify the potential functions and pathways related to EMT-RGs. In GO enrichment

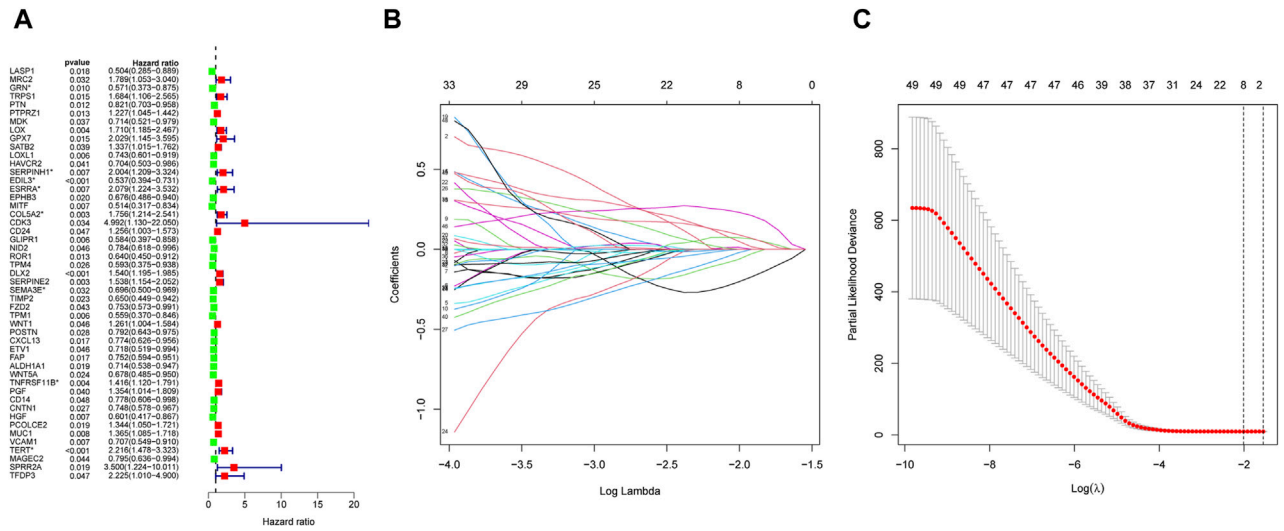

FIGURE 5
Construction of the EMT-Related risk model. **(A)** 49 EMT-RGs were shown to be connected to OS patients' overall survival by univariate Cox regression. **(B, C)** Eight prognostic EMT-RGs were screened by LASSO Cox regression and used for constructing the risk signature. "*" was used to highlight the eight genes.

analysis, we noted that these genes were positively related with "B cell mediated immunity," "immunoglobulin mediated immune response," "immunoglobulin complex," "antigen binding," and "immunoglobulin reception binding" (Figure 4A). KEGG analysis revealed three pathways where these genes enriched in, including "wnt signaling pathway," "potential digestion and absorption," and "retinol metabolism" and other pathways (Figure 4B). In addition, through GO GSEA enrichment analysis, we found that the main enriched pathways in the EMT-low subgroup included "detection of stimulus involved in sensory perception," "sensory perception of chemical Stimulus" and "sensory perception of smell." EMT-high subgroup, on the other hand, were mainly enriched by other pathways including "B cell receptor signaling pathway," "immunoglobulin complex" and "immnoglobulin complex circulating" (Figure 4C). These enriched terms and pathways might be important in the development of tumor cells.

Construction of the EMT-Related risk signature

We identified 49 prognosis-related genes that were correlated with OS patient's overall survival. The expression of 28 genes was linked to extended overall survival of OS patients, whereas 21 genes was linked to reduced overall survival of OS patients (Figure 5A). Eight genes obtained by LASSO analysis as more important genes (including GRN, SERPINH1, EDIL3, ESRRA, COL5A2, SEMA3E, TNFRSF11B, and TERT) were used to establish the risk model (Figures 5B,C).

Predictive performance evaluation of the EMT-Related risk signature

In the training cohort, the risk model's prognostic value was initially ascertained, and then verified by the GSE21257 validation cohort. Patients in the training and validation cohorts were separated into the high- and low-risk categories based on the median risk score. The high-risk group had a higher quantity of deaths in both cohorts, indicating poorer prognosis of patients in this group (Figures 6A, B). As shown by the K-M survival analysis, the overall survival rate of the high-risk group of patients was lower than that of the low-risk group (Figures 6C, D). Utilizing ROC analysis, OS patients in the training cohort showed 1-, 3-, and 5-year survival rates with AUC values of 0.823, 0.793, and 0.808, respectively (Figure 6E). Similarly, the AUC values of the risk model were 0.750, 0.683, and 0.677 for the validation cohort at 1-, 3-, and 5-years, respectively (Figure 6F). Collectively, these findings suggest that the risk model demonstrated a high level of predictive accuracy in both the training and validation cohorts.

EMT-Related risk signature as an independent predictive factor for OS

Employing the multifaceted Cox regression analysis, the study unequivocally established that patients with OS may be able to use the risk score as an independent predictor of their overall prognosis (Figure 7A). Additionally, to help better predict the clinical outcomes of OS patients, a nomogram was created with the scoring system depicted in the top part and the prediction system in the bottom part (Figure 7B). From Calibration curves, we could find that the predicted survival time could be very close to the actual survival time at 1-, 3-, and 5-years (Figure 7C). The findings above suggested that the EMT-Related risk signature could be considered as an independent predictor of OS and had a lot of promise for therapeutic applications.

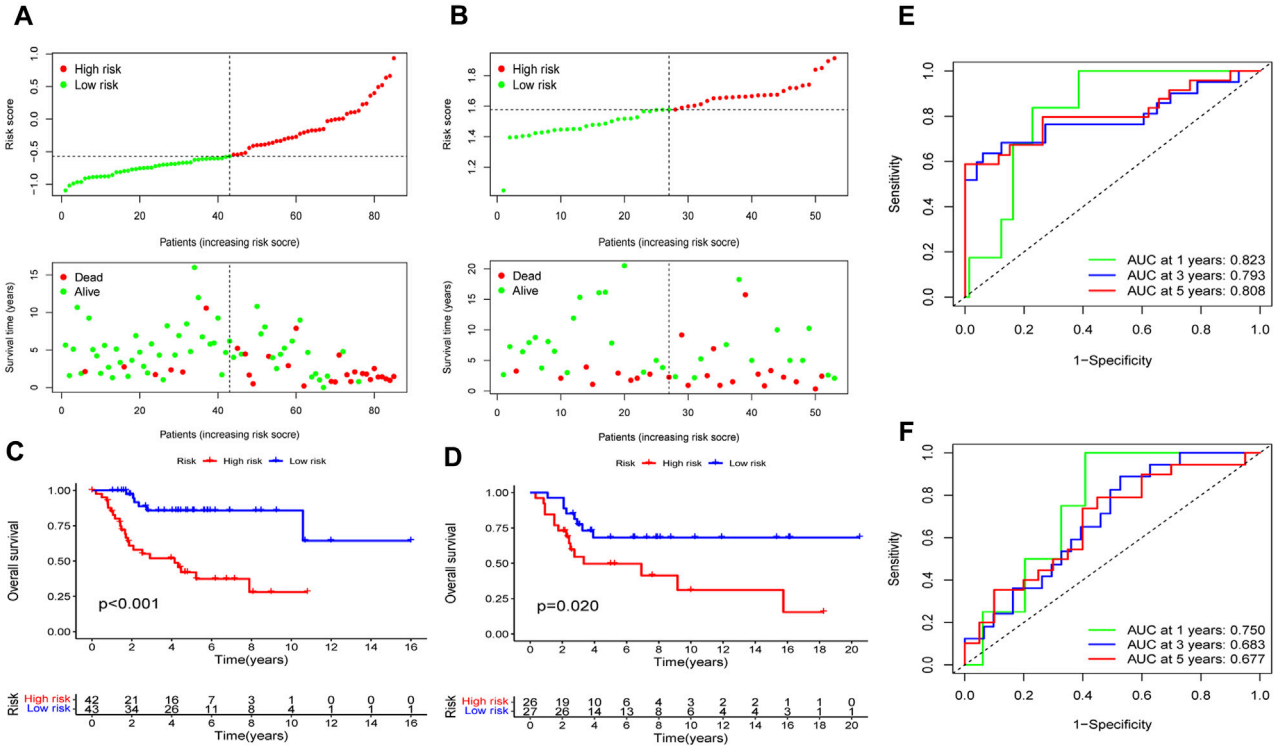

FIGURE 6
Assess the EMT-Related risk signature's prediction performance. The training **(A)** and validation **(B)** cohorts of OS patients were classified as low-risk and high-risk subgroups based on the median risk score, and the high-risk group had a higher incidence of deaths in both cohorts. In the training **(C)** and validation **(D)** cohorts, the overall survival rates for OS patients in the high-risk groups was notably lower, according to K-M survival analyses. ROC analyses demonstrated the AUC values of the risk model for 1-, 3-, and 5-year survival rates of OS patients in the training **(E)** and validation **(F)** cohorts.

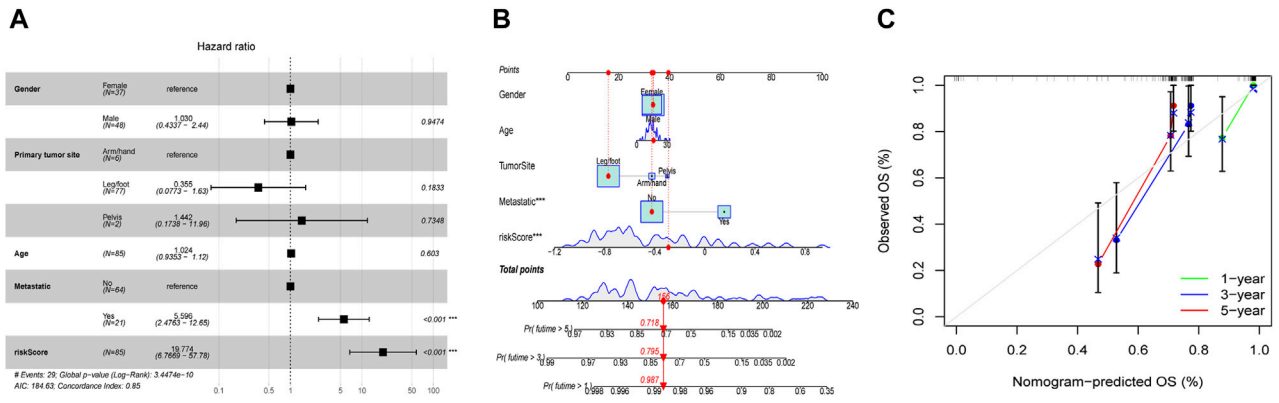

FIGURE 7
Independent prognostic evaluation and nomogram construction. **(A)** Multivariate Cox analysis demonstrated that the risk score may be used independently to predict OS patients' prognosis. **(B)** The nomogram for predicting the survival percentage of patients at 1-, 3-, and 5-years in TARGET was constructed using gender, age, tumor-site, metastatic situation, and risk score. **(C)** Calibration curves revealed that there may be a similarity between the nomogram-predicted overall survival of OS patients and their actual survival duration.

Evaluation of immunotherapy sensitivity

We first analyzed the immunological features between the high- and low-risk groups. We found that the low-risk group presented statistically higher stromal score, immune score, estimate score, and lower tumor purity (Figure 8A). Further analysis revealed that there was a positive relationship between the risk and with resting dendritic cell expression (R = 0.22, $P < 0.05$) while a negative relationship existed with activated memory CD4 T cell levels (R = −0.28, $P < 0.01$; Figure 8B). The MSI score was then

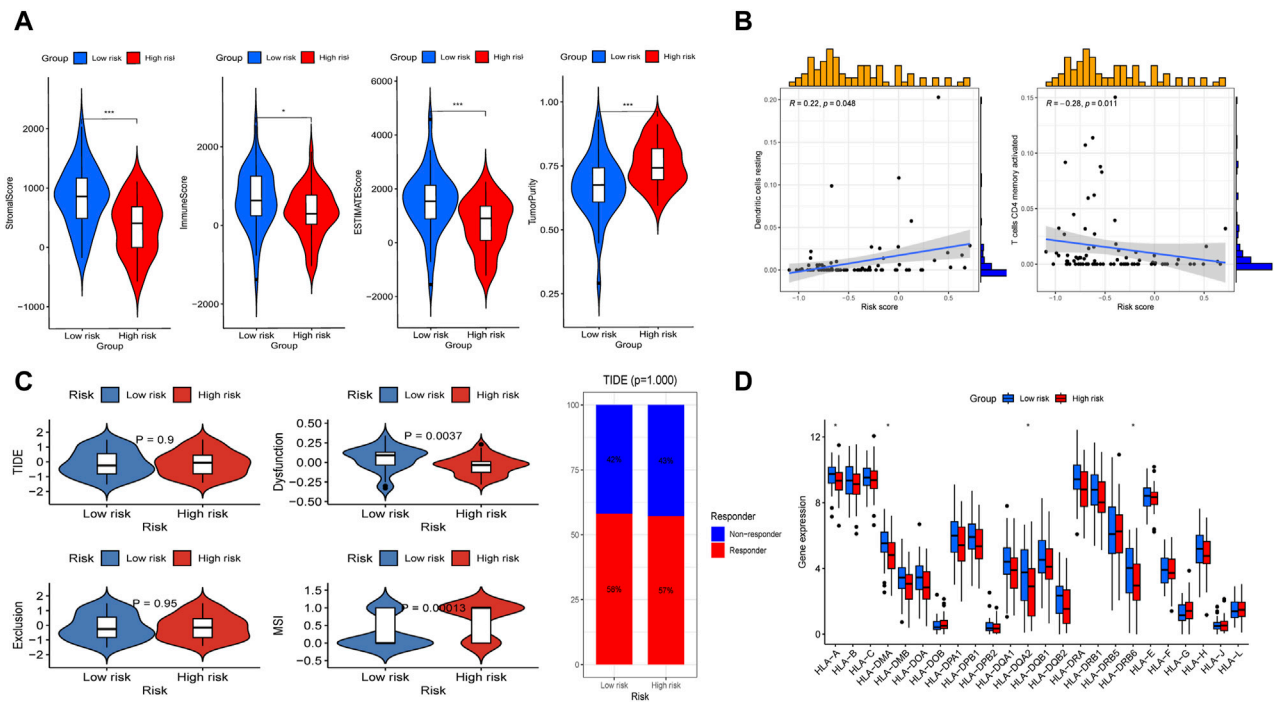

FIGURE 8
Evaluation of immunotherapy sensitivity in the high-risk and low-risk subgroups. **(A)** Comparisons between the two subgroups in terms of stromal-, immune-, estimate-scores, and tumor purity. **(B)** Spearman correlation study demonstrated the association between immune cells (including resting dendritic cell and active memory CD4 T cells) and risk score. **(C)** The differences of TIDE score, dysfuction score, exclusion score, MSI score, and the proportion of patients whether response to ICP between the two subgroups. **(D)** Box plot presented differential expression of HLA genes between the two subgroups.

calculated, and we discovered that the high-risk group had a substantially higher MSI score compared to the low-risk subgroup (Figure 8C). In addition, through TIDE analysis, we found that dysfunction score was decreased in the high-risk group, while TIDE and exclusion scores did not show apparent differences between the two subtypes (Figure 8C). And the percentage of ICB therapy non-responders was similar to that of responders, which indicated that patients with OS may be not sensitive to immunotherapy (Figure 8C). Furthermore, giving the significance of human leukocyte antigen (HLA) genes in anti-cancer immunity, we examined 24 HLA genes across different risk classes. Our findings indicated that most genes were downregulated in the high-risk subgroup (Figure 8D). This result suggested that potential association may existed between the risk score and HLA gene expression levels, which may serve as prospective immunotherapy biomarkers.

Prediction of potential chemotherapeutic agents

The correlation between the risk score and sensitivity of some chemotherapeutic agents was calculated by "oncoPredict" package in R software. And the results indicated lower IC50 values and better sensitivity of vorinostat, lapatinib, VSP34_8731, I-BRD9, and NVP-ADW742 in the high-risk group, which implied that aforementioned chemotherapeutic agents would be more beneficial for individuals with higher risk scores (Figure 9).

Single-cell landscape of hub genes

The cellular heterogeneity in tumor tissues of OS patients was characterized using scRNA-seq data analysis. In the UMAP plot, a total of 28 main cell clusters were displayed. Followed all clusters annotated using markers, the UMAP representing all sequenced cells revealed eight main cell types: CD4Tconv, CD8Tex, endothelial, fibroblasts, malignant, Mono/Macro, osteoblasts, and plasmocytes (Figure 10A). Among these cell types, Mono/Macro was found to occupy the highest proportion in the tumor microenvironment (Figure 10B). Furthermore, three prognostic hub genes were screened, including EDIL3, SEMA3E, and TNFRSF11B (Figure 10C). Further analysis demonstrated different expression patterns of each gene in various cell types. EDIL3 showed a high expression level in endothelial cells and fibroblasts, while SEMA3E in malignant cells, and TNFRSF11B in fibroblasts and malignant cells (Figure 10D).

Discussion

Osteosarcoma (OS) is a well-known malignant bone tumor with great harm in children and adolescents (Gilsenan et al., 2021; Rojas

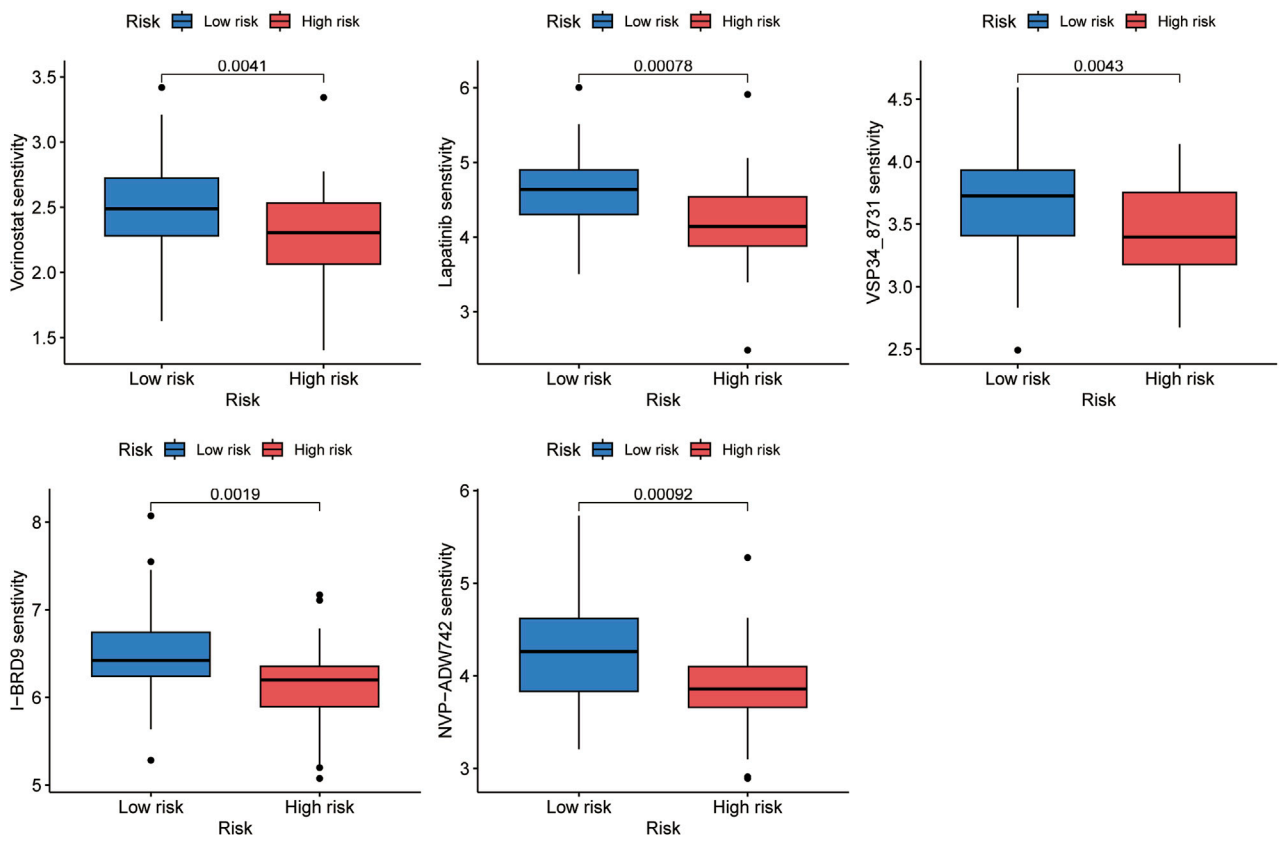

FIGURE 9
Five chemotherapeutic agents, including vorinostat, lapatinib, VSP34_8731, I-BRD9, and NVP-ADW742, were discovered to be more beneficial for OS patients with higher risk scores.

et al., 2021). Owing to this tumor's high malignancy, OS patients continue to have an unsatisfactory survival rate, with over half dying from tumor cell metastasis and resistance to chemotherapy (Chou and Gorlick, 2006; Benjamin, 2020). Consequently, gaining a more profound understanding of the possible biomechanisms linked to the advancement of OS is especially crucial, thus creating novel therapies to improve the clinical outcomes for patients with OS. EMT, a cellular process, has been identified to be closely associated with the initiation and migration of cancers, including breast and bladder cancers (Chen et al., 2021; Kong et al., 2021). It has also been proved to result in drug resistance in lung and breast cancers (Luo et al., 2018; Tulchinsky et al., 2019). Moreover, many studies have demonstrated the connection between EMT and immunity in human cancers (Lou et al., 2016; Mak et al., 2016). Recently, there are studies showing that EMT plays a important role in the progression of OS, potentially elucidating why EMT leads to poorer clinical results in OS patients (Jiang et al., 2019). A multitude of distinct prognostic EMT-RGs have been investigated (Zhang Y. et al., 2019; Chen et al., 2019). Here, we explored the prognostic value of EMT-RGs by bioinformatics analysis and constructed created a novel EMT-Related risk signature. It has been shown that prognostic-related gene signatures from sequencing data play important roles in the identification of risk stratification and prediction of survival, developing precise treatment strategies for cancer patients (Gong et al., 2023).

Our research revealed that patients with OS can be divided into two distinct categories based on the EMT-Related DEGs, exhibiting significant differences in somatic mutations, immune responses, and possible mechanisms. The stromal score of the EMT-high subgroup was significantly higher, indicating that stromal cells inside the tumor microenvironment may be the source of EMT-RG expression in OS. This idea was also supported by earlier research on colorectal, urothelial, and OS cancers (Isella et al., 2015; Wang et al., 2018). The EMT-high subtype was related to positive clinical results along with an active immune reaction. Peng et al. (2020) revealed that a high EMT score was linked to significantly poor overall survival in OS patients, which was contrary to the result of this study. But judging by the results of the immune response, we could discover that immune cells, such as plasma cells and activated memory CD4 T cells, were increased in the EMT-high subtype, while resting dendritic cells were lower than the EMT-low subgroup. The anti-tumor immunity and immunosurveillance against cancer are beneficially mediated by plasma cells and CD4 T cells, and the enhancement of their responses may make cancer immunotherapies more effective (Wouters and Nelson, 2018; Yamamoto et al., 2020). By processing immune signals and presenting antigens to T cells, activated dendritic cells can initiate immunological cascades, which may explain lower levels of immunoreaction in patients with higher amounts of resting dendritic cells (Gardner and Ruffell, 2016; Hato et al., 2024). PDCD1LG2 was also discovered to be higher in the EMT-high subgroup by ICP expression analysis. It's been established that improved general survival in hepatocellular

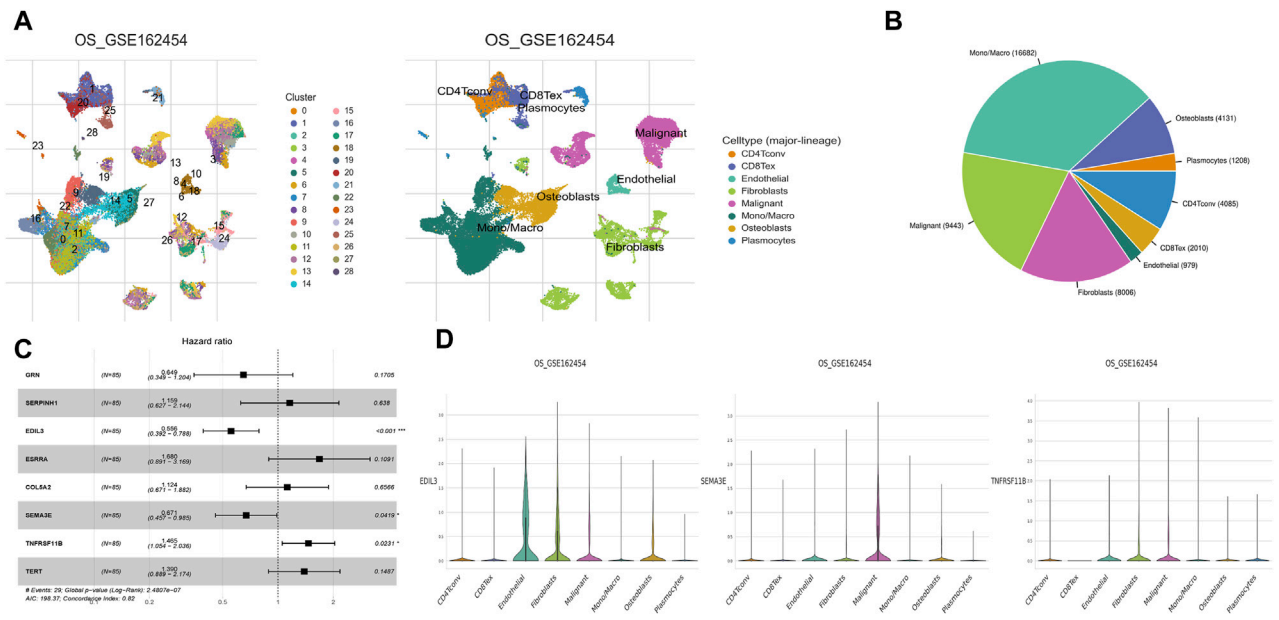

FIGURE 10
Single-cell landscape of hub genes. **(A)** UMAP plots displayed 28 main cell clusters and eight main cell types. **(B)** Pie chart displayed the immune cell composition of OS samples. Mono/Macro was found to dominate the tumour immune microenvironment. **(C)** Multivariate Cox regression identified three hub genes that affected the prognosis of OS, including EDIL3, SEMA3E, and TNFRSF11B. **(D)** Violin plots showing hub EDIL3, SEMA3E, and TNFRSF11B at the single-cell level in each of the eight main cell types.

carcinoma is linked to this gene expression (Lei et al., 2021). All these above could explain the better overall survival in the EMT-high subgroup to some extent. Therefore, we speculated that the prognosis of OS patients may be not directly related to the expression of EMT-RGs, but associated with the immune response accompanying the process of EMT, and active immune response may contribute to better clinical outcomes in OS patients.

To acquire a deeper insight into the possible pathways of EMT-RGs in OS development, functional enrichment studies were subsequently carried out. The results of GO analysis showed possible mechanisms in the progression of OS affected by EMT-RGs. To be specific, abnormal activation of B cells promoted by antigen binding, induce immunoglobulin production which bind to the corresponding receptors, leading to abnormal immune responses ultimately. In KEGG analysis, pathways mainly enriched were metabolic process related pathways, implying a coordinated interaction of these processes in OS. In light of the possible link between GO analysis outcomes and immune-related pathways, GSEA was employed in the two EMT-Related subgroups. And the results indicated a very close relationship between EMT-RGs and immunity in the occurrence and development of OS. These results could provide implications when developing new treatment methods for OS, especially immunotherapy.

Furthermore, we constructed a predictive risk signature using eight EMT-RGs, including GRN, SERPINH1, EDIL3, ESRRA, COL5A2, SEMA3E, TNFRSF11B, and TERT. GRN, by encoding granulin precursor, mainly controls the survival and differentiation of neurons, and is linked to immune, inflammatory, and stress reactions in the nervous system (Chu et al., 2023; Cai et al., 2024). SERPINH1, also known as HSP47, is noteworthy in the development of several kinds of human malignancies, including breast cancer, cervical cancer and other malignancies (Nagata et al., 1986; Yamamoto et al., 2013; Yoneda et al., 2020). Xia et al. (2024) revealed than SERPINH1 could enhance the malignancy of OS via PI3K-Akt signaling pathway. EDIL3 acts as a pro-angiogenic factor and associates with worse clinical outcomes of several cancers, such as gastric, breast and pancreatic cancers (Jiang et al., 2016; Kun et al., 2019; Zhang et al., 2020). There are studies suggesting that EDIL3 may promote EMT in cancer cells by facilitating autocrine or paracrine signaling (Gasca et al., 2020). ESRRA, full name estrogen related receptor alpha, is considered as an orphan nuclear receptor (Li FN. et al., 2021). Earlier research indicates a link between the over expression of ESRRA and unfavorable cancer outcomes, as it hastens the cancer cell proliferation and improves their ability to migrate and invade (Zhang L. et al., 2019; Wang L. et al., 2020). COL5A2 is crucial for regulating the immune system, promoting angiogenesis, and facilitating tumor metastasis (Ding et al., 2021). It was found by Han et al. (2022) that COL5A2 could prevent the malignant progression of OS. SEMA3E was found to play an important role in OS metastasis induced by UHRF1 overexpression. TNFRSF11B, also called osteoprotegerin (OPG), has been confirmed to participate in OS growth. Marley et al. (2015) revealed that OPG could increase proliferation in human derived OS cell lines. TERT, fully known as telomerase reverse transcriptase, is a catalytic subunit of telomerase, abnormal expression of which can activate the telomerase and play a key role in the cancer formation (Zou et al., 2020). A vitro study by Xie et al. (2023) indicated that inhibiting TERT may reduce the motility, metastasis, and proliferation of OS cells.

According to survival analyses, eight previously listed genes showed a strong correlation with the prognosis of OS patients and the high-risk individuals had a worse prognosis. The predictive

precision of the risk model underwent additional validation by ROC curves. Moreover, multivariate Cox regression analysis provided convincing proof of the independence of the risk model. In order to improve the prediction of OS patients' prognosis, we created a nomogram that incorporated clinical features such as gender, age, tumor-site, and metastatic situation. In the training cohort, the nomogram's predictive performance was demonstrated with effectiveness, evidenced by survival rates at 1-, 3-, and 5-years, which further proved the risk model's prediction effectiveness.

MSI score of tumor tissues can show how well ICB is working as a treatment, and the higher the score, the better the effects (Lichtenstern et al., 2020; Lin et al., 2020; Jiang et al., 2021). The high-risk group exhibited a higher MSI score in our research, suggesting that patients in this category may benefit more from ICB. However, upon comparing the immunological characteristics of the two risk groups, we discovered that patients with higher risk scores presented poorer immune infiltration. Additionally, we discovered the risk score was positively related with the expression levels of resting dendritic cells, while negatively correlated with activated memory CD4 T cells. Integrating all of these factors, we speculated that while high MSI scores would induce immune reactions, missing activated dendritic cells would eventually prohibit T cells from activation to efficiently attack cancer cells. A study by Pan et al. (2022) also has the similar speculation. The following TIDE analysis showed that the percentage of patients who responded to immunotherapy and those who did not shown any discernible variation. To summarize the above, we could suspect that OS patients may be not very sensitive to immunotherapy. In reality, OS is regarded as a "cold" tumor that may not respond well to ICP inhibitor therapy or be receptive to ICB (Wu et al., 2020; Li X. et al., 2021). Finally, upon conducting oncoPredict, it was discovered that patients in the high-risk subtype had lower IC50 values and greater sensitivity for five drugs, including vorinostat, lapatinib, VSP34_8731, I-BRD9, and NVP-ADW742. These findings may help guide individualized treatments for OS patients.

Data from scRNA-seq represents a novel method in cancer studies, aimed at identifying tumor cell composition and analyzing gene expression changes at the individual cell scale (Guo et al., 2024). This study revealed Mono/Macro as the predominant cell type in the tumor microenvironment, indicating their potential critical roles in the pathogenesis of OS. Further analysis of scRNA-seq data indicated that the cell types in which three hub genes highly expressed were not exactly same. These discoveries gain comprehensive insight on the molecular and cellular variations of OS, and have significant ramifications for developing novel treatment approaches that target particular cell types and genes. Nonetheless, more studies are required to corroborate these findings and ascertain their clinical relevance.

However, this study has several limitations. First of all, the training cohort of this study contains only 85 OS samples from the TARGET database, making the sample size small. Also, our model needs to be further validated using datasets outside of the GSE21257. Moreover, eight genes we have identified that may influence the prognosis of OS patients require further experiments *in vivo* and *in vitro* to elucidate their exact mechanisms of action. Nevertheless, our findings emphasize the significance of EMT-Related gene classifications in assessing the tumor immune microenvironment as well as predicting the prognosis of patients with OS. These findings not only contribute to the development of new treatment methods, but also help clinicians better predict the clinical outcomes of patients.

Conclusion

In summary, our study analyzed the tumor immune microenvironment, immune response and biological functions in EMT-Related subtypes. And the prognosis of OS patients could be independently predicted by the risk signature constructed based on eight EMT-Related DEGs. Our results may give physicians novel perspectives into how to evaluate the prognosis of OS patients and develop more customized and efficient therapy regimens for OS patients, yet further study is still needed to validate our findings.

Data availability statement

The original contributions presented in the study are included in the article/Supplementary Material, further inquiries can be directed to the corresponding author.

Ethics statement

The studies involving humans were approved by Ethics Committee of Guangzhou First People's Hospital. The studies were conducted in accordance with the local legislation and institutional requirements. The human samples used in this study were acquired from the data that support the findings of this study are available from the corresponding author upon reasonable request. Written informed consent for participation was not required from the participants or the participants' legal guardians/next of kin in accordance with the national legislation and institutional requirements.

Author contributions

M-PL: Conceptualization, Formal Analysis, Investigation, Software, Writing–original draft, Writing–review and editing. S-PL: Conceptualization, Formal Analysis, Resources, Validation, Writing–original draft, Writing–review and editing. W-CL: Conceptualization, Methodology, Software, Validation, Writing–original draft, Writing–review and editing. KL: Data curation, Software, Validation, Writing–review and editing. X-HG: Conceptualization, Funding acquisition, Project administration, Resources, Visualization, Writing–review and editing.

Funding

The author(s) declare that financial support was received for the research, authorship, and/or publication of this article. This work

was supported by Science and Technology Projects in Guangzhou (No. 2023A03J0968).

Conflict of interest

The authors declare that the research was conducted in the absence of any commercial or financial relationships that could be construed as a potential conflict of interest.

Publisher's note

All claims expressed in this article are solely those of the authors and do not necessarily represent those of their affiliated organizations, or those of the publisher, the editors and the reviewers. Any product that may be evaluated in this article, or claim that may be made by its manufacturer, is not guaranteed or endorsed by the publisher.

References

Bakir, B., Chiarella, A. M., Pitarresi, J. R., and Rustgi, A. K. (2020). EMT, MET, plasticity, and tumor metastasis. *Trends Cell Biol.* 30 (10), 764–776. doi:10.1016/j.tcb.2020.07.003

Benjamin, R. S. (2020). Adjuvant and neoadjuvant chemotherapy for osteosarcoma: a historical perspective. *Adv. Exp. Med. Biol.* 1257, 1–10. doi:10.1007/978-3-030-43032-0_1

Brown, H. K., Tellez-Gabriel, M., and Heymann, D. (2017). Cancer stem cells in osteosarcoma. *Cancer Lett.* 386, 189–195. doi:10.1016/j.canlet.2016.11.019

Cai, J., Hu, Y., Ye, Z., Ye, L., Gao, L., Wang, Y., et al. (2022). Immunogenic cell death-related risk signature predicts prognosis and characterizes the tumour microenvironment in lower-grade glioma. *Front. Immunol.* 13, 1011757. doi:10.3389/fimmu.2022.1011757

Cai, Y., Peng, Z., He, Q., and Sun, P. (2024). Behavioral variant frontotemporal dementia associated with GRN and ErbB4 gene mutations: a case report and literature review. *BMC Med. Genomics* 17 (1), 43. doi:10.1186/s12920-024-01819-5

Chen, J., Liu, G., Wu, Y., Ma, J., Wu, H., Xie, Z., et al. (2019). CircMYO10 promotes osteosarcoma progression by regulating miR-370-3p/RUVBL1 axis to enhance the transcriptional activity of β-catenin/LEF1 complex via effects on chromatin remodeling. *Mol. Cancer* 18 (1), 150. doi:10.1186/s12943-019-1076-1

Chen, X., Chen, R. X., Wei, W. S., Li, Y. H., Feng, Z. H., Tan, L., et al. (2021). Correction: PRMT5 circular RNA promotes metastasis of urothelial carcinoma of the bladder through sponging miR-30c to induce epithelial-mesenchymal transition. *Clin. Cancer Res.* 27 (9), 2664. doi:10.1158/1078-0432.CCR-21-0936

Chou, A. J., and Gorlick, R. (2006). Chemotherapy resistance in osteosarcoma: current challenges and future directions. *Expert Rev. Anticancer Ther.* 6 (7), 1075–1085. doi:10.1586/14737140.6.7.1075

Chu, M., Nan, H., Jiang, D., Liu, L., Huang, A., Wang, Y., et al. (2023). Progranulin gene mutations in Chinese patients with frontotemporal dementia: a case report and literature review. *J. Alzheimers Dis.* 93 (1), 225–234. doi:10.3233/JAD-230052

Derynck, R., and Weinberg, R. A. (2019). EMT and cancer: more than meets the eye. *Dev. Cell* 49 (3), 313–316. doi:10.1016/j.devcel.2019.04.026

Ding, Y. L., Sun, S. F., and Zhao, G. L. (2021). COL5A2 as a potential clinical biomarker for gastric cancer and renal metastasis. *Med. Baltim.* 100 (7), e24561. doi:10.1097/MD.0000000000024561

Gardner, A., and Ruffell, B. (2016). Dendritic cells and cancer immunity. *Trends Immunol.* 37 (12), 855–865. doi:10.1016/j.it.2016.09.006

Gasca, J., Flores, M. L., Jiménez-Guerrero, R., Sáez, M. E., Barragán, I., Ruíz-Borrego, M., et al. (2020). EDIL3 promotes epithelial-mesenchymal transition and paclitaxel resistance through its interaction with integrin αVβ3 in cancer cells. *Cell Death Discov.* 6, 86. doi:10.1038/s41420-020-00322-x

Gilsenan, A., Midkiff, K., Harris, D., Kellier-Steele, N., McSorley, D., and Andrews, E. B. (2021). Teriparatide did not increase adult osteosarcoma incidence in a 15-year US postmarketing surveillance study. *J. Bone Min. Res.* 36 (2), 244–251. doi:10.1002/jbmr.4188

Gong, H., Tao, Y., Xiao, S., Li, X., Fang, K., Wen, J., et al. (2023). Identification of an EMT-related gene-based prognostic signature in osteosarcoma. *Cancer Med.* 12 (11), 12912–12928. doi:10.1002/cam4.5942

Gong, L., Zhang, D., Dong, Y., Lei, Y., Qian, Y., Tan, X., et al. (2018). Integrated bioinformatics analysis for identificating the therapeutic targets of aspirin in small cell lung cancer. *J. Biomed. Inf.* 88, 20–28. doi:10.1016/j.jbi.2018.11.001

Groisberg, R., Hong, D. S., Behrang, A., Hess, K., Janku, F., Piha-Paul, S., et al. (2017). Characteristics and outcomes of patients with advanced sarcoma enrolled in early phase immunotherapy trials. *J. Immunother. Cancer* 5 (1), 100. doi:10.1186/s40425-017-0301-y

Guo, C., Yang, X., and Li, L. (2024). Pyroptosis-related gene signature predicts prognosis and response to immunotherapy and medication in pediatric and young adult osteosarcoma patients. *J. Inflamm. Res.* 17, 417–445. doi:10.2147/JIR.S440425

Han, Y. L., Luo, D., Habaxi, K., Tayierjiang, J., Zhao, W., Wang, W., et al. (2022). COL5A2 inhibits the TGF-β and wnt/β-catenin signaling pathways to inhibit the invasion and metastasis of osteosarcoma. *Front. Oncol.* 12, 813809. doi:10.3389/fonc.2022.813809

Hato, L., Vizcay, A., Eguren, I., Pérez-Gracia, J. L., Rodríguez, J., Gállego Pérez-Larraya, J., et al. (2024). Dendritic cells in cancer immunology and immunotherapy. *Cancers (Basel)* 16 (5), 981. doi:10.3390/cancers16050981

Isella, C., Terrasi, A., Bellomo, S. E., Petti, C., Galatola, G., Muratore, A., et al. (2015). Stromal contribution to the colorectal cancer transcriptome. *Nat. Genet.* 47 (4), 312–319. doi:10.1038/ng.3224

Ji, T., Shi, Q., Mei, S., Xu, J., Liang, H., Xie, L., et al. (2023). Integrated analysis of single-cell and bulk RNA sequencing data reveals an immunostimulatory microenvironment in tumor thrombus of osteosarcoma. *Oncogenesis* 12 (1), 31. doi:10.1038/s41389-023-00474-2

Jiang, M., Jia, K., Wang, L., Li, W., Chen, B., Liu, Y., et al. (2021). Alterations of DNA damage response pathway: biomarker and therapeutic strategy for cancer immunotherapy. *Acta Pharm. Sin. B* 11 (10), 2983–2994. doi:10.1016/j.apsb.2021.01.003

Jiang, S. H., Wang, Y., Yang, J. Y., Li, J., Feng, M. X., Wang, Y. H., et al. (2016). Overexpressed EDIL3 predicts poor prognosis and promotes anchorage-independent tumor growth in human pancreatic cancer. *Oncotarget* 7 (4), 4226–4240. doi:10.18632/oncotarget.6772

Jiang, X., Zhang, Z., Song, C., Deng, H., Yang, R., Zhou, L., et al. (2019). Glaucocalyxin A reverses EMT and TGF-β1-induced EMT by inhibiting TGF-β1/Smad2/3 signaling pathway in osteosarcoma. *Chem. Biol. Interact.* 307, 158–166. doi:10.1016/j.cbi.2019.05.005

Kager, L., Tamamyan, G., and Bielack, S. (2017). Novel insights and therapeutic interventions for pediatric osteosarcoma. *Future Oncol.* 13 (4), 357–368. doi:10.2217/fon-2016-0261

Kong, D., Zhou, H., Neelakantan, D., Hughes, C. J., Hsu, J. Y., Srinivasan, R. R., et al. (2021). VEGF-C mediates tumor growth and metastasis through promoting EMT-epithelial breast cancer cell crosstalk. *Oncogene* 40 (5), 964–979. doi:10.1038/s41388-020-01539-x

Kun, Z., Xin, G., Tao, W., Chenglong, Z., Dongsheng, W., Liang, T., et al. (2019). Tumor derived EDIL3 modulates the expansion and osteoclastogenesis of myeloid derived suppressor cells in murine breast cancer model. *J. Bone Oncol.* 16, 100238. doi:10.1016/j.jbo.2019.100238

Lei, T., Qian, H., Lei, P., and Hu, Y. (2021). Ferroptosis-related gene signature associates with immunity and predicts prognosis accurately in patients with osteosarcoma. *Cancer Sci.* 112 (11), 4785–4798. doi:10.1111/cas.15131

Li, F. N., Zhang, Q. Y., Li, O., Liu, S. L., Yang, Z. Y., Pan, L. J., et al. (2021a). ESRRA promotes gastric cancer development by regulating the CDC25C/CDK1/CyclinB1 pathway via DSN1. *Int. J. Biol. Sci.* 17 (8), 1909–1924. doi:10.7150/ijbs.57623

Li, X., Luo, L., Jiang, M., Zhu, C., Shi, Y., Zhang, J., et al. (2021b). Cocktail strategy for 'cold' tumors therapy via active recruitment of CD8+ T cells and enhancing their function. *J. Control Release* 334, 413–426. doi:10.1016/j.jconrel.2021.05.002

Lichtenstern, C. R., Ngu, R. K., Shalapour, S., and Karin, M. (2020). Immunotherapy, inflammation and colorectal cancer. *Cells* 9 (3), 618. doi:10.3390/cells9030618

Lin, A., Zhang, J., and Luo, P. (2020). Crosstalk between the MSI status and tumor microenvironment in colorectal cancer. *Front. Immunol.* 11, 2039. doi:10.3389/fimmu.2020.02039

Liu, C., Xie, J., Lin, B., Tian, W., Wu, Y., Xin, S., et al. (2024). Pan-cancer single-cell and spatial-resolved profiling reveals the immunosuppressive role of APOE+ macrophages in immune checkpoint inhibitor therapy. *Adv. Sci. (Weinh).* 11, e2401061. doi:10.1002/advs.202401061

Liu, P., Deng, X., Zhou, H., Xie, J., Kong, Y., Zou, Y., et al. (2023). Multi-omics analyses unravel DNA damage repair-related clusters in breast cancer with experimental validation. *Front. Immunol.* 14, 1297180. doi:10.3389/fimmu.2023.1297180

Lou, Y., Diao, L., Cuentas, E. R., Denning, W. L., Chen, L., Fan, Y. H., et al. (2016). Epithelial-mesenchymal transition is associated with a distinct tumor microenvironment including elevation of inflammatory signals and multiple immune checkpoints in lung adenocarcinoma. *Clin. Cancer Res.* 22 (14), 3630–3642. doi:10.1158/1078-0432.CCR-15-1434

Lu, X. Q., Zhang, J. Q., Zhang, S. X., Qiao, J., Qiu, M. T., Liu, X. R., et al. (2021). Identification of novel hub genes associated with gastric cancer using integrated bioinformatics analysis. *BMC Cancer* 21 (1), 697. doi:10.1186/s12885-021-08358-7

Luo, J., Yao, J. F., Deng, X. F., Zheng, X. D., Jia, M., Wang, Y. Q., et al. (2018). 14, 15-EET induces breast cancer cell EMT and cisplatin resistance by up-regulating integrin αvβ3 and activating FAK/PI3K/AKT signaling. *J. Exp. Clin. Cancer Res.* 37 (1), 23. doi:10.1186/s13046-018-0694-6

Maeser, D., Gruener, R. F., and Huang, R. S. (2021). oncoPredict: an R package for predicting *in vivo* or cancer patient drug response and biomarkers from cell line screening data. *Brief. Bioinform* 22 (6), bbab260. doi:10.1093/bib/bbab260

Mak, M. P., Tong, P., Diao, L., Cardnell, R. J., Gibbons, D. L., William, W. N., et al. (2016). A patient-derived, pan-cancer EMT signature identifies global molecular alterations and immune target enrichment following epithelial-to-mesenchymal transition. *Clin. Cancer Res.* 22 (3), 609–620. doi:10.1158/1078-0432.CCR-15-0876

Marley, K., Bracha, S., and Seguin, B. (2015). Osteoprotegerin activates osteosarcoma cells that co-express RANK and RANKL. *Exp. Cell Res.* 338 (1), 32–38. doi:10.1016/j.yexcr.2015.08.001

Matsuoka, T., and Yashiro, M. (2024). Bioinformatics analysis and validation of potential markers associated with prediction and prognosis of gastric cancer. *Int. J. Mol. Sci.* 25 (11), 5880. doi:10.3390/ijms25115880

Miwa, S., Shirai, T., Yamamoto, N., Hayashi, K., Takeuchi, A., Igarashi, K., et al. (2019). Current and emerging targets in immunotherapy for osteosarcoma. *J. Oncol.* 2019, 7035045. doi:10.1155/2019/7035045

Nagata, K., Saga, S., and Yamada, K. M. (1986). A major collagen-binding protein of chick embryo fibroblasts is a novel heat shock protein. *J. Cell Biol.* 103 (1), 223–229. doi:10.1083/jcb.103.1.223

Pan, R., Pan, F., Zeng, Z., Lei, S., Yang, Y., Yang, Y., et al. (2022). A novel immune cell signature for predicting osteosarcoma prognosis and guiding therapy. *Front. Immunol.* 13, 1017120. doi:10.3389/fimmu.2022.1017120

Park, S. Y. (2018). Nomogram: an analogue tool to deliver digital knowledge. *J. Thorac. Cardiovasc Surg.* 155 (4), 1793. doi:10.1016/j.jtcvs.2017.12.107

Peng, Y. X., Yu, B., Qin, H., Xue, L., Liang, Y. J., and Quan, Z. X. (2020). EMT-related gene expression is positively correlated with immunity and may be derived from stromal cells in osteosarcoma. *PeerJ* 8, e8489. doi:10.7717/peerj.8489

Rojas, G. A., Hubbard, A. K., Diessner, B. J., Ribeiro, K. B., and Spector, L. G. (2021). International trends in incidence of osteosarcoma (1988-2012). *Int. J. Cancer* 149 (5), 1044–1053. doi:10.1002/ijc.33673

Ruh, M., Stemmler, M. P., Frisch, I., Fuchs, K., van Roey, R., Kleemann, J., et al. (2021). The EMT transcription factor ZEB1 blocks osteoblastic differentiation in bone development and osteosarcoma. *J. Pathol.* 254 (2), 199–211. doi:10.1002/path.5659

Shao, S., Piao, L., Guo, L., Wang, J., Wang, L., Wang, J., et al. (2022). Tetraspanin 7 promotes osteosarcoma cell invasion and metastasis by inducing EMT and activating the FAK-Src-Ras-ERK1/2 signaling pathway. *Cancer Cell Int.* 22 (1), 183. doi:10.1186/s12935-022-02591-1

Shi, D., Wu, F., Mu, S., Hu, B., Zhong, B., Gao, F., et al. (2019). LncRNA AFAP1-AS1 promotes tumorigenesis and epithelial-mesenchymal transition of osteosarcoma through RhoC/ROCK1/p38MAPK/Twist1 signaling pathway. *J. Exp. Clin. Cancer Res.* 38 (1), 375. doi:10.1186/s13046-019-1363-0

Sommer, B., Inoue, D., and Baaden, M. (2022). Design X Bioinformatics: a community-driven initiative to connect bioinformatics and design. *J. Integr. Bioinform* 19 (2), 20220037. doi:10.1515/jib-2022-0037

Su, M., Pan, T., Chen, Q. Z., Zhou, W. W., Gong, Y., Xu, G., et al. (2022). Data analysis guidelines for single-cell RNA-seq in biomedical studies and clinical applications. *Mil. Med. Res.* 9 (1), 68. doi:10.1186/s40779-022-00434-8

Tulchinsky, E., Demidov, O., Kriajevska, M., Barlev, N. A., and Imyanitov, E. (2019). EMT: a mechanism for escape from EGFR-targeted therapy in lung cancer. *Biochim. Biophys. Acta Rev. Cancer* 1871 (1), 29–39. doi:10.1016/j.bbcan.2018.10.003

Wang, L., Saci, A., Szabo, P. M., Chasalow, S. D., Castillo-Martin, M., Domingo-Domenech, J., et al. (2018). EMT- and stroma-related gene expression and resistance to PD-1 blockade in urothelial cancer. *Nat. Commun.* 9 (1), 3503. doi:10.1038/s41467-018-05992-x

Wang, L., Yang, M., Guo, X., Yang, Z., Liu, S., Ji, Y., et al. (2020b). Estrogen-related receptor-α promotes gallbladder cancer development by enhancing the transcription of Nectin-4. *Cancer Sci.* 111 (5), 1514–1527. doi:10.1111/cas.14344

Wang, M., Song, W. M., Ming, C., Wang, Q., Zhou, X., Xu, P., et al. (2022). Guidelines for bioinformatics of single-cell sequencing data analysis in Alzheimer's disease: review, recommendation, implementation and application. *Mol. Neurodegener.* 17 (1), 17. doi:10.1186/s13024-022-00517-z

Wang, Q., Zhao, S., Gan, L., and Zhuang, Z. (2020a). Bioinformatics analysis of prognostic value of PITX1 gene in breast cancer. *Biosci. Rep.* 40 (9). doi:10.1042/BSR20202537

Wouters, M. C. A., and Nelson, B. H. (2018). Prognostic significance of tumor-infiltrating B cells and plasma cells in human cancer. *Clin. Cancer Res.* 24 (24), 6125–6135. doi:10.1158/1078-0432.CCR-18-1481

Wu, C. C., Beird, H. C., Andrew Livingston, J., Advani, S., Mitra, A., Cao, S., et al. (2020). Immuno-genomic landscape of osteosarcoma. *Nat. Commun.* 11 (1), 1008. doi:10.1038/s41467-020-14646-w

Xia, K., Huang, X., Zhao, Y., Yang, I., and Guo, W. (2024). SERPINH1 enhances the malignancy of osteosarcoma via PI3K-Akt signaling pathway. *Transl. Oncol.* 39, 101802. doi:10.1016/j.tranon.2023.101802

Xie, J., Deng, X., Xie, Y., Zhu, H., Liu, P., Deng, W., et al. (2020). Multi-omics analysis of disulfidptosis regulators and therapeutic potential reveals glycogen synthase 1 as a disulfidptosis triggering target for triple-negative breast cancer. *MedComm* 5 (3), e502. doi:10.1002/mco2.502

Xie, J., Zheng, S., Zou, Y., Tang, Y., Tian, W., Wong, C. W., et al. (2022). Turning up a new pattern: identification of cancer-associated fibroblast-related clusters in TNBC. *Front. Immunol.* 13, 1022147. doi:10.3389/fimmu.2022.1022147

Xie, L., Yin, W., Tang, F., and He, M. (2023). Pan-cancer analysis of TERT and validation in osteosarcoma cell lines. *Biochem. Biophys. Res. Commun.* 639, 106–116. doi:10.1016/j.bbrc.2022.11.068

Yamamoto, N., Kinoshita, T., Nohata, N., Yoshino, H., Itesako, T., Fujimura, L., et al. (2013). Tumor-suppressive microRNA-29a inhibits cancer cell migration and invasion via targeting HSP47 in cervical squamous cell carcinoma. *Int. J. Oncol.* 43 (6), 1855–1863. doi:10.3892/ijo.2013.2145

Yamamoto, Y., Iwahori, K., Funaki, S., Matsumoto, M., Hirata, M., Yoshida, T., et al. (2020). Immunotherapeutic potential of CD4 and CD8 single-positive T cells in thymic epithelial tumors. *Sci. Rep.* 10 (1), 4064. doi:10.1038/s41598-020-61053-8

Yang, B., Su, Z., Chen, G., Zeng, Z., Tan, J., Wu, G., et al. (2021). Identification of prognostic biomarkers associated with metastasis and immune infiltration in osteosarcoma. *Oncol. Lett.* 21 (3), 180. doi:10.3892/ol.2021.12441

Yang, G., Yuan, J., and Li, K. (2013). EMT transcription factors: implication in osteosarcoma. *Med. Oncol.* 30 (4), 697. doi:10.1007/s12032-013-0697-2

Yoneda, A., Minomi, K., and Tamura, Y. (2020). HSP47 promotes metastasis of breast cancer by interacting with myosin IIA via the unfolded protein response transducer IRE1α. *Oncogene* 39 (23), 4519–4537. doi:10.1038/s41388-020-1311-7

Yoshihara, K., Shahmoradgoli, M., Martínez, E., Vegesna, R., Kim, H., Torres-Garcia, W., et al. (2013). Inferring tumour purity and stromal and immune cell admixture from expression data. *Nat. Commun.* 4, 2612. doi:10.1038/ncomms3612

Zhang, L., Peng, K. W., Wang, B., Yang, X. F., and Zhang, Z. M. (2020). EDIL3 regulates gastric cancer cell migration, invasion and epithelial-mesenchymal transition via TGF-β1/XIST/miR-137 feedback loop. *Transl. Cancer Res.* 9 (10), 6313–6330. doi:10.21037/tcr-19-2967b

Zhang, L., Zhu, Y., Cheng, H., Zhang, J., Zhu, Y., Chen, H., et al. (2019b). The increased expression of estrogen-related receptor α correlates with Wnt5a and poor prognosis in patients with glioma. *Mol. Cancer Ther.* 18 (1), 173–184. doi:10.1158/1535-7163.MCT-17-0782

Zhang, N., Ng, A. S., Cai, S., Li, Q., Yang, L., and Kerr, D. (2021). Novel therapeutic strategies: targeting epithelial-mesenchymal transition in colorectal cancer. *Lancet Oncol.* 22 (8), e358–e368. doi:10.1016/S1470-2045(21)00343-0

Zhang, Y., Cheng, H., Li, W., Wu, H., and Yang, Y. (2019a). Highly-expressed P2X7 receptor promotes growth and metastasis of human HOS/MNNG osteosarcoma cells via PI3K/Akt/GSK3β/β-catenin and mTOR/HIF1α/VEGF signaling. *Int. J. Cancer* 145 (4), 1068–1082. doi:10.1002/ijc.32207

Zhang, Y., Li, Y., Zuo, Z., Li, T., An, Y., and Zhang, W. (2023). An epithelial-mesenchymal transition-related mRNA signature associated with the prognosis, immune infiltration and therapeutic response of colon adenocarcinoma. *Pathol. Oncol. Res.* 29, 1611016. doi:10.3389/pore.2023.1611016

Zhou, S., Lu, Y., Chen, Y., and Gan, W. (2023). Identification of an immunogenic cell death-related gene signature predicts survival and sensitivity to immunotherapy in clear cell renal carcinoma. *Sci. Rep.* 13 (1), 4449. doi:10.1038/s41598-023-31493-z

Zou, Y., Cong, Y. S., and Zhou, J. (2020). Implications of telomerase reverse transcriptase in tumor metastasis. *BMB Rep.* 53 (9), 458–465. doi:10.5483/BMBRep.2020.53.9.108

frontiers | Frontiers in Pharmacology

TYPE Original Research
PUBLISHED 09 August 2024
DOI 10.3389/fphar.2024.1434988

Check for updates

OPEN ACCESS

EDITED BY
Hailin Tang,
Sun Yat-sen University Cancer Center (SYSUCC), China

REVIEWED BY
Rong Xu,
The First People's Hospital of Changde City, China
Hao Wu,
Sun Yat-sen University Cancer Center (SYSUCC), China
Bin Yang,
University of Pittsburgh, United States

*CORRESPONDENCE
Qiang Li,
Liqressh1962@163.com
Feilong Wang,
wang_feilong@tongji.edu.cn

†These authors have contributed equally to this work

RECEIVED 19 May 2024
ACCEPTED 22 July 2024
PUBLISHED 09 August 2024

CITATION
Zhang J, He W, Liu D, Zhang W, Qin H, Zhang S, Cheng A, Li Q and Wang F (2024), Phosphoenolpyruvate carboxykinase 2-mediated metabolism promotes lung tumorigenesis by inhibiting mitochondrial-associated apoptotic cell death.
Front. Pharmacol. 15:1434988.
doi: 10.3389/fphar.2024.1434988

COPYRIGHT
© 2024 Zhang, He, Liu, Zhang, Qin, Zhang, Cheng, Li and Wang. This is an open-access article distributed under the terms of the Creative Commons Attribution License (CC BY). The use, distribution or reproduction in other forums is permitted, provided the original author(s) and the copyright owner(s) are credited and that the original publication in this journal is cited, in accordance with accepted academic practice. No use, distribution or reproduction is permitted which does not comply with these terms.

Phosphoenolpyruvate carboxykinase 2-mediated metabolism promotes lung tumorigenesis by inhibiting mitochondrial-associated apoptotic cell death

Jing Zhang[1†], Wenjuan He[2†], Dongmei Liu[3], Wenyu Zhang[2], Huan Qin[2], Song Zhang[4], Ailan Cheng[5], Qiang Li[1*] and Feilong Wang[1*]

[1]Department of Pulmonary and Critical Care Medicine, Shanghai East Hospital, School of Medicine, Tongji University, Shanghai, China, [2]School of Medicine, Tongji University, Shanghai, China, [3]Nanjing Medical University, Nanjing, China, [4]Department of Cardiovascular Medicine, Mayo Clinic, Rochester, MN, United States, [5]Department of Radiology, Shanghai East Hospital, School of Medicine, Tongji University, Shanghai, China

Background: It is unknown how cancer cells override apoptosis and maintain progression under nutrition-deprived conditions within the tumor microenvironment. Phosphoenolpyruvate carboxykinase (PEPCK or PCK) catalyzes the first rate-limiting reaction in gluconeogenesis, which is an essential metabolic alteration that is required for the proliferation of cancer cells under glucose-limited conditions. However, if PCK-mediated gluconeogenesis affects apoptotic cell death of non small cell lung cancer (NSCLC) and its potential mechanisms remain unknown.

Methods: RNA-seq, Western blot and RT-PCR were performed in A549 cell lines cultured in medium containing low or high concentrations of glucose (1 mM vs. 20 mM) to gain insight into how cancer cells rewire their metabolism under glucose-restriction conditions. Stable isotope tracing metabolomics technology (LC-MS) was employed to allow precise quantification of metabolic fluxes of the TCA cycle regulated by PCK2. Flow Cytometry was used to assess the rates of early and later apoptosis and mitochondrial ROS in NSCLC cells. Transwell assays and luciferase-based *in vivo* imaging were used to determine the role of PCK2 in migration and invasion of NSCLC cells. Xenotransplants on BALB/c nude mice to evaluate the effects of PCK2 on tumor growth *in vivo*. Western blot, Immunohistochemistry and TUNEL assays to evaluate the protein levels of mitochondrial apoptosis.

Results: This study report that the mitochondrial resident PCK (PCK2) is upregulated in dependent of endoplasmic reticulum stress-induced expression of activating transcription factor 4 (ATF4) upon glucose deprivation in NSCLC cells. Further, the study finds that PCK2-mediated metabolism is required to decrease the burden of the TCA cycles and oxidative phosphorylation as well as the production of mitochondrial reactive oxygen species. These metabolic alterations in turn reduce the activation of

Caspase9-Caspase3-PARP signal pathway which drives apoptotic cell death. Importantly, silencing PCK2 increases apoptosis of NSCLC cells under low glucose condition and inhibits tumor growth both *in vitro* and *in vivo*.

Conclusion: In summary, PCK2-mediated metabolism is an important metabolic adaptation for NSCLC cells to acquire resistance to apoptosis under glucose deprivation.

KEYWORDS

phosphoenolpyruvate carboxykinase 2, metabolic reprogramming, lung tumorigenesis, mitochondrial apoptosis, reactive oxygen species

1 Introduction

Apoptosis is a form of programmed cell death which plays a critical role in tissue homeostasis. Of note, cancer cells could acquire the ability to evade apoptosis, which enables their excessive proliferation and survival under stressful conditions (Bertheloot et al., 2021; Attwaters, 2022; Tong et al., 2022). Among various mechanisms that contribute to the evasion of apoptosis in cancer, metabolism reprogramming is emerging as one of key factors (Schiliro and Firestein, 2021; Li et al., 2022). Cancer cells exhibit distinct metabolic signatures from non-malignant cells. Under nutritionally adequate conditions, cancer cells consume much more glucose than normal cells even in the presence of plenty oxygen, a phenomenon called Warburg effect or aerobic glycolysis (Abdel-Wahab et al., 2019). The enhanced glycolysis generates many macromolecular building blocks to sustain a high proliferation rate and metastatic capacity in cancer cells (Dey et al., 2021). During solid tumor progression, however, cancer cells inevitably encounter a nutrient-deprived tumor microenvironment. For instance, the intratumoral glucose level is 3- to 10-fold lower than in normal tissues (Rocha et al., 2015). Nutrient deprivation causes apoptotic cell death in many types of cancer cells (Onodera et al., 2020; Sa-Nongdej et al., 2021). As the major carbon source for cancer cells, glucose deprivation has been recognized as a key inducer of apoptotic cell death (Garlapati et al., 2021; Wang et al., 2022). The impaired glycolysis in cancer cells leads to inadequate production of metabolic intermediates, which are required to meet the cellular demand for the synthesis of many biological macromolecules (DeBerardinis et al., 2008). Moreover, the downregulation of pentose phosphate pathway due to glucose deprivation is unable to produce enough NADPH to sustain reduction–oxidation homeostasis, which ultimately trigger the activation of apoptosis signaling (Moon et al., 2020). However, how cancer cells overcome apoptosis and maintain their capacity to proliferate under glucose-limited conditions remains poorly understood.

Gluconeogenesis is the metabolic process by which organisms generate glucose from noncarbohydrate substrates such as lactate and amino acids. While principally occurs in the liver and kidneys in humans and mice, gluconeogenesis can also be induced to compensate for the decreased glycolysis in several types of cancer cells (Grasmann et al., 2019; Yu et al., 2021; Legouis et al., 2022; Paulusma et al., 2022). Phosphoenolpyruvate carboxykinase (PEPCK or PCK), which is composed of cytoplasmic form (PCK1) and mitochondrial form (PCK2), catalyzes the first rate-limiting reaction in gluconeogenesis (Wang and Dong, 2019). Of note, previous studies demonstrated that PCK2-mediated production of phosphoenolpyruvate (PEP) from glutamine-derived oxaloacetate enables glucose-independent proliferation in non small cell lung cancer (NSCLC) cells (Vincent et al., 2015; Smolle et al., 2020). Moreover, PCK2 is essential for the synthesis of glycerol phosphate which is required for NSCLC cells growth (Leithner et al., 2018). However, it remains unknown the role of PCK2-mediated gluconeogenesis in the evasion of apoptotic cell death in NSCLC cells in the low glucose condition. PCK2 paves a critical way to move TCA cycle carbons to cytoplasm, which has potential impacts on metabolic reprogramming in mitochondria upon glucose restriction (Vincent et al., 2015; Luo et al., 2017; Yu et al., 2021). Therefore, it would be of interest to investigate if and how PCK2-meditated metabolism affects mitochondrial apoptosis induced by glucose deprivation in NSCLC cells.

In the present study, we found that glucose deprivation increases PCK2 expression in NSCLC cells through the induction of endoplasmic reticulum stress (ER stress). Isotope tracing metabolomics showed that PCK2 is a key mediator of gluconeogenesis in NSCLC cells upon glucose restriction. Of note, silencing of PCK2 significantly enhances apoptotic cell death *in vitro* and inhibits NSCLC tumor growth in a xenograft mouse model, indicating that PCK2-mediated gluconeogenesis is critical for NSCLC cells to override apoptosis. Mechanistically, silencing of PCK2 leads to increased burden of the TCA cycle and oxidative phosphorylation, which in turn disrupts the redox balance to induce the activation of Caspase9-Caspase3-PARP signal pathway.

2 Results

2.1 Glucose restriction increases PCK2 expression through the activation of ER stress signaling in NSCLC cell lines

To gain insight into how cancer cells rewire their metabolism under glucose-restriction conditions, RNA-seq was performed in NSCLC cell line A549 cultured in medium containing low or high concentrations of glucose (1 mM vs. 20 mM) for 24 h. As shown in Figures 1A, B, glucose restriction induced a global metabolic adaptation as indicated by the increased the expression of enzymes in several metabolic pathways, including PCK2, hexokinase 2 (HK2), asparagine synthetase (ASNS), isocitrate dehydrogenase 1 (IDH1) and phosphoglycerate dehydrogenase (PHGDH). Of note, the expression of PCK2 rather than other

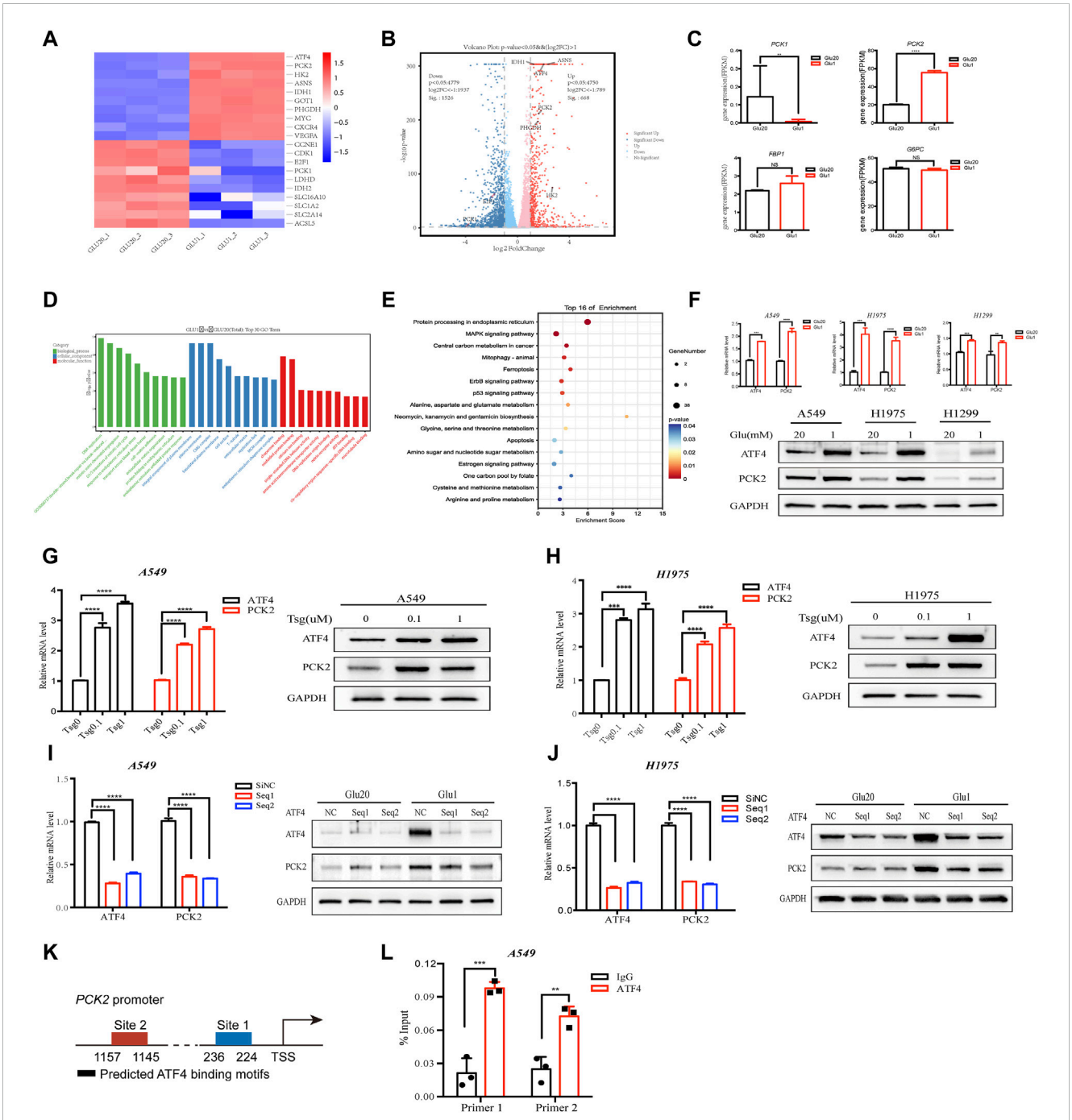

FIGURE 1
Glucose restriction increases PCK2 expression through the activation of ER stress signaling in NSCLC cell lines. **(A)** Heat map of gene expression in A549 cells cultured in medium containing high (20 mM) and low (1 mM) concentrations of glucose for 24 h. **(B)** Volcano plots of gene expression in A549 cells cultured in medium containing high (20 mM) and low (1 mM) concentrations of glucose for 24 h. FC, fold change. **(C)** Gene expression of gluconeogenic enzymes in A549 cells cultured in medium containing high (20 mM) and low (1 mM) concentrations of glucose for 24 h $^{**}p < 0.01$, $^{****}p < 0.0001$; ns, no significant difference. Data are representative of three independent experiments (n = 3, mean ± SEM). **(D)** GO analysis of differentially expressed genes (DEGs) in A549 cells cultured in medium containing high (20 mM) and low (1 mM) concentrations of glucose for 24 h **(E)** KEGG enrichment analysis of differentially expressed genes (DEGs) in A549 cells cultured in medium containing high (20 mM) and low (1 mM) concentrations of glucose for 24 h. **(F)** Expression of ATF4 and PCK2 mRNA and protein in A549, H1975 and H1299 cells cultured in medium containing high (20 mM) and low (1 mM) concentrations of glucose for 24 h (mRNA) or 48 h (protein). $^{**}p < 0.01$, $^{***}p < 0.001$, $^{****}p < 0.0001$. Data are representative of three independent experiments (n = 3, mean ± SEM). **(G)** Expression of ATF4 and PCK2 mRNA and protein in A549 cells treated with different concentrations of thapsigargin for 24 h (mRNA) or 48 h (protein). $^{****}p < 0.0001$. Data are representative of three independent experiments (n = 3, mean ± SEM). **(H)** Expression of ATF4 and PCK2 mRNA and protein in H1975 cells treated with different concentrations of thapsigargin for 24 h (mRNA) or 48 h (protein). Data are representative of three independent experiments. **(I)** Expression of ATF4 and PCK2 mRNA and protein in A549 cells transfected with control or ATF4 siRNA for 24 h (mRNA) or 48 h (protein). $^{****}p < 0.0001$. Data are representative of three independent experiments (n = 3, mean ± SEM). **(J)** Expression of ATF4 and PCK2 mRNA and protein in H1975 cells transfected with control or

(*Continued*)

FIGURE 1 (Continued)
ATF4 siRNA for 24 h (mRNA) or 48 h (protein). Data are representative of three independent experiments. **(K)** Two putative ATF binding sites were predicted on the promoter of PCK2 using JASPAR database. **(L)** ATF4 directly bound to the PCK2 promoter. A549 cells were applied to ChIP assay. Data are representative of three independent experiments. $^{**}p < 0.01$, $^{***}p < 0.001$; Data are representative of three independent experiments.

gluconeogenic enzymes (PCK1, Fructose-1,6-bisphosphatase 1, glucose-6-phosphatases) were significantly increased by glucose restriction (Figures 1B, C), indicating that PCK2-mediated metabolism might be required for NSCLC cells to adapt to a low glucose environment. We next explored the underlying mechanisms of how PCK2 expression was induced by glucose deprivation. Gene Ontology (GO) analysis showed that differentially expressed genes (DEGs) were significantly enriched in ER stress-related process, including ER stress response, protein folding in ER and ER stress unfolded protein response, under the biological process category (Figure 1D). In addition, KEGG enrichment analysis of DEGs showed that the protein processing in ER had the highest enrichment score among the top 16 most significant pathways (Figure 1E). These data indicated that glucose-restriction induces ER stress and its related cellular responses in NSCLC cells, which is well-known as the key inducer of transcriptional signaling to promote adaptive cellular responses to stress (Chen and Cubillos-Ruiz, 2021). A key downstream transcription factor of ER stress is the activating transcription factor 4 (ATF4) which mediates the expression of genes that allow cells to adapt cellular stress (Andrews et al., 2021). Indeed, the expression of ATF4 was significantly increased by glucose-restriction in A549, H1975 and H1299 cells (Figure 1F). Consistently, ATF4 was upregulated upon the treatment of thapsigargin which is a classical chemical inducer of ER stress (Figures 1G, H). Of note, a clear trend of co-expression of PCK2 and ATF4 was observed in A549 and H1975 cell lines (Figures 1F–H). To further determine the role of ATF4 in the induction of PCK2, we knocked down ATF4 through small interfering RNA (siRNA) and the expression of PCK2 was evaluated. As shown in Figures 1I, J, knockdown of ATF4 reduced both mRNA and protein levels of PCK2 in A549 and H1975 cells under glucose restriction conditions, indicating that the upregulation of PCK2 is dependent on ATF4. Then, we identified two putative ATF4 binding sites on the promoter of PCK2 through JASPAR database (Figure 1K). The ATF4 and PCK2 DNA direct interaction was experimentally demonstrated using ChIP assay (Figure 1L). Taken together, these data show that PCK2 is upregulated by glucose deprivation through ER stress-induced ATF4 expression in NSCLC cells.

2.2 Glucose deprivation enhances the glutamine fueling of the TCA cycle and gluconeogenesis

As enhanced glycolysis is essential for cancer cells to meet the demand for energy production, building blocks generation and redox homeostasis, how these cells maintain proliferation and energy supply under glucose restriction conditions remains poorly understood. Previous studies demonstrated that cancer cells increase oxidative phosphorylation to compensate for the reduced glycolysis, in which glutamine was used as an alternative substrate to supply the TCA cycle (Jin et al., 2023). To test if the contribution of glutamine to the TCA cycle is elevated by glucose deprivation in NSCLC cells, we employed stable isotope tracing metabolomics technology which allow precise quantification of metabolic fluxes of glutamine. As shown in Figures 2A–F, flux contribution of glutamine carbons to the TCA cycle was significantly increased by glucose deprivation as indicated by the enhanced ^{13}C-labeled glutamate and TCA cycle metabolites including succinate, fumarate, malate and citrate. The TCA cycle links gluconeogenesis through the conversion of oxaloacetate into phosphoenolpyruvate by PCK2 in cytosol (Figure 2A). We then assessed the alteration of gluconeogenesis by quantifying the flux contribution of glutamine to metabolites belonging to the glycolysis/gluconeogenesis pathways. Importantly, we found an elevated ^{13}C-labeled metabolites in the gluconeogenetic pathway, including fructose-1,6-bisphosphate (FBP) and fructose 6-phosphate (F-6-P) (Figures 2G, H). Aspartate, which is a key metabolite that supports nucleotide and asparagine synthesis in cancer cells, also increased its ^{13}C-labelled part under glucose restriction conditions (Figure 2I). Moreover, an increased glutamine-dependent serine biosynthesis through gluconeogenesis was also observed after glucose deprivation (Figure 2J). The labeling ratios of gluconeogenetic metabolites were lower than that of malate, further indicating that these metabolites were the downstream intermediates of the TCA cycle. Collectively, these data demonstrate that NSCLC cells increase glutamine utilization under glucose restriction conditions, which in turn maintains TCA cycle operation and promote gluconeogenesis.

2.3 PCK2-mediated gluconeogenesis protects NSCLC cells against mitochondrial apoptosis under glucose-restriction conditions

Having shown that more glutamine contributes to the TCA cycle and gluconeogenesis in response to glucose deprivation, we next asked if this metabolic alteration affects the fate of cancer cells. As PCK2 is a rate-limiting enzyme of gluconeogenesis that converts oxaloacetate into phosphoenolpyruvate, we knocked down PCK2 by the small hairpin RNA (shRNA) to evaluate the role of PCK2-mediated gluconeogenesis in cell proliferation as well as cell death. The knockdown efficacy was confirmed at both the mRNA and protein levels (Figures 3A, B). While silencing of PCK2 did not affect the viability of A549 and H1975 cells cultured in regular medium, it significantly reduced the viability of these cells cultured in medium containing 1 mM glucose, indicating that PCK2-mediated gluconeogenesis is required for the optimal growth of NSCLC cell under glucose-restriction conditions (Figure 3C). In addition, PCK2 silencing reduced the migration abilities of A549 and

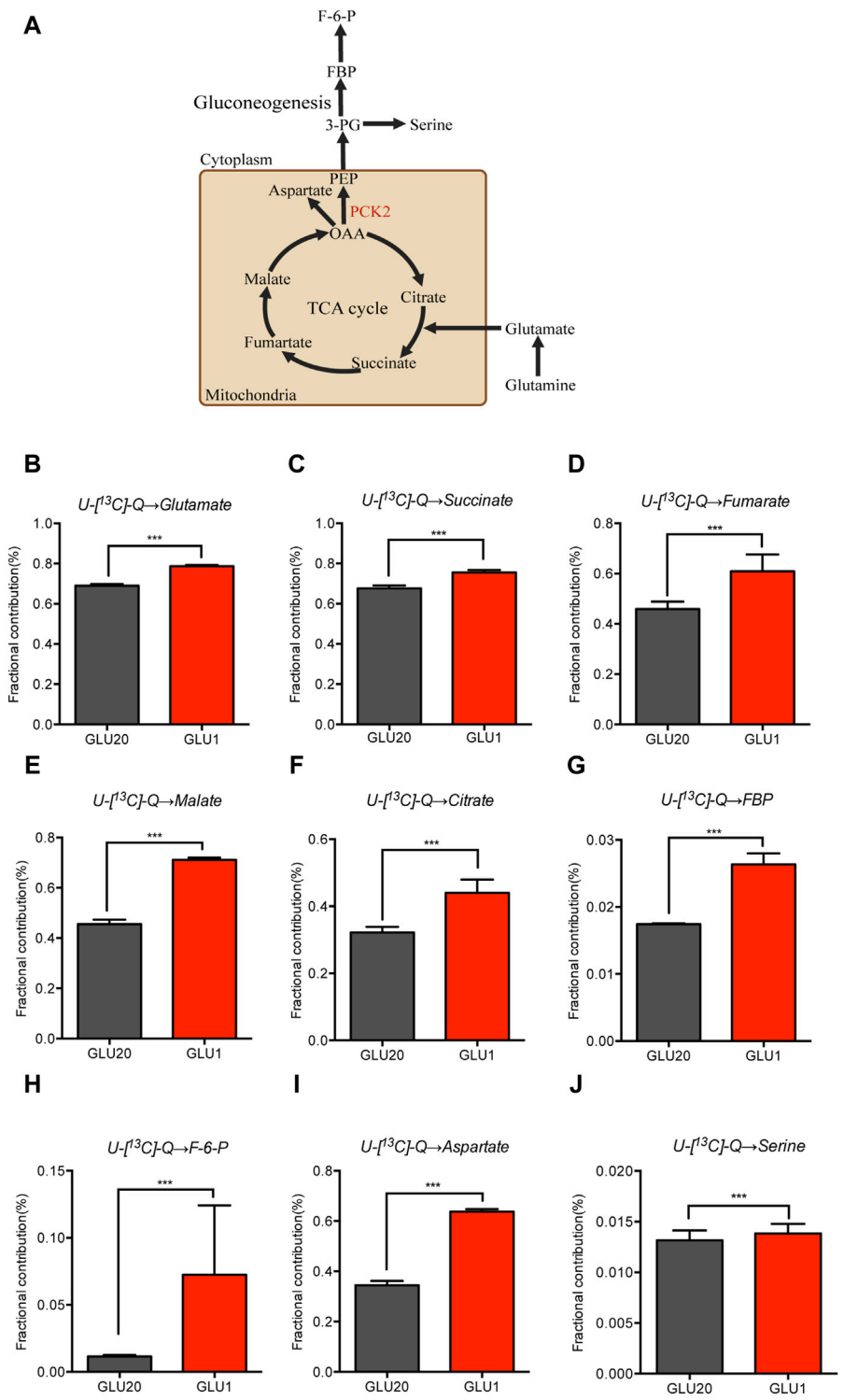

FIGURE 2
Glucose deprivation enhances the glutamine fueling of the TCA cycle and gluconeogenesis. **(A–J)** U-[13C]-glutamine-labelled glutamate **(B)**, TCA cycle metabolites **(C–F)**, gluconeogenesis metabolites **(G,H)**, Aspartate **(I)** and Serine **(J)** in A549 cells cultured in medium containing high (20 mM) and low (1 mM) concentrations of glucose for 12 h ***$p < 0.001$. (n = 4, mean ± SEM). U-[13C]-Q, U-[13C]-glutamine.

H1975 cells, suggesting that PCK2-mediated gluconeogenesis is also essential for the invasion activity of NSCLC cells (Figure 3D). Numerous studies found that glucose restriction and sustained ER stress lead to the activation of pro-apoptotic signaling to drive apoptotic cell death (Chen and Cubillos-Ruiz, 2021; Fu et al., 2021). Indeed, we found that both early and later apoptosis rates of A549 and H1975 cells were slightly increased under glucose-restricted conditions (Figures 3E, F). Importantly, silencing of

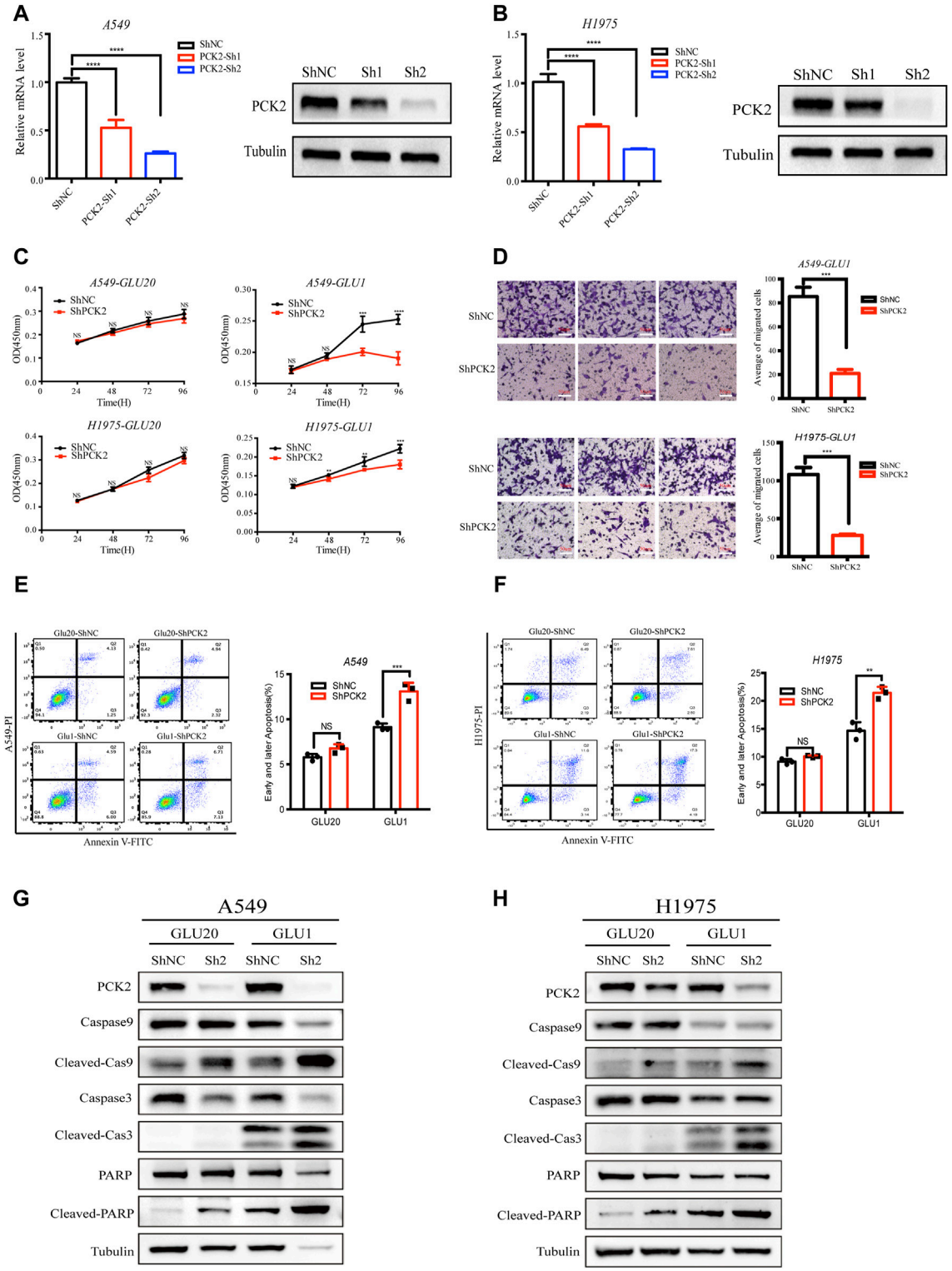

FIGURE 3
PCK2-mediated gluconeogenesis protects NSCLC cells against mitochondrial apoptosis under glucose-restriction conditions. **(A)** Expression of *PCK2* mRNA and protein in A549 transfected with control or PCK2 shRNA. ****$p < 0.0001$. Data are representative of three independent experiments (n = 3, mean ± SEM). **(B)** Expression of PCK2 mRNA and protein in H1975 cells transfected with control or PCK2 shRNA. Data are representative of three independent experiments. **(C)** Cell viability of A549 and H1975 cells transfected with control or PCK2 shRNA and cultured in medium containing high (20 mM) and low (1 mM) concentrations of glucose for 96 h **$p < 0.01$, ***$p < 0.001$, ****$p < 0.0001$. Data are representative of three independent experiments (n = 5, mean ± SEM). **(D)** Right: Representative images of transwell assays of A549 and H1975 cells transfected with control or PCK2 shRNA and cultured in medium containing 1 mM glucose for 48 h. Left: Statistics of cell migration of A549 and H1975 cells treated as in (Right). ***$p < 0.001$. Data are representative of three independent experiments (n = 3, mean ± SEM). **(E)** Right: Flow cytometry analysis of early and later apoptosis of A549 cells (*Continued*)

FIGURE 3 (Continued)
transfected with control or PCK2 shRNA and cultured in medium containing high (20 mM) and low (1 mM) concentrations of glucose for 48 h. Left: Statistics of early and later apoptosis of A549 cells treated as in (Right). ***$p < 0.001$; ns, no significant difference. Data are representative of three independent experiments (n = 3, mean ± SEM). **(F)** Right: Flow cytometry analysis of early and later apoptosis of H1975 cells transfected with control or PCK2 shRNA and cultured in medium containing high (20 mM) and low (1 mM) concentrations of glucose for 48 h. Left: Statistics of early and later apoptosis of A549 cells treated as in (Right). **$p < 0.01$; ns, no significant difference. Data are representative of three independent experiments (n = 3, mean ± SEM). **(G,H)** Expression of Caspase-9, Caspase-3, PARP and their cleaved forms in A549 **(G)** and H1975 **(H)** cells transfected with control or PCK2 shRNA and cultured in medium containing high (20 mM) and low (1 mM) concentrations of glucose for 48 h. Data are representative of three independent experiments.

PCK2 significantly enhanced apoptosis rates of cancer cells cultured in glucose-restricted medium rather than in regular culture conditions (Figures 3E, F). These data demonstrate that PCK2-mediated gluconeogenesis is critical for NSCLC cells to acquire resistance to apoptosis under glucose restriction conditions.

Apoptosis is a process of cellular self-destruction catalyzed by many proteolytic enzymes, among which caspases play key roles in carrying out the cleavage of apoptosis-executive proteins (Boice and Bouchier-Hayes, 2020; Carneiro and El-Deiry, 2020). The activation of caspase three and caspase nine lead to the cleavage of Poly (ADP-ribose) polymerase (PARP) which is a hallmark of mitochondrial apoptosis (Carneiro and El-Deiry, 2020; Morana et al., 2022). To further investigate how PCK2-mediated gluconeogenesis inhibits apoptotic cell death of NSCLC cells, we tested the expressions of caspase 9, caspase 3, PARP and their cleaved forms in A549 and H1975 after PCK2 silencing. We found that the cleavages of caspase-9, caspase-3 and PARP were clearly induced in NSCLC cells cultured in medium containing l mM glucose but not in those cultured in regular medium (Figures 3G, H), confirming that glucose restriction trigger the activation of mitochondrial apoptotic signaling. Importantly, PCK2 silencing further increased the cleavages of caspase-9, caspase-3 and PARP (Figures 3G, H), indicating that PCK2-mediated gluconeogenesis is required to prevent the activation of mitochondrial pro-apoptotic signaling in NSCLC cells.

2.4 PCK2-mediated gluconeogenesis is required to reduce the burden of the TCA cycle and to rebalance redox equilibrium

PCK2 mediates transport of oxaloacetate from the TCA cycle and decarboxylation to PEP, which has been recognized as an important metabolic adaptation for cancer cells in response to nutrition deprivations. However, little is known about how this metabolic alteration affects apoptotic caspases signaling. Since glucose restriction resulted in the accumulation of glutamine-derived TCA cycle metabolites (Figures 2C–F), we hypothesized that PCK2-mediated gluconeogenesis is required to remove excess intermediates of the TCA cycle and in turn alleviate mitochondria-associated cellular dysfunction which is a key driver of apoptotic cell death. In support of this hypothesis, we found that ^{13}C-glutamine labeled glutamate and TCA cycle metabolites, including citrate, succinate, fumarate and malate, were increased by PCK2 silencing in A549 cells cultured in medium containing low (1 mM) concentrations of glucose. (Figures 4A–E). Conversely, ^{13}C-glutamine derived serine as well as metabolites involved in pentose phosphate pathway including ribulose-5-phosphate and ribose-5-phosphate were reduced by PCK2 silencing (Figures 4F–H).

The accumulation of TCA cycle metabolites is associated with increased oxidative phosphorylation and reactive oxygen species (ROS) production (Chakrabarty and Chandel, 2021). As PCK2-mediated gluconeogenesis is required to reduce the burden of the TCA cycle in NSCLC cells under glucose-restriction conditions, we tested if PCK2 silencing affects ATP generation and mitochondrial ROS(mtROS) production in this setting. As shown in Figures 4I–K, the levels of both ATP and mtROS were elevated by PCK2 silencing in A549 and H1975 cells. The increased ATP level after PCK2 silencing is likely due to the enhanced oxidative phosphorylation as ATP generation through glycolysis has been impaired by glucose restriction in this setting. The mitochondrial respiratory chain is the main generator of mtROS which is considered as byproduct of oxidative phosphorylation during ATP synthesis. The increased level of mtROS after PCK2 silencing suggests that either more mtROS was generated due to enhanced OXPHOS, as indicated above, or less mtROS was detoxified. In addition, or less gluconeogenesis is required to reduce the production of mtROS maintain redox balance in NSCLC cells upon glucose deprivation (Figures 4J, K). The later was supported by the findings that PCK2 silencing decreased glutamine-derived metabolites within the pentose phosphate pathway (Figures 4G, H), through which nicotinamide adenine dinucleotide phosphate (NADPH) was generated for ROS detoxification (Hayes et al., 2020). To further confirm this, we measured the NADPH/NADP ratio in NSCLC cells after silencing of PCK2. We found that NADPH/NADP ratio was reduced by PCK2 silencing in both A549 and H1975 cells, showing that cellular redox balance was disrupted (Figure 4L).

As mtROS is an important inducer of apoptotic cell death, we next tested if the protective role of PCK2-mediated gluconeogenesis in NSCLC cells upon glucose deprivation is through inhibiting mtROS production. To this end, A549 and H1975 cells were incubated in glucose starvation medium containing N-acetyl cysteine (NAC), which is a direct oxidant scavenger of ROS, before the evaluation of the activation of mitochondrial pro-apoptotic signaling. As shown in Figures 4M, N, the increased cleavages of caspase-3 and PARP by PCK2 silencing under glucose restriction conditions were largely attenuated by NAC, conforming that mtROS is the key mediator of mitochondrial apoptosis in this setting. Taken together, these data showed that PCK2-mediated gluconeogenesis is required to reduce the accumulation of TCA cycle metabolites and the level of oxidative phosphorylation, which in turn decreases mtROS production and apoptotic cell death of NSCLC cells upon glucose restriction.

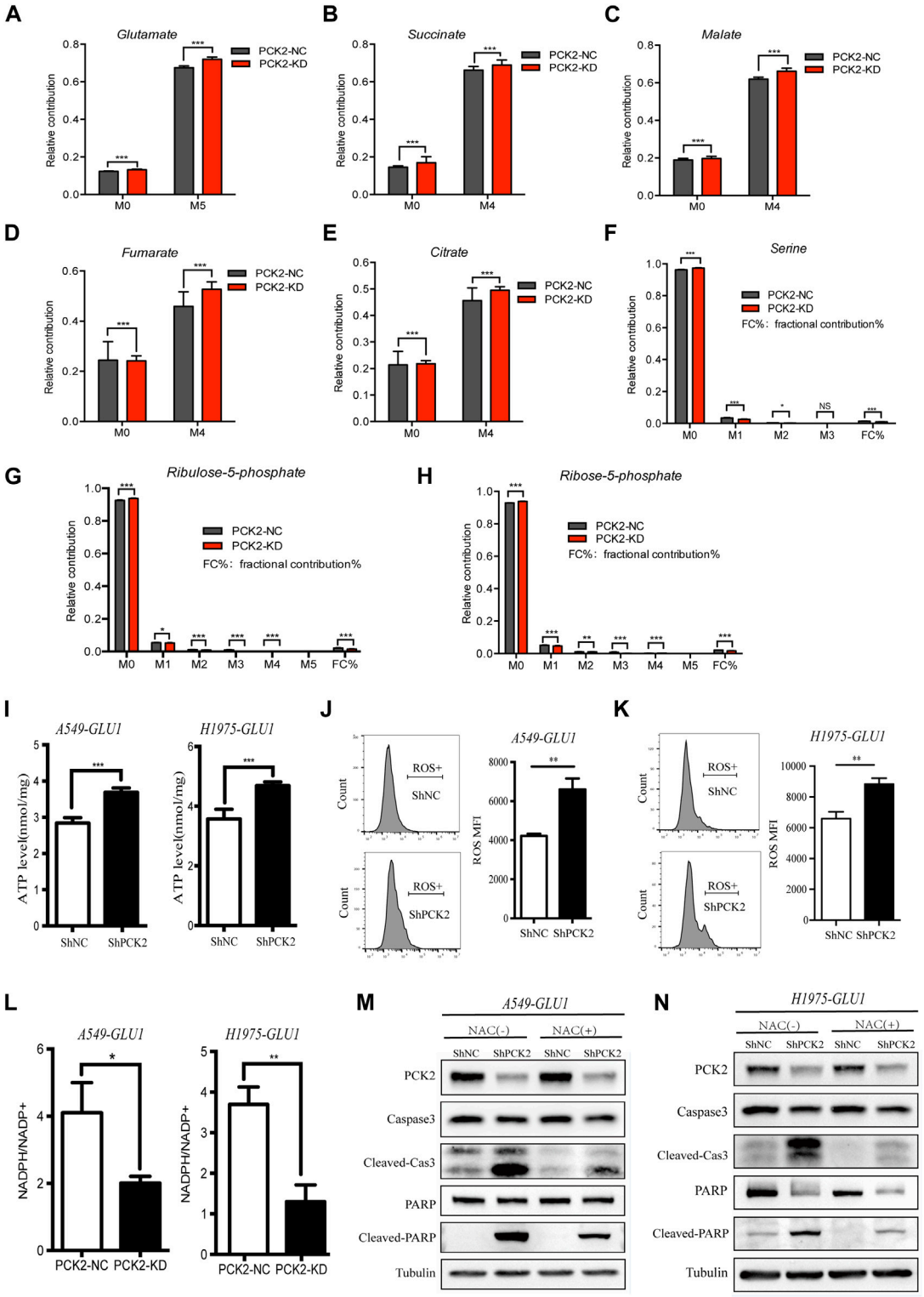

FIGURE 4
PCK2-mediated gluconeogenesis is required to reduce the burden of TCA cycle and to rebalance redox equilibrium. **(A–H)** U-[^{13}C]-glutamine-labelled metabolites in A549 cells transfected with control or PCK2 shRNA and cultured in medium containing low (1 mM) concentrations of glucose for 12 h *$p < 0.05$, **$p < 0.01$, ***$p < 0.001$; ns, no significant difference. (n = 4, mean ± SEM). **(I)** Intracellular ATP levels of A549 and H1975 cells transfected with control or PCK2 shRNA and cultured in medium containing low (1 mM) concentrations of glucose for 48 h ***$p < 0.001$. (n = 3, mean ± SEM). **(J,K)** Flow cytometry analysis of mitochondrial ROS in A549 **(J)** and H1975 **(K)** cells transfected with control or PCK2 shRNA and culture in 1 mM glucose for 48 h **$p < 0.01$. Data are representative of three independent experiments (n = 3, mean ± SEM). **(L)** NADPH/NADP + ratio in A549 and H1975 cells
(*Continued*)

FIGURE 4 (Continued)
transfected with control or PCK2 shRNA and cultured in medium containing 1 mM glucose for 48 h *$p < 0.05$, **$p < 0.01$. Data are representative of three independent experiments (n = 3, mean ± SEM). **(M,N)** Expression of PCK2 and Caspase-3, PARP and their cleaved forms in A549 **(M)** and H1975 **(N)** cells transfected with control or PCK2 shRNA, cultured in medium containing 1 mM glucose and 5 mM NAC for 48 h. NAC, N-acetyl cysteine. Data are representative of three independent experiments.

2.5 PCK2 promotes lung tumorigenesis and metastasis *in vivo*

To assess the impact of PCK2-mediated metabolism on tumor growth *in vivo*, A549 and H1975 cells expressing either control or PCK2-specific shRNAs were injected into the flanks of nude mice, and tumor growth was assessed every 2 days. We found that tumor volumes and weights of both A549-shPCK2 and H1975-shPCK2 were significantly decreased compared to those of control cells, indicating the critical role of PCK2 in the growth of NSCLC cells *in vivo* (Figures 5A–F). We next evaluated if PCK2-mediated gluconeogenesis affects metastatic capacity of NSCLC cells. To this end, we intravenously injected luciferase-expressing A549 and H1975 cells transfected with either control or PCK2-specific shRNAs in mice and lung metastasis was evaluated after 45 days. Strikingly, both A549-shPCK2 and H1975-shPCK2 dramatically reduced their metastatic capacity compared to control cells as indicated by the significantly reduced percentage of tumor area within the lung (Figures 5G, H). Importantly, the expression of cleaved caspase-3 and the number of TUNEL positive cells were increased in both A549-shPCK2 and H1975-shPCK2 tumor tissues (Figures 5I–K), confirming that loss of PCK2 promotes apoptosis in NSCLC cells *in vivo* in the low glucose. Moreover, there were less Ki67-positive cells within tumor tissue upon PCK2 knocking down, suggesting a reduced proliferative capacity of these cells (Figures 5J, K). Taken together, our data show that PCK2-mediated gluconeogenesis promotes tumorigenesis of NSCLC *in vivo* by protecting lung cancer cells against apoptosis. We also assessed PCK2 mRNA and protein levels in tumor samples isolated from human NSCLC patients. Real-time PCR revealed a significant increase in PCK2 mRNA expression levels in lung tumors compared with adjacent normal tissue (Figure 5L). Examples of PCK2 protein expression in normal and tumor tissue from the lungs of six NSCLC patients are shown in Figure 5M. These data indicate that PCK2 expression is enriched in the tumor tissues of NSCLC. A working model of PCK2-mediated metabolism promotes lung tumorigenesis has been shown in Figure 6.

3 Discussion

Solid tumors frequently encounter nutrient deprivation during growth due to insufficient blood supply (Martínez-Reyes and Chandel, 2021). Since cancer cells prefer the process of glycolysis as the source of ATP generation and macromolecular synthesis (Vander Heiden et al., 2009), it is unclear how these cells maintain viability and proliferation in the microenvironment with limited availability of glucose. In this study, we demonstrate that PCK2 is upregulated in NSCLC cells in response to glucose deprivation through ER stress-induced ATF4 expression. PCK2-mediated gluconeogenesis protects NSCLC cells against mitochondrial apoptosis by reducing the burden of the TCA cycle and restoring cellular redox balance. Importantly, silencing of PCK2 inhibits the growth of NSCLC cells both *in vitro* and *in vivo* in the low glucose condition, suggesting that PCK2 is a potential therapeutic target for NSCLC. To date, there has been little focus on PCK2 in the context of cancer. Elevated expression of the upstream gluconeogenesis enzyme PCK2 has been noted in many tumor types include colon cancer, NSCLC and hepatocellular carcinoma. In this light, targeting PCK2 may be an effective strategy for certain cancer subtypes. However, recently, several studies had suggested that PCK2 overexpression could suppress the progression of renal cell carcinoma and melanoma (Luo et al., 2017; Xiong et al., 2020). The tumor-promoting or tumor-suppressive roles of PCK2 in different studies depend on the cancer type and context. Thus, the diversity of PCK2 expression in different cancer models make it a challenging therapeutic target and it is required to fully investigate the underlying molecular mechanisms of PCK2-mediated tumor development in different tissues and disease stages (Yu et al., 2023). Additionally, to identify specific tumor types that can be effectively treated by targeting PCK2, it is imperative to develop the biomarkers to predict the response of tumor cells against PCK2 inhibitors. It is worth noting that PCK2-mediated metabolic downstream pathways play an important role to maintain physiology functions of liver and insulin-producing β-cells (Stark et al., 2009; Stark et al., 2014), whether targeting PCK2 could affect these normal organs and tissues is still undermined and need to be addressed in future studies.

Gluconeogenesis is required for cancer cells to generate glycolytic intermediates in adapting to a glucose-deprived tumor microenvironment (Wang and Dong, 2019). A key step in gluconeogenesis is the conversion of oxaloacetate to phosphoenolpyruvate, which is catalyzed by PCK1 in the cytoplasm or by PCK2 in the mitochondrial (Grasmann et al., 2019). While PCK1 is the dominant form of PCK in the liver, the active and functional form of PCK in cancer cells is dependent on tumor types (Bian et al., 2022). PCK1 is upregulated and required for optimal growth of human pancreatic cancer cells, hepatocellular carcinoma cells and melanoma cells (Xu et al., 2020). Conversely, PCK2 was shown to be critical for the proliferation of lung cancer cells, kidney renal clear cancer cells and breast cancer cells (Chen et al., 2023; Hsu et al., 2023). In line with previous studies (Leithner et al., 2015), we found that PCK2 rather than PCK1 is upregulated in NSCLC cells upon glucose deprivation. Importantly, we uncovered that glucose restriction-induced ER stress and its downstream ATF4 upregulation are the key drivers of PCK2 expression in NSCLC cells. Glucose deprivation induces ER stress in cancer cells via multiple ways. The compromised glycolysis impairs the production of uridine diphosphate-N-acetylglucosamine (UDP-GlcNAc) which is required for N-linked glycosylation and protein folding in the ER (Xiang et al., 2021). In addition, glucose restriction leads to defected calcium flux in the

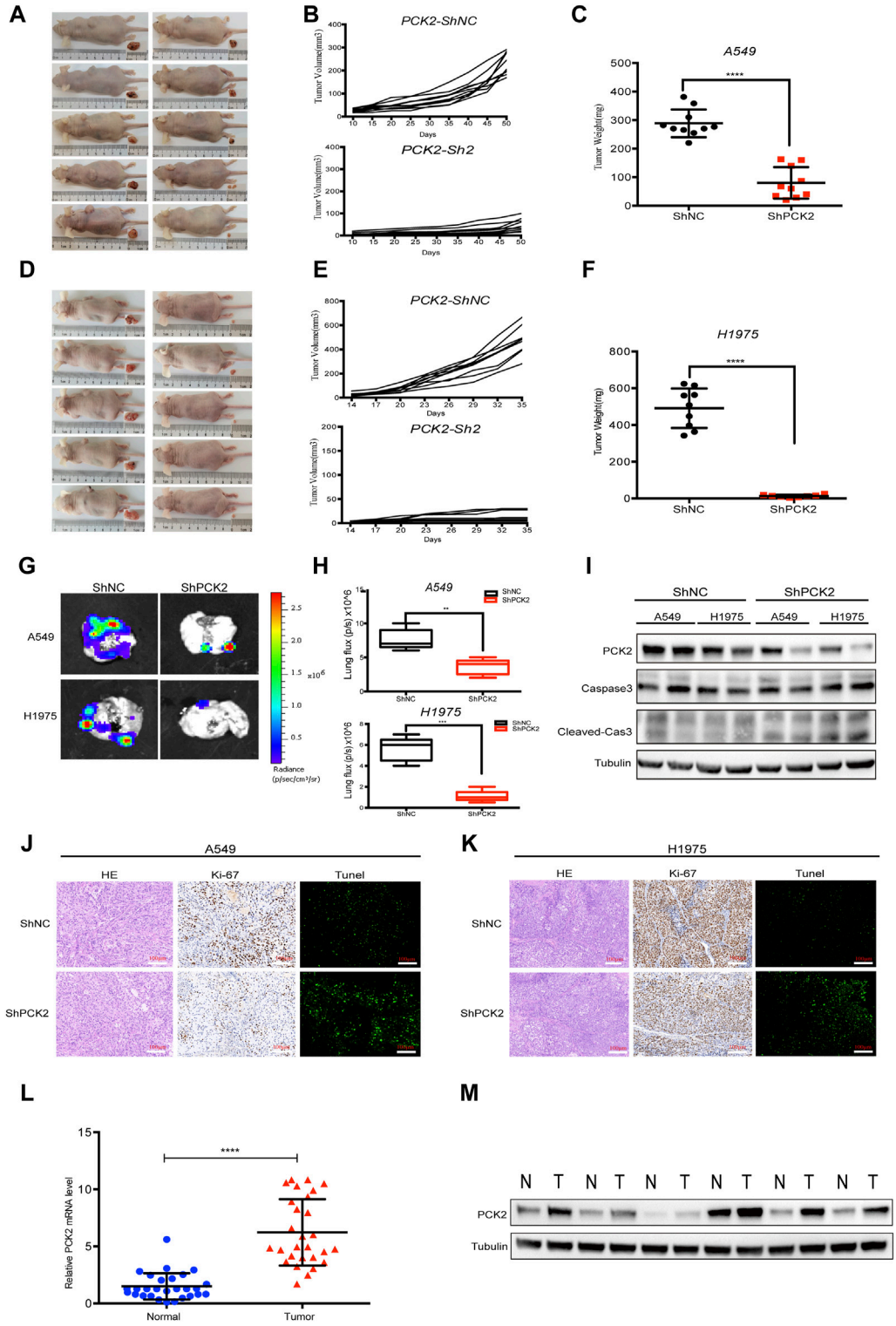

FIGURE 5
PCK2 promotes lung tumorigenesis and metastasis *in vivo*. **(A–C)** Representative photographs of tumors, tumor volume and weight in xenografts mice models after 50 days subcutaneously injection of A549 cells transfected with control or PCK2 shRNA. ****$p < 0.0001$. (n = 10 mice, mean ± SEM). **(D–F)** Representative photographs of tumors, tumor volume and weight in xenografts mice models after 35 days subcutaneously injection of H1975 cells transfected with control or PCK2 shRNA. ****$p < 0.0001$. (n = 10 mice, mean ± SEM). **(G,H)** Representative photographs of lung metastasis of mice after 45 days injection of A549 and H1975 cells transfected with control or PCK2 shRNA. **$p < 0.01$, ***$p < 0.001$; ns, no significant difference. (n = 5 mice, mean ± SEM). **(I)** Expression of PCK2, Caspase-3, cleaved-Caspase-3 in subcutaneously implanted tumor tissues of A549 and H1975 cells transfected with control or PCK2 shRNA. Data are representative of three independent experiments with ten mice tested in each group. **(J,K)** Representative images of HE,

(*Continued*)

FIGURE 5 (Continued)
Ki67 and Tunel staining of the tumor sections in subcutaneously implanted tumors of A549 **(J)** and H1975 **(K)** cells transfected with control or PCK2 shRNA. Images are obtained from ten mice in each group. **(L)** Quantification of PCK2 mRNA expression from tumor samples and matched adjacent normal lung tissues of NSCLC patients (n = 29). *$p < 0.0001$. **(M)** Immunoblot for PCK2 on six individual samples of normal and tumor tissue samples from NSCLC patients. Tubulin was used as a control for protein loading. Data are representative of three independent experiments.

ER (Li et al., 2019). Although it is well established that ER stress leads to a decrease in global protein translation, it also upregulates specific proteins to reduce the burden of unfolded proteins via the transcription factor ATF4 (Balsa et al., 2019). In this study, we confirmed that glucose deprivation leads to ER stress and ATF4 upregulation in NSCLC cells. Of note, we found that the induction of PCK2 is dependent on ATF4 expression, revealing a novel mechanism of how PCK2 is induced under nutrient deprivation conditions in NSCLC cells. Since PCK2-mediated metabolism is critical for the survival of NSCLC cells, targeting ER stress-ATF4 signaling pathway could be a therapeutic approach for the treatment of NSCLC.

Apoptotic cell death is an important form of regulated cell death which plays a pivotal role in cancer development (Kashyap et al., 2021). Evasion of apoptosis is not only a common characteristic of many types of cancer cells, but also is a crucial ability for these cells to maintain optimal growth under nutrient-deprived tumor microenvironment (Shahar and Larisch, 2020). Of note, mitochondria are critical to trigger apoptotic signaling. Unlike extrinsic pathway of apoptosis, mitochondrial apoptosis is induced by diverse cellular stresses such as growth-factor deprivation, DNA damage or glucose deprivation (Caro-Maldonado et al., 2010; Luo et al., 2020). In this study, we confirmed that glucose deprivation promotes mitochondrial apoptosis in NSCLC cells. Intriguingly, the extent of this form of apoptosis was significantly increased by PCK2 silencing in NSCLC cells under glucose-limited conditions but not in cells grown in regular culture medium, indicating that PCK2 is essential for NSCLC cells to acquire resistance to mitochondrial apoptosis upon nutrient deprivation. We further revealed that PCK2-mediated gluconeogenesis removes abundance TCA cycle metabolites and restores redox balance in NSCLC cells upon glucose deprivation, showing the fine-tuning metabolic switches in cancer cells in response to nutrient-deprived tumor microenvironment. Given the induction of apoptosis has been recognized as a promising approach for the treatment of cancers (Mohammad et al., 2015), the current study provides a new therapeutic target to inhibit tumor growth of NSCLC by promoting apoptosis.

In summary, our study demonstrates that PCK2-mediated gluconeogenesis is critical for NSCLC cells to maintain survival under glucose-limited conditions. Targeting PCK2 could be used as a potential therapeutic strategy for the treatment of non-small-cell lung cancer.

4 Materials and methods

4.1 Cell lines and culture

The Human NSCLC cell lines (A549, H1299, and H1975) were obtained from the American Type Culture Collection. Cells were cultured in DMEM (A549 cells) or RPMI 1640 (H1299 and H1975) medium supplemented with 10% fetal calf serum (FCS) and antibiotics (100 U/mL penicillin and 0.1 mg/mL streptomycin) at 37°C in a humidified incubator containing 5% CO2. For high and low glucose experiments, glucose- and glutamine-free DMEM (Gibco) were supplemented with 2 mM glutamine and 1/20 mM (low/high) glucose, 10% FCS and antibiotics. All cell lines were tested for *mycoplasma* contamination before use and validated by short tandem repeat profiling.

4.2 Isotope-tracing experiments

Metabolic tracing analysis of U-[^{13}C]-glutamine (Cat#CLM-1822-H, Cambridge Isotope Laboratories) in A549 cells were determined by GC–MS or LC–MS. Briefly, 1 × 106 A549 cells were seeded in 3.5 cm dishes in regular medium (DMEM supplemented with 10% FCS and antibiotics) for 18 h. Cells were then washed twice with phosphate buffered saline (PBS) and incubated in medium containing 1 mM or 20 mM glucose with 2 mM glutamine for 24 h. After 3 times wishing by PBS, cells were incubated in medium containing 1 mM or 20 mM glucose as well as 2 mM U-[^{13}C]-glutamine for 12 h. Cells were then collected and processed as described for intracellular metabolites. Metabolites were quantitated by Metabo-Profile Biotechnology (Shanghai, China). To determine ^{13}C-labelling, mass information for known fragments of labelled metabolites was retrieved. These fragments contained either the whole or partial carbon skeleton of the metabolite. For each fragment, the retrieved data consisted of mass intensities for the lightest isotopomer (without any heavy isotopes, M + 0) and isotopomers with increasing unit mass (up to M + 6) relative to M0. These mass distributions were normalized by dividing by the sum of M0 to M6 and corrected for the natural abundance of heavy isotopes, using matrix-based probabilistic methods as described previously, (Lee et al., 1991), and implemented in Microsoft Excel. ^{13}C-labelling data are expressed as fractional abundance of each isotopolog of a measured metabolite pool or relevant enrichment of each metabolite. Fractional contribution (%) is determined by the formula (FC% = (M1*1 + M2*2+. . .+Mn*n)/n) as described in the previous literature. (Buescher et al., 2015).

4.3 RNA-sequence

Total RNA was extracted using the TRIzol reagent (Invitrogen, CA, USA) according to the manufacturer's protocol. RNA purity and quantification were evaluated using the NanoDrop 2000 spectrophotometer (Thermo Scientific, USA). RNA integrity was assessed using the Agilent 2,100 Bioanalyzer (Agilent Technologies, Santa Clara, CA, USA). The libraries were

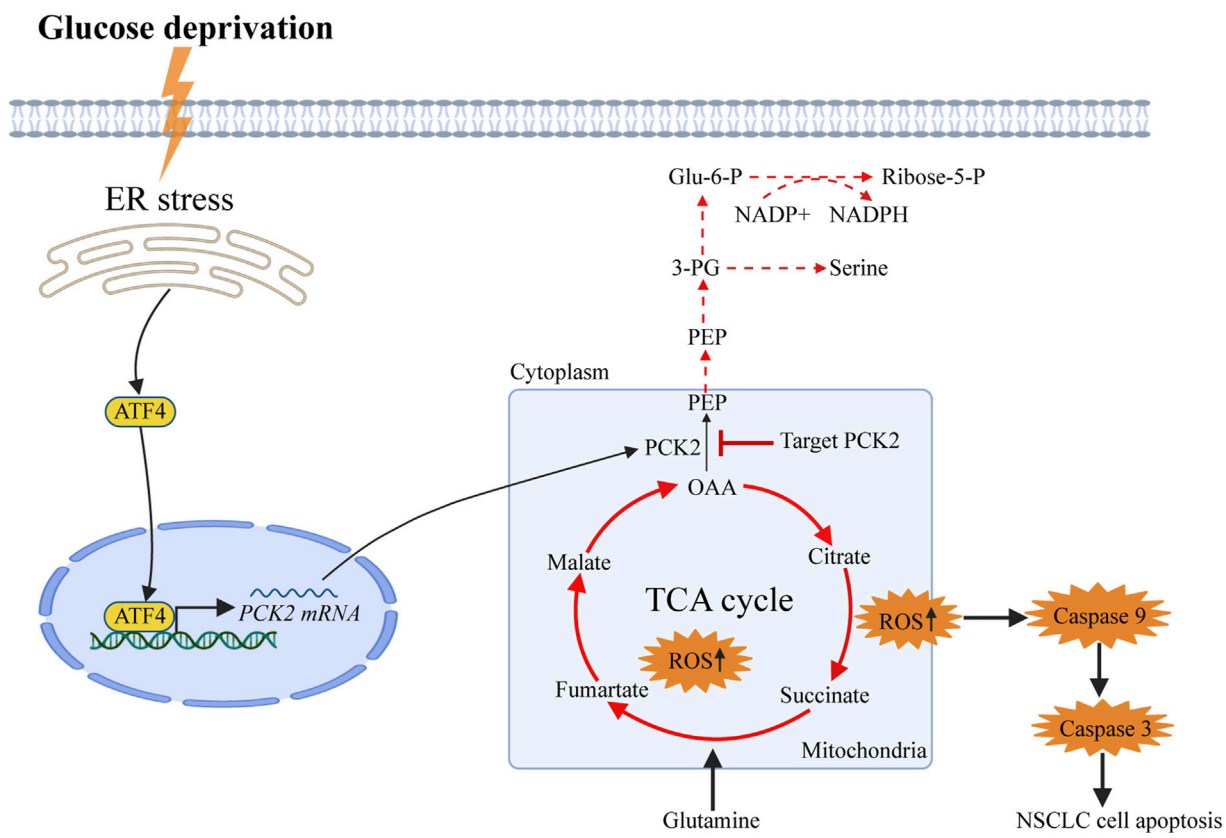

FIGURE 6
Working model of PCK2-mediated metabolism promotes lung tumorigenesis. Phosphoenolpyruvate Carboxykinase 2 (PCK2) is upregulated in dependent of endoplasmic reticulum stress-induced expression of activating transcription factor 4 (ATF4) upon glucose deprivation in NSCLC cells. PCK2-mediated metabolism is required to decrease the burden of the TCA cycles and oxidative phosphorylation as well as the production of mitochondrial reactive oxygen species, in turn reduce the activation of Caspase9-Caspase3-PARP mitochondrial apoptotic pathway.

constructed using VAHTS universal V6 RNA-seq Library Prep Kit according to the manufacturer's instructions. The transcriptome sequencing and analysis were conducted by OE Biotech Co., Ltd. (Shanghai, China). The libraries were sequenced on an Illumina HiSeq X Ten platform and 150 bp paired-end reads were generated. Raw reads for each sample were generated. Raw data (raw reads) of fastq format were firstly processed using Trimmomatic (Bolger et al., 2014) and the low quality reads were removed to obtain the clean reads. The clean reads for each sample were then retained for subsequent analyses. The clean reads were mapped to the human genome (GRCh38) using HISAT2 (Kim et al., 2015). FPKM (Roberts et al., 2011) of each gene was calculated using Cufflinks (Trapnell et al., 2010), and the read counts of each gene were obtained by HTSeq-count (Anders et al., 2015). Differential expression analysis was performed using the DESeq (2012) R package. p-value <0.05 and foldchange >2 or foldchange <0.5 was set as the threshold for significantly differential expression. Hierarchical cluster analysis of differentially expressed genes (DEGs) was performed to demonstrate the expression pattern of genes in different groups and samples. GO enrichment and KEGG (Kanehisa et al., 2008) pathway enrichment analysis of DEGs were performed respectively using R based on the hypergeometric distribution.

4.4 Quantitative real-time PCR

Total RNA was isolated from NSCLC cell lines using RNeasy Plus Mini Kit (Cat#74134, QIAGEN), and 2,000 ng of RNA was used for the cDNA synthesis using a PCR cDNA kit according to manufacturer's protocol (Cat#K1622, Thermofisher). Quantitative real-time PCR was performed using the PowerUp SYBR Green Master Mix (Thermo Fisher Scientific) on a QuantStudio 6 Flex System (Applied Biosystems). All samples were measured in triplicate and the mean value was used. The gene expression levels were calculated according to the $2^{-\Delta\Delta CT}$ method and normalized to 18S rRNA. The primers sequence used for gene expression analysis in this study were listed in Supplementary Table S1.

4.5 Western blotting

After different treatments and stimulation, cells were lysed in RIPA buffer containing Complete Mini EDTA-Free protease inhibitor cocktail and phosphatase inhibitor cocktail (Roche). Protein concentrations of cell lysate were measured by Pierce BCA protein assay kit (Thermo Fisher Scientific) and equal amounts of total protein from different samples were used. Cell

lysate was then boiled in SDS sample buffer for 5 min at 95°C–100°C, separated by SDS–PAGE and transferred to PVDF membranes (Bio-Rad). The membrane was then blocked in TBST plus 5% non-fat dry milk (Bio-Rad) for 1hincubated with primary antibodies at 4°C overnight. After three times washing with TBST, the membranes were incubated with HRP-linked secondary antibodies for 1 h at room temperature (RT) and visualized with Clarity Western ECL substrates (Thermo Fisher Scientific). Bands of interest were developed by using an autoradiographic film. The antibodies used for the immunoblotting studies are listed in Supplementary Table S2.

4.6 Cell proliferation, migration and invasion

To test cell proliferation rate, NSCLC cells were seeded in a 96-well plates at the density of 5×10^4/well in 100 μL complete medium for 18–24 h. Cells were then washed twice with PBS and incubated in the medium containing high glucose or low concentrations of glucose. Cell viability was assessed at 24, 48, 72 and 96 h using a Cell Counting K-8 kit-8 (Dojindo, Japan) according to the manufacturer's instructions.

To test migration and invasion of lung cancer cells, 3×10^5/well NSCLC cells were seeded on the top chamber of the transwell plate (Corning) in serum-free mediun containing high glucose or low concentrations of glucose medium, and medium supplemented with 10% FCS was added to the bottom chamber. After 48 h of incubation at 37°C, the chambers were fixed with methanol for 30 min, followed by staining with crystal violet (C0121, Beyotime, China) for another 30 min. The average number of migrated cells per representative field was calculated by ImageJ software.

4.7 Gene silencing by siRNA or shRNA transfection

Small interfering RNAs (SiRNAs) were used to induce transient knockdown of ATF4 and PCK2 in NSCLC cells. All siRNA duplexes were purchased from GenePharma (GenePharma, Shanghai, China). Briefly, the human NSCLC cell lines were seeded in the six-well plates at a density of 3×10^5 cells/well for 18–24 h in regular medium. The cells were then washed twice with PBS and cultured in the medium containing high glucose or low concentrations of glucose. Before transfection, diluted siRNA was mixed with diluted Lipofectamine™ RNAiMAX in OptiMEM medium (Cat#13778150, Invitrogen, USA) and was incubated for 15 min at room temperature. The mixtures were added to the culture medium with the final concentration of SiRNA at 50 nM. Cells were transfected with different siRNA for 48 h before further experimentation.

PCK2 shRNAs and nonsense control shRNA were inserted into the plasmid vector GV248 and lentiviruses were constructed, which were purchased from Shanghai GeneChem Co., Ltd. The name of the empty plasmid was hU6-MCS-Ubiquitin-EGFP-IRES-puromycin. The scrambled or shPCK2 constructs were transfected with 293T cells with the pack-aging plasmids PMD2G and psPAX2 using Lipofectamine 2000 (Invitrogen Life Technologies) for 48 h according to the manufacturer's instructions. Later, the retrovirus titer in the culture supernatant was collected. 1.5 mL of viral supernatant and 1.5 mL of fresh medium were then added to in the six-well plate containing A549 and H1975 cell lines in the presence of hexadimethrine bromide (polybrene), respectively. After 48 h, positively infected cells were selected using puromycin at 2 μg/mL. All siRNA or shRNA sequences are shown in Supplementary Table S3.

4.8 Flow cytometric analysis of cell apoptosis

A549 and H1975 cell lines were seeded in the six-well plates at a density of 5×10^5 cells/well for 18–24 h in regular medium. After twice washing with PBS, cells were cultured in the medium containing high or low concentrations of glucose for 48 h. Cells were then harvested and stained with Annexin V-FITC and Propidium iodide (PI) (E-CK-A217, Elabscience, China) for 20 min at room temperature in the dark. The percentage of apoptotic cells for each sample was immediately analyzed by flow cytometer (CytoFlex, BeckmanCoulter).

4.9 Detection of mitochondrial ROS

To measure mitochondrial reactive oxygen species, cells were seeded in the 6-well paltes for 18 h in regular medium, followed by incubating in the medium containing low concentrations of glucose (1 mM) for 48 h. Cells were then collected and incubated with 5 μM of MitoSox (M36008, Invitrogen, USA) for 30 min at 37°C. After washing with warm PBS, cells were resuspended in PBS and analyzed by flow cytometry (CytoFlex, BeckmanCoulter).

4.10 Determination of ATP and NADPH/NADP + ratio

Intracellular ATP levels were determined using an ATP assay kit (S0026B, Beyotime, China) according to the manufacturer's instructions. Briefly, NSCLC cells were plated overnight and cultured in the medium containing low concentrations (1 mM) of glucose for 48 h. The cells were then washed with cold PBS and lyzed in 200 μL ATP lysis buffer. The lysate was centrifuged at 12,000 g for 5 min, and the supernatants were used to analyze with the ATP level using ATP assay kit.

The NADPH/NADP + ratio was measured using NADP+/NADPH Assay Kit with WST-8 (S0179, Beyotime, China) according to the manufacturer's instructions. Briefly, NSCLC cells were plated overnight and then cultured in the medium containing low concentrations (1 mM) of glucose for 48 h. The cells were then collected and lysed by three freeze-thaw cycles. The lysates were used to determine NADPH and NADP + respectively. The NADPH/NADP + ratio was calculated by the following formula: (NADPH)/($NADP_{total}$–NADPH).

4.11 Mouse strains

Sex- and age-matched C57 BALB/c nude mice (Vital River Laboratory Animal Technology Co. Ltd., Beijing, China) aged

6–8 weeks were used in this study. The mice were bred and maintained under specific pathogen-free conditions with *ad libitum* access to food and water. All the animal experiments were approved by the approval of the animal care and use of committee of Tongji University (Approval number: TJBB03723107).

4.12 Subcutaneous growth of xenotransplants and lung metastasis in nude mice

To evaluate the growth of NSCLC cells *in vivo*, A549 and H1975 cells expressing either ShNC or ShPCK2 (5×10^6) suspended in 200 μL PBS were injected subcutaneously into the right flanks of athymic nude mice (age 6–8 weeks). Tumor length (L) and width (W) was measured every 2 days with a digital caliper and tumor volume (V) was calculated ($V = L \times W^2/2$). At the end of the experiments, mice were sacrificed, and tumors were dissected out and *ex vivo* weighted. Tumor tissues were collected for further experimentation.

To evaluate lung metastasis of NSCLC cells, 5×10^6 luciferase-expressing A549 and H1975 ShNC or ShPCK2 cells suspended in 200 μL PBS were injected into the tail vein of the athymic nude mice (age 6–8 weeks). After 45 days, the mice were anesthetized with phenobarbital sodium and 150 mg/kg D-luciferin (Cat#D9390, Solarbio, China) was injected intraperitoneally. The mice were then scanned and monitored by bioluminescence imaging using the IVIS system. Finally, all nude mice were sacrificed, and the lungs were dissected out and photographed.

4.13 Immunohistochemistry and TUNEL assay

Tumor tissues for immunohistochemistry were fixed with neutral formalin and embedded in paraffin. Tumor sections were stained immunohistochemically with anti-Ki67 antibody (Cat#ab16667, Abcam, United Kingdom) as well as hematoxylin. The staining was visualized by adding 3, 3′-Diaminobenzidine (DAB) (Cat#8059, Cell Signaling Technology, USA).

TUNEL assay was performed on tumor sections by using TUNEL assay kit (Cat#25869, Cell Signaling Technology, USA) following the manufacturer's instructions. Briefly, tumor sections were deparaffinized with xylene and rehydrated gradually using ethanol. The sections were then permeabilized with Proteinase K and labeled with Terminal Deoxynucleotidyl Transferase, Recombinant, (rTdT) enzyme. Fluorescent detection of apoptotic cells was achieved by using fluorescence microscopy (NIKON ECLIPSE TI-SR) and NIKON DS-U3 Imaging System.

4.14 Chromatin immunoprecipitation (CHIP)-PCR

Putative binding sites of ATF4 on PCK2 promoter were predicted using online JASPAR database (https://jaspar.elixir.no/). A549 cells were subjected to ChIP assay to verify the potential protein-DNA interaction using a commercial kit (P2080S; Beyotime, Shanghai, China) following the manufacturer's protocol. Briefly, cells were firstly treated with 1% formaldehyde for 10 min to cross link proteins and genomic DNA, then sonicated on ice to break down DNA into 400–800 base pairs. 1% of the lysed samples were taken as the input. Then, samples were pretreated with protein A/G magnetic beads to block non-specific bindings. Each sample was divided into two equal parts and incubated with anti-ATF4 (D4B8, Cell Signaling Technology) and anti-IgG (30000-0-AP; Proteintech, Wuhan, China) antibodies at 4°C overnight, respectively. Subsequently, samples were added with protein A/G magnetic beads, rotated at 4°C for 1 h and washed with the corresponding buffers. A small part of samples was subjected to Western blot assay to ensure immunoprecipitation efficiency. The rest samples were purified and subjected to quantitative PCR. Two primers were designed based on the putative binding sites. Primer 1: forward: 5'-TTCCTAGCTTGTTTGCCACCTA-3′, reverse: 5′-CCAGCC GCACATGATGTAACTT-3'; primer 2: forward: 5′- ACACAA AAGTTGGCTAAGCTGC-3′, reverse: 5′- GGAACCATCTCC TCAGTCTGT-3'.

4.15 Clinical NSCLC specimens

Tumour and adjacent normal tissues were freshly collected during the surgery. All patients were pathologically and clinically diagnosed as NSCLC. Three distinct samples of lung tumor tissue and adjacent normal lung from the resection margin were taken, flash-frozen in liquid nitrogen, and stored at −80°C until further analysis. Only NSCLC tumor samples comprising at least 90% of tumor tissue were analyzed. Each tissue sample weighing approximately 50 mg were homogenized in 500 mL lysis buffer (cat#78510, thermo scientific) using a tissuelyser (JXFSTPRP-32L, Shanghai Jingxin) to generate tissue lysates for real-time PCR and Western blot. Patients' consent and approval from the Ethics Committee of the East Affiliated Hospital of Tongji University were obtained before using these tissue materials for research purposes (Grant number:2023037).

4.16 Statistical analysis

All the data were presented as means ± standard error of the mean (S.E.M). Analyses were performed by using GraphPad Prism Software 6.0 (San Diego, CA, USA). Student t-test were used for two groups, and One-way ANOVA followed by Tukey's test was used to compare more than two groups. Statistical significance is represented in figures as follows: $^{*}p < 0.05$, $^{**}p < 0.01$, $^{***}p < 0.001$ and $^{****}p < 0.0001$.

Data availability statement

The raw RNA sequence data reported in this paper have been deposited in the Sequence Read Archive Database in the NCBI (Accession number: PRJNA1111007). Further inquiries can be directed to the corresponding authors.

Ethics statement

All the animal experiments were approved by the approval of the animal care and use of committee of Tongji University (Approval number: TJBB03723107). The study was conducted in accordance with the local legislation and institutional requirements.

Author contributions

JZ: Funding acquisition, Investigation, Methodology, Writing–original draft, Writing–review and editing. WH: Investigation, Methodology, Writing–original draft. DL: Methodology, Writing–original draft. WZ: Methodology, Writing–review and editing. HQ: Methodology, Writing–review and editing. SZ: Writing–review and editing. AC: Writing–original draft, Methodology. QL: Conceptualization, Funding acquisition, Supervision, Writing–review and editing. FW: Conceptualization, Funding acquisition, Supervision, Writing–review and editing.

Funding

The author(s) declare that financial support was received for the research, authorship, and/or publication of this article. This study was supported by the Shanghai Municipal Health Commission (grant no. 20234Y0215 to JZ), the National Natural Science Foundation of China (grant nos 81970073 and 82170090 to FW), the Shanghai Science and Technology Commission (grant no. 21Y11901100 to FW, grant no. 19411950400 to QL), the Top-level Clinical Discipline Project of Shanghai Pudong (grant no. PWYgf 2021-05 to QL) and the Academic Leaders Training Program of Pudong Health and Family Planning Commission of Shanghai (grant no. PWRd 2019-02 to FW).

Conflict of interest

The authors declare that the research was conducted in the absence of any commercial or financial relationships that could be construed as a potential conflict of interest.

Publisher's note

All claims expressed in this article are solely those of the authors and do not necessarily represent those of their affiliated organizations, or those of the publisher, the editors and the reviewers. Any product that may be evaluated in this article, or claim that may be made by its manufacturer, is not guaranteed or endorsed by the publisher.

Supplementary material

The Supplementary Material for this article can be found online at: https://www.frontiersin.org/articles/10.3389/fphar.2024.1434988/full#supplementary-material

References

Abdel-Wahab, A. F., Mahmoud, W., and Al-Harizy, R. M. (2019). Targeting glucose metabolism to suppress cancer progression: prospective of anti-glycolytic cancer therapy. *Pharmacol. Res.* 150, 104511. doi:10.1016/j.phrs.2019.104511

Anders, S., Pyl, P. T., and Huber, W. (2015). HTSeq–a Python framework to work with high-throughput sequencing data. *Bioinformatics* 31 (2), 166–169. doi:10.1093/bioinformatics/btu638

Andrews, A. M., Tennant, M. D., and Thaxton, J. E. (2021). Stress relief for cancer immunotherapy: implications for the ER stress response in tumor immunity. *Cancer Immunol. Immunother.* 70 (5), 1165–1175. doi:10.1007/s00262-020-02740-3

Attwaters, M. (2022). Persisting through apoptosis. *Nat. Rev. Mol. Cell Biol.* 23 (11), 697. doi:10.1038/s41580-022-00544-0

Balsa, E., Soustek, M. S., Thomas, A., Cogliati, S., García-Poyatos, C., Martín-García, E., et al. (2019). ER and nutrient stress promote assembly of respiratory chain supercomplexes through the PERK-eIF2α Axis. *Mol. Cell* 74 (5), 877–890. doi:10.1016/j.molcel.2019.03.031

Bertheloot, D., Latz, E., and Franklin, B. S. (2021). Necroptosis, pyroptosis and apoptosis: an intricate game of cell death. *Cell Mol. Immunol.* 18 (5), 1106–1121. doi:10.1038/s41423-020-00630-3

Bian, X., Jiang, H., Meng, Y., Li, Y. P., Fang, J., and Lu, Z. (2022). Regulation of gene expression by glycolytic and gluconeogenic enzymes. *Trends Cell Biol.* 32 (9), 786–799. doi:10.1016/j.tcb.2022.02.003

Boice, A., and Bouchier-Hayes, L. (2020). Targeting apoptotic caspases in cancer. *Biochim. Biophys. Acta Mol. Cell Res.* 1867 (6), 118688. doi:10.1016/j.bbamcr.2020.118688

Bolger, A. M., Lohse, M., and Usadel, B. (2014). Trimmomatic: a flexible trimmer for Illumina sequence data. *Bioinformatics* 30 (15), 2114–2120. doi:10.1093/bioinformatics/btu170

Buescher, J. M., Antoniewicz, M. R., Boros, L. G., Burgess, S. C., Brunengraber, H., Clish, C. B., et al. (2015). A roadmap for interpreting (13)C metabolite labeling patterns from cells. *Curr. Opin. Biotechnol.* 34, 189–201. doi:10.1016/j.copbio.2015.02.003

Carneiro, B. A., and El-Deiry, W. S. (2020). Targeting apoptosis in cancer therapy. *Nat. Rev. Clin. Oncol.* 17 (7), 395–417. doi:10.1038/s41571-020-0341-y

Caro-Maldonado, A., Tait, S. W. G., Ramírez-Peinado, S., Ricci, J. E., Fabregat, I., Green, D. R., et al. (2010). Glucose deprivation induces an atypical form of apoptosis mediated by caspase-8 in Bax-Bak-deficient cells. *Cell Death Differ.* 17 (8), 1335–1344. doi:10.1038/cdd.2010.21

Chakrabarty, R. P., and Chandel, N. S. (2021). Mitochondria as signaling organelles control mammalian stem cell fate. *Cell Stem Cell* 28 (3), 394–408. doi:10.1016/j.stem.2021.02.011

Chen, X., and Cubillos-Ruiz, J. R. (2021). Endoplasmic reticulum stress signals in the tumour and its microenvironment. *Nat. Rev. Cancer* 21 (2), 71–88. doi:10.1038/s41568-020-00312-2

Chen, Y., Wang, Z., Deng, Q., and Liang, H. (2023). Mitochondrial phosphoenolpyruvate carboxykinase inhibits kidney renal clear cell carcinoma malignant progression, leading to cell energy metabolism imbalance. *Am. J. Cancer Res.* 13 (3), 886–899.

DeBerardinis, R. J., Lum, J. J., Hatzivassiliou, G., and Thompson, C. B. (2008). The biology of cancer: metabolic reprogramming fuels cell growth and proliferation. *Cell Metab.* 7 (1), 11–20. doi:10.1016/j.cmet.2007.10.002

Dey, P., Kimmelman, A. C., and DePinho, R. A. (2021). Metabolic codependencies in the tumor microenvironment. *Cancer Discov.* 11 (5), 1067–1081. doi:10.1158/2159-8290.CD-20-1211

Fu, X., Cui, J., Meng, X., Jiang, P., Zheng, Q., Zhao, W., et al. (2021). Endoplasmic reticulum stress, cell death and tumor: association between endoplasmic reticulum stress and the apoptosis pathway in tumors (Review). *Oncol. Rep.* 45 (3), 801–808. doi:10.3892/or.2021.7933

Garlapati, C., Joshi, S., Turaga, R. C., Mishra, M., Reid, M. D., Kapoor, S., et al. (2021). Monoethanolamine-induced glucose deprivation promotes apoptosis through metabolic rewiring in prostate cancer. *Theranostics* 11 (18), 9089–9106. doi:10.7150/thno.62724

Grasmann, G., Smolle, E., Olschewski, H., and Leithner, K. (2019). Gluconeogenesis in cancer cells - repurposing of a starvation-induced metabolic pathway? *Biochim. Biophys. Acta Rev. Cancer* 1872 (1), 24–36. doi:10.1016/j.bbcan.2019.05.006

Hayes, J. D., Dinkova-Kostova, A. T., and Tew, K. D. (2020). Oxidative stress in cancer. *Cancer Cell* 38 (2), 167–197. doi:10.1016/j.ccell.2020.06.001

Hsu, H. P., Chu, P. Y., Chang, T. M., Huang, K. W., Hung, W. C., Jiang, S. S., et al. (2023). Mitochondrial phosphoenolpyruvate carboxykinase promotes tumor growth in estrogen receptor-positive breast cancer via regulation of the mTOR pathway. *Cancer Med.* 12 (2), 1588–1601. doi:10.1002/cam4.4969

Jin, J., Byun, J. K., Choi, Y. K., and Park, K. G. (2023). Targeting glutamine metabolism as a therapeutic strategy for cancer. *Exp. Mol. Med.* 55 (4), 706–715. doi:10.1038/s12276-023-00971-9

Kanehisa, M., Araki, M., Goto, S., Hattori, M., Hirakawa, M., Itoh, M., et al. (2008). KEGG for linking genomes to life and the environment. *Nucleic Acids Res.* 36, D480–D484. doi:10.1093/nar/gkm882

Kashyap, D., Garg, V. K., and Goel, N. (2021). Intrinsic and extrinsic pathways of apoptosis: role in cancer development and prognosis. *Adv. Protein Chem. Struct. Biol.* 125, 73–120. doi:10.1016/bs.apcsb.2021.01.003

Kim, D., Langmead, B., and Salzberg, S. L. (2015). HISAT: a fast spliced aligner with low memory requirements. *Nat. Methods* 12 (4), 357–360. doi:10.1038/nmeth.3317

Lee, W. N., Byerley, L. O., Bergner, E. A., and Edmond, J. (1991). Mass isotopomer analysis: theoretical and practical considerations. *Biol. Mass Spectrom.* 20 (8), 451–458. doi:10.1002/bms.1200200804

Legouis, D., Faivre, A., Cippà, P. E., and de Seigneux, S. (2022). Renal gluconeogenesis: an underestimated role of the kidney in systemic glucose metabolism. *Nephrol. Dial. Transpl.* 37 (8), 1417–1425. doi:10.1093/ndt/gfaa302

Leithner, K., Hrzenjak, A., Trötzmüller, M., Moustafa, T., Köfeler, H. C., Wohlkoenig, C., et al. (2015). PCK2 activation mediates an adaptive response to glucose depletion in lung cancer. *Oncogene* 34 (8), 1044–1050. doi:10.1038/onc.2014.47

Leithner, K., Triebl, A., Trötzmüller, M., Hinteregger, B., Leko, P., Wieser, B. I., et al. (2018). The glycerol backbone of phospholipids derives from noncarbohydrate precursors in starved lung cancer cells. *Proc. Natl. Acad. Sci. U. S. A.* 115 (24), 6225–6230. doi:10.1073/pnas.1719871115

Li, M., Zhang, C. S., Zong, Y., Feng, J. W., Ma, T., Hu, M., et al. (2019). Transient receptor potential V channels are essential for glucose sensing by aldolase and AMPK. *Cell Metab.* 30 (3), 508–524. doi:10.1016/j.cmet.2019.05.018

Li, X., Liu, M., Liu, H., and Chen, J. (2022). Tumor metabolic reprogramming in lung cancer progression (Review). *Oncol. Lett.* 24 (2), 287. doi:10.3892/ol.2022.13407

Luo, S., Ma, R., Liu, J., Xu, P., and Zhang, H. (2017). Downregulation of PCK2 remodels tricarboxylic acid cycle in tumor-repopulating cells of melanoma. *Oncogene* 36 (25), 3609–3617. doi:10.1038/onc.2016.520

Luo, Y., Ma, J., and Lu, W. (2020). The significance of mitochondrial dysfunction in cancer. *Int. J. Mol. Sci.* 21 (16), 5598. doi:10.3390/ijms21165598

Martínez-Reyes, I., and Chandel, N. S. (2021). Cancer metabolism: looking forward. *Nat. Rev. Cancer* 21 (10), 669–680. doi:10.1038/s41568-021-00378-6

Mohammad, R. M., Muqbil, I., Lowe, L., Yedjou, C., Hsu, H. Y., Lin, L. T., et al. (2015). Broad targeting of resistance to apoptosis in cancer. *Semin. Cancer Biol.* 35, S78–s103. doi:10.1016/j.semcancer.2015.03.001

Moon, S. J., Dong, W., Stephanopoulos, G. N., and Sikes, H. D. (2020). Oxidative pentose phosphate pathway and glucose anaplerosis support maintenance of mitochondrial NADPH pool under mitochondrial oxidative stress. *Bioeng. Transl. Med.* 5 (3), e10184. doi:10.1002/btm2.10184

Morana, O., Wood, W., and Gregory, C. D. (2022). The apoptosis paradox in cancer. *Int. J. Mol. Sci.* 23 (3), 1328. doi:10.3390/ijms23031328

Onodera, T., Momose, I., Adachi, H., Yamazaki, Y., Sawa, R., Ohba, S. I., et al. (2020). Human pancreatic cancer cells under nutrient deprivation are vulnerable to redox system inhibition. *J. Biol. Chem.* 295 (49), 16678–16690. doi:10.1074/jbc.RA120.013893

Paulusma, C. C., Lamers, W. H., Broer, S., and van de Graaf, S. F. J. (2022). Amino acid metabolism, transport and signalling in the liver revisited. *Biochem. Pharmacol.* 201, 115074. doi:10.1016/j.bcp.2022.115074

Roberts, A., Trapnell, C., Donaghey, J., Rinn, J. L., and Pachter, L. (2011). Improving RNA-Seq expression estimates by correcting for fragment bias. *Genome Biol.* 12 (3), R22. doi:10.1186/gb-2011-12-3-r22

Rocha, C. M., Barros, A. S., Goodfellow, B. J., Carreira, I. M., Gomes, A., Sousa, V., et al. (2015). NMR metabolomics of human lung tumours reveals distinct metabolic signatures for adenocarcinoma and squamous cell carcinoma. *Carcinogenesis* 36 (1), 68–75. doi:10.1093/carcin/bgu226

Sa-Nongdej, W., Chongthammakun, S., and Songthaveesin, C. (2021). Nutrient starvation induces apoptosis and autophagy in C6 glioma stem-like cells. *Heliyon* 7 (2), e06352. doi:10.1016/j.heliyon.2021.e06352

Schiliro, C., and Firestein, B. L. (2021). Mechanisms of metabolic reprogramming in cancer cells supporting enhanced growth and proliferation. *Cells* 10 (5), 1056. doi:10.3390/cells10051056

Shahar, N., and Larisch, S. (2020). Inhibiting the inhibitors: targeting anti-apoptotic proteins in cancer and therapy resistance. *Drug Resist Updat* 52, 100712. doi:10.1016/j.drup.2020.100712

Smolle, E., Leko, P., Stacher-Priehse, E., Brcic, L., El-Heliebi, A., Hofmann, L., et al. (2020). Distribution and prognostic significance of gluconeogenesis and glycolysis in lung cancer. *Mol. Oncol.* 14 (11), 2853–2867. doi:10.1002/1878-0261.12780

Stark, R., Guebre-Egziabher, F., Zhao, X., Feriod, C., Dong, J., Alves, T. C., et al. (2014). A role for mitochondrial phosphoenolpyruvate carboxykinase (PEPCK-M) in the regulation of hepatic gluconeogenesis. *J. Biol. Chem.* 289 (11), 7257–7263. doi:10.1074/jbc.C113.544759

Stark, R., Pasquel, F., Turcu, A., Pongratz, R. L., Roden, M., Cline, G. W., et al. (2009). Phosphoenolpyruvate cycling via mitochondrial phosphoenolpyruvate carboxykinase links anaplerosis and mitochondrial GTP with insulin secretion. *J. Biol. Chem.* 284 (39), 26578–26590. doi:10.1074/jbc.M109.011775

Tong, X., Tang, R., Xiao, M., Xu, J., Wang, W., Zhang, B., et al. (2022). Targeting cell death pathways for cancer therapy: recent developments in necroptosis, pyroptosis, ferroptosis, and cuproptosis research. *J. Hematol. Oncol.* 15 (1), 174. doi:10.1186/s13045-022-01392-3

Trapnell, C., Williams, B. A., Pertea, G., Mortazavi, A., Kwan, G., van Baren, M. J., et al. (2010). Transcript assembly and quantification by RNA-Seq reveals unannotated transcripts and isoform switching during cell differentiation. *Nat. Biotechnol.* 28 (5), 511–515. doi:10.1038/nbt.1621

Vander Heiden, M. G., Cantley, L. C., and Thompson, C. B. (2009). Understanding the Warburg effect: the metabolic requirements of cell proliferation. *Science* 324 (5930), 1029–1033. doi:10.1126/science.1160809

Vincent, E. E., Sergushichev, A., Griss, T., Gingras, M. C., Samborska, B., Ntimbane, T., et al. (2015). Mitochondrial phosphoenolpyruvate carboxykinase regulates metabolic adaptation and enables glucose-independent tumor growth. *Mol. Cell* 60 (2), 195–207. doi:10.1016/j.molcel.2015.08.013

Wang, Y., Lei, J., Zhang, S., Wang, X., Jin, J., Liu, Y., et al. (2022). 4EBP1 senses extracellular glucose deprivation and initiates cell death signaling in lung cancer. *Cell Death Dis.* 13 (12), 1075. doi:10.1038/s41419-022-05466-5

Wang, Z., and Dong, C. (2019). Gluconeogenesis in cancer: function and regulation of PEPCK, FBPase, and G6Pase. *Trends Cancer* 5 (1), 30–45. doi:10.1016/j.trecan.2018.11.003

Xiang, J., Chen, C., Liu, R., Gou, D., Chang, L., Deng, H., et al. (2021). Gluconeogenic enzyme PCK1 deficiency promotes CHK2 O-GlcNAcylation and hepatocellular carcinoma growth upon glucose deprivation. *J. Clin. Invest.* 131 (8), e144703. doi:10.1172/JCI144703

Xiong, Z., Yuan, C., Shi, J., Xiong, W., Huang, Y., Xiao, W., et al. (2020). Restoring the epigenetically silenced PCK2 suppresses renal cell carcinoma progression and increases sensitivity to sunitinib by promoting endoplasmic reticulum stress. *Theranostics* 10 (25), 11444–11461. doi:10.7150/thno.48469

Xu, D., Wang, Z., Xia, Y., Shao, F., Xia, W., Wei, Y., et al. (2020). The gluconeogenic enzyme PCK1 phosphorylates INSIG1/2 for lipogenesis. *Nature* 580 (7804), 530–535. doi:10.1038/s41586-020-2183-2

Yu, S., Meng, S., Xiang, M., and Ma, H. (2021). Phosphoenolpyruvate carboxykinase in cell metabolism: roles and mechanisms beyond gluconeogenesis. *Mol. Metab.* 53, 101257. doi:10.1016/j.molmet.2021.101257

Yu, Y., Li, J., and Ren, K. (2023). Phosphoenolpyruvate carboxykinases as emerging targets in cancer therapy. *Front. Cell Dev. Biol.* 11, 1196226. doi:10.3389/fcell.2023.1196226

frontiers | Frontiers in Oncology

TYPE Original Research
PUBLISHED 09 September 2024
DOI 10.3389/fonc.2024.1428937

Check for updates

OPEN ACCESS

EDITED BY
Hailin Tang,
Sun Yat-sen University Cancer Center (SYSUCC), China

REVIEWED BY
Jie Luo,
The First Affiliated Hospital of Guangdong Pharmaceutical University, China
Wenxiao Zheng,
University of Pittsburgh, United States
Xuefeng Chen,
No.1 People's Hospital of Xiangshan, China
Ujjal Bhawal,
Nihon University, Japan

*CORRESPONDENCE
Qiaoying Chen
cqyjlh222@163.com

RECEIVED 07 May 2024
ACCEPTED 26 June 2024
PUBLISHED 09 September 2024

CITATION
Chen Q (2024) Efficacy of different medications in the treatment of gynaecological tumours: a clinical meta-analysis.
Front. Oncol. 14:1428937.
doi: 10.3389/fonc.2024.1428937

COPYRIGHT
© 2024 Chen. This is an open-access article distributed under the terms of the Creative Commons Attribution License (CC BY). The use, distribution or reproduction in other forums is permitted, provided the original author(s) and the copyright owner(s) are credited and that the original publication in this journal is cited, in accordance with accepted academic practice. No use, distribution or reproduction is permitted which does not comply with these terms.

Efficacy of different medications in the treatment of gynaecological tumours: a clinical meta-analysis

Qiaoying Chen*

Department of Gynecology, Women's and Children's Hospital of Ningbo University, Ningbo, Zhejiang, China

Background: A gynaecological tumour is one of the world's leading causes of death for women globally. Among women, cancer is the 8th most common cause of death. Since there are no such programmes, the majority of women who are diagnosed with the condition are either in advanced stages or do not respond well to current treatments. Even if patients react to the treatments, they still risk having the cancer return, at which point any further medical intervention is met with resistance.

Method: For this study, we selected the systemic reviews and articles that have the use of different medications used for the treatment of gynaecological tumours.

Results: Regarding metformin use, this study found a positive relationship between higher survival and metformin use. Five of the studies that examined the use of statins revealed a link between statin use and higher overall and/or progression-free survival rates. Individuals on lipophilic and hydrophilic statins would do better. Research evaluating beta-blocker use during neoadjuvant treatment revealed a time-varying effect, with improved survival seen across all users early in the follow-up period. However, only non-selective beta-blocker users demonstrated a correlation with higher survival after five years. One study found that the benefits of aspirin use were significant, but the advantage for continuous users (both before and after diagnosis) was minimal.

Conclusion: Conclusions on the association between gynaecological tumour survival and NA-NSAIDs, metformin, beta-blockers, and aspirin cannot be drawn due to insufficient evidence. However, the vast majority of statin studies have demonstrated that users had higher rates of survival. Bias, however, bias may affect the results of the studies.

KEYWORDS

gynaecologic neoplasms, drug therapy, survival rate, non-steroidal anti-inflammatory agents (NSAIDs), metformin

Introduction

One of the leading causes of death among females worldwide is the tumour of the gynaecological system (1). Cancer-related deaths among females are the eighth leading cause. At present, no such population-based programs are screening that help in detecting these cancers early (2). Because there are no such programs, most of the women when diagnosed with the disease in advanced stages or their response towards the treatments that exist is not well. Even if they respond to the treatments, they also face a recurrence of that cancer, which then resists any treatment (3).

Screening for gynaecological cancers or any other kind of cancer is very important. A public health service for the population that seems to be in good health is screening. A test is provided to identify those who are at risk so that more research or therapy can reduce the likelihood of a certain disease or its consequences. Although early discovery of a dangerous ailment might save lives or improve quality of life, screening is not a foolproof procedure and does not ensure protection. The idea behind cancer screening initiatives is that early detection of the disease would lead to better results. Effective illness treatment and a good screening test that is acceptable to the community being tested are prerequisites. There should be few false positives and false negatives overall, and the program should be cost-effective. Different gynaecological cancers include the following:

Cervical cancer

Cervical cancer is the second most common malignant tumour in women worldwide. Countries with a well-established screening strategy have seen a decrease in the incidence and death of cervical cancer. Cervical cancer pathogenesis is shown in Figure 1. 4 The primary method of screening for cervical cancer is exfoliative cytology. By detecting pre-invasive cervical cancer, Papanicolaou (Pap) smear screening significantly lowers the incidence of invasive disease (4). Despite being a useful screening tool, the test's low sensitivity means that cervical cancer cannot be completely cured. More advanced techniques have been created recently to enhance detection (5).

Cervical cancer is commonly treated with a combination of surgery, chemotherapy, and radiation therapy. Chemotherapy drugs such as cisplatin, paclitaxel, and topotecan are often used either alone or in combination to target and kill cancer cells. Targeted therapies such as bevacizumab have also shown promise in treating advanced cervical cancer by blocking the blood supply to the tumour Immunotherapy drugs like pembrolizumab are being increasingly investigated for their potential in treating recurrent or metastatic cervical cancer by boosting the body's immune response against the cancer cells. Overall, a multimodal approach combining different treatment modalities has shown the most effective outcomes in managing cervical cancer.

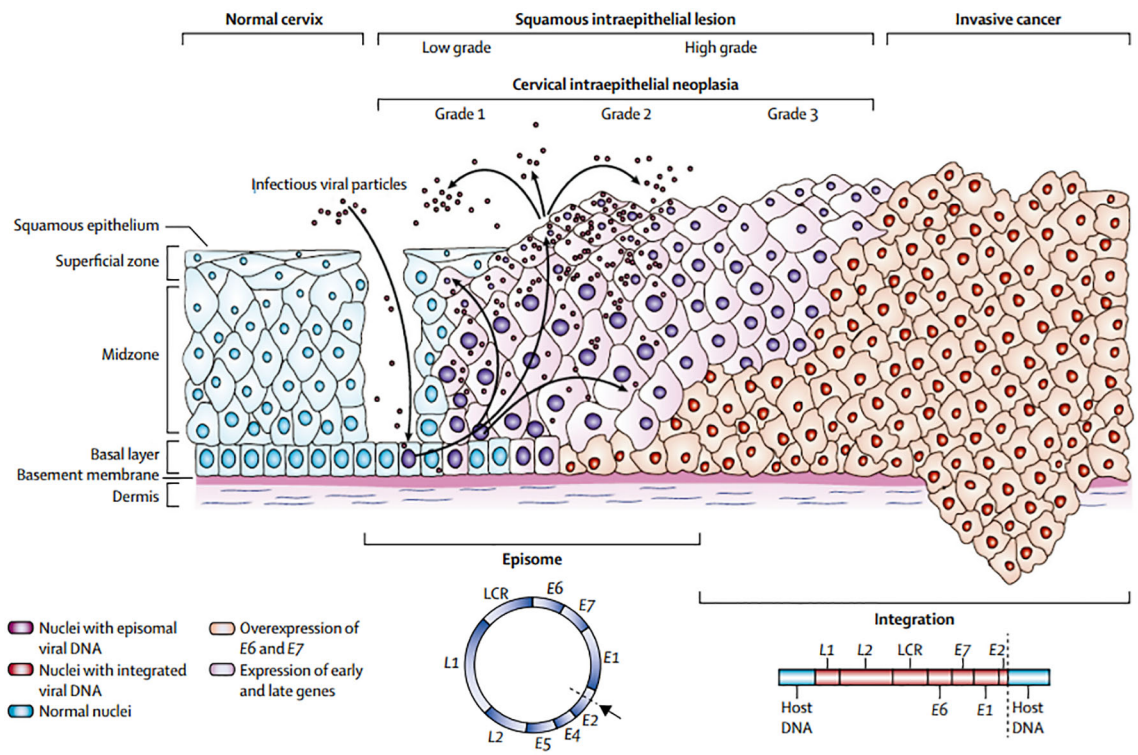

FIGURE 1
Cervical cancer's pathogenesis (34).

Fallopian tube and ovarian cancer

In affluent nations, ovarian cancer is the most prevalent cause of cancer-related fatalities among women and the primary cause of death from gynaecological cancer (6). Different histological subtypes of ovarian cancer can be distinguished based on distinct risk factors, cell origin, molecular makeup, clinical characteristics, and treatment approaches (Table 1). The need for investigating screening for this disease is supported by strong data that an early diagnosis leads to over 90% 5-year survival rates (7). The screening process is restricted to identifying low-volume illness since no premalignant lesions have been found yet (8).

Endometrial cancer

Ten per cent of all malignancies diagnosed in women are endometrial cancers, which are the most prevalent tumours of the vaginal tract. It is presently not advised to screen for this disorder in the general population or in women who are at elevated risk because of obesity, infertility, diabetes, or tamoxifen usage because the majority of women present with irregular bleeding in an early stage (9). The use of pipeline biopsy for endometrial screening in patients with breast cancer using tamoxifen has been investigated. But before endorsing routine office endometrial biopsies as a common screening procedure for individuals with breast cancer using tamoxifen, further research is needed (10). At the moment, screening is only advised for females who have a genetic susceptibility to the illness as a result of having hereditary nonpolyposis colorectal cancer (HNPCC) syndrome. For these women, their lifelong risk of cancer of the endometrium might range from 40 to 60%. If a preventive colectomy is planned, these women should be advised to undergo a prophylactic hysterectomy and a bilateral salpingo-oophorectomy, particularly if they have previously had children. According to certain research, women who have or are at risk of developing HNPCC do not substantially differ in their chances of surviving endometrial cancer from those in the general population (11, 12).

Vulval cancer or vaginal cancer

There isn't much information in the literature on these uncommon malignancies. Elevations of the urine core fragment of the HCG beta subunit, SCC, and tissue polypeptide specific antigen (TPS) have been seen in certain investigations. No research has been done on the benefits of screening (12).

When the diagnosis of these conditions is made in females, less than 50% of the females survive for at least five years. Many studies have been published attributing how the use of common medications impacts the survival of these patients (3). Commonly used medications used by these patients include metformin, beta-blockers, statins, aspirin as well as non-steroidal anti-inflammatory medicines (NSAIDs) (13). Many systemic reviews have been published that demonstrate these medicines positively affect the survival of patients with tumours and improve survival chances.

TABLE 1 Ovarian cancer features based on histology, genetics, and active therapy 8.

Histological subtype	Clinical findings	Genetic characteristics	Treatment options
High-grade serous carcinoma and high-grade endometrioid carcinoma	Can present with peritoneal carcinomatosis, ascites and/or pelvic mass	Deficiencies in homologous recombination (50% of tumours)	Platinum-based chemotherapy and poly (ADP-ribose) polymerase inhibitors
	typically advanced stage at presentation	Associated with *BKCA* and *TP53* mutations	Tumours are initially sensitive to platinum-based chemotherapy. but most patients with advanced-stage cancer will recur
Low-grade serous carcinoma	Presents in younger patients (median reported age: 43-55 years)	Associated with *KRAF* and *BRAF* mutations	MEK inhibitors (currently being tested in clinical traits) and hormonal therapies
	Can be early or late stage at presentation	Tumours have genomic stability	
Low-grade endometrioid carcinoma	Can be associated with endometriosis	Associated with *PTEN*, *ARJDIA* and *PIK3CA* mutations	Possible hormonal therapies (not yet established)
		Can have microsatellite instability	
Clear-cell carcinoma	Can present with parenchymal metastases (in the liver and the lungs)	Associated with *AKID1A* and *PIK3CA* mutations	Immunotherapy agents.
	Can be associated with hypercoagulability and hypercalcaemia		Can be resistant to platinum-based chemotherapy
Mucinous carcinoma	Presents in younger patients and is typically early stage of presentation	Associated with *KRAS* mutations.	Tends to be insensitive to chemotherapy but is still treated initially with cytotoxic chemotherapy

Also, there are a few studies which also suggest that the effects that these medicines bring can also vary because of the subtypes of the medication like statins of lipophilic or hydrophilic nature, or selective beta blockers or non-selective beta blockers (14). The period to which these medicines are being used also affects the impact that they brings (15).

More than two-thirds of patients with advanced cancer report having significant pain, and as many as half of them say their pain is not well managed. Patients with gynaecologic oncology may also feel acute discomfort due to the burden of their disease or the course of their cancer therapy (16).

Regardless of speciality, gynaecologic oncologists may help stop the opioid crisis by treating patients' pain with awareness and purpose. This can start with developing improved recovery protocols and performing a greater percentage of minimally invasive operations to handle gynaecologic cancers surgically (17).

Gynaecologic oncologists should provide a pain evaluation to individuals with either acute or ongoing cancer or pain linked to therapy at every visit. The location of the pain, aggravating and mitigating variables, current therapies, and any prior treatments should all be covered in this evaluation. Clinicians should also check if drug demands are rising, steady or decreasing. It is important to rule out recurring or progressive illness in individuals presenting with new or worsening pain (18).

In addition, the administration of beta-adrenergic receptor antagonists, or beta-blockers, during cancer treatment has been suggested to have potential benefits based on experimental and epidemiological findings. This may be because the sympathomimetic neurotransmitters norepinephrine (NE) and epinephrine (E) are inhibited in their ability to act. These neurotransmitters may play a significant role in the development of secondary tumours and may be involved in some of the eight recognized characteristics of cancer, such as metastasis (19).

Since beta blockers are thought to be inexpensive, safe, and effective medications, it would be extremely advantageous to explore any possible adverse effects before using them (19).Nevertheless, data from relevant epidemiological studies have yielded conflicting results, and it has been proposed that immortal time bias—a period of cohort follow-up during which a population cannot experience an event because of the definition of drug exposure—may be partially to blame for the apparent discrepancies in study results (20).

Adults in the US take statins often to decrease their low-density lipoprotein (LDL) levels of cholesterol and avoid cardiovascular disease; in 2012, 28% of those over 40 reported using a statin. There have been documented non-cardiovascular advantages of statin usage, such as possible anti-tumour actions in a broad range of cancers. Statin users had a substantial 15% lower incidence of mortality from cancer and a 15% lower frequency of death from any cause, according to population-based observational research of 295,925 individuals in the Danish Cancer Registry (21).

We found a substantial 30- 40% increase in overall survival when statin usage was independently associated with this large prospective cohort of older women with ovarian cancer. This is consistent with smaller retrospective datasets that were previously reported and showed increased overall and disease-free survival in patients receiving concomitant statin medication for primary peritoneal, fallopian tube, or epithelial ovarian carcinomas (19).

The survival rate specific to ovarian cancer was statistically substantially higher for women who reported recent use of aspirin and non-aspirin nonsteroidal anti-inflammatory drugs (NSAIDs) in the time following diagnosis for the NHS recent for the NHSII, with identical timeframes for the evaluation of NSAIDs. These findings call for more research, and if they are validated, it could be interesting to evaluate the use of anti-inflammatory drugs after diagnosis in randomized trials in addition to conventional ovarian cancer treatments to enhance patient outcomes (22).

Another study suggested that Even though there is significant variability, cancer patients who take metformin have longer survival than those who do not (23). Met24 Metformin is linked to non-significantly higher survival times for malignancies of the prostate, lung, liver, larynx, and bladder, but substantially longer survival times for breast, colorectal, endometrial, and ovarian cancers (24). The main drawback is the high degree of study heterogeneity and the paucity of data for some cancer types (25).

Methods

For this study, we selected the systemic reviews and articles that have the use of different medications used for the treatment of gynaecological tumours. Controlling for bias and compensating for missing values were explored in our study, which in turn led to a more statistically rigorous article and a more conclusive article.

Search strategy

The search was done on Embase (Elsevier), PubMed (National Library of Medicine, Web of Science and Google Scholar. Some research was also done on the list of references of the articles that were eligible for this study. Each article was thoroughly studied for relevant information and then the information was extracted from it and stored in a secure database.

Eligibility criteria

Exposures

Multiple terminologies were used throughout the studies regarding the use of medications in tumours. However, we classify the exposures as ever or never use of any sort of medications before or after the diagnosis.

Study population

The population of this study were the women who have experienced any gynaecological tumour (ovarian, fallopian tube or primary peritoneal) and went through the use of medicine for it.

Study selection and data extraction

All the studies that were identified were stored in an endnote file. Each study was assessed for its eligibility and after reviewing the

titles and the abstracts of different studies. For the studies that remained, we obtained full-text papers wherever possible, and we eliminated those that had ineligible individuals or samples. When a research or dataset had numerous publications, we included the report with the biggest sample size, the most comprehensive data, or the most extended follow-up period. For this purpose, we utilized 10 studies to be included in this analysis and they were studied for their characteristics and hazard ratios (95% CI). We tried our best to resolve any type of discrepancies from the studies. The disagreements of reviewers were put into question throughout the study duration, and conflicts of interest were addressed during the process of data extraction so that no questions could be raised after the study was completed.

Quality assessment

A reviewer independently evaluated each study's quality using the Cochrane ROBINS-I method, which assigns a risk of bias (ROB) score of low (quality comparable to a randomized clinical trial), moderate, serious, or critical. Since none of the included research was deemed to have low ROB, we categorized the investigations based on whether or not they had substantial ROB. The Cochrane ROB, as a revised version of the current evidence appraisal, categorizes the quality of evidence in the included literature more accurately, increasing the overall quality of this paper.

Statistical analysis

To create pooled hazard ratios (pHR), we employed random-effects models and the inverse variance approach. When required, we estimated the pertinent confidence bounds using the provided P-value (P). To avoid all kinds of reverse causation from the studies, in those studies where hazard ratios were available for both times diagnosis and post-diagnosis, we utilized the data of pre-diagnosis assuming that the patient must have continued the use of medication after the diagnosis as well. The analysis was done using SPSS version 22 and STATA 15.

Results

Metformin

The survival rates of women taking metformin were compared to those of non-users who were either women with diabetes, women without diabetes, or women with both diabetes and non-diabetes combined. In all, three studies found a correlation between the usage of metformin and increased survival; nevertheless, they were all thought to have ITB. The two trials that were graded as ITB-free indicated that there was no overall survival advantage linked to the use of metformin; however, the research that assessed usage within six months before or following diagnosis found that metformin users had improved survival 30 months after diagnosis. The combined estimate of all research, including those classified as possibly having ITB, indicated a positive correlation between metformin usage and better survival (pHR: 0.66, 95%CI: 0.44–1.00) as well as better survival among users (pHR: 0.45, 95%CI: 0.33–0.60). See Table 2 for details and Figure 2.

Statin

Among the studies that were focused on the use of statins, 5 studies suggested a correlation between statins and increased survival rates overall and/or progression-free. A correlation between statins and increased survival was revealed by pooling the data from the eight ITB-free trials (pHR: 0.76, 95%CI: 0.68–0.85). Publication bias was not evident (P=0.059). Based on the exposure timing, we categorized the research. A relationship between statin usage and increased survival was revealed by the calculated pHRs based on pre-diagnosis use (three studies, pHR: 0.77, 95%CI: 0.67–0.87), perioperative use (two studies, pHR: 0.60, 95%CI: 0.48–0.72), and post-diagnosis use (three studies, pHR: 0.81, 95%CI: 0.74–0.89). The studies also revealed a correlation between statin use and a lower death rate (pHR: 0.63, 95%CI: 0.37–1.09). Two of the three studies that examined the survival results of lipophilic and hydrophilic statins independently were assessed as ITB-free; yet, one of the studies categorized atorvastatin as hydrophilic even though its characteristics are mostly lipophilic. The results of the three trials indicated that patients using hydrophilic and lipophilic statins would fare better. See Table 3 for details and Figure 3.

Beta-blockers

A time-varying impact for beta-blockers was shown in research assessing usage during neoadjuvant treatment, with better survival observed amongst all users early in the follow-up period. However after five years, only non-selective beta-blocker users showed a relationship with increased survival, and the association was larger in women without hypertension. Another study had provided HRs for exposures both before and after diagnosis. A meta-analysis of six ITB-free trials that included the pre-diagnosis estimate produced a pooled HR of 1.07 (95%CI: 0.96–1.21), indicating no survival advantage for beta-blockers. There was no correlation between usage and survival, according to the combined findings of the three trials that assessed PFS (pHR: 0.97, 95%CI: 0.78–1.20). Nevertheless, combining the findings from the other two trials assessing perioperative usage revealed a potential link between use

TABLE 2 Metformin studies and its characteristics.

Metformin Studies	Population	HR (95% CI)
USA 2017 (Garcia)	2291	0.88 (0.66, 1.17)
USA 2012 (Romero)	341	0.58 (0.23, 0.83)
Israel 2016 (Bar)	2016	0.78 (0.40, 1.42)

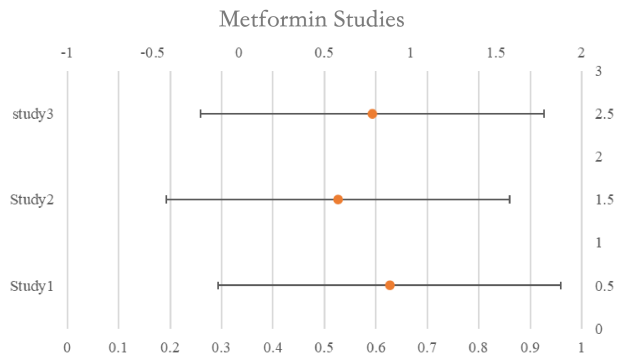

FIGURE 2
Rest plot for the meta-analysis regarding hazard ratio among the patients using metformin.

TABLE 3 Statin studies and its characteristics.

Statin Studies	Population	HR (CI 95%)
USA 2008 (Elmore)	126	0.45 (0.23, 0.88)
Belgium 2017 (Couttenier)	4895	0.82 (0.72, 0.93)
China 2016 (Chen)	60	0.57 (0.21, 1.55)

and enhanced PFS (pHR: 0.87, 95%CI: 0.69–1.09) and overall (pHR: 0.82, 95%CI: 0.60–1.12). See Table 4 for details and Figure 4.

Aspirin & NSAID's

One of the studies assessed survival rates using data from both pre- and post-diagnosis periods. When the HRs assessing pre-diagnosis usage were included in the initial meta-analysis, we saw no correlation between aspirin use. Use both before and after diagnosis was evaluated in two trials.

Aspirin, HR: 0.44, 95%CI: 0.26–0.74; NSAIDs, 0.46, 95%CI: 0.29–0.73) and post-diagnosis survival benefit was shown to be significant in one study, while the advantage to continuous users (pre- and post-diagnosis) was low. The second research found no evidence that ongoing low-dose aspirin treatment improved overall survival (HR: 1.01, 95%CI: 0.84–1.22). See Table 5 for details and Figure 5.

Discussion

Studies on statin usage showed that users might live longer (26). The combined findings of beta-blocker trials indicated a potential advantage linked to perioperative usage but no improvement in overall survival (27). The small number of trials revealed no survival advantages linked to metformin, and the evidence supporting a relationship between aspirin and NSAIDs was weak, although more research is needed. Studies addressing the possibility of Immortal

TABLE 4 Beta-blocker studies and their characteristics.

Beta-blockers studies	Population	HR (CI 95%)
Denmark 2013 (Johannesdottir)	6626	1.17 (1.02, 1.34)
Germany 2017 (Heltz)	801	0.94 (0.69. 1.29)
South Korea 2018 (Baek)	866	1.05 (0.80, 1.37)

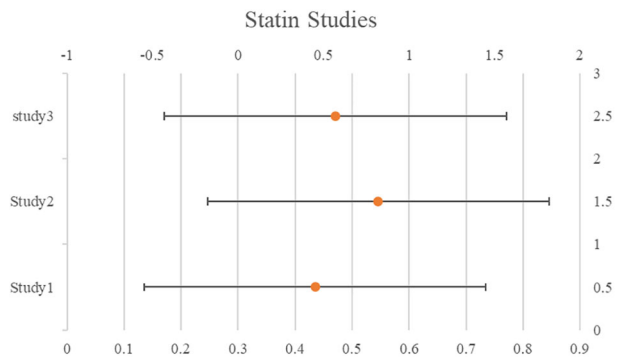

FIGURE 3
Forest plot for the meta-analysis regarding hazard ratio among the patients using Statin.

FIGURE 4
Forest plot for the meta-analysis regarding hazard ratio among the patients using beta-blockers.

Time Biased were generally more likely to demonstrate links with the drugs and increased survival (28).

An essential enzyme in the mevalonate pathway, 3-hydroxy-3-methylglutaryl-coenzyme A (HMG-CoA) reductase, is inhibited by statins25 The primary byproduct of the mevalonate pathway in liver cells, cholesterol, is reduced by this restriction, but it also has an impact on several non-sterol side products necessary for cell division, survival, and repair. Studies conducted *in vitro* have revealed that certain cancer cells, such as those from the breast and ovary, have abnormally elevated expression of the HMG-CoA reductase gene. Tumour cells can proliferate more rapidly and survive longer than normal cells due to altered metabolism. One proposed mechanism is that statins, by inhibiting the mevalonate pathway and reducing its downstream products, may induce apoptosis, or cell death, thereby impeding tumour growth.

TABLE 5 Aspirin & NSAIDs studies and their characteristics.

Aspirin & NSAIDs studies	Population	HR (CI 95%)
USA 2018 (Merritt)	1022	0.99 (0.79, 1.25)
USA 2017 (Wield)	77	0.13 (0.02, 0.95)
Denmark 2018 (Verdoot)	4117	0.97 (0.87, 1.08)

Additionally, preclinical studies have demonstrated that combining statins with chemotherapy drugs enhances the effectiveness of cancer treatment (24).

All things considered; these findings imply that it would be worthwhile to look at the possible effects of statins in a study that also assesses whether statins might increase survival rates among women without hyperlipidaemia.

Experimental research has indicated that using beta-blockers during surgery may improve survival, mostly by limiting the possibility of cell migration and metastases (29).

A limitation of the included studies is that they could only assess medication use in women with the specific medical condition necessitating the medication (18).

Furthermore, the severity of the ailment being treated as well as the prognosis of the cancer may have an impact on the usage of chronic illness drugs during cancer therapy or following diagnosis, both of which can also have an impact on survival rates. Because the expected benefit would be small, women with poorer cancer prognoses could decide not to start preventative medicine or stop taking it altogether. (30) This may pose a special challenge for assessments of new usage after diagnosis and help to explain some of the substantial correlations observed between the new use of NSAIDs and aspirin after diagnosis and increased survival (31).

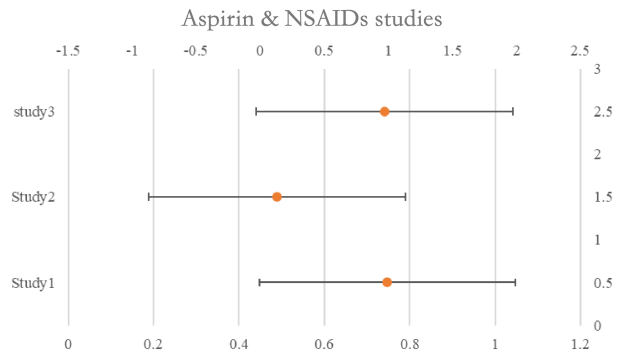

FIGURE 5
Forest plot for the meta-analysis regarding hazard ratio among the patients using Aspirin & NSAIDs.

Certain confounding factors also impose a tricky situation for the researcher to conduct the research. Such confounding factors like parity and oral contraceptive use can also play a vital role in the medication used for the treatment of gynaecological cancers.

Conclusion

In conclusion, there is not enough data available to make any judgements on the relationship between gynaecological tumour survival and metformin, beta-blockers, aspirin, and NA-NSAIDs. On the other hand, the majority of research on statins has shown that users had better survival rates. However, bias might have an impact on observational study outcomes. Moreover, they are only able to evaluate statin usage in women who are prescribed these drugs, often for hypercholesterolemia; they are unable to evaluate statin use in women whose cholesterol levels are normal. Randomized studies are necessary to ascertain if administering statins as an adjuvant therapy to women with gynaecological cancer during or after chemotherapy could enhance their likelihood of survival.

Data availability statement

The original contributions presented in the study are included in the article/supplementary material. Further inquiries can be directed to the corresponding author.

Author contributions

QC: Conceptualization, Data curation, Methodology, Project administration, Supervision, Validation, Writing – original draft, Writing – review & editing.

Funding

The author(s) declare that no financial support was received for the research, authorship, and/or publication of this article.

Conflict of interest

The author declares that the research was conducted in the absence of any commercial or financial relationships that could be construed as a potential conflict of interest.

Publisher's note

All claims expressed in this article are solely those of the authors and do not necessarily represent those of their affiliated organizations, or those of the publisher, the editors and the reviewers. Any product that may be evaluated in this article, or claim that may be made by its manufacturer, is not guaranteed or endorsed by the publisher.

References

1. Ferlay J, Ervik M, Lam F, Colombet M, Mery L, Piñeros M, et al. Global cancer observatory: cancer today. *Lyon France: Int agency Res Cancer*. (2018) 3(20):2019.

2. Bottoni P, Scatena R. The role of CA 125 as tumor marker: biochemical and clinical aspects. *Adv Cancer Biomarkers: From Biochem to clinic Crit revision*. (2015), 229–44. doi: 10.1007/978-94-017-7215-0_14

3. Göbel A, Breining D, Rauner M, Hofbauer LC, Rachner TD. Induction of 3-hydroxy-3-methylglutaryl-CoA reductase mediates statin resistance in breast cancer cells. *Cell Death Dis*. (2019) 10(2):91. doi: 10.1038/s41419-019-1322-x

4. Canavan TP, Doshi NR. Cervical cancer. *Am Family physician*. (2000) 61:1369–76.

5. Moore DH. Cervical cancer. *Obstetrics Gynecology*. (2006) 107:1152–61. doi: 10.1097/01.AOG.0000215986.48590.79

6. Jayson GC, Kohn EC, Kitchener HC, Ledermann JA. Ovarian cancer. *Lancet*. (2014) 384(9951):1376–88. doi: 10.1016/S0140-6736(13)62146-7

7. Matulonis UA, Sood AK, Fallowfield L, Howitt BE, Sehouli J, Karlan BY. Ovarian cancer. *Nat Rev Dis Primers*. (2016) 2(1):1–22. doi: 10.1038/nrdp.2016.61

8. Permuth-Wey J, Sellers TA. Epidemiology of ovarian cancer. *Cancer epidemiology: modifiable factors*. (2009), 413–37. doi: 10.1007/978-1-60327-492-0_20

9. Amant F, Moerman P, Neven P, Timmerman D, Van Limbergen E, Vergote I. Endometrial cancer. *Lancet*. (2005) 366(9484):491–505. doi: 10.1016/S0140-6736(05)67063-8

10. Braun MM, Overbeek-Wager EA, Grumbo RJ. Diagnosis and management of endometrial cancer. *Am Family physician*. (2016) 93:468–74.

11. Burke WM, Orr J, Leitao M, Salom E, Gehrig P, Olawaiye AB, et al. Endometrial cancer: a review and current management strategies: part II. *Gynecologic Oncol*. (2014) 134(2):393–402. doi: 10.1016/j.ygyno.2014.06.003

12. Majidi A, Na R, Dixon-Suen S, et al. Common medications and survival in women with ovarian cancer: A systematic review and meta-analysis. *Gynecologic Oncol*. (2020) 157:678–85. doi: 10.1016/j.ygyno.2020.03.028

13. Jang H-I, Lim S-H, Lee Y-Y, et al. Perioperative administration of propranolol to women undergoing ovarian cancer surgery: A pilot study. *Obstetrics gynecology Sci*. (2017) 60:170. doi: 10.5468/ogs.2017.60.2.170

14. Mei Z, Liang M, Li L, et al. Effects of statins on cancer mortality and progression: a systematic review and meta-analysis of 95 cohorts including 1,111,407 individuals. *Int J Cancer*. (2017) 140:1068–81. doi: 10.1002/ijc.30526

15. Na Z, Qiao X, Hao X, Fan L, Xiao Y, Shao Y, et al. The effects of beta-blocker use on cancer prognosis: a meta-analysis based on 319,006 patients. *OncoTargets Ther*. (2018), 4913–44. doi: 10.2147/OTT

16. Ravnskov U, McCully K, Rosch P. The statin-low cholesterol-cancer conundrum. *QJM: Int J Med*. (2012) 105:383–88. doi: 10.1093/qjmed/hcr243

17. Sterne JA, Hernán MA, Reeves BC, Savović J, Berkman ND, Viswanathan M, et al. ROBINS-I: a tool for assessing risk of bias in non-randomised studies of interventions. *bmj*. (2016), 355. doi: 10.1136/bmj.i4919

18. Watkins JL, Thaker PH, Nick AM, et al. Clinical impact of selective and nonselective beta-blockers on survival in patients with ovarian cancer. *Cancer*. (2015) 121:3444–51. doi: 10.1002/cncr.29392

19. Al-Niaimi A, Dickson EL, Albertin C, et al. The impact of perioperative β blocker use on patient outcomes after primary cytoreductive surgery in high-grade epithelial ovarian carcinoma. *Gynecologic Oncol*. (2016) 143:521–25. doi: 10.1016/j.ygyno.2016.09.019

20. Bar D, Lavie O, Stein N, Feferkorn I, Shai A. The effect of metabolic comorbidities and commonly used drugs on the prognosis of patients with ovarian cancer. *Eur J Obstetrics Gynecology Reprod Biol*. (2016) 207:227–31. doi: 10.1016/j.ejogrb.2016.09.005

21. Altwairgi AK. Statins are potential anticancerous agents. *Oncol Rep*. (2015) 33:1019–39. doi: 10.3892/or.2015.3741

22. Merritt MA, Rice MS, Barnard ME, Hankinson SE, Matulonis UA, Poole EM, et al. Pre-diagnosis and post-diagnosis use of common analgesics and ovarian cancer prognosis (NHS/NHSII): a cohort study. *Lancet Oncol*. (2018) 19(8):1107–16. doi: 10.1016/S1470-2045(18)30373-5

23. Clayton L, Keene S, Stansel SP, Jiang M, Aldrich M, Xu H, et al. Abstract C19: Assessing metformin use and ovarian cancer survival from electronic medical records. *Cancer Epidemiology Biomarkers Prev*. (2016) 25:C19–9. doi: 10.1158/1538-7755.DISP15-C19

24. Mo H, Elson CE. Studies of the isoprenoid-mediated inhibition of mevalonate synthesis applied to cancer chemotherapy and chemoprevention. *Exp Biol Med*. (2004) 229:567–85. doi: 10.1177/153537020422900701

25. Romero IL, McCormick A, McEwen KA, Park S, Karrison T, Yamada SD, et al. Relationship of type II diabetes and metformin use to ovarian cancer progression, survival, and chemosensitivity. *Obstetrics Gynecol*. (2012) 119(1):61–7. doi: 10.1097/AOG.0b013e3182393ab3

26. Chen Y, Han L, Zheng A. Association between statin use and the risk, prognosis of gynecologic cancer: A meta-analysis. *Eur J Obstetrics Gynecology Reprod Biol*. (2022) 268:74–81. doi: 10.1016/j.ejogrb.2021.11.013

27. Xie W, Ning L, Huang Y, Liu Y, Zhang W, Hu Y, et al. Statin use and survival outcomes in endocrine-related gynecologic cancers: A systematic review and meta-analysis. *Oncotarget*. (2017) 8(25):41508. doi: 10.18632/oncotarget.v8i25

28. Liu Y, Qin A, Li T, et al. Effect of statin on risk of gynecologic cancers: a meta-analysis of observational studies and randomized controlled trials. *Gynecologic Oncol*. (2014) 133:647–55. doi: 10.1016/j.ygyno.2014.04.007

29. Modzelewska B, Jóźwik M, Kleszczewski T, et al. Myometrial responses to beta-adrenoceptor antagonists in gynecological Malignancies. *Gynecologic Obstetric Invest*. (2021) 86:162–69. doi: 10.1159/000513718

30. Brøns N, Baandrup L, Dehlendorff C, Kjaer SK. Use of nonsteroidal anti-inflammatory drugs and risk of endometrial cancer: a nationwide case–control study. *Cancer Causes Control*. (2015) 26:973–81. doi: 10.1016/j.ygyno.2018.09.022

31. Hannibal CG, Dehlendorff C, Kjaer SK. Use of paracetamol, low-dose aspirin, or non-aspirin non-steroidal anti-inflammatory drugs and risk of ovarian borderline tumors in Denmark. *Gynecologic Oncol*. (2018) 151(3):513–18. doi: 10.1016/j.ygyno.2018.09.022

frontiers | Frontiers in Pharmacology

TYPE Original Research
PUBLISHED 16 September 2024
DOI 10.3389/fphar.2024.1466779

Check for updates

OPEN ACCESS

EDITED BY
Hailin Tang,
Sun Yat-sen University Cancer Center (SYSUCC), China

REVIEWED BY
Yufan Chen,
Sun Yat-sen University Cancer Center (SYSUCC), China
Lang He,
Chengdu Fifth People's Hospital, China

*CORRESPONDENCE
Qing Zhou,
zhangyuxuan1117@hotmail.com
Haiyan Zhu,
xiaoyanzibj301@163.com
Fan Yin,
yinfancying@163.com

†These authors have contributed equally to this work

RECEIVED 18 July 2024
ACCEPTED 27 August 2024
PUBLISHED 16 September 2024

CITATION
Peng Y, Wang L, Yang J, Wu Q, Sun X, Zhang J, Yu Y, Zhang L, Gao J, Zhou Q, Zhu H and Yin F (2024) Integrated analyses reveal IDO1 as a prognostic biomarker coexpressed with PD-1 on tumor-associated macrophages in esophageal squamous cell carcinoma. *Front. Pharmacol.* 15:1466779. doi: 10.3389/fphar.2024.1466779

COPYRIGHT
© 2024 Peng, Wang, Yang, Wu, Sun, Zhang, Yu, Zhang, Gao, Zhou, Zhu and Yin. This is an open-access article distributed under the terms of the Creative Commons Attribution License (CC BY). The use, distribution or reproduction in other forums is permitted, provided the original author(s) and the copyright owner(s) are credited and that the original publication in this journal is cited, in accordance with accepted academic practice. No use, distribution or reproduction is permitted which does not comply with these terms.

Integrated analyses reveal IDO1 as a prognostic biomarker coexpressed with PD-1 on tumor-associated macrophages in esophageal squamous cell carcinoma

Yaojun Peng[1,2†], Lingxiong Wang[3,4†], Juan Yang[5†], Qiyan Wu[3,4], Xiaoxuan Sun[6,7], Jinying Zhang[8], Yanju Yu[4], Liping Zhang[1], Jie Gao[9], Qing Zhou[10]*, Haiyan Zhu[1]* and Fan Yin[9]*

[1]Department of Emergency, The First Medical Center, Chinese People's Liberation Army (PLA) General Hospital, Beijing, China, [2]Medical School of Chinese People's Liberation Army (PLA), Beijing, China, [3]Lab of the Oncology Department, The First Medical Center, Chinese People's Liberation Army (PLA) General Hospital, Beijing, China, [4]Institute of Oncology, The Fifth Medical Centre, Chinese People's Liberation Army (PLA) General Hospital, Beijing, China, [5]Department of Cardiothoracic Surgery, Tianjin Fourth Center Hospital, Tianjin, China, [6]National Clinical Research Center for Cancer, Key Laboratory of Cancer Prevention and Therapy, Tianjin's Clinical Research Center for Cancer, Tianjin Medical University Cancer Institute and Hospital, Tianjin, China, [7]Department of Oncology Surgery, Tianjin Cancer Hospital Airport Free Trade Zone Hospital, Tianjin, China, [8]Department of Basic Medicine, Medical School of Chinese People's Liberation Army (PLA), Beijing, China, [9]Department of Oncology, The Second Medical Center and National Clinical Research Center of Geriatric Disease, Chinese People's Liberation Army (PLA) General Hospital, Beijing, China, [10]Department of Gastroenterology, The Second Medical Center and National Clinical Research Center of Geriatric Disease, Chinese People's Liberation Army (PLA) General Hospital, Beijing, China

Background: Inhibition of indolamine-2,3-dioxygenase 1 (IDO1) has been proposed as a promising strategy for cancer immunotherapy; however, it has failed in clinical trials. Macrophages in the tumor microenvironment (TME) contribute to immune escape and serve as potential therapeutic targets. This study investigated the expression pattern of IDO1 in TME and its impact on prognosis and therapeutic response of patients with esophageal squamous cell carcinoma (ESCC).

Methods: RNA sequencing data from 95 patients with ESCC from The Cancer Genome Atlas (TCGA) database were used to explore the prognostic value of IDO1. Bioinformatics tools were used to estimate scores for stromal and immune cells in tumour tissues, abundance of eight immune cell types in TME, and sensitivity of chemotherapeutic drugs and immune checkpoint (IC) blockage.

Abbreviations: IDO1, Indolamine-2,3-dioxygenase 1; TME, tumor microenvironment; ESCC, esophageal squamous cell carcinoma; TCGA, The Cancer Genome Atlas; IC, immune checkpoint; PD-1, programmed cell death 1; PD-L1, programmed cell death 1 ligand 1; OS, overall survival; FFPE, formalin-fixed paraffin-embedded; CAF, cancer associated fibroblast; scRNA-seq, single-cell RNA sequencing; TIDE, Tumor Immune Dysfunction and Exclusion; DEGs, differentially expressed genes; GO, Gene Ontology; KEGG, Kyoto Encyclopedia of Genes and Genomes; WSI, whole-slide image; HR, hazard ratio; CI, confidence interval; TAMs, tumor-associated macrophages; DCs, dendritic cells; Tregs, regulatory T cells; MDSCs, myeloid-derived suppressor cells; IC50, half-maximal inhibitory concentration.

The results were validated using digitalized immunohistochemistry and multiplexed immunofluorescence in ESCC tissue samples obtained from our clinical center.

Results: TCGA and validation data suggested that high expression of IDO1 was associated with poor patient survival, and IDO1 was an independent prognostic factor. IDO1 expression positively correlated with macrophages in TME and PDCD1 within diverse IC genes. Single-cell RNA sequencing data analysis and multiplexed immunofluorescence verified the coexpression of IDO1 and PD-1 in tumor-associated macrophages (TAMs). Patients with high IDO1 expression showed increased sensitivity to various chemotherapeutic drugs, while were more likely to resist IC blockage.

Conclusion: This study identifies IDO1 as an independent prognostic indicator of OS in patients with ESCC, reveals a compelling connection of IDO1, PD-1, and TAMs, and explores the sensitivity of patients with high IDO1 expression to chemotherapeutic drugs and their resistance to IC blockade. These findings open new avenues for potential targets in ESCC immunotherapy.

KEYWORDS

immune checkpoint, esophageal squamous cell carcinoma, macrophage, immune microenvironment, PD-1, IDO1

Introduction

Esophageal cancer is a major public health concern worldwide, with a poor prognosis (Sung et al., 2021). Esophageal squamous cell carcinoma (ESCC) is the predominant histological subtype of esophageal cancer, accounting for approximately 90% of all cases. ESCC has a unique etiology, molecular profile, and clinicopathological features (Rustgi and El-Serag, 2014; Ooki et al., 2023). Many patients are diagnosed at an advanced stage, delaying treatment initiation (Liang et al., 2017). Despite the implementation of early cancer screening strategies and multimodal treatments, the high incidence and low survival rate of ESCC remain urgent issues that need to be addressed (Fong et al., 2020). Therefore, it is important to identify novel molecular markers and develop effective therapeutic strategies.

The development and approval of immune checkpoint (programmed cell death protein 1 [PD-1], programmed cell death-ligand 1 [PD-L1], and cytotoxic T-lymphocyte associated protein 4 [CTLA4]) inhibitors leaded to dramatic changes in the landscape of cancer therapy (Robert, 2020). However, only a small proportion of patients exhibit long-lasting responses, and most patients treated with an immune checkpoint inhibitor, especially with a monotherapy approach, will demonstrate either primary or acquired resistance (Sharma et al., 2017). Multiple mechanisms of resistance have been proposed, among which L-tryptophan (Trp) catabolism was suggested as a critical contributor (Fujiwara et al., 2022).

Trp is an essential amino acid, playing a vital role in cell growth and protein synthesis (Badawy, 2017). Trp generally participants in three main metabolic processes: production of proteins, incorporation into serotonin anabolism, and transformation into kynurenine (Kyn) (Platten et al., 2012). Three enzymes (indoleamine 2,3-dioxygenase [IDO] 1, IDO2, and tryptophan 2,3-dioxygenase [TDO]) catalyze the rate-limiting step of the Kyn pathway. In particular, IDO1 is overexpressed and constitutes a poor prognostic marker in many tumours including endometrial cancer (Ino et al., 2006), laryngeal squamous cell carcinoma (Ye et al., 2013), melanomas (Speeckaert et al., 2012), gastric cancer (Li et al., 2019), hepatocarcinoma (Pan et al., 2008), and cervical cancer (Inaba et al., 2010). As for esophageal cancer, IDO1 was shown to be associated with immune tolerance and poor prognosis in patients with surgically resected tumours (Kiyozumi et al., 2019a). Zhou et al. (2020) revealed that IDO1 and PD-L1 expression and CD8 density increased significantly after neoadjuvant chemoradiation therapy in ESCC, and could serve as prognostic biomarkers for survival. IDO1 promoter hypomethylation was found to regulate its mRNA upregulation in esophageal cancer (Kiyozumi et al., 2019b). Mechanically, IDO1 facilitated esophageal carcinoma progression by driving the direct binding of NF-κB and CXCL10 (Yao et al., 2023). Nonetheless, the link between IDO1 and ESCC has not yet been fully elucidated, and further research on its role in the tumor microenvironment (TME) is needed. Therefore, this study aimed to investigate the expression pattern of IDO1 in TME and its impact on prognosis and therapeutic response of patients with ESCC based on publicly available datasets and experimental validation in ESSC samples from our clinical center.

Materials and methods

TCGA ESCC dataset and ESCC tissue samples

The RNA sequencing data for 95 newly diagnosed ESCC patients from the TCGA database (https://cancergenome.nih.gov/) were downloaded from the UCSC Xena platform (https://xenabrowser.net/datapages/). Tumour samples were collected before chemotherapy, targeted therapy, or radiotherapy. Clinicopathologic characteristics, including age, sex, tumour grade, TNM stage, overall survival (OS) time, and survival status, were obtained (summarized in Supplementary Table S1). The TCGA ESCC dataset was designated as the discovery cohort.

Formalin-fixed paraffin-embedded (FFPE) tissue samples were collected from 77 patients with ESCC after surgical resection at the First Medical Center of the Chinese PLA General Hospital between 18 July 2010, and 27 May 2011. These patients did not undergo chemotherapy, targeted therapy, or radiotherapy before surgical resection. Patients' clinicopathologic characteristics were summarized in Supplementary Table S1. This group of patients was designated as the validation cohort. This study was approved by the Ethics Committee of the Chinese PLA General Hospital (No. S2019-228-02). All experimental procedures were performed in accordance with the principles of the Declaration of Helsinki.

Survival analysis

A total of 78 immunomodulators was retrieved from a published study (Thorsson et al., 2018). These immunomudulators were classified into seven categories: antigen presentation, cell adhesion, co-inhibitors, co-stimulators, ligands, receptors, and others (summarized in Supplementary Table S2). The expression of these immunomodulators was extracted from the mRNA matrix of TCGA ESCC, and integrated with their corresponding survival information. Univariate Cox regression analysis was performed to identify immunomodulators with prognostic value utilizing the "survival" package of R software (version 4.1.2).

The prognostic value of IDO1 in patients with ESCC was evaluated using the Kaplan-Meier method and the log-rank test. The "maxstat" R package was used to calculate the best cutoff point of IDO1 expression for subgrouping patients. The minimum sample size for low- and high-IDO1 subgroups was set as more than 25% of the total count of the entire cohort. A Cox proportional hazards model was used to explore whether IDO1 was an independent determinant of OS in patients with ESCC.

Evaluation of tumour purity

The ESTIMATE algorithm computes scores for the infiltration of stromal and immune cells in tumour tissues based on RNA-seq data (Yoshihara et al., 2013). Stroma, immune, and ESTIMATE scores of TCGA ESCC samples were retrieved from the ESTIMATE website, (https://bioinformatics.mdanderson.org/estimate/).

Estimation of immune cell infiltration

The abundance of eight types of cells (B cells, cancer-associated fibroblasts [CAFs], CD4 T cells, CD8 T cells, endothelial cells, macrophages, natural killer [NK] cells, and uncharacterized [UC] cells) in TME of TCGA ESSC estimated by the EPIC method (Racle et al., 2017) was downloaded from the TIMER2.0 website (http://timer.comp-genomics.org/) (Li et al., 2020).

Analysis of single-cell RNA sequencing data

The IMMUcan scDB database (https://immucanscdb.vital-it.ch/) is an accessible and supportive tool for deciphering tumour-associated single-cell RNA sequencing (scRNA-seq) data, allowing researchers to maximize the use of these data to provide new insights into cancer biology (Camps et al., 2023). scRNA-seq datasets of ESCC were searched within this database. The cell type compositions of each sample were explored by selecting the "UAMP Plot" panel with a given annotation, such as immune cell type assignment. The "Gene X vs. Gene Y expression" panel was used to evaluate gene coexpression at the cell type resolution.

In silico prediction of therapeutic response

The sensitivity of 13 commonly used chemotherapeutic medications (cisplatin, docetaxel, doxorubicin, gefitinib, gemcitabine, nilotinib, paclitaxel, rapamycin, roscovitine, sorafenib, sunitinib, vinblastine, and vorinostat) was evaluated using the "pRRophetic" R package (Geeleher et al., 2014b; Geeleher et al., 2014a). The half-maximal inhibitory concentration (IC50) was an indicator of the response rate of chemotherapeutic drugs. Additionally, we employed the Tumour Immune Dysfunction and Exclusion (TIDE) algorithm (Jiang et al., 2018) (http://tide.dfci.harvard.edu/) to evaluate T-cell dysfunction and exclusion in TCGA ESCC to infer their therapeutic response to immune checkpoint (IC) blockade.

Pathway enrichment

Metascape is a well-recognized and web-based tool for gene annotation (http://metascape.org) (Zhou et al., 2019), which was employed to explore signaling pathways associated with IDO1 in this study. Firstly, differentially expressed genes (DEGs) between the low- and high-IDO1 subgroups were screened using the "limma" R package. The filtering criteria were set as $\log_2$ |fold change| ≥ 1 and adjusted *P*-value <0.05. The DEGs obtained in the first step were then subjected to Metascape for Gene Ontology (GO) and Kyoto Encyclopedia of Genes and Genomes (KEGG) analyses. All genes in the genome were used as the enrichment background. Terms with a *P*-value less than 0.01, a minimum count of three, and an enrichment factor (defined as the ratio between the observed counts and the counts expected by chance) greater than 1.5 were selected. Finally, terms that were significantly enriched in the second step were grouped into clusters based on their membership similarities, and the most statistically significant term within each cluster was selected to represent the cluster.

Immunohistochemistry and digital pathology assessment

Four-micrometer sections were prepared from the FFPE samples. The sections were deparaffinized and rehydrated using graded ethanol. The sections were then subjected to heat-induced epitope retrieval using a citrate buffer solution. Endogenous peroxidase activity was quenched using 0.3% H_2O_2 and non-specific binding was achieved by blocking with 5% goat serum. Next, the sections were incubated with an anti-IDO1 antibody (1:800, CST, #86630) at 4°C overnight, followed by incubation with a

secondary antibody for 30 min at 37°C. IDO1 staining was visualized with 3,3′-diaminobenzidine (DAB, ZSGB-BIO, ZLI-9018) and counterstained with hematoxylin.

An Olympus SLIDEVIEW VS200 research slide scanner was used to capture images of the stained slides, and these pathological images were rendered in a whole-slide image (WSI) format. The quantitative analysis of all WSIs was performed using QuPath (version 0.4.2) (Bankhead et al., 2017), as previously described in Zheng et al. (2022). In brief, the watershed cell detection method was used to identify and segment cells in a slide. Representative specific regions were manually selected to classify tumour cells and stroma cells. A random tree classifier was applied to the training process to produce the best cell classification, which required multiple rounds of optimization. The trained classifier was then applied to all WSIs, and the number of cells and the area of each type were counted for quantification in the tumour parenchyma and stroma. The quality of cell segmentation and classification in the training course is of great importance for QuPath analysis, which was quality controlled by experienced pathologists.

Multiplexed immunofluorescence

Six-color multiplex immunohistochemistry was performed using an OPAL Polaris system (Akoya Biosciences). Four-micrometer sections of FFPE tumours were routinely deparaffinized and hydrated. Heat-induced epitope retrieval in citrate buffer was performed before non-specific binding was blocked. Sections were sequentially stained with each primary antibody (anti-CK [1:1,500, Abcam, ab215838], anti-IDO1 [1:1,000, CST, #86630], anti-CD68 [1:600, Gen Tech, GM081429], anti-CD163 [1:800, Gen Tech, GT207729], and anti-PD-1 [1:200, CST, #43248]), corresponding horseradish peroxidase-conjugated secondary antibody, tyramide signal amplification, and OPAL fluorophore. OPAL 520 (CK), 570 (IDO1), 620 (PD-1), 690 (CD163), and 780 (CD68) dyes were used. The sections were then counterstained with spectral DAPI (Akoya Biosciences). A Vectra Polaris multispectral imaging system (Akoya Biosciences) was used to scan and image the fluorescence signals. The scanned images were annotated and visualized using PhenoChart (version 1.1.0, Akoya Biosciences), and analyzed using inForm software (version 2.5.0, Akoya Biosciences). The tumour parenchyma areas were identified using CK as a marker. CD68 and CD163 were used as pan-macrophage and M2 macrophage markers, respectively.

Statistical analysis

The Mann-Whitney test and Wilcoxon matched-pairs signed rank test were used to compare differences between unpaired and paired two groups, respectively. The correlation between IDO1 expression and other relevant genes or the abundance of putative infiltrating immune cells was evaluated using Spearman correlation analysis. Statistical analysis was performed using R software (version 3.6.3) or GraphPad Prism (version 9.0.0). A P-value <0.05 was considered statistically significant. All statistical tests were two-sided.

Results

Survival analysis of IDO1 in patients with ESCC

We first analyzed the prognostic importance of a panel of immunomodulators in TCGA ESCC dataset (n = 95), which was designated as the discovery cohort. Univariate Cox regression analysis revealed that the mRNA expression levels of CD27, CXCL9, GZMA, HLA-A, HLA-B, HLA-C, HLA-DPB1, IDO1, ITGB2, and SLAMF7 were significantly correlated with OS (all $P < 0.05$; Figure 1A).

Ample evidence suggests that IDO1 is an immunosuppressive molecule in TME, and therapeutic strategies targeting the Trp-IDO1-Kyn signaling using IDO1 inhibitors are currently being assessed in clinical trials; therefore, we focused on IDO1 in subsequent analyses. To further evaluate the prognostic value of IDO1, Kaplan-Meier survival analysis was used to examine the survival differences in ESCC patients with varying IDO1 expression. ESCC patients were divided into low- (n = 68) and high-IDO1 (n = 27) subgroups according to the optimal cut-off value of IDO1 expression levels in the Kaplan-Meier survival analysis. ESCC patients with higher IDO1 expression had significantly shorter OS ($P = 0.014$; Figure 1B).

Notably, the mRNA expression level does not always match the protein level; therefore, we detected IDO1 protein in the validation cohort using immunohistochemistry staining, and quantified its expression level in a digitalized manner using QuPath software. Heterogeneous protein expression of IDO1 was observed in different ESCC samples, even in different parts (parenchyma and stroma) within a certain sample (Figure 1C). Poor OS was observed in patients with high total IDO1 protein expression ($P = 0.040$; Figure 1D, left panel) and high stroma IDO1 protein expression ($P < 0.001$; Figure 1D, middle panel). However, no significant difference in OS was observed in patients with different parenchymal IDO1 protein expression ($P = 0.566$; Figure 1D, right panel).

IDO1 is an independent prognostic indicator of OS in patients with ESCC

To further explore the clinical significance of IDO1 in ESCC, univariate Cox regression analysis with IDO1 expression and multiple clinicopathologic characteristics included was performed in the discovery cohort. The results showed that IDO1 mRNA (hazard ratio [HR] = 2.356, 95% confidence interval [CI]: 1.164 to 4.768, $P = 0.017$) and TNM stage (HR = 2.390, 95% CI: 1.165 to 4.903, $P = 0.017$) were significantly associated with OS in the discovery cohort. Multivariate Cox regression analysis showed that IDO1 mRNA (HR = 2.462, 95% CI: 1.188 to 5.099, $P = 0.015$) and TNM stage (HR = 2.221, 95% CI: 1.087 to 4.575, $P = 0.030$) were independent prognostic factors (Table 1). Above findings were confirmed in the validation cohort. Univariate Cox regression analysis showed that total IDO1 protein (HR = 2.484, 95% CI: 1.069 to 5.770, $P = 0.034$), stroma IDO1 protein (HR = 4.881, 95% CI: 1.805 to 13.196, $P = 0.034$), and TNM stage (HR = 3.363, 95% CI: 1.408 to 8.030, $P = 0.006$) were significantly associated with OS in the validation cohort. Multivariate Cox regression analysis showed that stroma IDO1 protein (HR = 3.539, 95% CI: 1.208 to 10.365, $P = 0.021$) and TNM stage (HR = 4.554, 95% CI: 1.723 to 12.041, $P = 0.002$) were independent prognostic factors

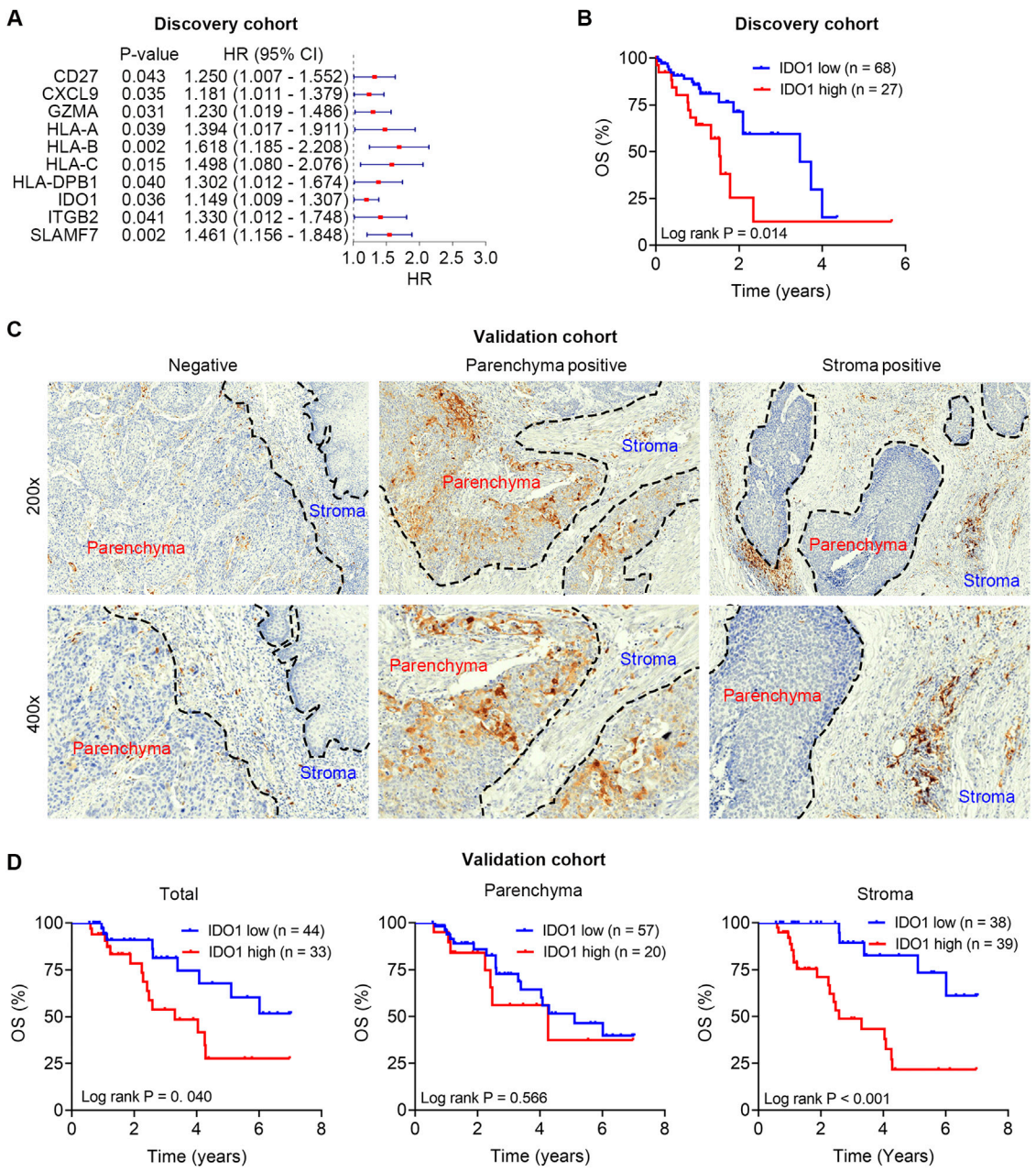

FIGURE 1
Survival analysis of IDO1 in the discovery and validation cohorts. **(A)** Univariate cox regression analysis to screen prognostic immunomodulators in the discovery cohort. **(B)** Kaplan-Meier analysis of ESCC patients' OS in the discovery cohort (n = 95) stratified by IDO1 mRNA expression. **(C)** Representative immunohistochemistry micrographs of IDO1 protein expression in tumour parenchyma and stroma. **(D)** Kaplan-Meier analyses of ESCC patients' OS in the validation cohort (n = 77) stratified by IDO1 protein expression level in total tumour (left panel), tumour parenchyma (middle panel), and tumour stroma (right panel). HR, hazard ratio; CI, confidential interval.

(Table 2). Overall, these data suggest that IDO1 is an independent prognostic indicator of OS in patients with ESCC.

Association between IDO1 expression and immunological characteristics

Next, we explored the role of IDO1 in TME remodeling and immune cell regulation. According to the ESTIMATE algorithm, patients in the high-IDO1 subgroup had higher immune scores, indicating significantly higher infiltration of immune cells into TME ($P < 0.001$; Figure 2A). Correlation analysis also revealed a positive correlation between IDO1 expression and immune score (Rho = 0.67, $P < 0.001$; Figure 2B). Using the EPIC algorithm to calculate tumour-infiltrating immune cells (Figure 2C), we further investigated the difference in specific infiltrating immune cells between the two groups. The high-IDO1 subgroup had a significantly higher number of macrophages and NK cells and

TABLE 1 Univariate and multivariate regression analysis of IDO1 mRNA expression in the discovery cohort.

Variables	Univariate regression		Multivariate regression	
	HR (95% CI)	*P*-value	HR (95% CI)	*P*-value
Age (<60 vs. ≥60)	1.710 (0.806–3.629)	0.162		
Gender (Female vs. Male)	3.866 (0.911–10.713)	0.062		
Grade (G1 + G2 vs. G3)	0.718 (0.271–1.903)	0.505		
TNM stage (I + II vs. III + IV)	2.390 (1.165–4.903)	**0.017**	2.221 (1.078–4.575)	**0.030**
IDO1 mRNA (Low vs. High)	2.356 (1.164–4.768)	**0.017**	2.462 (1.188–5.099)	**0.015**

HR, hazard ratio; CI, confidence interval; *P*-value bold if <0.05.

TABLE 2 Univariate and multivariate regression analysis of IDO1 protein expression in the validation cohort.

Variables	Univariate regression		Multivariate regression	
	HR (95% CI)	*P*-value	HR (95% CI)	*P*-value
Age (<60 vs. ≥ 60)	1.630 (0.727–3.656)	0.236		
Gender (Female vs. Male)	1.572 (0.697–3.542)	0.276		
Grade (G1+G2 vs. G3)	1.557 (0.642–3.774)	0.327		
TNM stage (I + II vs. III + IV)	3.363 (1.408–8.030)	**0.006**	4.554 (1.723–12.041)	**0.002**
Total IDO1 protein (Low vs. High)	2.484 (1.069–5.770)	**0.034**	2.171 (0.789–5.975)	0.133
Parenchyma IDO1 protein (Low vs. High)	1.361 (0.559–3.314)	0.497		
Stroma IDO1 protein (Low vs. High)	4.881 (1.805–13.196)	**0.002**	3.539 (1.208–10.365)	**0.021**

HR, hazard ratio; CI, confidence interval; *P*-value bold if <0.05.

fewer CAFs (Figure 2D). Correlation analysis also revealed positive correlations between IDO1 expression and the number of macrophages and NK cells, and a negative correlation between IDO1 expression and the number of CAFs (Figure 2E). In particular, macrophages were most significantly correlated with IDO1 expression (Rho = 0.43, $P < 0.001$; Figure 2F). Therefore, we further explored the potential role of IDO1 in macrophage polarization. The relationship between IDO1 and marker genes of tumor-associated macrophages (TAMs; CCL5, CD68, and IL10), M1 (IRF5, NOS2, and PTGS2), and M2 (CD163, VSIG4, and MS4A4A) macrophages was analyzed. The Spearman correlation analysis showed that IDO1 was strongly correlated with marker genes of TAMs (CCL5 and CD68) and M2 macrophages (CD163, VSIG4, and MS4A4A) (all Rho > 0.3, all $P < 0.001$; Figures 2G–I). These results suggest that IDO1 may play a role in the regulation of macrophage polarization in ESSC.

In TME, ICs are co-inhibitors effectively engaged by tumour cells, immune cells, and stromal cells that bind to the ligands expressed on the cell surface of $CD8^+$ T cells, triggering inhibitory signaling pathways and leading to the quiescence or exhaustion of $CD8^+$ T cells (Palucka and Coussens, 2016). Patients in the high-IDO1 subgroup had higher expression of a range of ICs, including ADORA2A, BTLA, C10orf54, CD274, CTLA4, HAVCR2, IL10, IL13, KIR2DL1, KIR2DL3, LAG3, MICA, MICB, PDCD1, PDCD1LG2, SLAMF7, and TIGIT (all $P < 0.05$; Figure 3A). Additionally, the correlation analysis revealed that IDO1 had a strong correlation with ADORA2A, BTLA, CD274, CTLA4, HAVCR2, IL13, KIR2DL1, KIR2DL3, LAG3, MICB, PDCD1, PDCD1LG2, SLAMF7 and TIGIT (all Rho > 0.3, all $P < 0.001$; Figure 3B), among which PDCD1, TIGIT, and LAG3 were most positively correlated with IDO1 (Figures 3C–E). These results imply that ESCC with high IDO1 expression possesses a suppressive TME.

Coexpression of IDO1 and PD-1 on macrophages

In the above analyses, we found that IDO1 expression was positively correlated with the number of macrophages in TME (Figure 2F), as well as the expression of PDCD1 within a range of ICs (Figure 3C), prompting us to further investigate the cellular distribution of IDO1 and PDCD1 in macrophages. We performed scRNA-seq data analysis using the IMMUcan scDB database. GSE154763 containing seven pairs of esophageal tumours and adjacent tissues was searched and selected. Five cell clusters (dendritic cells [DCs], macrophages, mast cells, monocytes, and neutrophils) within the GSE154763 were dissected by scRNA-seq analysis (Figure 4A). The cell compositions of ESCC samples and adjacent tissues are shown in Figure 4B. Monocytes and neutrophils were significantly downregulated in ESCC samples compared with those in adjacent tissues (both $P < 0.05$; Figure 4C), whereas no

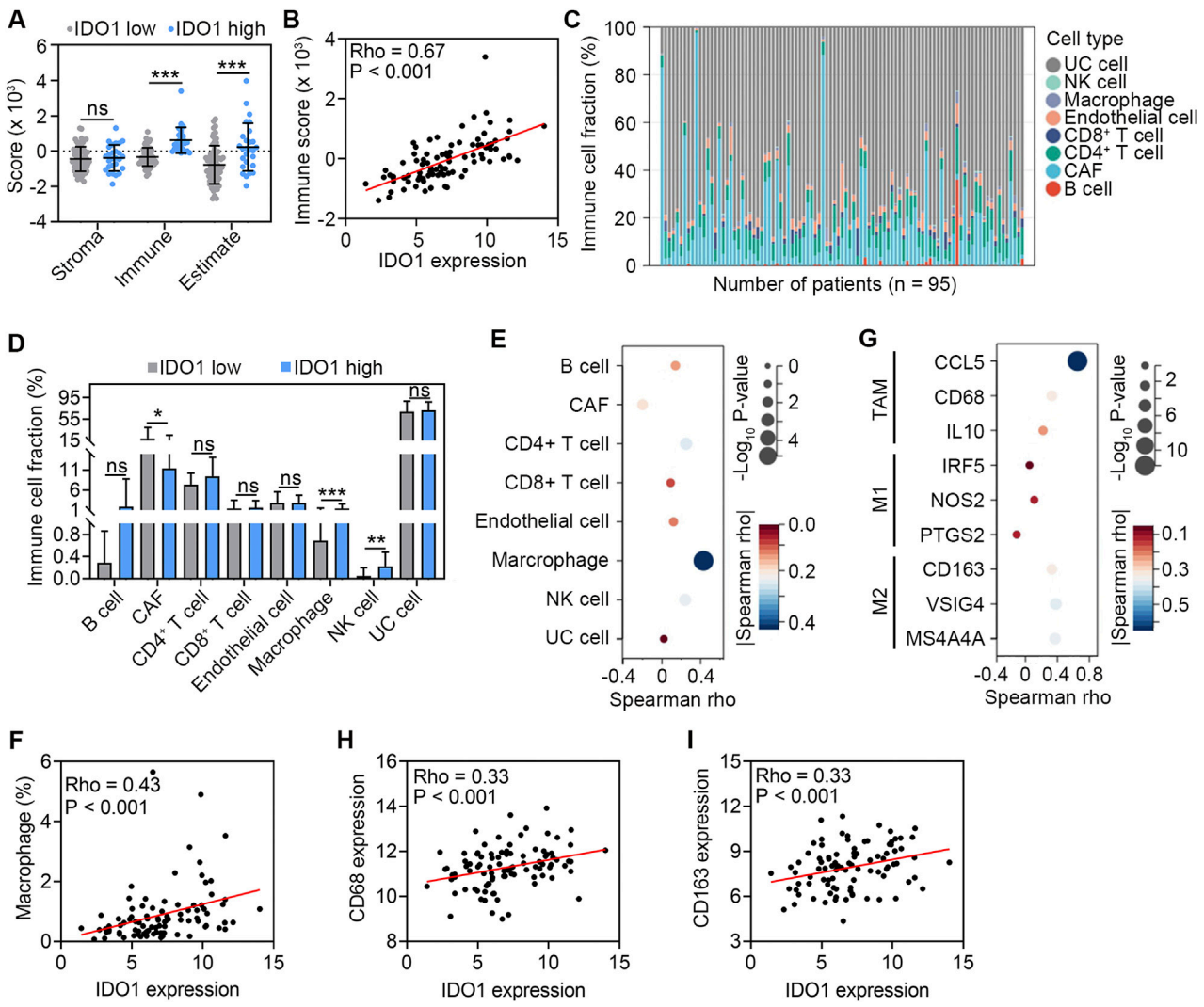

FIGURE 2
Association between IDO1 expression and immune cell abundance in TME. **(A)** Comparison of stroma score, immune score, and estimate score estimated by the ESTIMATE algorithm between ESCC patients with low (n = 68) and high (n = 27) IDO1 expression. **(B)** Scatter plot showing Spearman correlation between IDO1 mRNA expression and immune score. **(C)** Profile of eight types of cells in TME of ESCC samples (n = 95) estimated by the EPIC algorithm. **(D)** Comparison of the abundance of eight types of cells between ESCC patients with low (n = 68) and high (n = 27) IDO1 expression. **(E)** Bubble chart showing Spearman correlation between IDO1 mRNA expression and the abundance of eight types of cells. **(F)** Scatter plot showing Spearman correlation between IDO1 mRNA expression and the abundance of macrophages. **(G)** Bubble chart showing Spearman correlation between mRNA expression levels of IDO1 and marker genes of TAMs (CCL5, CD68, and IL10), M1 (IRF5, NOS2, and PTGS2), and M2 (CD163, VSIG4, and MS4A4A) macrophages. Scatter plot showing Spearman correlation between mRNA expression levels of IDO1 and CD68 **(H)**, IDO1 and CD163 **(I)** CAF, cancer-associated fibroblast; NK, nature killer; UC, uncharacterized cell. Values are means ± SD. Mann-Whitney test **(A, D)**. ns, no significance. *$P < 0.05$; **$P < 0.01$; ***$P < 0.001$.

difference was found in cell fractions of DCs, macrophages, and mast cells (all $P > 0.05$; Figure 4C). Coexpression analysis revealed a highly significant overlap of IDO1 and PDCD1 in DCs ($P < 0.001$; Figure 4D) and macrophages ($P < 0.05$; Figure 4D), but not in monocytes, mast cells, and neutrophils (all $P > 0.05$; Figure 4D). To further validate the results of scRNA-seq analyses, we conducted multiplexed immunofluorescence to analyze IDO1 and PD-1 expression in TME. We observed colocalization of IDO1, PD-1, CD68 (marker of TAMs), and CD163 (marker of M2 macrophages) in the tumour stroma (Figures 4E, F). In aggregate, these data suggest that IDO1 and PD-1 are coexpressed on macrophages in TME of ESSC.

Association between IDO1 expression and therapeutic response

The differences of drug sensitivity between the low- and high-IDO1 subgroups in 13 commonly used chemotherapeutic medications (Figure 5A) were analyzed using the "pRRophetic" R package. The high-IDO1 subgroup showed significantly increased sensitivity to doxorubicin ($P < 0.05$), gefitinib ($P < 0.05$), gemcitabine ($P < 0.01$), roscovitine ($P < 0.001$), and sunitinib ($P < 0.001$) (Figure 5B).

Two stages of T cell dysfunction have been found, and anti-PD-1 treatment can deteriorate early stage dysfunctional T cells; however, late-stage dysfunctional T cells are resistant to IC

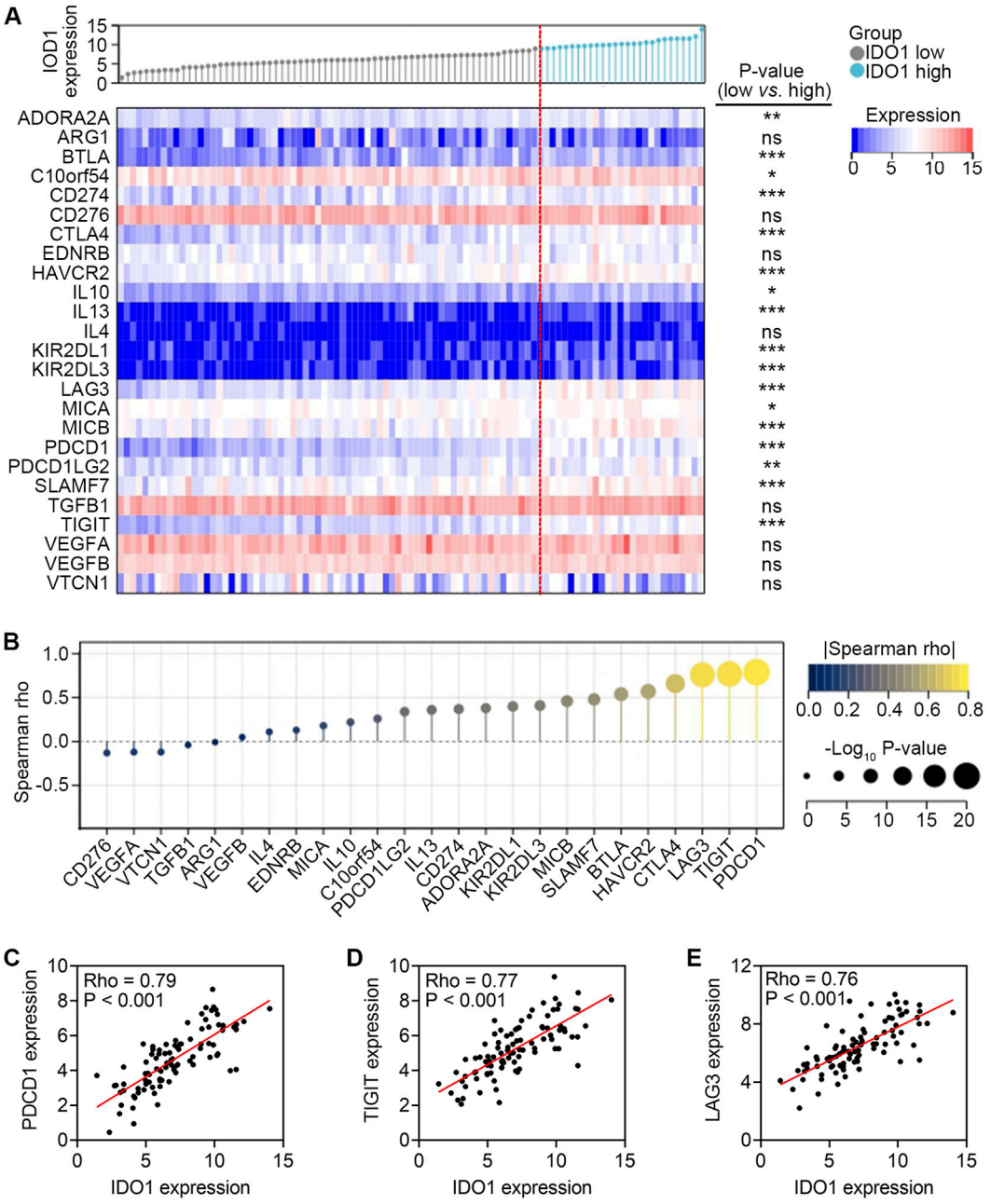

FIGURE 3
Association between mRNA expression levels of IDO1 and IC genes. **(A)** Comparison of mRNA expression levels of IC genes between ESCC patients with low (n = 68) and high (n = 27) IDO1 expression. **(B)** Lollipop chart showing Spearman correlation between mRNA expression levels of IDO1 and IC genes. Scatter plot showing Spearman correlation between mRNA expression levels of IDO1 and PDCD1 **(C)**, IDO1 and TIGIT **(D)**, IDO1 and LAG3 **(E)** Mann-Whitney test **(A)**. ns, no significance. *$P < 0.05$; **$P < 0.01$; ***$P < 0.001$.

blockage reprogramming (Philip et al., 2017). TIDE dysfunction signatures were able to infer dysfunctional T cells in the late stages based on gene expression profiles (Jiang et al., 2018); therefore, we used the TIDE algorithm to estimate T cell dysfunction in patients. Compared with those in the low-IDO1 subgroup, patients in the high-IDO1 subgroup had higher T-cell dysfunction but lower T-cell exclusion scores (both $P < 0.001$; Figure 5C), reflecting the profiles of dysfunctional T cells in the late stages. Collectively, these data indicate that ESSC patients with higher IDO1 expression show increased sensitivity to a range of chemotherapeutic drugs, while are more likely to resist IC inhibitor administration.

Exploring the signaling pathways associated with IDO1

Finally, we explored the signaling pathways associated with IDO1 to elucidate the possible underlying molecular mechanisms

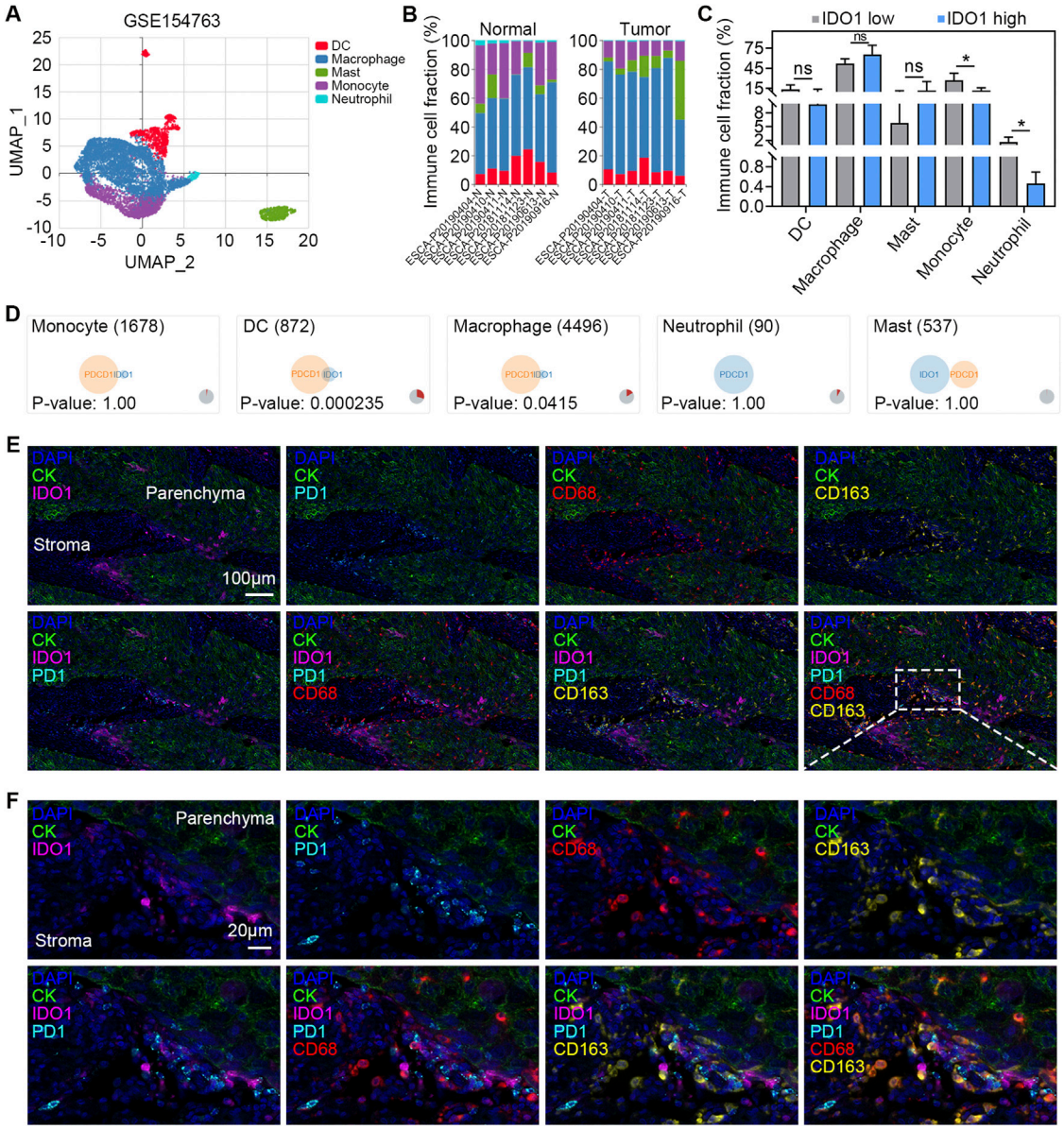

FIGURE 4
Coexpression of IDO1 and PD-1 on macrophages. **(A)** UMAP plot of GSE154763 scRNA-seq dataset. The cells are colored according to their immune annotation. **(B)** Bar plots of the percentage of cells per cell types in tumour (n = 6) and adjacent normal (n = 6) samples. **(C)** Paired comparison of the percentage of cells per cell type in tumour (n = 6) and adjacent normal (n = 6) samples. **(D)** Venn diagram showing the coexpression of IDO1 and PDCD1 in different types of immune cells. Representative multiplexed immunofluorescence micrographs **(E)** and the detail with enlarged scale **(F)** showing expression of IDO1 (pink), PD-1 (cyan), CD68 (red), and CD163 (yellow) in tumour parenchyma and stroma. DAPI (blue) and CK (green) were used for nuclear and tumour parenchyma staining, respectively. Scale bar = 100 μm in **(E)**, and 20 μm in **(F)**. Values are means ± SD. Wilcoxon matched-pairs signed rank test **(C)**. ns, no significance. *$P < 0.05$.

of IDO1 in ESCC. Differential analysis using the "limma" R package revealed a total of 440 DEGs between low- and high-IDO1 subgroups, with 403 genes upregulated and 37 genes downregulated (Figure 6A). The expression profiles of the top 10 dysregulated DEGs are shown in Figure 6B. These DEGs were further subjected to Metascape for signaling pathway exploration. Genes enriched for biological processes in GO analysis were mainly associated with leukocyte activation and innate and adaptive immune responses (top 10 terms shown in Figure 6C). Genes enriched for cellular components in the GO analysis were principally associated with side of membrane, vesicle membrane, and MHC protein complex (top 10 terms shown in Figure 6D). Genes enriched for molecular functions in GO analysis were predominantly associated with immune receptor activity, MHC protein binding, and cytokine receptor activity (top 10 terms shown in Figure 6E). Genes enriched in KEGG analysis were generally associated with antigen processing and presentation, cell adhesion molecules, and cytokine-cytokine receptor interactions (top 10 terms shown in Figure 6F). These enriched terms were further classified into 20 clusters based on their membership similarities (Figure 6G).

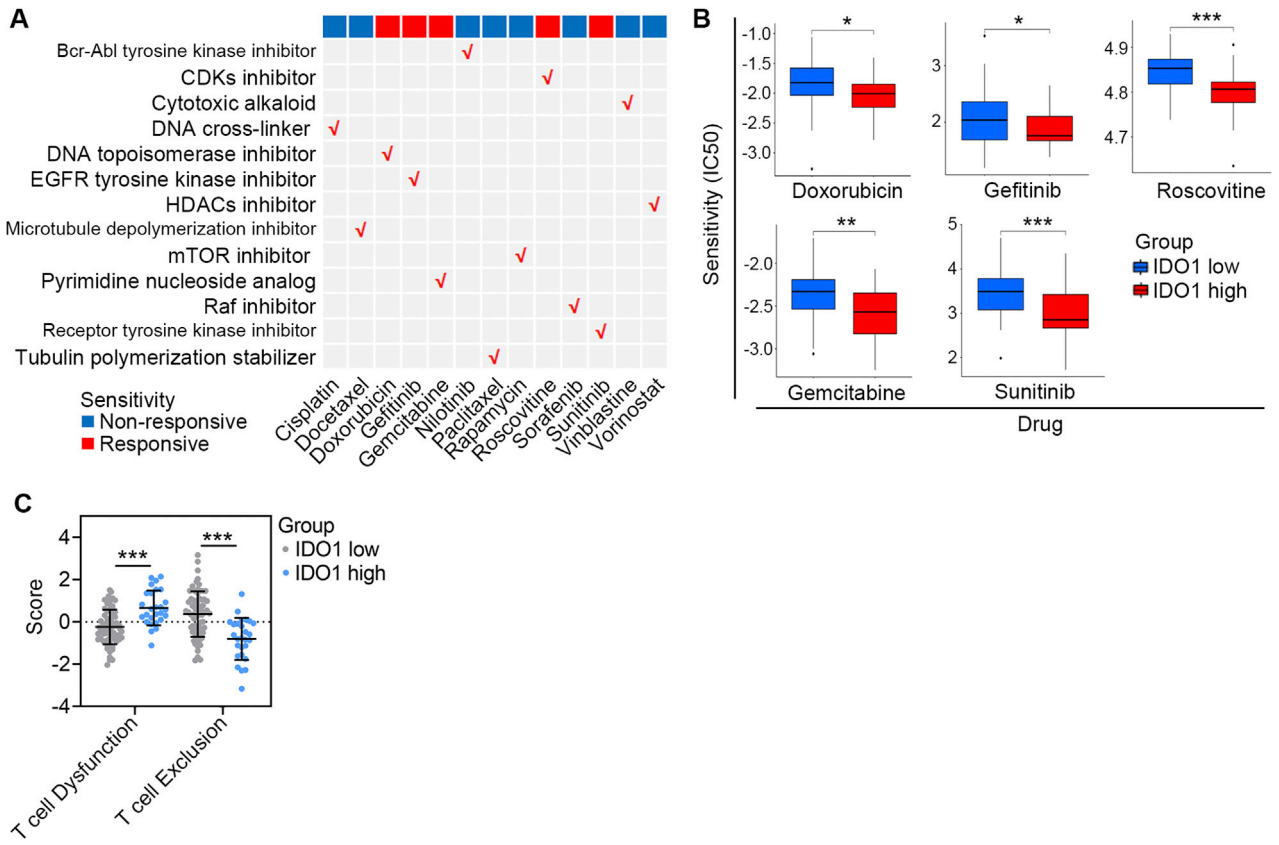

FIGURE 5
Association between IDO1 expression and therapeutic response. **(A)** Summary of the sensitivity of chemotherapeutic drugs with different mechanisms in ESCC patients with disparate IDO1 expression. **(B)** Bar plots of the IC50 in IDO1 low (n = 68) and high (n = 27) ESCC patients. **(C)** Comparison of T cell dysfunction and T cell exclusion scores estimated by the TIDE algorithm between ESCC patients with low (n = 68) and high (n = 27) IDO1 expression. IC50, half maximal inhibitory concentration. Values are means ± SD. Mann-Whitney test **(B, C)**. *$P < 0.05$; **$P < 0.01$; ***$P < 0.001$.

Discussion

In recent years, cancer immunotherapy has emerged as a groundbreaking approach, and the inhibition of IDO1 has been explored as a potential strategy (Charehjoo et al., 2023). Despite initial promise, clinical trials in this area have faced challenges (Peyraud et al., 2022). Our research addresses this issue by shifting the focus toward the role of macrophages in TME as potential therapeutic targets. Based on the analysis of RNA sequencing data from 95 patients with ESCC from TCGA database, our study delved into the prognostic significance of IDO1. Utilizing a range of bioinformatics tools, we not only established the association of IDO1 with poor patient survival but also highlighted its independent prognostic value. We validated the expression of IDO1 in the stroma and parenchyma of tumour samples from our clinical center in a computer-guided digital manner with QuPath software. Moreover, we comprehensively explored TME of ESSC through estimating scores for stromal and immune cells, and assessing the abundance of various immune cell types within TME. Our findings demonstrated a positive correlation between IDO1 expression and macrophages in TME. Furthermore, our scRNA-seq data analysis and multiplexed immunofluorescence revealed a compelling connection between IDO1 and PD-1, particularly coexpressed on TAMs. This observation opens new avenues for potential targets in ESCC immunotherapy. We also explored the sensitivity of patients with high IDO1 expression to chemotherapeutic drugs and their resistance to immune checkpoint blockade, providing valuable insights for future clinical strategies.

TME is a complex and dynamic entity that has been extensively implicated in tumourignesis. It harbors tumour cells that interact with surrounding cells, especially immune cells, to influence tumour growth, metastasis, and response to therapy. Previous studies have demonstrated the immunomodulatory effects of IDO1 on multiple types of immune cells, including tumor-associated DCs, regulatory T cells (Tregs), myeloid-derived suppressor cells (MDSCs), NK cells, and TAMs. In particular, TAMs are the most abundant cell types in solid tumours and usually exhibit an M2-like phenotype that participates in tumour immunosuppression and leads to the immune escape of cancer cells. IDO1 expressing immune cells, especially macrophages, were found to be more abundant in malignant tissues and associated with worse prognosis of many cancer types, such as penile squamous cell carcinoma (Zhou et al., 2020), oral squamous cell carcinoma of advanced stages (Struckmeier et al., 2023), and classical Hodgkin lymphoma (Karihtala et al., 2020). Moreover, increased numbers of $IDO1^+$ TAMs in breast cancer patients upregulated pro-tumourigenic factors associated with resistance to immunosuppressive therapy after anti-PD-1 treatment (Chang et al., 2024). The results in our study were complied with above findings, adding fundamental evidences to the combination of IDO1 inhibition and IC blockage for cancer treatment, though the much-

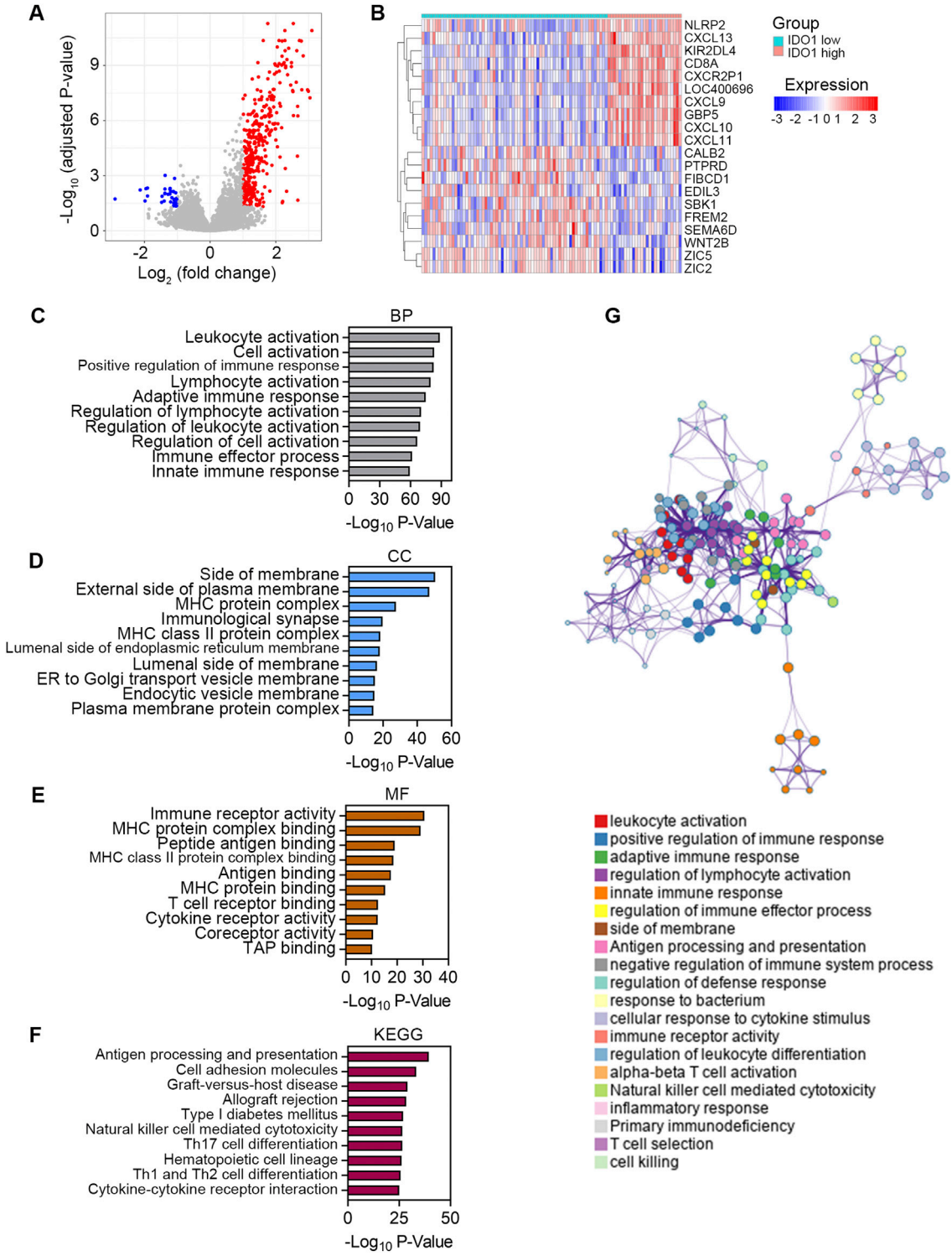

FIGURE 6
Exploring the signaling pathways associated with IDO1. **(A)** Volcano plot showing DEGs between ESCC patients with low (n = 68) and high (n = 27) IDO1 expression. The screening criteria were set as adjusted $P < 0.05$ and $|\log_2 (\text{fold change})| \geq 1$. **(B)** Expression profile of top 10 DEGs. Bar plots showing top 10 significantly enriched terms related to BP **(C)**, CC **(D)**, and MF **(E)** based on GO analysis. **(F)** Bar plot showing top 10 significantly enriched terms based on KEGG analysis. **(G)** Network plot showing relationships between the enriched terms. Nodes represent enriched gene sets that are grouped and annotated by their similarity according to related gene sets. Node size is proportional to the total number of genes within each gene set. Proportion of shared genes between gene sets is represented as the thickness of the connecting line between nodes. BP, Biological Process; CC, Cellular Component; MF, Molecular Function; KEGG, Kyoto Encyclopedia of Genes and Genomes.

anticipated phase III clinical trial (ECHO-301/KEYNOTE-252) of IDO1 inhibitor compound **29** combined with PD-1 inhibitor failed (Long et al., 2019). Future research should focus on comprehensive understanding of the role of IDO1 in TME, especially the immunosuppression caused by IDO1$^+$ TAMs in immunotherapy.

Limitations

This study has several limitations. With the convenience of large-scale datasets, bioinformatics offers valuable insights into cancer research; however, the introduction of big data analytics inevitably produces unique biases and sources of variation, which need to be carefully considered and addressed. Consequently, bioinformatics results may not precisely mirror the effect observed in practical clinical settings (Baykal et al., 2024).

Another limitation arises from the diversity and the relatively small sample size of the study cohorts. The discovery cohort (n = 95) is collected from TCGA database that contains individuals of differing races, while the validation cohort (n = 77) population is recruited from our clinical center consisting solely of East Asians. The discrepancy in population backgrounds and the relatively insufficient participants could result in potential bias.

It is noteworthy that prognosis is influenced by multiple factors, including specific genetic profiles, tumour stages, and treatment modalities. Consequently, survival outcomes may be affected by other potential confounding variables that were not incorporated into the prognostic analysis. In the context of the study's focus on chemotherapy and immunotherapy, the therapeutic response in both the discovery and validation datasets may serve as a more pertinent phenotype than survival. However, it is a fact that the follow-up information of treatment response in the discovery and validation cohorts is incomplete.

Moreover, treatment response was initially assessed using computational approaches. While this approach identifies potential drug targets, it does not guarantee their effectiveness in clinical settings. Experimental validation and clinical trials are necessary to confirm the findings.

Finally, there is few experimental data regarding the role of IDO1 in macrophages. To this end, subsequent experimental exploration is necessary to unveil the function and molecular mechanism of IDO1 in macrophages.

Suggestions for future research directions

In light of the study's limitations, several suggestions can guide future research directions in this critical area. Firstly, future investigations should aim to compose a set of recommended standards and guidelines aimed at promoting reproducibility in bioinformatics, and enhancing translation of bioinformatics findings into medical practice.

Secondly, to improve the generalizability of our findings, future studies should include a larger patient cohorts consisting of individuals with different genetic backgrounds. In addition, more detailed clinicopathological characteristics should be recoded on file.

Lastly, it is important to note that therapeutic response achieved through *in silico* prediction does not guarantee their effectiveness in clinical settings. Furthermore, the role of IDO1 in macrophages remained unveiled. Therefore, experimental explorations and clinical trials should be designed to address above issues.

Conclusion

In conclusion, this research integrated bioinformatics analyses and digital pathology assessment to identify IDO1 as an independent prognostic indicator of OS in patients with ESCC. Moreover, our research revealed a compelling connection between IDO1 and PD-1, particularly coexpressed on TAMs through comprehensive exploration of TME and multiplexed immunofluorescence validation in tumour samples. We also explored the sensitivity of patients with high IDO1 expression to chemotherapeutic drugs and their resistance to IC blockade. Our study contributes to the understanding of the complex interplay of IDO1, PD-1, and macrophages in TME of ESCC. These observations open new avenues for potential targets in ESCC immunotherapy. Further research and clinical trials are needed to explore the role IDO1 in macrophages, and to elaborate the clinical findings of the present study.

Data availability statement

The original contributions presented in the study are included in the article/Supplementary Material, further inquiries can be directed to the corresponding authors.

Ethics statement

The studies involving humans were approved by Ethics Committee of the Chinese PLA General Hospital. The studies were conducted in accordance with the local legislation and institutional requirements. The participants provided their written informed consent to participate in this study.

Author contributions

YP: Formal Analysis, Validation, Writing–original draft. LW: Formal Analysis, Writing–original draft. JY: Formal Analysis, Writing–original draft. QW: Data curation, Writing–original draft. XS: Validation, Writing–original draft. JZ: Conceptualization, Supervision, Writing–original draft. YY: Validation, Writing–original draft. LZ: Data curation, Writing–original draft. JG: Data curation, Writing–original draft. QZ: Writing–review and editing. HZ: Conceptualization, Supervision, Writing–review and editing. FY: Conceptualization, Supervision, Writing–review and editing.

Funding

The authors declare that financial support was received for the research, authorship, and/or publication of this article. This work was supported by National Nature Science Foundation of China

(No. 81972902), and Major Science and Technology Program of Hainan Province (No. ZDKJ202004).

Acknowledgments

We would like to thank Editage (www.editage.cn) for English language editing.

Conflict of interest

The authors declare that the research was conducted in the absence of any commercial or financial relationships that could be construed as a potential conflict of interest.

Publisher's note

All claims expressed in this article are solely those of the authors and do not necessarily represent those of their affiliated organizations, or those of the publisher, the editors and the reviewers. Any product that may be evaluated in this article, or claim that may be made by its manufacturer, is not guaranteed or endorsed by the publisher.

Supplementary material

The Supplementary Material for this article can be found online at: https://www.frontiersin.org/articles/10.3389/fphar.2024.1466779/full#supplementary-material

References

Badawy, A. A. (2017). Kynurenine pathway of tryptophan metabolism: regulatory and functional aspects. *Int. J. Tryptophan Res.* 10, 1178646917691938. doi:10.1177/1178646917691938

Bankhead, P., Loughrey, M. B., Fernández, J. A., Dombrowski, Y., McArt, D. G., Dunne, P. D., et al. (2017). QuPath: open source software for digital pathology image analysis. *Sci. Rep.* 7, 16878. doi:10.1038/s41598-017-17204-5

Baykal, P. I., Łabaj, P. P., Markowetz, F., Schriml, L. M., Stekhoven, D. J., Mangul, S., et al. (2024). Genomic reproducibility in the bioinformatics era. *Genome Biol.* 25, 213. doi:10.1186/s13059-024-03343-2

Camps, J., Noël, F., Liechti, R., Massenet-Regad, L., Rigade, S., Götz, L., et al. (2023). Meta-analysis of human cancer single-cell RNA-seq datasets using the IMMUcan database. *Cancer Res.* 83, 363–373. doi:10.1158/0008-5472.CAN-22-0074

Chang, K., Jiao, Y., Zhang, B., Hou, L., He, X., Wang, D., et al. (2024). MGP(+) and Ido1(+) tumor-associated macrophages facilitate immunoresistance in breast cancer revealed by single-cell RNA sequencing. *Int. Immunopharmacol.* 131, 111818. doi:10.1016/j.intimp.2024.111818

Charehjoo, A., Majidpoor, J., and Mortezaee, K. (2023). Indoleamine 2,3-dioxygenase 1 in circumventing checkpoint inhibitor responses: updated. *Int. Immunopharmacol.* 118, 110032. doi:10.1016/j.intimp.2023.110032

Fong, L. Y., Taccioli, C., Palamarchuk, A., Tagliazucchi, G. M., Jing, R., Smalley, K. J., et al. (2020). Abrogation of esophageal carcinoma development in miR-31 knockout rats. *Proc. Natl. Acad. Sci. U. S. A.* 117, 6075–6085. doi:10.1073/pnas.1920333117

Fujiwara, Y., Kato, S., Nesline, M. K., Conroy, J. M., DePietro, P., Pabla, S., et al. (2022). Indoleamine 2,3-dioxygenase (Ido) inhibitors and cancer immunotherapy. *Cancer Treat. Rev.* 110, 102461. doi:10.1016/j.ctrv.2022.102461

Geeleher, P., Cox, N., and Huang, R. S. (2014a). pRRophetic: an R package for prediction of clinical chemotherapeutic response from tumor gene expression levels. *PLoS One* 9, e107468. doi:10.1371/journal.pone.0107468

Geeleher, P., Cox, N. J., and Huang, R. S. (2014b). Clinical drug response can be predicted using baseline gene expression levels and *in vitro* drug sensitivity in cell lines. *Genome Biol.* 15, R47. doi:10.1186/gb-2014-15-3-r47

Inaba, T., Ino, K., Kajiyama, H., Shibata, K., Yamamoto, E., Kondo, S., et al. (2010). Indoleamine 2,3-dioxygenase expression predicts impaired survival of invasive cervical cancer patients treated with radical hysterectomy. *Gynecol. Oncol.* 117, 423–428. doi:10.1016/j.ygyno.2010.02.028

Ino, K., Yoshida, N., Kajiyama, H., Shibata, K., Yamamoto, E., Kidokoro, K., et al. (2006). Indoleamine 2,3-dioxygenase is a novel prognostic indicator for endometrial cancer. *Br. J. Cancer* 95, 1555–1561. doi:10.1038/sj.bjc.6603477

Jiang, P., Gu, S., Pan, D., Fu, J., Sahu, A., Hu, X., et al. (2018). Signatures of T cell dysfunction and exclusion predict cancer immunotherapy response. *Nat. Med.* 24, 1550–1558. doi:10.1038/s41591-018-0136-1

Karihtala, K., Leivonen, S. K., Brück, O., Karjalainen-Lindsberg, M. L., Mustjoki, S., Pellinen, T., et al. (2020). Prognostic impact of tumor-associated macrophages on survival is checkpoint dependent in classical Hodgkin lymphoma. *Cancers (Basel)* 12, 877. doi:10.3390/cancers12040877

Kiyozumi, Y., Baba, Y., Okadome, K., Yagi, T., Ishimoto, T., Iwatsuki, M., et al. (2019a). Ido1 expression is associated with immune tolerance and poor prognosis in patients with surgically resected esophageal cancer. *Ann. Surg.* 269, 1101–1108. doi:10.1097/SLA.0000000000002754

Kiyozumi, Y., Baba, Y., Okadome, K., Yagi, T., Ogata, Y., Eto, K., et al. (2019b). Indoleamine 2, 3-dioxygenase 1 promoter hypomethylation is associated with poor prognosis in patients with esophageal cancer. *Cancer Sci.* 110, 1863–1871. doi:10.1111/cas.14028

Li, F., Sun, Y., Huang, J., Xu, W., Liu, J., and Yuan, Z. (2019). CD4/CD8 + T cells, DC subsets, Foxp3, and Ido expression are predictive indictors of gastric cancer prognosis. *Cancer Med.* 8, 7330–7344. doi:10.1002/cam4.2596

Li, T., Fu, J., Zeng, Z., Cohen, D., Li, J., Chen, Q., et al. (2020). TIMER2.0 for analysis of tumor-infiltrating immune cells. *Nucleic Acids Res.* 48, W509-W514–w514. doi:10.1093/nar/gkaa407

Liang, H., Fan, J. H., and Qiao, Y. L. (2017). Epidemiology, etiology, and prevention of esophageal squamous cell carcinoma in China. *Cancer Biol. Med.* 14, 33–41. doi:10.20892/j.issn.2095-3941.2016.0093

Long, G. V., Dummer, R., Hamid, O., Gajewski, T. F., Caglevic, C., Dalle, S., et al. (2019). Epacadostat plus pembrolizumab versus placebo plus pembrolizumab in patients with unresectable or metastatic melanoma (ECHO-301/KEYNOTE-252): a phase 3, randomised, double-blind study. *Lancet Oncol.* 20, 1083–1097. doi:10.1016/S1470-2045(19)30274-8

Ooki, A., Osumi, H., Chin, K., Watanabe, M., and Yamaguchi, K. (2023). Potent molecular-targeted therapies for advanced esophageal squamous cell carcinoma. *Ther. Adv. Med. Oncol.* 15, 17588359221138377. doi:10.1177/17588359221138377

Palucka, A. K., and Coussens, L. M. (2016). The basis of oncoimmunology. *Cell* 164, 1233–1247. doi:10.1016/j.cell.2016.01.049

Pan, K., Wang, H., Chen, M. S., Zhang, H. k., Weng, D. s., Zhou, J., et al. (2008). Expression and prognosis role of indoleamine 2,3-dioxygenase in hepatocellular carcinoma. *J. Cancer Res. Clin. Oncol.* 134, 1247–1253. doi:10.1007/s00432-008-0395-1

Peyraud, F., Guegan, J. P., Bodet, D., Cousin, S., Bessede, A., and Italiano, A. (2022). Targeting tryptophan catabolism in cancer immunotherapy era: challenges and perspectives. *Front. Immunol.* 13, 807271. doi:10.3389/fimmu.2022.807271

Philip, M., Fairchild, L., Sun, L., Horste, E. L., Camara, S., Shakiba, M., et al. (2017). Chromatin states define tumour-specific T cell dysfunction and reprogramming. *Nature* 545, 452–456. doi:10.1038/nature22367

Platten, M., Wick, W., and Van den Eynde, B. J. (2012). Tryptophan catabolism in cancer: beyond Ido and tryptophan depletion. *Cancer Res.* 72, 5435–5440. doi:10.1158/0008-5472.CAN-12-0569

Racle, J., de Jonge, K., Baumgaertner, P., Speiser, D. E., and Gfeller, D. (2017). Simultaneous enumeration of cancer and immune cell types from bulk tumor gene expression data. *Elife* 6, e26476. doi:10.7554/eLife.26476

Robert, C. (2020). A decade of immune-checkpoint inhibitors in cancer therapy. *Nat. Commun.* 11, 3801. doi:10.1038/s41467-020-17670-y

Rustgi, A. K., and El-Serag, H. B. (2014). Esophageal carcinoma. *N. Engl. J. Med.* 371, 2499–2509. doi:10.1056/NEJMra1314530

Sharma, P., Hu-Lieskovan, S., Wargo, J. A., and Ribas, A. (2017). Primary, adaptive, and acquired resistance to cancer immunotherapy. *Cell* 168, 707–723. doi:10.1016/j.cell.2017.01.017

Speeckaert, R., Vermaelen, K., van Geel, N., Autier, P., Lambert, J., Haspeslagh, M., et al. (2012). Indoleamine 2,3-dioxygenase, a new prognostic marker in sentinel lymph nodes of melanoma patients. *Eur. J. Cancer* 48, 2004–2011. doi:10.1016/j.ejca.2011.09.007

Struckmeier, A. K., Radermacher, A., Fehrenz, M., Bellin, T., Alansary, D., Wartenberg, P., et al. (2023). Ido1 is highly expressed in macrophages of patients in advanced tumour stages of oral squamous cell carcinoma. *J. Cancer Res. Clin. Oncol.* 149, 3623–3635. doi:10.1007/s00432-022-04277-7

Sung, H., Ferlay, J., Siegel, R. L., Laversanne, M., Soerjomataram, I., Jemal, A., et al. (2021). Global cancer statistics 2020: GLOBOCAN estimates of incidence and mortality worldwide for 36 cancers in 185 countries. *CA Cancer J. Clin.* 71, 209–249. doi:10.3322/caac.21660

Thorsson, V., Gibbs, D. L., Brown, S. D., Wolf, D., Bortone, D. S., Ou Yang, T. H., et al. (2018). The immune landscape of cancer. *Immunity* 48, 812–830.e14. doi:10.1016/j.immuni.2018.03.023

Yao, W., Cui, X., Peng, H., Zhang, Y., Jia, X., Wu, S., et al. (2023). Ido1 facilitates esophageal carcinoma progression by driving the direct binding of NF-κB and CXCL10. *Cell Death Discov.* 9, 403. doi:10.1038/s41420-023-01689-3

Ye, J., Liu, H., Hu, Y., Li, P., and Zhang, G. (2013). Tumoral indoleamine 2,3-dioxygenase expression predicts poor outcome in laryngeal squamous cell carcinoma. *Virchows Arch.* 462, 73–81. doi:10.1007/s00428-012-1340-x

Yoshihara, K., Shahmoradgoli, M., Martínez, E., Vegesna, R., Kim, H., Torres-Garcia, W., et al. (2013). Inferring tumour purity and stromal and immune cell admixture from expression data. *Nat. Commun.* 4, 2612. doi:10.1038/ncomms3612

Zheng, Q., Yang, R., Ni, X., Yang, S., Jiao, P., Wu, J., et al. (2022). Quantitative assessment of tumor-infiltrating lymphocytes using machine learning predicts survival in muscle-invasive bladder cancer. *J. Clin. Med.* 11, 7081. doi:10.3390/jcm11237081

Zhou, Q. H., Han, H., Lu, J. B., Liu, T. Y., Huang, K. B., Deng, C. Z., et al. (2020b). Up-regulation of indoleamine 2,3-dioxygenase 1 (Ido1) expression and catalytic activity is associated with immunosuppression and poor prognosis in penile squamous cell carcinoma patients. *Cancer Commun. (Lond)* 40, 3–15. doi:10.1002/cac2.12001

Zhou, S., Yang, H., Zhang, J., Wang, J., Liang, Z., Liu, S., et al. (2020a). Changes in indoleamine 2,3-dioxygenase 1 expression and CD8+ tumor-infiltrating lymphocytes after neoadjuvant chemoradiation therapy and prognostic significance in esophageal squamous cell carcinoma. *Int. J. Radiat. Oncol. Biol. Phys.* 108, 286–294. doi:10.1016/j.ijrobp.2020.01.020

Zhou, Y., Zhou, B., Pache, L., Chang, M., Khodabakhshi, A. H., Tanaseichuk, O., et al. (2019). Metascape provides a biologist-oriented resource for the analysis of systems-level datasets. *Nat. Commun.* 10, 1523. doi:10.1038/s41467-019-09234-6

frontiers | Frontiers in Pharmacology

TYPE Original Research
PUBLISHED 17 September 2024
DOI 10.3389/fphar.2024.1464145

Check for updates

OPEN ACCESS

EDITED BY
Hailin Tang,
Sun Yat-sen University Cancer Center (SYSUCC), China

REVIEWED BY
Zhipeng Ye,
Guangzhou Medical University, China
Ruo Wang,
Shanghai Jiao Tong University, China

*CORRESPONDENCE
Wei Zhuang,
612032@fjmu.edu.cn
Xiaoping Su,
suhb_007@163.com
Junyi Chen,
chenjunyidoctor@163.com
Weihui Liu,
lwh200591@163.com

†These authors have contributed equally to this work

RECEIVED 13 July 2024
ACCEPTED 19 August 2024
PUBLISHED 17 September 2024

CITATION
He Q, Su Q, Wei C, Zhang P, Liu W, Chen J, Su X and Zhuang W (2024) Extrachromosomal circular DNAs in prostate adenocarcinoma: global characterizations and a novel prediction model.
Front. Pharmacol. 15:1464145.
doi: 10.3389/fphar.2024.1464145

COPYRIGHT
© 2024 He, Su, Wei, Zhang, Liu, Chen, Su and Zhuang. This is an open-access article distributed under the terms of the Creative Commons Attribution License (CC BY). The use, distribution or reproduction in other forums is permitted, provided the original author(s) and the copyright owner(s) are credited and that the original publication in this journal is cited, in accordance with accepted academic practice. No use, distribution or reproduction is permitted which does not comply with these terms.

Extrachromosomal circular DNAs in prostate adenocarcinoma: global characterizations and a novel prediction model

Qingliu He[1†], Qingfu Su[1†], Chengcheng Wei[2†], Pu Zhang[3†], Weihui Liu[1*], Junyi Chen[1*], Xiaoping Su[1,4*] and Wei Zhuang[1*]

[1]Department of Urology, The Second Affiliated Hospital of Fujian Medical University, Quanzhou, China, [2]Department of Urology, The First Affiliated Hospital of Chongqing Medical University, Chongqing, China, [3]Department of Urology, Sichuan Provincial People's Hospital, School of Medicine, University of Electronic Science and Technology of China, Chengdu, China, [4]Department of Nursing, The Second Affiliated Hospital of Fujian Medical University, Quanzhou, China

Background: The role of focal amplifications and extrachromosomal circular DNA (eccDNA) is still uncertain in prostate adenocarcinoma (PRAD). Here, we first mapped the global characterizations of eccDNA and then investigate the characterization of eccDNA-amplified key differentially expressed encoded genes (eKDEGs) in the progression, immune response and immunotherapy of PRAD.

Methods: Circular_seq was used in conjunction with the TCGA-PRAD transcriptome dataset to sequence, annotate, and filter for eccDNA-amplified differentially expressed coding genes (eDEGs) in PRAD and para-cancerous normal prostate tissues. Afterwards, risk models were created and eKDEGs linked to the PRAD prognosis were identified using Cox and Lasso regression analysis. The immune microenvironment of the risk model was quantified using a variety of immunological algorithms, which also identified its characteristics with regard to immunotherapy, immune response, and immune infiltration.

Results: In this research, there was no significant difference in the size, type, and chromosomal distribution of eccDNA in PRAD and para-cancerous normal prostate tissues. However, 4,290 differentially expressed eccDNAs were identified and 1,981 coding genes were amplified. Following that, 499 eDEGs were tested in conjunction with the transcriptome dataset from TCGA-PRAD. By using Cox and Lasso regression techniques, ZNF330 and PITPNM3 were identified as eKDEGs of PRAD, and a new PRAD risk model was conducted based on this. Survival analysis showed that the high-risk group of this model was associated with poor prognosis and validated in external data. Immune infiltration analysis showed that the model risks affected immune cell infiltration in PRAD, not only mediating changes in immune cell function, but also correlating with immunophenotyping. Furthermore, the high-risk group was negatively associated with anti-*CTLA-4*/anti-*PD-1* response and mutational burden. In addition, Tumor Immune Dysfunction and Exclusion analyses showed that high-risk group was more prone to immune escape. Drug sensitivity analyses identified 10 drugs, which were instructive for PRAD treatment.

Conclusion: *ZNF330* and *PITPNM* are the eKDEGs for PRAD, which can be used as potential new prognostic markers. The two-factor combined risk model can

effectively assess the survival and prognosis of PRAD patients, but also can predict the different responses of immunotherapy to PRAD patients, which may provide new ideas for PRAD immunotherapy.

KEYWORDS

prostate adenocarcinoma, extrachromosomal circular DNA, risk model, immune infiltration, immunotherapy

1 Introduction

Prostate adenocarcinoma (PRAD) is the second most common cancer and the fifth cause of cancer deaths in men throughout the world (Sung et al., 2021), with its incidence increasing by 3% per year since 2014 (Siegel et al., 2024). According to statistics, in the United States, PRAD cases will be responsible for 11% of all fatalities and 29% of all male cancer cases by 2024 (Siegel et al., 2024). Despite the availability of several treatment options, including androgen restriction, surgery, radiation, chemotherapy, and endocrine therapy, 20%–30% of cases of PRAD advance to metastatic prostate cancer (mPCa) (Sandhu et al., 2021) which ultimately develops into metastatic prostate cancer that is resistant to denudation (mCRPC) until death. The emerging research in immunotherapy holds great promise for improving the lives of PRAD patients (Rebello et al., 2021). Recent data indicates that the tumour microenvironment (TME) has a major role in determining the prognosis of PRAD (Xu et al., 2022). A better prognosis for patients and enhanced immunological control of PRAD are linked to immune infiltration in the TME (Fridman et al., 2012). Immunotherapies, including immune checkpoint inhibitors (ICIs) and chimeric antigen receptor T-cell therapies, can improve anti-tumour outcomes and overall survival (OS) in patients with advanced PRAD (Abida et al., 2019). Immunotherapy for PRAD has made great progress in recent years. A mendelian randomisation study has provided evidence for a causal relationship between immune cells and PRAD, with important implications for clinical diagnosis and treatment (Ye et al., 2024). In addition, Recent studies have highlighted the potential of PD-1 and PD-L1 inhibitors in treating metastatic castration-resistant prostate cancer (Antonarakis et al., 2020; Philippou et al., 2020). New vaccine strategies have emerged, building on the success of sipuleucel-T (Sutherland et al., 2021). Recent trials have explored vaccines targeting prostate-specific antigens (PSA) (Lopez-Bujanda et al., 2021). Furthermore, advances in cell-based therapies, such as chimeric antigen receptor (CAR) T-cell therapy (Narayan et al., 2022) and tumor-infiltrating lymphocytes (TILs) (Kaur et al., 2022), have been reported. But only a small percentage of mPCa patients respond to immunotherapies (Abida et al., 2019) for the main possible reason that PRAD is an immunocold tumour with defective tumour suppression and poor immune infiltration (Melo et al., 2021). Consequently, it is critical to look for novel biomarkers, targets, and characteristics in order to develop fresh treatment approaches for breaking through the immunotherapeutic obstacles associated with PRAD.

The unique topology and genetic characteristics of extrachromosomal circular DNA (eccDNA), a circular DNA derived from chromosomes that may be chromosome-independent (Hotta and Bassel, 1965), have led to new understandings of cancer surveillance, diagnosis, treatment, and prediction. EccDNA has been implicated in the development and progression of cancer (Ling et al., 2021). For example, Turner KM et al. (Turner et al., 2017) demonstrated that eccDNAs could act as enhancer elements to mediate overexpression of oncogenes and amplify more copies of oncogenes. Andrisani O et al. (Andrisani, 2024; Zou et al., 2024) found that eccDNAs acted as miR-17–92 amplicons in hepatocellular carcinomas (HCCs), which is a risk factor for poor prognosis of patients. In addition, eccDNA is frequently found in a variety of cancers (Chen et al., 2024a), including PRAD.

Increasing evidence has revealed the immunostimulatory activity of eccDNA in tumours, as well as its route and possible therapeutic implications in the immune response (Wang et al., 2021). For example, Ying Zhang et al. (Zhang et al., 2023) found that risk models generated by eccDNA-amplified encoded genes (eGenes) may affect the prognosis of ovarian cancer patients by modulating some immune cells or immune checkpoints, suggesting that eGenes are important factors in the immune infiltration and immune response of tumour cells.

However, the expression profile of eccDNA in PRAD has received little attention. Although Chen JP et al. (Chen JP et al., 2024) and Luo X et al. (Luo et al., 2023) have identified the potential of eccDNA in the diagnosis of PRAD, it is not clear whether there are specific eccDNAs that are exclusively involved in the immune response to PRAD. Therefore, in this study, in this investigation, we developed a novel risk model based on eKDEGs in PRAD, which was tested by sequencing eccDNA from PRAD and paracancerous normal prostate tissues with the TCGA-PRAD transcriptome dataset. We investigate the predictive features and their involvement in immune infiltration and immune response, with the goal of discovering new biomarkers and therapeutic targets for PRAD immunotherapy.

2 Methods

2.1 Tissue specimen collection

This experimental study was approved by the Ethics Committee of our hospital, and three cases of patients with limited prostate adenocarcinoma were collected from the Department of Urology of our hospital in the year of 2022, under the guidance of the physicians of the Department of Pathology. The PRAD tumour tissue specimens were used as the tumour group, and the paracancerous normal prostate tissue specimens were used as the normal group. Tissue specimens were collected and stored in liquid nitrogen to send for eccDNA sequencing.

2.2 eccDNA sequencing

PRAD and paracancerous normal prostate tissue specimens were subjected to eccDNA sequencing assisted by CloudSeq Biotech Inc. (Shanghai, China) using the circle-seq (Møller et al., 2018) method. Briefly, cell deposits were resuspended in L1 buffer (Plasmid Mini AX; A&A Biotechnology) supplemented with protease K (ThermoFisher) prior to digestion at 50°C overnight. Digested samples were alkali-treated and column-purified by following the instructions of the Plasmid Mini AX kit. Column-purified DNA samples were digested by FastDigest MssI (ThermoFisher) at 37°C for 16 h to remove mitochondrial circular DNA. Then, the samples were incubated with Plasmid-Safe ATP-dependent DNase (Epicentre) at 37°Cfor 1 week to remove the remaining linear DNA. The samples were then supplemented with 30U of DNase and a proportional amount of ATP every 24 h. The treated samples were used as templates for eccDNA amplification by using the RCA DNA Amplification Kit (GenSeq Inc.), followed by purification with the MinElute Reaction Cleanup Kit (Qiagen). Library preparation of purified DNA was performed with the GenSeq® Rapid DNA Lib Prep Kit (GenSeq Inc.). High-throughput sequencing was performed on an Illumina NovaSeq 6000 sequencer in 150 bp double-ended mode to obtain the raw data. Quality control was performed with Q30 as following sequence, low-quality reads were removed firstly by using cutadapt software (v1.9.1), and high-quality clean reads were aligned to the reference genome by using bwa software (v0.7.12). Next, all eccDNAs were identified with circle-map software (v1.1.4) and then raw soft-clipped read counts of the break point were obtained by using SAMtools (v1.9) software. Normalisation and differential analysis were performed by using DESeq2 [7] (v1.38.3) software. Annotation of eccDNA was performed by using bedtools software (v2.27.1) and enrichment analyses were performed by using the eDEGs. eccDNA visualisation was performed by using IGV (v2.4.10) software.

2.3 Analysis of TCGA-PRAD dataset

Transcriptional profiles, clinical features, tumour mutation burden (TMB) and microsatellite instability (MSI) scores of PRAD were downloaded from The Cancer Genome Atlas Program (TCGA, https://portal.gdc.cancer.gov/) database. Validation set data were obtained from cBioPortal-SU2C/PCF (https://www.cbioportal.org/) and GEO70770 (https://www.ncbi.nlm.nih.gov/geo/). Data preprocessing and DEGs analysis were perfoemed by the "limma" and "affay" packages in the R environment. The coding genes amplified by differential eccDNA were taken to intersect with the DEGs of TCGA-PRADt to obtain eccDNA-amplified differentially expressed coding genes (eDEGs). Gene Ontology (GO), Kyoto Encyclopedia of Genes and Genomes (KEGG) functional enrichment analyses were performed using the "clusterProfiler" package. GO enrichment analysis described the potential functions of genes in terms of Molecular Function (MF), Cellular Component (CC) and Biological Process (BP). KEGG analysed the major metabolic and signal transduction pathways in which the genes were involved through pathway annotation. Cox regression analysis and Lasso analysis were used to further identify prognostic genes and construct risk models. Cox regression analysis was performed using the "survival" package and Lasso analysis was performed using the "glmnet" package. Kaplan-Meier (KM) survival analysis plots and risk factor association plots based on the risk models were constructed using the "survival" and "ggplot2" packages. Nomograms were used to visualise the 1-year, 3-year, and 5-year survival predictions of the risk model. Time-dependent ROC curves were used to verify the model accuracy. Gene Set Enrichment Analysis (GSEA) was performed using the "Cluster Profiler," "org. Hs.eg.db", and "enrichplot" package to identify biological processes and enrichment pathways of the key gene. Quantification of the immune microenvironment was performed using XCELL, MCPCOUNTER, CIBERSORT, TIMER, EPIC, and QUANTISEQ algorithms. Identify the characteristics and differences in immune infiltration (performed with the "CIBERSORT" and "reshape2" packages), immune function (performed with the "RColorBrewer" package), and immune subtypes (performed with the "RColorBrewer" package) of risk models based on quantitative immune microenvironment results. ESTIMATE analysis identified specific signals associated with stromal and immune cell infiltration in tumour tissue and predicted the level of infiltrating stromal and immune cells by calculating stromal and immune scores, which were performed with the "utils" package. Gene mutation frequency and mutation burden of the risk models were analyzed with the"maftools" package. Immunophenotype score (IPS) was obtained from The Cancer Immunome Database (TCIA) (Charoentong et al., 2017), which was used to show the response of PRAD patients to immunotherapy. Also, Tumor Immune Dysfunction and Exclusion (TIDE) (Jiang et al., 2018) algorithm was used to assess patients' immunotherapy response. Data for drug sensitivity analysis were obtained from Genomics of Drug Sensitivity in Cancer (GDSC) (Yang et al., 2013) by using the "oncoPredict" package. All the above data visualisations relied on R language implementation.

3 Results

3.1 Genome-wide analysis of eccDNA in prostate adenocarcinoma tumor tissues and parecancerous normal prostate tissues

The eccDNA expression profiles in PRAD tumour tissues and paracancerous normal prostate tissues were obtained by eccDNA sequencing. The results showed that the tumour group contained 76,636 eccDNAsand 11,967 eGenes (Figure 1A; Supplementary Table 1), and 58,781 eccDNAs and 10,694 eGenes were identified in the normal group (Figure 1A; Supplementary Table 2). The eccDNA can encode some or all exons of a gene to affect protein expression, and different eccDNA can encode the same gene. In the normal group, we found 9,460 eGenes derived from 1-5 eccDNAs, 885 eGenes derived from 6–10 eccDNAs, 216 eGenes derived from 11–15 eccDNAs, 74 eGenes derived from 16–20 eccDNAs, 33 eGenes derived from 21–25 eccDNA derivatives, 17 eGenes were derived from 26–30 eccDNA types, 5 eGenes were derived from 31–35 eccDNA types, 3 eGenes were derived from 36–40 eccDNA types. The number of eccDNA types amplifying the CNTNAP2 gene are even more than 45, reaching up to 47

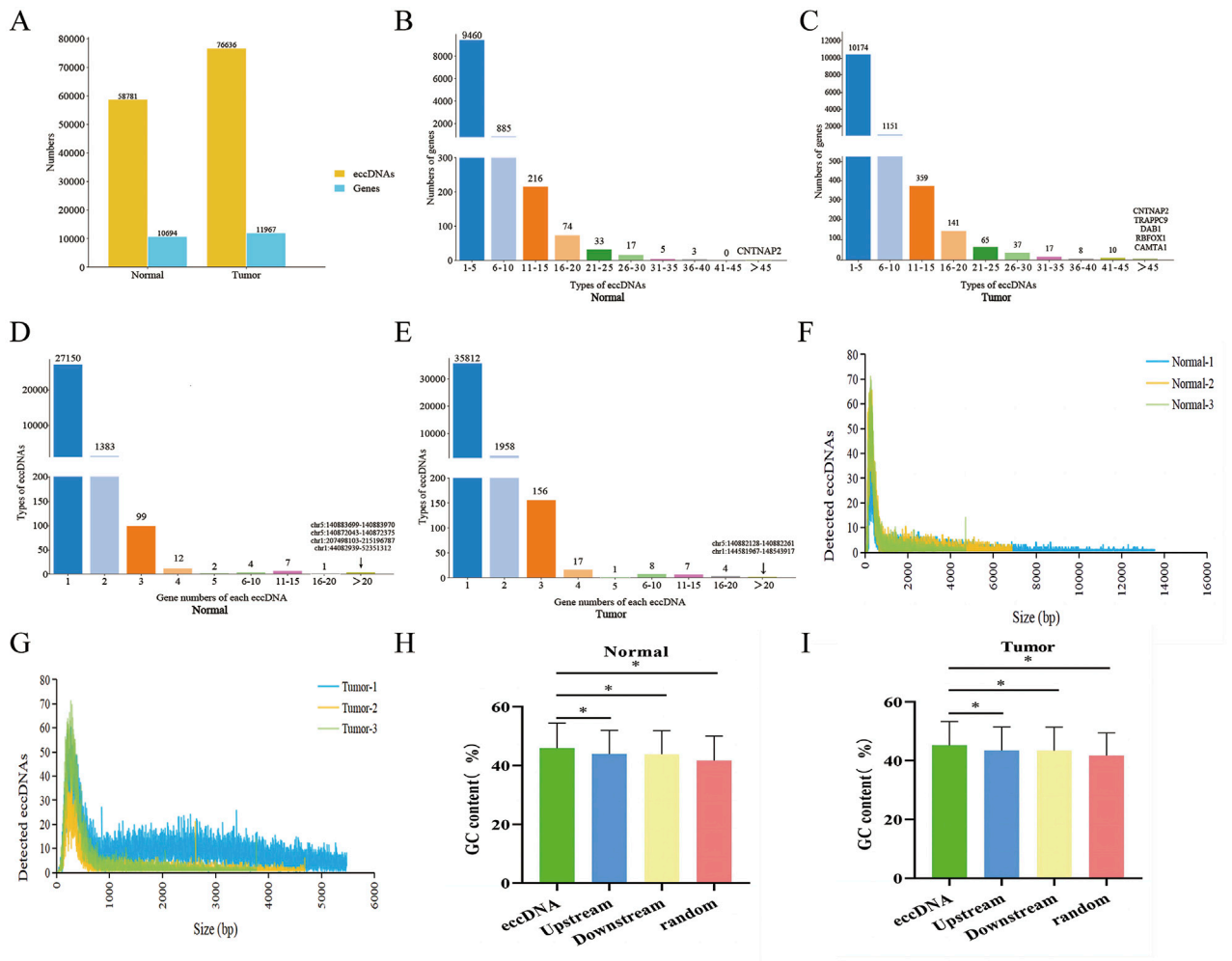

FIGURE 1
Features of eccDNAs detected in PRAD and paracancerous normal prostate tissues. **(A)** Number of eccDNA types and amplified genes from PRAD (tumor) and paracancerous normal prostate (normal) groups. **(B)** Number of genes derived from 1 to 45 and more than 45 different types of eccDNAs in normal groups. **(C)** Number of genes derived from 1 to 45 and more than 45 different types of eccDNAs in tumor groups. **(D)** Number of eccDNA types amplifying 1 to 20 and more than 20 different genes in normal groups. **(E)** Number of eccDNA types amplifying 1 to 20 and more than 20 different genes in tumor groups. **(F)** Size of eccDNA in normal groups. **(G)** Size of eccDNA in tumor groups. **(H–I)** GC contents compared to the genomic average in eccDNA, upstream, downstream and random groups from the genomic locus and regions. H, normal groups. I, tumor groups.

(Figure 1B; Supplementary Table 3). In the PRAD tumour group, 10,174 eGenes were detected to be derived from 1-5 eccDNA types, 1,151 eGenes were derived from 6–10 eccDNA types, 359 eGenes were derived from 11–15 eccDNA types, 141 eGenes were derived from 16–20 eccDNA types, 65 eGenes were derived from 21–25 eccDNAs, 37 eGenes were derived from 26–30 eccDNAs, 17 eGenes were derived from 31–35 eccDNAs, 8 eGenes were derived from 36–40 eccDNAs, 10 eGenes were derived from 40–45 eccDNAs, and five eGenes were derived from more than 45 eccDNA types, namely CNTNAP2, TRAPPC9, DAB1, RBFOX1 and CAMTA1 (Figure 1C; Supplementary Table 4).

At the same time, multiple coding genes could be amplified from the same eccDNA. In the normal group, there were 27,150 eccDNAs amplified 1 eGene, 1,983 eccDNAs amplified 2 eGenes, 99 eccDNAs amplified 3 eGenes, 12 eccDNAs amplified 4 eGenes, 2 eccDNAs amplified 5 eGenes, and 4 eccDNAs amplified 6–10 eGenes, 7 eccDNAs amplified 11–15 eGenes, 1 eccDNA amplified 16–20 eGenes, and 4 eccDNAs amplified more than 20 eGenes (Figure 1D; Supplementary Table 5). In the PRAD tumour group, there were 35,812 eccDNAs amplified 1 eGene, 1,958 eccDNAs amplified 2 eGenes, 156 eccDNAs amplified 3 eGenes, 17 eccDNAs amplified 4 eGenes, 1 eccDNA amplified 5 eGenes, and 8 eccDNAs amplified 6 to 10 eGenes, 7 eccDNAs amplified 11–15 eGenes, 4 eccDNAs amplified 16–20 eGenes, and 2 eccDNAs amplified more than 20 eGenes (Figure 1E; Supplementary Table 5).

In addition, we found that the size distribution of eccDNA in the normal group ranged from 10 bp to 14,000 kb (Figure 1F), and that in the tumour group ranged from 10 to 6,000 bp (Figure 1G). Both groups had an emergent peak at 300 bp (Supplementary Figures S1A–C), and there was no significant difference in the size distribution of eccDNA between the tumour and normal groups (Supplementary Figure S1D). The GC content enrichment of eccDNA in normal and tumour tissue were both significantly higher than other genomic regions (Figures 1H, I).

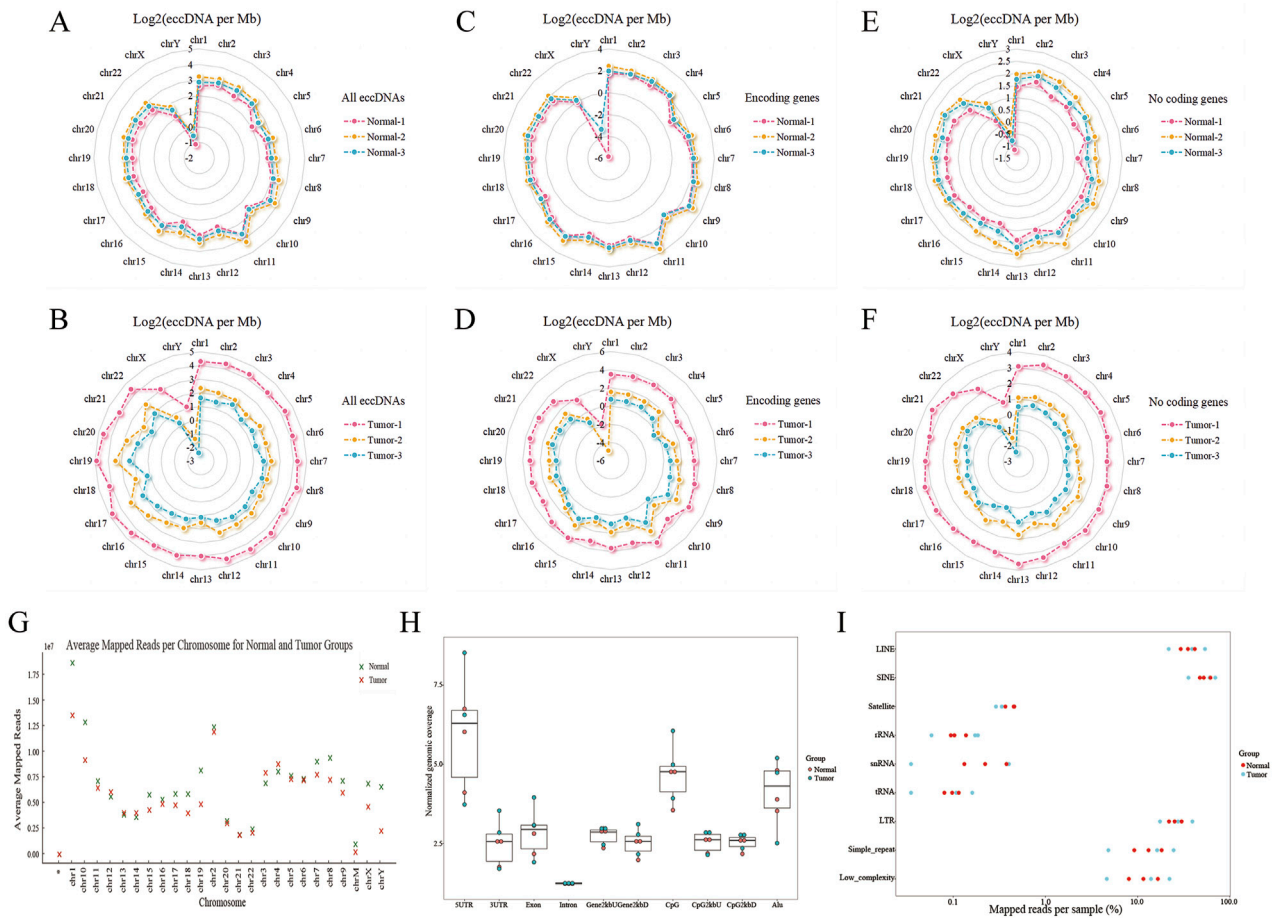

FIGURE 2
Characterization of the chromosomal and genomic distribution of eccDNAs in tumor and normal groups. **(A–F)** The radar plots showing chromosomal genome distribution of all eccDNAs, eccDNAs with and without encoding genes. A, all eccDNAs in normal group. B, all eccDNAs in tumor group. C, eccDNA with encoding genes in normal group. D, eccDNAs with encoding genes in tumor group. E, eccDNA without encoding genes in normal groups. F, eccDNAs without encoding genes in tumor groups. **(G)** EccDNA frequency counted with average mapped reads per Mb of all chromosomes in normal and tumor groups. **(H)** Genomic distributions of eccDNAs in normal and tumor groups. CpG2kbD, 2 kb downstream of CpG islands; CpG2kbU, 2 kb upstream of CpG islands; Gene2kbD, 2 kb downstream of genes; Gene2kbU, 2 kb upstream of genes. **(I)** Repetitive regions from total mapped reads for eccDNAs derived from each sample.

3.2 Genomic distribution of eccDNA on different chromosomes

We further analyzed the genomic distribution of eccDNA on different chromosomes, including intact eccDNA (Figures 2A, B), eccDNA amplifying coding genes (Figures 2C, D), and eccDNA with unamplifying coding genes (Figures 2E, F). The results show that gene-rich chromosome contributed to a higher average frequency of eccDNAs per Mb than other chromosomes, such as chromosome 1, while gene-poor chromosome contributed to a lower average frequency of eccDNAs per Mb, such as chromosome Y. It suggests that regions with gene-rich are more preferentially producing eccDNA. eccDNA distribution on chromosomes between the normal group and PRAD tumour group was not significant differentiation (Figure 2G).

Finally, we explored the possible origins of eccDNAs by mapping the eccDNAs to different genomic elements (Figure 2H) and repetitive elements (Figure 2I). Notably, eccDNA was more significantly enriched in both 5′ UTR genomic region and repetitive elements, such as long interspersed elements (LINEs) and short interspersed elements (SINE), suggesting that these regions are more preferentially producing eccDNA in PRAD.

3.3 Differential expression of eccDNA in tumour and normal tissues

Based on the eccDNA sequencing results, a total of 4,290 differentially expressed eccDNA were screened in PRAD tissues compared with normal tissues (Figure 3A; Supplementary Tables 6, 7). Among them, 1,667 eccDNAs were higher expressed in the tumour tissues, and these eccDNAs amplified 798 eGenes. 2,623 eccDNAs were lowly expressed and amplified 1,183 eGenes ($|FC(\text{fold change})| \geq 2$, $P < 0.05$) (Supplementary Figures S1E, F). The transcriptome data of PRAD and normal samples were

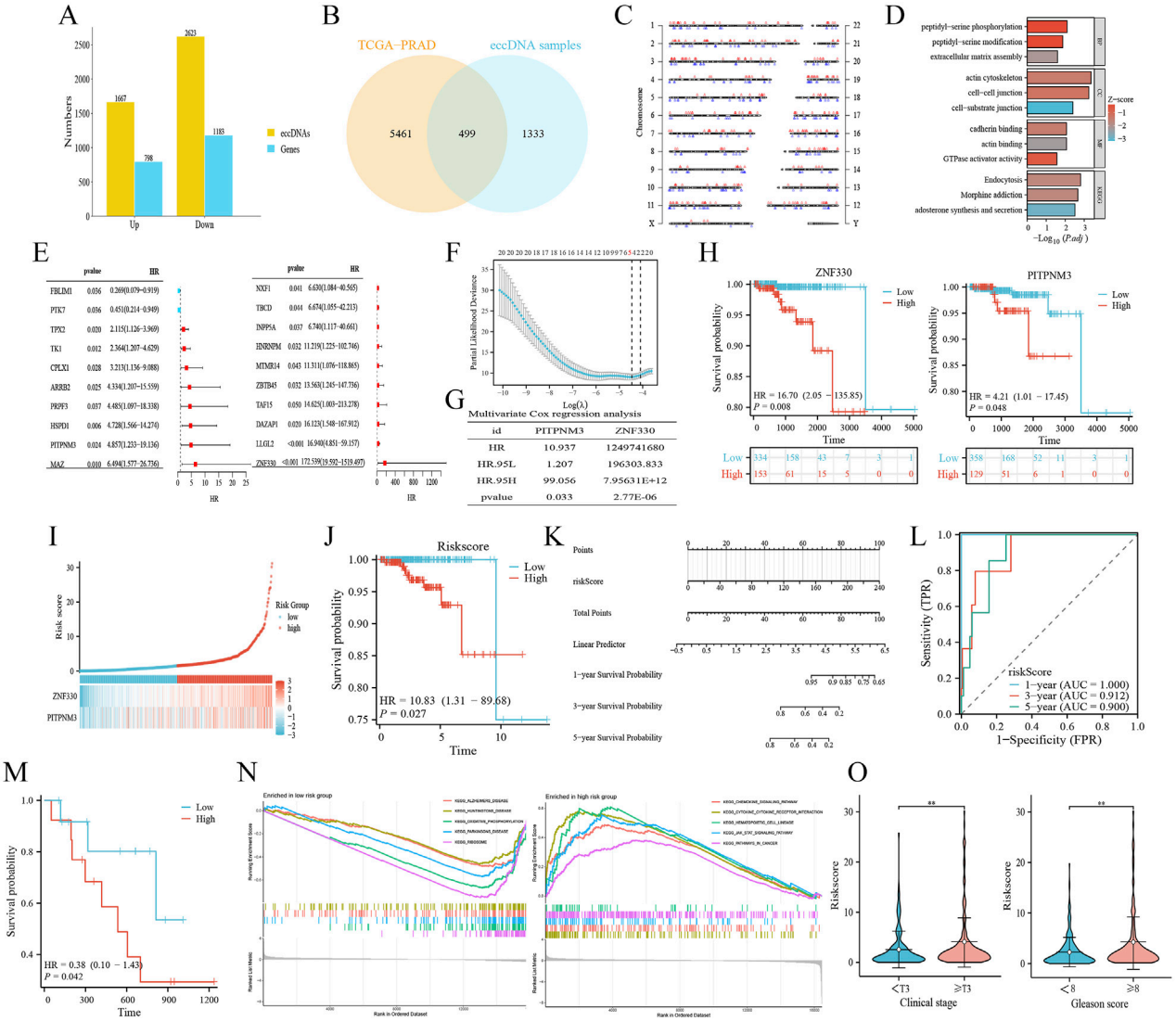

FIGURE 3
Construction of a novel PRAD risk prediction model based on differentially expressed genes amplified by eccDNA. **(A)** Number of differentially expressed eccDNAs and amplified coding genes obtained based on Circle-Seq results. **(B)** Differential eccDNA amplified coding genes and TCGA-PRAD differentially expressed genes were taken to intersect to obtain 499 eccDNA-associated differentially expressed genes (eDEGs). **(C)** Distribution of the 499 eDEGs on the chromosomes. Red, high expression; blue, low expression. **(D)** eDEGs were analyzed for functional enrichment. BP, Biological Process; CC, Cellular Component; MF, Molecular Function; KEGG, Kyoto Encyclopedia of Genes and Genomes. **(E–G)** eDEGs were sequentially subjected to different analysis. E, univariate Cox regression analysis; F, Lasso analysis; G, multivariate Cox regression analysis. **(H)** Survival analysis of ZNF330, PITPNM3. **(I)** Construction of the novel prostate risk model based on ZNF330, PITPNM3 and drawing risk factor plots. **(J)** Survival analysis of the risk model. **(K)** Prognostic nomogram based on risk score. **(L)** Time-dependent ROC curves demonstrated the predictive performance of nomogram. **(M)** Survival analysis of the validation group cBioPortal-SU2C/PCF. **(N)** GSEA functional enrichment analysis of the risk model. **(O)** The clinical correlation analysis between risk model and risk factors of PRAD.

obtained from the TCGA database, and 5,960 DEGs were obtained by screening (Supplementary Figure S1G). The coding genes amplified by differential eccDNA and the DEGs of TCGA-PRAD were taken to be intersected (Figure 3B), and 499 eDEGs were obtained. Further analysis of the distribution of eDEGs on chromosomes (Figure 3C) showed that eDEGs were enriched on chromosomes 1 to 22 without appear on the Y chromosome. Functional enrichment analysis of eDEGs (Figure 3D) showed that their roles were mainly focused on post-translational modification, signal transduction, and cell intercellular communication pathways.

To further explore the eKDEGs of PRAD, this study combined the TCGA-PRAD transcriptome dataset and further performed one-way Cox regression analyses (Figure 3E), LASSO analyses (Figure 3F), and multifactorial Cox regression analyses (Figure 3G) on the eDEGs. ZNF330 and PITPNM3 were finally identified as eKDEGs and independent risk factors for PRAD. ZNF330 was highly expressed and PITPNM3 was lowly expressed in PRAD (Supplementary Figure S1H), which corresponded to eccDNA sources of ZNF330$^{circle142141735-142142329}$, PITPNM3$^{circle6458635-6459156}$. In addition, the differential expression was validated in the GSE70770 dataset set (Supplementary Figure S1I) with consistent results.

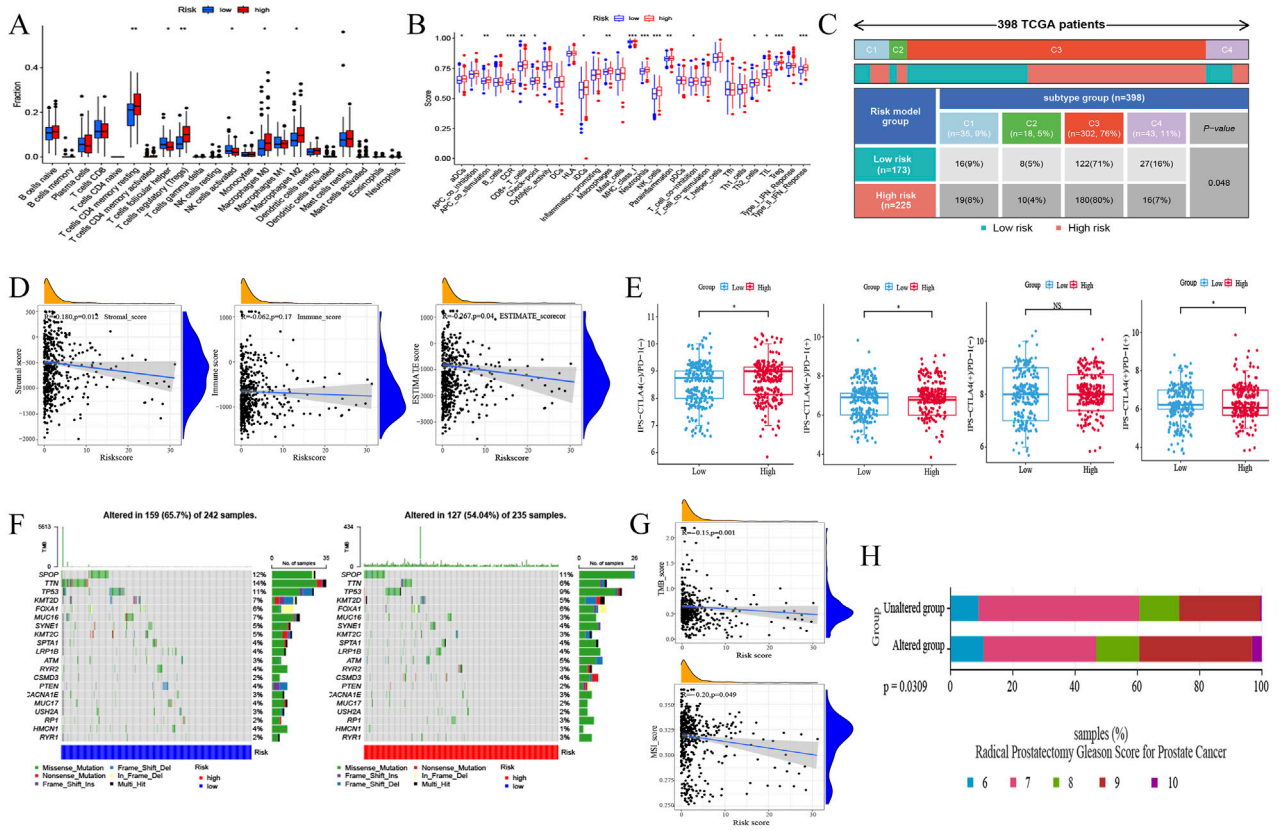

FIGURE 4
The immune landscape and mutation of risk model. **(A)** Immune infiltration analysis of risk model. **(B)** Immune function analysis of risk model. **(C)** Immunophenotyping analysis of risk model. C1, wound-healing phenotype; C2, IFN-γ dominant phenotype; C3, inflammatory phenotype; C4, lymphocyte-depleted phenotype. **(D)** Correlation of risk model with stromal score, immune score and estimate score. **(E)** Correlation of risk model and IPS score. **(F)** Waterfall plot showing the most frequently mutated genes in the risk model. **(G)** Mutation analysis of risk model. TMB, tumor mutation burden; MSI, microsatellite instability. **(H)** Correlation analysis of mutations and Gleason score ratio in PRAD under radical prostatectomy.

3.4 Analysis of critical eccDNA ZNF330$^{circle142141735-142142329}$ and PITPNM3$^{circle6458635-6459156}$ at the transcriptome level

Survival analysis (Figure 3H) showed that PRAD patients with high expression of ZNF330, PITPNM3 had lower overall survival (OS), which suggested that ZNF330, PITPNM3 may be a risk factor for poor prognosis. A novel PRAD risk model was constructed by basing on these two genes, and it was found that the risk score of patients increased with higher expression of ZNF330 and PITPNM3 (Figure 3I). Patients were classified into high and low risk groups based on the risk scores, and the higher risk group had lower OS (Figure 3J), which may lead to poor prognosis. Nomograms were plotted to predict patient survival based on risk scores (Figure 3K), and the 1-year, 3-year and 5-year survival rates of patients gradually decreased with increasing risk scores. The area under the curve (AUC) of the time-dependent ROC at 1-year, 3-year and 5- years were 1.000, 0.912, and 0.900 respectively (Figure 3L), suggesting that the risk model had good predictive performance. cBioPortal-SU2C/PCF data set validated the model, and survival analysis still showed that the high-risk group was associated with poor prognosis (Figure 3M). GSEA analysis (Figure 3N) showed that the high-risk group was significantly enriched in the cytokine signalling pathway (KEGG_CYTOKINE_CYTOKINE_RECEPTOR_INTERACTION, KEGG_HEMATOPOIETIC_CELL_LINEAGE) and cancer-related pathways (KEGG_JAK_STAT_SIGNALING_PATHWAY). Meanwhile, clinical correlation analysis (Figure 3O) showed that high risk scores were positively correlated with later clinical T stage and higher Gleason scores, suggesting that PRAD in the high-risk group were more malignant. KEGG_HEMATOPOIETIC_CELL_LINEAGE) and cancer-related pathways (KEGG_JAK_STAT_SIGNALING_PATHWAY). Meanwhile, clinical correlation analysis (Figure 3O) showed that high risk scores were positively correlated with later clinical T stage and higher Gleason scores, suggesting that PRAD in the high-risk group were more malignant.

3.5 Risk model can reshape PRAD immune microenvironment

Quantitative analysis of the immune microenvironment was performed on the PRAD risk model based on multiple immunological algorithms. Different immune infiltration patterns were observed in patients with the high and low-risk groups. The

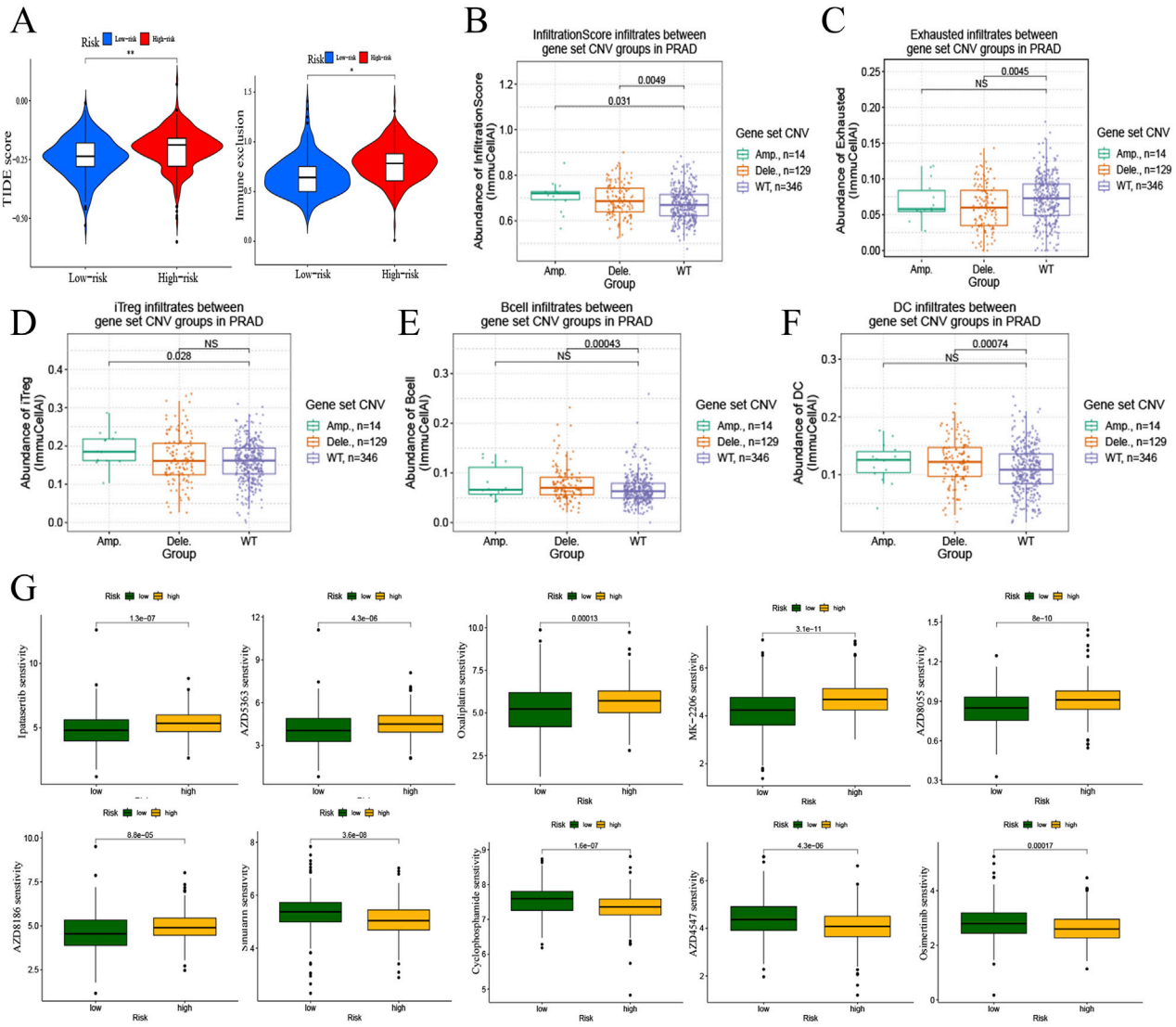

FIGURE 5
Immunotherapy and drug sensitivity to PRAD of risk model. **(A)** Correlation of risk model with TIDE score and immune exclusion. **(B–F)** Correlation analysis of mutations and immune infiltration in PRAD with gene set CNV. B, infiltrationscore infiltrates. C, exhausted infiltrates. D, iTreg infiltrates. E, B cell infiltrates. F, DC cell infiltrates. **(G)** Correlation of risk model and drug sensitivity to PRAD.

immune infiltration analysis (Figure 4A) showed that the immune microenvironment in the high-risk group had increased levels of T cells CD4 memory resting, Macrophages M0, Macrophages M2 and Tregs, and decreased levels of T cells follicular helper and NK cells activated. Meanwhile, the infiltration abundance of some immune cells correlated with prognosis (B cells naive and Tregs infiltration were associated with poor prognosis, and Macrophages M1 and M2 infiltration were associated with better prognosis) (Supplementary Figure S2A). Single gene immune infiltration analysis of ZNF330 and PITPNM3 (Supplementary Figures S2B, C) also revealed multiple immune cell content changes. Interestingly, differential analysis of immune cell function showed that the majority of immune cells were functionally active in the high-risk group (Figure 4B), and altered immune function was associated with patient prognosis (DCs functionally active was associated with a poorer prognosis, and APC_co_inhibition, Mast_cells and Tfh functionally active were associated with a better prognosis) (Supplementary Figure S2D). In addition, there were differences of immune subtypes distribution in the risk model (Figure 4C). ESTIMATE analysis found a negative correlation between the risk model and stromal score, immune score and estimated scores (Figure 4D), suggesting that tumour purity was higher in the high-risk group. IPS scores were calculated to predict response of PRAD patients to two ICIs, anti-CTLA-4 and anti-PD-1 (Figure 4E). We found a positive correlation between the high-risk group andips-CTLA4 (−)/PD1 (−), while a negative correlation was existed between the high-risk group and ips-CTLA4 (−)/PD1 (+) and ips-CTLA4 (+)/PD1 (+) in, indicating that the PRAD model risk can influence the immunotherapy response and the high-risk group of PRAD patients had poor responses to ICIs. These results suggested that tumour immunity may play a key role in PRAD.

3.6 Correlation analysis of mutation with immunotherapy response in risk models

TMB and MSI are molecular markers for determining the suitability of immunotherapy for tumour patients, which also suggest genomic instability. In the risk model, we observed that the mutation rate was lower in the high-risk group (Figure 4F), and the same five most mutated genes in two risk groups were SPOP, TTN, TP53, KMT2D, and FOXA1. What's more, the TMB and MSI scores were negatively correlated with the risk scores (TMB: R = −0.15; MSI: R = −0.2) (Figure 4G). In addition, Correlation analysis of mutations in the risk model gene set and Gleason scores (Figure 4H) showed that advanced Gleason scores were higher ratioin the mutation group in PRAD patients, which may be associated with a poor prognosis.

Subsequently, the TIDE score and immune exclusion was calculated for each PRAD patient based on the TIDE analysis (Figure 5A), and the risk scores were positively correlated with them. It is suggested that patients in the high-risk group are more likely to experience immune escape and poor immunotherapy. Based on the previous analysis, we found that both immune infiltration and mutation have important roles in the risk model. Therefore, we further explored the correlation between mutation and immune phenotype through the mutation profile of the gene set in the risk model. Both gene amplification (Amp) and deletion (Dele) were types of copy number variation (CNV) (Zhang et al., 2009), which were belongs to mutations. The results showed that the infiltration score was higher in the gene amplification and deletion groups compared with the wild type (WT) (Figure 5B), and the deletion group had lower exhausted abundance, whereas there was no significant difference in exhausted abundance between the wild type and amplification group (Figure 5C). The abundance of iTreg (Figure 5D) in the amplification group, and B cell (Figure 5E) and DC cell (Figure 5F) in the deletion group were higher compared to the wild type.

Drug sensitivity analysis based on the PRAD risk model gene set (Figure 5G) revealed that the high- Drug sensitivity analysis based on the PRAD risk model gene set (Figure 5G) revealed that the high-risk group decrease the sensibility of Ipatasertib, AZD5363, Oxaliplatin, MK-2206, AZD8055, and AZD8186in PRAD, and increase the sensibility of Sinularin, Cyclophosphamide, AZD4547, and Osimertinib in PRAD.

4 Discussion

EccDNA has long been discovered in both normal and malignant cells (Ling et al., 2021). Using circle-seq, we investigated the eccDNA profiles of PRAD and para-cancerous normal prostate tissues. It was found that ZNF330$^{circle142141735-142142329}$ was significantly upregulated in PRAD and PITPNM3$^{circle6458635-6459156}$ was significantly downregulated, which may be potential biomarkers in PRAD patients. We observed some conclusions that are consistent with past investigations (Kumar et al., 2017; Noer et al., 2022). For example, the size and type of eccDNA did not change significantly between PRAD tumours and normal tissues, with size distribution peaks of around 300 bp. At the same time, we discovered that the amount of amplified eGenes was identical, despite the fact that the number of eccDNA varied dramatically between these two tissues. We then investigated the matching shedding sites of eccDNA on chromosomes and discovered that there was no significant change in the chromosomal distribution of eccDNA across tissues. However, the number of eccDNA loci differed substantially among chromosomes, with chromosome 1 being the most prevalent and the Y chromosome being the least common. In the differential expression analysis of eccDNAs from PRAD tumours and normal tissues, we found that 4,290 eccDNAs were differentially expressed, and these eccDNAs amplified 1,981 eGenes. Some previous studies (Jiang et al., 2023) have shown that the expression of eccDNAs varies between cancer and normal tissues, eccDNA-amplified eGenes may not be differentially expressed. This indicates that not all differentially expressed eccDNAs play a role in disease progression. Therefore, we further explored the changes in expression levels of eccDNA-amplified eGenes in PRAD and their underlying molecular mechanisms.

This study identified eccDNA-amplified eGenes ZNF330 and PITPNM3 as key genes in PRAD. ZNF330$^{circle142141735-142142329}$ was significantly amplified in PRAD, and ZNF330 was also consistently highly expressed in PRAD Whereas, PITPNM3$^{circle6458635-6459156}$ was upregulated in PRAD, but PITPNM3 was lowly expressed in PRAD. This shows that eccDNA amplification may be an important, although not determining, factor influencing eGenes expression (Koche et al., 2020). Survival analysis revealed that high levels of both ZNF330 and PITPNM3 were associated with a bad prognosis, implying that they are independent risk factors for PRAD prognosis. In one study, ZNF330 was identified as a potential oncogenic factor in breast cancer (Zhang et al., 2021), and we also found that high expression of ZNF330 in PRAD led to worse clinical prognosis, which was associated with the occurrence of PRAD progressive disease (PD), DSS event (Supplementary Figures S2E, F). PITPNM3 has also been found to promote the progression of various tumours, such as breast (Zeng et al., 2023) and pancreatic cancer (Meng et al., 2015), which is an emerging therapeutic target in cancer (Torphy et al., 2022). Our work also reveals that PITPNM3 is a predictive risk factor for PRAD, and high expression of PITPNM3 is related with poor clinical stage (Supplementary Figure S2G). Thus, PITPNM3 may be related with PRAD at the transcriptional level, which requires further investigation with other samples. The above findings show that ZNF330 and PITPNM3 could be predictive indicators for PRAD.

The PRAD risk model, which was based on ZNF330 and PITPNM3, revealed that high risk was associated with a poor prognosis, and the ROC curve indicated that the model was prognostically reliable. Functional enrichment analysis revealed that the high-risk group was primarily enriched for post-translational modifications, cytokine signalling, and cancer-related pathways. More crucially, we discovered that the risk model might influence the immunological microenvironment (TME) of PRAD, directing the immunotherapy response.

Cancer development is highly correlated with the physiological state of TME (Roma-Rodrigues et al., 2019). In our study, we found that high risk was positively with the increase level of T cells CD4 memory resting, Macrophages M0, Macrophages M2, Tregs contents, and negatively with the decrease level of T cells follicular helper, NK cells in PRAD microenvironment. Tregs infiltration is also found in ZNF330 and PITPNM3 single gene immune infiltration analyses

(Supplementary Figures S2B, C), which is a major mechanism of tumour immune escape, and its phenotypic and functional diversity affects its response to therapy (Kang and Zappasodi, 2023). A study of hepatocellular carcinoma (HCC) (Chen et al., 2024b) demonstrated that SOX18 overexpression mediated infiltration of Tregs and promoted HCC progression and metastasis. Macrophages M2 polarisation is a driver of tumour progression (Christofides et al., 2022), and T cells follicular helper (King, 2021) and NK cells activated (Park et al., 2023) play an important role in anti-tumour immunity. The reduction of these cells may allow tumour cells to escape immune surveillance. Meanwhile, immune cell function was active in the high-risk group. These results suggest that the risk model may be able to reshape the immune microenvironment in PRAD patients. In addition, we found that risk models influence immune subtyping, and different immune subtypes may affect the response to immunotherapy (Petralia et al., 2024).

Therefore, the impact of risk models on immunotherapy response are highly concerned. PD-1, CTLA4, TMB and MSI are all important markers for predicting the efficacy of immunotherapy. High levels of PD-1 with or without CTLA4 are generally associated with enhanced response to the corresponding targeted therapy (Yarchoan et al., 2019), and patients with high TMB and MSI scores are also more likely to benefit from immunotherapy (Valero et al., 2021). The study found that high-risk groups responded poorly to anti-PD-1 and anti-CTLA-4 therapies, which are common immune checkpoint inhibitors. This suggests that combining these immunotherapies with agents that target ZNF330 and PITPNM3, or drugs that modulate the TME, could potentially overcome resistance and improve patient outcomes. PD-1 and TMB evaluation are mainly based on the characteristics of the tumour cells, while ignoring the influence of the tumour microenvironment and immune components, such as the tumour cells themselves, the T lymphocytes and the antigen-presenting cells and other multiple immune cells' expression (Bruni et al., 2020). Moreover, relevant factors such as tumour heterogeneity may also lead to false-negative PD-1/PD-L1 expression. Therefore, we also need to assess the tumour response to immunotherapy in terms of other factors. Higher TIDE and immunological exclusion scores in the high-risk group indicate a greater likelihood of immune escape, suggesting that these patients may require more aggressive or combination immunotherapy approaches. Additionally, the low ESTIMATE scores imply higher tumor purity, which could be factored into the development of pharmacological interventions aimed at enhancing immune infiltration and activity. These findings emphasize the need for a multifaceted approach in treating PRAD, integrating novel genetic markers, immune modulation, and personalized pharmacotherapy to improve patient prognosis and response to treatment. The research identified several drugs with varying sensitivities based on the PRAD risk model. High-risk patients showed decreased sensitivity to drugs like Ipatasertib and AZD5363 but increased sensitivity to drugs such as Sinularin and Osimertinib. This highlights the importance of personalized medicine, where drug selection is tailored based on the genetic and molecular profile of the tumor.

Although our analysis is based on precise sequencing and high-quality analyses, there are several limitations that must be acknowledged. First, putative eccDNA-amplified genes were selected and confirmed, excluding non-coding genes, which would be investigated further. Second, additional *in vitro* investigations are required to confirm the expression of ZNF330 and PITPNM3 in PRAD. Moreover, the fundamental mechanism by which eccDNA increases PRAD's malignant tendencies is unknown and requires further investigation. Finally, although eccDNA sequencing was performed in this study, some of the analyses still originated from data in public databases, so the results await more experimental validation. We partially tested the two genes and confirmed their role in prostate cancer, while more basic research is needed in the future to better understand the role of eccDNA in PRAD.

5 Conclusion

In this study, we sequenced PRAD's eccDNA and examined its size distribution, chromosomal position, and expression level. Based on eccDNA sequencing and transcriptome analysis, the important coding genes ZNF330 and PITPNM were identified as potentially transcribed from eccDNA. A unique PRAD risk model based on the two-factor combination of ZNF330 and PITPNM3 was developed, which not only predicts survival but also predicts the immunotherapy responses of PRAD patients of varying risk. These findings highlight the utility of the eccDNA-based PRAD risk model in clinical settings.

Data availability statement

The data presented in the study are deposited in the OMIX repository, accession number OMIX007219 (https://ngdc.cncb.ac.cn/omix/release/OMIX007219).

Ethics statement

The studies involving humans were approved by Ethics Committee of the Second Affiliated Hospital of Fujian Medical University (2021–148). The studies were conducted in accordance with the local legislation and institutional requirements. The participants provided their written informed consent to participate in this study. No potentially identifiable images or data are presented in this study.

Author contributions

QH: Writing–review and editing, Writing–original draft, Methodology, Funding acquisition, Formal Analysis, Data curation, Conceptualization. QS: Writing–review and editing, Visualization, Software, Methodology, Conceptualization. CW: Writing–review and editing, Methodology, Conceptualization. PZ: Writing–review and editing, Methodology, Conceptualization. WL: Writing–review and editing, Supervision, Software, Funding acquisition. JC: Writing–review and editing, Methodology, Formal Analysis, Conceptualization. XS: Writing–review and editing, Supervision, Funding acquisition, Conceptualization. WZ: Writing–review and editing, Writing–original draft, Supervision, Methodology, Funding acquisition.

Funding

The author(s) declare that financial support was received for the research, authorship, and/or publication of this article. This research was funded by the Natural Science Foundation of Fujian Province (No.2021J01276), the Science and Technology Program of Fujian Provincial Health Commission (No.2021GGA038) and the Quanzhou City Science and Technology Program of China (No. 2022NS078, No. 2023C008YR), and Joint funds for the innovation of science and technology, Fujian Province (No.2023Y9228).

Conflict of interest

The authors declare that the research was conducted in the absence of any commercial or financial relationships that could be construed as a potential conflict of interest.

Publisher's note

All claims expressed in this article are solely those of the authors and do not necessarily represent those of their affiliated organizations, or those of the publisher, the editors and the reviewers. Any product that may be evaluated in this article, or claim that may be made by its manufacturer, is not guaranteed or endorsed by the publisher.

Supplementary material

The Supplementary Material for this article can be found online at: https://www.frontiersin.org/articles/10.3389/fphar.2024.1464145/full#supplementary-material

SUPPLEMENTARY FIGURE S1
(A–D) Comparison of eccDNA size distribution between tumor and normal groups. A, group 1. B, group 2. C, group 3. D, all groups. **(E)** Heatmap of differentially expressed eccDNAs. Red, high expression; Green, low expression. **(F)** Distribution of differentially expressed eccDNAs on all chromosomes. **(G)** Volcano plot of eccDNA amplified differentially expressed genes. Red, high expression; Green, low expression. **(H–I)** Relative RNA expression of eKDEGs (ZNF330, PITPNM3). H, TCGA-PRAD. I, validation dataset GSE70770.

SUPPLEMENTARY FIGURE S2
(A) Immune infiltration and survival analysis. **(B–C)** Single gene immune infiltration analysis of ZNF330 and PITPNM3. **(D)** Immune function and survival analysis. **(E–F)** Clinical correlation analysis of ZNF330. E, primary therapy outcome. F, DSS event. **(G)** Correlation analysis between PITPNM3 and clinical T stage.

SUPPLEMENTARY FIGURE S3
The expression and effect of ZNF330 in prostate cancer. **(A)** The mRNA expressions of ZNF330 and PITPNM3 in prostate normal and cancer tissues by qRT-PCR. **(B)** The protein expression of ZNF330 and PITPNM3 in prostate normal and cancer tissues from HPA database. **(C)** The mRNA expression of ZNF330 in prostate epithelial and tumor cell lines. **(D)** The mRNA and protein expression of ZNF330 with silencing ZNF330 in 22Rv1. **(E)** The effect of silencing ZNF330 and apoptosis inhibitor Z-VAD-FMK on cell proliferation of 22Rv1 with heat shock. **(F–G)** The Co-immunoprecipitation of ZNF330 with HSPA1 and HSPA8 in 22Rv1 cells.

References

Abida, W., Cheng, M. L., Armenia, J., Middha, S., Autio, K. A., Vargas, H. A., et al. (2019). Analysis of the prevalence of microsatellite instability in prostate cancer and response to immune checkpoint blockade. *JAMA Oncol.* 5, 471–478. doi:10.1001/jamaoncol.2018.5801

Andrisani, O. (2024). Two important players in poor-prognosis hepatocellular carcinoma: extrachromosomal circular DNA (eccDNA) and its passenger, the oncogenic miR-17~92 locus. *Hepatology* 79, 6–8. doi:10.1097/HEP.0000000000000453

Antonarakis, E. S., Piulats, J. M., Gross-Goupil, M., Goh, J., Ojamaa, K., Hoimes, C. J., et al. (2020). Pembrolizumab for treatment-refractory metastatic castration-resistant prostate cancer: multicohort, open-label phase II KEYNOTE-199 study. *J. Clin. Oncol.* 38, 395–405. doi:10.1200/JCO.19.01638

Bruni, D., Angell, H. K., and Galon, J. (2020). The immune contexture and Immunoscore in cancer prognosis and therapeutic efficacy. *Nat. Rev. Cancer* 20, 662–680. doi:10.1038/s41568-020-0285-7

Charoentong, P., Finotello, F., Angelova, M., Mayer, C., Efremova, M., Rieder, D., et al. (2017). Pan-cancer immunogenomic analyses reveal genotype-immunophenotype relationships and predictors of response to checkpoint blockade. *Cell Rep.* 18, 248–262. doi:10.1016/j.celrep.2016.12.019

Chen, J., Feng, W., Sun, M., Huang, W., Wang, G., Chen, X., et al. (2024b). TGF-β1-Induced SOX18 elevation promotes hepatocellular carcinoma progression and metastasis through transcriptionally upregulating PD-L1 and CXCL12. *Gastroenterology* 167, 264–280. doi:10.1053/j.gastro.2024.02.025

Chen, J. P., Diekmann, C., Wu, H., Chen, C., Della Chiara, G., Berrino, E., et al. (2024a). scCircle-seq unveils the diversity and complexity of extrachromosomal circular DNAs in single cells. *Nat. Commun.* 15, 1768. doi:10.1038/s41467-024-45972-y

Christofides, A., Strauss, L., Yeo, A., Cao, C., Charest, A., and Boussiotis, V. A. (2022). The complex role of tumor-infiltrating macrophages. *Nat. Immunol.* 23, 1148–1156. doi:10.1038/s41590-022-01267-2

Fridman, W. H., Pagès, F., Sautès-Fridman, C., and Galon, J. (2012). The immune contexture in human tumours: impact on clinical outcome. *Nat. Rev. Cancer* 12, 298–306. doi:10.1038/nrc3245

Hotta, Y., and Bassel, A. (1965). Molecular size and circularity of dna in cells of mammals and higher plants. *Proc. Natl. Acad. Sci. U. S. A.* 53, 356–362. doi:10.1073/pnas.53.2.356

Jiang, P., Gu, S., Pan, D., Fu, J., Sahu, A., Hu, X., et al. (2018). Signatures of T cell dysfunction and exclusion predict cancer immunotherapy response. *Nat. Med.* 24, 1550–1558. doi:10.1038/s41591-018-0136-1

Jiang, X., Pan, X., Li, W., Han, P., Yu, J., Li, J., et al. (2023). Genome-wide characterization of extrachromosomal circular DNA in gastric cancer and its potential role in carcinogenesis and cancer progression. *Cell Mol. Life Sci.* 80, 191. doi:10.1007/s00018-023-04838-0

Kaur, H. B., Vidotto, T., Mendes, A. A., Salles, D. C., Isaacs, W. B., Antonarakis, E. S., et al. (2022). Association between pathogenic germline mutations in BRCA2 and ATM and tumor-infiltrating lymphocytes in primary prostate cancer. *Cancer Immunol. Immunother.* 71, 943–951. doi:10.1007/s00262-021-03050-y

Kang, J. H., and Zappasodi, R. (2023). Modulating Treg stability to improve cancer immunotherapy. *Trends Cancer* 9, 911–927. doi:10.1016/j.trecan.2023.07.015

King, C. (2021). Tfh cells set the stage for tumor control. *Immunity* 54, 2690–2692. doi:10.1016/j.immuni.2021.11.013

Koche, R. P., Rodriguez-Fos, E., Helmsauer, K., Burkert, M., MacArthur, I. C., Maag, J., et al. (2020). Extrachromosomal circular DNA drives oncogenic genome remodeling in neuroblastoma. *Nat. Genet.* 52, 29–34. doi:10.1038/s41588-019-0547-z

Kumar, P., Dillon, L. W., Shibata, Y., Jazaeri, A. A., Jones, D. R., and Dutta, A. (2017). Normal and cancerous tissues release extrachromosomal circular DNA (eccDNA) into the circulation. *Mol. Cancer Res.* 15, 1197–1205. doi:10.1158/1541-7786.MCR-17-0095

Ling, X., Han, Y., Meng, J., Zhong, B., Chen, J., Zhang, H., et al. (2021). Small extrachromosomal circular DNA (eccDNA): major functions in evolution and cancer. *Mol. Cancer* 20, 113. doi:10.1186/s12943-021-01413-8

Lopez-Bujanda, Z. A., Obradovic, A., Nirschl, T. R., Crowley, L., Macedo, R., Papachristodoulou, A., et al. (2021). TGM4: an immunogenic prostate-restricted antigen. *J. Immunother. Cancer* 9, e001649. doi:10.1136/jitc-2020-001649

Luo, X., Zhang, L., Cui, J., An, Q., Li, H., Zhang, Z., et al. (2023). Small extrachromosomal circular DNAs as biomarkers for multi-cancer diagnosis and monitoring. *Clin. Transl. Med.* 13, e1393. doi:10.1002/ctm2.1393

Melo, C. M., Vidotto, T., Chaves, L. P., Lautert-Dutra, W., Reis, R. B. D., and Squire, J. A. (2021). The role of somatic mutations on the immune response of the tumor microenvironment in prostate cancer. *Int. J. Mol. Sci.* 22, 9550. doi:10.3390/ijms22179550

Meng, F., Li, W., Li, C., Gao, Z., Guo, K., and Song, S. (2015). CCL18 promotes epithelial-mesenchymal transition, invasion and migration of pancreatic cancer cells in pancreatic ductal adenocarcinoma. *Int. J. Oncol.* 46, 1109–1120. doi:10.3892/ijo.2014.2794

Møller, H. D., Mohiyuddin, M., Prada-Luengo, I., Sailani, M. R., Halling, J. F., Plomgaard, P., et al. (2018). Circular DNA elements of chromosomal origin are

common in healthy human somatic tissue. *Nat. Commun.* 9, 1069. doi:10.1038/s41467-018-03369-8

Narayan, V., Barber-Rotenberg, J. S., Jung, I. Y., Lacey, S. F., Rech, A. J., Davis, M. M., et al. (2022). PSMA-targeting TGFβ-insensitive armored CAR T cells in metastatic castration-resistant prostate cancer: a phase 1 trial. *Nat. Med.* 28, 724–734. doi:10.1038/s41591-022-01726-1

Noer, J. B., Hørsdal, O. K., Xiang, X., Luo, Y., and Regenberg, B. (2022). Extrachromosomal circular DNA in cancer: history, current knowledge, and methods. *Trends Genet.* 38, 766–781. doi:10.1016/j.tig.2022.02.007

Park, M. D., Reyes-Torres, I., LeBerichel, J., Hamon, P., LaMarche, N. M., Hegde, S., et al. (2023). TREM2 macrophages drive NK cell paucity and dysfunction in lung cancer. *Nat. Immunol.* 24, 792–801. doi:10.1038/s41590-023-01475-4

Petralia, F., Ma, W., Yaron, T. M., Caruso, F. P., Tignor, N., Wang, J. M., et al. (2024). Pan-cancer proteogenomics characterization of tumor immunity. *Cell* 187, 1255–1277.e27. doi:10.1016/j.cell.2024.01.027

Philippou, Y., Protheroe, A. S., and Bryant, R. J. (2020). Re: pembrolizumab for treatment-refractory metastatic castration-resistant prostate cancer: multicohort, open-label phase II KEYNOTE-199 study. *Eur. Urol.* 77, 759–760. doi:10.1016/j.eururo.2020.02.026

Rebello, R. J., Oing, C., Knudsen, K. E., Loeb, S., Johnson, D. C., Reiter, R. E., et al. (2021). Prostate cancer. *Nat. Rev. Dis. Prim.* 7, 9. doi:10.1038/s41572-020-00243-0

Roma-Rodrigues, C., Mendes, R., Baptista, P. V., and Fernandes, A. R. (2019). Targeting tumor microenvironment for cancer therapy. *Int. J. Mol. Sci.* 20, 840. doi:10.3390/ijms20040840

Sandhu, S., Moore, C. M., Chiong, E., Beltran, H., Bristow, R. G., and Williams, S. G. (2021). Prostate cancer. *Lancet* 398, 1075–1090. doi:10.1016/S0140-6736(21)00950-8

Siegel, R. L., Giaquinto, A. N., and Jemal, A. (2024). Cancer statistics, 2024. *CA Cancer J. Clin.* 74, 12–49. doi:10.3322/caac.21820

Sung, H., Ferlay, J., Siegel, R. L., Laversanne, M., Soerjomataram, I., Jemal, A., et al. (2021). Global cancer statistics 2020: GLOBOCAN estimates of incidence and mortality worldwide for 36 cancers in 185 countries. *CA Cancer J. Clin.* 71, 209–249. doi:10.3322/caac.21660

Sutherland, S. I. M., Ju, X., Horvath, L. G., and Clark, G. J. (2021). Moving on from sipuleucel-t: new dendritic cell vaccine strategies for prostate cancer. *Front. Immunol.* 12, 641307. doi:10.3389/fimmu.2021.641307

Torphy, R. J., Yee, E. J., Schulick, R. D., and Zhu, Y. (2022). Atypical chemokine receptors: emerging therapeutic targets in cancer. *Trends Pharmacol. Sci.* 43, 1085–1097. doi:10.1016/j.tips.2022.09.009

Turner, K. M., Deshpande, V., Beyter, D., Koga, T., Rusert, J., Lee, C., et al. (2017). Extrachromosomal oncogene amplification drives tumour evolution and genetic heterogeneity. *Nature* 543, 122–125. doi:10.1038/nature21356

Valero, C., Lee, M., Hoen, D., Wang, J., Nadeem, Z., Patel, N., et al. (2021). The association between tumor mutational burden and prognosis is dependent on treatment context. *Nat. Genet.* 53, 11–15. doi:10.1038/s41588-020-00752-4

Wang, Y., Wang, M., Djekidel, M. N., Chen, H., Liu, D., Alt, F. W., et al. (2021). eccDNAs are apoptotic products with high innate immunostimulatory activity. *Nature* 599, 308–314. doi:10.1038/s41586-021-04009-w

Xu, Z., Chen, S., Zhang, Y., Liu, R., and Chen, M. (2022). Roles of m5C RNA modification patterns in biochemical recurrence and tumor microenvironment characterization of prostate adenocarcinoma. *Front. Immunol.* 13, 869759. doi:10.3389/fimmu.2022.869759

Yang, W., Soares, J., Greninger, P., Edelman, E. J., Lightfoot, H., Forbes, S., et al. (2013). Genomics of Drug Sensitivity in Cancer (GDSC): a resource for therapeutic biomarker discovery in cancer cells. *Nucleic Acids Res.* 41, D955–D961. doi:10.1093/nar/gks1111

Yarchoan, M., Albacker, L. A., Hopkins, A. C., Montesion, M., Murugesan, K., Vithayathil, T. T., et al. (2019). PD-L1 expression and tumor mutational burden are independent biomarkers in most cancers. *JCI Insight* 4, e126908. doi:10.1172/jci.insight.126908

Ye, Z., Deng, X., Zhang, J., Shao, R., Song, C., Zhao, J., et al. (2024). Causal relationship between immune cells and prostate cancer: a Mendelian randomization study. *Front. Cell Dev. Biol.* 12, 1381920. doi:10.3389/fcell.2024.1381920

Zeng, W., Xiong, L., Wu, W., Li, S., Liu, J., Yang, L., et al. (2023). CCL18 signaling from tumor-associated macrophages activates fibroblasts to adopt a chemoresistance-inducing phenotype. *Oncogene* 42, 224–237. doi:10.1038/s41388-022-02540-2

Zhang, F., Carvalho, C. M., and Lupski, J. R. (2009). Complex human chromosomal and genomic rearrangements. *Trends Genet.* 25, 298–307. doi:10.1016/j.tig.2009.05.005

Zhang, J., Lu, H., Zhang, S., Wang, T., Zhao, H., Guan, F., et al. (2021). Leveraging methylation alterations to discover potential causal genes associated with the survival risk of cervical cancer in TCGA through a two-stage inference approach. *Front. Genet.* 12, 667877. doi:10.3389/fgene.2021.667877

Zhang, Y., Dong, K., Jia, X., Du, S., Wang, D., Wang, L., et al. (2023). A novel extrachromosomal circular DNA related genes signature for overall survival prediction in patients with ovarian cancer. *BMC Med. Genomics* 16, 140. doi:10.1186/s12920-023-01576-x

Zou, S., Chen, S., Rao, G., Zhang, G., Ma, M., Peng, B., et al. (2024). Extrachromosomal circular MiR-17-92 amplicon promotes HCC. *Hepatology* 79, 79–95. doi:10.1097/HEP.0000000000000435

frontiers | Frontiers in Pharmacology

TYPE Review
PUBLISHED 30 September 2024
DOI 10.3389/fphar.2024.1469830

Check for updates

OPEN ACCESS

EDITED BY
Hailin Tang,
Sun Yat-sen University Cancer Center (SYSUCC), China

REVIEWED BY
Cheng Hu,
Third Affiliated Hospital of Sun Yat-sen University, China
Renjun Gu,
Nanjing University of Chinese Medicine, China
Jin Zhang,
University of Mississippi Medical Center, United States

*CORRESPONDENCE
Qin Deng,
300352@hospital.cqmu.edu.cn
Yanjun Liu,
liuyanjun_001@163.com

†These authors have contributed equally to this work

RECEIVED 24 July 2024
ACCEPTED 13 September 2024
PUBLISHED 30 September 2024

CITATION
Tang Y, Ju W, Liu Y and Deng Q (2024) The role of SIRT1 in autophagy and drug resistance: unveiling new targets and potential biomarkers in cancer therapy.
Front. Pharmacol. 15:1469830.
doi: 10.3389/fphar.2024.1469830

COPYRIGHT
© 2024 Tang, Ju, Liu and Deng. This is an open-access article distributed under the terms of the Creative Commons Attribution License (CC BY). The use, distribution or reproduction in other forums is permitted, provided the original author(s) and the copyright owner(s) are credited and that the original publication in this journal is cited, in accordance with accepted academic practice. No use, distribution or reproduction is permitted which does not comply with these terms.

The role of SIRT1 in autophagy and drug resistance: unveiling new targets and potential biomarkers in cancer therapy

Yujing Tang[1,2†], Wantao Ju[1,2†], Yanjun Liu[1,2*] and Qin Deng[3*]

[1]School of Life Science and Engineering, Southwest Jiaotong University, Chengdu, China, [2]Obesity and Metabolism Medicine-Engineering Integration Laboratory, Department of General Surgery, The Third People's Hospital of Chengdu, Affiliated Hospital of Southwest Jiaotong University, Chengdu, Sichuan, China, [3]Department of Breast and Thyroid Surgery, The Second Affiliated Hospital of Chongqing Medical University, Chongqing, China

Cancer, the world's second leading cause of death after cardiovascular diseases, is characterized by hallmarks such as uncontrolled cell growth, metastasis, angiogenesis, hypoxia, and resistance to therapy. Autophagy, a cellular process that can both support and inhibit cancer progression, plays a critical role in cancer development and progression. This process involves the formation of autophagosomes that ultimately fuse with lysosomes to degrade cellular components. A key regulator of this process is Sirtuin 1 (SIRT1), which significantly influences autophagy. This review delves into the role of SIRT1 in modulating autophagy and its broader impacts on carcinogenesis. SIRT1 regulates crucial autophagy mediators, such as AMP-activated protein kinase (AMPK) and mammalian target of rapamycin (mTOR), effectively promoting or suppressing autophagy. Beyond its direct effects on autophagy, SIRT1's regulatory actions extend to other cell death processes, including apoptosis and ferroptosis, thereby influencing tumor cell proliferation, metastasis, and chemotherapy responses. These insights underscore the complex interplay between SIRT1 and autophagy, with significant implications for cancer therapy. Targeting SIRT1 and its associated pathways presents a promising strategy to manipulate autophagy in cancer treatment. This review underscores the potential of SIRT1 as a therapeutic target, opening new avenues for enhancing cancer treatment efficacy.

KEYWORDS

autophagy, apoptosis, ferroptosis, drug resistance, sirtuin family, SIRT1

Highlights

- As a cell death mechanism, autophagy regulates initiation and progression of carcinogenesis.
- Sirutin family has various cellular functions in which SIRT1 is the most well-known one.
- SIRT1 modulates autophagy and other selective types including mitophagy and lipophagy.
- SIRT-mediated autophagy can regulate apoptosis occurrence in tumor cells.

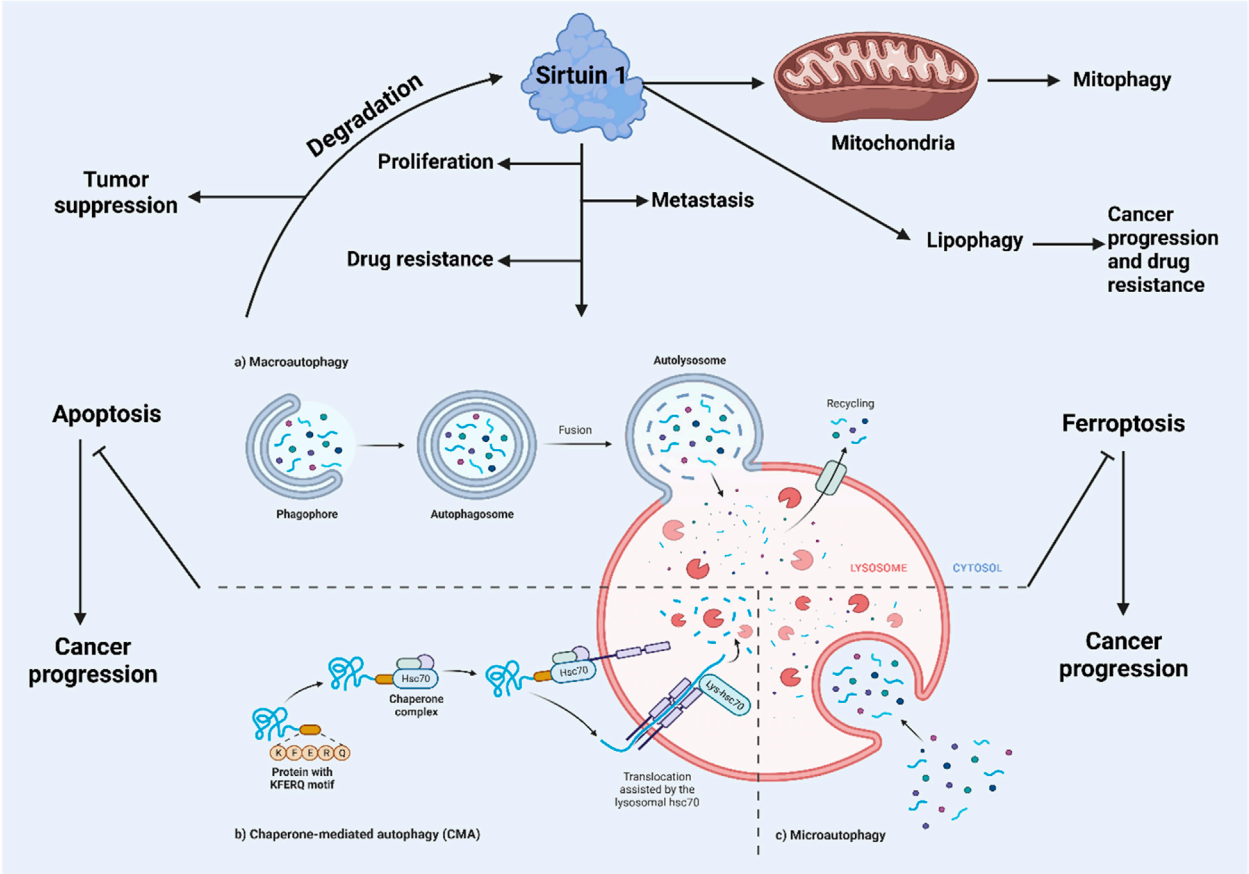

GRAPHICAL ABSTRACT

- SIRT1-mediated autophagy regulation determines the response to cancer chemotherapy.

1 Introduction

Cells utilize autophagy and the ubiquitin-proteasome degradation pathway to dispose of toxic, misfolded, damaged, or unnecessary proteins (Wirawan et al., 2012). Unlike the proteasome, autophagy can degrade a vast array of substrates, including large protein aggregates and entire organelles. Beyond proteins, autophagy also breaks down lipids, DNA, and nuclear RNA, generating new pools of amino acids, fatty acids, and nucleosides for use in anabolic processes. This continual turnover facilitates a cycle of cellular breakdown and renewal (Rabinowitz and White, 2010). Autophagic degradation is carried out by lysosomes, which contain acidic hydrolases such as peptidases, lipases, and nucleases, breaking down large molecules into simpler components. Although all autophagic pathways converge at the lysosomal compartment (or vacuole in yeast), several routes exist to reach these lysosomes. In mammalian cells, three primary autophagy processes are recognized: chaperone-mediated autophagy (CMA), microautophagy, and macroautophagy (Cuervo, 2004). CMA targets proteins with a KFERQ-like motif to the lysosomes, facilitated by heat shock cognate 70 and its co-chaperones, with the lysosomal-associated membrane protein 2 (LAMP-2A) (Kaushik et al., 2011) mediating their subsequent breakdown. Microautophagy involves the lysosomal membrane invaginating to engulf cytoplasmic material, which is then degraded. Macroautophagy, on the other hand, involves the formation of autophagic vacuoles through the creation of autophagic membranes (phagophores) that evolve into double-membraned vesicles called autophagosomes. This form of autophagy is evolutionarily conserved across all eukaryotic cells and has been extensively studied, particularly through mouse models focusing on macroautophagy.

Cancer remains one of the most prevalent diseases globally, irrespective of economic status, with approximately 18.1 million new cases and 9.1 million deaths reported in 2018 (Bray et al., 2018). The extensive research over the past decades into cancer development, progression, detection, and treatment has highlighted the critical nature of early diagnosis and intervention. Without these, cancer often proves fatal. Despite significant advancements, cancer multidrug resistance continues to be a significant obstacle in effective cancer treatment. Chemotherapy remains a cornerstone for treating various malignancies across different stages. Researchers often grapple with understanding the development and potential treatments of cancer, not foreseeing the emergence of drug resistance within their studies. Drug resistance in cancer is complex and broad, making it a challenging phenomenon to elucidate. The

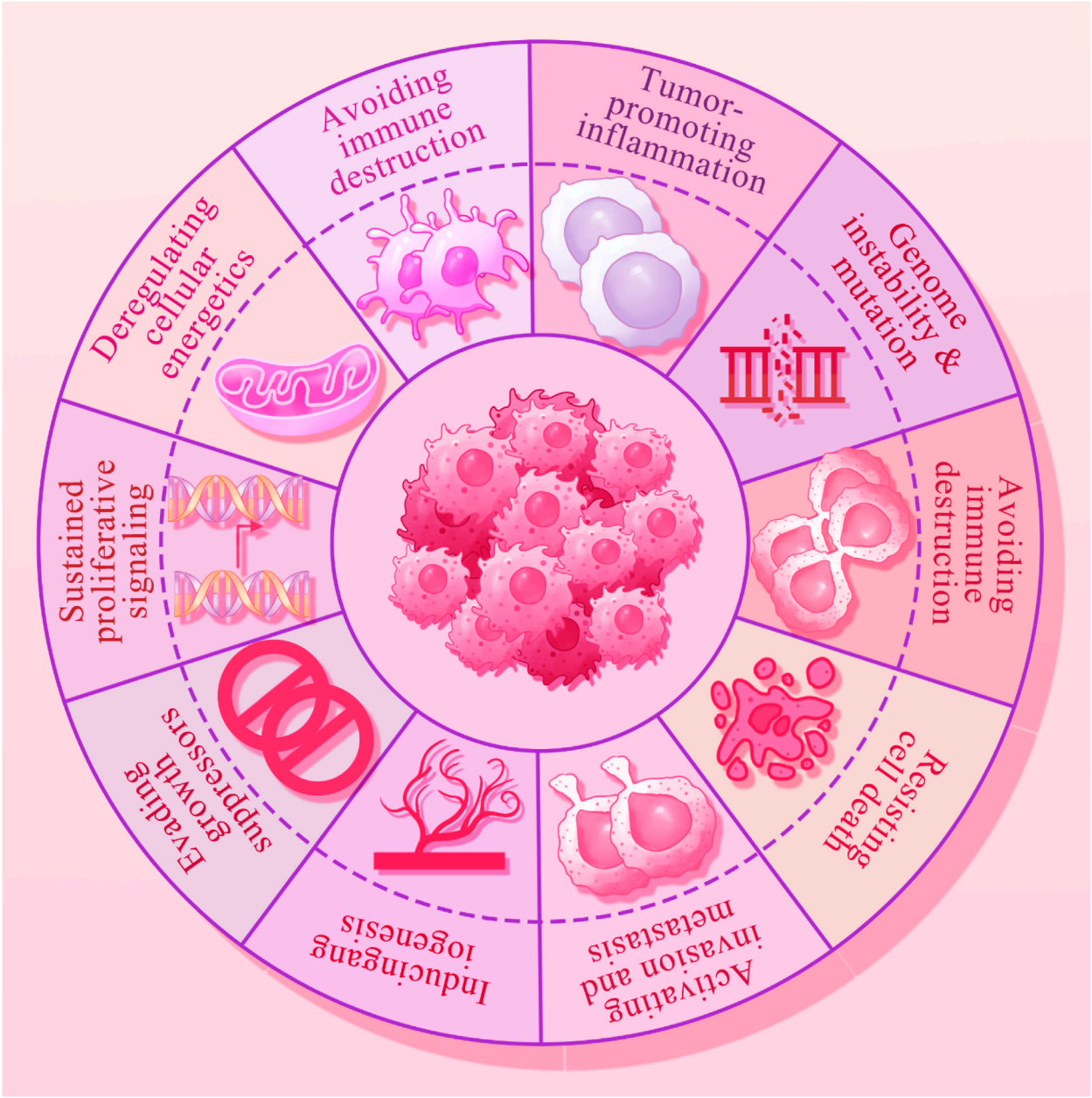

FIGURE 1
The hallmarks of cancer that include the immune escape, epigenetic alterations, oncogenic inflammation, genomic instability, increased proliferation, angiogenesis, metastasis, cell death resistance and replicative immortality.

understanding of chemotherapeutic resistance mechanisms has expanded greatly, yet the scientific explanations remain limited. The strategies by which tumor cells manage their metabolic pathways and signaling can influence treatment outcomes, such as preventing drug penetration into cancer cells and promoting drug efflux. Numerous studies have also explored whether specific genes are upregulated to foster drug resistance, examining aspects like drug transport through tumor cells, membrane transport protein pathways, target molecule overexpression, direct gene transcription, anti-apoptosis, and enhanced DNA repair, all of which have been implicated in the promotion of drug resistance (Harguindey et al., 2005; Housman et al., 2014; Liang Z. et al., 2014).

Dysregulation of cell death mechanisms is a common feature in carcinogenesis (Figure 1), influencing tumor cell survival, viability, proliferation, metastasis, and response to therapy. Autophagy, a cellular catabolic process, involves the breakdown and recycling of proteins and organelles. It starts with the formation of an autophagosome, a vesicle that fuses with a lysosome containing hydrolytic enzymes. Unlike mitophagy, which specifically targets intracellular organelles, macroautophagy is a non-selective form of autophagy. The

complex molecular process of autophagy, which includes nucleation, elongation, and fusion, is facilitated by various proteins, including the autophagy-related (ATG) protein family (Ferro et al., 2020; Ichimura et al., 2000; Mizushima et al., 1998; Zaffagnini and Martens, 2016). Autophagy plays a critical role in balancing environmental substrate availability with cellular metabolic demands. It is activated by nutrient deprivation and oxidative stress through well-regulated pathways linked to energy metabolism, involving key regulators such as mTORC1 and AMPK (Hosokawa et al., 2009; Jung et al., 2009; Egan et al., 2011; Kim et al., 2011). The two primary physiological roles of autophagy are the degradation of defective proteins or organelles for quality control and the recycling of macromolecules under conditions of nutritional stress to meet metabolic needs (Kim and Lee, 2014; Mizushima and Komatsu, 2011).

In recent years, research has increasingly focused on the role of autophagy in both physiological and pathological contexts. Autophagy serves a dual and crucial role in cancer, where it can either promote or inhibit tumorigenesis. While commonly recognized as a mechanism of cell death, autophagy also influences metastasis and resistance to therapy (Qin et al., 2023; Ashrafizadeh et al., 2022). Consequently, it has become a promising target for pharmacological compounds and nanoparticles in cancer treatment (Ashrafizadeh et al., 2020a; Paskeh et al., 2022). With a better understanding of various autophagy regulators now available, this review concentrates on the role of SIRT1 in autophagy regulation within human cancers. It explores SIRT1's association with cancer hallmarks and its interactions with apoptosis and ferroptosis.

2 A history of cell death

Cell death is essential for eliminating undesirable or damaged cells, playing a crucial role in animal development, tissue homeostasis, and stress response (Chen et al., 2016). Improper regulation of cell death contributes to various human diseases, including cancer and inflammatory disorders. Oncogenic transformation allows neoplastic cells to develop resistance to cell death, aiding their survival and the accumulation of mutations that promote cancer development (Hanahan and Weinberg, 2011). Many chemotherapeutic drugs work by inducing cell death, making it a fundamental strategy in cancer treatment. Consequently, targeting cell death mechanisms offers a promising approach for developing new anticancer drugs. Cell death can be classified based on morphological and biochemical characteristics into several primary types, such as apoptosis, necrosis, autophagic death, and mitotic catastrophe (Galluzzi et al., 2012). Historically, necrosis was considered a passive and uncontrolled process, while apoptosis was understood as a highly regulated, programmed cell death. However, the past 2 decades of research have revised this view, revealing a regulated form of necrosis. It was discovered that in some cells, inhibiting caspases, which are crucial for apoptosis, did not stop cell death but instead shifted it towards necrotic symptoms (Vercammen et al., 1998). Further studies identified receptor-interacting kinase 1 (RIP1; RIPK1) as a key regulator of this form of necrosis (Holler et al., 2000). Chemical biology research led to the identification of small-molecule inhibitors targeting this cell death pathway (Degterev et al., 2005), specifically inhibiting RIP1 (Degterev et al., 2008). Recent studies have established that RIP3 acts as a downstream mediator of RIP1 (Cho et al., 2009; He et al., 2009; Zhang et al., 2009), with the Mixed Lineage Kinase Domain-Like (MLKL) protein playing a central role in executing cell death (Sun et al., 2012). The physiological and clinical relevance of necrosis has been underscored by various studies in living organisms (Belizário et al., 2015). This regulated form of cell death, now termed necroptosis, involves RIP1, RIP3, and MLKL (Galluzzi et al., 2012) and is essential for its execution. Increasing evidence suggests that necroptosis acts as a protective mechanism by eliminating cancer cells that are resistant to apoptosis, highlighting its significant role in both the biology and therapy of cancer. Table 1 summarizes the dysregulation of cell death mechanisms in human cancers.

3 Different types of autophagy machinery

3.1 Macroautophagy

Macroautophagy, the most extensively examined type of autophagy, plays a crucial role in the breakdown and recycling of cellular components. This process is advantageous in numerous diseases, such as the removal of protein aggregates found in neurodegenerative disorders. Furthermore, macroautophagy has been recognized as a potential therapeutic target in cancer treatment, with its effectiveness depending on the stage of the tumor, its biological characteristics, and the tumor's microenvironment (Debnath et al., 2023). Autophagosome formation, which involves creating a double-membrane vesicle, is the first step in autophagosomal vesicle generation. These autophagosomes, containing a variety of ATG products, subsequently merge with lysosomes. Lysosomal hydrolases then degrade the autophagosome's contents. Key protein kinases, ULK1 and ULK2, along with their subunits FIP200, ATG13, and ATG101, initiate autophagosome formation in response to nutritional and energy signals, primarily from mTORC1 signaling. The recruitment of ATG7 and ATG3 is essential when phosphatidylinositol 3-phosphate is activated, facilitating the production of PS3P on autophagic membranes by the specialized Vps34 complex I, which includes Vps34, Beclin-1, ATG14, and Vps15. This complex is vital for cargo recruitment and autophagosome maturation (Zhao et al., 2021; Nakatogawa, 2020). Members of the ATG8 family, divided into two human subfamilies (microtubule-associated protein 1A/1B-light chain 3 (LC3) and GABARAP), are involved in lipid conjugation produced by the Vps34 complex I. Macroautophagy can non-selectively incorporate various materials into autophagosomes, especially under conditions of nutrient scarcity, thereby recycling essential molecules like lipids and amino acids. Consequently, macroautophagy is segmented into four phases: initiation, autophagosome formation, elongation, and fusion of the autophagosome with lysosomes,

TABLE 1 A summary of dysregulated cell death mechanisms in tumors.

Cell death	Cancer	Remark	Reference
Ferroptosis	Colorectal cancer	This study identifies METTL17 as a key regulator of mitochondrial function and ferroptosis resistance in CRC, showing that its depletion sensitizes CRC cells to ferroptosis and inhibits tumor growth	Li et al. (2024a)
Ferroptosis	-	USP8 stabilizes GPX4 to counteract ferroptosis, and its inhibition sensitizes cancer cells to ferroptosis	Li et al. (2024b)
Ferroptosis	Breast cancer	This study identifies Acod1 as a key metabolic enzyme in tumor-infiltrating neutrophils (TINs) that protects them from ferroptosis and promotes metastasis	Zhao et al. (2023a)
Autophagy	-	YY1 promotes gastric cancer progression by enhancing autophagy through ATG4B transactivation, and is regulated by ALKBH5 and YTHDF1 via m6A modification	Wang et al. (2023a)
Autophagy	Colon cancer	KLF4 suppresses 5-FU resistance in colon cancer cells by inhibiting autophagy through targeting RAB26, and its overexpression reduces proliferation and drug resistance	Zheng et al. (2023)
Autophagy	Pancreatic cancer	The fructose metabolism, mediated by GLUT5, supports pancreatic ductal adenocarcinoma (PDAC) progression by enhancing cell survival, proliferation, and metabolic plasticity, while inhibiting autophagic cell death through the AMPK-mTORC1 pathway	Cui et al. (2023)
Autophagy	Bladder cancer	The loperamide inhibits bladder cancer cell proliferation by inducing autophagy and apoptosis through the ROS-mediated JNK pathway, and combining loperamide with autophagy inhibitor CQ enhances its anti-cancer effects	Wu et al. (2023)
Autophagy	Pancreatic cancer	Inhibiting CAF autophagy suppresses tumor development and enhances anti-tumor immunity by reducing CD274/PDL1 expression in PDAC, with targeted CAF autophagy inhibition via chloroquine diphosphate-loaded MSC-liposomes improving immunochemotherapy efficacy	Zhang et al. (2024a)
Autophagy	B-cell malignancy	The cancer-intrinsic autophagy, involving key genes like ATG3, BECN1, and RB1CC1, protects tumor cells from CD19 CAR-T cell-mediated cytotoxicity, and its inhibition sensitizes B-cell leukemia and lymphoma cells to CAR-T therapy	Tang et al. (2024)
Apoptosis	Gastric cancer	DHRS4-AS1 is significantly downregulated in GC, inhibiting GC cell proliferation and promoting apoptosis by degrading the pro-oncogenic DHX9 and disrupting the DHX9-ILF3 interaction that activates NF-kB signalling	Xiao et al. (2023)
Apoptosis	Pancreatic cancer	This study introduces CK21, a novel pro-drug of triptolide, which demonstrates potent anti-proliferative effects on pancreatic cancer by inhibiting the NF-κB pathway, increasing oxidative stress, and inducing mitochondrial-mediated apoptosis, while showing minimal toxicity	Tian et al. (2023)
Apoptosis	Cervical cancer	The galectin-7 enhances cisplatin-induced apoptosis in cervical cancer by promoting mitochondrial dysfunction and ROS generation, while reducing chemoresistance by facilitating stress granule clearance via the galectin-7/RACK1/G3BP1 axis	Liu et al. (2023)
Apoptosis	Colorectal cancer	5-MTP promotes apoptosis, induces cell cycle arrest, and inhibits cell proliferation in colorectal cancer (CRC) cells, with these effects significantly enhanced when combined with PI3K/Akt/FoxO3a signaling pathway inhibitors	Zhao et al. (2023b)
Apoptosis	Ovarian cancer	METTL3 is highly expressed in EOC and promotes cell proliferation, while its silencing induces cell cycle arrest and apoptosis through the FAS/FADD and mitochondrial pathways. Sulfuretin (Sul) enhances apoptosis in EOC cells by downregulating METTL3 and reversing the effects of METTL3 overexpression	Yu et al. (2023a)
Apoptosis Ferroptosis	Hepatocellular carcinoma	Celastrol (Cel) targets VDAC2 to induce mitochondria-dependent apoptosis and ROS-mediated ferroptosis in hepatocellular carcinoma (HCC), while its encapsulation in alkyl glucoside-modified liposomes (AGCL) enhances its anti-tumor efficacy and reduces side effects	Luo et al. (2023a)

(Continued on following page)

TABLE 1 (*Continued*) A summary of dysregulated cell death mechanisms in tumors.

Cell death	Cancer	Remark	Reference
Apoptosis Ferroptosis	Colorectal cancer	CAPG is significantly overexpressed in CRC and correlates with poor prognosis, while its knockdown inhibits CRC cell growth, induces cell cycle arrest, and promotes apoptosis and ferroptosis via the upregulation of the P53 pathway	Zhao et al. (2023c)
Apoptosis	Gastric cancer	TRIM17 is upregulated in GC and promotes tumor cell proliferation and survival by ubiquitinating and degrading BAX, thereby inhibiting BAX-dependent apoptosis	Shen et al. (2023)
Ferroptosis	Cervical cancer	Matrine inhibits tumor growth and induces ferroptosis in SiHa cells by reducing GPX4 levels and increasing intracellular Fe2+, ROS, and lipid peroxides, while upregulating Piezo1 expression and promoting calcium influx	Jin et al. (2024)
Ferroptosis	Breast cancer	TAM resistance in breast cancer is driven by RelB, which inhibits TAM-induced ferroptosis by upregulating GPX4, and that reducing RelB or GPX4 levels can resensitize TAM-resistant cells by promoting ferroptosis	Xu et al. (2023a)
Ferroptosis	Colorectal cancer	The drug-resistant colorectal cancer organoids exhibit elevated LGR4 expression and Wnt signaling activation, which confer resistance by upregulating SLC7A11 to inhibit ferroptosis. Targeting LGR4 with a monoclonal antibody (LGR4-mAb) sensitizes cancer cells to chemotherapy-induced ferroptosis	Zheng et al. (2024a)
Ferroptosis	-	GSTP1 provides a GPX4- and FSP1-independent defense against ferroptosis by detoxifying lipid hydroperoxides, and its degradation via the SMURF2/GSTP1 axis sensitizes cancer cells to ferroptosis-inducing drugs and immune checkpoint inhibitors	Zhang et al. (2023a)
Ferroptosis	Colorectal cancer	ATF3-CBS signaling axis as a key mechanism that enables colorectal cancer cells to evade ferroptosis under cystine deprivation by regulating the mitochondrial TCA cycle. Blocking this axis sensitizes cancer cells to ferroptosis	Liu et al. (2024a)

with each stage meticulously controlled. The final step, fusion, is mediated by SNARE proteins that facilitate the merging with the lysosome.

3.2 Microautophagy

Microautophagy includes two forms: selective and non-selective (Wang L. et al., 2023). Similarly, macroautophagy can also engage in either selective or non-selective absorption and degradation of cargoes. The cellular context influences whether microautophagy targets specific cargoes or functions non-selectively (Mijaljica et al., 2011). Historical studies primarily focused on microautophagy in rat liver before the discovery of ATG genes. In these studies, rat liver lysosomes were observed to invaginate their membranes and engulf various cargoes such as hemoglobin, ovalbumin, lysozyme, ferritin, and Percoll particles, facilitated by their acidic internal pH (Ahlberg et al., 1982; Marzella et al., 1981; Ahlberg and Glaumann, 1985). Certain drugs known as lysosomotropic agents, such as chloroquine, can inhibit the breakdown of these materials within the lysosomes. Findings indicate that the main autophagic response to starvation and refeeding in mice and rat livers is microautophagy (de Waal et al., 1986; Mortimore et al., 1988; Mortimore et al., 1983). However, these studies primarily utilized electron microscopy to observe morphological changes and lacked detailed biochemical evidence of alterations in autophagic activity or the molecular pathways involved. Macroautophagy can selectively target specific cargoes based on environmental conditions. Various selective forms of macroautophagy have been identified, including xenophagy for microorganisms, aggregephagy for protein aggregates, mitophagy for mitochondria, reticulophagy for the endoplasmic reticulum, lysophagy for lysosomes, and ribophagy for ribosomes (Kirkin and Rogov, 2019; Anding and Baehrecke, 2017). Recent research has also highlighted different types of selective microautophagy such as endosomal microautophagy (eMI), micronucleophagy, and micromitophagy, each believed to be regulated by distinct molecular pathways and serving unique functions.

While the direct role of microautophagy in cancer progression modulation has been overlooked, the pathways it influences are better understood (Wang L. et al., 2023). The Wnt signaling pathway regulates various biological processes including development, self-renewal, and immune surveillance (Galluzzi et al., 2019; Nusse and Clevers, 2017). Inhibition of GSK3 triggers the Wnt pathway, and microproteophagy contributes to the degradation of GSK3 and its associated substrate, SMAD4 (Albrecht et al., 2018; Taelman et al., 2010). The degradation of GSK3 by Wnt, facilitated through microproteophagy, depends on the availability of methionine (Albrecht et al., 2019). This establishes a link between microautophagy's role and the regulation of pathways that influence the proliferation and survival of cancer cells. Furthermore, tumor cells may utilize MDV-induced micromitophagy to enhance their adaptability and survival, underscoring that targeting both macromitophagy and micromitophagy could enhance the efficacy of cancer therapies (Towers et al., 2021).

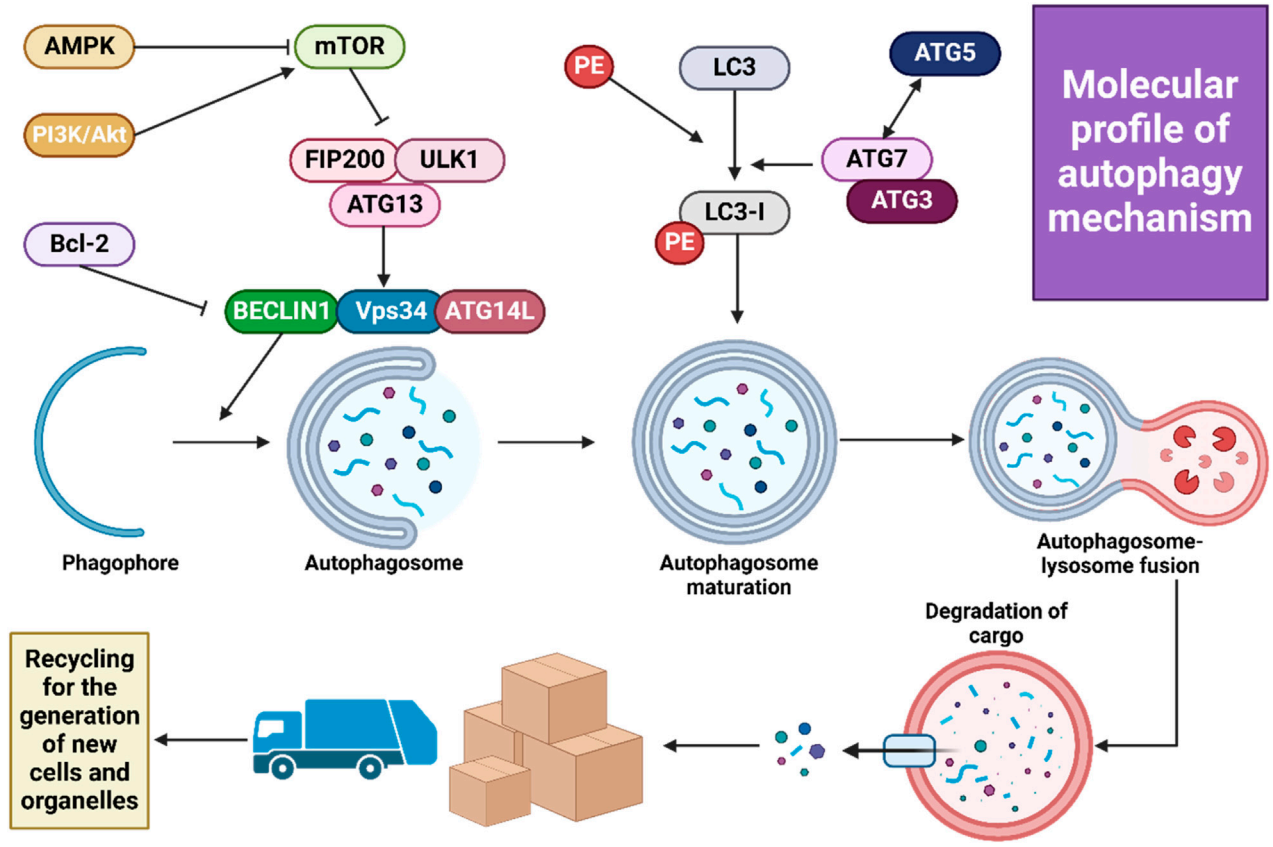

FIGURE 2
A schematic illustration of autophagy mechanism.

3.3 CMA

Three types of intracellular lysosomal degradation and autophagy exist, among which CMA is one (Assaye and Gizaw, 2022). CMA specifically targets proteins that are damaged or abnormal for degradation. It distinguishes itself from the other two types of autophagic processes in two keyways. Firstly, it uniquely requires the specific translocation of cargo proteins directly across the lysosomal membrane without enclosing them in a vesicle, allowing these proteins to enter directly into the lysosomal lumen (Auzmendi-Iriarte and Matheu, 2020). Secondly, CMA selectively degrades specific proteins from a larger pool, facilitated by a recognition motif similar to KFERQ found in proteins it targets (Xilouri and Stefanis, 2015). This selectivity enables CMA to degrade only the damaged or abnormal proteins without affecting the normal proteins, even if these are part of a multi-protein complex (Cuervo and Wong, 2014). Furthermore, CMA plays a crucial role in regulating various cellular processes by influencing levels of intracellular enzymes, transcription factors, and cell maintenance proteins. This impacts proteostasis, cellular energetics, and immune system functionality, depending on which proteins are selected for degradation at any given time (Auzmendi-Iriarte and Matheu, 2020; Cuervo and Wong, 2014). Figure 2 illustrates the macroautophagy mechanism.

The role of CMA in cancer therapy has garnered attention. For instance, FDW028 has been found to inhibit lysosomal proteolysis via CMA, which in turn can hinder metastasis in colorectal cancer (Wang M. et al., 2023). Additionally, CMA-mediated degradation of Dicer has been linked to increased metastasis in breast cancer cells (Su CM. et al., 2023). These findings suggest that CMA's function extends beyond promoting cell death; it also plays a critical role in regulating metastasis and invasion in cancer cells. In prostate cancer, the protein TPD52 has been observed to activate CMA through its interaction with HSPA8/HSC70, leading to enhanced substrate degradation. The upregulation of TPD52 is crucial for promoting growth and stress resistance in prostate cancer cells (Fan et al., 2021). Beyond influencing metastasis, CMA is implicated in regulating growth and drug resistance in various cancers (Ichikawa et al., 2020). Furthermore, CMA is capable of degrading IGF-1Rβ in pancreatic cancer, demonstrating its impact on other significant factors (Xue et al., 2019).

4 Autophagy machinery function in oncology

Studies involving cell cultures and pre-clinical animal models have demonstrated that autophagy, along with genome integrity and anti-inflammatory signaling pathways, plays a crucial role in maintaining tissue homeostasis and preventing pro-oncogenic conditions (Amaravadi et al., 2016; Mathew et al., 2009; Long and McWilliams, 2020). Although there are instances of polymorphisms and altered expression levels of ATG proteins, key autophagy genes are generally unmutated in human cancers (Jiang and Mizushima, 2014).

Additionally, autophagy genes are associated with either promoting or inhibiting tumor growth (White, 2015). The discovery of frequent loss of the autophagy regulator Beclin-1 (BECN1) in many cases of human breast, ovarian, and prostate cancers has shed light on the role of autophagy in oncology, suggesting that BECN1 may act as a tumor suppressor gene, particularly in individuals with only one functional copy (Yue et al., 2003; Qu et al., 2003; Karantza-Wadsworth et al., 2007). This theory is supported by findings in heterozygote Becn1 mice, which exhibit an elevated risk of developing hepatic, breast, and lymphoid tumors (Karantza-Wadsworth et al., 2007). While the status of BECN1 as a *bona fide* tumor suppressor remains under debate, its significant cellular role is undeniable (Li et al., 2017). In recent research, scientists created knock-in mice with a constitutively active Beclin-1 variant (Becn1F121A/F121A) that disrupts the interaction between endogenous Beclin-1 and its inhibitor Bcl-2. This alteration led to increased autophagic activity, improved overall health, extended lifespan, and a lower incidence of age-related spontaneous cancers in these mice (Fernández et al., 2018).

Research has identified patterns of overstimulated, understimulated, and deregulated autophagy (Ozpolat and Benbrook, 2015). The role of autophagy in cancer—whether it is oncogenic or tumor-suppressing—is still a subject of debate (Kroemer and Jäättelä, 2005; Ogier-Denis and Codogno, 2003; Scott et al., 2007; Dalby et al., 2010; Golstein and Kroemer, 2007; Tóth et al., 2002). Autophagy in cancer cells is influenced by various cellular factors, including gene mutations, abnormalities, the activation or inactivation of signaling pathways, and the level of cellular stress. Cancer cells often exhibit a higher rate of autophagy compared to normal cells, which can accelerate their proliferation. For instance, while normal breast epithelial cells typically display high levels of the Beclin-1 protein, these levels are significantly reduced or absent in breast cancer cells (Liang et al., 1999). Beclin-1 is monoallelically deleted in 40%–70% of human breast, prostate, and ovarian cancers (Liang et al., 1999; Qu et al., 2003; Karantza-Wadsworth et al., 2007; Saito et al., 1993), though biallelic mutations in Beclin-1 are rare in human tumors. Instead, other malignancies often show monoallelic deletions. In high-grade malignancies, such as prostate and ovarian cancers, autophagy tends to be downregulated (Liang et al., 2001; Gao et al., 1995). An initial study indicated that inhibiting Beclin-1 accelerated the progression of premalignant lesions caused by agents like the hepatitis B virus, enhanced the emergence of spontaneous cancers in the lung, liver, and lymphomas, and promoted mammary hyperplasia (Liang et al., 1999). This highlights how dysregulation of Beclin-1 and autophagy genes contributes to the development of human cancers. Subsequent research has linked abnormal autophagy to inflammation, DNA damage, genetic instability, insufficient cell turnover, and the production of reactive oxygen species (ROS), all of which are precursors to tumorigenesis and cancer (Table 2) (Karantza-Wadsworth et al., 2007).

5 Chemoresistance regulation by autophagy

Autophagy plays a role in drug resistance in cancer, with chemotherapeutic drugs often limited in their effectiveness due to their induction of protective autophagy, leading to chemoresistance (Hill and Wang, 2020). For instance, cisplatin, commonly used in treating various cancers including ovarian cancer, activates autophagy through the ERK pathway, thereby promoting drug resistance in these cells (Wang and Wu, 2014). Inhibition of autophagy has been shown to sensitize cancer cells to cisplatin (Bao et al., 2015; You et al., 2019), with similar results in lung cancer (Lee et al., 2015). In esophageal cancer, cisplatin-induced autophagy via the class III PI3K pathway enhances treatment efficacy when combined with the autophagy inhibitor 3-Methyladenine (Liu et al., 2011). Similarly, 5-FU, which inhibits DNA synthesis (Park et al., 2013), also induces autophagy leading to chemoresistance (Shuhua et al., 2015). Blocking autophagy has enhanced the effectiveness of 5-FU in colorectal cancer, where ATG genes have been linked to multi-drug resistance (Li et al., 2010). Activation of c-Jun N-terminal kinases (JNK) and phosphorylation of Bcl-2 are key mechanisms in 5-FU-induced autophagy in colon cancer, providing protection to cancer cells (Park et al., 2013). This phenomenon is also observed in gallbladder carcinoma, where inhibiting autophagy with chloroquine enhances the cytotoxic effects of 5-FU (Liang X. et al., 2014). In estrogen receptor-positive breast cancer, suppression of autophagy can resensitize cells to tamoxifen (Samaddar et al., 2008). In prostate cancer, elevated levels of the tumor suppressor candidate gene, nitrogen permease regulator-like 2, increase resistance to Everolimus by enhancing autophagy via the mTOR pathway (Chen et al., 2019). Autophagy also interacts with apoptosis, often protecting cancer cells from drug-induced cell death. In breast cancer, treatment with Epirubicin induces autophagy in MCF-7 cells, shielding them from apoptosis. However, inhibition of autophagy can resensitize these drug-resistant cells to therapy (Sun et al., 2011). In osteosarcoma, common chemotherapeutics induce overexpression of HSP90AA1, regulating autophagy through the PI3K/Akt/mTOR pathway and apoptosis through JNK/p38, highlighting the intricate interactions of these pathways in drug resistance (Xiao et al., 2018). A comprehensive understanding of these mechanisms is vital for developing new treatments. Novel strategies are emerging that target drug resistance by inhibiting autophagy, enhancing the efficacy of chemotherapy (An et al., 2015; O'Donovan et al., 2011; Zhang et al., 2016; Zhang et al., 2010; Fan et al., 2010; Ahn and Lee, 2011; Carew et al., 2007; Ge et al., 2014). Combining anti-cancer drugs with autophagy inhibitors, such as using cisplatin with autophagy suppression, has increased cytotoxicity in cells (Su et al., 2017; Claerhout et al., 2010). Similarly, pairing 5-FU with the autophagy inhibitor hydroxychloroquine has shown increased effects in colon cancer (Sasaki et al., 2010).

Autophagy is thought to play a crucial role in both the development of cancers and their treatment (Pu et al., 2022). Although many patients experience significant benefits from chemotherapy, acquired drug resistance has become a major obstacle to successful treatment. Numerous studies have demonstrated that a variety of chemotherapeutic agents can induce autophagy (Condello et al., 2020; Ashrafizadeh et al., 2020b), which is linked to increased resistance to chemotherapy. Chemotherapy typically triggers apoptosis in cancer cells, but these cells often

initiate autophagy as a defense mechanism to avoid apoptosis, thereby reducing the efficacy of the treatment. Liu et al. (2013) used MTT and Hoechst 33342 staining, along with flow cytometry, to detect apoptosis in A549 lung cancer cells post-chemotherapy. They also employed the autophagy inhibitor 3-methyladenine (3-MA) to explore the relationship between autophagy and apoptosis. Their findings indicated that drugs like cisplatin (DDP) and paclitaxel can induce both autophagy and apoptosis in A549 cells. Additionally, studies have revealed that autophagy can render salivary gland adenoid cystic carcinoma cells resistant to DDP, often leading to chemotherapy failure (Tan et al., 2020). Using transmission electron microscopy, the autophagy marker LC3 can be identified, and the presence of minimal levels of p62 also suggests autophagy triggered by DDP. Moreover, downregulating Beclin-1 using 3-MA or RNA interference has been shown to increase apoptosis induced by DDP. As a result, the activation of protective autophagy by chemotherapy contributes to an increase in chemotherapeutic resistance in tumor cells.

6 SIRT1: Cellular functions and oncological importance

6.1 Structure and cellular functions

Sirtuins are characterized by a conserved catalytic domain, NAD + binding domains, and variable NH2- and COOH-terminal sections (Jiao and Gong, 2020; Frye, 1999; Yamamoto et al., 2007). These proteins differ in their functions, catalytic activities, and cellular localizations, influenced by their distinct amino acid sequences. Human sirtuins are classified into four categories: Class I, closely related to yeast Sir2, includes SIRT1, SIRT2, and SIRT3; Class II consists of SIRT4; Class III is represented by SIRT5; and Class IV includes both SIRT6 and SIRT7 (Frye, 2000). SIRT1, which is composed of 747 amino acids, features the longest terminal extensions, including a conserved catalytic core (244–512 residues), a COOH-terminal region (1–180 residues), and an NH2-terminal region (513–747 residues) (Kumar and Chauhan, 2016). The nuclear localization signal (KRKKRK) within the 41–46th residues of SIRT1 explains its presence in the nucleus (Frye, 1999). However, SIRT1 is also found in the cytoplasm in some cell types, indicating dual localization (Jin et al., 2007; Moynihan et al., 2005; Stünkel et al., 2007). SIRT1's ability to shuttle between the nucleus and cytoplasm (Yanagisawa et al., 2018) is regulated by nuclear import and export sequences within its NH2-terminal region (Tanno et al., 2007). Other sirtuins have distinct subcellular locations: SIRT2 typically resides in the cytoplasm, though it can shuttle to the nucleus (North et al., 2003; Inoue et al., 2007); SIRT3, SIRT4, and SIRT5 are primarily mitochondrial, with SIRT3 being shown to move to the mitochondria from the nucleus post UV exposure or etoposide treatment (Scher et al., 2007). SIRT6 and SIRT7, like SIRT1, are located in the nucleus, with SIRT7 localized specifically to the nucleolus and SIRT6 associated with chromatin (Michishita et al., 2005). SIRT1 plays a significant role in regulating various biological and cellular processes, such as aging, metabolism, and inflammation (Chen et al., 2021). Figure 3 illustrates the functions of SIRT1 in these biological events.

6.2 Role in cancer

Despite the cellular functions of SIRT1, increasing evidence has underscored its role as a potential regulator of tumorigenesis. SIRT1 interacts with various signaling networks to influence the carcinogenesis process. It is upregulated in colorectal cancer and downregulates p53 expression through deacetylation, reducing miR-101 levels, while enhancing KPNA3 expression to promote metastasis and drug resistance (Wang XW. et al., 2023). Additionally, cytoplasmic SIRT1 may contribute to the formation and survival of polypoid giant tumor cells, leading to paclitaxel resistance in ovarian tumors (Xu H. et al., 2023). Conditions such as glucose deprivation and oxidative stress can trigger SIRT1 upregulation, which mediates β-catenin deacetylation, facilitating its transfer from the nucleus to the cytoplasm to decrease glycolysis and enhance fatty acid oxidation (Wei et al., 2023). Importantly, USP14 can increase the stability of SIRT1 by preventing its deubiquitination, promoting fatty acid oxidation in macrophages, which leads to M2 polarization and tumorigenesis (He et al., 2023). In terms of SIRT1's oncogenic role, inhibiting it can disrupt tumorigenesis; for instance, LITAF increases FOXO1 levels, leading to SIRT1 downregulation, which diminishes the stemness and malignant phenotype of tumor cells (Guan et al., 2023). SIRT1 also regulates fatty acid oxidation in tumor cells. NSD2 boosts SIRT1 expression through interaction with AROS, enhancing fatty acid oxidation and reducing responsiveness to radiotherapy (Luo H. et al., 2023). Propofol's potential as an anti-cancer agent in reducing tumor metastasis is partly attributed to the downregulation of SIRT1 (Wang R. et al., 2023). The transfer of SIRT1 via extracellular vesicles can activate the CD24/Siglec-10 axis, increasing apoptosis in $CD8^+$ T cells and accelerating carcinogenesis (Zheng Q. et al., 2024). Moreover, SIRT1 regulates cell death mechanisms in cancers, such as inhibiting ferroptosis via p53 downregulation, thereby enhancing the survival of gastric tumor cells (Zhao H. et al., 2023). The following sections will delve deeper into the role of SIRT1 in autophagy regulation and associated molecular pathways (Table 3).

When compared to the non-cancerous tissues that were next to EC tissues, ENST00000534735 in EC tissues was dramatically downregulated (Shan et al., 2024). In addition to facilitating apoptosis and pyroptosis, the ectopic expression of ENST00000534735 significantly stopped the capacity of lung cancer cells to proliferate and migrate. The elevation of OSBPL3 through the APMK/SIRT1/NF-κB pathway was able to counteract the tumor-suppressing effects of ENST00000534735 overexpression. This was accomplished by knocking down ENST00000534735, which resulted in an increase in OSBPL3 expression. An excessive amount of ENST00000534735 expression was shown to inhibit the development of EC in the *in vivo* tumorigenic experiments that were carried out on nude mice. Another study identifies SIRT1 as a target of ISGylation, a post-translational modification by ISG15, which enhances SIRT1's deacetylase activity by disrupting its interaction with the inhibitor DBC1 (Kang et al., 2024). SIRT1 ISGylation promotes lung cancer progression and reduces the sensitivity of lung cancer cells to DNA damage-based therapies. Elevated ISG15 and SIRT1 levels in lung cancer tissues correlate with poor patient prognosis, suggesting that these biomarkers could aid

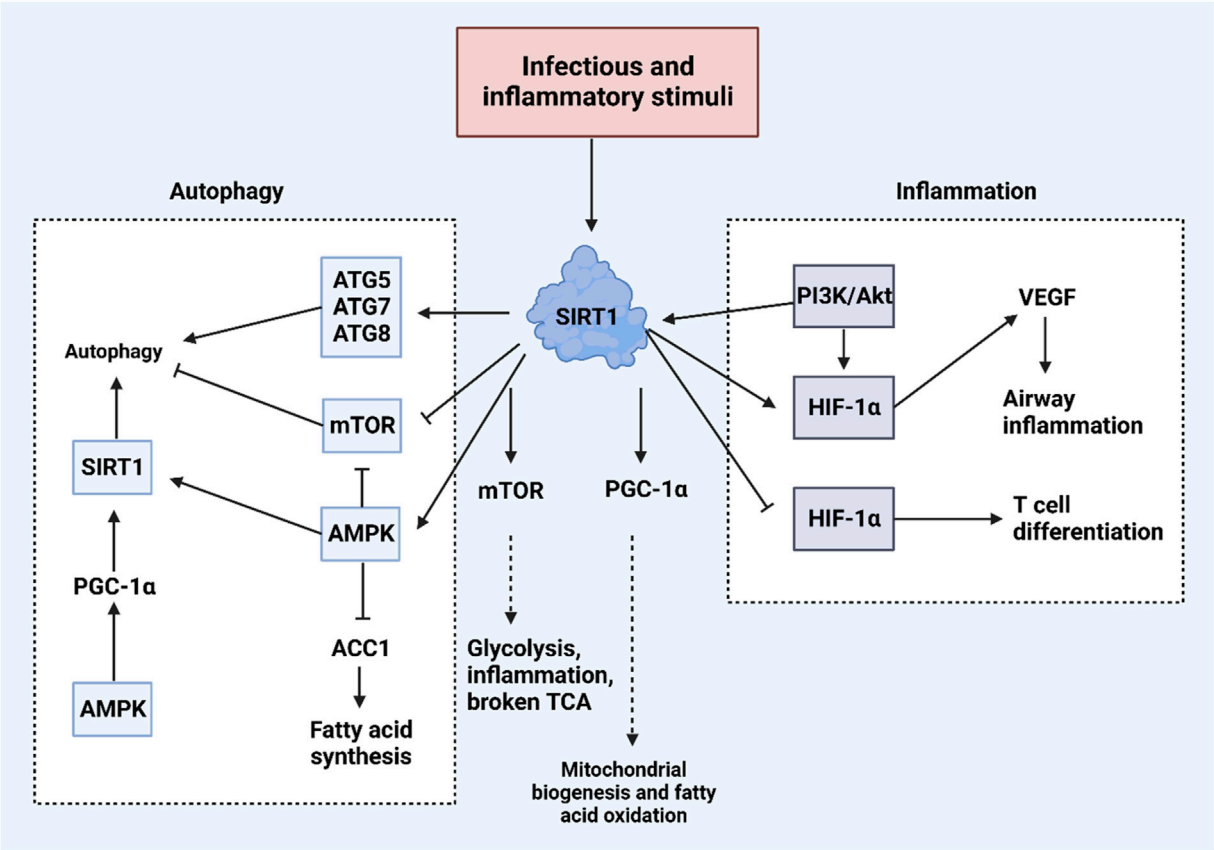

FIGURE 3
An overview of biological and cellular functions of SIRT1. Exposure to infectious and inflammatory stimuli can lead to an increase in SIRT1 expression, which plays a crucial role in regulating both inflammation and autophagy within cells. SIRT1 enhances autophagy by increasing the levels of ATG proteins such as ATG5, ATG7, and ATG8. Additionally, SIRT1 activates AMPK and suppresses mTOR, further promoting autophagy. In terms of regulating inflammation, SIRT1 interacts with the PI3K/Akt pathway and HIF-1α, illustrating its comprehensive role in cellular response mechanisms. (Kim et al., 2022).

in patient stratification and outcome evaluation. SIRT1 downregulation in oral cancer cells leads to mitochondrial hyperfusion and drug resistance, while SIRT1 overexpression or activation by gallic acid reverses this effect, promoting apoptosis and restoring cisplatin sensitivity (Patra et al., 2023a). SPC-180002, a novel dual inhibitor of SIRT1/3, disrupts redox homeostasis and mitochondrial function, leading to cell cycle arrest and strong inhibition of cancer cell growth (Cho et al., 2023). MiR-653–3p promotes genomic instability, proliferation, migration, and chemoresistance in colorectal cancer cells by inhibiting SIRT1 and activating the TWIST1 signaling pathway (Wang H. et al., 2023). Doxorubicin-induced SIRT1 promotes redox imbalance and chemoresistance in breast cancer by enhancing cell proliferation, angiogenesis, and metastasis through NRF2 activation and increased glutathione levels (Sahoo et al., 2024). SIRT1 deacetylates and enhances KRASMut activity in lung cancer, and inhibiting SIRT1 or activating p300, which acetylates KRASMut, sensitizes tumors to cisplatin and erlotinib, offering a potential combination therapy for KRASMut lung cancer (Shin et al., 2023). Resveratrol inhibits neutrophil extracellular trap formation by targeting SIRT1, thereby reducing breast cancer metastasis and promoting $CD8^+$ T cell infiltration in a murine model (Yu W. et al., 2023). Therefore, increasing evidences highlight the function of SIRT1 in the regulation of cancer progression and interaction with various molecular pathways (Wang XW. et al., 2023; Xu H. et al., 2023; Li X. et al., 2023; Zhang X. et al., 2023; Liu S. et al., 2024).

7 General discussion of SIRT1 in autophagy regulation in cancer

The process of mitotic chromosomal condensation is largely dependent on the presence of condensin (Hirano, 2002). Condensin I and condensin II are the names given to the two distinct forms of condensin complexes that may be found in a wide variety of eukaryotic cells (Hirano et al., 1997). The conventional condensin complex is composed of three distinct non-SMC subunits in addition to the same pair of core subunits that are referred to as structural maintenance of chromosomes (SMC) family proteins (Kimura and Hirano, 2000). Within human cells, the non-SMC subunits of condensin I are denoted by the letters NCAPD2, NCAPG, and NCAPH. On the other hand, the comparable subunits in the condensin II complex are denoted by the letters NCAPD3,

TABLE 2 Autophagy with dual function in cancer progression and suppression.

Autophagy action	Highlight	Reference
Pro-death	CircTICRR suppresses autophagy through HuR binding and increasing GLUD1 stability Silencing circTICRR induces autophagy to increase apoptosis	Zhu et al. (2022)
Pro-death	Autophagy can reduce the oncogenic function of YAP in pancreatic tumor	Sun et al. (2021a)
Pro-death	COPZ1 deficiency increases NCOA4 expression to induce autophagy and ferroptosis in glioblastoma	Zhang et al. (2021)
Pro-survival	Platycodin D impairs autophagy through LDLR overexpression to facilitate cell death in glioblastoma	Lee et al. (2022a)
Pro-death	Sendeng-4 stimulates autophagy and apoptosis to reduce the progression of melanoma	Du et al. (2021)
Pro-death	TSPAN9 accelerates autophagy to elevate 5-fluorouracil sensitivity in gastric cancer	Qi et al. (2020)
Pro-survival	The suppression of protective autophagy promotes apoptosis induction by melatonin in the treatment of glioblastoma	Zhou et al. (2019)
Pro-survival	Angelicin stimulates mTOR signaling to inhibit autophagy in cancer therapy	Wang et al. (2019a)
Pro-survival	LncRNA MITA1 mediates protective autophagy in lung cancer in elevating gefitinib resistance	Hu et al. (2021)
Pro-death	TIGAR downregulation by decitabine can promote apoptosis and autophagy in leukemia	Li et al. (2021)

NCAPG2, and NCAPH2 (Hirano et al., 1997). Condensin I has three non-SMC subunits, and one of them is called NCAPD2. This component may be found on chromosome 12p13.3. Previous research on NCAPD2 has mostly concentrated on its role in mitotic chromosomal condensation and segregation. This is because NCAPD2 is an essential component of the cell cycle. In addition, a number of studies have demonstrated that NCAPD2 is linked to a number of neurodevelopmental diseases, including Alzheimer's disease, autism, Parkinson's disease, and others, which suggests that it may have a function in the development of the central nervous system (Lee et al., 2008; Li et al., 2009; Sanders et al., 2012; Zhang et al., 2014). The abnormal expression of NCAPD2 in triple-negative breast cancer has the potential to function as an independent prognostic factor (Zhang et al., 2020). Through its involvement in the Ca2+/CAMKK/AMPK/mTORC1 pathway and the PARP-1/SIRT1 axis, NCAPD2 is able to suppress autophagy and impede autophagic flux. NCAPD2 is a tumor promoter that may be found in both *in vitro* and *in vivo* settings. In an AOM/DSS-induced mouse model, suppression of the development of colorectal cancer by NCAPD2 deletion is seen (Jing et al., 2021). 4-dmH targets tNOX and SIRT1, inhibiting their activity and inducing apoptosis (Islam et al., 2024a). SIRT1 in EML4-ALK G1202R and EML4-ALK L1196M mutant drug-resistant cells was downregulated compared with EML4-ALK NSCLC cells (Yang et al., 2024). The high expression of SIRT1 was related to the longer survival time of patients with lung cancer. Activation of SIRT1 induced autophagy and suppressed the invasion and migration of mutant cells. Further experiments indicated that the activation of SIRT1 inhibited the phosphorylation level of mTOR and S6K by upregulating the expression of AMPK, thus activating autophagy. SIRT1 can significantly enhanced the sensitivity of mutant cells to crizotinib, improved its ability to promote apoptosis of mutant cells, and inhibited cell proliferation.

A number of transcription factors, including p53, E2F1, FOXO, NF-θβ, and c-Myc, have been identified as targets for SIRT1 (Mao et al., 2014). These interactions are responsible for the formation of cancer and the spread of disease to other parts of the body in a variety of malignancies (Ayob and Ramasamy, 2018; Wong et al., 2021; Ong and Ramasamy, 2018). Overexpression of SIRT1 in HCC has the potential to contribute to the survival and proliferation of tumor cells (Chen et al., 2011; Jang KY. et al., 2012; Molla et al., 2020), as well as to the promotion of metastasis (Hao et al., 2014). SIRT1 is mostly found in the nucleus, where it plays a function in the development of tumors. However, it has been suggested that cytoplasmic sirtuin 1 may play a role in the suppression of tumors in HCC (Farcas et al., 2019; Song et al., 2014). SIRT1 is also known to influence chemoresistance in a variety of malignancies, including ovarian, breast, and gastric cancers (An et al., 2020; Mvunta et al., 2017; Wang et al., 2019b). However, the involvement of SIRT1 in the chemoresistance of HCC is not well understood. A study investigates the role of SIRT1 in sorafenib-resistant HCC, revealing that increased SIRT1 levels promote autophagy and activate NF-κβ signaling in resistant cells (Chan et al., 2024). Silencing SIRT1 downregulates autophagy and restores NF-κβ activity by failing to deacetylate key proteins, suggesting that the SIRT1/autophagy/NF-κβ axis plays a crucial role in HCC progression and resistance, with potential implications for therapeutic strategies.

There was a significant amount of RACGAP1 found in the cells of stomach cancer. Gastric cancer cell proliferation, migration, and invasion were all enhanced when RACGAP1 was overexpressed (Yan et al., 2024). In addition, the inhibition of RACGAP1 led to the induction of autophagy and death in cells. In addition, the expression of SIRT1 and Mfn2 was also inhibited by RACGAP1. In the tissues of EC tumors, FIRRE and SIRT1 were found to be elevated, whereas miR-199b-5p was shown to be downregulated. By

sponging miR-199b-5p and suppressing autophagy, FIRRE knockdown was able to improve the susceptibility of EC cells to radiation doses (Cai et al., 2024). The microRNA known as miR-199b-5p was able to act as a negative regulator of SIRT1. In the absence of this information, SIRT1 has the potential to deacetylate BECN1 protein and take part in FIRRE-mediated autophagy. The activation of FIRRE resulted in an enhancement in the sensitivity of EC radiation *in vivo*. By inhibiting autophagy and proliferation, as well as inducing apoptosis in HCT116 and HT29 cells, ZMIZ1 knockdown was found to have a substantial therapeutic effect (Huang et al., 2024). Both the mRNA level of SIRT1 and the protein level of the SIRT1-specific substrate, acetylated FOXO3a, were considerably reduced as a result of ZMIZ1 knockdown. However, the mRNA level of SIRT1 was not changed by the knockdown. The relationship between SIRT1 and ZMIZ1 in HCT116 and HT29 cells was brought to light by immunoprecipitation tests. There was an increase in the intracellular ubiquitination of SIRT1 due to ZMIZ1. The effects of ZMIZ knockdown on proliferation, autophagy, and apoptosis in HCT116 and HT29 cells were reduced by targeting SIRT1 by knockdown or pharmacological inhibition. The drug-resistant oesophageal cancer cells exhibit increased autophagy and SIRT1 expression, both of which are linked to enhanced cell migration and the EMT (Zhang et al., 2024b). Inhibiting autophagy or SIRT1 reduced these processes. Additionally, a SIRT1 inhibitor effectively suppressed tumor growth in a mouse xenograft model without significant toxicity, suggesting that SIRT1 plays a key role in autophagy-driven drug resistance in oesophageal cancer. The adipose triglyceride lipase (ATGL) is highly expressed in CRC and is associated with poor prognosis (Su BC. et al., 2023). ATGL promotes CRC cell proliferation by inhibiting the mTOR signaling pathway and activating autophagy. Additionally, ATGL regulates autophagy by increasing SIRT1 expression. These findings suggest that ATGL contributes to CRC growth through the upregulation of autophagy and SIRT1. The electro-acupuncture (EA) can alleviate CRC in mice by reducing inflammation and promoting autophagy through the SIRT1/miR-215/Atg14 axis (Li J. et al., 2023). EA treatment decreased tumor numbers, inflammation, and DAI scores, while increasing body weight and SIRT1 expression. SIRT1 overexpression was shown to suppress miR-215 and enhance Atg14 expression, suggesting that EA exerts its anti-CRC effects by regulating this molecular pathway. The ubiquitin-conjugating enzyme E2C (UBE2C) promotes the malignant progression of endometrial cancer by inhibiting autophagy (Zhao R. et al., 2023). UBE2C suppresses autophagy by inducing ubiquitination and degradation of SIRT1, leading to reduced expression of autophagy-related genes. Knockdown of UBE2C in cancer cells enhanced autophagy and increased apoptosis, while overexpression of UBE2C promoted tumor growth in a mouse model. However, rapamycin, an autophagy activator, reversed the tumor growth and apoptosis inhibition caused by UBE2C overexpression. SIRT1 regulates mitotic catastrophe (MC) through autophagy and BubR1 signaling. Degradation of SIRT1 increased MC, while overexpression of SIRT1 reduced MC by decreasing apoptotic and multinuclear cells and promoting autophagy. Additionally, SIRT1 was shown to bind to the promoter of BubR1, a key component of the spindle assembly checkpoint, increasing its expression and reducing MC (Zhao et al., 2022).

8 SIRT1/AMPK axis in autophagy regulation

AMPK, a crucial metabolic regulator, restores depleted ATP levels and maintains energy balance, especially when cells are stressed. Targeting AMPK has shown promise in treating metabolic syndrome and type 2 diabetes (Steinberg and Kemp, 2009; Yuan et al., 2023). AMPK enhances metabolic processes by inhibiting glucose production in the liver, improving insulin sensitivity, reducing fatty acid synthesis and esterification, increasing glucose uptake in muscles, and reducing proinflammatory changes (Ruderman and Prentki, 2004). Small molecules such as cellular AMP allosterically activate AMPK by binding to the CBS1 domain, while AMP or ADP binding to CBS3 alters AMPK's phosphorylation status (Xiao et al., 2011). These interactions trigger structural changes in the AMPK complex, enabling phosphorylation at the Thr-172 site on the AMPKα subunit (Hawley et al., 1996; STEIN et al., 2000), and are further enhanced by various upstream kinases that also phosphorylate the Thr-172 site, fully activating AMPK (Liu et al., 2014). AMPK acts as a regulator of autophagy in various cancers, with growing evidence suggesting that SIRT1 serves as an upstream mediator of AMPK in this role. Quercetin, a natural compound, induces apoptosis and toxic autophagy in lung cancer, where increased SIRT1 levels upregulate AMPK, leading to autophagy-mediated apoptosis (Guo et al., 2021). Similarly, ghrelin enhances SIRT1 expression to activate AMPK and induce autophagy, although this SIRT1/AMPK-mediated autophagy does not significantly trigger apoptosis (Heshmati et al., 2020). The SIRT1/AMPK axis has been studied across different tumor types, influencing tumorigenesis progression. For example, diallyl trisulfide induces pro-death autophagy in hepatocellular carcinoma through the AMPK/SIRT1 axis (Sun et al., 2022). Additionally, since mTOR is downstream of AMPK, SIRT1's regulation of AMPK impacts mTOR, a key autophagy regulator (Ye et al., 2017). Calycosin activates the SIRT1/AMPK axis to inhibit the Akt/mTOR pathway, stimulating autophagy-mediated apoptosis in cancer cells (El-Kott et al., 2019). Nitrosative stress can also induce autophagy in breast cancer by upregulating SIRT1 and its interaction with AMPK (Chakraborty et al., 2019). Thus, SIRT1 is integral in regulating AMPK and downstream targets, influencing autophagy in human cancers.

9 SIRT1/mTOR axis in autophagy regulation

mTOR, a highly conserved serine/threonine kinase, orchestrates cellular metabolism, proliferation, and apoptosis (Xie et al., 2023). It forms two distinct complexes: mTOR complex 1 (mTORC1) and mTOR complex 2 (mTORC2), with mTORC1 being more sensitive to rapamycin and containing the regulatory-associated protein of mTOR (RAPTOR) (Ben-Sahra and Manning, 2017). mTOR responds to three main types of upstream signals: immune activation, environmental stress, and nutrient availability (Chi, 2012). These signals can either upregulate or downregulate mTOR, influencing cell growth, division, and survival, as well as regulating protein synthesis and catabolism. Downstream of mTOR, translational regulation is mediated by factors such as the eIF4E binding protein 1 (4E-BP1) and p70S6 Kinase (S6 Kinase),

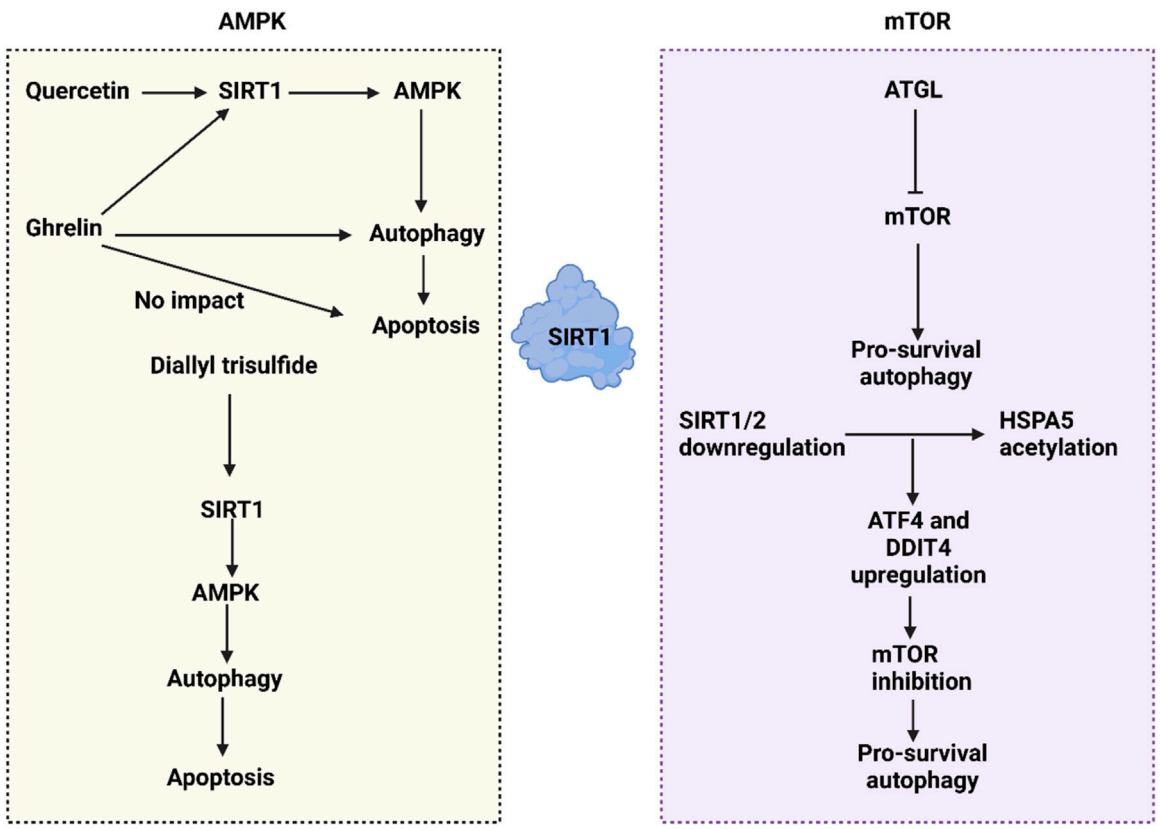

FIGURE 4
The SIRT1-mediated autophagy regulation in cancer through affecting mTOR and AMPK pathways. The interaction between SIRT1 and AMPK clearly illustrates that SIRT1 upregulates AMPK to promote autophagy. Various compounds influence the SIRT1/AMPK axis; for example, quercetin activates the SIRT1/AMPK/autophagy pathway to stimulate apoptosis. Ghrelin also activates the SIRT1/AMPK/autophagy axis, though it does not lead to cell death. Additionally, the downregulation of SIRT1/2 enhances the acetylation of HSPA5, which in turn increases ATF4 and DDIT4 levels, leading to the downregulation of mTOR and facilitating pro-survival autophagy.

illustrating another facet of mTOR signaling (Zou et al., 2020; Tan and Miyamoto, 2016; Kennedy and Lamming, 2016). SIRT1 interacts with mTOR to regulate autophagy in human cancers. For instance, ATGL, identified as an oncogenic factor in colorectal tumors, promotes proliferation and correlates with poor prognosis by downregulating mTOR, thus facilitating pro-survival autophagy (Su BC. et al., 2023). SIRT1 regulators have emerged as autophagy modulators in cancer. MHY2245, an inhibitor of SIRT1, suppresses the PKM2/mTOR axis, stimulating autophagy and accelerating apoptosis, which leads to growth reduction in ovarian tumors (Yousafzai et al., 2021). The downregulation of SIRT1/2 can induce protective autophagy in lung cancer by increasing the acetylation of HSPA5, which in turn elevates ATF4 and DDIT4 levels, suppressing mTOR and promoting pro-survival autophagy (Mu et al., 2019). Thus, both AMPK and mTOR play significant roles in the regulation of autophagy in human cancers (Figure 4).

10 SIRT1-mediated autophagy regulation in cancer drug resistance

A major challenge in oncology is the issue of drug resistance, a problem that shares similarities with antimicrobial therapy in terms of rapidly adapting threats, primarily originating from within, such as cancerous cells, and to a lesser extent from external sources like bacteria. Early chemotherapeutics such as nitrogen mustard and aminopterin were initially effective, putting many tumors into remission. However, similar to antimicrobial chemotherapy, they often led to drug resistance and disease relapse. Drawing on strategies from antimicrobial therapy, oncology first attempted to overcome resistance through polychemotherapy, which involves administering a sequence of drugs, each with a different mechanism of action. This approach has been empirically successful in treating certain diseases like some types of lymphoma, breast cancer, and testicular cancer. Consequently, combination chemotherapy became the foundation of systemic cancer treatment, frequently used alongside surgery and tailored radiation therapy. Over time, these combinations grew more complex, and dose intensity strategies were introduced to enhance antitumor efficacy. This involved reducing intervals between chemotherapy cycles or increasing drug dosages, supported by myeloid and other growth factors to manage drug-induced myelotoxicity and sustain ongoing treatment. Despite nearly 5 decades of success, by the early 21st century, it became evident that surgery, radiation, and combination chemotherapy were not curative for many types of tumors (Vasan et al., 2019; Goodman et al., 1946; Farber and Diamond, 1948; Crofton, 1959;

DeVita et al., 1980; Bonadonna et al., 1976; Bosl et al., 1986; Hryniuk and Bush, 1984; Citron et al., 2003; Sternberg et al., 2001).

Chemotherapy drugs induce mitochondrial dysfunction to trigger apoptosis in tumor cells. Conversely, CDK9 inhibitors enhance the stability and dephosphorylation of SIRT1. Subsequently, elevated SIRT1 levels lead to the degradation of FOXO3, which in turn suppresses BNIP3-induced stability of PINK1. Additionally, CDK9 inhibitors can inhibit the SIRT1/FOXO9/BNIP3 axis and the PINK1/PRKN pathway, thereby suppressing mitophagy. This inhibition of mitophagy by CDK9 inhibitors contributes to increased mitochondrial dysfunction, ultimately promoting apoptosis in hepatocellular carcinoma (Yao et al., 2022). Despite evidence suggesting that increased stability and upregulation of SIRT1 can suppress mitophagy and enhance apoptosis, some findings overexpressed SIRT1 can facilitate drug resistance in tumor cells. Specifically, SIRT1 can mediate the deacetylation of Beclin-1, which activates protective autophagy and promotes resistance to cisplatin in bladder cancer (Sun et al., 2023).

Autophagy induction during tumorigenesis serves to supply cancer cells with the necessary components for growth by degrading organelles and proteins (White et al., 2015). Modifying autophagy levels has emerged as a promising strategy in cancer treatment (Li et al., 2017). Lipophagy, a selective form of autophagy that degrades lipids, plays a role in modulating lipid metabolism and maintaining intracellular lipid homeostasis (Zhang et al., 2018). Various genes, enzymes, transcription regulators, and other molecules regulate lipophagy (Maan et al., 2018; Madrigal-Matute and Cuervo, 2016). Additionally, *de novo* lipogenesis is linked to the development of drug resistance in cancer (Zhang et al., 2018; Maan et al., 2018; Beloribi-Djefaflia et al., 2016). For instance, low expression of miR-425 can elevate SIRT1 levels, thereby stimulating pro-survival lipophagy and enhancing resistance to sorafenib in liver cancer (Sun G. et al., 2021). Conversely, the independent regulation of SIRT1 and autophagy can also influence drug resistance. Jaridon 6, for example, inhibits the PI3K/Akt/mTOR axis to induce autophagy and reduces SIRT1 expression, weakening drug resistance in gastric tumors (Fu et al., 2021). A notable aspect of SIRT1-mediated autophagy is its role in various human cancers. The lncRNA H19, which has oncogenic properties in colorectal cancer, mediates 5-fluorouracil resistance by sponging miR-194–5p to elevate SIRT1 expression, thus promoting autophagy-induced resistance to 5-fluorouracil in colorectal tumors (Wang et al., 2018). Thus, the interaction between SIRT1 and autophagy plays a critical role in determining the responsiveness of tumor cells to chemotherapy.

11 SIRT1-mediated autophagy and apoptosis crosstalk

11.1 Basics of apoptosis

During the initiation and intermediate stages of apoptosis, a variety of metabolic activities occur alongside significant morphological changes. These changes include cytoplasmic filament aggregation, nuclear membrane shrinkage, cell fragmentation, the formation of apoptotic bodies, and plasma membrane blebbing (Elmore, 2007; Power et al., 2002). These changes are mainly observed in the nucleus, cell membrane, cytoplasm, and mitochondria, and can be detected through microscopic, light, and fluorescence microscopy methods (Elmore, 2007; Savill and Fadok, 2000). Apoptosis is triggered by environmental signals originating from two primary sources: external signals from other cells and signals from physical contact with adjacent cells. At the onset of apoptosis, cells begin to lose contact with neighboring cells and tightly pack their internal components without releasing them outside, thus preventing inflammation and contamination in the surrounding environment (Rosenblatt et al., 2001; Ferri and Kroemer, 2001). Surrounding cells recognize these apoptotic cells and facilitate their internalization and degradation without triggering an inflammatory response. Apoptosis proceeds via two major pathways: intrinsic and extrinsic. The extrinsic pathway is activated by the interaction of death receptors with their ligands, leading to the activation of caspase 8. This activation can directly induce cell death or further activate caspase 3 or Bid, a process that can be inhibited by cellular FLICE-like inhibitory proteins (cFLIP) (Kiraz et al., 2016). The intrinsic pathway, on the other hand, is initiated by genomic damage and proceeds via the mitochondrial pathway. This involves the activation of Bax, a pro-apoptotic member of the Bcl-2 family. At the mitochondrial membrane, anti-apoptotic proteins such as Bcl-2 and Bcl-XL inhibit Bax's activity. The release of cytochrome c from mitochondria leads to the formation of apoptosomes, complexes involving cytochrome c, APAF-1, and procaspase 9. The assembly of these complexes triggers the caspase activation cascade, converting procaspase-3 to active caspase 3. Bid, another pro-apoptotic Bcl-2 family member, facilitates communication between the intrinsic and extrinsic pathways. Caspase 8 cleavage of Bid enhances the release of mitochondrial cytochrome C, further driving the apoptotic process (Kiraz et al., 2016).

11.2 SIRT1-mediated autophagy and apoptosis crosstalk

The interactions between autophagy and apoptosis play a crucial role in human cancers, with SIRT1 acting as a key mediator. This section discusses the relationship between SIRT1-induced autophagy and apoptosis. SIRT1 upregulation is essential for initiating autophagy. UBE2C promotes the ubiquitination of SIRT1, leading to its degradation and decreased stability, which in turn reduces H4K16 deacetylation, suppressing autophagy at an epigenetic level. In endometrial cancer, autophagy is critical for inducing apoptosis, hence UBE2C's regulation of autophagy affects the autophagy-apoptosis interplay (Zhao R. et al., 2023). In some cases, autophagy can inhibit apoptosis in human cancers. For instance, SIRT1 translocation from the nucleus to the cytoplasm increases Beclin-1 expression, thereby promoting autophagy. This protective autophagy then inhibits the release of cytochrome C from mitochondria, suppressing the caspase-3/PARP pathway and preventing apoptosis in bladder cancer (Sun et al., 2023). Additionally, the response of autophagy to cellular stress is pivotal, as evidenced by increased SIRT1 and FoxO1 levels under glucose deprivation in gastric cancer, which boosts Rab7 expression

and autophagy, supporting tumor cell survival. Conversely, inhibiting autophagy can enhance apoptosis, underscoring the supportive role of autophagy in this context (Zhu M. et al., 2023). In colorectal cancer, SIRT1 typically stimulates autophagy to inhibit apoptosis. However, using catalpol, a natural product with anticancer and epigenetic properties, leads to miR-34a upregulation, which suppresses the SIRT1/autophagy axis and triggers apoptosis in colorectal tumor cells (Qiao et al., 2020). Although SIRT1 is primarily seen as an upstream autophagy mediator in cancers, autophagy can also influence SIRT1, impacting tumorigenesis regulation. For example, autophagy-induced SIRT1 degradation can enhance radiotherapy-mediated apoptosis in prostate cancer, showing its potential to reduce radio-resistance (Wang et al., 2022). Epigenetic modifications and miRNA dysregulation in tumor cells also affect cancer progression and treatment responses (Ashrafizadeh et al., 2021). In lung cancer, miR-124 and miR-142 downregulation of SIRT1 suppresses supportive autophagy, enhancing cisplatin sensitivity and promoting apoptosis (Song et al., 2019). Furthermore, the anticancer compound elaiophylin decreases SIRT1 and its downstream target Nrf2, inhibiting mitophagy and accelerating apoptosis in lung tumors (Ji et al., 2022). Thus, the interplay between SIRT1-mediated autophagy and apoptosis is integral to the regulation of carcinogenesis (Figure 4).

12 SIRT1-mediated autophagy and ferroptosis crosstalk: New perspectives

Ferroptosis, an iron-dependent form of regulated cell death characterized by the accumulation of lipid peroxides on cellular membranes, was first identified in a proteomics study by the Stockwell laboratory and colleagues in 2012 (Dixon et al., 2012; Lei et al., 2022). This process is distinct from apoptosis and other forms of cell death in several ways, including its unique mechanisms and morphological characteristics. Cells undergoing ferroptosis do not exhibit chromatin condensation or form apoptotic bodies; instead, they typically have smaller mitochondria with fewer mitochondrial cristae compared to normal or apoptosis-resistant cells (Dixon et al., 2012; Stockwell et al., 2017). These cells also accumulate harmful lipid peroxides (Jiang et al., 2021), arising from an imbalance between antioxidant activities that prevent ferroptosis and the pro-ferroptotic processes. When the imbalance exceeds the cell's capacity to cope, leading to a critical overload of lipid peroxides, ferroptosis is triggered (Yang et al., 2014; Bersuker et al., 2019; Doll et al., 2019; Kraft et al., 2020; Soula et al., 2020; Mao et al., 2021; Ingold et al., 2018). Additionally, ferroptosis differs in its molecular mechanisms from other types of cell death, which involve specific executioner proteins like caspase in apoptosis, gasdermin D in pyroptosis, or MLKL in necroptosis. Furthermore, the oxidized phospholipid profiles are distinctive to ferroptosis, setting it apart from other cell death types (Galluzzi et al., 2018; Wiernicki et al., 2020; Kagan et al., 2017).

Recent research has underscored the interplay between autophagy and ferroptosis in various human cancers, illuminating their roles in tumorigenesis regulation. In lung cancer, inducing ferroptosis has been shown to curb tumor growth, with curcumin enhancing this process by promoting toxic autophagy in lung tumor cells (Tang X. et al., 2021). In ovarian cancer, studies have investigated the expression levels of C-MYC and NCOA4 and their relationship with cancer malignancy. Findings indicate a significant correlation, where C-MYC appears to suppress NCOA4 expression by directly interacting with its mRNA, influencing ferroptosis negatively. This interaction reduces NCOA4 levels, decreases ROS production, and inhibits mitophagy, leading to increased proliferation and invasion of ovarian cancer cells. Furthermore, C-MYC is implicated in reducing NCOA4-mediated ferroptosis, enhancing cancer cell invasion and immune evasion (Jin et al., 2022). In head and neck cancer, the induction of ferritinophagy, a specific form of autophagy, is crucial for promoting ferroptosis (Lee J. et al., 2022). Conversely, in cervical cancer, Cdc25A enhances PKM2 dephosphorylation, which upregulates ErB2 expression and inhibits autophagy-induced ferroptosis (Wang et al., 2021). Additionally, in bladder cancer, although GPX4 acts to inhibit ferroptosis, autophagy facilitates the degradation of GPX4, augmenting the efficacy of Fin56 in stimulating ferroptosis (Sun Y. et al., 2021). These findings highlight the complex interactions and crosstalk between autophagy and ferroptosis in cancer regulation. Given the role of SIRT1 as a regulator of autophagy, further exploration into how SIRT1-mediated autophagy might influence ferroptosis is warranted, offering potential new avenues for cancer therapy.

13 SIRT1 modulators in cancer

There are various types of sirtuins, with SIRT1 being particularly well-studied for its dual role in cancer progression and inhibition. Researchers have explored pathways to activate or inhibit SIRT1, given its critical regulatory impact on tumor promotion and suppression (Carafa et al., 2019). Recent studies have identified several chemotherapeutic agents that target SIRT1, derived from both synthetic and natural bioactive compounds (Patra et al., 2023b). Among these, the polyphenolic antioxidant resveratrol has been highlighted for its anticancer properties, including antioxidant, immunomodulatory, anti-inflammatory, and pro-apoptotic effects. Resveratrol has shown effectiveness against multiple solid tumors and is known to influence autophagy, suggesting that it might trigger autophagic cell death (ACD) as an alternative cell death mechanism when apoptosis is compromised (Patra et al., 2022; Patra et al., 2021). This activation of SIRT1 by resveratrol could be particularly useful in treating drug-resistant cancer cells and eliminating cancer stem cells (Pervaiz and Holme, 2009). Another agent, gallic acid, known for inhibiting autophagy flux, can also activate SIRT1 and induce ATG cell death (Patra et al., 2020a; Patra et al., 2020b; Chang et al., 2021). Additionally, synthetic compound 5 has been shown to induce autophagic and mitophagic cell death in glioblastoma cells through SIRT1 activation (Yao et al., 2018). Indirect evidence also suggests that SRT1720, SRT2183, and SRT1460, as activators of SIRT1, may modulate autophagy to initiate cancer cell death pathways (Pacholec et al., 2010). Abrus agglutinin, another SIRT1 activator, mediates lipophagy leading to apoptotic cell death through ROS production induced by free fatty acids (Panda et al., 2020). Increased SIRT1 expression is associated

TABLE 3 Summarizing the underlying mechanisms involved in SIRT1-mediated cancer regulation.

Targets	Highlights	References
SIRT1/WEE1	SIRT1 mediates WEE1 deacetylation to increase sensitivity to WEE1 suppression	Zhu et al. (2023a)
NCAPD2/PARP-1/SIRT1	NCAPD2 disrupts autophagy mechanism through controlling PARP-1/SIRT1 axis	Jing et al. (2021)
SIRT1	The overexpression of SIRT1 in liver cancer enhances energy homeostasis and regulates antioxidant response	Varghese et al. (2023)
SIRT1/p53/miR-101/KPNA3	SIRT1 induces drug resistance in colorectal tumor through p53 downregulation to reduce miR-101 levels in upregulating KPNA3	Wang et al. (2023d)
SIRT1	SIRT1 enhances tumorigenesis in colorectal cancer via enhancing glucolipid metabolic conversion	Wei et al. (2023)
SIRT1	Cytoplasmic SIRT1 promotes the formation and viability of polyploidy giant cancer cells to mediate paclitaxel resistance in ovarian cancer	Xu et al. (2023b)
LITAF/FOXO1/SIRT1	LITAF inhibits SIRT1 by FOXO1 to reduce proliferation and metastasis in colorectal tumor	Guan et al. (2023)
SIRT1/STAT3/MMP-13	SIRT3 disrupts the growth and invasion of gastric cancer through STAT3 inhibition to induce MMP-13 expression	Zhang et al. (2019)
NSD2/AROS/SIRT1	NSD2 facilitates AROS methylation to upregulate SIRT1	Li et al. (2023a)

TABLE 4 The regulation of autophagy by SIRT1 in cancer.

Targets	Highlights	References
CDK9	The downregulation of CDK9 suppresses PINK1/PRKN-induced mitophagy to promote mitochondrial dysfunction in hepatocellular carcinoma	Yao et al. (2022)
UBE2C	UBE2C increases SIRT1 ubiquitination to suppress autophagy in endometrial cancer	Zhao et al. (2023e)
SIRT1/AMPK	Quercetin stimulates SIRT1/AMPK axis to mediate autophagy-induced apoptosis	Guo et al. (2021)
SIRT1/FoxO1/Rab7	SIRT1 increases Rab7 expression to induce autophagy in gastric cancer	Zhu et al. (2023b)
SIRT1	SIRT1 stimulates the Beclin-1/autophagy axis in cisplatin resistance in bladder tumor	Sun et al. (2023)
SIRT1	Downregulation of SIRT1 induces autophagy-mediated radiosensitivity in prostate cancer	Wang et al. (2022)
miR-34a	miR-34a is upregulated by catalpol to suppress SIRT1/autophagy in colorectal cancer treatment	Qiao et al. (2020)
Ube2v1	Ube2v1 increases SIRT1 degradation to enhance metastasis of colorectal cancer by autophagy inhibition	Shen et al. (2018)
SIRT/HSPA5	SIRT1/2 downregulation promotes HSPA5 acetylation and mediates protective autophagy in lung cancer	Mu et al. (2019)
miR-138/SIRT1	miR-138 suppresses SIRT1 to inhibit growth, invasion, and autophagy	Ye et al. (2017)
SIRT1	SIRT1 inhibition increases ULK1 acetylation to promote ROS-induced autophagy in colon cancer	Islam et al. (2024b)
miR-124 miR-142	miR-124 and miR-142 downregulate SIRT1 to increase cisplatin sensitivity by autophagy inhibition in lung cancer	Song et al. (2019)
H19/SIRT1	LncRNA H19 stimulates the SIRT1/autophagy axis to induce drug resistance in colorectal cancer	Wang et al. (2018)

with the onset of carcinogenesis and malignant transformation, making SIRT1 inhibition a potential therapeutic strategy. The SIRT1 inhibitor EX527, for example, can acetylate p53 in the presence of etoposide (Solomon et al., 2006), potentially triggering apoptotic cell death and inhibiting protective autophagy (Brooks and Gu, 2008). Despite its mixed results in cancer therapy, EX527 has progressed to phase three clinical trials for Huntington's disease. The combination of chemotherapy with other SIRT1 inhibitors, such as suramins, JGB1741, tenovins, salermide, sirtinol, and other class III HDAC inhibitors, might enhance the efficacy of cancer treatments by regulating autophagy and inducing associated cell death (Lin and Fang, 2013; Heltweg et al., 2006; Lara et al., 2009; Kalle et al., 2010; Lain et al., 2008; Asaka et al., 2015). The latest inhibitor, MHY2245, affects PKM2/mTOR signaling in ovarian cancer cells, promoting autophagy alongside cell cycle arrest in the G2/M phase and potentially initiating autophagy-associated cell death (Table 4) (Tae et al., 2020).

A chemical known as silybin has been shown to inhibit SIRT1 and increase p53 acetylation, in addition to its anticancer properties (Yousafzai et al., 2021). Moreover, silybin and the SIRT1 inhibitor cambinol were produced in mice and employed for *in vitro* research according to dosage and time dependent parameters. When it comes to lung adenocarcinoma, silybin has been demonstrated to be an efficient inhibitor of adenocarcinoma, and it has the potential to be utilized as a therapeutic intervention (Liang Z. et al., 2014). HDACs inhibitor tenovin-6 induces apoptosis, suppresses cell migration and invasion, and eliminates cancer stem cells (CSCs) in uveal melanoma (Dai et al., 2016). The progression of uveal melanoma (UM) and the diagnosis have remained pitiful. Tenovin-6 has all of these effects. Inducing a senescence-like growth arrest, perhaps having anticancer potential, and causing an impairment in the activation of the Ras/MAPK pathway are all outcomes of sirtinol, which is another inhibitor. Despite this, sirtinol was found to have an influence on the activation of Akt/PKB as well as the tyrosine phosphorylation of receptors for EGF and IGF-I on the receptors (Ota et al., 2006). On the other hand, SIRT1 suppression by EX527 dramatically decreased the tumor growth of HEC1B and HHUA endometrial cancer. This was due to the fact that SIRT1 overexpression caused cisplatin resistance in HHUA cells, which in turn accelerated carcinogenesis in nude mice. In the treatment of cisplatin-resistant cancer, a combination of EX527 and cisplatin has the potential to be an effective targeted therapy (Asaka et al., 2015). According to computational docking studies, EX527 is solely specific for SIRT1 rather than other sirtuin members. However, Sirtinol, Nicotinamide, and Salermide are all direct targets of inhibitors SIRT1 and 2, and they all have the specific inhibitory action for SIRT1. Salermide is also a direct target of SIRT2. EX527 enhanced carcinogenesis in SCID mice in comparison to the control group, regardless of whether it induces apoptosis and DNA damage *in vitro* (Oon et al., 2015). This suggests that the current method to inhibiting SIRT1 by EX527 *in vitro* and *in vivo* both pancreatic tumor models is unexpectedly the opposite of what was seen *in vitro*. In addition, a study that used short interfering RNA to target SIRT1 found that knocking down SIRT1 can result in the death of cells in the MCF-7 patient line (Peck et al., 2010). MiR-29c overexpression in cisplatin-resistant cancer cells was shown to directly target SIRT1 mRNA and suppress SIRT1 expression. This was demonstrated by Zhang et al. to regulate cell progression and apoptosis, as well as to restore chemosensitivity to cisplatin (Zhang and Luo, 2018). MiR-34a mediated SIRT1 suppression mediates apoptotic activation and chemosensitivity (Herbert et al., 2014). In addition, it is believed that SIRT1 is responsible for accelerating cell growth. In the study of SIRT1's cellular processes in colorectal cancer, clinical data and patient samples were combined, and a mechanical technique was discovered to regulate p53 and FRA-1 via SIRT1. This approach was verified to be directly related with EMT (Cheng et al., 2016).

14 Function of SIRT1 as biomarker

In terms of genetic and epigenetic background, dietary habits, and environmental influences, it has been demonstrated that there are substantial disparities between the populations of Asians and Caucasians (Hur et al., 2008; Tarabay et al., 2016). Not only are these elements necessary for the beginning and advancement of cancer, but they are also necessary for the spread of cancer to other parts of the body (Chatterjee et al., 2018; Pavlidis and Pavlidis, 2018). Mutations and widespread polymorphisms of SIRT1 were discovered in cancer lines produced by Chinese and Japanese individuals (Shimoyama et al., 2011; Shimoyama et al., 2012; Chen et al., 2015; Lv et al., 2017) as well as 41 cancer lines (Han J. et al., 2013). We suggest that differences in SIRT1 mutations and polymorphisms may be one of the causes for differences in predicting OS and TNM stage and lymphatic metastasis of cancer on the basis of SIRT1 expression. This is despite the fact that the data on SIRT1 mutations and polymorphisms are extremely uncommon. It is important to conduct further research on this (Mei et al., 2016). It is well knowledge that metastasis is a factor that may be used to independently predict a bad prognosis for a variety of cancer types (Tsutsumi et al., 2012; Funazo et al., 2017; Ambe et al., 2018). There was a correlation between the higher expression of SIRT1 and OS, DFS, EFS, and PFS. There is a correlation between SIRT1 overexpression and TNM stage, lymph node metastasis, and distant metastasis (Sun et al., 2019); however, there is no correlation with tumor size, tissue invasion depth, differentiation, gender, or age. The overexpression of SIRT1 was found to be predictive with a worse overall survival, as well as a higher TNM stage and lymphatic metastases, in the Asian population, particularly in China. Consequently, the overexpression of SIRT1 may lead to lymphatic metastasis of malignancies, which in turn results in poor overall survival, disease-free survival, event-free survival, and progression-free survival statistics. One of the possible underlying mechanisms for metastasis is the presence of molecular events and biological processes that are mediated by SIRT1. The results of our meta-analysis are in agreement with the findings of SIRT1 being upregulated more frequently in T3 + T4, lymph node metastases, and TNM stage of colorectal cancer patients (Jiang et al., 2014). SIRT1 expression was not connected with these clinicopathological aspects, but rather a poor predictive biomarker of colorectal cancer patients (Byles et al., 2012). This is despite the fact that SIRT1 over-expression was proven to be associated with distant metastasis and histological grade (Jang S-H. et al., 2012). There was a propensity for a high SIRT1 expression to be related with positive lymph node metastasis, despite the fact that a study did not find any significant differences in lymph node metastasis compared to other studies (Otsuka et al., 2022). A high expression of SIRT1 was shown to be strongly linked with lymph node metastasis, according to the findings of two studies that were included in this comparative analysis. In breast cancer (Wu et al., 2012) and colorectal cancer (Zu et al., 2016), there has been reported to be a connection between SIRT1 expression and lymph node metastasis. Furthermore, it has been revealed that SIRT1 expression is implicated in cell migration in prostate cancer (Byles et al., 2012) and non-small-cell lung cancer (Han L. et al., 2013).

SIRT1, as a key regulator of cellular processes such as DNA repair, apoptosis, autophagy, and metabolism, has become a potential therapeutic target in cancer therapy, where both SIRT1 inducers and inhibitors are being explored for different cancer contexts. SIRT1 inducers are of particular interest in cancers where SIRT1 functions as a tumor suppressor. In many

cancers, SIRT1 activation promotes genomic stability and DNA repair by deacetylating important regulators such as p53 and FOXO proteins, thereby reducing the accumulation of DNA damage. This function helps prevent oncogenesis by preserving the integrity of the genome. Inducers of SIRT1, such as resveratrol and other small molecules, have been shown to activate SIRT1's deacetylase activity, which leads to the suppression of tumor progression through the inhibition of cancer cell proliferation and the promotion of apoptosis. Resveratrol, a naturally occurring polyphenol, has garnered attention for its ability to activate SIRT1 and its subsequent anti-cancer effects, particularly in cancers like breast and prostate cancer, where SIRT1's tumor-suppressive role has been documented. In addition to promoting apoptosis, SIRT1 activation also stimulates autophagy, a process that allows cancer cells to degrade damaged organelles and proteins, thus reducing oxidative stress and promoting cell survival under stress conditions. This duality makes SIRT1 inducers promising for cancers where oxidative stress plays a significant role, offering a cytoprotective effect in normal tissues while targeting cancerous growth. On the other hand, SIRT1 inhibitors are being explored in cancer types where SIRT1 acts as a tumor promoter, particularly in cases of drug resistance and aggressive cancers. For example, in cancers such as hepatocellular carcinoma, pancreatic cancer, and some forms of leukemia, SIRT1 is often upregulated, which leads to enhanced survival of cancer cells through the suppression of apoptosis and the activation of pro-survival pathways. In such cases, inhibiting SIRT1 can restore the cell's sensitivity to apoptosis-inducing therapies. SIRT1 inhibitors, such as EX527 and nicotinamide, have been shown to enhance the effectiveness of chemotherapeutic agents like cisplatin by increasing the acetylation and activity of pro-apoptotic factors such as p53. By preventing SIRT1 from deacetylating key regulators of apoptosis and cell death, these inhibitors can sensitize cancer cells to treatment, overcoming resistance and leading to more effective cancer eradication. Additionally, SIRT1 inhibitors may interfere with the autophagic survival pathways, further increasing cancer cell susceptibility to stress and cytotoxicity. However, the use of SIRT1 inhibitors must be approached cautiously, as prolonged inhibition of SIRT1 can disrupt normal cellular homeostasis, potentially leading to adverse effects such as metabolic dysregulation or damage to normal tissues. Therefore, identifying the cancer-specific roles of SIRT1 and tailoring the application of its inducers and inhibitors is critical for developing precise and effective cancer therapies.

15 Conclusion and future perspectives

The sirtuin family, particularly SIRT1, plays a crucial role in regulating cellular and biological processes. While SIRT1 is essential for normal physiological functions, its dysregulation has been linked to the pathogenesis of various diseases, including cancer. Recent studies have shown that SIRT1 is dysregulated in multiple tumor types, including brain, gastrointestinal, gynecological, and reproductive tumors. Given SIRT1's influence on numerous pathways and its regulation by diverse upstream mediators, it is critical to delineate the specific mechanisms through which SIRT1 modulates tumorigenesis. Additionally, autophagy, a process extending beyond cell death, has been recognized for its role in tumor cell behavior, impacting cell death, growth, viability, metastasis, and therapy resistance. This review focuses on the interaction between autophagy and SIRT1 in regulating tumorigenesis. Notably, while autophagy generally contributes to protein degradation, it can specifically regulate SIRT1 by targeting it for degradation, thereby suppressing its activity. However, most research has concentrated on how SIRT1 regulates autophagy, with findings that SIRT1 can activate autophagy, including specialized forms like mitophagy and lipophagy. Such regulation can contribute to drug resistance in cancer. The impact of SIRT1-mediated autophagy on cancer drug resistance is yet to be thoroughly investigated across different cancer types and with various chemotherapeutic agents, including topoisomerases. Moreover, SIRT1's regulation of autophagy often involves major autophagy regulators such as AMPK and mTOR. Intriguingly, SIRT1-mediated autophagy can influence apoptosis in cancer cells; for example, SIRT1-induced pro-survival autophagy can decrease apoptosis, whereas toxic autophagy can enhance it. Despite the development of several SIRT1 regulators, their direct effects on autophagy have not been extensively studied. Future research should focus on drug discovery and the development of small molecules that target SIRT1 to modulate autophagy in cancer treatment.

SIRT1 plays a dual role in cancer, acting as both a tumor suppressor and a tumor promoter depending on the cellular context. As a tumor suppressor, SIRT1 deacetylates and activates key regulatory proteins such as p53, FOXO transcription factors, and RB, which are involved in cell cycle arrest, DNA repair, and apoptosis. This promotes cellular homeostasis and reduces the likelihood of oncogenic transformation. Additionally, SIRT1's role in maintaining genomic stability and preventing oxidative stress further supports its tumor-suppressive functions, particularly in early stages of cancer development. In various cancer types, SIRT1 overexpression has been linked to reduced tumorigenicity and enhanced sensitivity to chemotherapy. Conversely, SIRT1 can also act as a tumor promoter, particularly in advanced cancers, where it aids in tumor progression by promoting cell survival and resistance to stress. SIRT1 has been shown to inhibit apoptosis by deacetylating and inactivating pro-apoptotic factors, such as p53 and E2F1, leading to enhanced tumor cell survival. It also contributes to the activation of oncogenic pathways, including those involving NF-κB and MYC, which drive cancer cell proliferation and metastasis. Moreover, SIRT1 has been implicated in promoting drug resistance by modulating autophagy and DNA repair pathways, making tumors more resilient to conventional therapies. This dual nature of SIRT1 highlights the importance of context in determining its role in cancer progression.

SIRT's role in autophagy is tightly linked to several key molecular pathways, such as the mTOR (mechanistic target of rapamycin) and AMPK (AMP-activated protein kinase) pathways. SIRT1 influences these pathways in ways that either promote or regulate autophagy, depending on the cellular context. SIRT1 activates autophagy primarily by deacetylating various proteins involved in the autophagic machinery, such as ATG5, ATG7, and ATG8, and also deacetylates the transcription factor FOXO3, promoting the expression of autophagy-related genes, including LC3. In the mTOR pathway, a major negative regulator of autophagy, SIRT1 indirectly inhibits mTOR, promoting autophagy. This inhibition occurs through the activation of TSC1/2, a negative regulator of mTORC1, and by activating AMPK, which

enhances the inhibition of mTORC1. Under nutrient-rich conditions, mTOR suppresses autophagy by preventing autophagosome formation, but SIRT1-mediated inhibition of mTOR reverses this effect. On the other hand, SIRT1 activates AMPK by deacetylating liver kinase B1 (LKB1), which leads to the phosphorylation of TSC2 and RAPTOR, thus promoting autophagy. Activated AMPK also directly phosphorylates ULK1, an initiator of autophagy. This interaction between SIRT1 and AMPK is critical in energy-deficient states, allowing cells to initiate autophagy to survive under stress. SIRT1 also affects autophagy through its interaction with p53, a tumor suppressor that inhibits autophagy when acetylated. By deacetylating and inactivating cytoplasmic p53, SIRT1 reduces its inhibitory effects on autophagy. Furthermore, SIRT1 modulates FOXO transcription factors, particularly FOXO1 and FOXO3, which promote the expression of autophagy-related genes when deacetylated by SIRT1. This enhances autophagic processes, especially during stress conditions. Additionally, SIRT1 influences mitochondrial autophagy (mitophagy) by deacetylating and activating PGC-1α, a key regulator of mitochondrial biogenesis and energy metabolism. Another important autophagy regulator influenced by SIRT1 is Beclin-1, a key protein in autophagosome formation. SIRT1 interacts with and enhances the activity of Beclin-1, further promoting autophagy. Moreover, SIRT1 affects multiple molecular pathways, such as its interaction with mTOR and AMPK, highlighting its central role in coordinating cellular energy homeostasis and stress responses. By integrating signals from various pathways, including mTOR, AMPK, FOXO, and p53, SIRT1 balances cell survival and degradation under stress conditions. These mechanisms demonstrate the significant role of SIRT1 in promoting autophagy, making it a crucial factor in cellular health, energy regulation, and potential therapeutic targets for diseases linked to autophagy dysfunction.

As a NAD + -dependent deacetylase, SIRT1 influences cancer cell survival by modulating stress responses, DNA repair, and the tumor microenvironment, contributing to the development of resistance to chemotherapy and targeted therapies. Understanding the relationship between SIRT1 and drug resistance, particularly through autophagy, is essential to developing effective therapeutic strategies. SIRT1 contributes to drug resistance in multiple cancer types by promoting cancer cell survival under stress. It deacetylates and activates various transcription factors, such as p53, FOXO, and NF-κB, which are involved in cellular stress responses and apoptosis. Through these interactions, SIRT1 enhances the ability of cancer cells to withstand chemotherapeutic agents and resist apoptosis. For example, in breast cancer, SIRT1 has been shown to deacetylate and inhibit p53, a tumor suppressor, allowing cancer cells to escape apoptosis induced by DNA-damaging agents. Additionally, in hepatocellular carcinoma (HCC), SIRT1-mediated pathways are associated with resistance to sorafenib, a common drug used in HCC treatment. Autophagy is a cellular degradation process that plays a dual role in cancer, acting as a tumor suppressor in early stages and a survival mechanism in advanced cancers. SIRT1 is a key regulator of autophagy, particularly under conditions of stress, such as nutrient deprivation or chemotherapy. By deacetylating autophagy-related proteins (ATGs) and transcription factors like FOXO1/FOXO3, SIRT1 promotes the formation of autophagosomes and enhances the autophagic flux, allowing cancer cells to recycle cellular components and sustain energy production during chemotherapy-induced stress. The SIRT1-autophagy axis has been implicated in drug resistance across various cancer types. For instance, in colorectal cancer, SIRT1 activation enhances autophagy, which protects cancer cells from chemotherapy-induced apoptosis by degrading damaged organelles and proteins. In drug-resistant esophageal cancer cells, SIRT1 upregulation has been linked to increased autophagy, leading to enhanced cell survival and resistance to chemotherapy. In these cases, inhibition of SIRT1 or autophagy sensitizes cancer cells to chemotherapy, indicating the pivotal role of the SIRT1-autophagy pathway in mediating drug resistance. SIRT1 promotes autophagy by deacetylating key regulators of the autophagic process, such as Beclin-1 and LC3. It also regulates autophagy-related miRNAs, including miR-34a and miR-215, which affect the expression of autophagy proteins like Atg14. Furthermore, SIRT1 inhibits mTOR (mechanistic target of rapamycin), a negative regulator of autophagy, through pathways involving AMPK activation, thus promoting autophagy under stress conditions. This activation of autophagy by SIRT1 enables cancer cells to maintain cellular homeostasis and evade the cytotoxic effects of chemotherapy. In drug-resistant cancer cells, increased SIRT1-mediated autophagy allows the cells to clear damaged components and maintain survival despite the presence of chemotherapeutic agents. For example, in ovarian cancer, SIRT1-mediated autophagy has been shown to contribute to resistance to cisplatin, while in gastric cancer, SIRT1 enhances autophagy to protect cancer cells from apoptosis induced by 5-fluorouracil. Blocking SIRT1 or inhibiting autophagy in these models reverses drug resistance, further highlighting the importance of this pathway in maintaining cancer cell survival during treatment.

The research on SIRT1 and its role in autophagy has advanced significantly, but its complexity presents several limitations. One key challenge is the dual role of SIRT1 in cancer, where it can function as both a tumor suppressor and promoter depending on the context. In some cancers, SIRT1 activation supports autophagy and cell survival, while in others, it triggers apoptosis and suppresses tumor growth. The context-specific roles of SIRT1, as well as the dual nature of autophagy, complicate the development of generalized therapeutic strategies. This complexity makes it difficult to predict when SIRT1-mediated autophagy would either aid or hinder treatment, especially given the need to target specific cellular environments in cancer. Another limitation stems from the incomplete understanding of the molecular mechanisms behind SIRT1's regulation of autophagy. While SIRT1's interactions with autophagy-related proteins like Beclin-1 and FOXO have been noted, the precise pathways it influences remain unclear. This knowledge gap limits the ability to fully exploit SIRT1 as a therapeutic target. Furthermore, SIRT1 is involved in various cellular pathways, including those regulating metabolism and DNA repair, which complicates its therapeutic targeting. The potential for off-target effects or unwanted consequences from influencing multiple pathways simultaneously represents a significant challenge in developing SIRT1-targeted therapies. Currently available SIRT1 activators and inhibitors lack the specificity needed for effective clinical application. Compounds such as resveratrol and EX527 not only target SIRT1 but also affect other members of the sirtuin family and related pathways, leading to

potential side effects. Furthermore, finding the optimal dosage and timing of SIRT1 modulation is challenging because over-activation or inhibition of SIRT1 can either promote survival or induce apoptosis in cancer cells. This delicate balance underscores the need for more selective and precise pharmacological tools to modulate SIRT1 activity in a controlled manner. Translating promising preclinical results into clinical practice has proven difficult, particularly due to differences between animal models and human physiology. Tumor heterogeneity further complicates the development of SIRT1-targeted therapies, as the role of SIRT1 and autophagy can vary not only between different cancer types but also within different regions of the same tumor. Additionally, cancer cells can develop resistance to SIRT1 modulators, limiting the long-term effectiveness of these treatments. Understanding and overcoming these resistance mechanisms will be essential for successful clinical application. Finally, the long-term safety of SIRT1-targeted therapies remains uncertain. SIRT1 is involved in many critical cellular processes, including aging and DNA repair, so long-term inhibition or activation could have adverse effects, such as metabolic disorders or neurodegenerative diseases. Moreover, reliable biomarkers to predict patient response to SIRT1-targeted therapies are lacking, making it difficult to assess which patients would benefit most from these treatments. Addressing these limitations will be crucial to advancing SIRT1-targeted therapies into clinical practice, offering new hope for effective cancer treatments.

Although the function of SIRT1 in the regulation of autophagy was covered in the present review, there are also other members of SIRT family participating in the regulation of autophagy. SIRT2, primarily localized in the cytoplasm, has been shown to regulate autophagy through its deacetylation of key autophagic proteins and its involvement in energy metabolism. SIRT2 can deacetylate FOXO1 and FOXO3, transcription factors that upregulate autophagy-related genes. Additionally, SIRT2 affects autophagy by modulating the acetylation of LC3, a key autophagy marker. By promoting LC3 deacetylation, SIRT2 enhances autophagosome formation and autophagic flux. SIRT2 has also been linked to the regulation of mTOR, a key negative regulator of autophagy. By inhibiting mTOR activity, SIRT2 indirectly promotes autophagy under conditions of nutrient stress. However, SIRT2's role in autophagy can be complex, as in some contexts, it has been observed to inhibit autophagy and promote cell proliferation, particularly in cancer. SIRT3, SIRT4, and SIRT5 are mitochondrial sirtuins that regulate autophagy through their effects on mitochondrial function and metabolism. SIRT3 is the most well-studied of the three and plays a key role in regulating mitophagy, a specific form of autophagy that targets damaged mitochondria for degradation. SIRT3 deacetylates several mitochondrial proteins, enhancing mitochondrial respiration and reducing oxidative stress, which can influence autophagy activation. In response to cellular stress, SIRT3 can enhance autophagy by deacetylating and activating FOXO3, which upregulates autophagy-related genes such as Beclin-1 and LC3. Additionally, SIRT3 inhibits mTOR signaling by promoting the activation of AMPK, an energy sensor that stimulates autophagy. SIRT4, while less studied, has been shown to inhibit autophagy through its role in regulating mitochondrial glutamine metabolism. By inhibiting glutamate dehydrogenase (GDH), SIRT4 suppresses the production of ATP and thus limits the energy supply needed for autophagy, leading to decreased autophagic activity. SIRT5, a mitochondrial lysine demalonylase and desuccinylase, can also regulate mitochondrial function and oxidative stress, although its direct involvement in autophagy is still under investigation. SIRT6 is primarily a nuclear sirtuin involved in DNA repair and metabolic regulation, but it also influences autophagy. SIRT6 can enhance autophagy by promoting the activation of the AMPK pathway, leading to the inhibition of mTOR, thus stimulating autophagy. Additionally, SIRT6 regulates autophagy by deacetylating histones at the promoters of autophagy-related genes, promoting their transcription. For example, SIRT6-mediated deacetylation of histone H3 at lysine 9 (H3K9) near the promoter region of genes such as ATG5 and ATG12 enhances autophagy induction. SIRT6 also affects the autophagy-lysosomal pathway, which is critical for maintaining cellular homeostasis, particularly during stress. SIRT7, another nuclear sirtuin, has a more indirect role in autophagy regulation. SIRT7 primarily regulates ribosomal RNA (rRNA) transcription and protein synthesis, which affects cellular growth and metabolism. By modulating metabolic pathways, SIRT7 influences the availability of nutrients and energy, which can impact autophagy activation. Interestingly, SIRT7's suppression of autophagy has been linked to its role in cancer, where it promotes cancer cell survival by limiting autophagic processes. SIRT7 has been observed to deacetylate and inhibit proteins involved in autophagy initiation, thus reducing autophagic flux in certain cancer contexts. More information about SIRT2, SIRT3, SIRT4, SIRT5, SIRT6 and SIRT7 can be found in these reviews (Chen et al., 2020; Wang et al., 2019c; Torrens-Mas et al., 2017; Alhazzazi et al., 2011; Wang et al., 2020; Tomaselli et al., 2020; Bringman-Rodenbarger et al., 2018; Lagunas-Rangel, 2023; Fiorentino et al., 2021; Tang M. et al., 2021).

Author contributions

YT: Conceptualization, Data curation, Investigation, Methodology, Project administration, Resources, Software, Supervision, Validation, Visualization, Writing–original draft, Writing–review and editing. WJ: Conceptualization, Data curation, Formal Analysis, Investigation, Methodology, Project administration, Resources, Software, Supervision, Validation, Visualization, Writing–original draft, Writing–review and editing. YL: Conceptualization, Data curation, Formal Analysis, Investigation, Methodology, Project administration, Resources, Software, Supervision, Validation, Writing–original draft, Writing–review and editing. QD: Conceptualization, Data curation, Investigation, Methodology, Project administration, Resources, Software, Supervision, Validation, Writing–original draft, Writing–review and editing.

Funding

The author(s) declare that no financial support was received for the research, authorship, and/or publication of this article.

Conflict of interest

The authors declare that the research was conducted in the absence of any commercial or financial relationships that could be construed as a potential conflict of interest.

Publisher's note

All claims expressed in this article are solely those of the authors and do not necessarily represent those of their affiliated organizations, or those of the publisher, the editors and the reviewers. Any product that may be evaluated in this article, or claim that may be made by its manufacturer, is not guaranteed or endorsed by the publisher.

References

Ahlberg, J., and Glaumann, H. (1985). Uptake--microautophagy--and degradation of exogenous proteins by isolated rat liver lysosomes. Effects of pH, ATP, and inhibitors of proteolysis. *Exp. Mol. pathology* 42 (1), 78–88. doi:10.1016/0014-4800(85)90020-6

Ahlberg, J., Marzella, L., and Glaumann, H. (1982). Uptake and degradation of proteins by isolated rat liver lysosomes. Suggestion of a microautophagic pathway of proteolysis. *Laboratory investigation; a J. Tech. methods pathology* 47 (6), 523–532.

Ahn, J. H., and Lee, M. (2011). Suppression of autophagy sensitizes multidrug resistant cells towards Src tyrosine kinase specific inhibitor PP2. *Cancer Lett.* 310 (2), 188–197. doi:10.1016/j.canlet.2011.06.034

Albrecht, L. V., Bui, M. H., and De Robertis, E. M. (2019). Canonical Wnt is inhibited by targeting one-carbon metabolism through methotrexate or methionine deprivation. *Proc. Natl. Acad. Sci. U. S. A.* 116 (8), 2987–2995. doi:10.1073/pnas.1820161116

Albrecht, L. V., Ploper, D., Tejeda-Muñoz, N., and De Robertis, E. M. (2018). Arginine methylation is required for canonical Wnt signaling and endolysosomal trafficking. *Proc. Natl. Acad. Sci. U. S. A.* 115 (23), E5317–e5325. doi:10.1073/pnas.1804091115

Alhazzazi, T. Y., Kamarajan, P., Verdin, E., and Kapila, Y. L. (2011). SIRT3 and cancer: tumor promoter or suppressor? *Biochimica Biophysica Acta (BBA)-Reviews Cancer* 1816 (1), 80–88. doi:10.1016/j.bbcan.2011.04.004

Amaravadi, R., Kimmelman, A. C., and White, E. (2016). Recent insights into the function of autophagy in cancer. *Genes and Dev.* 30 (17), 1913–1930. doi:10.1101/gad.287524.116

Ambe, P. C., Gödde, D., Stoerkel, S., Zirngibl, H., and Bönicke, L. (2018). Extra nodular metastasis is a poor prognostic factor for overall survival in node-positive patients with colorectal cancer. *Int. J. Colorectal Dis.* 33, 403–409. doi:10.1007/s00384-018-2991-0

An, Y., Wang, B., Wang, X., Dong, G., Jia, J., and Yang, Q. (2020). SIRT1 inhibits chemoresistance and cancer stemness of gastric cancer by initiating an AMPK/FOXO3 positive feedback loop. *Cell death and Dis.* 11 (2), 115. doi:10.1038/s41419-020-2308-4

An, Y., Zhang, Z., Shang, Y., Jiang, X., Dong, J., Yu, P., et al. (2015). miR-23b-3p regulates the chemoresistance of gastric cancer cells by targeting ATG12 and HMGB2. *Cell death and Dis.* 6 (5), e1766. doi:10.1038/cddis.2015.123

Anding, A. L., and Baehrecke, E. H. (2017). Cleaning house: selective autophagy of organelles. *Dev. Cell* 41 (1), 10–22. doi:10.1016/j.devcel.2017.02.016

Asaka, R., Miyamoto, T., Yamada, Y., Ando, H., Mvunta, D. H., Kobara, H., et al. (2015). Sirtuin 1 promotes the growth and cisplatin resistance of endometrial carcinoma cells: a novel therapeutic target. *Laboratory investigation; a J. Tech. methods pathology* 95 (12), 1363–1373. doi:10.1038/labinvest.2015.119

Ashrafizadeh, M., Ahmadi, Z., Farkhondeh, T., and Samarghandian, S. (2020a). Autophagy regulation using luteolin: new insight into its anti-tumor activity. *Cancer Cell Int.* 20 (1), 537. doi:10.1186/s12935-020-01634-9

Ashrafizadeh, M., Paskeh, M. D. A., Mirzaei, S., Gholami, M. H., Zarrabi, A., Hashemi, F., et al. (2022). Targeting autophagy in prostate cancer: preclinical and clinical evidence for therapeutic response. *J. Exp. and Clin. Cancer Res.* 41 (1), 105. doi:10.1186/s13046-022-02293-6

Ashrafizadeh, M., Tavakol, S., Ahmadi, Z., Roomiani, S., Mohammadinejad, R., and Samarghandian, S. (2020b). Therapeutic effects of kaempferol affecting autophagy and endoplasmic reticulum stress. *Phytotherapy Res. PTR* 34 (5), 911–923. doi:10.1002/ptr.6577

Ashrafizadeh, M., Zarrabi, A., Hushmandi, K., Hashemi, F., Moghadam, E. R., Owrang, M., et al. (2021). Lung cancer cells and their sensitivity/resistance to cisplatin chemotherapy: role of microRNAs and upstream mediators. *Cell. Signal.* 78, 109871. doi:10.1016/j.cellsig.2020.109871

Assaye, M. A., and Gizaw, S. T. (2022). Chaperone-mediated autophagy and its implications for neurodegeneration and cancer. *Int. J. general Med.* 15, 5635–5649. doi:10.2147/IJGM.S368364

Auzmendi-Iriarte, J., and Matheu, A. (2020). Impact of chaperone-mediated autophagy in brain aging: neurodegenerative diseases and glioblastoma. *Front. aging Neurosci.* 12, 630743. doi:10.3389/fnagi.2020.630743

Ayob, A. Z., and Ramasamy, T. S. (2018). Cancer stem cells as key drivers of tumour progression. *J. Biomed. Sci.* 25 (1), 20. doi:10.1186/s12929-018-0426-4

Bao, L., Jaramillo, M. C., Zhang, Z., Zheng, Y., Yao, M., Zhang, D. D., et al. (2015). Induction of autophagy contributes to cisplatin resistance in human ovarian cancer cells. *Mol. Med. Rep.* 11 (1), 91–98. doi:10.3892/mmr.2014.2671

Belizário, J., Vieira-Cordeiro, L., and Enns, S. (2015). Necroptotic cell death signaling and execution pathway: lessons from knockout mice. *Mediat. Inflamm.* 2015, 128076. doi:10.1155/2015/128076

Beloribi-Djefaflia, S., Vasseur, S., and Guillaumond, F. (2016). Lipid metabolic reprogramming in cancer cells. *Oncogenesis* 5 (1), e189. doi:10.1038/oncsis.2015.49

Ben-Sahra, I., and Manning, B. D. (2017). mTORC1 signaling and the metabolic control of cell growth. *Curr. Opin. Cell Biol.* 45, 72–82. doi:10.1016/j.ceb.2017.02.012

Bersuker, K., Hendricks, J. M., Li, Z., Magtanong, L., Ford, B., Tang, P. H., et al. (2019). The CoQ oxidoreductase FSP1 acts parallel to GPX4 to inhibit ferroptosis. *Nature* 575 (7784), 688–692. doi:10.1038/s41586-019-1705-2

Bonadonna, G., Brusamolino, E., Valagussa, P., Rossi, A., Brugnatelli, L., Brambilla, C., et al. (1976). Combination chemotherapy as an adjuvant treatment in operable breast cancer. *N. Engl. J. Med.* 294 (8), 405–410. doi:10.1056/NEJM197602192940801

Bosl, G. J., Gluckman, R., Geller, N. L., Golbey, R. B., Whitmore, W. F., Jr., Herr, H., et al. (1986). VAB-6: an effective chemotherapy regimen for patients with germ-cell tumors. *J. Clin. Oncol. official J. Am. Soc. Clin. Oncol.* 4 (10), 1493–1499. doi:10.1200/JCO.1986.4.10.1493

Bray, F., Ferlay, J., Soerjomataram, I., Siegel, R. L., Torre, L. A., and Jemal, A. (2018). Global cancer statistics 2018: GLOBOCAN estimates of incidence and mortality worldwide for 36 cancers in 185 countries. *CA a cancer J. Clin.* 68 (6), 394–424. doi:10.3322/caac.21492

Bringman-Rodenbarger, L. R., Guo, A. H., Lyssiotis, C. A., and Lombard, D. B. (2018). Emerging roles for SIRT5 in metabolism and cancer. *Antioxidants and redox Signal.* 28 (8), 677–690. doi:10.1089/ars.2017.7264

Brooks, C. L., and Gu, W. (2008). p53 Activation: a case against Sir. *Cancer Cell* 13 (5), 377–378. doi:10.1016/j.ccr.2008.04.009

Byles, V., Zhu, L., Lovaas, J. D., Chmilewski, L. K., Wang, J., Faller, D. V., et al. (2012). SIRT1 induces EMT by cooperating with EMT transcription factors and enhances prostate cancer cell migration and metastasis. *Oncogene* 31 (43), 4619–4629. doi:10.1038/onc.2011.612

Cai, J., Wang, R., Chen, Y., Zhang, C., Fu, L., and Fan, C. (2024). LncRNA FIRRE regulated endometrial cancer radiotherapy sensitivity via the miR-199b-5p/SIRT1/BECN1 axis-mediated autophagy. *Genomics* 116 (1), 110750. doi:10.1016/j.ygeno.2023.110750

Carafa, V., Altucci, L., and Nebbioso, A. (2019). Dual tumor suppressor and tumor promoter action of sirtuins in determining malignant phenotype. *Front. Pharmacol.* 10, 38. doi:10.3389/fphar.2019.00038

Carew, J. S., Nawrocki, S. T., Kahue, C. N., Zhang, H., Yang, C., Chung, L., et al. (2007). Targeting autophagy augments the anticancer activity of the histone deacetylase inhibitor SAHA to overcome Bcr-Abl-mediated drug resistance. *Blood* 110 (1), 313–322. doi:10.1182/blood-2006-10-050260

Chakraborty, S., Datta, S., and Ghosh, S. (2019). Induction of autophagy under nitrosative stress: a complex regulatory interplay between SIRT1 and AMPK in MCF7 cells. *Cell. Signal.* 64, 109411. doi:10.1016/j.cellsig.2019.109411

Chan, H. Y., Ramasamy, T. S., Chung, F. F., and Teow, S. Y. (2024). Role of sirtuin 1 (SIRT1) in regulation of autophagy and nuclear factor-kappa Beta (NF-κβ) pathways in sorafenib-resistant hepatocellular carcinoma (HCC). *Cell Biochem. biophysics* 82 (2), 959–968. doi:10.1007/s12013-024-01247-3

Chang, W.-T., Huang, S.-C., Cheng, H.-L., Chen, S.-C., and Hsu, C.-L. (2021). Rutin and gallic acid regulates mitochondrial functions via the SIRT1 pathway in C2C12 myotubes. *Antioxidants* 10 (2), 286. doi:10.3390/antiox10020286

Chatterjee, A., Rodger, E. J., and Eccles, M. R. (2018). "Epigenetic drivers of tumourigenesis and cancer metastasis," in *Seminars in cancer biology* (Elsevier), 149–159.

Chen, D., Yu, J., and Zhang, L. (2016). Necroptosis: an alternative cell death program defending against cancer. *Biochimica Biophysica Acta (BBA) - Rev. Cancer* 1865 (2), 228–236. doi:10.1016/j.bbcan.2016.03.003

Chen, G., Huang, P., and Hu, C. (2020). The role of SIRT2 in cancer: a novel therapeutic target. *Int. J. cancer* 147 (12), 3297–3304. doi:10.1002/ijc.33118

Chen, J., Chen, H., and Pan, L. (2021). SIRT1 and gynecological malignancies (Review). *Oncol. Rep.* 45 (4), 43. doi:10.3892/or.2021.7994

Chen, J., Zhang, B., Wong, N., Lo, A. W., To, K. F., Chan, A. W., et al. (2011). Sirtuin 1 is upregulated in a subset of hepatocellular carcinomas where it is essential for

telomere maintenance and tumor cell growth. *Cancer Res.* 71 (12), 4138–4149. doi:10.1158/0008-5472.CAN-10-4274

Chen, Z., Jiang, Q., Zhu, P., Chen, Y., Xie, X., Du, Z., et al. (2019). NPRL2 enhances autophagy and the resistance to Everolimus in castration-resistant prostate cancer. *Prostate* 79 (1), 44–53. doi:10.1002/pros.23709

Chen, Z., Zhai, Y., Zhang, W., Teng, Y., and Yao, K. (2015). Single nucleotide polymorphisms of the sirtuin 1 (SIRT1) gene are associated with age-related macular degeneration in Chinese han individuals: a case–control pilot study. *Medicine* 94 (49), e2238. doi:10.1097/MD.0000000000002238

Cheng, F., Su, L., Yao, C., Liu, L., Shen, J., Liu, C., et al. (2016). SIRT1 promotes epithelial–mesenchymal transition and metastasis in colorectal cancer by regulating Fra-1 expression. *Cancer Lett.* 375 (2), 274–283. doi:10.1016/j.canlet.2016.03.010

Chi, H. (2012). Regulation and function of mTOR signalling in T cell fate decisions. *Nat. Rev. Immunol.* 12 (5), 325–338. doi:10.1038/nri3198

Cho, Y., Challa, S., Moquin, D., Genga, R., Ray, T. D., Guildford, M., et al. (2009). Phosphorylation-driven assembly of the RIP1-RIP3 complex regulates programmed necrosis and virus-induced inflammation. *Cell* 137 (6), 1112–1123. doi:10.1016/j.cell.2009.05.037

Cho, Y., Hwang, J. W., Park, N. J., Moon, J., Ali, K. H., Seo, Y. H., et al. (2023). SPC-180002, a SIRT1/3 dual inhibitor, impairs mitochondrial function and redox homeostasis and represents an antitumor activity. *Free Radic. Biol. and Med.* 208, 73–87. doi:10.1016/j.freeradbiomed.2023.07.033

Citron, M. L., Berry, D. A., Cirrincione, C., Hudis, C., Winer, E. P., Gradishar, W. J., et al. (2003). Randomized trial of dose-dense versus conventionally scheduled and sequential versus concurrent combination chemotherapy as postoperative adjuvant treatment of node-positive primary breast cancer: first report of Intergroup Trial C9741/Cancer and Leukemia Group B Trial 9741. *J. Clin. Oncol. official J. Am. Soc. Clin. Oncol.* 21 (8), 1431–1439. doi:10.1200/JCO.2003.09.081

Claerhout, S., Verschooten, L., Van Kelst, S., De Vos, R., Proby, C., Agostinis, P., et al. (2010). Concomitant inhibition of AKT and autophagy is required for efficient cisplatin-induced apoptosis of metastatic skin carcinoma. *Int. J. cancer* 127 (12), 2790–2803. doi:10.1002/ijc.25300

Condello, M., Mancini, G., and Meschini, S. (2020). The exploitation of liposomes in the inhibition of autophagy to defeat drug resistance. *Front. Pharmacol.* 11, 787. doi:10.3389/fphar.2020.00787

Crofton, J. (1959). Chemotherapy of pulmonary tuberculosis. *Br. Med. J.* 1 (5138), 1610–1614. doi:10.1136/bmj.1.5138.1610

Cuervo, A. M. (2004). Autophagy: many paths to the same end. *Mol. Cell. Biochem.* 263 (1-2), 55–72. doi:10.1023/b:mcbi.0000041848.57020.57

Cuervo, A. M., and Wong, E. (2014). Chaperone-mediated autophagy: roles in disease and aging. *Cell Res.* 24 (1), 92–104. doi:10.1038/cr.2013.153

Cui, Y., Tian, J., Wang, Z., Guo, H., Zhang, H., Wang, Z., et al. (2023). Fructose-induced mTORC1 activation promotes pancreatic cancer progression through inhibition of autophagy. *Cancer Res.* 83 (24), 4063–4079. doi:10.1158/0008-5472.CAN-23-0464

Dai, W., Zhou, J., Jin, B., and Pan, J. (2016). Class III-specific HDAC inhibitor Tenovin-6 induces apoptosis, suppresses migration and eliminates cancer stem cells in uveal melanoma. *Sci. Rep.* 6, 22622. doi:10.1038/srep22622

Dalby, K. N., Tekedereli, I., Lopez-Berestein, G., and Ozpolat, B. (2010). Targeting the prodeath and prosurvival functions of autophagy as novel therapeutic strategies in cancer. *Autophagy* 6 (3), 322–329. doi:10.4161/auto.6.3.11625

Debnath, J., Gammoh, N., and Ryan, K. M. (2023). Autophagy and autophagy-related pathways in cancer. *Nat. Rev. Mol. Cell Biol.* 24 (8), 560–575. doi:10.1038/s41580-023-00585-z

Degterev, A., Hitomi, J., Germscheid, M., Ch'en, I. L., Korkina, O., Teng, X., et al. (2008). Identification of RIP1 kinase as a specific cellular target of necrostatins. *Nat. Chem. Biol.* 4 (5), 313–321. doi:10.1038/nchembio.83

Degterev, A., Huang, Z., Boyce, M., Li, Y., Jagtap, P., Mizushima, N., et al. (2005). Chemical inhibitor of nonapoptotic cell death with therapeutic potential for ischemic brain injury. *Nat. Chem. Biol.* 1 (2), 112–119. doi:10.1038/nchembio711

DeVita, V. T., Simon, R. M., Hubbard, S. M., Young, R. C., Berard, C. W., Moxley, J. H., et al. (1980). Curability of advanced Hodgkin's disease with chemotherapy. Long-term follow-up of MOPP-treated patients at the National Cancer Institute. *Ann. Intern. Med.* 92 (5), 587–595. doi:10.7326/0003-4819-92-5-587

de Waal, E. J., Vreeling-Sindelárová, H., Schellens, J. P., Houtkooper, J. M., and James, J. (1986). Quantitative changes in the lysosomal vacuolar system of rat hepatocytes during short-term starvation. A morphometric analysis with special reference to macro- and microautophagy. *Cell tissue Res.* 243 (3), 641–648. doi:10.1007/BF00218073

Dixon, S. J., Lemberg, K. M., Lamprecht, M. R., Skouta, R., Zaitsev, E. M., Gleason, C. E., et al. (2012). Ferroptosis: an iron-dependent form of nonapoptotic cell death. *Cell* 149 (5), 1060–1072. doi:10.1016/j.cell.2012.03.042

Doll, S., Freitas, F. P., Shah, R., Aldrovandi, M., da Silva, M. C., Ingold, I., et al. (2019). FSP1 is a glutathione-independent ferroptosis suppressor. *Nature* 575 (7784), 693–698. doi:10.1038/s41586-019-1707-0

Du, R., Zhao, P., Wu, S., Gao, Y., Wu, R., Yang, M., et al. (2021). Sendeng-4 suppressed melanoma growth by induction of autophagy and apoptosis. *Evidence-based complementary Altern. Med. eCAM* 2021, 5519973. doi:10.1155/2021/5519973

Egan, D. F., Shackelford, D. B., Mihaylova, M. M., Gelino, S., Kohnz, R. A., Mair, W., et al. (2011). Phosphorylation of ULK1 (hATG1) by AMP-activated protein kinase connects energy sensing to mitophagy. *Sci. (New York, NY)* 331 (6016), 456–461. doi:10.1126/science.1196371

El-Kott, A. F., Al-Kahtani, M. A., and Shati, A. A. (2019). Calycosin induces apoptosis in adenocarcinoma HT29 cells by inducing cytotoxic autophagy mediated by SIRT1/AMPK-induced inhibition of Akt/mTOR. *Clin. Exp. Pharmacol. and physiology* 46 (10), 944–954. doi:10.1111/1440-1681.13133

Elmore, S. (2007). Apoptosis: a review of programmed cell death. *Toxicol. Pathol.* 35 (4), 495–516. doi:10.1080/01926230701320337

Fan, Q. W., Cheng, C., Hackett, C., Feldman, M., Houseman, B. T., Nicolaides, T., et al. (2010). Akt and autophagy cooperate to promote survival of drug-resistant glioma. *Sci. Signal.* 3 (147), ra81. doi:10.1126/scisignal.2001017

Fan, Y., Hou, T., Gao, Y., Dan, W., Liu, T., Liu, B., et al. (2021). Acetylation-dependent regulation of TPD52 isoform 1 modulates chaperone-mediated autophagy in prostate cancer. *Autophagy* 17 (12), 4386–4400. doi:10.1080/15548627.2021.1917130

Farber, S., and Diamond, L. K. (1948). Temporary remissions in acute leukemia in children produced by folic acid antagonist, 4-aminopteroyl-glutamic acid. *N. Engl. J. Med.* 238 (23), 787–793. doi:10.1056/NEJM194806032382301

Farcas, M., Gavrea, A. A., Gulei, D., Ionescu, C., Irimie, A., Catana, C. S., et al. (2019). SIRT1 in the development and treatment of hepatocellular carcinoma. *Front. Nutr.* 6, 148. doi:10.3389/fnut.2019.00148

Fernández, Á. F., Sebti, S., Wei, Y., Zou, Z., Shi, M., McMillan, K. L., et al. (2018). Disruption of the beclin 1–BCL2 autophagy regulatory complex promotes longevity in mice. *Nature* 558 (7708), 136–140. doi:10.1038/s41586-018-0162-7

Ferri, K. F., and Kroemer, G. (2001). Organelle-specific initiation of cell death pathways. *Nat. Cell Biol.* 3 (11), E255–E263. doi:10.1038/ncb1101-e255

Ferro, F., Servais, S., Besson, P., Roger, S., Dumas, J.-F., and Brisson, L. (2020). Autophagy and mitophagy in cancer metabolic remodelling. *Seminars Cell and Dev. Biol.* 98, 129–138. doi:10.1016/j.semcdb.2019.05.029

Fiorentino, F., Carafa, V., Favale, G., Altucci, L., Mai, A., and Rotili, D. (2021). The two-faced role of SIRT6 in cancer. *Cancers* 13 (5), 1156. doi:10.3390/cancers13051156

Frye, R. A. (1999). Characterization of five human cDNAs with homology to the yeast SIR2 gene: Sir2-like proteins (sirtuins) metabolize NAD and may have protein ADP-ribosyltransferase activity. *Biochem. biophysical Res. Commun.* 260 (1), 273–279. doi:10.1006/bbrc.1999.0897

Frye, R. A. (2000). Phylogenetic classification of prokaryotic and eukaryotic Sir2-like proteins. *Biochem. biophysical Res. Commun.* 273 (2), 793–798. doi:10.1006/bbrc.2000.3000

Fu, L., Han, B. K., Meng, F. F., Wang, J. W., Wang, T. Y., Li, H. J., et al. (2021). Jaridon 6, a new diterpene from Rabdosia rubescens (Hemsl.) Hara, can display anti-gastric cancer resistance by inhibiting SIRT1 and inducing autophagy. *Phytotherapy Res. PTR* 35 (10), 5720–5733. doi:10.1002/ptr.7231

Funazo, T., Nomizo, T., and Kim, Y. H. (2017). Liver metastasis is associated with poor progression-free survival in patients with non–small cell lung cancer treated with nivolumab. *J. Thorac. Oncol.* 12 (9), e140–e141. doi:10.1016/j.jtho.2017.04.027

Galluzzi, L., Spranger, S., Fuchs, E., and López-Soto, A. (2019). WNT signaling in cancer immunosurveillance. *Trends Cell Biol.* 29 (1), 44–65. doi:10.1016/j.tcb.2018.08.005

Galluzzi, L., Vitale, I., Aaronson, S. A., Abrams, J. M., Adam, D., Agostinis, P., et al. (2018). Molecular mechanisms of cell death: recommendations of the nomenclature committee on cell death 2018. *Cell death Differ.* 25 (3), 486–541. doi:10.1038/s41418-017-0012-4

Galluzzi, L., Vitale, I., Abrams, J., Alnemri, E., Baehrecke, E., Blagosklonny, M., et al. (2012). Molecular definitions of cell death subroutines: recommendations of the Nomenclature Committee on Cell Death 2012. *Cell Death and Differ.* 19 (1), 107–120. doi:10.1038/cdd.2011.96

Gao, X., Zacharek, A., Salkowski, A., Grignon, D. J., Sakr, W., Porter, A. T., et al. (1995). Loss of heterozygosity of the BRCA1 and other loci on chromosome 17q in human prostate cancer. *Cancer Res.* 55 (5), 1002–1005.

Ge, J., Chen, Z., Huang, J., Chen, J., Yuan, W., Deng, Z., et al. (2014). Upregulation of autophagy-related gene-5 (ATG-5) is associated with chemoresistance in human gastric cancer. *PloS one* 9 (10), e110293. doi:10.1371/journal.pone.0110293

Golstein, P., and Kroemer, G. (2007). Cell death by necrosis: towards a molecular definition. *Trends Biochem. Sci.* 32 (1), 37–43. doi:10.1016/j.tibs.2006.11.001

Goodman, L. S., Wintrobe, M. M., Dameshek, W., Goodman, M. J., Gilman, A., and McLennan, M. T. (1946). Nitrogen mustard therapy; use of methyl-bis (beta-chloroethyl) amine hydrochloride and tris (beta-chloroethyl) amine hydrochloride for Hodgkin's disease, lymphosarcoma, leukemia and certain allied and miscellaneous disorders. *J. Am. Med. Assoc.* 132, 126–132. doi:10.1001/jama.1946.02870380008004

Guan, J., Zhang, Z. Y., Sun, J. H., Wang, X. P., Zhou, Z. Q., and Qin, L. (2023). LITAF inhibits colorectal cancer stemness and metastatic behavior by regulating FOXO1-mediated SIRT1 expression. *Clin. and Exp. metastasis* 40 (4), 309–320. doi:10.1007/s10585-023-10213-x

Guo, H., Ding, H., Tang, X., Liang, M., Li, S., Zhang, J., et al. (2021). Quercetin induces pro-apoptotic autophagy via SIRT1/AMPK signaling pathway in human lung cancer cell lines A549 and H1299 *in vitro*. *Thorac. cancer* 12 (9), 1415–1422. doi:10.1111/1759-7714.13925

Han, J., Hubbard, B. P., Lee, J., Montagna, C., Lee, H.-W., Sinclair, D. A., et al. (2013a). Analysis of 41 cancer cell lines reveals excessive allelic loss and novel mutations in the SIRT1 gene. *Cell Cycle* 12 (2), 263–270. doi:10.4161/cc.23056

Han, L., Liang, X. H., Chen, L. X., Bao, S. M., and Yan, Z. Q. (2013b). SIRT1 is highly expressed in brain metastasis tissues of non-small cell lung cancer (NSCLC) and in positive regulation of NSCLC cell migration. *Int. J. Clin. Exp. pathology* 6 (11), 2357–2365.

Hanahan, D., and Weinberg, R. A. (2011). Hallmarks of cancer: the next generation. *Cell* 144 (5), 646–674. doi:10.1016/j.cell.2011.02.013

Hao, C., Zhu, P. X., Yang, X., Han, Z. P., Jiang, J. H., Zong, C., et al. (2014). Overexpression of SIRT1 promotes metastasis through epithelial-mesenchymal transition in hepatocellular carcinoma. *BMC cancer* 14, 978. doi:10.1186/1471-2407-14-978

Harguindey, S., Orive, G., Luis Pedraz, J., Paradiso, A., and Reshkin, S. J. (2005). The role of pH dynamics and the Na+/H+ antiporter in the etiopathogenesis and treatment of cancer. Two faces of the same coin--one single nature. *Biochimica biophysica acta* 1756 (1), 1–24. doi:10.1016/j.bbcan.2005.06.004

Hawley, S. A., Davison, M., Woods, A., Davies, S. P., Beri, R. K., Carling, D., et al. (1996). Characterization of the AMP-activated protein kinase kinase from rat liver and identification of threonine 172 as the major site at which it phosphorylates AMP-activated protein kinase. *J. Biol. Chem.* 271 (44), 27879–27887. doi:10.1074/jbc.271.44.27879

He, F., Chen, Y., He, D., and He, S. (2023). USP14-mediated deubiquitination of SIRT1 in macrophage promotes fatty acid oxidation amplification and M2 phenotype polarization. *Biochem. biophysical Res. Commun.* 646, 19–29. doi:10.1016/j.bbrc.2022.12.076

He, S., Wang, L., Miao, L., Wang, T., Du, F., Zhao, L., et al. (2009). Receptor interacting protein kinase-3 determines cellular necrotic response to TNF-alpha. *Cell* 137 (6), 1100–1111. doi:10.1016/j.cell.2009.05.021

Heltweg, B., Gatbonton, T., Schuler, A. D., Posakony, J., Li, H., Goehle, S., et al. (2006). Antitumor activity of a small-molecule inhibitor of human silent information regulator 2 enzymes. *Cancer Res.* 66 (8), 4368–4377. doi:10.1158/0008-5472.CAN-05-3617

Herbert, K. J., Cook, A. L., and Snow, E. T. (2014). SIRT1 inhibition restores apoptotic sensitivity in p53-mutated human keratinocytes. *Toxicol. Appl. Pharmacol.* 277 (3), 288–297. doi:10.1016/j.taap.2014.04.001

Heshmati, M., Soltani, A., Sanaei, M. J., Nahid-Samiei, M., Shirzad, H., Jami, M. S., et al. (2020). Ghrelin induces autophagy and CXCR4 expression via the SIRT1/AMPK axis in lymphoblastic leukemia cell lines. *Cell. Signal.* 66, 109492. doi:10.1016/j.cellsig.2019.109492

Hill, C., and Wang, Y. (2020). The importance of epithelial-mesenchymal transition and autophagy in cancer drug resistance. *Cancer drug Resist. (Alhambra, Calif.)* 3 (1), 38–47. doi:10.20517/cdr.2019.75

Hirano, T. (2002). The ABCs of SMC proteins: two-armed ATPases for chromosome condensation, cohesion, and repair. *Genes and Dev.* 16 (4), 399–414. doi:10.1101/gad.955102

Hirano, T., Kobayashi, R., and Hirano, M. (1997). Condensins, chromosome condensation protein complexes containing XCAP-C, XCAP-E and a Xenopus homolog of the Drosophila Barren protein. *Cell* 89 (4), 511–521. doi:10.1016/s0092-8674(00)80233-0

Holler, N., Zaru, R., Micheau, O., Thome, M., Attinger, A., Valitutti, S., et al. (2000). Fas triggers an alternative, caspase-8–independent cell death pathway using the kinase RIP as effector molecule. *Nat. Immunol.* 1 (6), 489–495. doi:10.1038/82732

Hosokawa, N., Hara, T., Kaizuka, T., Kishi, C., Takamura, A., Miura, Y., et al. (2009). Nutrient-dependent mTORC1 association with the ULK1–Atg13–FIP200 complex required for autophagy. *Mol. Biol. Cell* 20 (7), 1981–1991. doi:10.1091/mbc.e08-12-1248

Housman, G., Byler, S., Heerboth, S., Lapinska, K., Longacre, M., Snyder, N., et al. (2014). Drug resistance in cancer: an overview. *Cancers* 6 (3), 1769–1792. doi:10.3390/cancers6031769

Hryniuk, W., and Bush, H. (1984). The importance of dose intensity in chemotherapy of metastatic breast cancer. *J. Clin. Oncol. official J. Am. Soc. Clin. Oncol.* 2 (11), 1281–1288. doi:10.1200/JCO.1984.2.11.1281

Hu, J., Dong, S. W., Pei, Y., Wang, J., Zhang, J., and Wei, X. P. (2021). LncRNA MITA1 promotes gefitinib resistance by inducing autophagy in lung cancer cells. *Biochem. biophysical Res. Commun.* 551, 21–26. doi:10.1016/j.bbrc.2021.02.130

Huang, M., Wang, J., Zhang, Z., and Zuo, X. (2024). ZMIZ1 regulates proliferation, autophagy and apoptosis of colon cancer cells by mediating ubiquitin-proteasome degradation of SIRT1. *Biochem. Genet.* 62 (4), 3245–3259. doi:10.1007/s10528-023-10573-9

Hur, Y., Kaprio, J., Iacono, W., Boomsma, D., McGue, M., Silventoinen, K., et al. (2008). Genetic influences on the difference in variability of height, weight and body mass index between Caucasian and East Asian adolescent twins. *Int. J. Obes.* 32 (10), 1455–1467. doi:10.1038/ijo.2008.144

Ichikawa, A., Fujita, Y., Hosaka, Y., Kadota, T., Ito, A., Yagishita, S., et al. (2020). Chaperone-mediated autophagy receptor modulates tumor growth and chemoresistance in non-small cell lung cancer. *Cancer Sci.* 111 (11), 4154–4165. doi:10.1111/cas.14629

Ichimura, Y., Kirisako, T., Takao, T., Satomi, Y., Shimonishi, Y., Ishihara, N., et al. (2000). A ubiquitin-like system mediates protein lipidation. *Nature* 408 (6811), 488–492. doi:10.1038/35044114

Ingold, I., Berndt, C., Schmitt, S., Doll, S., Poschmann, G., Buday, K., et al. (2018). Selenium utilization by GPX4 is required to prevent hydroperoxide-induced ferroptosis. *Cell* 172 (3), 409–422. doi:10.1016/j.cell.2017.11.048

Inoue, T., Hiratsuka, M., Osaki, M., Yamada, H., Kishimoto, I., Yamaguchi, S., et al. (2007). SIRT2, a tubulin deacetylase, acts to block the entry to chromosome condensation in response to mitotic stress. *Oncogene* 26 (7), 945–957. doi:10.1038/sj.onc.1209857

Islam, A., Chang, Y. C., Chen, X. C., Weng, C. W., Chen, C. Y., Wang, C. W., et al. (2024a). Water-soluble 4-(dimethylaminomethyl)heliomycin exerts greater antitumor effects than parental heliomycin by targeting the tNOX-SIRT1 axis and apoptosis in oral cancer cells. *eLife* 12. doi:10.7554/eLife.87873

Islam, A., Chang, Y. C., Tsao, N. W., Wang, S. Y., and Chueh, P. J. (2024b). Calocedrus formosana essential oils induce ROS-mediated autophagy and apoptosis by targeting SIRT1 in colon cancer cells. *Antioxidants (Basel, Switz.)* 13 (3), 284. doi:10.3390/antiox13030284

Jang, K. Y., Noh, S. J., Lehwald, N., Tao, G. Z., Bellovin, D. I., Park, H. S., et al. (2012a). SIRT1 and c-Myc promote liver tumor cell survival and predict poor survival of human hepatocellular carcinomas. *PloS one* 7 (9), e45119. doi:10.1371/journal.pone.0045119

Jang, S.-H., Min, K.-W., Paik, S. S., and Jang, K.-S. (2012b). Loss of SIRT1 histone deacetylase expression associates with tumour progression in colorectal adenocarcinoma. *J. Clin. pathology* 65 (8), 735–739. doi:10.1136/jclinpath-2012-200685

Ji, J., Wang, K., Meng, X., Zhong, H., Li, X., Zhao, H., et al. (2022). Elaiophylin inhibits tumorigenesis of human lung adenocarcinoma by inhibiting mitophagy via suppression of SIRT1/nrf2 signaling. *Cancers* 14 (23), 5812. doi:10.3390/cancers14235812

Jiang, K., Lyu, L., Shen, Z., Zhang, J., Zhang, H., Dong, J., et al. (2014). Overexpression of SIRT1 is a poor prognostic factor for advanced colorectal cancer. *Chin. Med. J.* 127 (11), 2021–2024. doi:10.3760/cma.j.issn.0366-6999.20140044

Jiang, P., and Mizushima, N. (2014). Autophagy and human diseases. *Cell Res.* 24 (1), 69–79. doi:10.1038/cr.2013.161

Jiang, X., Stockwell, B. R., and Conrad, M. (2021). Ferroptosis: mechanisms, biology and role in disease. *Nat. Rev. Mol. Cell Biol.* 22 (4), 266–282. doi:10.1038/s41580-020-00324-8

Jiao, F., and Gong, Z. (2020). The beneficial roles of SIRT1 in neuroinflammation-related diseases. *Oxidative Med. Cell. Longev.* 2020, 6782872. doi:10.1155/2020/6782872

Jin, J., Fan, Z., Long, Y., Li, Y., He, Q., Yang, Y., et al. (2024). Matrine induces ferroptosis in cervical cancer through activation of piezo1 channel. *Phytomedicine Int. J. phytotherapy Phytopharm.* 122, 155165. doi:10.1016/j.phymed.2023.155165

Jin, Q., Yan, T., Ge, X., Sun, C., Shi, X., and Zhai, Q. (2007). Cytoplasm-localized SIRT1 enhances apoptosis. *J. Cell. physiology* 213 (1), 88–97. doi:10.1002/jcp.21091

Jin, Y., Qiu, J., Lu, X., and Li, G. (2022). C-MYC inhibited ferroptosis and promoted immune evasion in ovarian cancer cells through NCOA4 mediated ferritin autophagy. *Cells* 11 (24), 4127. doi:10.3390/cells11244127

Jing, Z., He, X., Jia, Z., Sa, Y., Yang, B., and Liu, P. (2021). NCAPD2 inhibits autophagy by regulating Ca(2+)/CAMKK2/AMPK/mTORC1 pathway and PARP-1/SIRT1 axis to promote colorectal cancer. *Cancer Lett.* 520, 26–37. doi:10.1016/j.canlet.2021.06.029

Jung, C. H., Jun, C. B., Ro, S.-H., Kim, Y.-M., Otto, N. M., Cao, J., et al. (2009). ULK-Atg13-FIP200 complexes mediate mTOR signaling to the autophagy machinery. *Mol. Biol. Cell* 20 (7), 1992–2003. doi:10.1091/mbc.e08-12-1249

Kagan, V. E., Mao, G., Qu, F., Angeli, J. P., Doll, S., Croix, C. S., et al. (2017). Oxidized arachidonic and adrenic PEs navigate cells to ferroptosis. *Nat. Chem. Biol.* 13 (1), 81–90. doi:10.1038/nchembio.2238

Kalle, A. M., Mallika, A., Badiger, J., Talukdar, P., and Sachchidanand, (2010). Inhibition of SIRT1 by a small molecule induces apoptosis in breast cancer cells. *Biochem. biophysical Res. Commun.* 401 (1), 13–19. doi:10.1016/j.bbrc.2010.08.118

Kang, J. A., Kim, Y. J., Jang, K. Y., Moon, H. W., Lee, H., Lee, S., et al. (2024). SIRT1 ISGylation accelerates tumor progression by unleashing SIRT1 from the inactive state to promote its deacetylase activity. *Exp. and Mol. Med.* 56 (3), 656–673. doi:10.1038/s12276-024-01194-2

Karantza-Wadsworth, V., Patel, S., Kravchuk, O., Chen, G., Mathew, R., Jin, S., et al. (2007). Autophagy mitigates metabolic stress and genome damage in mammary tumorigenesis. *Genes Dev.* 21 (13), 1621–1635. doi:10.1101/gad.1565707

Kaushik, S., Bandyopadhyay, U., Sridhar, S., Kiffin, R., Martinez-Vicente, M., Kon, M., et al. (2011). Chaperone-mediated autophagy at a glance. *J. Cell Sci.* 124 (Pt 4), 495–499. doi:10.1242/jcs.073874

Kennedy, B. K., and Lamming, D. W. (2016). The mechanistic target of rapamycin: the grand conducTOR of metabolism and aging. *Cell metab.* 23 (6), 990–1003. doi:10.1016/j.cmet.2016.05.009

Kim, J., Kundu, M., Viollet, B., and Guan, K.-L. (2011). AMPK and mTOR regulate autophagy through direct phosphorylation of Ulk1. *Nat. Cell Biol.* 13 (2), 132–141. doi:10.1038/ncb2152

Kim, J. K., Silwal, P., and Jo, E. K. (2022). Sirtuin 1 in host defense during infection. *Cells* 11 (18), 2921. doi:10.3390/cells11182921

Kim, K. H., and Lee, M.-S. (2014). Autophagy—a key player in cellular and body metabolism. *Nat. Rev. Endocrinol.* 10 (6), 322–337. doi:10.1038/nrendo.2014.35

Kimura, K., and Hirano, T. (2000). Dual roles of the 11S regulatory subcomplex in condensin functions. *Proc. Natl. Acad. Sci.* 97 (22), 11972–11977. doi:10.1073/pnas.220326097

Kiraz, Y., Adan, A., Kartal Yandim, M., and Baran, Y. (2016). Major apoptotic mechanisms and genes involved in apoptosis. *Tumor Biol.* 37 (7), 8471–8486. doi:10.1007/s13277-016-5035-9

Kirkin, V., and Rogov, V. V. (2019). A diversity of selective autophagy receptors determines the specificity of the autophagy pathway. *Mol. Cell* 76 (2), 268–285. doi:10.1016/j.molcel.2019.09.005

Kraft, V. A. N., Bezjian, C. T., Pfeiffer, S., Ringelstetter, L., Müller, C., Zandkarimi, F., et al. (2020). GTP cyclohydrolase 1/tetrahydrobiopterin counteract ferroptosis through lipid remodeling. *ACS central Sci.* 6 (1), 41–53. doi:10.1021/acscentsci.9b01063

Kroemer, G., and Jäättelä, M. (2005). Lysosomes and autophagy in cell death control. *Nat. Rev. Cancer* 5 (11), 886–897. doi:10.1038/nrc1738

Kumar, A., and Chauhan, S. (2016). How much successful are the medicinal chemists in modulation of SIRT1: a critical review. *Eur. J. Med. Chem.* 119, 45–69. doi:10.1016/j.ejmech.2016.04.063

Lagunas-Rangel, F. A. (2023). Role of SIRT5 in cancer. Friend or foe? *Biochimie* 209, 131–141. doi:10.1016/j.biochi.2023.02.008

Lain, S., Hollick, J. J., Campbell, J., Staples, O. D., Higgins, M., Aoubala, M., et al. (2008). Discovery, *in vivo* activity, and mechanism of action of a small-molecule p53 activator. *Cancer Cell* 13 (5), 454–463. doi:10.1016/j.ccr.2008.03.004

Lara, E., Mai, A., Calvanese, V., Altucci, L., Lopez-Nieva, P., Martinez-Chantar, M., et al. (2009). Salermide, a Sirtuin inhibitor with a strong cancer-specific proapoptotic effect. *Oncogene* 28 (6), 781–791. doi:10.1038/onc.2008.436

Lee, J., You, J. H., and Roh, J. L. (2022b). Poly(rC)-binding protein 1 represses ferritinophagy-mediated ferroptosis in head and neck cancer. *Redox Biol.* 51, 102276. doi:10.1016/j.redox.2022.102276

Lee, J. G., Shin, J. H., Shim, H. S., Lee, C. Y., Kim, D. J., Kim, Y. S., et al. (2015). Autophagy contributes to the chemo-resistance of non-small cell lung cancer in hypoxic conditions. *Respir. Res.* 16, 138. doi:10.1186/s12931-015-0285-4

Lee, J. H., Cheng, R., Rogaeva, E., Meng, Y., Stern, Y., Santana, V., et al. (2008). Further examination of the candidate genes in chromosome 12p13 locus for late-onset alzheimer disease. *Neurogenetics* 9, 127–138. doi:10.1007/s10048-008-0122-8

Lee, S. J., Choi, Y. J., Kim, H. I., Moon, H. E., Paek, S. H., Kim, T. Y., et al. (2022a). Platycodin D inhibits autophagy and increases glioblastoma cell death via LDLR upregulation. *Mol. Oncol.* 16 (1), 250–268. doi:10.1002/1878-0261.12966

Lei, G., Zhuang, L., and Gan, B. (2022). Targeting ferroptosis as a vulnerability in cancer. *Nat. Rev. Cancer* 22 (7), 381–396. doi:10.1038/s41568-022-00459-0

Li, H., Sun, Y., Yao, Y., Ke, S., Zhang, N., Xiong, W., et al. (2024b). USP8-governed GPX4 homeostasis orchestrates ferroptosis and cancer immunotherapy. *Proc. Natl. Acad. Sci. U. S. A.* 121 (16), e2315541121. doi:10.1073/pnas.2315541121

Li, H., Yu, K., Hu, H., Zhang, X., Zeng, S., Li, J., et al. (2024a). METTL17 coordinates ferroptosis and tumorigenesis by regulating mitochondrial translation in colorectal cancer. *Redox Biol.* 71, 103087. doi:10.1016/j.redox.2024.103087

Li, J., Han, Y., Zhou, M., Liu, N., Li, H., Huang, G., et al. (2023b). Electroacupuncture ameliorates AOM/DSS-induced mice colorectal cancer by inhibiting inflammation and promoting autophagy via the SIRT1/miR-215/Atg14 axis. *Aging* 15 (22), 13194–13212. doi:10.18632/aging.205236

Li, J., Hou, N., Faried, A., Tsutsumi, S., and Kuwano, H. (2010). Inhibition of autophagy augments 5-fluorouracil chemotherapy in human colon cancer *in vitro* and *in vivo* model. *Eur. J. cancer (Oxford, Engl. 1990)* 46 (10), 1900–1909. doi:10.1016/j.ejca.2010.02.021

Li, L., Liu, W., Sun, Q., Zhu, H., Hong, M., and Qian, S. (2021). Decitabine downregulates TIGAR to induce apoptosis and autophagy in myeloid leukemia cells. *Oxidative Med. Cell. Longev.* 2021, 8877460. doi:10.1155/2021/8877460

Li, X., Song, D., Chen, Y., Huang, C., Liu, A., Wu, Q., et al. (2023a). NSD2 methylates AROS to promote SIRT1 activation and regulates fatty acid metabolism-mediated cancer radiotherapy. *Cell Rep.* 42 (10), 113126. doi:10.1016/j.celrep.2023.113126

Li, Y., Chu, L. W., Li, Z., Yik, P.-Y., and Song, Y.-Q. (2009). A study on the association of the chromosome 12p13 locus with sporadic late-onset alzheimer's disease in Chinese. *Dementia geriatric cognitive Disord.* 27 (6), 508–512. doi:10.1159/000218740

Li, Y. J., Lei, Y. H., Yao, N., Wang, C. R., Hu, N., Ye, W. C., et al. (2017). Autophagy and multidrug resistance in cancer. *Chin. J. cancer* 36 (1), 52. doi:10.1186/s40880-017-0219-2

Liang, X., Tang, J., Liang, Y., Jin, R., and Cai, X. (2014a). Suppression of autophagy by chloroquine sensitizes 5-fluorouracil-mediated cell death in gallbladder carcinoma cells. *Cell and Biosci.* 4 (1), 10. doi:10.1186/2045-3701-4-10

Liang, X. H., Jackson, S., Seaman, M., Brown, K., Kempkes, B., Hibshoosh, H., et al. (1999). Induction of autophagy and inhibition of tumorigenesis by beclin 1. *Nature* 402 (6762), 672–676. doi:10.1038/45257

Liang, X. H., Yu, J., Brown, K., and Levine, B. (2001). Beclin 1 contains a leucine-rich nuclear export signal that is required for its autophagy and tumor suppressor function. *Cancer Res.* 61 (8), 3443–3449.

Liang, Z., Yang, Y., Wang, H., Yi, W., Yan, X., Yan, J., et al. (2014b). Inhibition of SIRT1 signaling sensitizes the antitumor activity of silybin against human lung adenocarcinoma cells *in vitro* and *in vivo*. *Mol. cancer Ther.* 13 (7), 1860–1872. doi:10.1158/1535-7163.MCT-13-0942

Lin, Z., and Fang, D. (2013). The roles of SIRT1 in cancer. *Genes and cancer* 4 (3-4), 97–104. doi:10.1177/1947601912475079

Liu, C., Zhou, L., Chen, J., Yang, Z., Chen, S., Wang, X., et al. (2023). Galectin-7 promotes cisplatin efficacy by facilitating apoptosis and G3BP1 degradation in cervical cancer. *Biochem. Pharmacol.* 217, 115834. doi:10.1016/j.bcp.2023.115834

Liu, D., Yang, Y., Liu, Q., and Wang, J. (2011). Inhibition of autophagy by 3-MA potentiates cisplatin-induced apoptosis in esophageal squamous cell carcinoma cells. *Med. Oncol. N. Lond. Engl.* 28 (1), 105–111. doi:10.1007/s12032-009-9397-3

Liu, F., Liu, D., Yang, Y., and Zhao, S. (2013). Effect of autophagy inhibition on chemotherapy-induced apoptosis in A549 lung cancer cells. *Oncol. Lett.* 5 (4), 1261–1265. doi:10.3892/ol.2013.1154

Liu, J., Lu, X., Zeng, S., Fu, R., Wang, X., Luo, L., et al. (2024a). ATF3-CBS signaling axis coordinates ferroptosis and tumorigenesis in colorectal cancer. *Redox Biol.* 71, 103118. doi:10.1016/j.redox.2024.103118

Liu, S., Wang, Z., Hu, L., Ye, C., Zhang, X., Zhu, Z., et al. (2024b). Pan-cancer analysis of super-enhancer-induced LINC00862 and validation as a SIRT1-promoting factor in cervical cancer and gastric cancer. *Transl. Oncol.* 45, 101982. doi:10.1016/j.tranon.2024.101982

Liu, X., Chhipa, R. R., Nakano, I., and Dasgupta, B. (2014). The AMPK inhibitor compound C is a potent AMPK-independent antiglioma agent. *Mol. cancer Ther.* 13 (3), 596–605. doi:10.1158/1535-7163.MCT-13-0579

Long, M., and McWilliams, T. G. (2020). Monitoring autophagy in cancer: from bench to bedside. *Seminars Cancer Biol.* 66, 12–21. doi:10.1016/j.semcancer.2019.05.016

Luo, H., Zhang, H., Mao, J., Cao, H., Tao, Y., Zhao, G., et al. (2023b). Exosome-based nanoimmunotherapy targeting TAMs, a promising strategy for glioma. *Cell death and Dis.* 14 (4), 235. doi:10.1038/s41419-023-05753-9

Luo, P., Zhang, Q., Shen, S., An, Y., Yuan, L., Wong, Y. K., et al. (2023a). Mechanistic engineering of celastrol liposomes induces ferroptosis and apoptosis by directly targeting VDAC2 in hepatocellular carcinoma. *Asian J. Pharm. Sci.* 18 (6), 100874. doi:10.1016/j.ajps.2023.100874

Lv, Y., Lin, S., and Peng, F. (2017). *SIRT1 gene polymorphisms and risk of lung cancer*. Cancer management and research 2017 9, 381–386.

Maan, M., Peters, J. M., Dutta, M., and Patterson, A. D. (2018). Lipid metabolism and lipophagy in cancer. *Biochem. biophysical Res. Commun.* 504 (3), 582–589. doi:10.1016/j.bbrc.2018.02.097

Madrigal-Matute, J., and Cuervo, A. M. (2016). Regulation of liver metabolism by autophagy. *Gastroenterology* 150 (2), 328–339. doi:10.1053/j.gastro.2015.09.042

Mao, B., Hu, F., Cheng, J., Wang, P., Xu, M., Yuan, F., et al. (2014). SIRT1 regulates YAP2-mediated cell proliferation and chemoresistance in hepatocellular carcinoma. *Oncogene* 33 (11), 1468–1474. doi:10.1038/onc.2013.88

Mao, C., Liu, X., Zhang, Y., Lei, G., Yan, Y., Lee, H., et al. (2021). DHODH-mediated ferroptosis defence is a targetable vulnerability in cancer. *Nature* 593 (7860), 586–590. doi:10.1038/s41586-021-03539-7

Marzella, L., Ahlberg, J., and Glaumann, H. (1981). Autophagy, heterophagy, microautophagy and crinophagy as the means for intracellular degradation. *Virchows Arch. B, Cell Pathol. Incl. Mol. Pathol.* 36 (2-3), 219–234. doi:10.1007/BF02912068

Mathew, R., Karp, C. M., Beaudoin, B., Vuong, N., Chen, G., Chen, H.-Y., et al. (2009). Autophagy suppresses tumorigenesis through elimination of p62. *Cell* 137 (6), 1062–1075. doi:10.1016/j.cell.2009.03.048

Mei, Z., Duan, C., Li, C., Cui, L., and Ogino, S. (2016). Prognostic role of tumor PIK3CA mutation in colorectal cancer: a systematic review and meta-analysis. *Ann. Oncol.* 27 (10), 1836–1848. doi:10.1093/annonc/mdw264

Michishita, E., Park, J. Y., Burneskis, J. M., Barrett, J. C., and Horikawa, I. (2005). Evolutionarily conserved and nonconserved cellular localizations and functions of human SIRT proteins. *Mol. Biol. Cell* 16 (10), 4623–4635. doi:10.1091/mbc.e05-01-0033

Mijaljica, D., Prescott, M., and Devenish, R. J. (2011). Microautophagy in mammalian cells: revisiting a 40-year-old conundrum. *Autophagy* 7 (7), 673–682. doi:10.4161/auto.7.7.14733

Mizushima, N., and Komatsu, M. (2011). Autophagy: renovation of cells and tissues. *Cell* 147 (4), 728–741. doi:10.1016/j.cell.2011.10.026

Mizushima, N., Noda, T., Yoshimori, T., Tanaka, Y., Ishii, T., George, M. D., et al. (1998). A protein conjugation system essential for autophagy. *Nature* 395 (6700), 395–398. doi:10.1038/26506

Molla, M. D., Dessie, G., Akalu, Y., and Ayelign, B. (2020). Hepatocellular expression of SIRT1 and its effect on hepatocellular carcinoma progression: a future therapeutic perspective. *Int. J. hepatology* 2020, 2374615. doi:10.1155/2020/2374615

Mortimore, G. E., Hutson, N. J., and Surmacz, C. A. (1983). Quantitative correlation between proteolysis and macro- and microautophagy in mouse hepatocytes during starvation and refeeding. *Proc. Natl. Acad. Sci. U. S. A.* 80 (8), 2179–2183. doi:10.1073/pnas.80.8.2179

Mortimore, G. E., Lardeux, B. R., and Adams, C. E. (1988). Regulation of microautophagy and basal protein turnover in rat liver. Effects of short-term starvation. *J. Biol. Chem.* 263 (5), 2506–2512. doi:10.1016/s0021-9258(18)69235-x

Moynihan, K. A., Grimm, A. A., Plueger, M. M., Bernal-Mizrachi, E., Ford, E., Cras-Méneur, C., et al. (2005). Increased dosage of mammalian Sir2 in pancreatic beta cells enhances glucose-stimulated insulin secretion in mice. *Cell metab.* 2 (2), 105–117. doi:10.1016/j.cmet.2005.07.001

Mu, N., Lei, Y., Wang, Y., Wang, Y., Duan, Q., Ma, G., et al. (2019). Inhibition of SIRT1/2 upregulates HSPA5 acetylation and induces pro-survival autophagy via ATF4-DDIT4-mTORC1 axis in human lung cancer cells. *Apoptosis Int. J. Program. Cell death* 24 (9-10), 798–811. doi:10.1007/s10495-019-01559-3

Mvunta, D. H., Miyamoto, T., Asaka, R., Yamada, Y., Ando, H., Higuchi, S., et al. (2017). SIRT1 regulates the chemoresistance and invasiveness of ovarian carcinoma cells. *Transl. Oncol.* 10 (4), 621–631. doi:10.1016/j.tranon.2017.05.005

Nakatogawa, H. (2020). Mechanisms governing autophagosome biogenesis. *Nat. Rev. Mol. Cell Biol.* 21 (8), 439–458. doi:10.1038/s41580-020-0241-0

North, B. J., Marshall, B. L., Borra, M. T., Denu, J. M., and Verdin, E. (2003). The human Sir2 ortholog, SIRT2, is an NAD+-dependent tubulin deacetylase. *Mol. Cell* 11 (2), 437–444. doi:10.1016/s1097-2765(03)00038-8

Nusse, R., and Clevers, H. (2017). Wnt/β-Catenin signaling, disease, and emerging therapeutic modalities. *Cell* 169 (6), 985–999. doi:10.1016/j.cell.2017.05.016

O'Donovan, T. R., O'Sullivan, G. C., and McKenna, S. L. (2011). Induction of autophagy by drug-resistant esophageal cancer cells promotes their survival and recovery following treatment with chemotherapeutics. *Autophagy* 7 (5), 509–524. doi:10.4161/auto.7.6.15066

Ogier-Denis, E., and Codogno, P. (2003). Autophagy: a barrier or an adaptive response to cancer. *Biochimica biophysica acta* 1603 (2), 113–128. doi:10.1016/s0304-419x(03)00004-0

Ong, A. L. C., and Ramasamy, T. S. (2018). Role of Sirtuin1-p53 regulatory axis in aging, cancer and cellular reprogramming. *Ageing Res. Rev.* 43, 64–80. doi:10.1016/j.arr.2018.02.004

Oon, C. E., Strell, C., Yeong, K. Y., Östman, A., and Prakash, J. (2015). SIRT1 inhibition in pancreatic cancer models: contrasting effects *in vitro* and *in vivo*. *Eur. J. Pharmacol.* 757, 59–67. doi:10.1016/j.ejphar.2015.03.064

Ota, H., Tokunaga, E., Chang, K., Hikasa, M., Iijima, K., Eto, M., et al. (2006). Sirt1 inhibitor, Sirtinol, induces senescence-like growth arrest with attenuated Ras-MAPK signaling in human cancer cells. *Oncogene* 25 (2), 176–185. doi:10.1038/sj.onc.1209049

Otsuka, R., Sakata, H., Murakami, K., Kano, M., Endo, S., Toyozumi, T., et al. (2022). SIRT1 expression is a promising prognostic biomarker in esophageal squamous cell carcinoma: a systematic review and meta-analysis. *Cancer Diagnosis and Prognosis* 2 (2), 126–133. doi:10.21873/cdp.10086

Ozpolat, B., and Benbrook, D. M. (2015). Targeting autophagy in cancer management - strategies and developments. *Cancer Manag. Res.* 7, 291–299. doi:10.2147/CMAR.S34859

Pacholec, M., Bleasdale, J. E., Chrunyk, B., Cunningham, D., Flynn, D., Garofalo, R. S., et al. (2010). SRT1720, SRT2183, SRT1460, and resveratrol are not direct activators of SIRT1◆. *J. Biol. Chem.* 285 (11), 8340–8351. doi:10.1074/jbc.M109.088682

Panda, P. K., Patra, S., Naik, P. P., Praharaj, P. P., Mukhopadhyay, S., Meher, B. R., et al. (2020). Deacetylation of LAMP1 drives lipophagy-dependent generation of free fatty acids by Abrus agglutinin to promote senescence in prostate cancer. *J. Cell. physiology* 235 (3), 2776–2791. doi:10.1002/jcp.29182

Park, J. M., Huang, S., Wu, T. T., Foster, N. R., and Sinicrope, F. A. (2013). Prognostic impact of Beclin 1, p62/sequestosome 1 and LC3 protein expression in colon carcinomas from patients receiving 5-fluorouracil as adjuvant chemotherapy. *Cancer Biol. and Ther.* 14 (2), 100–107. doi:10.4161/cbt.22954

Paskeh, M. D. A., Entezari, M., Clark, C., Zabolian, A., Ranjbar, E., Farahani, M. V., et al. (2022). Targeted regulation of autophagy using nanoparticles: new insight into cancer therapy. *Biochimica Biophysica Acta (BBA) - Mol. Basis Dis.* 1868 (3), 166326. doi:10.1016/j.bbadis.2021.166326

Patra, S., Bhol, C. S., Panigrahi, D. P., Praharaj, P. P., Pradhan, B., Jena, M., et al. (2020b). Gamma irradiation promotes chemo-sensitization potential of gallic acid through attenuation of autophagic flux to trigger apoptosis in an NRF2 inactivation signalling pathway. *Free Radic. Biol. Med.* 160, 111–124. doi:10.1016/j.freeradbiomed.2020.06.022

Patra, S., Mishra, S. R., Behera, B. P., Mahapatra, K. K., Panigrahi, D. P., Bhol, C. S., et al. (2022). "Autophagy-modulating phytochemicals in cancer therapeutics: current evidences and future perspectives," in *Seminars in cancer biology* (Elsevier), 205–217.

Patra, S., Panda, P. K., Naik, P. P., Panigrahi, D. P., Praharaj, P. P., Bhol, C. S., et al. (2020a). Terminalia bellirica extract induces anticancer activity through modulation of apoptosis and autophagy in oral squamous cell carcinoma. *Food Chem. Toxicol.* 136, 111073. doi:10.1016/j.fct.2019.111073

Patra, S., Pradhan, B., Nayak, R., Behera, C., Rout, L., Jena, M., et al. (2021). "Chemotherapeutic efficacy of curcumin and resveratrol against cancer: chemoprevention, chemoprotection, drug synergism and clinical pharmacokinetics," in *Seminars in cancer biology* (Elsevier), 310–320.

Patra, S., Praharaj, P. P., Singh, A., and Bhutia, S. K. (2023b). Targeting SIRT1-regulated autophagic cell death as a novel therapeutic avenue for cancer prevention. *Drug Discov. Today* 28 (9), 103692. doi:10.1016/j.drudis.2023.103692

Patra, S., Singh, A., Praharaj, P. P., Mohanta, N. K., Jena, M., Patro, B. S., et al. (2023a). SIRT1 inhibits mitochondrial hyperfusion associated mito-bulb formation to sensitize oral cancer cells for apoptosis in a mtROS-dependent signalling pathway. *Cell death and Dis.* 14 (11), 732. doi:10.1038/s41419-023-06232-x

Pavlidis, E. T., and Pavlidis, T. E. (2018). Current molecular and genetic aspects of pancreatic cancer, the role of metastasis associated proteins (MTA): a review. *J. Investigative Surg.* 31 (1), 54–66. doi:10.1080/08941939.2016.1269854

Peck, B., Chen, C. Y., Ho, K. K., Di Fruscia, P., Myatt, S. S., Coombes, R. C., et al. (2010). SIRT inhibitors induce cell death and p53 acetylation through targeting both SIRT1 and SIRT2. *Mol. cancer Ther.* 9 (4), 844–855. doi:10.1158/1535-7163.MCT-09-0971

Pervaiz, S., and Holme, A. L. (2009). Resveratrol: its biologic targets and functional activity. *Antioxidants and redox Signal.* 11 (11), 2851–2897. doi:10.1089/ars.2008.2412

Power, C., Fanning, N., and Redmond, H. P. (2002). Cellular apoptosis and organ injury in sepsis: a review. *Shock* 18 (3), 197–211. doi:10.1097/00024382-200209000-00001

Pu, Y., Wang, J., and Wang, S. (2022). Role of autophagy in drug resistance and regulation of osteosarcoma. *Mol. Clin. Oncol.* 16 (3), 1–6.

Qi, Y., Qi, W., Liu, S., Sun, L., Ding, A., Yu, G., et al. (2020). TSPAN9 suppresses the chemosensitivity of gastric cancer to 5-fluorouracil by promoting autophagy. *Cancer Cell Int.* 20, 4. doi:10.1186/s12935-019-1089-2

Qiao, P. F., Yao, L., and Zeng, Z. L. (2020). Catalpol-mediated microRNA-34a suppresses autophagy and malignancy by regulating SIRT1 in colorectal cancer. *Oncol. Rep.* 43 (4), 1053–1066. doi:10.3892/or.2020.7494

Qin, Y., Ashrafizadeh, M., Mongiardini, V., Grimaldi, B., Crea, F., Rietdorf, K., et al. (2023). Autophagy and cancer drug resistance in dialogue: pre-clinical and clinical evidence. *Cancer Lett.* 570, 216307. doi:10.1016/j.canlet.2023.216307

Qu, X., Yu, J., Bhagat, G., Furuya, N., Hibshoosh, H., Troxel, A., et al. (2003). Promotion of tumorigenesis by heterozygous disruption of the beclin 1 autophagy gene. *J. Clin. Invest.* 112 (12), 1809–1820. doi:10.1172/JCI20039

Rabinowitz, J. D., and White, E. (2010). Autophagy and metabolism. *Sci. (New York, NY)* 330 (6009), 1344–1348. doi:10.1126/science.1193497

Rosenblatt, J., Raff, M. C., and Cramer, L. P. (2001). An epithelial cell destined for apoptosis signals its neighbors to extrude it by an actin-and myosin-dependent mechanism. *Curr. Biol.* 11 (23), 1847–1857. doi:10.1016/s0960-9822(01)00587-5

Ruderman, N., and Prentki, M. (2004). AMP kinase and malonyl-CoA: targets for therapy of the metabolic syndrome. *Nat. Rev. Drug Discov.* 3 (4), 340–351. doi:10.1038/nrd1344

Sahoo, S., Kumari, S., Pulipaka, S., Chandra, Y., and Kotamraju, S. (2024). SIRT1 promotes doxorubicin-induced breast cancer drug resistance and tumor angiogenesis via regulating GSH-mediated redox homeostasis. *Mol. Carcinog.* doi:10.1002/mc.23809

Saito, H., Inazawa, J., Saito, S., Kasumi, F., Koi, S., Sagae, S., et al. (1993). Detailed deletion mapping of chromosome 17q in ovarian and breast cancers: 2-cM region on 17q21.3 often and commonly deleted in tumors. *Cancer Res.* 53 (14), 3382–3385.

Samaddar, J. S., Gaddy, V. T., Duplantier, J., Thandavan, S. P., Shah, M., Smith, M. J., et al. (2008). A role for macroautophagy in protection against 4-hydroxytamoxifen-induced cell death and the development of antiestrogen resistance. *Mol. cancer Ther.* 7 (9), 2977–2987. doi:10.1158/1535-7163.MCT-08-0447

Sanders, S. J., Murtha, M. T., Gupta, A. R., Murdoch, J. D., Raubeson, M. J., Willsey, A. J., et al. (2012). *De novo* mutations revealed by whole-exome sequencing are strongly associated with autism. *Nature* 485 (7397), 237–241. doi:10.1038/nature10945

Sasaki, K., Tsuno, N. H., Sunami, E., Tsurita, G., Kawai, K., Okaji, Y., et al. (2010). Chloroquine potentiates the anti-cancer effect of 5-fluorouracil on colon cancer cells. *BMC cancer* 10, 370. doi:10.1186/1471-2407-10-370

Savill, J., and Fadok, V. (2000). Corpse clearance defines the meaning of cell death. *Nature* 407 (6805), 784–788. doi:10.1038/35037722

Scher, M. B., Vaquero, A., and Reinberg, D. (2007). SirT3 is a nuclear NAD+-dependent histone deacetylase that translocates to the mitochondria upon cellular stress. *Genes Dev.* 21 (8), 920–928. doi:10.1101/gad.1527307

Scott, R. C., Juhász, G., and Neufeld, T. P. (2007). Direct induction of autophagy by Atg1 inhibits cell growth and induces apoptotic cell death. *Curr. Biol. CB* 17 (1), 1–11. doi:10.1016/j.cub.2006.10.053

Shan, S., Wang, X., Qian, L., Wang, C., and Zhao, S. (2024). ENST00000534735 inhibits proliferation and migration, promotes apoptosis and pyroptosis of endometrial cancer via OSBPL3 through APMK/SIRT1/NF-κB pathway. *Heliyon* 10 (4), e25281. doi:10.1016/j.heliyon.2024.e25281

Shen, J., Yang, H., Qiao, X., Chen, Y., Zheng, L., Lin, J., et al. (2023). The E3 ubiquitin ligase TRIM17 promotes gastric cancer survival and progression via controlling BAX stability and antagonizing apoptosis. *Cell death Differ.* 30 (10), 2322–2335. doi:10.1038/s41418-023-01221-1

Shen, T., Cai, L. D., Liu, Y. H., Li, S., Gan, W. J., Li, X. M., et al. (2018). Ube2v1-mediated ubiquitination and degradation of Sirt1 promotes metastasis of colorectal cancer by epigenetically suppressing autophagy. *J. Hematol. and Oncol.* 11 (1), 95. doi:10.1186/s13045-018-0638-9

Shimoyama, Y., Mitsuda, Y., Tsuruta, Y., Suzuki, K., Hamajima, N., and Niwa, T. (2012). SIRTUIN 1 gene polymorphisms are associated with cholesterol metabolism and coronary artery calcification in Japanese hemodialysis patients. *J. Ren. Nutr.* 22 (1), 114–119. doi:10.1053/j.jrn.2011.10.025

Shimoyama, Y., Suzuki, K., Hamajima, N., and Niwa, T. (2011). Sirtuin 1 gene polymorphisms are associated with body fat and blood pressure in Japanese. *Transl. Res.* 157 (6), 339–347. doi:10.1016/j.trsl.2011.02.004

Shin, D. H., Jo, J. Y., Choi, M., Kim, K. H., Bae, Y. K., and Kim, S. S. (2023). Oncogenic KRAS mutation confers chemoresistance by upregulating SIRT1 in non-small cell lung cancer. *Exp. and Mol. Med.* 55 (10), 2220–2237. doi:10.1038/s12276-023-01091-0

Shuhua, W., Chenbo, S., Yangyang, L., Xiangqian, G., Shuang, H., Tangyue, L., et al. (2015). Autophagy-related genes Raptor, Rictor, and Beclin1 expression and relationship with multidrug resistance in colorectal carcinoma. *Hum. Pathol.* 46 (11), 1752–1759. doi:10.1016/j.humpath.2015.07.016

Solomon, J. M., Pasupuleti, R., Xu, L., McDonagh, T., Curtis, R., DiStefano, P. S., et al. (2006). Inhibition of SIRT1 catalytic activity increases p53 acetylation but does not alter cell survival following DNA damage. *Mol. Cell. Biol.* 26 (1), 28–38. doi:10.1128/MCB.26.1.28-38.2006

Song, S., Luo, M., Song, Y., Liu, T., Zhang, H., and Xie, Z. (2014). Prognostic role of SIRT1 in hepatocellular carcinoma. *J. Coll. Physicians Surg. Pak* 24 (11), 849–854.

Song, X., Kong, F., Zong, Z., Ren, M., Meng, Q., Li, Y., et al. (2019). miR-124 and miR-142 enhance cisplatin sensitivity of non-small cell lung cancer cells through repressing autophagy via directly targeting SIRT1. *RSC Adv.* 9 (9), 5234–5243. doi:10.1039/c8ra09914f

Soula, M., Weber, R. A., Zilka, O., Alwaseem, H., La, K., Yen, F., et al. (2020). Metabolic determinants of cancer cell sensitivity to canonical ferroptosis inducers. *Nat. Chem. Biol.* 16 (12), 1351–1360. doi:10.1038/s41589-020-0613-y

Stein, S. C., Woods, A., Jones, N. A., Davison, M. D., and Carling, D. (2000). The regulation of AMP-activated protein kinase by phosphorylation. *Biochem. J.* 345 (3), 437–443. doi:10.1042/0264-6021:3450437

Steinberg, G. R., and Kemp, B. E. (2009). AMPK in health and disease. *Physiol. Rev.* 89 (3), 1025–1078. doi:10.1152/physrev.00011.2008

Sternberg, C. N., de Mulder, P. H., Schornagel, J. H., Théodore, C., Fossa, S. D., van Oosterom, A. T., et al. (2001). Randomized phase III trial of high-dose-intensity methotrexate, vinblastine, doxorubicin, and cisplatin (MVAC) chemotherapy and recombinant human granulocyte colony-stimulating factor versus classic MVAC in advanced urothelial tract tumors: European Organization for Research and Treatment of Cancer Protocol no. 30924. *J. Clin. Oncol. official J. Am. Soc. Clin. Oncol.* 19 (10), 2638–2646. doi:10.1200/JCO.2001.19.10.2638

Stockwell, B. R., Friedmann Angeli, J. P., Bayir, H., Bush, A. I., Conrad, M., Dixon, S. J., et al. (2017). Ferroptosis: a regulated cell death nexus linking metabolism, redox biology, and disease. *Cell* 171 (2), 273–285. doi:10.1016/j.cell.2017.09.021

Stünkel, W., Peh, B. K., Tan, Y. C., Nayagam, V. M., Wang, X., Salto-Tellez, M., et al. (2007). Function of the SIRT1 protein deacetylase in cancer. *Biotechnol. J.* 2 (11), 1360–1368. doi:10.1002/biot.200700087

Su, B. C., Xiao, K. M., Wang, K. L., Yang, S. F., Huang, Z. X., and Luo, J. W. (2023b). ATGL promotes colorectal cancer growth by regulating autophagy process and SIRT1 expression. *Med. Oncol. N. Lond. Engl.* 40 (12), 350. doi:10.1007/s12032-023-02148-w

Su, C. M., Hsu, T. W., Chen, H. A., Wang, W. Y., Huang, C. Y., Hung, C. C., et al. (2023a). Chaperone-mediated autophagy degrade Dicer to promote breast cancer metastasis. *J. Cell. physiology* 238 (4), 829–841. doi:10.1002/jcp.30979

Su, Z., Li, G., Liu, C., Ren, S., Deng, T., Zhang, S., et al. (2017). Autophagy inhibition impairs the epithelial-mesenchymal transition and enhances cisplatin sensitivity in nasopharyngeal carcinoma. *Oncol. Lett.* 13 (6), 4147–4154. doi:10.3892/ol.2017.5963

Sun, G., Yang, L., Wei, S., Jin, H., Li, B., and Li, H. (2021b). miR-425 regulates lipophagy via SIRT1 to promote sorafenib resistance in liver cancer. *Oncol. Lett.* 22 (4), 695. doi:10.3892/ol.2021.12956

Sun, L., Wang, H., Wang, Z., He, S., Chen, S., Liao, D., et al. (2012). Mixed lineage kinase domain-like protein mediates necrosis signaling downstream of RIP3 kinase. *Cell* 148 (1), 213–227. doi:10.1016/j.cell.2011.11.031

Sun, M., Du, M., Zhang, W., Xiong, S., Gong, X., Lei, P., et al. (2019). Survival and clinicopathological significance of SIRT1 expression in cancers: a meta-analysis. *Front. Endocrinol.* 10, 121. doi:10.3389/fendo.2019.00121

Sun, S., Liu, X., Wei, X., Zhang, S., and Wang, W. (2022). Diallyl trisulfide induces pro-apoptotic autophagy via the AMPK/SIRT1 signalling pathway in human hepatocellular carcinoma HepG2 cell line. *Food and Nutr. Res.* 66. doi:10.29219/fnr.v66.8981

Sun, T., Peng, H., Mao, W., Ma, L., Liu, H., Mai, J., et al. (2021a). Autophagy-mediated negative feedback attenuates the oncogenic activity of YAP in pancreatic cancer. *Int. J. Biol. Sci.* 17 (13), 3634–3645. doi:10.7150/ijbs.61795

Sun, W. L., Chen, J., Wang, Y. P., and Zheng, H. (2011). Autophagy protects breast cancer cells from epirubicin-induced apoptosis and facilitates epirubicin-resistance development. *Autophagy* 7 (9), 1035–1044. doi:10.4161/auto.7.9.16521

Sun, Y., Berleth, N., Wu, W., Schlütermann, D., Deitersen, J., Stuhldreier, F., et al. (2021c). Fin56-induced ferroptosis is supported by autophagy-mediated GPX4 degradation and functions synergistically with mTOR inhibition to kill bladder cancer cells. *Cell death and Dis.* 12 (11), 1028. doi:10.1038/s41419-021-04306-2

Sun, Y., Liu, X., Tong, H., Yin, H., Li, T., Zhu, J., et al. (2023). SIRT1 promotes cisplatin resistance in bladder cancer via Beclin1 deacetylation-mediated autophagy. *Cancers* 16 (1), 125. doi:10.3390/cancers16010125

Tae, I. H., Son, J. Y., Lee, S. H., Ahn, M.-Y., Yoon, K., Yoon, S., et al. (2020). A new SIRT1 inhibitor, MHY2245, induces autophagy and inhibits energy metabolism via PKM2/mTOR pathway in human ovarian cancer cells. *Int. J. Biol. Sci.* 16 (11), 1901–1916. doi:10.7150/ijbs.44343

Taelman, V. F., Dobrowolski, R., Plouhinec, J. L., Fuentealba, L. C., Vorwald, P. P., Gumper, I., et al. (2010). Wnt signaling requires sequestration of glycogen synthase kinase 3 inside multivesicular endosomes. *Cell* 143 (7), 1136–1148. doi:10.1016/j.cell.2010.11.034

Tan, Q., Liu, Y., Deng, X., Chen, J., Tsai, P. J., Chen, P. H., et al. (2020). Autophagy: a promising process for the treatment of acetaminophen-induced liver injury. *Archives Toxicol.* 94 (9), 2925–2938. doi:10.1007/s00204-020-02780-9

Tan, V. P., and Miyamoto, S. (2016). Nutrient-sensing mTORC1: integration of metabolic and autophagic signals. *J. Mol. Cell. Cardiol.* 95, 31–41. doi:10.1016/j.yjmcc.2016.01.005

Tang, L., Zhang, H., Zhou, F., Wei, Q., Du, M., Wu, J., et al. (2024). Targeting autophagy overcomes cancer-intrinsic resistance to CAR-T immunotherapy in B-cell malignancies. *Cancer Commun. Lond. Engl.* 44 (3), 408–432. doi:10.1002/cac2.12525

Tang, M., Tang, H., Tu, B., and Zhu, W.-G. (2021b). SIRT7: a sentinel of genome stability. *Open Biol.* 11 (6), 210047. doi:10.1098/rsob.210047

Tang, X., Ding, H., Liang, M., Chen, X., Yan, Y., Wan, N., et al. (2021a). Curcumin induces ferroptosis in non-small-cell lung cancer via activating autophagy. *Thorac. cancer* 12 (8), 1219–1230. doi:10.1111/1759-7714.13904

Tanno, M., Sakamoto, J., Miura, T., Shimamoto, K., and Horio, Y. (2007). Nucleocytoplasmic shuttling of the NAD+-dependent histone deacetylase SIRT1. *J. Biol. Chem.* 282 (9), 6823–6832. doi:10.1074/jbc.M609554200

Tarabay, M., Elshazli, R., and Settin, A. (2016). African vs. Caucasian and Asian difference for the association of interleukin-10 promotor polymorphisms with type 2 diabetes mellitus (a meta-analysis study). *Meta gene* 9, 10–17. doi:10.1016/j.mgene.2016.02.006

Tian, Q., Zhang, P., Wang, Y., Si, Y., Yin, D., Weber, C. R., et al. (2023). A novel triptolide analog downregulates NF-κB and induces mitochondrial apoptosis pathways in human pancreatic cancer. *eLife* 12, e85862. doi:10.7554/eLife.85862

Tomaselli, D., Steegborn, C., Mai, A., and Rotili, D. (2020). Sirt4: a multifaceted enzyme at the crossroads of mitochondrial metabolism and cancer. *Front. Oncol.* 10, 474. doi:10.3389/fonc.2020.00474

Torrens-Mas, M., Oliver, J., Roca, P., and Sastre-Serra, J. (2017). SIRT3: oncogene and tumor suppressor in cancer. *Cancers* 9 (7), 90. doi:10.3390/cancers9070090

Tóth, S., Nagy, K., Pálfia, Z., and Réz, G. (2002). Cellular autophagic capacity changes during azaserine-induced tumour progression in the rat pancreas. Up-regulation in all premalignant stages and down-regulation with loss of cycloheximide sensitivity of segregation along with malignant transformation. *Cell tissue Res.* 309 (3), 409–416. doi:10.1007/s00441-001-0506-7

Towers, C. G., Wodetzki, D. K., Thorburn, J., Smith, K. R., Caino, M. C., and Thorburn, A. (2021). Mitochondrial-derived vesicles compensate for loss of LC3-mediated mitophagy. *Dev. Cell* 56 (14), 2029–2042.e5. doi:10.1016/j.devcel.2021.06.003

Tsutsumi, S., Watanabe, R., Tabe, Y., Fujii, T., Morita, H., Kigure, W., et al. (2012). Extranodal metastasis predicts poor survival in advanced colorectal cancer. *Hepato-gastroenterology* 59 (114), 372–374. doi:10.5754/hge10139

Varghese, B., Chianese, U., Capasso, L., Sian, V., Bontempo, P., Conte, M., et al. (2023). SIRT1 activation promotes energy homeostasis and reprograms liver cancer metabolism. *J. Transl. Med.* 21 (1), 627. doi:10.1186/s12967-023-04440-9

Vasan, N., Baselga, J., and Hyman, D. M. (2019). A view on drug resistance in cancer. *Nature* 575 (7782), 299–309. doi:10.1038/s41586-019-1730-1

Vercammen, D., Beyaert, R., Denecker, G., Goossens, V., Van Loo, G., Declercq, W., et al. (1998). Inhibition of caspases increases the sensitivity of L929 cells to necrosis mediated by tumor necrosis factor. *J. Exp. Med.* 187 (9), 1477–1485. doi:10.1084/jem.187.9.1477

Wang, C., Liu, Y., Zhu, Y., and Kong, C. (2020). Functions of mammalian SIRT4 in cellular metabolism and research progress in human cancer. *Oncol. Lett.* 20 (4), 11–1. doi:10.3892/ol.2020.11872

Wang, C., Zeng, J., Li, L. J., Xue, M., and He, S. L. (2021). Cdc25A inhibits autophagy-mediated ferroptosis by upregulating ErbB2 through PKM2 dephosphorylation in cervical cancer cells. *Cell death and Dis.* 12 (11), 1055. doi:10.1038/s41419-021-04342-y

Wang, H., Liang, Y., Zhao, L., Deng, J., Li, Y., Zhao, H., et al. (2023f). miR-653-3p promotes genomic instability of colorectal cancer cells via targeting SIRT1/TWIST1 signaling pathway. *Biochimica biophysica acta Mol. basis Dis.* 1869 (8), 166821. doi:10.1016/j.bbadis.2023.166821

Wang, J., and Wu, G. S. (2014). Role of autophagy in cisplatin resistance in ovarian cancer cells. *J. Biol. Chem.* 289 (24), 17163–17173. doi:10.1074/jbc.M114.558288

Wang, K. X., Yan, C., Yang, X., Zhu, P. Y., Cui, W. W., Ye, C., et al. (2022). Enhanced autophagy promotes radiosensitivity by mediating Sirt1 downregulation in RM-1 prostate cancer cells. *Biochem. biophysical Res. Commun.* 609, 84–92. doi:10.1016/j.bbrc.2022.03.142

Wang, L., Klionsky, D. J., and Shen, H.-M. (2023b). The emerging mechanisms and functions of microautophagy. *Nat. Rev. Mol. Cell Biol.* 24 (3), 186–203. doi:10.1038/s41580-022-00529-z

Wang, M., Han, D., Yuan, Z., Hu, H., Zhao, Z., Yang, R., et al. (2018). Long non-coding RNA H19 confers 5-Fu resistance in colorectal cancer by promoting SIRT1-mediated autophagy. *Cell death and Dis.* 9 (12), 1149. doi:10.1038/s41419-018-1187-4

Wang, M., Zhang, Z., Chen, M., Lv, Y., Tian, S., Meng, F., et al. (2023c). FDW028, a novel FUT8 inhibitor, impels lysosomal proteolysis of B7-H3 via chaperone-mediated autophagy pathway and exhibits potent efficacy against metastatic colorectal cancer. *Cell death and Dis.* 14 (8), 495. doi:10.1038/s41419-023-06027-0

Wang, R., Li, S., Hou, Q., Zhang, B., Chu, H., Hou, Y., et al. (2023e). Propofol inhibits colon cancer cell stemness and epithelial-mesenchymal transition by regulating SIRT1, Wnt/β-catenin and PI3K/AKT/mTOR signaling pathways. *Discov. Oncol.* 14 (1), 137. doi:10.1007/s12672-023-00734-y

Wang, S., Nie, J., Xu, K., Liu, Y., Tong, W., Li, A., et al. (2023a). YY1 is regulated by ALKBH5-mediated m6A modification and promotes autophagy and cancer progression through targeting ATG4B. *Aging* 15 (18), 9590–9613. doi:10.18632/aging.205037

Wang, X. W., Jiang, Y. H., Ye, W., Shao, C. F., Xie, J. J., and Li, X. (2023d). SIRT1 promotes the progression and chemoresistance of colorectal cancer through the p53/miR-101/KPNA3 axis. *Cancer Biol. and Ther.* 24 (1), 2235770. doi:10.1080/15384047.2023.2235770

Wang, Y., Chen, Y., Chen, X., Liang, Y., Yang, D., Dong, J., et al. (2019a). Angelicin inhibits the malignant behaviours of human cervical cancer potentially via inhibiting autophagy. *Exp. Ther. Med.* 18 (5), 3365–3374. doi:10.3892/etm.2019.7985

Wang, Y., Yang, J., Hong, T., Chen, X., and Cui, L. (2019c). SIRT2: controversy and multiple roles in disease and physiology. *Ageing Res. Rev.* 55, 100961. doi:10.1016/j.arr.2019.100961

Wang, Y., Zeng, J., Wu, W., Xie, S., Yu, H., Li, G., et al. (2019b). Nicotinamide N-methyltransferase enhances chemoresistance in breast cancer through SIRT1 protein stabilization. *Breast cancer Res. BCR* 21 (1), 64. doi:10.1186/s13058-019-1150-z

Wei, Z., Xia, J., Li, J., Cai, J., Shan, J., Zhang, C., et al. (2023). SIRT1 promotes glucolipid metabolic conversion to facilitate tumor development in colorectal carcinoma. *Int. J. Biol. Sci.* 19 (6), 1925–1940. doi:10.7150/ijbs.76704

White, E. (2015). The role for autophagy in cancer. *J. Clin. investigation* 125 (1), 42–46. doi:10.1172/JCI73941

White, E., Mehnert, J. M., and Chan, C. S. (2015). Autophagy, metabolism, and cancer. *Clin. cancer Res. official J. Am. Assoc. Cancer Res.* 21 (22), 5037–5046. doi:10.1158/1078-0432.CCR-15-0490

Wiernicki, B., Dubois, H., Tyurina, Y. Y., Hassannia, B., Bayir, H., Kagan, V. E., et al. (2020). Excessive phospholipid peroxidation distinguishes ferroptosis from other cell death modes including pyroptosis. *Cell death and Dis.* 11 (10), 922. doi:10.1038/s41419-020-03118-0

Wirawan, E., Berghe, T. V., Lippens, S., Agostinis, P., and Vandenabeele, P. (2012). Autophagy: for better or for worse. *Cell Res.* 22 (1), 43–61. doi:10.1038/cr.2011.152

Wong, M. M., Chan, H. Y., Aziz, N. A., Ramasamy, T. S., Bong, J. J., Ch'ng, E. S., et al. (2021). Interplay of autophagy and cancer stem cells in hepatocellular carcinoma. *Mol. Biol. Rep.* 48 (4), 3695–3717. doi:10.1007/s11033-021-06334-9

Wu, J., Guo, Q., Li, J., Yuan, H., Xiao, C., Qiu, J., et al. (2023). Loperamide induces protective autophagy and apoptosis through the ROS/JNK signaling pathway in bladder cancer. *Biochem. Pharmacol.* 218, 115870. doi:10.1016/j.bcp.2023.115870

Wu, M., Wei, W., Xiao, X., Guo, J., Xie, X., Li, L., et al. (2012). Expression of SIRT1 is associated with lymph node metastasis and poor prognosis in both operable triple-negative and non-triple-negative breast cancer. *Med. Oncol. N. Lond. Engl.* 29 (5), 3240–3249. doi:10.1007/s12032-012-0260-6

Xiao, B., Sanders, M. J., Underwood, E., Heath, R., Mayer, F. V., Carmena, D., et al. (2011). Structure of mammalian AMPK and its regulation by ADP. *Nature* 472 (7342), 230–233. doi:10.1038/nature09932

Xiao, L., Zhang, Y., Luo, Q., Guo, C., Chen, Z., and Lai, C. (2023). DHRS4-AS1 regulate gastric cancer apoptosis and cell proliferation by destabilizing DHX9 and inhibited the association between DHX9 and ILF3. *Cancer Cell Int.* 23 (1), 304. doi:10.1186/s12935-023-03151-x

Xiao, X., Wang, W., Li, Y., Yang, D., Li, X., Shen, C., et al. (2018). HSP90AA1-mediated autophagy promotes drug resistance in osteosarcoma. *J. Exp. and Clin. cancer Res. CR* 37 (1), 201. doi:10.1186/s13046-018-0880-6

Xie, Y., Lei, X., Zhao, G., Guo, R., and Cui, N. (2023). mTOR in programmed cell death and its therapeutic implications. *Cytokine and Growth Factor Rev.* 71-72, 66–81. doi:10.1016/j.cytogfr.2023.06.002

Xilouri, M., and Stefanis, L. (2015). Chaperone mediated autophagy to the rescue: a new-fangled target for the treatment of neurodegenerative diseases. *Mol. Cell. Neurosci.* 66 (Pt A), 29–36. doi:10.1016/j.mcn.2015.01.003

Xu, H., Zeng, S., Wang, Y., Yang, T., Wang, M., Li, X., et al. (2023b). Cytoplasmic SIRT1 promotes paclitaxel resistance in ovarian carcinoma through increased formation and survival of polyploid giant cancer cells. *J. pathology* 261 (2), 210–226. doi:10.1002/path.6167

Xu, Z., Wang, X., Sun, W., Xu, F., Kou, H., Hu, W., et al. (2023a). RelB-activated GPX4 inhibits ferroptosis and confers tamoxifen resistance in breast cancer. *Redox Biol.* 68, 102952. doi:10.1016/j.redox.2023.102952

Xue, N., Lai, F., Du, T., Ji, M., Liu, D., Yan, C., et al. (2019). Chaperone-mediated autophagy degradation of IGF-1Rβ induced by NVP-AUY922 in pancreatic cancer. *Cell. Mol. life Sci. CMLS* 76 (17), 3433–3447. doi:10.1007/s00018-019-03080-x

Yamamoto, H., Schoonjans, K., and Auwerx, J. (2007). Sirtuin functions in health and disease. *Mol. Endocrinol. (Baltim. Md)* 21 (8), 1745–1755. doi:10.1210/me.2007-0079

Yan, T., Lu, G., Shang, R., Hu, J., Zhu, C., and Jin, L. (2024). RACGAP1 drives proliferation, migration and invasion and suppresses autophagy of gastric cancer cells via inhibiting SIRT1/Mfn2. *Physiol. Int.* 111 (1), 35–46. doi:10.1556/2060.2023.00235

Yanagisawa, S., Baker, J. R., Vuppusetty, C., Koga, T., Colley, T., Fenwick, P., et al. (2018). The dynamic shuttling of SIRT1 between cytoplasm and nuclei in bronchial epithelial cells by single and repeated cigarette smoke exposure. *PloS one* 13 (3), e0193921. doi:10.1371/journal.pone.0193921

Yang, Q., Sun, K., Gao, T., Gao, Y., Yang, Y., Li, Z., et al. (2024). SIRT1 silencing promotes EMT and Crizotinib resistance by regulating autophagy through AMPK/mTOR/S6K signaling pathway in EML4-ALK L1196M and EML4-ALK G1202R mutant non-small cell lung cancer cells. *Mol. Carcinog.* doi:10.1002/mc.23799

Yang, W. S., SriRamaratnam, R., Welsch, M. E., Shimada, K., Skouta, R., Viswanathan, V. S., et al. (2014). Regulation of ferroptotic cancer cell death by GPX4. *Cell* 156 (1-2), 317–331. doi:10.1016/j.cell.2013.12.010

Yao, J., Wang, J., Xu, Y., Guo, Q., Sun, Y., Liu, J., et al. (2022). CDK9 inhibition blocks the initiation of PINK1-PRKN-mediated mitophagy by regulating the SIRT1-FOXO3-BNIP3 axis and enhances the therapeutic effects involving mitochondrial dysfunction in hepatocellular carcinoma. *Autophagy* 18 (8), 1879–1897. doi:10.1080/15548627.2021.2007027

Yao, Z.-q., Zhang, X., Zhen, Y., He, X.-Y., Zhao, S., Li, X.-F., et al. (2018). A novel small-molecule activator of Sirtuin-1 induces autophagic cell death/mitophagy as a potential therapeutic strategy in glioblastoma. *Cell death and Dis.* 9 (7), 767. doi:10.1038/s41419-018-0799-z

Ye, Z., Fang, B., Pan, J., Zhang, N., Huang, J., Xie, C., et al. (2017). miR-138 suppresses the proliferation, metastasis and autophagy of non-small cell lung cancer by targeting Sirt1. *Oncol. Rep.* 37 (6), 3244–3252. doi:10.3892/or.2017.5619

You, Y., Bi, F. F., Jiang, Y., Xu, Y. T., An, Y. Y., Li, D., et al. (2019). BRCA1 affects the resistance and stemness of SKOV3-derived ovarian cancer stem cells by regulating autophagy. *Cancer Med.* 8 (2), 656–668. doi:10.1002/cam4.1975

Yousafzai, N. A., Jin, H., Ullah, M., and Wang, X. (2021). Recent advances of SIRT1 and implications in chemotherapeutics resistance in cancer. *Am. J. cancer Res.* 11 (11), 5233–5248.

Yu, H. Y., Yang, L., Liu, Y. C., and Yu, A. J. (2023a). Sulforaphene suppressed cell proliferation and promoted apoptosis of COV362 cells in endometrioid ovarian cancer. *PeerJ* 11, e16308. doi:10.7717/peerj.16308

Yu, W., Wang, Z., Dai, P., Sun, J., Li, J., Han, W., et al. (2023b). The activation of SIRT1 by resveratrol reduces breast cancer metastasis to lung through inhibiting neutrophil extracellular traps. *J. drug Target.* 31 (9), 962–975. doi:10.1080/1061186X.2023.2265585

Yuan, W., Fang, W., Zhang, R., Lyu, H., Xiao, S., Guo, D., et al. (2023). Therapeutic strategies targeting AMPK-dependent autophagy in cancer cells. *Biochimica Biophysica Acta (BBA) - Mol. Cell Res.* 1870 (7), 119537. doi:10.1016/j.bbamcr.2023.119537

Yue, Z., Jin, S., Yang, C., Levine, A. J., and Heintz, N. (2003). Beclin 1, an autophagy gene essential for early embryonic development, is a haploinsufficient tumor suppressor. *Proc. Natl. Acad. Sci.* 100 (25), 15077–15082. doi:10.1073/pnas.2436255100

Zaffagnini, G., and Martens, S. (2016). Mechanisms of selective autophagy. *J. Mol. Biol.* 428 (9), 1714–1724. doi:10.1016/j.jmb.2016.02.004

Zhang, B., Shen, P., Yin, X., Dai, Y., Ding, M., and Cui, L. (2020). Expression and functions of cellular prion proteins in immunocytes. *Scand. J. Immunol.* 91 (3), e12854. doi:10.1111/sji.12854

Zhang, D.-W., Shao, J., Lin, J., Zhang, N., Lu, B.-J., Lin, S.-C., et al. (2009). RIP3, an energy metabolism regulator that switches TNF-induced cell death from apoptosis to necrosis. *Sci. (New York, NY)* 325 (5938), 332–336. doi:10.1126/science.1172308

Zhang, L. H., Yang, A. J., Wang, M., Liu, W., Wang, C. Y., Xie, X. F., et al. (2016). Enhanced autophagy reveals vulnerability of P-gp mediated epirubicin resistance in triple negative breast cancer cells. *Apoptosis Int. J. Program. Cell death* 21 (4), 473–488. doi:10.1007/s10495-016-1214-9

Zhang, N., Qi, Y., Wadham, C., Wang, L., Warren, A., Di, W., et al. (2010). FTY720 induces necrotic cell death and autophagy in ovarian cancer cells: a protective role of autophagy. *Autophagy* 6 (8), 1157–1167. doi:10.4161/auto.6.8.13614

Zhang, P., Liu, L., Huang, J., Shao, L., Wang, H., Xiong, N., et al. (2014). Non-SMC condensin I complex, subunit D2 gene polymorphisms are associated with Parkinson's disease: a Han Chinese study. *Genome* 57 (5), 253–257. doi:10.1139/gen-2014-0032

Zhang, S., Yang, Y., Huang, S., Deng, C., Zhou, S., Yang, J., et al. (2019). SIRT1 inhibits gastric cancer proliferation and metastasis via STAT3/MMP-13 signaling. *J. Cell. physiology* 234 (9), 15395–15406. doi:10.1002/jcp.28186

Zhang, W., Dai, J., Hou, G., Liu, H., Zheng, S., Wang, X., et al. (2023a). SMURF2 predisposes cancer cell toward ferroptosis in GPX4-independent manners by promoting GSTP1 degradation. *Mol. Cell* 83 (23), 4352–4369.e8. doi:10.1016/j.molcel.2023.10.042

Zhang, W., and Luo, P. (2018). MicroRNA-29c restores cisplatin sensitivity in liver cancer through direct inhibition of sirtuin 1 expression. *Oncol. Lett.* 16 (2), 1543–1550. doi:10.3892/ol.2018.8801

Zhang, X., Dong, Y., Li, W., He, M., Shi, Y., Han, S., et al. (2024b). The mechanism by which SIRT1 regulates autophagy and EMT in drug-resistant oesophageal cancer cells. *Life Sci.* 343, 122530. doi:10.1016/j.lfs.2024.122530

Zhang, X., Lao, M., Yang, H., Sun, K., Dong, Y., He, L., et al. (2024a). Targeting cancer-associated fibroblast autophagy renders pancreatic cancer eradicable with immunochemotherapy by inhibiting adaptive immune resistance. *Autophagy* 20 (6), 1314–1334. doi:10.1080/15548627.2023.2300913

Zhang, X., Wu, X., Yao, W., and Wang, Y. H. (2023b). A tumor-suppressing role of TSPYL2 in thyroid cancer: through interacting with SIRT1 and repressing SIRT1/AKT pathway. *Exp. Cell Res.* 432 (1), 113777. doi:10.1016/j.yexcr.2023.113777

Zhang, Y., Kong, Y., Ma, Y., Ni, S., Wikerholmen, T., Xi, K., et al. (2021). Loss of COPZ1 induces NCOA4 mediated autophagy and ferroptosis in glioblastoma cell lines. *Oncogene* 40 (8), 1425–1439. doi:10.1038/s41388-020-01622-3

Zhang, Z., Yao, Z., Chen, Y., Qian, L., Jiang, S., Zhou, J., et al. (2018). Lipophagy and liver disease: new perspectives to better understanding and therapy. *Biomed. and Pharmacother. = Biomedecine and Pharmacother.* 97, 339–348. doi:10.1016/j.biopha.2017.07.168

Zhao, H., Ding, Y., and Zhang, L. (2023d). SIRT1/APE1 promotes the viability of gastric cancer cells by inhibiting p53 to suppress ferroptosis. *Open Med. Wars. Pol.* 18 (1), 20220620. doi:10.1515/med-2022-0620

Zhao, R., Liu, Y., Wang, Z., Zhang, J., Zhang, W., Zhou, X., et al. (2023e). UBE2C-mediated autophagy inhibition via ubiquitination of SIRT1 contributes to endometrial cancer progression. *Mol. cancer Res. MCR* 21 (6), 564–577. doi:10.1158/1541-7786.MCR-22-0825

Zhao, T. L., Qi, Y., Wang, Y. F., Wang, Y., Liang, H., and Pu, Y. B. (2023b). 5-methoxytryptophan induced apoptosis and PI3K/Akt/FoxO3a phosphorylation in colorectal cancer. *World J. gastroenterology* 29 (47), 6148–6160. doi:10.3748/wjg.v29.i47.6148

Zhao, W., Wang, Q., Li, L., Xie, C., Wu, Y., Gautam, M., et al. (2022). SIRT1 regulates mitotic catastrophe via autophagy and BubR1 signaling. *Mol. Cell. Biochem.* 477 (12), 2787–2799. doi:10.1007/s11010-022-04470-9

Zhao, Y., Liu, Z., Liu, G., Zhang, Y., Liu, S., Gan, D., et al. (2023a). Neutrophils resist ferroptosis and promote breast cancer metastasis through aconitate decarboxylase 1. *Cell metab.* 35 (10), 1688–1703.e10. doi:10.1016/j.cmet.2023.09.004

Zhao, Y., Ma, R., Wang, C., Hu, R., Wu, W., Sun, X., et al. (2023c). CAPG interference induces apoptosis and ferroptosis in colorectal cancer cells through the P53 pathway. *Mol. Cell. probes* 71, 101919. doi:10.1016/j.mcp.2023.101919

Zhao, Y. G., Codogno, P., and Zhang, H. (2021). Machinery, regulation and pathophysiological implications of autophagosome maturation. *Nat. Rev. Mol. Cell Biol.* 22 (11), 733–750. doi:10.1038/s41580-021-00392-4

Zheng, H., Liu, J., Cheng, Q., Zhang, Q., Zhang, Y., Jiang, L., et al. (2024a). Targeted activation of ferroptosis in colorectal cancer via LGR4 targeting overcomes acquired drug resistance. *Nat. cancer* 5 (4), 572–589. doi:10.1038/s43018-023-00715-8

Zheng, Q., Du, X., Zhang, J., Liu, Y., Dong, W., Dai, X., et al. (2024b). Delivery of SIRT1 by cancer-associated adipocyte-derived extracellular vesicles regulates immune response and tumorigenesis of ovarian cancer cells. *Clin. and Transl. Oncol.* 26 (1), 190–203. doi:10.1007/s12094-023-03240-3

Zheng, Y., Wu, J., Chen, H., Lin, D., Chen, H., Zheng, J., et al. (2023). KLF4 targets RAB26 and decreases 5-FU resistance through inhibiting autophagy in colon cancer. *Cancer Biol. and Ther.* 24 (1), 2226353. doi:10.1080/15384047.2023.2226353

Zhou, N., Wei, Z. X., and Qi, Z. X. (2019). Inhibition of autophagy triggers melatonin-induced apoptosis in glioblastoma cells. *BMC Neurosci.* 20 (1), 63. doi:10.1186/s12868-019-0545-1

Zhu, M., Wei, C., Wang, H., Han, S., Cai, L., Li, X., et al. (2023b). SIRT1 mediated gastric cancer progression under glucose deprivation through the FoxO1-Rab7-autophagy axis. *Front. Oncol.* 13, 1175151. doi:10.3389/fonc.2023.1175151

Zhu, T., Cen, Y., Chen, Z., Zhang, Y., Zhao, L., Wang, J., et al. (2022). Oncogenic circTICRR suppresses autophagy via binding to HuR protein and stabilizing GLUD1 mRNA in cervical cancer. *Cell death and Dis.* 13 (5), 479. doi:10.1038/s41419-022-04943-1

Zhu, X., Su, Q., Xie, H., Song, L., Yang, F., Zhang, D., et al. (2023a). SIRT1 deacetylates WEE1 and sensitizes cancer cells to WEE1 inhibition. *Nat. Chem. Biol.* 19 (5), 585–595. doi:10.1038/s41589-022-01240-y

Zou, Z., Tao, T., Li, H., and Zhu, X. (2020). mTOR signaling pathway and mTOR inhibitors in cancer: progress and challenges. *Cell and Biosci.* 10 (1), 31–11. doi:10.1186/s13578-020-00396-1

Zu, G., Ji, A., Zhou, T., and Che, N. (2016). Clinicopathological significance of SIRT1 expression in colorectal cancer: a systematic review and meta analysis. *Int. J. Surg.* 26, 32–37. doi:10.1016/j.ijsu.2016.01.002

frontiers | Frontiers in Pharmacology

TYPE Original Research
PUBLISHED 09 October 2024
DOI 10.3389/fphar.2024.1459520

Check for updates

OPEN ACCESS

EDITED BY
Hailin Tang,
Sun Yat-sen University Cancer Center (SYSUCC), China

REVIEWED BY
Zhonggao Gao,
China Academy of Chinese Medical Sciences, China
Peng Ren,
Beijing Institute of Basic Medicine Sciences, China
Qinong Ye,
Beijing Institute of Biotechnology, China

*CORRESPONDENCE
Zhang Xuewu,
zhangxuewu@ybu.edu.cn

RECEIVED 04 July 2024
ACCEPTED 30 August 2024
PUBLISHED 09 October 2024

CITATION
Chen J, Cheng H, Bai C, Wang D, Fu J, Hao J, Wang Y and Xuewu Z (2024) *Sorbaria sorbifolia* flavonoid derivative induces mitochondrial apoptosis in human hepatoma cells through Bclaf1.
Front. Pharmacol. 15:1459520.
doi: 10.3389/fphar.2024.1459520

COPYRIGHT
© 2024 Chen, Cheng, Bai, Wang, Fu, Hao, Wang, Xuewu. This is an open-access article distributed under the terms of the Creative Commons Attribution License (CC BY). The use, distribution or reproduction in other forums is permitted, provided the original author(s) and the copyright owner(s) are credited and that the original publication in this journal is cited, in accordance with accepted academic practice. No use, distribution or reproduction is permitted which does not comply with these terms.

Sorbaria sorbifolia flavonoid derivative induces mitochondrial apoptosis in human hepatoma cells through Bclaf1

Jiaxin Chen, Haoyi Cheng, Chunhua Bai, Dandan Wang, Jinghao Fu, Jinge Hao, Yixuan Wang and Zhang Xuewu*

College of Medicine, Yanbian University, Yanji, China

4′,5,7-Trihydroxy-8-methoxyflavone is an anticancer monomer component isolated from the traditional Chinese medicine *Sorbaria sorbifolia*. 4′,5-Dihydroxy-7-piperazinemethoxy-8-methoxy flavonoids (DMF) with good solubility and anti-tumor effects was obtained by chemical modification in the early stage. This study explored the mechanism by which DMF regulates the mitochondrial apoptosis of human hepatoma cells through Bcl-2-associated transcription factor 1 (Bclaf1). DMF inhibited the proliferation of human hepatoma cells in a concentration- and time-dependent manner and induced cell mitochondrial apoptosis. The molecular docking and cell assay results demonstrated that DMF inhibits Bclaf1 expression by binding to its active site. Lentivirus transfection was used to construct cells with stable knockout and overexpression of Bclaf1, and a Hep3B xenograft model was constructed in nude mice. The mechanism by which DMF induced the mitochondrial apoptosis of human hepatoma cells through Bclaf1 was further verified *in vitro* and *in vivo*. These findings indicated that DMF induced human hepatoma cell mitochondrial apoptosis through Bclaf1.

KEYWORDS

***Sorbaria sorbifolia*, 4′,5-Dihydroxy-7-piperazinemethoxy-8-methoxy flavonoids, liver cancer, bcl-2-associated transcription factor 1, mitochondrial apoptosis**

1 Introduction

Liver cancer is one of the most common malignant tumors globally. At present, interventional ablation, chemoradiotherapy, and biological immunotherapy are the main treatment methods, but they have severe side effects (Anwanwan et al., 2020; Sankar et al., 2020). Traditional Chinese medicine, used as an adjuvant therapy, offers advantages such as lower toxicity, reduced side effects, and more targets, which has attracted much attention from researchers in recent years.

Sorbaria sorbifolia is a Rosaceae plant, known for promoting blood circulation, reducing swelling, relieving pain, and treating the effects of traumatic injury. Its main components are flavonoids. In the early stage of our research, we isolated a compound from *S. sorbifolia* ethyl acetate extract and identified it as 5,2′,4′-trihydroxy-6,7,5′-trimethoxyflavone (TTF1). The compound was found to induce apoptosis in HepG2 cells through the mitochondrial pathway (Li et al., 2011), inhibit tumor angiogenesis (Liu et al., 2011), induce ERS-mediated apoptosis and inhibition of

human hepatoma cells (Xiao et al., 2016b) in the form of the nanoparticles, inhibit angiogenesis, cell migration, and cell invasion in human hepatoma cells by regulating STAT3 (Xiao et al., 2016a), and induce protective autophagy during apoptosis by inhibiting the Akt/mTOR pathway and activating JNK in human hepatoma cells (Zhang et al., 2018). It exhibits a good anti-liver cancer effect. Our research group extracted and obtained 4′,5,7-trihydroxy-8-methoxyflavone from *S. sorbifolia*. Due to the poor solubility, after chemical modification, 4′,5-Dihydroxy-7-piperazinemethoxy-8-methoxy flavonoids (DMF) was screened as a compound with good anti-tumor effects. However, the anti-tumor mechanism remains unclear.

Bcl-2-associated transcription factor 1 (Bclaf1, also known as BTF) is a multifunctional protein located on human chromosome 6q23.3, and it encodes 17 transcriptional variants of different subtypes (Jiang et al., 2022). Bclaf1 is mainly localized in the nucleus, with a small distribution in the cytoplasm. The notable features of the Bclaf1 structure include its arginine–serine domain, bZIP domain, and MYB DNA-binding domain (Yu et al., 2022). It has been found that upregulated SMYD3 promoted bladder cancer progression by targeting Bclaf1 and activating autophagy (Shen et al., 2016). Bclaf1 binds to SPOP, thereby inhibiting PD-L1 ubiquitination and degradation and making cancer cells sensitive to checkpoint therapy, suggesting that Bclaf1 is a novel therapeutic target for enhancing anti-tumor immunity in HCC (Yu et al., 2024). Bclaf1 could bind to CircZFR, thereby preventing its ubiquitination and degradation to promote colorectal cancer cell proliferation and metastasis (Chen et al., 2024). Our previous studies found that Bclaf1 was the upstream regulator of HIF-1α in anoxic microenvironments. In addition, ginsenoside CK significantly inhibited the binding of Bclaf1 and HIF-1α, thereby suppressing HIF-1α-mediated glycolysis in anoxic human hepatoma cells and inhibiting their proliferation (Zhang et al., 2020). Curcumin induced mitochondrial apoptosis in human hepatoma cells by inhibiting Bclaf1 expression (Bai et al., 2022), which suggested that Bclaf1 is closely related to the development of hepatoma. To explore deeply the anti-tumor mechanisms of DMF through Bclaf1, this study explored the mitochondrial apoptosis effect by which DMF regulated Bclaf1 by *in vivo* and *in vitro* experiments, providing a theoretical and experimental basis for the development and utilization of *S. sorbifolia* flavonoid derivatives.

2 Materials and methods

2.1 Reagents

5-Fluorouracil (5-FU) was purchased from Yuanye Co., Ltd. (Shanghai, China). HPLC ≥ 98% (No. B25419), Dulbecco's modified Eagle medium (DMEM) (No. 11965092), penicillin–streptomycin (No. 15140122), and fetal bovine serum (No. 302220F) were purchased from Gibco (Grand Island, NY, United States). The Cell Counting Kit-8 (No. 302220F) was purchased from APE×BIO (Houston, United States). The ECL chemiluminescence kit (No. WBK1S0100) was purchased from Millipore (Billerica, Massachusetts, United States). The ATP content kit (No. BC0305) and JC-1 mitochondrial membrane potential detection kit (No. C2006) were purchased from Solarbio (Beijing, China). Antibodies Bcl-2 (No. ab182858), Bax (No. ab32503), cytochrome C (Cyt-c) (No. ab133504), cleaved caspase-3 (No. ab32042), and Bclaf1 (No. ab181240) were purchased from Abcam (Cambridge, MA, United States). β-Actin (No. AC026) was purchased from ABclonal (Beijing, China). Horseradish-labeled goat anti-rabbit IgG (No. ZB-2306) was purchased from Zhongshan Jinqiao Co., Ltd. (Beijing, China). Horseradish-labeled goat anti-mouse IgG (No. 31430) was purchased from Thermo Co., Ltd. (Beijing, China).

2.2 Experimental animals

Thirty 5-week-old female BALB/C-NU mice, 17–19 g, were provided by Beijing Weitong Lihua Laboratory Animal Co., Ltd. (experimental animal production license: SCXK (Beijing) 2021-0006; certificate number: 110011221112896151; experimental animal use license: SYXK (Hubei) 2018-0101). The experiment program was approved by the Institutional Animal Care and Use Committee of Yanbian University (resolution number: 201501022).

2.3 Experimental cells

Human hepatoma cells HepG2 (No. FH0076), Hep3B (No. FH0861), and THLE-2 (No. FH1249) were purchased from Fuheng Biotechnology (Shanghai, China). QSG-7701(No. CL0264) was purchased from Fenghui Biotechnology Co., Ltd. (Changsha, Hunan, China).

2.4 Preparation of 4′,5,7-trihydroxy-8-methoxy flavone

First, commercial 2-methoxybenzene-1,3,5-triol (1.00 g, 5 mmol) was dissolved in CH_2Cl_2, anhydrous aluminum chloride was added at a catalytic amount, and chloroacetyl chloride was slowly dripped at room temperature (0.6 mL, 6 mmol) and refluxed for reaction at 40°C for 1 h. Thin-layer chromatography [unfolding agent: CH_2Cl_2 (v):MeOH (v) = 10:1] was used to monitor the reaction process. The reaction liquid dropped to room temperature, and a hydrochloric acid and ice water solution at a concentration of 1:1 was added to the mixture to begin the third extraction with ether. The organic layer was filtered and dried with the proper quantity of anhydrous sodium sulfate. The purification of 2-chloro-1-(2,4,6-trihydroxy-3-methoxyphenyl) thanone was obtained by column chromatography separation [eluent: v (CH_2Cl_2):v (petroleum ether) = 1:1].

Then, at room temperature, compound 2-chloro-1-(2,4,6-trihydroxy-3-methoxyphenyl) thanone reacted with p-hydroxybenzaldehyde (0.53 g, 5 mmol) and underwent an alkaline catalytic reaction in an ethanol solution for 24 h (pH = 11). Thin-layer chromatography was used to monitor the reaction process. After the reaction was completed, a 10% HCl solution was added to adjust the pH of the solution to neutral, and a bright yellow precipitate was observed, which was recrystallized with ethanol to obtain compound 4′,5,7-trihydroxy-8-methoxyflavone with a yield of 60%.

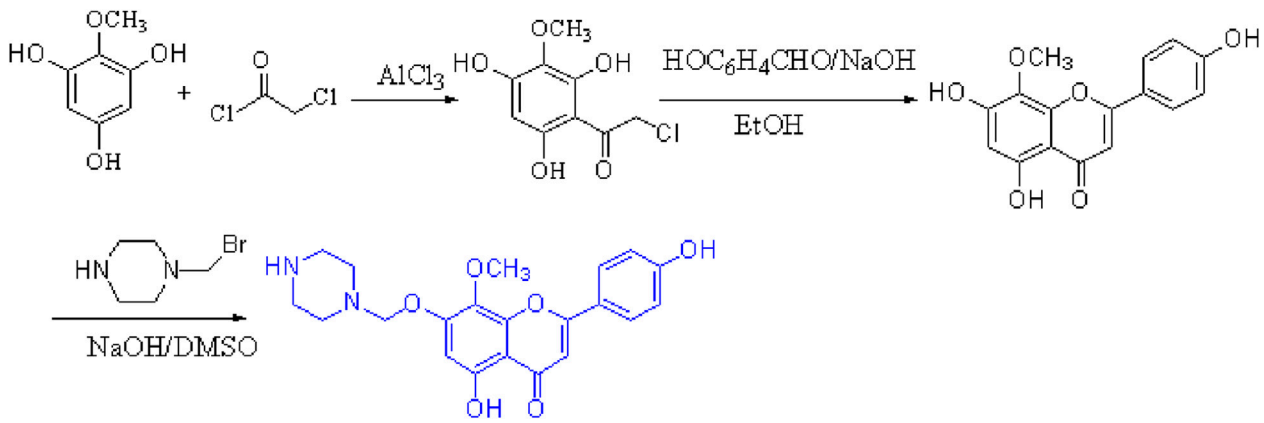

FIGURE 1
4′,5-Dihydroxy-7-piperazinemethoxy-8-methoxy flavonoids.

2.5 Preparation of 4′,5-dihydroxy-7-piperazinemethoxy-8-methoxy flavonoid

To a stirred solution of 4′,5,7-trihydroxy-8-methoxyflavone (1.0 g, 5 mmol) in dry dimethyl sulfoxide, a solution of 1-(bromomethyl) piperazine (0.6 g, 5 mmol) and NaOH (0.13 g, 5 mmol) was added at 0°C. The resulting mixture was stirred at room temperature for 5 h (reaction progress was monitored by TLC); after the reaction was completed, a 10% HCl solution was added to adjust the pH of the solution to neutral, resulting in the formation of a yellow precipitate, which was purified by recrystallization with EtOH to yield compound 4′,5-DMF. The yield was 71%. The structure of the target compound DMF was identified by IR, MS, 1H-NMR, and 13C-NMR (Figure 1).

2.6 Cell culture and proliferation experiment

HepG2, Hep3B, and THLE-2 cells were cultured in a culture medium (DMEM:fetal bovine serum:penicillin–streptomycin = 100:1:1). QSG-7701 cells were cultured in a culture medium (RPMI:fetal bovine serum:penicillin–streptomycin = 100:1:1) in a humid incubator (37°C, 5% CO_2). When the cells reached the logarithmic growth phase, CCK-8 was used to detect cell proliferation ability, and 100 μL of cell suspension was added to the pores of the 96-well plate so that the cell density in each hole was 5×10^3 cells/mL. After the cells were attached to the wall, the HepG2 and Hep3B cells were divided into the following groups: control group, DMF treatment group (25, 50, 100, 200, and 250 μM), sgRNA group, and sgRNA + DMF group. The THLE-2 and QSG-7701 cells were divided into the following groups: control group and DMF treatment group (50, 100, and 200 μM). Each group was set up with five compound pores, and 10 μL CCK-8 solution was added to each group and incubated for 1 h. OD values of each pore solution were detected at a wavelength of 490 nm using an enzyme-labeled instrument, and the data were recorded to calculate the cell growth inhibition rate.

Cell growth inhibition rate (%) = 1−[(experimental group OD value−blank group OD value)/(negative control group OD value−blank group OD value)] × 100%.

Cell viability (%) = (experimental group OD value−blank group OD value)/(negative control group OD value−blank group OD value)] × 100%.

2.7 Determination of the ATP content

The cells of the logarithmic growth stage were divided into DMF treatment groups (0, 50, 100, and 200 μM) and a positive control group (5-FU). After administering the drug, 5×10^6 cells were taken from each group; 1 mL of extraction solution was added, crushed using ultrasonic waves, and then centrifuged for 10 min. The supernatant was obtained, and chloroform was added to the mix. The supernatant was obtained after centrifugation.

According to the instructions of the ATP test kit, the corresponding reagent was added to each tube in turn and then fully mixed. The absorbance value A1 at 10 s was determined at 340 nm, and then the sample was placed in a 37-C water bath for 3 min. The absorbance value was immediately measured and recorded as A2. The ATP content of the sample was tested according to the manufacturer's instructions.

2.8 CRISPR/Cas9-mediated *Bclaf1* gene knockout experiment

HepG2 and Hep3B cells were divided into a blank control group and an sgRNA group. The next day, 1 mL of high-sugar medium was replaced, and 20 μL of lentivirus vector was added to the sgRNA group. The complete culture medium was replaced after incubation for 12 h. After incubation for 48 h, 6 μg/mL of mycillin was added to each well for screening, and stable cell lines with the *Bclaf1* gene knocked out were obtained (Chen et al., 2022).

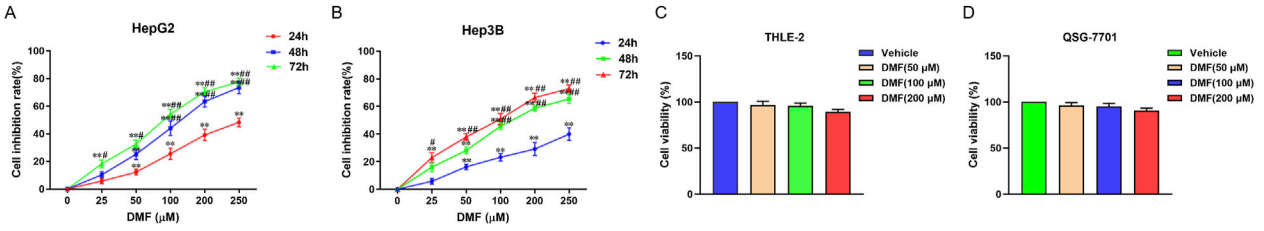

FIGURE 2
Effects of DMF on the proliferation of human hepatoma cells and normal hepatocytes. **(A)** HepG2; **(B)** Hep3B; **(C)** THLE-2; **(D)** QSG-7701, data were mean ± SD, n = 3; the results were compared with vehicle, $^{**}P < 0.01$, the results were compared with 24h groups, $^{\#}P < 0.05$, $^{\#\#}P < 0.01$.

2.9 Western blotting

The cell or tumor tissue proteins were extracted, and then, the protein concentration was determined using the BCA method. The loading volume was calculated according to the sample concentration. After separation by sodium dodecyl sulfate polyacrylamide gel electrophoresis (at 100 V for 120 min), the corresponding polyvinylidene fluoride (PVDF) membrane was clipped according to the molecular weight of the transferred target protein. The proteins were transferred to the PVDF membrane (100 V, 30–90 min). The membrane was then blocked with 5% skim milk. The primary antibody was diluted with TBST: Bcl-2 (1:2,500), Bax (1:2,500), Cyt-c (1:2,000), cleaved caspase-3 (1:2,000), Bclaf1 (1:2,500), and β-actin (1:30,000) and was incubated overnight at 4°C. On day 2, the anti-rabbit secondary antibody (1:5,000) was incubated for 2 h, and ECL chemiluminescence solution was added. The protein was detected using a bioanalytical imaging system (Cycloud, Beijing, China).

2.10 Annexin V/FITC double staining

HepG2 and Hep3B cells were inoculated in 6-well plates with 1×10^6 cells per well and divided into an unstained group, Annexin V group, PI group, DMF (0, 50, 100, and 200 μM) administration group, 5-FU (10 μM) group, sgRNA group, sgRNA + DMF group, Bclaf1-overexpression group, and Bclaf1-overexpression + DMF group. They were digested with a pancreatic enzyme without EDTA, and pre-cooled PBS was added to prepare the cell suspension and centrifuged at 3,000 g for 2 min. Then, 1 mL PBS was added to the cell mass. Centrifugation was performed at 3,000 g for 2 min, after which PBS was discarded. Next, 100 μL 1 × binding buffer was added, and 10 μL was removed from each tube. Subsequently, 5 μL Annexin V was added and incubated for 20 min, followed by the addition of 5 μL PI, which was incubated in the dark for 5 min. Finally, 400 μL 1 × binding buffer was added to each tube, and the apoptosis rate of cells was detected by flow cytometry (Beckman Coulter Corporation, United States).

2.11 JC-1 fluorescent probe method

HepG2 and Hep3B cells were divided into a negative control group, DMF (100 μM) administration group, 5-FU (10 μM) administration group, sgRNA group, and sgRNA + DMF group, Bclaf1-overexpression group, Bclaf1-overexpression + DMF group, and carbonyl cyanide 3-chlorophenylhydrazone (CCCP) group. After incubating for 48 h, the cells in the CCCP group were treated with the JC-1 staining solution for 40 min. The culture medium was discarded, and the JC-1 dyeing solution was added to each well and incubated for 60 min. The JC-1 buffer was diluted with distilled water (1:4), washed with the diluted JC-1 buffer, and then photographed under a 400× fluorescence microscope (Olympus, Japan) (Chen et al., 2022).

2.12 Immunofluorescence

HepG2 and Hep3B cells were inoculated in the 6-well plate; the next day, the blank control group, DMF (0, 50, 100, and 200 μM) group, and 5-FU (10 μM) group were treated with drugs and culture medium and incubated for 48 h. The culture medium was discarded, and 4% paraformaldehyde was incubated for 10 min. After infiltration of 0.2% Triton X-100 for 20 min, an appropriate amount of 5% BSA was added to each well and closed for 1 h. Then, 100 μL Bclaf1 (1:200) was uniformly dripped onto the tablet, which was then placed in a wet box sheltered from light and refrigerated at 4°C overnight. The next day, 200 μL fluorescein (1:100) was added away from light and incubated at 37°C for 1 h. Then, DAPI was cleaned with PBS, stained for 5 min under a 400× fluorescence microscope, and photographed.

2.13 Construction of a stable transmutation strain with the overexpression of Bclaf1

HepG2 and Hep3B cells were inoculated in 6-well plates. The next day, the viral stock solution was melted and diluted with fresh medium containing 8 μg/mL polybrene according to the appropriate MOI value. The lentivirus diluent was added to the cells. The next day, 2 μg/mL puromycin was added to the cells and cultured in an incubator for 24 h. Cells with stable overexpression of Bclaf1 were screened, and the infection effect was verified by Western blotting.

2.14 Establishment of a nude mouse transplanted tumor model

In nude mice, 1×10^7 Hep3B cells were inoculated in the right armpit (forelimb), and when the tumor grew to an average volume of

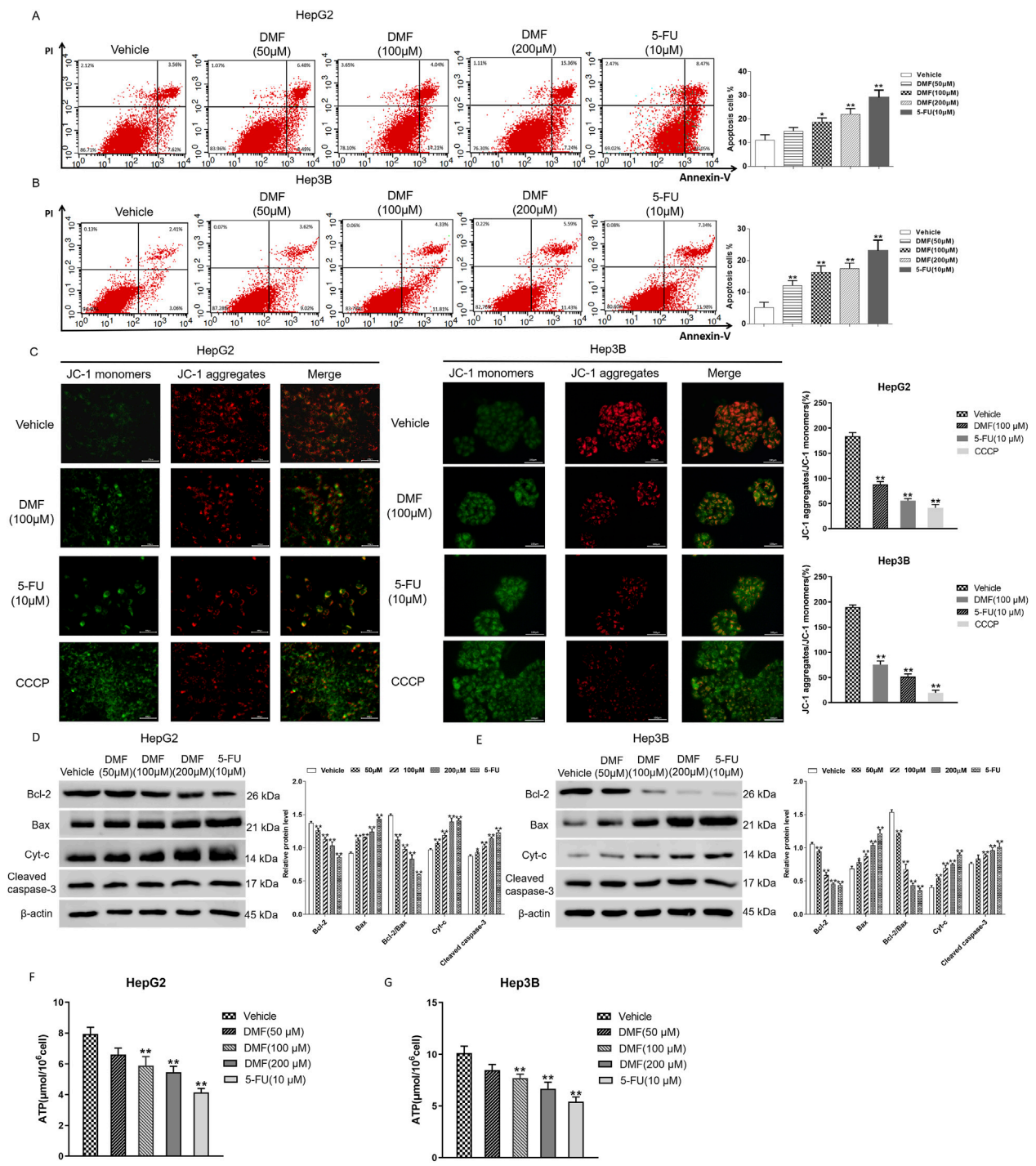

FIGURE 3
DMF induced mitochondrial apoptosis in human hepatoma cells. **(A,B)** Flow cytometry was used to detect the effect of DMF on apoptosis rates. **(C)** The JC-1 fluorescent probe method was used to detect changes in the mitochondrial membrane potential (400×). **(D,E)** Western blotting detected the expression levels of proteins, and the results were statistically analyzed. **(F,G)** Content of ATP in the cells; all the results were compared with those of the vehicle. $*p < 0.05$ and $**p < 0.01$.

80–100 mm^3, the drug was administered (intravenous injection). Before administration, the nude mice were weighed, and the tumor volume was measured. The nude mice were divided into the lysozyme control group, DMF (5, 10, and 20 mg/kg) group, and positive drug 5-FU (15 mg/kg) group. In the experiment, if the tumor volume of a single mouse exceeded 2,000 mm^3, the experiment was terminated. When the mean tumor volume of mice in the control group exceeded 1,000 mm^3 or when the tumor size of the control group and the experimental group mice was different, all nude mice were euthanized. The anesthetic was 20% urethane, intraperitoneally injected at a dose of 200 μL/20 g. The weight and tumor volume of nude mice were measured, and the tumors were collected.

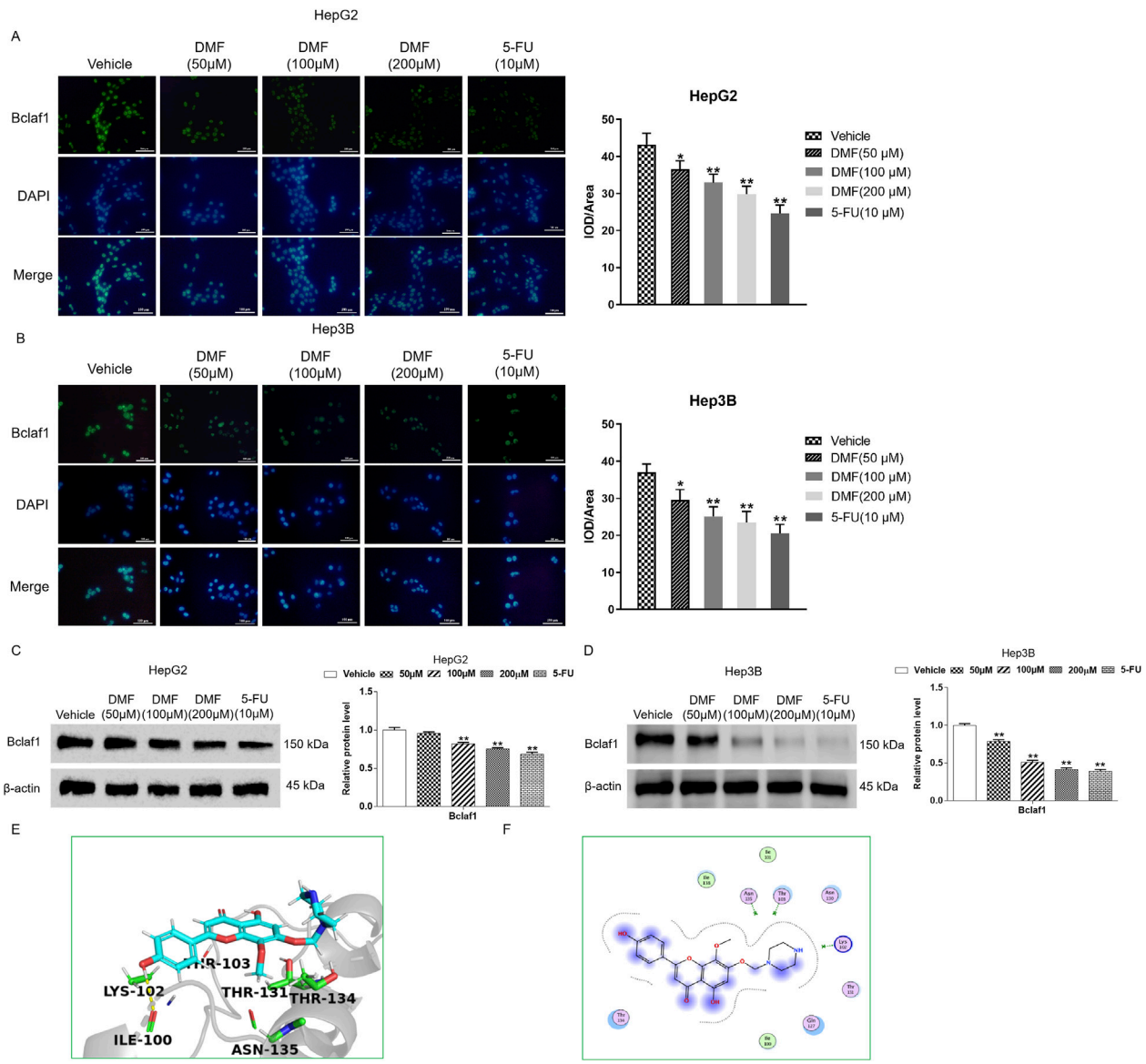

FIGURE 4
DMF inhibited Bclaf1 expression in human hepatoma cells. **(A,B)** Immunofluorescence was used to detect the expression of Bclaf1 after the cells were treated with DMF (400×). **(C,D)** Western blotting was used to detect the expression level of Bclaf1, and the results were statistically analyzed. All the results are compared with those of the vehicle. *$p < 0.05$ and **$p < 0.01$. **(E,F)** Docking result of DMF and Bclaf1 (PDB ID: 7RJR).

Tumor volume calculation formula: tumor volume (mm^3) = 1/2 × (tumor long diameter × tumor short diameter^2).

2.15 Immunohistochemical experiments

Tissue wax blocks were prepared by transplanting tumors in nude mice. After the sections were soaked in xylene for 10 min and dehydrated in a gradient, the antigen repair solution was added. The sections were kept in a slightly boiling state for 30 min. Two drops of 3% hydrogen peroxidation–methanol solution were added to the sections for 10 min, and 200 μL 5% BSA was then added to the sections for 20 min. Each slice was added with 100 μL of primary antibody Bclaf1 (1:200), incubated at 37°C in a wet box for 2 h, then dropped using an 80-μL enhancer, and placed for 30 min. Then, 100 μL of secondary antibody was added and incubated at 37°C for 30 min. Then, 50 μL of the DAB solution and hematoxylin dye solution were added to the tissue sections for 10 min, dehydrated with an ethanol gradient, and transplanted with xylene for 20 min. Then, neutral gum was added to seal the tablets.

2.16 Molecular docking experiments of target compounds

Molecular simulation and docking experiments were carried out using the PyRx docking program. The protein crystal structure

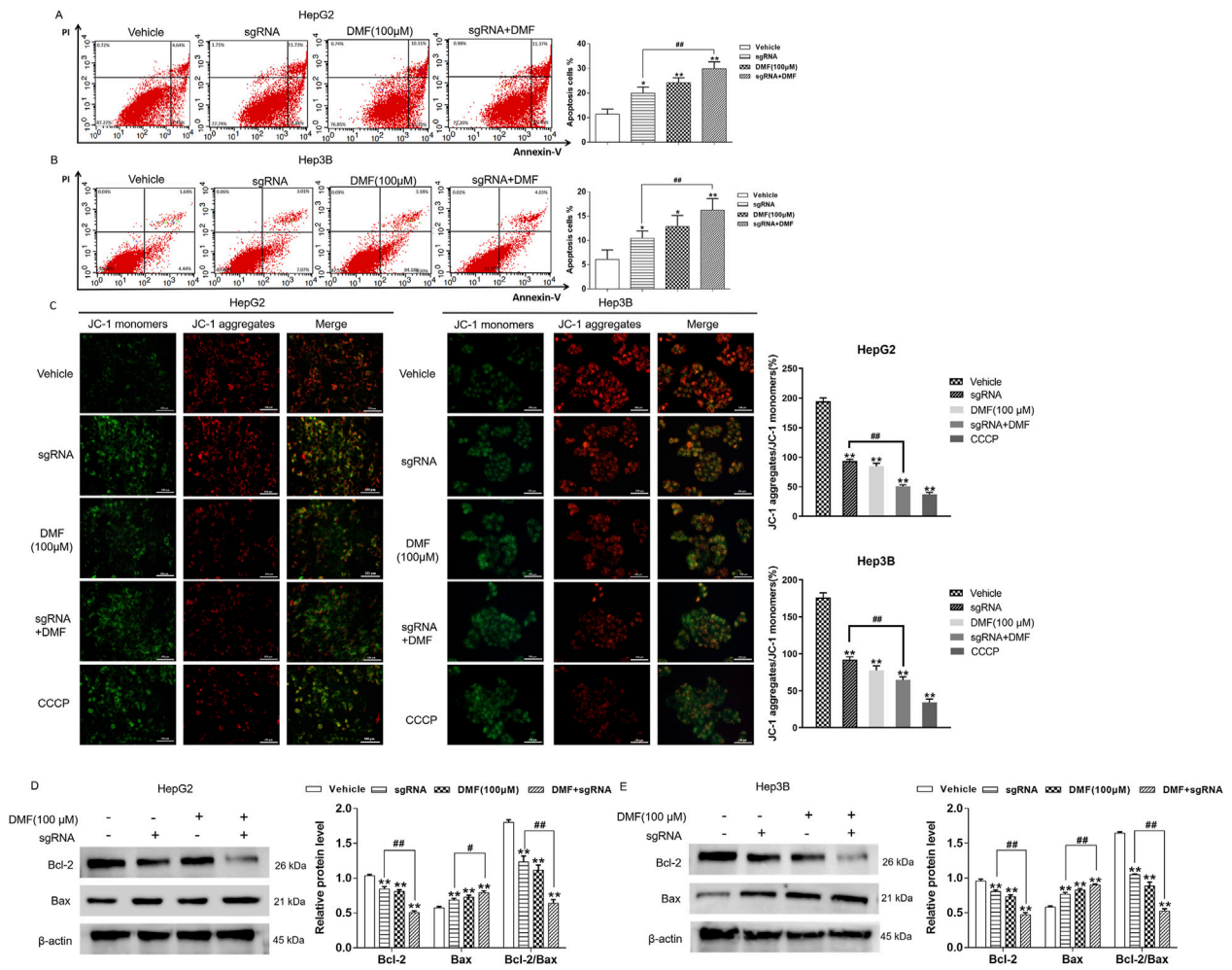

FIGURE 5
DMF induced mitochondrial apoptosis in human hepatoma cells with stable Bclaf1 knockout. **(A,B)** Flow cytometry was used to detect the changes in apoptosis rates. **(C)** The JC-1 fluorescence probe was used to detect the effect of DMF on the mitochondrial membrane potential (400×). **(D,E)** Western blotting was used to detect the expression of mitochondrial apoptosis-related proteins, Bcl-2 and Bax. Statistical analysis was performed; the results were compared with those of the vehicle. $^{*}p < 0.05$ and $^{**}p < 0.01$. The sgRNA group was compared with the sgRNA + DMF group. $^{\#}p < 0.05$ and $^{\#\#}p < 0.01$.

of Bclaf1 was obtained from the Protein Crystal Database (PDB ID: 7RJR) with a resolution of 1.45 Å. The initial structure of the Bclaf1 protein crystal was treated with default parameters. Here, 1, 2-ethylene glycol was used as the ligand center, and the optimized protein crystal structure and compound were simulated. The score (−5.4290) of the result was treated using PyMOL to evaluate the effect of the compound at the molecular level.

2.17 Statistical analysis

Data analysis was performed using GraphPad Prism 6. The data were expressed as the mean ± standard deviation (SD). Differences between groups were analyzed by one-way analysis of variance and Student's t-test. $p < 0.05$ was considered statistically significant, and $p < 0.01$ was considered a highly significant difference.

3 Results

3.1 DMF inhibited human hepatoma cell proliferation

The effects of DMF on the proliferation of HepG2 and Hep3B cells were detected using the CCK-8 assay. The cells were treated with DMF (25, 50, 100, 200, or 250 μM) for 24, 48, or 72 h. The results indicated that DMF inhibited the proliferation of human hepatoma cells in a time- and concentration-dependent manner. The IC_{50} values of DMF after treatment for 48 h in HepG2 and Hep3B cells were 121.7 and 130.4 μM, respectively (Figures 2A, B). The DMF concentration gradient selected for subsequent experiments was 50, 100, and 200 μM. The toxicity of DMF to normal hepatocytes was further examined, and the results showed that there was no significant difference in cell viability between TELE-2 and QSG-7701 normal hepatocytes after DMF treatment (Figures 2C, D).

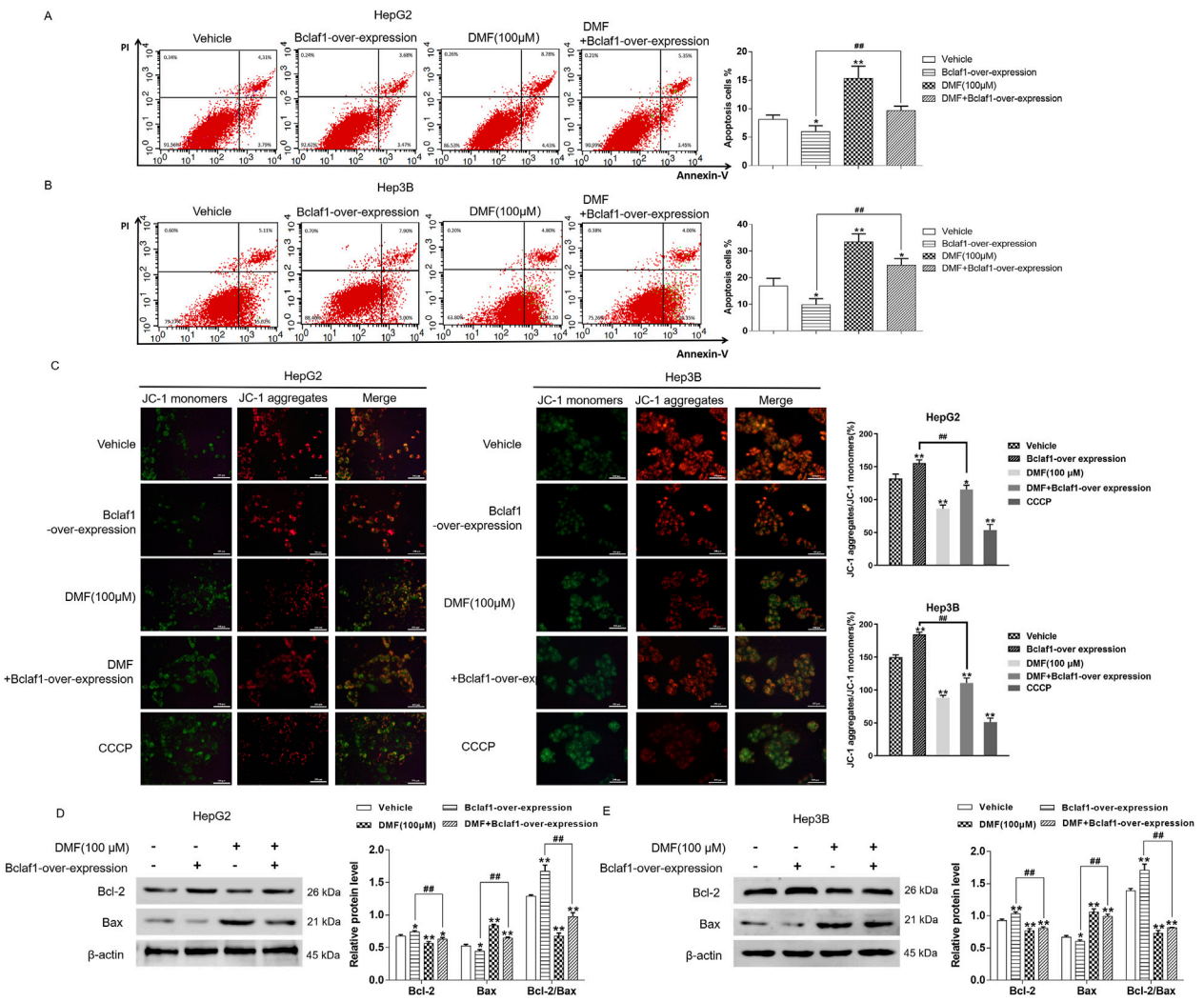

FIGURE 6
Overexpression of Bclaf1 inhibited mitochondrial apoptosis in human hepatoma cells. **(A,B)** Flow cytometry was used to detect the changes in apoptosis rates. Statistical analysis was performed. **(C)** The JC-1 fluorescence probe method was used to detect the effect of DMF on the mitochondrial membrane potential (400×). **(D,E)** Western blotting was used to detect the expression of mitochondrial apoptosis-related proteins, Bcl-2 and Bax. Statistical analysis was performed. The results were compared with those of the vehicle. $^{*}p < 0.05$ and $^{**}p < 0.01$. The Bclaf1-overexpression group was compared with the DMF + Bclaf1-overexpression group. $^{\#\#}p < 0.01$.

3.2 DMF induced mitochondrial apoptosis in human hepatoma cells

Flow cytometry was used to detect the change in the apoptosis rate in cells treated with DMF for 48 h. The experimental results indicated that the percentage of apoptotic cells increased in a DMF concentration-dependent manner. The percentages of apoptotic HepG2 cells after treatment with 50, 100, and 200 μM DMF and positive drug 5-FU were 11.06%, 14.85%, 18.66%, 21.96%, and 29.08%, respectively, and the percentages of apoptotic Hep3B cells after these treatments were 5.11%, 12.04%, 16.24%, 17.45%, and 23.10%, respectively (Figures 3A, B). HepG2 and Hep3B cells were examined using the JC-1 fluorescence probe method after DMF treatment. Following treatment, the red fluorescence was weakened, whereas the green fluorescence was enhanced, indicating decreased mitochondrial membrane potential and increased cell permeability (Figure 3C). To further explore the effects of DMF on mitochondrial apoptosis in human hepatoma cells, Western blotting was performed to detect the expression of Bcl-2, Bax, Cyt-c, and cleaved caspase-3 after DMF treatment. The results illustrated that the Bcl-2/Bax ratio was significantly decreased after DMF treatment compared with the findings in the negative control group ($P < 0.01$), whereas Cyt-c and cleaved caspase-3 expression was increased. Similar results were obtained after 5-FU treatment (Figures 3D, E). ATP is the main energy molecule in the cells, and its content can reflect the energy production capacity of mitochondria. The experimental results showed that compared with the control group, the content of ATP in the cells decreased significantly after DMF treatment (Figures 3F, G), indicating that DMF destroyed the integrity of the mitochondria and affected the function.

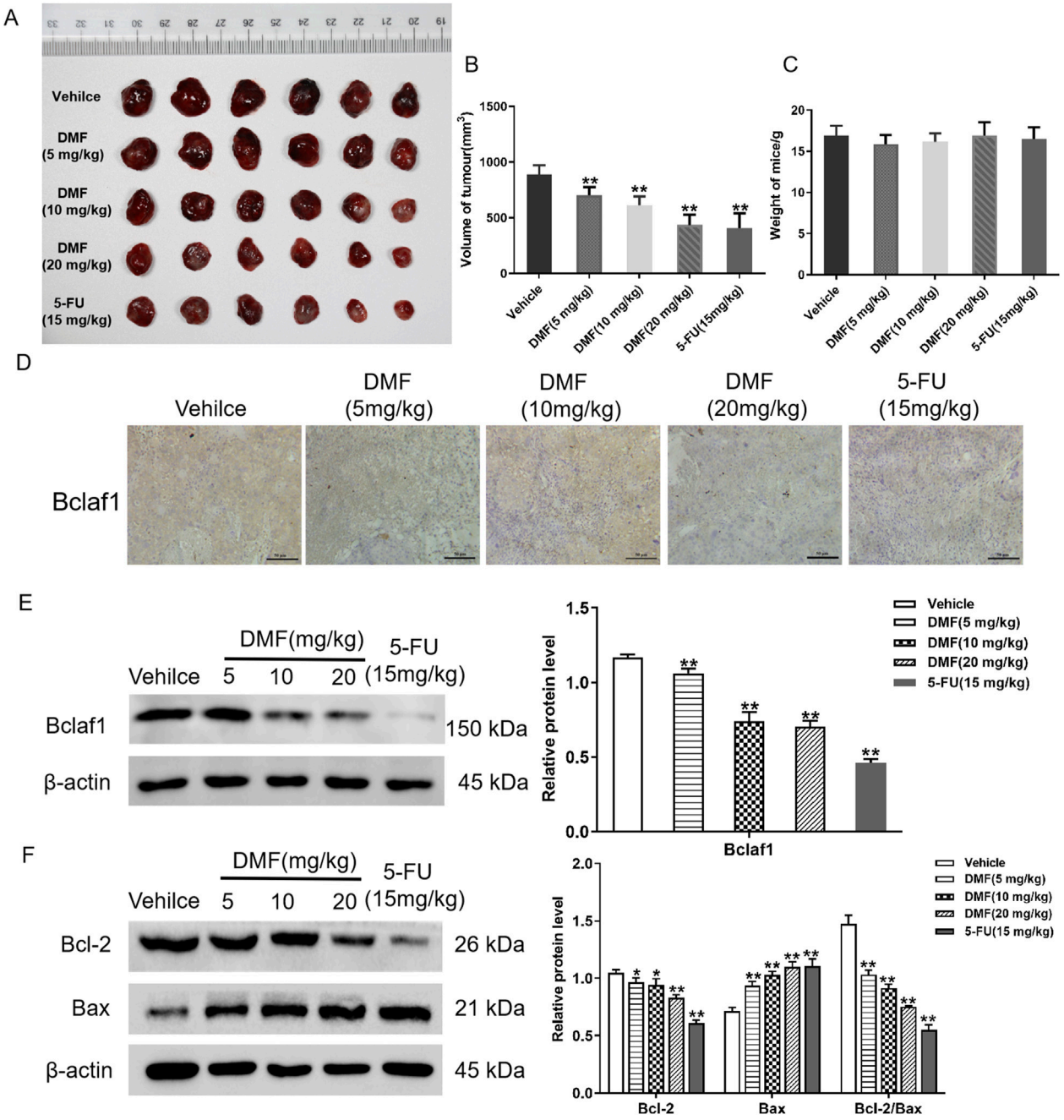

FIGURE 7
DMF inhibited the growth of transplanted tumors in nude mice. **(A)** Photograph of transplanted tumors taken from nude mice. The concentrations of DMF used to treat nude mice are 5 mg/kg, 10 mg/kg, and 20 mg/kg. The concentration of the positive control, 5-FU, was 15 mg/kg. **(B)** Volume of the transplanted tumor in nude mice (mm^3). **(C)** Changes in body weight after nude mice were treated with DMF (5, 10, and 20 mg/kg) or 5-FU (15 mg/kg). **(D)** Immunohistochemical of Bclaf1 expression in tumor tissue (200×). **(E)** Western blot analysis of Bclaf1 expression in tumor tissue. **(F)** Western blot detection of the expression of Bcl-2 and Bax in tumor tissues; the results were compared with those of the vehicle. $*p < 0.05$ and $**p < 0.01$.

3.3 DMF inhibited Bclaf1 expression in human hepatoma cells

Immunofluorescence detection revealed that Bclaf1 was expressed in both the nucleus and cytoplasm of untreated human hepatoma cells. After DMF treatment, the fluorescence intensity of Bclaf1 decreased in a concentration-dependent manner (Figures 4A, B). Western blotting illustrated that DMF significantly decreased Bclaf1 expression versus the control ($p < 0.01$; Figures 4C, D). The molecular docking of DMF in Bclaf1 was studied *in vitro*. The results demonstrated the optimal binding location and interaction between the receptor and target (Figures 4E, F). The 4′- and 5-hydroxyl groups of DMF formed hydrogen bonds with ILE-100 and THR-134 in the active center of Bclaf1, respectively, and the oxygen atoms at positions 1 and 7 of DMF formed hydrogen bonds with the amino acid residues THR-103 and THR-131 of Bclaf1, respectively. The

-NH moiety of the DMF piperazine ring formed a hydrogen bond with LYS-102 of Bclaf1.

3.4 DMF induced mitochondrial apoptosis in human hepatoma cells with stable Bclaf1 knockout

Annexin V/FITC double-staining revealed that the apoptosis rate of human hepatoma cells was increased after Bclaf1 knockout compared with the vehicle ($p < 0.05$). The apoptosis rate of HepG2 cells was further increased by DMF treatment, and rates in the groups were 11.37%, 19.96%, 24.19%, and 29.91%, respectively. The apoptosis rates of Hep3B cells in all groups were 6.10%, 10.47%, 12.85%, and 16.24%, respectively (Figures 5A, B). To further explore the role of DMF in inducing mitochondrial apoptosis in human hepatoma cells through Bclaf1, the fluorescence probe method was applied. Bclaf1 knockout resulted in increased green fluorescence, decreased red fluorescence, and decreased mitochondrial membrane potential in cells, indicating that Bclaf1 knockout induced mitochondrial apoptosis in human hepatoma cells. After DMF treatment in cells with stable Bclaf1 knockout, the mitochondrial membrane potential was further decreased (Figure 5C). After Bclaf1 knockout, Bcl-2 expression was downregulated, Bax expression was increased, and the Bcl-2/Bax ratio was decreased versus the control findings ($p < 0.01$), indicating that mitochondrial apoptosis was induced in human hepatoma cells after Bclaf1 knockout (Figures 5D, E).

3.5 Bclaf1 overexpression inhibited mitochondrial apoptosis in human hepatoma cells

Flow cytometry revealed that the apoptosis rate of human hepatoma cells was decreased by Bclaf1 overexpression ($P < 0.05$). DMF treatment significantly increased the apoptosis rate ($p < 0.01$) in HepG2 cells, and the apoptosis rates in all groups were 8.13%, 5.98%, 15.32%, and 9.67%, respectively. The apoptosis rates in the groups in Hep3B cells were 16.87%, 9.89%, 33.46%, and 24.71%, respectively (Figures 6A, B). In the JC-1 fluorescence probe assay, Bclaf1 overexpression resulted in decreased green fluorescence and increased red fluorescence, indicating that the mitochondrial membrane potential of human hepatoma cells was increased. Compared with the results in the blank control group, the green fluorescence was enhanced, the red fluorescence was weakened, and the mitochondrial membrane potential of the cells was decreased by DMF treatment (Figure 6C). After Bclaf1 overexpression was confirmed by Western blotting, the expression of Bcl-2, a key protein of mitochondrial apoptosis in hepatoma cells, was increased and that of Bax was decreased, and the Bcl-2/Bax ratio was increased compared with the findings in the blank control group (all $p < 0.01$). After DMF treatment, the Bcl-2/Bax ratio was decreased, indicating that mitochondrial apoptosis occurred in human hepatoma cells (Figures 6D, E).

3.6 DMF inhibited the growth of transplanted tumors and induced the mitochondrial apoptosis of the transplanted tumor in nude mice

To further verify the anti-tumor effects of DMF, the inhibitory effects of DMF (5, 10, and 20 mg/kg) and the positive control 5-FU (15 mg/kg) on the transplanted tumor were detected by establishing a nude mouse transplanted tumor model. The results illustrated that DMF significantly inhibited tumor growth ($p < 0.01$; Figures 7A, B), but there was no significant change in the body weight in each group (Figure 7C). Immunohistochemistry illustrated that compared with the vehicle, Bclaf1 expression was decreased by DMF treatment in a dose-dependent manner. Using extracted histones, Western blotting indicated that DMF inhibited the expression of Bclaf1 (Figures 7D, E). The tumor tissue protein was extracted, and Western blotting indicated that DMF treatment resulted in decreased Bcl-2 expression and increased Bax expression in tumor tissues, resulting in a lower Bcl-2/Bax ratio (all $p < 0.01$). The Bcl-2/Bax ratio was the smallest in the positive control group (Figure 7F).

4 Discussion

Liver cancer is the sixth most common cancer worldwide and the second leading cause of cancer-related death (Li et al., 2022). Traditional chemotherapy has strong side effects, and it is associated with low survival rates. Chinese medicine molecular targeted therapy has fewer overall side effects, making it an important adjuvant anti-tumor therapy for chemotherapy, radiotherapy, and surgery (Hao et al., 2021; Rodríguez-Landa et al., 2022). 4′,5,7-Trihydroxy-8-methoxyflavone was extracted from the traditional Chinese medicine *S. sorbifolia*, and after chemical modification, DMF was selected for the assessments of anti-tumor effects because of its better solubility. Following DMF treatment for 48 h, the growth inhibition rate of human hepatoma cells was significantly increased, and there was no significant difference in the activity of normal hepatocytes. In this study, HepG2 and Hep3B cells were targeted, and Annexin V/PI double-staining revealed that the apoptosis rate increased significantly after 100 μM DMF treatment compared with that in the blank control group, demonstrating that DMF can induce apoptosis of human hepatoma cells. Apoptosis can be categorized into the death receptor-mediated extrinsic pathway, mitochondrial pathway-mediated apoptosis, granzyme B-mediated apoptosis, and endoplasmic reticulum stress-induced apoptosis (Wang et al., 2018; Cheng and Ferrell, 2018). Further exploration of the apoptosis pathway induced by DMF revealed that DMF treatment decreased the mitochondrial membrane potential, as detected the by JC-1 probe. When cells are subjected to internal hypoxia, injury, and other damages, Bcl-2 family proteins are key regulatory factors activated in the mitochondrial apoptosis pathway, including the pro-apoptotic proteins Bax and Bak and the anti-apoptotic protein Bcl-2 (Schofield and Schafer, 2023; Bhosale et al., 2023). Bax reduces the membrane potential,

changes the membrane permeability, induces Cyt-c release in the cytoplasm, and forms an apoptosis complex with apoptotic protease-activating factor-1. Then, by recruiting and activating pro-caspase-9, the holoenzyme caspase 9 is formed, and caspases 3 and 7 are further activated as effectors. Consequently, the caspase cascade is initiated, and more than 100 substrates, such as actin, are cleaved, leading to apoptosis (Chu et al., 2021; Kashyap et al., 2021). Western blotting demonstrated that DMF decreased the Bcl-2/Bax ratio versus the control findings ($p < 0.01$). A decreased Bcl-2/Bax ratio is an important feature of mitochondrial apoptosis. Experimental detection demonstrated that Cyt-c and cleaved caspase-3 expression was increased. When mitochondrial apoptosis occurred in cells, the function of mitochondria was affected. A microanalysis found that after DMF treatment, the content of ATP in cells was significantly decreased, indicating that the integrity of mitochondria was destroyed. The above experimental results showed that after DMF treatment, the expression level of pro-apoptotic factor Bax increased, the expression level of anti-apoptotic factor Bcl-2 decreased, and the value of Bcl-2/Bax decreased, which decreased the mitochondrial membrane potential, opened the mitochondrial membrane permeability transition hole, promoted the release of pro-apoptotic proteins such as Cyt-c and cleaved caspase-3, and finally caused apoptosis.

Bclaf1, which is rich in arginine–serine-binding domains and contains MYB DNA-binding and bZIP domains, is involved in a variety of biological behaviors (Mou et al., 2020; Wen et al., 2019; Shao et al., 2016). This study revealed that Bclaf1 is highly expressed in human hepatoma cells and mainly distributed in the nucleus through immunofluorescence detection. DMF decreased Bclaf1 expression in a concentration-dependent manner. Molecular docking analysis showed that the 4′- and 5-hydroxyl groups of DMF formed hydrogen bonds with ILE-100 and THR-134, respectively, in the active center of Bclaf1, and the oxygen atoms at positions 1 and 7 of DMF formed hydrogen bonds with the amino acid residues THR-103 and THR-131 of Bclaf1, respectively. The -NH moiety of the DMF piperazine ring formed a hydrogen bond with LYS-102 of Bclaf1, which suggested that DMF could bind to the active site of Bclaf1 to inhibit its expression. Further probing the mechanism by which DMF induces mitochondrial apoptosis of human hepatoma cells through Bclaf1 showed that Bclaf1 knockout led to an increased apoptosis rate in human hepatoma cells by flow cytometry, and after the action and stability of DMF, the apoptosis rate was further increased. Bclaf1 knockout resulted in decreased mitochondrial membrane potential, which was further decreased in the DMF + sgRNA group, in addition to a decreased Bcl-2/Bax ratio. These results indicated that DMF could induce mitochondrial apoptosis in hepatoma cells through Bclaf1. To further verify this effect, after Bclaf1 overexpression, relevant indicators were detected. The results illustrated that Bclaf1 overexpression depressed mitochondrial apoptosis in human hepatoma cells and that DMF induced mitochondrial apoptosis in cells by inhibiting Bclaf1.

In vitro experiments demonstrated that DMF induced the mitochondrial apoptosis of human hepatoma cells through Bclaf1, thus inhibiting their proliferation. To verify the anti-tumor effects of DMF, a transplanted tumor model was constructed in nude mice, and the mice were euthanized after treatment with 5, 10, or 20 mg/kg DMF or 15 mg/kg 5-FU. The transplanted tumor was excised, and the tumor volume was calculated. DMF significantly inhibited tumor growth compared with the blank control group findings ($p < 0.01$), and the body weight of nude mice did not change significantly. To explore the mechanism by which DMF induced mitochondrial apoptosis through Bclaf1, immunohistochemical tests revealed that DMF treatment decreased Bclaf1 expression. Then, histones were extracted to detect Bcl-2 and Bax, and the results indicated that after DMF treatment, the Bcl-2/Bax ratio was decreased, indicating that DMF can induce mitochondrial apoptosis in liver cancer.

In summary, 4′,5,7-trihydroxy-8-methoxyflavone was extracted from *S. sorbifolia,* a traditional Chinese medicine, and structural modification resulted in the identification of DMF, which inhibited human hepatoma cell proliferation and induced mitochondrial apoptosis. The effect of DMF was linked to its targeting of the multi-functional protein Bclaf1. Inhibition of Bclaf1 expression can induce mitochondrial apoptosis in human hepatoma cells, and the anti-tumor effect of DMF was further verified through the construction of a nude mouse transplanted tumor model. Therefore, our study is expected to provide an experimental basis for DMF as an effective *S. sorbifolia* flavonoid derivative to treat liver cancer with Bclaf1 as its target and provide new ideas for the targeted therapy of liver cancer in clinical practice.

5 Conclusion

DMF induces mitochondrial apoptosis in human hepatoma cells through Bclaf1.

Data availability statement

The original contributions presented in the study are included in the article/Supplementary Material; further inquiries can be directed to the corresponding author.

Ethics statement

Ethical approval was not required for the studies on humans in accordance with the local legislation and institutional requirements because only commercially available established cell lines were used. The animal study was approved by the Institutional Animal Care and Use Committee of Yanbian University (resolution number: 201501022). The study was conducted in accordance with the local legislation and institutional requirements.

Author contributions

JC: conceptualization, data curation, formal analysis, methodology, software, writing–original draft, and

writing–review and editing. HC: conceptualization, data curation, formal analysis, software, writing–original draft, and writing–review and editing. CB: conceptualization, data curation, methodology, software, and writing–original draft. DW: investigation, methodology, software, and writing–review and editing. JF: data curation, formal analysis, investigation, software, and writing–review and editing. JH: formal analysis, methodology, software, validation, and writing–review and editing. YW: formal analysis, methodology, software, and writing–review and editing. ZX: conceptualization, data curation, funding acquisition, project administration, resources, and writing–review and editing.

Funding

The author(s) declare that financial support was received for the research, authorship, and/or publication of this article. This study was supported by the National Natural Science Foundation of China (No. 82260783, China).

Conflict of interest

The authors declare that the research was conducted in the absence of any commercial or financial relationships that could be construed as a potential conflict of interest.

Publisher's note

All claims expressed in this article are solely those of the authors and do not necessarily represent those of their affiliated organizations, or those of the publisher, the editors, and the reviewers. Any product that may be evaluated in this article, or claim that may be made by its manufacturer, is not guaranteed or endorsed by the publisher.

Supplementary material

The Supplementary Material for this article can be found online at: https://www.frontiersin.org/articles/10.3389/fphar.2024.1459520/full#supplementary-material

References

Anwanwan, D., Singh, S. K., Singh, S., Varma, S., and Rajesh, S. (2020). Challenges in liver cancer and possible treatment approaches. *Biochim. Biophys. Acta Rev. Cancer* 1873 (1), 188314. doi:10.1016/j.bbcan.2019.188314

Bai, C., Zhao, J., Su, J., Chen, J., Cui, X., Sun, M., et al. (2022). Curcumin induces mitochondrial apoptosis in human hepatoma cells through BCLAF1-mediated modulation of PI3K/AKT/GSK-3β signaling. *Life Sci.* 306, 120804. doi:10.1016/J.LFS.2022.120804

Bhosale, P. B., Kim, H. H., Abusaliya, A., Jeong, S. H., Park, M. Y., Kim, H. W., et al. (2023). Inhibition of cell proliferation and cell death by apigetrin through death receptor-mediated pathway in hepatocellular cancer cells. *Biomolecules* 13 (7), 1131. doi:10.3390/biom13071131

Chen, J., Sun, M., Cui, X., and Zhang, X. (2022). Ginsenoside compound K induces mitochondrial apoptosis in human hepatoma cells through Bclaf1-mediated modulation of ERK signaling. *Food Agric. Immunol.* 33 (1), 799–816. doi:10.1080/09540105.2022.2134313

Chen, J., Wang, H., Xu, J., Chen, E., Meng, Q., Wang, J., et al. (2024). CircZFR promotes colorectal cancer progression via stabilizing BCLAF1 and regulating the miR-3127-5p/RTKN2 axis. *Sci. China Life Sci.* 24, 1881–1898. doi:10.1007/s11427-023-2514-y

Cheng, X., and Ferrell, J. E. (2018). Apoptosis propagates through the cytoplasm as trigger waves. *Science* 361 (6402), 607–612. doi:10.1126/science.aah4065

Chu, Q., Gu, X., Zheng, Q., Wang, J., and Zhu, H. (2021). Mitochondrial mechanisms of apoptosis and necroptosis in liver diseases. *Anal. Cell. Pathol. (Amst)* 2021, 8900122. doi:10.1155/2021/8900122

Hao, X., Sun, G., Zhang, Y., Kong, X., Rong, D., Song, J., et al. (2021). Targeting immune cells in the tumor microenvironment of HCC: new opportunities and challenges. *Front. Cell. Dev. Biol.* 9, 775462. doi:10.3389/FCELL.2021.775462

Jiang, K., Ding, Y., Dong, C., Shan, F., Guo, K., Zhang, J., et al. (2022). BCLAF1, afunctional partner of BACH1, participates in DNA damage response. *DNA Repair (Amst)* 118, 103371. doi:10.1016/J.DNAREP.2022.103371

Kashyap, D., Garg, V. K., and Goel, N. (2021). Intrinsic and extrinsic pathways of apoptosis: role in cancer development and prognosis. *Adv. Protein Chem. Struct. Biol.* 125, 73–120. doi:10.1016/bs.apcsb.2021.01.003

Li, Q., Cao, M., Lei, L., Yang, F., Li, H., Yan, X., et al. (2022). Burden of liver cancer: from epidemiology to prevention. *Chin. J. Cancer Res.* 6 (3), 554–566. doi:10.21147/J.ISSN.1000-9604.2022.06.02

Li, Y., Bian, L., Cui, F., Li, L., and Zhang, X. (2011). TTF1-induced apoptosis of HepG-2 cells through a mitochondrial pathway. *Oncol. Rep.* 26 (3), 651–657. doi:10.3892/or.2011.1330

Liu, C., Li, X. W., Cui, L. M., Li, L. C., Chen, L. Y., and Zhang, X. W. (2011). Inhibition of tumor angiogenesis by TTF1 from extract of herbal medicine. *World J. Gastroenterol.* 17 (44), 4875–4882. doi:10.3748/wjg.v17.i44.4875

Mou, S. J., Yang, P. F., Liu, Y. P., Xu, N., Jiang, W. W., and Yue, W. J. (2020). BCLAF1 promotes cell proliferation, invasion and drug-resistance though targeting lncRNA NEAT1 in hepatocellular carcinoma. *Life Sci.* 242, 117177. doi:10.1016/j.lfs.2019.117177

Rodríguez-Landa, J. F., German-Ponciano, L. J., Puga-Olguín, A., and OlmosVázquez, O. J. (2022). Pharmacological, neurochemical, and behavioral mechanisms underlying the anxiolytic and antidepressant-likeEffects of flavonoid chrysin. *Molecules* 27 (11), 3551. doi:10.3390/MOLECULES27113551

Sankar, K., Pearson, A. N., Worlikar, T., Perricone, M. D., Holcomb, E. A., MendirattaLala, M., et al. (2020). Impact of immune tolerance mechanisms on the efficacy of immunotherapy in primary and secondary liver cancers. *Transl. Gastroenterol. Hepatol.* 8, 29. doi:10.21037/TGH-23-11

Schofield, J. H., and Schafer, Z. T. (2023). Regulators mount up: the metabolic roles of apoptotic proteins. *Front. Cell. Death* 2, 1223926. doi:10.3389/fceld.2023.1223926

Shao, A. W., Sun, H., Geng, Y., Peng, Q., Wang, P., Chen, J., et al. (2016). Bclaf1 is an important NF-κB signaling transducer and C/EBPβ regulator in DNA damage-induced senescence. *Cell. Death Differ.* 23 (5), 865–875. doi:10.1038/cdd.2015.150

Shen, B., Tan, M., Mu, X., Qin, Y., Zhang, F., Liu, Y., et al. (2016). Upregulated SMYD3 promotes bladder cancer progression by targeting BCLAF1 and activating autophagy. *Tumour Biol.* 37 (6), 7371–7381. doi:10.1007/s13277-015-4410-2

Wang, Y., Zhong, J., Bai, J., Tong, R., An, F., Jiao, P., et al. (2018). The application of natural products in cancer therapy by targeting apoptosis pathways. *Curr. Drug Metab.* 19 (9), 739–749. doi:10.2174/1389200219666180511154722

Wen, Y., Zhou, X., Lu, M., He, M., Tian, Y., Liu, L., et al. (2019). Bclaf1 promotes angiogenesis by regulating HIF-1α transcription in hepatocellular carcinoma. *Oncogene* 38 (11), 1845–1859. doi:10.1038/s41388-018-0552-1

Xiao, B., Lin, D., Zhang, X., Zhang, M., and Zhang, X. (2016a). TTF1, in the form of nanoparticles, inhibits angiogenesis, cell migration and cell invasion *in vitro* and *in vivo* in human hepatoma through STAT3 regulation. *Molecules* 21 (11), 1507. doi:10.3390/molecules21111507

Xiao, B., Liu, C., Liu, B. T., Zhang, X., Liu, R. R., and Zhang, X. W. (2016b). TTF1-NPs induce ERS-mediated apoptosis and inhibit human hepatoma cell growth *in vitro* and *in vivo*. *Oncol. Res.* 23 (6), 311–320. doi:10.3727/096504016X14567549091341

Yu, Z., Wu, X., Zhu, J., Yan, H., Li, Y., Zhang, H., et al. (2024). BCLAF1 binds SPOP to stabilize PD-L1 and promotes the development and immune escape of hepatocellular carcinoma. *Cell. Mol. Life Sci.* 81 (1), 82. doi:10.1007/s00018-024-05144-z

Yu, Z., Zhu, J., Wang, H., Li, H., and Jin, X. (2022). Function of BCLAF1 in human disease. *Oncol. Lett.* 23 (2), 58. doi:10.3892/OL.2021.13176

Zhang, S., Zhang, M., Chen, J., Zhao, J., Su, J., and Zhang, X. (2020). Ginsenoside compound K regulates HIF-1α-Mediated glycolysis through Bclaf1 to inhibit the proliferation of human liver cancer cells. *Front. Pharmacol.* 11, 583334. doi:10.3389/FPHAR.2020.583334

Zhang, X., Zhang, M., Xiao, B., Jiao, W., Zhang, S., and Zhang, X. (2018). TTF1-NP induces protective autophagy during apoptosis by inhibiting the Akt/mTOR pathway and activating JNK in human liver cancer cells. *Oncol. Rep.* 39 (3), 1423–1431. doi:10.3892/or.2018.6196

frontiers | Frontiers in Pharmacology

TYPE Review
PUBLISHED 11 October 2024
DOI 10.3389/fphar.2024.1459057

Check for updates

OPEN ACCESS

EDITED BY
Hailin Tang,
Sun Yat-sen University Cancer Center (SYSUCC), China

REVIEWED BY
Jinjun Wu,
Guangzhou University of Chinese Medicine, China
Xiaoning Gan,
Guangzhou First People's Hospital, China

*CORRESPONDENCE
Qunfeng Zhang,
xiaofeng29@163.com
Yukun Li,
yukun_li@foxmail.com
yukun_li@csu.edu.cn

†These authors have contributed equally to this work

RECEIVED 03 July 2024
ACCEPTED 16 September 2024
PUBLISHED 11 October 2024

CITATION
Song G, Liu J, Tang X, Zhong J, Zeng Y, Zhang X, Zhou J, Zhou J, Cao L, Zhang Q and Li Y (2024) Cell cycle checkpoint revolution: targeted therapies in the fight against malignant tumors. *Front. Pharmacol.* 15:1459057.
doi: 10.3389/fphar.2024.1459057

COPYRIGHT
© 2024 Song, Liu, Tang, Zhong, Zeng, Zhang, Zhou, Zhou, Cao, Zhang and Li. This is an open-access article distributed under the terms of the Creative Commons Attribution License (CC BY). The use, distribution or reproduction in other forums is permitted, provided the original author(s) and the copyright owner(s) are credited and that the original publication in this journal is cited, in accordance with accepted academic practice. No use, distribution or reproduction is permitted which does not comply with these terms.

Cell cycle checkpoint revolution: targeted therapies in the fight against malignant tumors

Guangming Song[1†], Jue Liu[1†], Xing Tang[2], Jie Zhong[1], Yuhuan Zeng[1], Xiaodi Zhang[1], Jianbin Zhou[1], Jie Zhou[1], Lu Cao[1], Qunfeng Zhang[1]* and Yukun Li[2]*

[1]Department of Obstetrics and Gynecology, The Second Affiliated Hospital, Hengyang Medical School, University of South China, Hengyang, Hunan, China, [2]Department of Assisted Reproductive Centre, The affiliated Zhuzhou hospital Xiangya medical college, Central South University, Zhuzhou, Hunan, China

Malignant tumors are among the most important causes of death worldwide. The pathogenesis of a malignant tumor is complex and has not been fully elucidated. Studies have shown that such pathogenesis is related to abnormal cell cycle progression. The expression levels of cyclins, cyclin-dependent kinases (CDKs), and CDK inhibitors as well as functions of the cell cycle checkpoints determine whether the cell cycle progression is smooth. Cell-cycle-targeting drugs have the advantages of high specificity, low toxicity, low side effects, and low drug resistance. Identifying drugs that target the cell cycle and applying them in clinical treatments are expected to promote chemotherapeutic developments against malignant tumors. This article aims to review drugs targeted against the cell cycle and their action mechanisms.

KEYWORDS

malignant tumor, cell cycle, cell cycle checkpoint, cyclin, cyclin-dependent kinase, chemotherapeutic drug

1 Introduction

The cell cycle refers to a series of events within a cell that cause it to divide into two new daughter cells. The typical cell cycle is divided into four phases, namely, G1, S, G2, and M phases. The function of the G1 phase is to prepare for the S phase and synthesize large amounts of RNA and proteins. The S phase mainly involves DNA replication. Small amounts of RNA and proteins are synthesized in the G2 phase. Finally, the cells undergo karyokinesis and cytokinesis in the M phase. In the process of cell life, various factors (environmental factors, self-factors, etc.) can easily affect the integrity of the genetic material of the cell (Barnum and O'Connell, 2014; Li et al., 2022). Cells have developed a series of regulatory mechanisms to ensure continuous cell division and accurate replication of the cellular genetic material known as the cell cycle regulatory system.

The cell cycle consists of three important nodes that we refer to as the cell cycle checkpoints. The first is the G1/S checkpoint between the G1 and S phases and is also called as the restriction point. The second is the G2/M checkpoint located between the G2 and M phases and is also called as the DNA damage checkpoint. The third is the mitotic spindle assembly checkpoint (SAC) (Khan and Wang, 2022). The cell cycle can function properly only through these checkpoints (Poon, 2016), and the three most critical types of proteins involved in regulating the cell cycle are the cyclins, cyclin-dependent kinases (CDKs), and CDK inhibitor proteins (Khan and Wang, 2022). Cyclins bind to the CDKs to form

TABLE 1 Cell-cycle-targeting drugs and tumor types treated.

Classification of the drug	Action period	Name of drug	Ki/IC50	Chemical structure	Tumor type	Reference
ATM inhibitors	S phase	AZD0156	IC50 = 0.58 nM	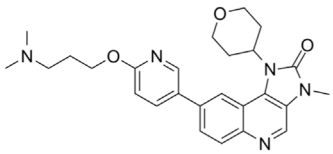	Advanced solid tumors	Imidazo 4,5-c quinolin-2-one compounds and their use in treating cancer (2019)
		AZD1390	IC50 = 0.78 nM	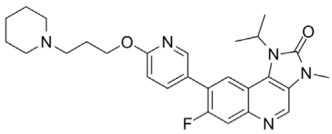	Brain tumors	Durant et al. (2018)
CDK2 inhibitors	S phase	Indisulam (E7070)	Wide range of IC50 values	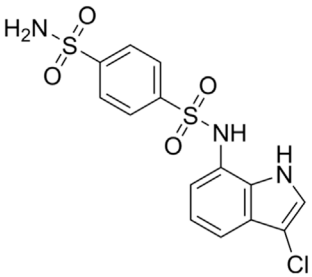	Lung cancer	Ozawa et al. (2001)
CDK4/6 inhibitors	G1 phase	Palbociclib	IC50 = 11 nM or 16 nM	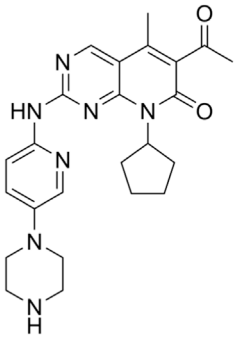	Breast cancer, lymphoma, etc.	Fry et al. (2004)
		Ribociclib	IC50 = 10 nM or 39 nM	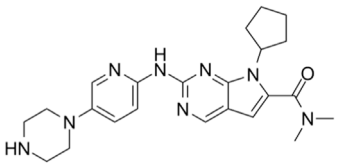	Breast cancer, liposarcoma, head and neck squamous cell carcinomas, melanoma, neuroblastoma, etc.	VanArsdale et al. (2015)
		Abemaciclib	IC50 = 2 nM or 10 nM	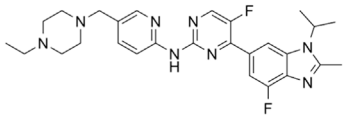	Breast cancer	Gelbert et al. (2014)
ATR inhibitors	S and G2 phases	M6620 (VX-970)	Ki = 0.2 nM	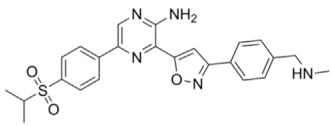	Brain metastases, solid tumors, esophageal cancer, ovarian cancer, primary peritoneal cancer, fallopian tube cancer, metastatic urothelial cancer, prostate cancer, metastatic gastric cancer, etc.	Fokas et al. (2012)

(Continued on following page)

TABLE 1 (*Continued*) Cell-cycle-targeting drugs and tumor types treated.

Classification of the drug	Action period	Name of drug	Ki/IC50	Chemical structure	Tumor type	Reference
		Ceralasertib (AZD6738)	IC50 = 1 nM	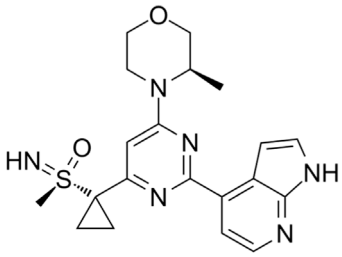	CLL, PLL, B-cell lymphoma, CML, MDS, NHL, head and neck squamous cell carcinoma, NSCLC, gastric cancer, TNBC, renal cell carcinoma, urothelial carcinoma, pancreatic cancer, SCLC, prostate cancer, melanoma advanced solid tumor, metastatic tumor, etc.	Vendetti et al. ()
		Elimusertib (BAY1895344)	IC50 = 7 nM	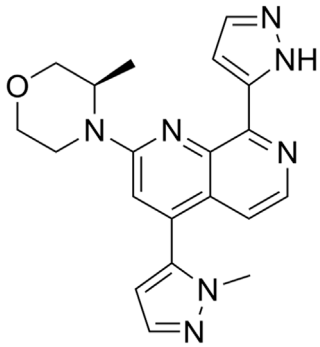	Advanced solid tumors, lymphoma, etc.	Ulrich et al. (2017)
		Gartisertib (VX-803)	IC50 = 8 nM	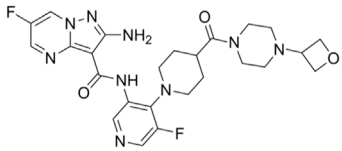	Advanced solid tumors	Zenke et al. (2019)
CHK1 inhibitors	S, G2, and M phases	SCH900776 (MK-8776)	IC50 = 3 nM	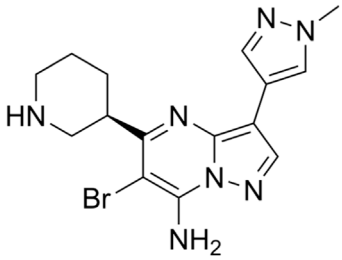	Acute leukemia, advanced solid tumors, etc.	Guzi et al. (2011)
		Prexasertib (LY2606368)	IC50 = 8 nM	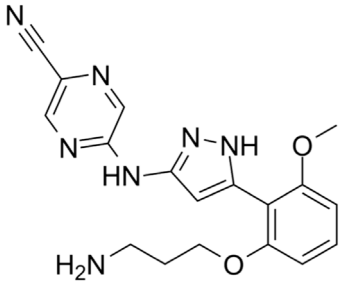	SCLC, platinum-resistant ovarian cancer, some solid tumors, breast cancer, prostate cancer, NSCSC, etc.	King et al. (2015)

(Continued on following page)

TABLE 1 (*Continued*) Cell-cycle-targeting drugs and tumor types treated.

Classification of the drug	Action period	Name of drug	Ki/IC50	Chemical structure	Tumor type	Reference
		CCT245737 (SRA737)	IC50 = 1.3 nM	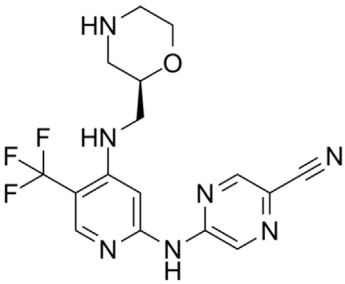	SCLC	Osborne et al. (2016)
Wee1 inhibitors	G2 phase	Adavosertib (AZD1775)	IC50 = 5.2 nM	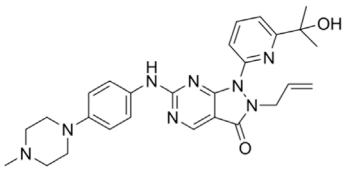	Ovarian cancer, SCLC, solid tumors, metastatic colorectal cancer, NSCLC, TNBC, acute myeloid leukemia, MDS, etc.	Bridges et al. (2011)
CDK1 inhibitors	G2/M phase	Ro-3306	Ki = 20 nM	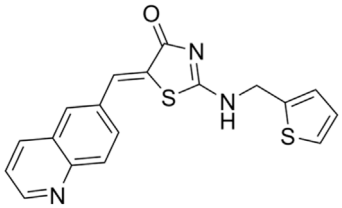	TNBC, ovarian cancer, etc.	Vassilev et al. (2006)
BUB1 kinase inhibitors	M phase	BAY 1816032	IC50 < 7 nM	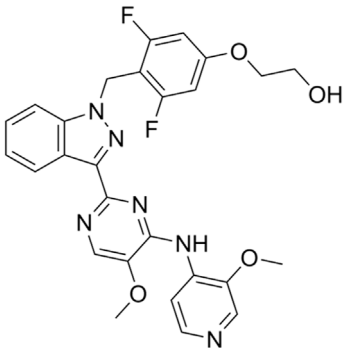	Cervical cancer, TNBC, NSCLC, glioblastoma, prostate cancer, osteosarcoma, etc.	Siemeister et al. (2017)
Inhibitors of tubulin synthesis	M phase	Indibulin	IC50 = 1 50 nM	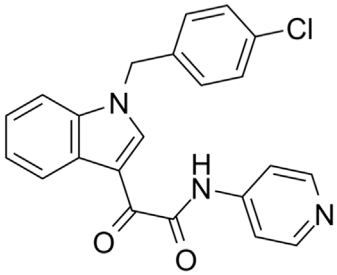	NSCLC, gastric cancer, breast cancer, head and neck cancer, etc.	Kapoor et al. (2018b)
CENP-E inhibitors	M phase	GSK923295	Ki = 3.2 ± 0.2 nM or 1.6 ± 0.1 nM	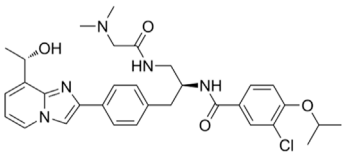	Solid tumors, hematological malignancies, etc.	Wood et al. (2010)

complexes that drive the cell cycle (Gao et al., 2020). Different complexes can act on different phases of the cell cycle. For example, the cyclinD–CDK4/6 and cyclinE–CDK2 complexes act on the G1 phase; the cyclinA–CDK2 complex acts on the S phase; the cyclinB–CDK1 complex acts on the G2 and M phases (Pan et al., 2023).

Malignant tumors are among the most important causes of death worldwide, and their incidence is increasing annually. In the 21st century, cancer is expected to become the leading cause of death in every country and imposes an enormous burden (Lin et al., 2021). The treatments for malignant tumors include surgery, radiotherapy, and chemotherapy; however, patients can relapse easily after treatment, and the mortality rate is high, which is a major problem for not only clinicians but also researchers. Studies have shown that the pathogenesis of a malignant tumor is related to abnormal cell cycle progression (Liu et al., 2022), and the search for targeted drugs acting on the cell cycle is expected to provide new avenues for the treatment of malignant tumors.

Herein, our main purpose is to explore the relationships between malignant tumors and cell cycle regulation as well as between the cell cycle and targeted drugs (Table 1); we also review these relationships to provide references and evidence for subsequent research on malignant tumors.

2 Differences between normal and malignant cells

In normal cells, the progression and termination of the cell cycle are determined by the cell cycle regulatory system (Khan and Wang, 2022). Once a given cell cycle ends, the commencement of the next cell cycle is dependent upon the needs of the body. Unlike normal cells, malignant tumor cells are relatively autonomous. Owing to the instability of the genome, regulated growth of the malignant tumor cells is disrupted, cell replication is dysregulated by the body, and cell apoptosis is hindered (Hanahan and Weinberg, 2011), which manifests as a cell cycle disorder. Studies have shown that cell cycle disorders in malignant tumors are associated with the cell cycle checkpoints. Malignant tumor cells can overcome the limitations of these checkpoints (Suski et al., 2021) by activating various signaling pathways and altering the expression levels of the intracellular proteins (Li et al., 2024; Zhang et al., 2024; Zhou et al., 2024), eventually leading to imbalances in cell cycle regulation.

3 Changes in the cyclin–CDK complexes during different cell cycle phases

3.1 G1 phase

The cell cycle ends when the last cell completes mitosis. Then, if the cell needs to undergo another round of mitosis, the new daughter cells will enter the G1 phase and start a new cell cycle. In the G1 phase, the cells synthesize proteins (such as the protein replication complex (pre-RC)), RNA, ribosomes, and other substances in preparation for DNA synthesis in the next phase (Bandura and Calvi, 2002). The cyclinD–CDK4/6 complex plays an important role in this phase; CDK4/6 binds to cyclinD to form a complex, which further activates CDK4/6 to continue the cell cycle. The cyclinD–CDK4/6 complex binds to members of the retinoblastoma (RB) protein family and phosphorylates them. The phosphorylated RB proteins stimulate downstream signaling pathways to release E2F transcription factors and activate the E2F-responsive genes. The E2F-mediated gene expression generates cyclinE, which interacts with CDK2 to form the cyclinE–CDK2 complex that phosphorylates RB, further activating the E2F genes and promoting the progression of the cell division cycle (Wang, 2022; Hamilton and Infante, 2016). The cyclinD–CDK4/6 and cyclinE–CDK2 complexes phosphorylate the RB proteins sequentially to release the restriction of the G1/S checkpoint (Liu et al., 2022); the cells then enter the S phase after passing the G1/S checkpoint.

3.2 S phase

In the S phase, the E2F-mediated gene expression stimulates the synthesis of a large number of proteins, and the generated cyclinA and CDK2 form the cyclinA–CDK2 complex (Hume et al., 2020). Moreover, the cyclinE–CDK2 and cyclinA–CDK2 complexes further activate CDK, eventually activating pre-RC and initiating DNA replication. The cells in the S phase complete DNA replication and then enter the G2 phase (Bandura and Calvi, 2002).

3.3 G2 phase

During the G2 phase, proteins and other substances are synthesized, and the cells grow in preparation for the next stage of mitosis (Wang, 2022). In the G2 phase, CDK1 interacts with cyclinA to form the cyclinA–CDK1 complex, which plays an irreplaceable role in the cell cycle (Santaguida and Nepveu, 2005). The cyclinA–CDK1 complex activates and stabilizes the cyclinB–CDK1 complex, steadily increasing the activity of the cyclinB–CDK1 complex and advancing the cell cycle to the next stage until mitosis is completed (Wang, 2022). The G2/M phase checkpoint is responsible for detecting DNA damage in the cells; DNA damage that occurs during DNA replication needs to be repaired before the cells enter the next stage to prevent errors in the genetic material (Khan and Wang, 2022).

3.4 M phase

The M phase is divided into mitotic and cytoplasmic divisions; here, mitosis is further divided into prophase, prometaphase, metaphase, anaphase, and telophase. Prophase is characterized by intracellular chromatin/chromosome aggregation, centrosome separation, and nuclear membrane rupture (Figure 1); once the chromosomes in the cell are condensed, the centrosomes separate and move toward the poles of the cell, following which the nuclear membrane ruptures. During the prometaphase, the spindle microtubules attach to the centromere of the chromosomal centromere. During metaphase, the centromere microtubules pull the chromosomes and align them along the equatorial plate to

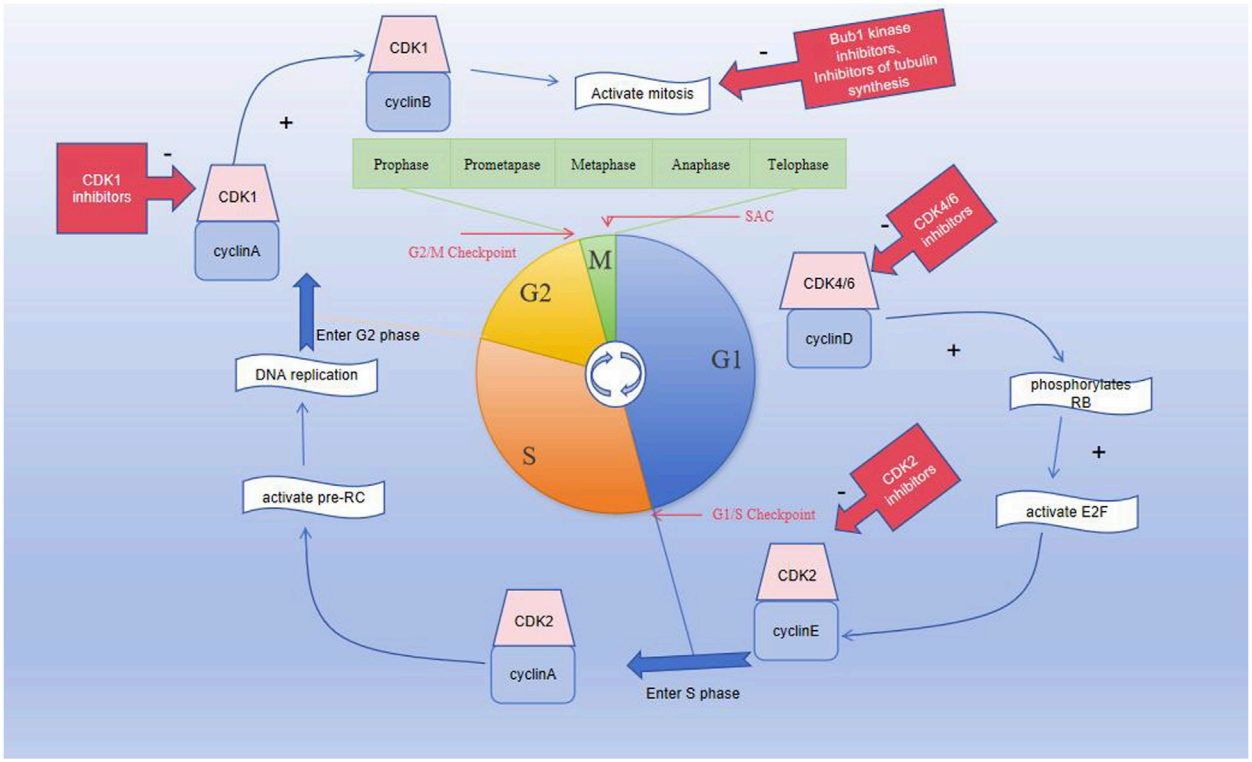

FIGURE 1
Graph showing the division of the cell cycle into G1, S, G2, and M phases; the M phase is further divided into prophase, prometaphase, metaphase, anaphase, and telophase. Three important checkpoints exist in the cell cycle, namely, the G1/S, G2/M, and spindle assembly checkpoints.

ensure accurate chromosomal separation. During this stage, SAC confirms that the chromosomes are in the proper positions along the equatorial plate, in addition to ensuring that the chromosomes are properly connected to the spindles (Poon, 2016) and that the microtubules are pulling in the correct direction. After passing the SAC, the cell cycle continues and enters the mitotic anaphase. During anaphase, the microtubules pull the chromatids toward each pole. During telophase, the chromosomes uncoil to become chromatin, and the nuclear membrane is formed again. Eventually, the cell membrane contracts inward, dividing the cytoplasm equally between the two cells and forming the two new daughter cells with identical genetic material (Wang, 2022). The cyclinB–CDK1 complex has an irreplaceable role in mitosis, and its activation is believed to trigger mitosis. The cyclinB–CDK1 complex is activated during prophase, degraded in the middle stage, and dephosphorylated in the late stage, until it drops below the threshold and the cell exits mitosis (Gavet and Pines, 2010).

4 DNA replication and damage repair during the cell cycle

Although DNA replication has high fidelity, the cells are affected by various damaging factors at all times, making DNA damage inevitable. The DNA-damaging factors can be divided into endogenous and exogenous factors. The endogenous factors include errors in base pairing during DNA replication, instability in the DNA structure, and reactive oxygen species produced by metabolism, among others. The exogenous factors can be roughly divided into biological, chemical, and physical factors. Biological factors mainly include viruses that can reverse transcribe directly to affect the DNA or its metabolites, damaging the integrity of the DNA. The common physical factors include electromagnetic radiation like X-rays, gamma rays, and ultraviolet rays. The chemical factors include free radicals, base analogs, and alkylating agents (Carusillo and Mussolino, 2020). DNA damage activates the DNA damage repair pathway in the body, and the intracellular checkpoint proteins are activated to provide the necessary time for DNA repair, following which the cell cycle continues. If the DNA damage exceeds the limit of repair, the cell will activate the apoptotic pathway and eventually undergo cell death. If the mutated DNA is not repaired and cell replication is not halted, the damaged genetic material will be passed on to the next generation of daughter cells, which will eventually develop into malignant cells. Cancer is believed to result from mutations in cellular DNA through mutations occurring in only a few genes (Basu, 2018).

During the replication of malignant cells, complete DNA replication depends on normal progression of the DNA replication forks. The arresting or deceleration of replication fork progression is called as replication stress, which is an important cause of instability of the genetic material in malignant tumor cells. Damaged DNA not only affects the progression of the DNA replication forks but also causes replication stress (da Costa et al., 2023). However, malignant tumor cells do not die easily from DNA

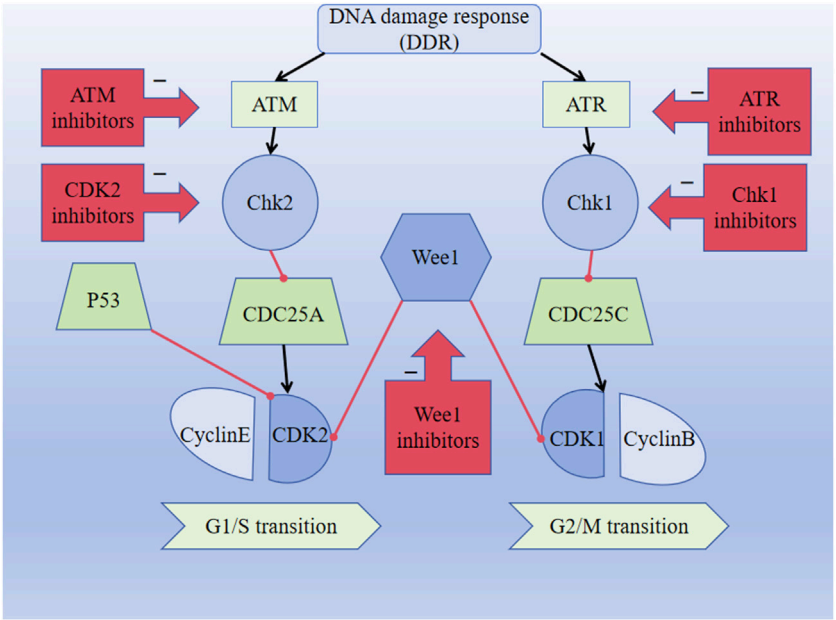

FIGURE 2
DNA damage response (DDR) pathway activates the ATM-CHK2-P53 signaling pathway and inhibits CDK2 expression, thereby affecting the G1/S transition. DDR pathway activates the ATR-CHK1-Wee1 signaling pathway and inhibits CDK1 expression, thus affecting the G2/M transition. The black lines indicate activation, and the red lines indicate inhibition.

damage because they have special damage repair mechanisms. Malignant tumor cells can repair damaged DNA replication forks through break-induced replication (BIR), thereby ensuring the integrity of the genetic material (Costantino et al., 2014). Understanding the specific DNA repair mechanisms of malignant tumors is thus helpful for identifying the causes of the difficulty with curing malignant tumors and chemotherapeutic resistance, providing new ideas for the development of targeted drugs in the future.

5 Cell cycle checkpoints and target drugs

5.1 G1/S checkpoint and target drugs

The G1/S checkpoint is an important cell cycle checkpoint that can detect DNA integrity. It prevents DNA damage from being replicated and determines whether the cells can easily enter the S phase. Ataxia telangiectasia mutation (ATM) is a type of DNA damage sensor, and the ATM-Chk2-p53 pathway is activated when DNA damage occurs. Activated ATM regulates the activities of CHK2 and P53, thereby affecting DNA repair and cell cycle progression. ATM phosphorylates CHK2, which then inhibits CDC25A dephosphorylation and ultimately inhibits CDK2, leading to cell cycle disruption (Figure 2). Research shows that ATM is lost in gastrointestinal, respiratory, and lymphatic malignancies, suggesting that the absence of ATM is associated with the development of malignant tumors (Smith et al., 2020). Moreover, studies have shown that the cyclinD–CDK4/6 complex is an important part of the cellular transition from G1 to S phases and that the expressions of the cyclinD–CDK4/6 complex change in various tumors, showing abnormal elevation (Hamilton and Infante, 2016; Chen et al., 2003). Blocking the signaling pathway downstream of cyclinD–CDK4/6 prevents RB protein phosphorylation, thereby preventing cells from entering the S phase and undergoing subsequent tumorigenesis (Hume et al., 2020). In conclusion, the ATM-Chk2-P53 pathway, CDK2, and CDK4/6 may constitute breakthroughs for which we can develop targeted drugs against the proteins; this is expected to improve the prognosis of patients with malignant tumors.

ATM inhibitors: Clinical trials of the ATM inhibitors, including M3541, AZD0156, and AZD1390, are underway. In phase I clinical trials, M3541 adjuvant radiotherapy has been used to treat solid tumors; AZD0156 combined with olaparib, irinotecan, fluorouracil, and folinic acid has been used to treat advanced solid tumors; AZD1390 combined with radiotherapy has been used to treat brain tumors (Smith et al., 2020).

CDK2 inhibitors: Indisulam (E7070) is a type of CDK2 inhibitor that inhibits the activation of cyclinE–CDK2 and the cell cycle, causing G1/S arrest. Ziva Pogacar et al. reported that indisulam combined with the CDK4/6 inhibitor palbociclib could cause senescence or death of lung cancer cells (Pogacar et al., 2022).

CDK4/6 inhibitors: At present, three CDK4/6 inhibitors are in clinical use or trials: abemaciclib (LY2835219), palbociclib (PD-0332991), and ribociclib (LEE011) (Hamilton and Infante, 2016). Palbociclib is currently used to treat perimenopausal or premenopausal patients with breast cancer and is relatively effective against hormone-receptor-positive (HR+) breast cancer cells. In patients with partial mantle cell lymphoma (MCL), palbociclib has been found to be clinically beneficial. Ribociclib can be used to treat tumors with abnormal activities of the

cyclinD–CDK complex and downstream pathways; some examples include neurological tumors, fat sarcomas, breast cancer, melanoma, and squamous cell carcinoma of the head and neck, with a certain safety profile. Abemaciclib can be used to treat postmenopausal women with breast cancer, with a clinical benefit rate of up to 72% for patients with HR+/HER2 breast cancers (Gao et al., 2020).

5.2 G2/M checkpoint and target agents

The G2/M checkpoint is responsible for monitoring DNA damage during cell cycle progression. The DNA damage response (DDR) is crucial for sustaining the integrity of the genetic material, and activation of the DDR pathway is closely coordinated with cell cycle arrest to prevent transmission of DNA damage to the next generation. Ataxia telangiectasia and Rad3 related (ATR) is a DNA damage sensor associated with phosphorylation and dephosphorylation that inactivates the CDKs, resulting in cessation of the cellular replication process. ATR is activated when the DNA is damaged by external or self-harmful factors. At this point, ATR fully activates the cell cycle checkpoint kinase 1 (CHK1) through serine phosphorylation. The overexpression of Wee1 has been observed in malignant tumor cells, including hepatic cell carcinomas, breast cancers, glioblastoma, respiratory tumors, and gastrointestinal tumors. The upregulation of the ATR-Chk1-Wee1 pathway in tumors may indicate poor prognosis, and the ATR-Chk1-Wee1 pathway is likely to be an attractive focus for the treatment of malignancies (Smith et al., 2020). Moreover, CHK1 inhibits the dephosphorylation functions of the CDC25 family of phosphatases and eventually inhibits CDK1, preventing cell entry into mitosis and thereby blocking the activity of the cyclinB–CDK1 complex (Figure 2) (Smith et al., 2010). Dysregulation of CDK1 expression is associated with the development of various malignant tumors and affects the survival probabilities of patients with different tumor types. Drugs targeting the ATR-Chk1-Wee1 pathway and CDK1 may thus be key strategies for the treatment of malignant tumors (Wang et al., 2023).

ATR inhibitors: Clinical trials of ATR inhibitors, including M6620 (VX-970), AZD6738, BAY1895344, and M4344 (VX-803), are underway. In phase I clinical trials, M6620 combined with radiotherapy was used to treat non-small cell lung carcinoma (NSCLC), small cell lung carcinoma (SCLC), and neural endocrine cancers that metastasized intracranially. M6620 combined with gemcitabine, cisplatin, carboplatin, paclitaxel, irinotecan, and other drugs have been used to treat late-stage solid tumors. M6620 combined with radiation and chemotherapy (cisplatin + capecitabine) has been used to treat esophageal cancer. AZD6738 monotherapy has been used for head and neck squamous cell carcinoma, chronic lymphocytic leukemia (CLL), prolymphocytic leukemia (PLL), B-cell lymphomas, chronic myeloid leukemia (CML), or myelodysplastic syndrome (MDS); AZD6738 combined with acalabrutinib has been prescribed for the treatment of non-Hodgkin lymphoma (NHL); AZD6738 combined with gemcitabine has been used in the treatment of late-stage solid tumors; AZD6738 with paclitaxel has been used to treat metastatic tumors for which standard chemotherapy has failed. BAY1895344 single therapy has been utilized for the treatment of late-stage solid tumors and lymphomas. M4344 (VX-803) is available as a standalone agent or is combination with cisplatin, carboplatin, and gemcitabine as a therapy for late-stage solid tumors. In phase I/II clinical trials, AZD6738 combined with carboplatin, olaparib, or durvalumab was used to treat NSCLC, breast cancer, squamous cell carcinoma of the head and neck, and gastrointestinal malignancies; AZD6738 was combined with acalcitoninib to treat refractory CLL. In phase II trials, M6620 combined with avelumab and carboplatin have been shown to treat primary peritoneal cancer and some malignant tumors of the female reproductive system, such as fallopian tube cancer and ovarian cancer; M6620 combined with cisplatin and gemcitabine has been used to treat metastatic urothelial carcinoma; M6620 combined with carboplatin/docetaxel has been used to treat prostate cancer; M6620 combined with gemcitabine has been used to treat recurrent ovarian cancer, primary peritoneal cancer, and fallopian tube cancer; M6620 combined with Irinotecan has been used to treat gastric or gastroesophageal junction cancers and metastatic gastric cancer. AZD6738 alone has been used to treat triple-negative mammary cancer (TNBC); AZD6738 combined with olaparib has been used in the treatment of nephrocellular carcinoma, urinary tract epithelial carcinoma, pancreatic carcinoma, recurrent ovarian carcinoma, SCLC, and carcinoma of the prostate, among others; AZD6738 and durvalumab combination has been used in the treatment of NSCLC, gastric cancer, and melanoma.

CHK1 inhibitors: At present, CHK1 inhibitors like MK-8776 (SCH900776) and LY2606368 (prexasertib) are used in clinical research. In phase I clinical trials, MK-8776 alone or in combination with cytarabine was used to treat acute leukemia; MK-8776 in combination with hydroxyurea was used to treat late-stage solid tumors. LY2606368 (prexasertib) alone or in combination with gemcitabine/pemetrexed or ralimetanib/olaparib/PD-L1 inhibitor was used to treat solid tumors; LY2606368 combined with cisplatin, cisplatin, cetuximab, or radiotherapy was used to treat head and neck cancers; LY2606368 and cytarabine has been used to treat myeloid leukemia. In phase I/II clinical trials, LY2606368 alone or in combination with gemcitabine was used to treat pancreatic cancer; LY2606368 combined with cisplatin or pemetrexed was used to treat NSCLC. MK-8776 as a single agent or in combination with cytarabine has been used to treat acute myeloid leukemia. In phase II clinical trials, LY2606368 monotherapy was used to treat SCLC, platinum-resistant ovarian cancer, some solid tumors, breast cancer, and prostate cancer; LY2606368 combined with pemetrexed has been used to treat NSCLC (Smith et al., 2020). SRA737 is an FDA-approved CHK1 inhibitor. Sen et al. (2019) reported that SRA737 and gemcitabine (LDG) could be combined to treat SCLC and other cancers (Sen et al., 2019).

Wee1 inhibitors: The Wee1 inhibitor AZD1775 (MK-1775) is currently in clinical trial. In phase I clinical trials, AZD1775 monotherapy has been used to treat ovarian cancer, SCLC, and solid tumors. AZD1775/paclitaxel and carboplatin/orapanitan/gemcitabine/cisplatin combinations have been used to treat solid tumors; AZD1775 combined with irinotecan has been used to treat metastatic colorectal cancer. In phase II clinical trials, AZD1775 monotherapy or in combination with carboplatin/taxol has been used to treat SCLC; AZD1775 and other combinations have

been used to treat NSCLC; AZD1775 combined with cisplatin has been used for the treatment of TNBC; the combination of AZD1775 and cytarabine has been used to treat advanced acute myeloid leukemia or MDS (Smith et al., 2020).

CDK1 inhibitors: Ro-3306 and CGP74514A are selective CDK1 inhibitors, and the elimination of CDK1 phosphorylation causes cell cycle arrest at the G2/M checkpoint (Ly et al., 2015). Chen et al. (2023) reported that RO-3306 could significantly reduce the multiplication, mobility, and invasiveness of TNBC while increasing the susceptibility of cancer cells to cisplatin and paclitaxel (Chen et al., 2023). Huang et al. (2023) investigated both an ovarian cancer cell line and a high-grade serous ovarian cancer in a genetically engineered mouse model and reported that CDK1 inhibition plays an antitumor role (Huang et al., 2023). Yang et al. (2021) reported that the combination of CGP74514A (CGP) and a broad-spectrum CDK inhibitor flavopiridol (pull pingdu) can synergistically inhibit acute myeloid leukemia cell proliferation and induce apoptosis (Yang et al., 2021).

5.3 SAC and target drugs

The SAC is an important mechanism for safeguarding mitotic fidelity to ensure the accuracy of karyotype numbers in meristematic cells. SAC impairment can cause destabilization of the chromosomes and also tumor development (Hosea et al., 2024). The major SAC components include *BUB1*, *BUBR1*, *MAD2*, *CENP-E*, and *CDC20*, among others. Mutations of the SAC components are associated with tumor progression, suggesting that the SAC components may be potential therapeutic targets for the treatment of malignant tumors (Bolanos-Garcia, 2009). BAY1816032 is a selective BUB1 kinase inhibitor, and Siemeister et al. (2019) reported that BAY1816032 can increase tumor cell sensitivity to paclitaxel, ATR inhibitors, and PARP inhibitors. In addition, the combination of BAY1816032 and paclitaxel has synergistic or additive antiproliferative effects during the treatment of malignancies, including cervical cancers, TNBC, NSCLC, prostate cancer, and intracranial malignant tumor cells (Siemeister et al., 2019). Huang et al. (2021) reported that BAY1816032 can significantly reduce the multiplication, aggressiveness, and migration of osteosarcoma cells and could be a novel therapeutic target for osteosarcoma (Huang et al., 2021). Indibulin is an inhibitor of tubulin synthesis that can activate the spindle assembly checkpoint proteins *MAD2* and *BUBR1* to halt the cell cycle. Kapoor et al. (2018a) observed that indibulin has favorable anticancer activity and less neural toxicity in both preclinical animal models and phase I clinical trials of carcinogenic chemistry; derivatives of indibulin have strong antiproliferative effects on different types of tumor cells, such as head and neck tumors, NSCLC, gastric cancer, and breast cancer (Kapoor et al., 2018a). Li et al. (2019) showed that the *CDC20-MAD2* complex could prevent apoptosis by preventing the early biodegradation of cyclin B1; M2I-1 is an MAD2 inhibitor that interferes with the interactions between *CDC20* and *MAD2*, thereby increasing the susceptibility of cancer cells to antiangiogenic drugs such as paclitaxel (Li et al., 2019). GSK923295 is a specific CENP-E inhibitor that causes chromosomal dislocation and interrupts mitotic progression (Qian et al., 2010). Chung et al. (2012) demonstrated that GSK923295 exhibits *in vitro* antitumor activity against several solid tumor cell lines and hematological malignant cell lines; it also exhibits *in vivo* antitumor activity against numerous solid tumor xenograft models, with very few grade 3 or 4 adverse reactions (Chung et al., 2012).

6 Traditional chemotherapeutic drugs

Chemotherapy is an important approach to treating malignant tumors. Based on the different mechanisms of operation, commonly used chemotherapy drugs can be classified into the categories listed below.

6.1 Drugs affecting DNA biosynthesis

Methotrexate: Methotrexate mainly affects the S phase of the cell cycle and DNA synthesis, thereby inhibiting the growth and proliferation of malignant tumor cells. Methotrexate is a dihydrofolate reductase inhibitor that prevents the conversion of dihydrofolate to tetrahydrofolate, ultimately reducing the synthesis of deoxythymidine acid and leading to impaired DNA synthesis (Olsen, 1991). Methotrexate is commonly used to treat acute leukemia and choriocarcinoma, and the common adverse reactions are myelosuppression, liver damage, and kidney damage, among others.

Fluorouracil: Fluorouracil mainly acts on the S phase of the cell cycle and can affect DNA synthesis in malignant tumor cells to inhibit the growth of malignant tumors. Fluorouracil is converted to fluorouracil deoxynucleotides in the cells, thereby inhibiting deoxythymidylate synthase and preventing the conversion of deoxyuridine acid to deoxythymidylate to interfere with DNA synthesis. Fluorouracil is mainly used to treat malignant tumors of the digestive system (such as colorectal cancer), breast cancer, and head and neck cancers. The common adverse reactions of this drug are bone marrow suppression and gastrointestinal damage (Longley et al., 2003).

Cytarabine: Cytarabine mainly targets the S phase of the cell cycle, affecting DNA synthesis and interfering with DNA replication to kill the malignant tumor cells. Cytarabine is a DNA polymerase inhibitor; after it enters the body, it produces metabolites such as cytarabine triphosphate, resulting in abnormal functions of DNA polymerase and interfering with DNA synthesis and replication to inhibit the proliferation of malignant tumor cells (Faruqi and Tadi, 2023). Cytarabine is commonly used to treat acute leukemia, and its common adverse reactions are myelosuppression and gastrointestinal reactions (Baker et al., 1991).

6.2 Drugs affecting DNA structure and functions

Cyclophosphamide: Cyclophosphamide is a cell cycle non-specific drug that acts by disrupting the structure of the cellular DNA. After cyclophosphamide enters the body, it produces phosphoramide nitrogen mustard, which can undergo alkylation reactions with the DNA in cells, cause DNA breakage, and destroy

the normal structure and functions of DNA. Cyclophosphamide is commonly used to treat multiple myeloma, leukemia, and solid tumors. The common adverse reactions of this drug are bone marrow suppression, nausea, and vomiting (Emadi et al., 2009).

Platinum-based drugs: Cisplatin is a cell cycle non-specific drug. After entering the body, cisplatin binds to the double strand of the DNA and forms intrastrand/interstrand crosslinks, which can prevent DNA replication or break the DNA strand. Cisplatin is commonly used to treat testicular cancer and ovarian cancer. The common adverse reactions of these drugs include gastrointestinal reactions, bone marrow suppression, and otonephrotoxicity (Dasari and Tchounwou, 2014).

6.3 Drugs affecting RNA and protein syntheses

Adriamycin: Adriamycin acts on cells in all phases of the cell cycle, but cells in the S phase are more sensitive to it. Adriamycin is an anthracycline antibiotic that can bind tightly to DNA, affecting not only DNA replication but also RNA transcription and synthesis. Adriamycin is commonly used to treat acute leukemia, breast cancer, and ovarian cancer. Its common adverse reactions are cardiotoxicity, bone marrow suppression, and gastrointestinal reactions (Tsukagoshi, 1988).

Vincristine: Vincristine mainly targets the M phase of the cell cycle and affects cell cycle progression by altering spindle filament formation. When vincristine binds to tubulin, it inhibits microtubule polymerization, blocks the generation of spindle filaments, and eventually leads to cell cycle arrest. Vincristine is commonly used to treat acute leukemia and lymphoma. Its common adverse reactions are neurotoxicity, bone marrow suppression, and gastrointestinal reactions.

Taxanes: Paclitaxel mainly acts on the M phase of the cell cycle and can affect the normal functions of the spindles. When paclitaxel enters the cell, it promotes tubulin polymerization and inhibits its depolymerization, thus causing a loss of function of the spindle and ultimately blocking cell mitosis to inhibit tumor cell growth. Paclitaxel is commonly used to treat ovarian and breast cancers. Its common adverse reactions are myelosuppression, neurotoxicity, and anaphylaxis (Alqahtani et al., 2019).

6.4 Other drugs

Minichromosome maintenance (MCM) complex inhibitors have also been developed. The MCM complex is closely linked to DNA duplication, and its dysfunction can lead to the development of malignant tumors. The inhibition of MCM or its downstream signaling pathway is expected to be a therapeutic target for treating malignant tumors (Li et al., 2021; Cao et al., 2020; Tang et al., 2023; Zeng et al., 2021).

7 Cell-cycle-targeting drugs reduce chemotherapeutic resistance

With the development of medicine and pharmacology, various chemotherapeutic drugs have been developed and applied clinically, but drug resistance or even multidrug resistance (MDR) can occur in patients during chemotherapy, whose mechanisms are not fully clear. At present, the possible resistance mechanisms listed below are considered.

7.1 Mutations in cell cycle regulatory genes

Mutations in the cell cycle regulatory genes may lead to cell cycle disorders, which potentially affect the efficacies of chemotherapeutic drugs and lead to drug resistance. For example, P53 is a protein that regulates the cell cycle and plays an important role in various malignant tumors. Frequent P53 mutations can eliminate the inhibitory effects on tumor cells and increase the DNA repair functions of malignant tumor cells such that the killing effects of chemotherapeutic drugs on DNA are reduced, leading to chemotherapeutic drug resistance (Alvarado-Ortiz et al., 2021).

7.2 Abnormal expressions of cyclins or altered functions of cell cycle checkpoints

The efficacy of a chemotherapeutic drug is closely related to the cell cycle of the malignant tumor cells, and interfering with the cell cycle affects the efficacy of the drug. The progression of the cell cycle is related to the expression levels of cyclins and functions of the cell cycle checkpoints. Malignant tumor cells can interfere with cellular processes by regulating the expressions of cyclins or altering the functions of the cell cycle checkpoints, thereby affecting the efficacies of the chemotherapeutic drugs and leading to resistance. For example, cyclinD expression affects the sensitivity of multiple myeloma cells to chemotherapeutic agents (Bustany et al., 2016). The overexpression of cyclinA is significantly associated with resistance to first-line platinum-based chemotherapy in ovarian cancer cells (Cybulski et al., 2015). The activities of cell cycle checkpoint kinases and functions of these checkpoints are altered in lung cancer cells, thereby interfering with cell cycle progression and leading to chemotherapeutic resistance (Ke et al., 2021).

7.3 Activation of antiapoptotic mechanisms

In the occurrence and development of malignant tumors, loss of control of the apoptotic signals and even activation of the antiapoptotic mechanisms can occur in tumor cells, which lead to failure of chemotherapy drugs that induce apoptosis (Mohammad et al., 2015). For example, mutations in the CHEK2 gene activate the P53 apoptotic pathway and induce apoptosis in TNMC cells, leading to chemotherapeutic resistance (Luo et al., 2018).

Cell-cycle-targeting drugs have advantages over traditional chemotherapeutic drugs. In particular, targeted drugs can act on target organs with high specificity and have fewer toxic side effects, which can improve the survival rates of patients (Lee et al., 2018). In contrast to traditional chemotherapy drugs, cell-cycle-targeting drugs have certain advantages in overcoming MDR. On the one hand, given the precise actions of cell-cycle-targeting drugs, the genes of the tumor cells do not readily mutate, thereby reducing the occurrence of drug resistance. On the other hand, cell-cycle-

targeting drugs act on cell cycle checkpoints and related pathways, do not directly damage the DNA of the malignant tumor cells, reduce the repair of DNA damage by tumor cells, and reduce the occurrence of chemotherapeutic resistance (Wu et al., 2014). Studies have shown that combination therapy not only reduces the toxic side effects of chemotherapeutic drugs on normal cells but also minimizes drug resistance (Mokhtari et al., 2017; Yue et al., 2021). Moreover, eradicating malignant tumor cells as much as possible and shrinking the tumor can reduce the occurrence of drug resistance (Chatterjee and Bivona, 2019). For example, in the treatment of SCLC, the combination of Wee1 inhibitors can ensure efficacy while reducing the side effects of chemotherapy (Meijer et al., 2022). In NSCLC, the use of a Wee1 inhibitor can increase the sensitivity of the tumor cells to sorafenib (Caiola et al., 2018). Ma et al. (2017) reported that the combination of the CDK4/6 inhibitor palbociclib and anastrozole can inhibit the proliferation of tumor cells and reduce drug resistance in patients with ER+/HER2- breast cancers (Ma et al., 2017).

8 Conclusions and perspectives

In this review, we summarize the pathological changes to the cell cycle in malignant tumors and the mechanisms of cell-cycle-targeting drugs. The action mechanisms of malignant tumors are very complex and are have not been fully elucidated thus far; these mechanisms are usually characterized by cell proliferation and are not subject to regulation or cell cycle disorders. Studies have shown that cell cycle progression, cell-cycle-related protein (cyclin, CDK, and CDK inhibitor) expressions, and activation of relevant proteins indicate that malignant tumors are potential therapeutic targets. In recent years, major advancements have been achieved in research on cell-cycle-targeting drugs, and some drugs such as the CDK4/6 inhibitors have been licensed for the clinical treatment of malignant tumors. Moreover, the combination of cell-cycle-targeting drugs and traditional chemotherapeutic drugs can significantly increase the therapeutic effects. However, methods to ensure the efficacy and safety of the drugs and resistance to subsequent treatment are still major problems that must be solved.

Therefore, future research efforts need to be focused on elucidating the pathogenesis of malignant tumors and developing cell-cycle-targeting drugs to formulate novel treatment options with increased scientific and clinical value while providing new hope for the treatment of malignant tumors in the future.

Author contributions

GS: writing–original draft and writing–review and editing. JL: writing–original draft and writing–review and editing. XT: writing–review and editing. JZ (4th author): writing–review and editing. YZ: writing–review and editing. XZ: writing–review and editing. JbZ: writing–review and editing. JZ (8th author): writing–review and editing. LC: writing–review and editing. QZ: writing–review and editing. YL: writing–review and editing.

Funding

The authors declare that no financial support was received for the research, authorship, and/or publication of this article.

Conflict of interest

The authors declare that the research was conducted in the absence of any commercial or financial relationships that could be construed as a potential conflict of interest.

Publisher's note

All claims expressed in this article are solely those of the authors and do not necessarily represent those of their affiliated organizations or those of the publisher, editors, and reviewers. Any product that may be evaluated in this article or claim that may be made by its manufacturer is not guaranteed or endorsed by the publisher.

References

Alqahtani, F. Y., Aleanizy, F. S., El Tahir, E., Alkahtani, H. M., and AlQuadeib, B. T. (2019). Paclitaxel. *Relat. Methodol.* 44, 205–238. doi:10.1016/bs.podrm.2018.11.001

Alvarado-Ortiz, E., de la Cruz-López, K. G., Becerril-Rico, J., Sarabia-Sánchez, M. A., Ortiz-Sánchez, E., and García-Carrancá, A. (2021). Mutant p53 gain-of-function: role in cancer development, progression, and therapeutic approaches. *Front. Cell Dev. Biol.* 8, 607670. Published 2021 Feb 11. doi:10.3389/fcell.2020.607670

Baker, W. J., Royer, G. L., Jr, and Weiss, R. B. (1991). Cytarabine and neurologic toxicity. *J. Clin. Oncol.* 9 (4), 679–693. doi:10.1200/JCO.1991.9.4.679

Bandura, J. L., and Calvi, B. R. (2002). Duplication of the genome in normal and cancer cell cycles. *Cancer Biol. Ther.* 1 (1), 8–13. doi:10.4161/cbt.1.1.31

Barnum, K. J., and O'Connell, M. J. (2014). Cell cycle regulation by checkpoints. *Methods Mol. Biol.* 1170, 29–40. doi:10.1007/978-1-4939-0888-2_2

Basu, A. K. (2018). DNA damage, mutagenesis and cancer. *Int. J. Mol. Sci.* 19 (4), 970. Published 2018 Mar 23. doi:10.3390/ijms19040970

Bolanos-Garcia, V. M. (2009). Assessment of the mitotic spindle assembly checkpoint (SAC) as the target of anticancer therapies. *Curr. Cancer Drug Targets* 9 (2), 131–141. doi:10.2174/156800909787580980

Bridges, K. A., Hirai, H., Buser, C. A., Brooks, C., Liu, H., Buchholz, T. A., et al. (2011). MK-1775, a novel Wee1 kinase inhibitor, radiosensitizes p53-defective human tumor cells. *Clin. Cancer Res.* 17 (17), 5638–5648. Epub 2011 Jul 28. doi:10.1158/1078-0432.CCR-11-0650

Bustany, S., Bourgeais, J., Tchakarska, G., Body, S., Hérault, O., Gouilleux, F., et al. (2016). Cyclin D1 unbalances the redox status controlling cell adhesion, migration, and drug resistance in myeloma cells. *Oncotarget* 7 (29), 45214–45224. doi:10.18632/oncotarget.9901

Caiola, E., Frapolli, R., Tomanelli, M., Valerio, R., Iezzi, A., Garassino, M. C., et al. (2018). Wee1 inhibitor MK1775 sensitizes KRAS mutated NSCLC cells to sorafenib. *Sci. Rep.* 8 (1), 948. Published 2018 Jan 17. doi:10.1038/s41598-017-18900-y

Cao, T., Yi, S. J., Wang, L. X., Zhao, J. X., Xiao, J., Xie, N., et al. (2020). Identification of the DNA replication regulator MCM complex expression and prognostic significance in hepatic carcinoma. *Biomed. Res. Int.* 2020, 3574261. Published 2020 Sep 9. doi:10.1155/2020/3574261

Carusillo, A., and Mussolino, C. (2020). DNA damage: from threat to treatment. *Cells* 9 (7), 1665. Published 2020 Jul 10. doi:10.3390/cells9071665

Chatterjee, N., and Bivona, T. G. (2019). Polytherapy and targeted cancer drug resistance. *Trends Cancer* 5 (3), 170–182. doi:10.1016/j.trecan.2019.02.003

Chen, J., Li, M., Liu, Y., Guan, T., Yang, X., Wen, Y., et al. (2023). PIN1 and CDK1 cooperatively govern pVHL stability and suppressive functions. *Cell Death Differ.* 30 (4), 1082–1095. doi:10.1038/s41418-023-01128-x

Chen, Q., Lin, J., Jinno, S., and Okayama, H. (2003). Overexpression of Cdk6-cyclin D3 highly sensitizes cells to physical and chemical transformation. *Oncogene* 22 (7), 992–1001. doi:10.1038/sj.onc.1206193

Chung, V., Heath, E. I., Schelman, W. R., Johnson, B. M., Kirby, L. C., Lynch, K. M., et al. (2012). First-time-in-human study of GSK923295, a novel antimitotic inhibitor of centromere-associated protein E (CENP-E), in patients with refractory cancer. *Cancer Chemother. Pharmacol.* 69 (3), 733–741. doi:10.1007/s00280-011-1756-z

Costantino, L., Sotiriou, S. K., Rantala, J. K., Magin, S., Mladenov, E., Helleday, T., et al. (2014). Break-induced replication repair of damaged forks induces genomic duplications in human cells. *Science* 343 (6166), 88–91. doi:10.1126/science.1243211

Cybulski, M., Jarosz, B., Nowakowski, A., Jeleniewicz, W., Kutarska, E., Bednarek, W., et al. (2015). Cyclin A correlates with YB1, progression and resistance to chemotherapy in human epithelial ovarian cancer. *Anticancer Res.* 35 (3), 1715–1721.

da Costa, AABA, Chowdhury, D., Shapiro, G. I., D'Andrea, A. D., and Konstantinopoulos, P. A. (2023). Targeting replication stress in cancer therapy. *Nat. Rev. Drug Discov.* 22 (1), 38–58. doi:10.1038/s41573-022-00558-5

Dasari, S., and Tchounwou, P. B. (2014). Cisplatin in cancer therapy: molecular mechanisms of action. *Eur. J. Pharmacol.* 740, 364–378. doi:10.1016/j.ejphar.2014.07.025

Durant, S. T., Zheng, L., Wang, Y., Chen, K., Zhang, L., Zhang, T., et al. (2018). The brain-penetrant clinical ATM inhibitor AZD1390 radiosensitizes and improves survival of preclinical brain tumor models. *Sci. Adv.* 4 (6), eaat1719. doi:10.1126/sciadv.aat1719

Emadi, A., Jones, R. J., and Brodsky, R. A. (2009). Cyclophosphamide and cancer: golden anniversary. *Nat. Rev. Clin. Oncol.* 6 (11), 638–647. doi:10.1038/nrclinonc.2009.146

Faruqi, A., and Tadi, P. (2023). "Cytarabine," in *StatPearls. Treasure island (FL)* (Treasure Island (FL): StatPearls Publishing).

Fokas, E., Prevo, R., Pollard, J. R., Reaper, P. M., Charlton, P. A., Cornelissen, B., et al. (2012). Targeting ATR *in vivo* using the novel inhibitor VE-822 results in selective sensitization of pancreatic tumors to radiation. *Cell Death Dis.* 3, e441. doi:10.1038/cddis.2012.181

Fry, D. W., Harvey, P. J., Keller, P. R., Elliott, W. L., Meade, M., Trachet, E., et al. (2004). Specific inhibition of cyclin-dependent kinase 4/6 by PD 0332991 and associated antitumor activity in human tumor xenografts. *Mol. Cancer Ther.* 3 (11), 1427–1438. doi:10.1158/1535-7163.1427.3.11

Gao, X., Leone, G. W., and Wang, H. (2020). Cyclin D-CDK4/6 functions in cancer. *Adv. Cancer Res.* 148, 147–169. doi:10.1016/bs.acr.2020.02.002

Gavet, O., and Pines, J. (2010). Progressive activation of CyclinB1-Cdk1 coordinates entry to mitosis. *Dev. Cell* 18 (4), 533–543. doi:10.1016/j.devcel.2010.02.013

Gelbert, L. M., Cai, S., Lin, X., Sanchez-Martinez, C., Del Prado, M., Lallena, M. J., et al. (2014). Preclinical characterization of the CDK4/6 inhibitor LY2835219: *in-vivo* cell cycle-dependent/independent anti-tumor activities alone/in combination with gemcitabine. *Invest New Drugs* 32 (5), 825–837. doi:10.1007/s10637-014-0120-7

Guzi, T. J., Paruch, K., Dwyer, M. P., Labroli, M., Shanahan, F., Davis, N., et al. (2011). Targeting the replication checkpoint using SCH 900776, a potent and functionally selective CHK1 inhibitor identified via high content screening. *Mol. Cancer Ther.* 10 (4), 591–602. doi:10.1158/1535-7163.MCT-10-0928

Hamilton, E., and Infante, J. R. (2016). Targeting CDK4/6 in patients with cancer. *Cancer Treat. Rev.* 45, 129–138. doi:10.1016/j.ctrv.2016.03.002

Hanahan, D., and Weinberg, R. A. (2011). Hallmarks of cancer: the next generation. *Cell* 144 (5), 646–674. doi:10.1016/j.cell.2011.02.013

Hosea, R., Duan, W., Meliala, I. T. S., Li, W., Wei, M., Hillary, S., et al. (2024). YY2/BUB3 Axis promotes SAC hyperactivation and inhibits colorectal cancer progression via regulating chromosomal instability. *Adv. Sci. (Weinh)* 11, e2308690. Published online April 29. doi:10.1002/advs.202308690

Huang, Y., Fan, Y., Zhao, Z., Zhang, X., Tucker, K., Staley, A., et al. (2023). Inhibition of CDK1 by RO-3306 exhibits anti-tumorigenic effects in ovarian cancer cells and a transgenic mouse model of ovarian cancer. *Int. J. Mol. Sci.* 24 (15), 12375. Published 2023 Aug 3. doi:10.3390/ijms241512375

Huang, Z., Wang, S., Wei, H., Chen, H., Shen, R., Lin, R., et al. (2021). Inhibition of BUB1 suppresses tumorigenesis of osteosarcoma via blocking of PI3K/Akt and ERK pathways. *J. Cell Mol. Med.* 25 (17), 8442–8453. doi:10.1111/jcmm.16805

Hume, S., Dianov, G. L., and Ramadan, K. (2020). A unified model for the G1/S cell cycle transition. *Nucleic Acids Res.* 48 (22), 12483–12501. doi:10.1093/nar/gkaa1002

Imidazo 4,5-c quinolin-2-one compounds and their use in treating cancer. (2019). US-10189834-B2. Issued 2019.

Kapoor, S., Srivastava, S., and Panda, D. (2018a). Indibulin dampens microtubule dynamics and produces synergistic antiproliferative effect with vinblastine in MCF-7 cells: implications in cancer chemotherapy. *Sci. Rep.* 8 (1), 12363. Published 2018 Aug 17. doi:10.1038/s41598-018-30376-y

Kapoor, S., Srivastava, S., and Panda, D. (2018b). Indibulin dampens microtubule dynamics and produces synergistic antiproliferative effect with vinblastine in MCF-7 cells: implications in cancer chemotherapy. *Sci. Rep.* 8 (1), 12363. doi:10.1038/s41598-018-30376-y

Ke, Z., Liang, A., and Liu, Y. (2021). *Zhongguo Fei Ai Za Zhi* 24 (4), 265–270. doi:10.3779/j.issn.1009-3419.2021.101.09

Khan, M. G. M., and Wang, Y. (2022). Cell cycle-related clinical applications. *Methods Mol. Biol.* 2579, 35–46. doi:10.1007/978-1-0716-2736-5_3

King, C., Diaz, H. B., McNeely, S., Barnard, D., Dempsey, J., Blosser, W., et al. (2015). LY2606368 causes replication catastrophe and antitumor effects through CHK1-dependent mechanisms. *Mol. Cancer Ther.* 14 (9), 2004–2013. doi:10.1158/1535-7163.MCT-14-1037

Lee, Y. T., Tan, Y. J., and Oon, C. E. (2018). Molecular targeted therapy: treating cancer with specificity. *Eur. J. Pharmacol.* 834, 188–196. doi:10.1016/j.ejphar.2018.07.034

Li, J., Dang, N., Martinez-Lopez, N., Jowsey, P. A., Huang, D., Lightowlers, R. N., et al. (2019). M2I-1 disrupts the *in vivo* interaction between CDC20 and MAD2 and increases the sensitivities of cancer cell lines to anti-mitotic drugs via MCL-1s. *Cell Div.* 14, 5. Published 2019 Jun 15. doi:10.1186/s13008-019-0049-5

Li, S., Wang, L., Wang, Y., Zhang, C., Hong, Z., and Han, Z. (2022). The synthetic lethality of targeting cell cycle checkpoints and PARPs in cancer treatment. *J. Hematol. Oncol.* 15 (1), 147. doi:10.1186/s13045-022-01360-x

Li, Y., Zou, J., Zhang, Q., Quan, F., Cao, L., Zhang, X., et al. (2021). Systemic analysis of the DNA replication regulator MCM complex in ovarian cancer and its prognostic value. *Front. Oncol.* 11, 681261. Published 2021 Jun 9. doi:10.3389/fonc.2021.681261

Li, Y. K., Gao, A. B., Zeng, T., Liu, D., Zhang, Q. F., Ran, X. M., et al. (2024). ANGPTL4 accelerates ovarian serous cystadenocarcinoma carcinogenesis and angiogenesis in the tumor microenvironment by activating the JAK2/STAT3 pathway and interacting with ESM1. *J. Transl. Med.* 22 (1), 46. doi:10.1186/s12967-023-04819-8

Lin, L., Li, Z., Yan, L., Liu, Y., Yang, H., and Li, H. (2021). Global, regional, and national cancer incidence and death for 29 cancer groups in 2019 and trends analysis of the global cancer burden, 1990-2019. *J. Hematol. Oncol.* 14 (1), 197. doi:10.1186/s13045-021-01213-z

Liu, J., Peng, Y., and Wei, W. (2022). Cell cycle on the crossroad of tumorigenesis and cancer therapy. *Trends Cell Biol.* 32 (1), 30–44. doi:10.1016/j.tcb.2021.07.001

Longley, D. B., Harkin, D. P., and Johnston, P. G. (2003). 5-fluorouracil: mechanisms of action and clinical strategies. *Nat. Rev. Cancer* 3 (5), 330–338. doi:10.1038/nrc1074

Luo, L., Gao, W., Wang, J., Wang, D., Peng, X., Jia, Z., et al. (2018). Study on the mechanism of cell cycle checkpoint kinase 2 (CHEK2) gene dysfunction in chemotherapeutic drug resistance of triple negative breast cancer cells. *Med. Sci. Monit.* 24, 3176–3183. Published 2018 May 15. doi:10.12659/MSM.907256

Ly, T., Endo, A., and Lamond, A. I. (2015). Proteomic analysis of the response to cell cycle arrests in human myeloid leukemia cells. *Elife* 4, e04534. Published 2015 Jan 2. doi:10.7554/eLife.04534

Ma, C. X., Gao, F., Luo, J., Northfelt, D. W., Goetz, M., Forero, A., et al. (2017). NeoPalAna: neoadjuvant palbociclib, a cyclin-dependent kinase 4/6 inhibitor, and anastrozole for clinical stage 2 or 3 estrogen receptor-positive breast cancer. *Clin. Cancer Res.* 23 (15), 4055–4065. doi:10.1158/1078-0432.CCR-16-3206

Meijer, J. J., Leonetti, A., Airò, G., Tiseo, M., Rolfo, C., Giovannetti, E., et al. (2022). Small cell lung cancer: novel treatments beyond immunotherapy. *Semin. Cancer Biol.* 86 (Pt 2), 376–385. doi:10.1016/j.semcancer.2022.05.004

Mohammad, R. M., Muqbil, I., Lowe, L., Yedjou, C., Hsu, H. Y., Lin, L. T., et al. (2015). Broad targeting of resistance to apoptosis in cancer. *Semin. Cancer Biol.* 35 (Suppl. l(0), S78-S103–S103. doi:10.1016/j.semcancer.2015.03.001

Mokhtari, R. B., Homayouni, T. S., Baluch, N., Morgatskaya, E., Kumar, S., Das, B., et al. (2017). Combination therapy in combating cancer. *Oncotarget* 8 (23), 38022–38043. doi:10.18632/oncotarget.16723

Olsen, E. A. (1991). The pharmacology of methotrexate. *J. Am. Acad. Dermatol* 25 (2 Pt 1), 306–318. doi:10.1016/0190-9622(91)70199-c

Osborne, J. D., Matthews, T. P., McHardy, T., Proisy, N., Cheung, K. M. J., Lainchbury, M., et al. (2016). Multiparameter lead optimization to give an oral checkpoint kinase 1 (CHK1) inhibitor clinical candidate: (R)-5-((4-((Morpholin-2-ylmethyl)amino)-5-(trifluoromethyl)pyridin-2-yl)amino)pyrazine-2-carbonitrile (CCT245737). *J. Med. Chem.* 59 (11), 5221–5237. doi:10.1021/acs.jmedchem.5b01938

Ozawa, Y., Sugi, N. H., Nagasu, T., Owa, T., Watanabe, T., Koyanagi, N., et al. (2001). E7070, a novel sulphonamide agent with potent antitumour activity *in vitro* and *in vivo*. *Eur. J. Cancer* 37 (17), 2275–2282. doi:10.1016/s0959-8049(01)00275-1

Pan, J., Shang, F., Ma, R., Rong, Y., and Zhang, Y. (2023). *Sheng Wu Gong Cheng Xue Bao* 39 (4), 1525–1547. doi:10.13345/j.cjb.220478

Pogacar, Z., Johnson, J. L., Krenning, L., De Conti, G., Jochems, F., Lieftink, C., et al. (2022). Indisulam synergizes with palbociclib to induce senescence through inhibition of CDK2 kinase activity. *PLoS One* 17 (9), e0273182. Published 2022 Sep 6. doi:10.1371/journal.pone.0273182

Poon, R. Y. (2016). Cell cycle control: a system of interlinking oscillators. *Methods Mol. Biol.* 1342, 3–19. doi:10.1007/978-1-4939-2957-3_1

Qian, X., McDonald, A., Zhou, H. J., Adams, N. D., Parrish, C. A., Duffy, K. J., et al. (2010). Discovery of the first potent and selective inhibitor of centromere-associated

protein E: GSK923295. *ACS Med. Chem. Lett.* 1 (1), 30–34. Published 2010 Jan 19. doi:10.1021/ml900018m

Santaguida, M., and Nepveu, A. (2005). Differential regulation of CDP/Cux p110 by cyclin A/Cdk2 and cyclin A/Cdk1. *J. Biol. Chem.* 280 (38), 32712–32721. doi:10.1074/jbc.M505417200

Sen, T., Della Corte, C. M., Milutinovic, S., Cardnell, R. J., Diao, L., Ramkumar, K., et al. (2019). Combination treatment of the oral CHK1 inhibitor, SRA737, and low-dose gemcitabine enhances the effect of programmed death ligand 1 blockade by modulating the immune microenvironment in SCLC. *J. Thorac. Oncol.* 14 (12), 2152–2163. doi:10.1016/j.jtho.2019.08.009

Siemeister, G., Mengel, A., Bone, W., Schröder, J., Zitzmann-Kolbe, S., Briem, H., et al. (2017). Abstract 287: BAY 1816032, a novel BUB1 kinase inhibitor with potent antitumor activity. *Cancer Res.* 77 (13 Suppl. l), 287. doi:10.1158/1538-7445.AM2017-287

Siemeister, G., Mengel, A., Fernández-Montalván, A. E., Bone, W., Schröder, J., Zitzmann-Kolbe, S., et al. (2019). Inhibition of BUB1 kinase by BAY 1816032 sensitizes tumor cells toward taxanes, ATR, and PARP inhibitors *in vitro* and *in vivo*. *Clin. Cancer Res.* 25 (4), 1404–1414. doi:10.1158/1078-0432.CCR-18-0628

Smith, H. L., Southgate, H., Tweddle, D. A., and Curtin, N. J. (2020). DNA damage checkpoint kinases in cancer. *Expert Rev. Mol. Med.* 22, e2. Published 2020 Jun 8. doi:10.1017/erm.2020.3

Smith, J., Tho, L. M., Xu, N., and Gillespie, D. A. (2010). The ATM-Chk2 and ATR-Chk1 pathways in DNA damage signaling and cancer. *Adv. Cancer Res.* 108, 73–112. doi:10.1016/B978-0-12-380888-2.00003-0

Suski, J. M., Braun, M., Strmiska, V., and Sicinski, P. (2021). Targeting cell-cycle machinery in cancer. *Cancer Cell* 39 (6), 759–778. doi:10.1016/j.ccell.2021.03.010

Tang, M., Chen, J., Zeng, T., Ye, D. M., Li, Y. K., Zou, J., et al. (2023). Systemic analysis of the DNA replication regulator origin recognition complex in lung adenocarcinomas identifies prognostic and expression significance. *Cancer Med.* 12 (4), 5035–5054. doi:10.1002/cam4.5238

Tsukagoshi, S. (1988). Gan to kagaku ryoho. *Gan To Kagaku Ryoho.* 15 (9), 2819–2827.

Ulrich, T. L., Lefranc, J., Wengner, A., Wortmann, L., Schick, H., Briem, H., et al. (2017). Abstract 983: identification of potent, highly selective and orally available ATR inhibitor BAY 1895344 with favorable PK properties and promising efficacy in monotherapy and combination in preclinical tumor models. *Cancer Res.* 77 (Issue 13 Suppl. ment), 983. doi:10.1158/1538-7445.am2017-983

VanArsdale, T., Boshoff, C., Arndt, K. T., and Abraham, R. T. (2015). Molecular pathways: targeting the cyclin D-CDK4/6 Axis for cancer treatment. *Clin. Cancer Res.* 21 (13), 2905–2910. doi:10.1158/1078-0432.CCR-14-0816

Vassilev, L. T., Tovar, C., Chen, S., Knezevic, D., Zhao, X., Sun, H., et al. (2006). Selective small-molecule inhibitor reveals critical mitotic functions of human CDK1. *Proc. Natl. Acad. Sci. U. S. A.* 103 (28), 10660–10665. doi:10.1073/pnas.0600447103

Vendetti, F. P., Lau, A., Schamus, S., Conrads, T. P., O'Connor, M. J., and Bakkenist, C. J. The orally active and bioavailable ATR kinase inhibitor AZD6738 potentiates the anti-tumor effects of CDDP to resolve ATM-deficient non-small cell lung cancer *in vivo*.

Wang, Q., Bode, A. M., and Zhang, T. (2023). Targeting CDK1 in cancer: mechanisms and implications. *NPJ Precis. Oncol.* 7 (1), 58. Published 2023 Jun 13. doi:10.1038/s41698-023-00407-7

Wang, Z. (2022). Cell cycle progression and synchronization: an overview. *Methods Mol. Biol.* 2579, 3–23. doi:10.1007/978-1-0716-2736-5_1

Wood, K. W., Lad, L., Luo, L., Qian, X., Knight, S. D., Nevins, N., et al. (2010). Antitumor activity of an allosteric inhibitor of centromere-associated protein-E. *Proc. Natl. Acad. Sci. U. S. A.* 107 (13), 5839–5844. doi:10.1073/pnas.0915068107

Wu, Q., Yang, Z., Nie, Y., Shi, Y., and Fan, D. (2014). Multi-drug resistance in cancer chemotherapeutics: mechanisms and lab approaches. *Cancer Lett.* 347 (2), 159–166. doi:10.1016/j.canlet.2014.03.013

Yang, Y., Dai, Y., Yang, X., Wu, S., and Wang, Y. (2021). DNMT3A mutation-induced CDK1 overexpression promotes leukemogenesis by modulating the interaction between EZH2 and DNMT3A. *Biomolecules* 11 (6), 781. Published 2021 May 22. doi:10.3390/biom11060781

Yue, S., Li, Y., Chen, X., Wang, J., Li, M., Chen, Y., et al. (2021). FGFR-TKI resistance in cancer: current status and perspectives. *J. Hematol. Oncol.* 14 (1), 23. Published 2021 Feb 10. doi:10.1186/s13045-021-01040-2

Zeng, T., Guan, Y., Li, Y. K., Wu, Q., Tang, X. J., Zeng, X., et al. (2021). The DNA replication regulator MCM6: an emerging cancer biomarker and target. *Clin. Chim. Acta* 517, 92–98. doi:10.1016/j.cca.2021.02.005

Zenke, F. T., Zimmermann, A., Dahmen, H., Elenbaas, B., and Blaukat, A. (2019). "Antitumor activity of M4344, a potent and selective ATR inhibitor, in monotherapy and combination therapy," in *Proceedings: AACR Annual Meeting 2019; March 29–April 3, 2019* (Atlanta, GA). doi:10.1158/1538-7445.AM2019-369

Zhang, J., Ouyang, F., Gao, A., Zeng, T., Li, M., Li, H., et al. (2024). ESM1 enhances fatty acid synthesis and vascular mimicry in ovarian cancer by utilizing the PKM2-dependent warburg effect within the hypoxic tumor microenvironment. *Mol. Cancer* 23 (1), 94. doi:10.1186/s12943-024-02009-8

Zhou, W., Zeng, T., Chen, J., Tang, X., Yuan, Y., Hu, D., et al. (2024). Aberrant angiogenic signaling pathways: accomplices in ovarian cancer progression and treatment. *Cell Signal* 120, 111240. doi:10.1016/j.cellsig.2024.111240

frontiers | Frontiers in Pharmacology

TYPE Review
PUBLISHED 24 October 2024
DOI 10.3389/fphar.2024.1442227

Check for updates

OPEN ACCESS

EDITED BY
Hailin Tang,
Sun Yat-sen University Cancer Center (SYSUCC), China

REVIEWED BY
Xiumei Wang,
Inner Mongolia Cancer Hospital & Affiliated People's Hospital of Inner Mongolia Medical University, China
Zhongyu Han,
Chengdu University of Traditional Chinese Medicine, China
Hai Huang,
Shanghai Jiao Tong University, China

*CORRESPONDENCE
Mingqing Zhang,
zmq2568@126.com

RECEIVED 01 June 2024
ACCEPTED 14 October 2024
PUBLISHED 24 October 2024

CITATION
Wang S, Bai Y, Ma J, Qiao L and Zhang M (2024) Long non-coding RNAs: regulators of autophagy and potential biomarkers in therapy resistance and urological cancers.
Front. Pharmacol. 15:1442227.
doi: 10.3389/fphar.2024.1442227

COPYRIGHT
© 2024 Wang, Bai, Ma, Qiao and Zhang. This is an open-access article distributed under the terms of the Creative Commons Attribution License (CC BY). The use, distribution or reproduction in other forums is permitted, provided the original author(s) and the copyright owner(s) are credited and that the original publication in this journal is cited, in accordance with accepted academic practice. No use, distribution or reproduction is permitted which does not comply with these terms.

Long non-coding RNAs: regulators of autophagy and potential biomarkers in therapy resistance and urological cancers

Shizong Wang[1,2], Yang Bai[1,2], Jie Ma[1,2], Liang Qiao[1,2] and Mingqing Zhang[1,2]*

[1]Department of Urology, Weifang People's Hospital, Weifang, Shandong, China, [2]Shangdong Provincial Key Laboratory for Prevention and Treatment of Urological Diseases in Medicine and Health, Weifang, Shandong, China

The non-coding RNAs (ncRNAs) comprise a large part of human genome that mainly do not code for proteins. Although ncRNAs were first believed to be non-functional, the more investigations highlighted tthe possibility of ncRNAs in controlling vital biological processes. The length of long non-coding RNAs (lncRNAs) exceeds 200 nucleotidesand can be present in nucleus and cytoplasm. LncRNAs do not translate to proteins and they have been implicated in the regulation of tumorigenesis. On the other hand, One way cells die is by a process called autophagy, which breaks down proteins and other components in the cytoplasm., while the aberrant activation of autophagy allegedly involved in the pathogenesis of diseases. The autophagy exerts anti-cancer activity in pre-cancerous lesions, while it has oncogenic function in advanced stages of cancers. The current overview focuses on the connection between lncRNAs and autophagy in urological cancers is discussed. Notably, one possible role for lncRNAs is as diagnostic and prognostic variablesin urological cancers. The proliferation, metastasis, apoptosis and therapy response in prostate, bladder and renal cancers are regulated by lncRNAs. The changes in autophagy levels can also influence the apoptosis, proliferation and therapy response in urological tumors. Since lncRNAs have modulatory functions, they can affect autophagy mechanism to determine progression of urological cancers.

KEYWORDS

prostate cancer, non-coding RNAs, autophagy and apoptosis, bladder cancer, renal cancer, biomarkers, therapy resistance

Highlights

- LncRNAs are considered as diagnostic, prognostic and therapeutic targets in urological cancers.
- Autophagy is programmed cell death pathway exerting dual function in cancer progresion.
- LncRNAs can change proliferation, metastasis and therapy response in urological cancers.
- The lncRNA-driven regulation of autophagy determines the progression of urological cancers.
- Both lncRNAs and autophagy possess dual function in urological cancers, making it difficult to target them in cancer therapy.

1 Introduction

Considering that cancer is an illness that is responsible for a high rate of death and morbidity rate all over the world, researchers have focused their attention over the past few decades on elucidating the function that signaling networks play in the illness. It is well accepted that abnormalities in molecular pathways are the cause of aberrant proliferation and spread of cancer cells (Mohan et al., 2018; Ang et al., 2021). These tumor-promoting molecular pathways, in point of fact, are responsible for the advancement of cancer by activating favorable variables that contribute to cancer survival. Mechanisms that inhibit tumor growth, in contrast, make cancer cells more susceptible to death and stop them from progressing and migrating. Molecular pathways of this kind have been discovered as a result of advancements in sequencing and bioinformatics, and ongoing research has led to the discovery of more new signaling networks that may have an impact on the development or reduction of cancer. The significance of elucidating such molecular pathways is critical because it opens the way for the creation of innovative therapies that are capable of effectively treating cancer. These treatments may be based on the development of genetic tools for the purpose of targeting molecular pathways or about the application of tiny molecules as medications for the purpose of inhibiting the advancement of cancer. In addition, natural compounds produced from plants have shown that they have the ability to target molecular pathways for chemotherapy for cancer. Cancer continues to be a significant obstacle for public health, and there should be an increase in the amount of research committed to gaining a fundamental and clinical knowledge of cancer (Mirzaei et al., 2022a; Paskeh et al., 2022; Wang Y. et al., 2024). It has been considered the gold standard for treating cancer in humans. t to understand the biological foundations of disease and to build plausible molecular therapeutics. Gene therapy is an essential means to attain a possible cure, and it is also one of the most significant ways to get this understanding (Wu Y. et al., 2023). Long noncoding RNAs, often known as LncRNAs, are RNAs that have a transcription length of greater than 200 nucleotides yet cannot code for proteins (Xiao et al., 2018). It is estimated what makes up about 20% of the human genome are genes that code for proteins. Furthermore, eighty percent of the human genome is translated into RNA; however, It is not possible for these RNA transcripts to code for proteins and are thus considered noncoding (Huang et al., 2018; Chen H. et al., 2024). Some elements of the biology of long noncoding RNA (LncRNA) are comparable to that of messenger RNA (mRNA), and RNA polymerase II (Pol II) is able to transcribe most long non-coding RNAs, despite the fact that LncRNA do not encode proteins (Bridges et al., 2021). Even though the amounts of long noncoding RNAs (LncRNAs) are typically lower than those of messenger RNAs (mRNAs), Their expression patterns are more unique to individual tissues. This provides more evidence that long non-coding RNAs (LncRNAs) are still involved in a wide variety of biological processes, such as transcriptional regulation, protein folding, RNA editing, gene modification, and microRNA (miRNA) regulation. (Guo et al., 2020; Si et al., 2021). It is commonly understood that a number of different long noncoding RNAs play a part in controlling cancer's energy metabolism (Tan et al., 2021). including LUCAT1 (Xing et al., 2021), DUXAP10 (Lin et al., 2021), GAS5 (Ma Y. et al., 2022), TTN-AS1 (Zheng et al., 2021), and others. Moreover, Whether lncRNAs are located in the nucleus or the cytoplasm determines their function. (Ashrafizadeh et al., 2022; Mirzaei et al., 2022b).

LncRNAs have the ability to interact with their targets in either a direct or indirect manner, and they may also act as a scaffold, guide, signal, or decoy to affect proteins, in addition to chromatin and other RNA molecules for the effects (Entezari et al., 2022; Gibb et al., 2011; Moran et al., 2012). LncRNAs have the ability to influence expression of genes simultaneously with those involved in post-transcriptional modifications in the nucleus and the cytoplasm. It should be noted that the role of long non-coding RNAs varies depending on whether they are located in the nucleus or the cytoplasm. Interacting with messenger RNAs (mRNAs), lncRNAs that are found in the cytoplasm are responsible for regulating gene expression at both the translational and post-transcriptional stages. In addition, long noncoding RNAs have the ability to interact with microRNAs by performing the function of competitive endogenous RNAs (ceRNAs) and lowering the production of miRNAs. On the other hand, long noncoding RNAs that are found in the nucleus have a distinct function and are able to associate with proteins and transcription factors; participate in DNA methylation; modify histones; remodel chromatin (Lu et al., 2021; Tang et al., 2023).

2 LncRNAs in oncology

Within the system that governs epigenetic regulation, lncRNAs play an essential function (Alharthi et al., 2024). By having an effect on the structure of chromatin (Xiang et al., 2014; Postepska-Igielska et al., 2015; Wang et al., 2011), the modification of histones (Sati et al., 2012; Grote et al., 2013), alternative transcription (Gonzalez et al., 2015), the suppression of X-chromosomes (Froberg et al., 2013), and the reimbursement of dosage (Samata and Akhtar, 2018). In addition to their ability to influence expression of genes during transcription, epigenetic modifications, and the post-transcriptional phase, lncRNAs have been linked to a wide range of cellular functions and molecular signaling cascades (Liz and Esteller, 2016; Jiang et al., 2021). Despite the fact that they are unable to produce translation proteins, lncRNAs are nevertheless able to make a contribution to affect transcription by manipulating transcription factors, enhancers, and initiators (Engreitz et al., 2016; Kim et al., 2010; Li W. et al., 2016). Furthermore, long noncoding RNAs have the ability to affect post-transcriptional changes in a manner that helps to preserve messenger RNAs and serves as a precursor for small noncoding RNAs (Jalali et al., 2012; Song et al., 2018; Yang et al., 2014). Alternatively, lncRNA) can be seen as contending for endogenous RNAs (ceRNAs), which compete with sponge microRNAs such that downstream gene targets can be addressed (Sen et al., 2014; Liang et al., 2015; Han et al., 2020; Thomson and Dinger, 2016; Jarlstad, 2021; Hussain et al., 2023; Xie et al., 2023). Several long non-coding RNAs have been associated with alterations that are associated with cancer. These lncRNAs also perform crucial activities in regulatory genes, which cause them to influence a variety of elements of the cellular homeostasis, which encompasses development, propagation, migration, and genetic integrity (Huarte, 2015). Evidence suggests that certain LncRNAs play a part in the stemness of tumors by controlling the establishment of transcription variables associated to malignant stem cells (Chen

et al., 2017; Liu B. et al., 2021). For example, the long noncoding RNA CCAT2, This represents an overexpressed gene in CRC, has the ability to activate the Wnt signaling cascade and regulate c-Myc transcription to improve tumor invasion and spread. (Ling et al., 2013). Given that c-Myc is responsible for the post-transcriptional activity, the long noncoding RNA known as CCAT1 has the potential to accelerate the progression of gastric cancer (GC) (Yang et al., 2013; Alharbi et al., 2022).

A large number of lncRNAs have recently been linked to cancer initiation and progression. It is possible for them to function act as either tumor suppressors or oncogenes (Martens-Uzunova et al., 2014). Many different forms of cancer have been linked to a large number of lncRNAs., including malignancies of the breast, ovary, pancreas, prostate, and other organs. TUG1, NEAT1,HOTAIR, and CCAT1are examples of lncRNAs that might potentially cause cancer. On the other hand, DANCR, GAS5, MALAT1, and UCA1 are examples of lncRNAs that could potentially inhibit cancer. These long noncoding RNAs have an effect on critical pathways that are related with the growth and spread of cancer, as well as EMT and MDR (Bhan et al., 2017; Braga et al., 2020; Arriaga-Canon et al., 2023; Adnane et al., 2022; Connerty et al., 2020). In addition, Prolonged noncoding RNAs (lncRNAs) have been demonstrated to play a role in significant regulatory actions inside the cell and have been connected to a variety of diseases, not the least of which is cancer. The medicinal relevance of long noncoding RNAs (lncRNAs) for use as diagnostic, therapeutic, and prognostic biological markers is now being researched. Additionally, lncRNA-based diagnostics and therapies are currently being developed in order to enhance personal healthcare and standard of living (Zhang and Tang, 2018; Bhat et al., 2023; Naderi-Meshkin et al., 2019; Hanly et al., 2018). Recent research has shown that long noncoding RNAs (lncRNAs) also play an important part in the molecular response of tumors (MRD) (Figure 4) (Majidinia and Yousefi, 2016). In light of these findings, it is possible that they might be utilized as target therapeutics in the battle against cancer.

The deregulation and functional involvement of lncRNAs in cancer provide novel opportunities for expanding the existing diagnostic and therapeutic toolbox for this complex disease (Begolli et al., 2019). Regarding diagnosis, the discovery of circulating oncogenic lncRNAs in tumor-derived exosomes, coupled with their specific spatiotemporal activation, currently holds great promise for the development of highly specific diagnostic markers (Xu et al., 2018; Kim et al., 2015). Exosomes are a group of extracellular vesicles that arise when intermediate endosomal compartments, known as multivesicular bodies (MVBs), fuse with the plasma membrane to release their contents (Edgar, 2016; Harding et al., 1983). Exosomes function as vehicles of cell-to-cell communication and have been implicated in various diseases, including cancer (Edgar, 2016; Milane et al., 2015). These vesicles, ranging from 30 to 100 nm in size, contain a wide assortment of molecular cargos such as proteins, lipids, and nucleic acids, including miRNAs, mRNAs, and lncRNAs (Shurtleff et al., 2017; Kogure et al., 2013). Several lncRNAs that epigenetically regulate cancer cells through various mechanisms are also part of the exosomal cargo secreted from tumors. Examples of lncRNAs that interact with the epigenetic machinery and have been detected in exosomes include MEG3 and HOTAIR, which are secreted specifically from cervical tumors but not from their normal counterparts, offering opportunities for developing RNA-centric diagnostic approaches (Zhang J. et al., 2016). Other examples of lncRNAs secreted from tumor exosomes include LUCAT1 and PVT1 in exosomes of liver cancer (Gramantieri et al., 2018; Yu et al., 2016). In contrast, secreted exosomes from normal intestines carry significantly higher levels of HOTTIP than their colon cancer counterparts, providing novel opportunities for monitoring disease onset (Oehme et al., 2019). Interestingly, exosomal packaging appears to increase the stability (and therefore detection threshold) of NEAT1 and certain other lncRNAs compared with their intracellular levels (Gezer et al., 2014). Evidence suggests that lncRNAs, apart from being secreted, can also exert significant control over the production of exosomes in cancer. For instance, lncRNA-APC1, which is downregulated in colorectal carcinoma cells (CRCs) due to mutations in its master regulator APC, is a tumor-suppressor transcript that inhibits angiogenesis, proliferation, and migration of cancer cells. With exosomes playing a vital role in the induction of angiogenesis in CRCs, it has been shown that lncRNA-APC1 exerts its function by decreasing the stability of Rab5b mRNA, an important regulator of the exosome production process, ultimately reducing overall exosome production (Wang FW. et al., 2019). Figure 1 demonstrates the potential of lncRNAs in the regulation of carcinogenesis.

3 Urological cancers: An overview

3.1 Prostate cancer

There are around 180,000 new instances of prostate cancer diagnosed on an annual basis in the USA, which is equivalent to approximately over 20% of newly diagnosed cancer cases (Siegel et al., 2018; Howard et al., 2019). Among male-specific malignancies, prostate cancer ranks high. Biological processes of drug resistance eventually limit therapies for metastatic sickness, notwithstanding the efficacy of prostatectomy or radiation therapy for early stage localized prostate cancer. This is the case even if these treatments are often effective. Orgasmic suppression treatment (ADT), upon which the androgen receptor pathway is focused, is the primary treatment dealing with men who have progressed to advanced stages of prostate cancer (Kirby et al., 2011; Huggins and Hodges, 1941). Being an illness, prostate cancer is the reason behind this. that is driven by androgens. Despite the fact that ADT is initially beneficial (Siegel et al., 2018; Ferlay et al., 2013), the vast majority of patients eventually develop resistance to the treatment, CRPC, which stands for castration-resistant prostate cancer, and androgen-independent prostate cancer. Crbazitaxel, sipuleucel-T, docetaxel, enzalutamide, radium-223, and abiraterone are some of the treatment choices that are available for metastatic CRPC for patients who have undergone ADT before. In addition, studies, including the one that we conducted, have shown that early combination treatment with ADT and docetaxel or ADT plus Abiraterone is beneficial to survival for some patients who had metastatic cancer (Sweeney et al., 2015; James et al., 2016; Fizazi et al., 2017; James et al., 2017). Despite the availability of all treatment options, metastatic CRPC continues to be incurable, and eventually medication resistance will emerge (Amaral et al., 2012; Chandrasekar et al., 2015).

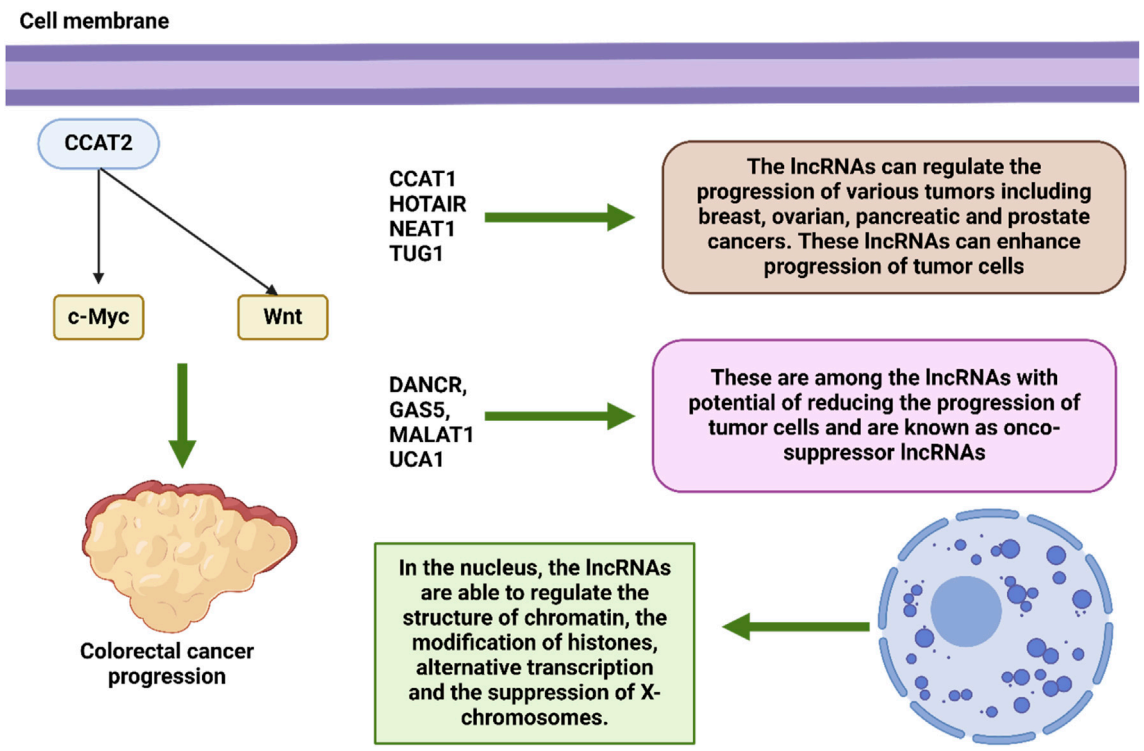

FIGURE 1
The mechanism of action of lncRNAs in the regulation of tumorigenesis.

Upregulation downstream of AR, alterations to AR splice variants and co-regulatory proteins, alterations to AR gene amplifications and mutations, and changes to the expression of AR steroid-generating enzymes are some of the processes that have been investigated as potential contributors to challenges in targeting the androgen receptor axis (Nakazawa et al., 2017).

Using morphologic criteria, the Gleason total score (Gleason, International Cancer Control Union) is used to describe the pathologic categorization of prostate cancer (Logothetis et al., 2013). This score is based on characteristics of the prostate. Regarding prostate cancer, it is the single most important indicator of prognosis. and the Gleason score is the primary way for classifying the tissue of prostate cancer (Gleason, 1966; Gleason and Mellinger, 1974). It is possible that intensive therapies are required if the Gleason score is high since it indicates that the development will be more fast. The Gleason score, on the other hand, does not offer any information on the choice of therapy. As a consequence of this, patients are presently classified in accordance with their current treatment state or clinical stage (for example, in the presence or absence of bone metastases, androgen ablation therapy resistance; chemotherapy efficacy). Through the use of this framework, patients that have similar prognoses are categorized (Ryan et al., 2006; McKenney et al., 2011; Ou et al., 2024). Therefore, the design of clinical trials is now determined by these parameters. This technique, on the other hand, lacks the molecular basis necessary to direct the proper molecularly targeted medication sequences or combinations. In addition, the current prostate cancer progression model does not take into consideration the finding that the state of cancer advancement is the determining factor in the efficacy of a particular medicine of choice. For instance, androgen ablation, chemotherapy-free, is more effective when administered at an earlier stage in the evolution of prostate cancer (Gravis et al., 2013). There is a paradoxical relationship between the latter phases of prostate cancer growth and the effectiveness of treatment (Efstathiou et al., 2010; Efstathiou and Logothetis, 2010; Millikan et al., 2008). The fact that the response to therapies varies depending on the stage of the disease suggests that prostate cancer goes through a progression that creates multiple states as the disease progresses. Additionally, the progression of prostate cancer is site-specific. which means that the prostate and bone are two favored locations of cancer that is either persistent or recurrent. Despite the fact that lymph nodes can potentially get affected by prostate cancer, these metastases are often not resistant to treatment. Based on these data, it appears that prostate cancer has a distinct association with the particular microenvironment that exists inside the prostate and bone (Loberg et al., 2005; Logothetis and Lin, 2005). Although every one of these characteristics is important from a therapeutic standpoint, they do not serve as a point of reference for choosing a therapy.

3.2 Bladder cancer

It is estimated that the number of newly diagnosed cases of bladder cancer in 2018 reached 549,393, making it the biggest cause of death throughout the globe (Mirzaei et al., 2022c; Bray et al., 2018). There are two subtypes of bladder cancer, which are referred

to as non-muscle invasive bladder cancer (NMIBC) and muscle-invasive balder cancer (MIBC). Both of these subtypes have different molecular patterns. It is still a cause of mortality, despite the fact that there have been advancements in the field of biology and medicine for the treatment and diagnosis of breast cancer. In an effort to enhance the prognosis and overall survival rate of patients with breast cancer, there have been efforts made to create clinical treatments. The advancements that have been made in the field of bioinformatics and large-scale gene expression have led to the introduction of molecular profiles as a basis for diagnosing breast cancer (Tran et al., 2021; Sim et al., 2019; Deng et al., 2024). There is a significant amount of application of surgery, chemotherapy, radiation, and immunotherapy for patients with breast cancer; yet, these patients continue to have a poor prognosis, and their overall survival rate over a period of 5 years is low (Parizi et al., 2020; Ashrafizadeh et al., 2020). Regarding the origin, the majority of BC originates from the urothelial layer, and this particular kind of BC is prevalent in the United States and Europe. On the other hand, BC in its non-epithelial variant is prevalent in other parts of the world due to the presence of persistent schistosomiasis (Rhea et al., 2021). Both nuclear anaplasia and architectural changes are taken into consideration when determining the BC grade (Epstein et al., 1998). The fact that individuals with NMIBC who are having therapy may have a return of the disease is something that should be mentioned since it demonstrates the significance of follow-up and subsequent medications. When compared to Migrant-inducible B-cells, of which the invasion and metastatic rates are quite high, which results in a high mortality rate among patients, recurrence is a growing concern among women whose breast cancer has not spread to the muscle (NMIBC) (Wang Y. et al., 2020). The high prevalence of gene mutations that are associated with breast cancer is one of the most intriguing aspects of this kind of cancer. This rate is equivalent to that of other types of cancer, such as lung and skin cancers, and have found that the gene encodes the enzyme TERT, which is involved in telomerase reverse transcription. is the most prevalent mutation that is identified in individuals with breast cancer (up to 70–80 percent) (Lawrence et al., 2013; Alexandrov et al., 2013; Rachakonda et al., 2013; Leão et al., 2019; Kurtis et al., 2016; Allory et al., 2014). The identification of molecular components that contribute to the initiation of breast cancer is thus of interest. Recent investigations have concentrated on identifying the elements that are responsible for the development of breast cancer and the therapeutic targeting of those factors. In addition, various molecular routes that are downregulated in breast cancer, and increasing the expression of these pathways is essential for the efficient elimination of cancer (Du et al., 2022; Wu et al., 2020; Shen et al., 2020; Liu et al., 2020; Li Y. et al., 2020).

3.3 Renal cancer

It is the 10th most prevalent cancer in the world (Grange et al., 2019; Petejova and Martinek, 2016) and the third most common urogenital malignancy (Williamson et al., 2019; Taneja and Williamson, 2018). Renal cell carcinoma (RCC) is responsible for around three percent of all adult cancers. The colorectal cancer (RCC) is one of the malignancies that is growing at the quickest rate, and it is anticipated that this trend will continue over the next 20 years (Znaor et al., 2015). Males have a greater risk of developing RCC. The majority of renal cell carcinomas are clear-cell varieties. accounting for up to 80 percent of all new instances of RCC. This is despite the fact that there are other histological subtypes of RCC that have been discovered. Histologically speaking, clear-cell rheumatoid carcinoma is distinguished through the existence of cancer cells with cytoplasm that is visible to the naked eye. This is because of cholesterol esters, phospholipids, glycogen, and a cell membrane's accumulation that is well defined (Rini et al., 2009). Papillary carcinoma, chromophobe reticulocellular carcinoma, and collecting-duct carcinoma are the additional subtypes. The best prognosis is for chromophobe renal cell carcinoma., is fairly uncommon (Patard et al., 2005), but papillary RCC, which accounts for fifteen percent of all cases of RCC, is the most common kind of cancer in kidney transplant patients.

It is known that a large number of genetic mutations have a role in the development and course of RCC, and the discovery of these mutations would help to improved diagnostics and prognoses (Schmidt and Linehan, 2016). One of the most important aspects of the process of developing new particular anti-cancer therapy techniques is this. The inactivation of the tumor suppressor von Hippel-Lindau (VHL) which can be caused by mutations, loss of heterozygosity, or promoter hypermethylation is the most frequent genetic aberration and was the first to be documented (Kim et al., 2018). Additionally, A multi-protein complex known as the E3 ubiquitin ligase includes the VHL protein. that is responsible for regulating the breakdown of proteins by proteasomes (Maxwell et al., 1999). As a result of an impairment in VHL, there is an increase in the expression of hypoxia inducible factors (HIF)-1α and 2α. These HIFs homodimerize and increase the production of proteins that promote angiogenesis, particularly platelet-derived growth factor (PDGF) and vascular endothelial growth factor (VEGF). (Brauch et al., 2000; Courtney and Choueiri, 2010). In particular, endothelial cell proliferation is enhanced by activating pathways linked to VEFG. as well as their migration and survival. The clear-cell RCC subtype is the most common location for this genetic mutation to be found. However, deactivating VHL is insufficient on its own to instigate the development of RCC (Petejova and Martinek, 2016; Brauch et al., 2000). The genes SET domain containing 2, BRCA1-related protein-1, lysine K-specific demethylase 6A, and PBRM1; the SWI/SNF chromatin-remodeling complex gene; are some of the other mutations that have been characterized as contributing to the onset and advancement of recurrent cervical cancer. Twelve. Furthermore, it has been demonstrated that the mammalian target of rapamycin (mTOR) pathway, which plays a role in the control of cell proliferation in response to hypoxia, is considerably elevated in RCC (Rausch et al., 2019). Studies on the patterns of microRNA (miRNA) expression in RCC tissue specimens have been conducted somewhat recently., and the results have shown that there is an overexpression of miRNAs where tumor-suppressors are targeted, whereas microRNAs that specifically target cancer genes are downregulated (Grange et al., 2014; Mytsyk et al., 2018). Deregulated microRNAs have an effect on critical molecules that are involved in the advancement of RCC, including HIF,mTOR, VEGF, VHL, and PTEN (Moch et al., 2015). The high risk of metastasis and the difficulty in diagnosis are two of the factors that contribute to the poor prognosis associated with RCC. In

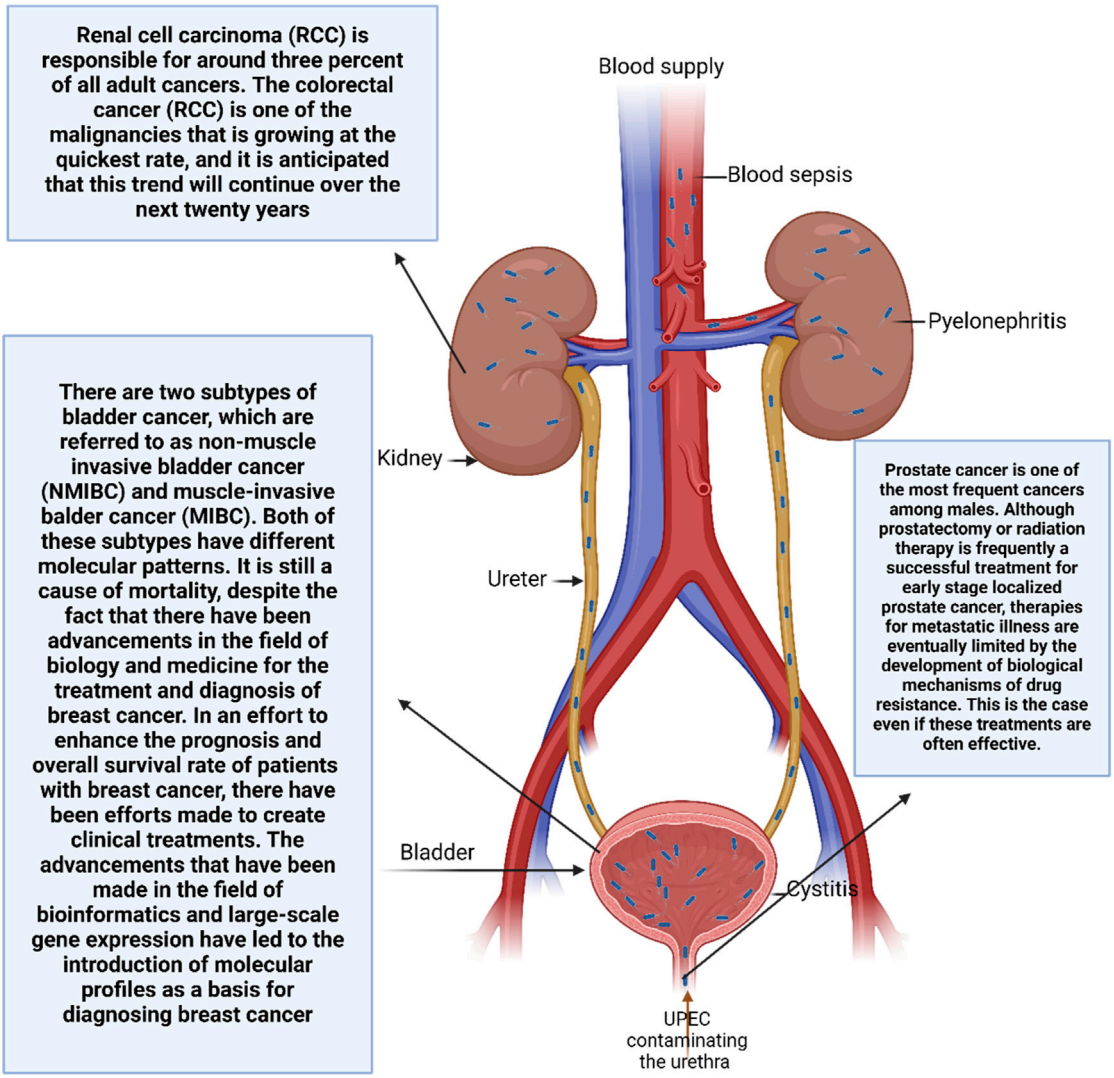

FIGURE 2
An overview of major urological cancers.

actuality, more than sixty percent of RCC are discovered by accident. It is estimated that around twenty to thirty percent of all patients already have illness that has spread throughout the body when diagnosed (Petejova and Martinek, 2016), and approximately thirty percent of patients who have been treated for localized RCC experience a recurrence in distant locations (Ahrens et al., 2019; Barata and Rini, 2017). This is despite the fact that imaging methods have been improving. There is a survival rate of fewer than 10% for individuals who have metastatic RCC (Cairns, 2011; Graves et al., 2013). This indicates that the prognosis for these patients is quite bad. The insufficient elimination of tumor cells is one of the variables that contribute to the failure of therapy, and this may be the result of the heterogeneity of the treated cells. Particularly, Researchers are becoming increasingly interested in the limited number of cancer stem cells (CSCs) because they are thought to be the main culprits behind tumor recurrence and medication resistance. (Figure 2) (Corro and Moch, 2018; Bussolati et al., 2008). This is because CSCs are the progenitor cells of cancer.

4 LncRNAs in prostate cancer

4.1 LncRNAs in prostate cancer progression

The little noncoding RNA known as CCAT1 is thought to be a tumor-promoting agent, and its significance in a variety of malignancies has been examined (Mirzaei et al., 2022b). The protein known as CCAT1 has been shown to promote the development of endometrial cancer, while simultaneously reducing the estrogen receptor-alpha (ERv) expression level and the molecular networks associated with it (Treeck et al., 2020). with example, CCAT1 has the ability to manage miRNA-138-5p and miRNA-181a-5p in pancreatic and colorectal malignancies through respectively, with the purpose of altering progression (Shang et al., 2020). This is supported by the growing body of data that supports the regulatory influence of the long noncoding RNA CCAT1 on the expression of miRNA in various malignancies. Within prostate tumors, CCAT1 is responsible for promoting tumor growth and

development. This explains why CCAT1 cytoplasmically interacts with miRNA-28-5p, which results in a decrease in the amount of expression, and this interaction lays the path for the advancement of prostate cancer (You et al., 2019). It is important to note that various upstream mediators in prostate cancer can have an effect on long noncoding RNAs (lncRNAs) in order to modulate their regulatory effects on microRNAs. This kind of behavior takes place with the long noncoding RNA FOXP4-AS1, which blocks cell death in prostate tumors. and dramatically boosts proliferation and metastasis. Paired box 5 (PAX5) has the ability to stimulate the production of FOXP4-AS1, which then acts as a ceRNA for miRNA-3184-5p. This ultimately results in the enhancement of FOXP4 expression and its post-transcriptional regulation, which is beneficial to the advancement of prostate cancer (Wu et al., 2019). It is necessary to conduct further experiments in order to investigate the complex molecular pathways that have emerged as a result of the regulation of long noncoding RNAs (lncRNAs) by upstream mediators and their interaction with the production of microRNAs. The long noncoding RNA LINC00665 is a newly discovered component in cancer that plays an important part in the regulation of a variety of cellular pathways. An additional experiment underlines the fact that increased expression of LINC00665 is associated with a worse prognosis for men with prostate cancer. (Eke et al., 2021). This is despite the fact that there is data suggesting that LINC00665 suppresses the growth of glioma through STAU1-mediated mRNA degradation (Ruan et al., 2020).

As a result, LINC00665 is capable of playing a role in the development of tumors in prostate cancer and may be considered a tool for diagnosis and prediction. In prostate cancer, STaphylococcal nuclease and Tudor domain containing 1 (SND1) overexpression is associated with the growth of the disease, and the expression of SND1 is downregulated by miRNA-1224-5p, which is responsible for stopping the advancement of cancer. Through the process of sponging miRNA-1224-5p and the consequent overexpression of SND1, it has been revealed that LINC00665 is responsible for the enhancement of tumor propagation, proliferation, and metastasis (Chen W. et al., 2020). As a result, It is well-known that lncRNAs can promote tumors by targeting microRNAs, which are a type of lncRNA. have the ability to influence their production by sponging in the process of influencing the growth of prostate cancer (Wu et al., 2019; Zhang et al., 2020). In a variety of malignancies, the long noncoding RNA SNHG4 acts as an oncogenic component. There is a multi-targeting capability of the long noncoding RNA SNHG4, which also influences a variety of pathways that promote tumor malignancy. By avoiding the arrest of the cell cycle and enhancing proliferation and spread of tumor cells, In gastric cancer, RRM2 is upregulated through miRNA-204-5p when SNHG4 is overexpressed. (Cheng et al., 2021). This action is taken in order to prevent cell cycle arrest. SNHG4, a long noncoding RNA, has a role in the process of boosting the metastasis of gastric tumor cells by the activation of EMT through the sponging of miRNA-204-5p (Wang et al., 2021). Additionally, it plays a role in the immune evasion of cancer cells (Zhou et al., 2021). When prostate cancer is present, the identical event takes place, and an upstream mediator known as SP1 causes SNHG4 to acquire an increased level of expression. Then, SNHG4 stimulates the production of ZIC5 by the sponging of miRNA-377, which has the effect of increasing the malignant behavior of tumor cells and enhancing their survival (Wang ZY. et al., 2020). In the event that a tumor-promoting long noncoding RNA is identified, the most effective methodology for decreasing the rate of prostate cancer's advancement is to knock it down. In the case of prostate cancer, for example, inhibiting the long noncoding RNA TUG1 is advantageous in terms of suppressing the disease and increasing radiosensitivity through the overexpression of miRNA-139-5p and the consequent overexpression of SMC1A (Xiu et al., 2020). In order to overcome the propensity of prostate tumor cells to mediate chemoresistance, further research is required (Quintanal-Villalonga et al., 2020). Because of the relationship between lncRNA and miRNA, treatment resistance in prostate tumors is determined. An increase in transcript levels of the long noncoding RNA the NEAT1 causes a resistance to docetaxel in prostate tumors. Increasing the expression of miRNA-204-5p and miRNA-34a-5p, which are both downregulated in prostate cancer, brings to an increase in chemosensitivity by inhibiting the expression of ACSL4. Because it acts as an upstream mediator, the long noncoding RNA NEAT1 brings down the levels of miRNA-204-5p and miRNA-34a-5p, which in turn raises the expression of ACSL4, which ultimately results in prostate tumor cells being resistant to docetaxel (Li X. et al., 2020).

Furthermore, additional lncRNAs that prostate cancer tissues, which are dysregulated, add to the advancement of the disease through processes that are completely distinct (Mitobe et al., 2018). HOX transcript antisense RNA, also known as HOTAIR, is a kind of long noncoding RNA that has been extensively studied and has been shown to be tumorigenic. The antisense strand of the HOXC gene cluster is where the transcription of HOTAIR takes place. According to the first findings of Rinn et al. (Rinn et al., 2007), PRC2-mediated histone H3 lysine-27 trimethylation at the HOXD gene locus requires HOTAIR. This interaction with PRC2 was determined to be crucial. The opposite is true, according to a paper that was published not too long ago (Portoso et al., 2017), which states that HOTAIR-mediated transcriptional suppression in breast cancer cells does not always need PRC2. As a predictive biomarker, HOTAIR has the potential to be utilized in a variety of cancer types. As an illustration, it was revealed that breast cancer patients exhibit high levels of HOTAIR. that has spread to other parts of the body (Gupta et al., 2010). Both the expression of genes and the invasiveness of cancer are controlled by HOTAIR, which is dependent on PRC2-mediated histone methylation. When it comes to prostate cancer, the expression of HOTAIR is strongly expressed in CRPC, while treatments with androgens suppress its expression. Blocking HOTAIR leads to a reduction in the proliferation and invasion of CRPC cells. The mechanism of action of HOTAIR involves direct interaction with AR, which serves to shield AR from the degradation of proteins This is carried out by MDM2, an E3 ubiquitin ligase. Therefore, the overexpression of HOTAIR causes an upregulation of AR target genes in a manner that is independent of androgens. This is one of the ways where HOTAIR could potentially aid in the development of castration-resistant diseases. (Zhang et al., 2015). Suppressor of cytokine signaling 2-antisense transcript 1, or SOCS2-AS1, is an antisense transcript of SOCS2. was shown to be activated by treatment with anandrogens and overexpressed in CRPC cell lines, according to the findings of a high-throughput sequencing

analysis that we conducted. Additionally, it was demonstrated that SOCS2-AS1 facilitated CRPC model cell migration and proliferation. Androgen signaling is enhanced when SOCS2-AS1 binds to AR, which in turn enhances AR-mediated epigenetic control of genes like TNFSF10, which are involved in apoptosis. (Misawa et al., 2016). This is accomplished by androgen signaling being activated. It was observed by Cui et al. that the expression of long noncoding RNA 1 (PlncRNA-1) was increased in prostate cancer. Furthermore, it was shown that disrupting the AR signaling pathway and killing cancer cells are both outcomes of lncRNA knockdown. (Cui et al., 2013). An additional research conducted not too long ago shown that PlncRNA-1 has a role in facilitating cell migration and invasion by enhancing the release of TGF-β1 (Jin et al., 2017).

A few examples of RNA-binding proteins are PSF, NONO, and paraspeckle component 1 (PSPC1). are involved in the formation of the paraspeckle structure in nuclear foci by nuclear-enriched abundant transcript 1 (NEAT1), which then controls transcription by sequestering these proteins (Hirose et al., 2014). When it comes to a number of different kinds of cancer, NEAT1 is frequently increased, and the levels of expression are related to the illness's severity (Yu et al., 2017). NEAT1 has been shown to rank among the ERα-regulated long noncoding RNAs that are most highly overexpressed in prostate cancer., according to an integrated study of ERα occupancy and signature in prostate cancer (Chakravarty et al., 2014). A greater expression of this long noncoding RNA (lncRNA) in prostate cancer contributes to the development of resilience in the face of AR inhibitors or androgen deprivation. Based on these findings, it appears that the combination of targeting ERαand NEAT1might potentially offer a revolutionary treatment approach for individuals who are afflicted in patients with advanced breast cancer. A transcript known as TRPM2-AS is antisense. that has been identified anywhere within the TRPM2 gene, which is a subfamily M cation channel. It has been shown to be increased with melanoma (Orfanelli et al., 2008) and prostate cancer (Lavorgna et al., 2015), and the expression level is connected with a bad clinical result. It has been demonstrated through knockdown experiments that TRPM2-AS is linked to both the growth of prostate cancer cells and the death of apoptotic cells (Orfanelli et al., 2015), but the specific biochemical mechanism underlying this association is not yet fully understood.

4.2 LncRNAs in prostate cancer drug resistance

The most significant challenge facing cancer treatment is known as MDR. Metastatic cancer cells have the ability to evade the effects of chemotherapeutics, which can be innate or acquired (Haghighi et al., 2023). This ability is referred to as chemoresistant cells (Alfarouk et al., 2015). The development of inherent drug resistance happens when cancer cells, following the administration of chemotherapeutic medicines, raise the expression level of tumor-promoting genes while decrease the expression level of tumor-suppressor genes. This results in an increase when it comes to cell division and proliferation, along with an inhibition of apoptosis. Genetic instability and evolutionary factors were also responsible for the acquisition of drug resistance in these organisms. Generally speaking, the channels for bypass signaling, drug efflux pumps, linkages, and epigenetic changes that exist in the tumor area have the potential to result in the establishment of chemoresistance (Zhong et al., 2021). According to the findings of the research, lncRNA plays a role in the development of chemoresistance in a variety of malignancies, particularly prostate cancer. Because of this, the influence of lncRNA on drug resistance might vary depending on the function of lncRNAs and the targets they target (Ding et al., 2021). The lncRNA HOXD-AS1 is one of the lncRNAs that are implicated in treatment resistance. It is shown to be increased in CRPC cells and has a strong correlation with lymph node metastases and life without progression. The downregulation of HOXD-AS1 reduced the growth of CRPC cells as well as the development of drug resistance in both *in vitro* and *in vivo* settings. Additionally, Some genes have been linked to the cell cycle, resistance to drugs, and castration resistance have been identified and stimulated transcriptionally through the use of HOXD-AS1. These genes include UBE2C, FOXM1,CDC25C, AURKA, and PLK1, among others; Aurora kinase A is also involved. It has been established that HOXD-AS1 utilized WDR5 in order to directly modify the expression of the target genes' expression. Overall, the recruitment of WDR5 by HOXD-AS1 is responsible for the promotion of cell division, resistance to chemotherapy, and resistance to castration in papillary carcinoma (Gu et al., 2017). A different research found that the long noncoding RNAs EGFR and LOXL1-AS1were expressed at a low level, but the doxorubicin-resistant prostate cancer DU-145 cells exhibited an overexpression of the microRNA miR-let-7a-5p. This microRNA has the potential to target the epidermal growth factor receptor (EGFR) as well as the long noncoding RNA LOXL1-AS1, which might have an impact on the course of prostate cancer. In general, The doxorubicin-resistant DU-145 cells' migration, apoptosis, and proliferation were all profoundly affected by the lncRNALOXL1-AS1/miR-let-7a-5p/EGFR axis. which may indicate a viable therapeutic strategy for patients with drug-resistant prostate cancer (Bai et al., 2019).

In docetaxel-resistant prostate cancer samples, NEAT1 was found to be overexpressed, as was indicated before. NEAT1 was silenced, which led to a reduction in the amount of cell proliferation and invasion that occurred in PCa cells that were resistant to docetaxel. Through the act of miR-34a-5p and miR-204-5p sponging in prostate cancer cells, NEAT1 plays a functional role in the development of docetaxel resistance (Jiang et al., 2020). This is accomplished by increasing the expression of ACSL4. The expressions of another long noncoding RNA, CCAT1, were demonstrated to be overexpressed in PCa cells that were resistant to either paclitaxel or PTX. Following treatment with PTX, the suppression of CCAT1 led to a reduction in the survival rate of cells and an increase in the rate of apoptosis (Li X. et al., 2020). The expression of the long noncoding RNA SNHG6 was also shown to be increased in drug-resistant prostate cancer tissues and cells. Experimentally and clinically, the suppression of SNHG6 led to an increase in the susceptibility of PTX-resistant prostate cancer cells to the drug. Additionally, the suppression of SNHG6 reduced PTX-resistant PCa cell migration, invasion, and proliferation *in vitro*. It has been suggested that SNHG6 may have the potential to be a therapeutic factor for prostate cancer (Cao C. et al., 2020). This is because reducing SNHG6 levels made

PTX-resistant PCa cells more vulnerable. to PTX by acting as a tumor suppressor against miR-186. There was also an increase in the expression of Linc00518 in PCa, which was associated with paclitaxel resistance. The lack of Linc00518 in PCa cell lines resulted in a reduction in their resistance to PTX (He et al., 2019). In PCa that was resistant to docetaxel or DTX, DANCR was shown to be highly elevated. Suppressing DANCR caused a rise in the effectiveness of DTX in PCa cells that were resistant to DTX (Ma et al., 2019).

The activation of alternative routes for AR signaling renders PC cells insensitive to ADT, leading to this outcome. which is a fundamental stance against. Castration-resistant prostate cancer (CRPC) is considered a more advanced type of cancer that coincides with the fact that patients have a low survival rate. LncRNA is responsible for controlling several of these routes. Xenograft tissues derived from patients with neuroendocrine prostate cancer (NEPC) who have developed a resistance to hormonal therapies show an overexpression of lncRNA-p21., according to a research that is rather intriguing. Additionally, it has been demonstrated that the antiandrogen enzalutamide (Enz), which is a medicine that is successful in increasing the survival rate of patients with CRPC, also enhances the expression of lncRNA-p21, as a result of which neuroendocrine differentiation (NED) occurs. In addition, functional *in vitro* investigation demonstrated that cell exposure to Enz resulted in the overexpression of lncRNA-p21 through the modulation of AR activity. This, in turn, led to the activation of STAT3 signaling through the Enhancer of zeste homolog 2 (EZH2) pathway. Several studies have shown that this particular signaling pathway plays a role in the process of fostering neuroendocrine differentiation. In addition, research that took place in living organisms revealed that inhibiting In mouse models, EZH2 was able to mitigate the neuroendocrine differentiation generated by Enz therapy. This finding suggests that targeting lncRNA-p21 could be an effective strategy for better management of patients with colorectal cancer who are battling the progression of non-epithelial squamous cell carcinoma (Luo et al., 2019). An further carcinogenic long noncoding RNA (lncRNA) that plays a role in the development of CRPC is called LncRNA-PCAT1. PTEN-deficient individuals experience castration resistance as a result of the activation of the AKT signaling pathway, which is caused by the inhibition of AR signaling signals. There is a report that LncRNA-PCAT1 has the capacity to interfere with a crucial regulatory complex that comprises an inhibitor of nuclear factor kappa B (IKKα) FKBP51,PHLPP, and PH domain. This disruption occurs through the interaction of LncRNA-PCAT1 with FKBP51, which results in the displacement of PHLPP from the complex. This, in turn, activates the signaling pathways of AKT and Nuclear factor kappa B (NF-κB).

4.3 LncRNAs as biomarkers in prostate cancer

PCA3, which was initially found in 1999 using prostate tissue and cell line differential display analysis, is considered to be one of the most precise biomarkers for prostate cancer (Bussemakers et al., 1999). While its expression was found to be sixty to one hundred times greater in more than ninety-five percent of prostate cancers in comparison to non-neoplastic tissues that were adjacent to the tumors, it was not detected in any other forms of malignancies. The fact that knocking down PCA3 reduces AR signaling, as well as cell growth and survival, suggests that modulating AR signaling in tumor cells may be possible by overexpression of PCA3. There is a partial elevation of epithelial indicators such as cytokeratin-18, claudin-3, and E-cadherin when PCA3 is knocked down, while there is a downregulation of the mesenchymal marker vimentin (Lemos et al., 2016). Additionally, PCA3 is responsible for regulating the expression of significant genes that are associated with cancer and are associated with mitogen-activated kinase 1, cell adhesion, signal transduction, apoptosis, and angiogenesis. (Lemos et al., 2016). Further, a PCA3 operational model is now under consideration. According to this model, PCA3 functions as a dominant-negative oncogene that suppresses the activity of the unidentified tumor suppressor Prune Homolog 2 (PRUNE2)), which is the prune gene in fruit fly hybrids with its human equivalent. The procedure relies on RNA editing, namely, the production of double-stranded RNA, to achieve this goal. that is PRUNE2/PCA3 (Salameh et al., 2015). When compared with serum PSA, the combination of urine PCA3 and fusion gene TMPRSS2-ERG has the potential to significantly reduce the number of prostate biopsies that are not necessary. This combination can also boost the specificity of the diagnosis of prostate cancer. The long noncoding RNA known as SChLAP1, which stands for second chromosomal locus associated with prostate is significantly expressed in twenty-five percent of prostate cancer cases (Prensner et al., 2013). There is a substantial correlation between its expression and the likelihood of mortality, clinical progression, biochemical recurrence, metastasis specifically related to prostate cancer. In cases of colorectal cancer, its expression is higher. By interacting with the Switch-Sucrose Non-Fermentable (SWI/SNF) complex for the purpose of chromatin remodeling, SChLAP1 is able to reverse the effects of SWI/SNF, which are known to decrease tumor growth (Prensner et al., 2013). Biochemical recurrence after radical prostatectomy can be independently predicted by this lncRNA., according to an analysis of SChLAP1 expression using *in situ* hybridization (ISH) (Mehra et al., 2014). This long non-coding RNA (lncRNA) is a useful biomarker for prostate cancer patients that is found in tissues. who are at a greater risk of CRPC advancement. Furthermore, the expression of SChLAP1 was found to connect with the progression of prostate cancer that was likely to be fatal (Mehra et al., 2016). In normal prostate tissues and non-cancerous prostate epithelial cells, the expression of the long noncoding RNA known as SPRY4 intronic transcript 1 (SPRY4-IT1) is seen to be much higher in patient samples and inPC3 cells (Lee et al., 2014). siRNA knockdown of SPRY4-IT1 decreased the spread of PC3 cells and their invasion, and also increased the number of cells that underwent apoptosis. According to the results of an RNA chromogenic ISH test, SPRY4-IT1 was easily identified in all prostate cancer samples with varying Gleason scores ranging from 6 to 10 (Lee et al., 2014). Due to its selectivity for prostate cancer and its ability to be easily detected using conventional clinical staining methods on tissue samples, this long noncoding

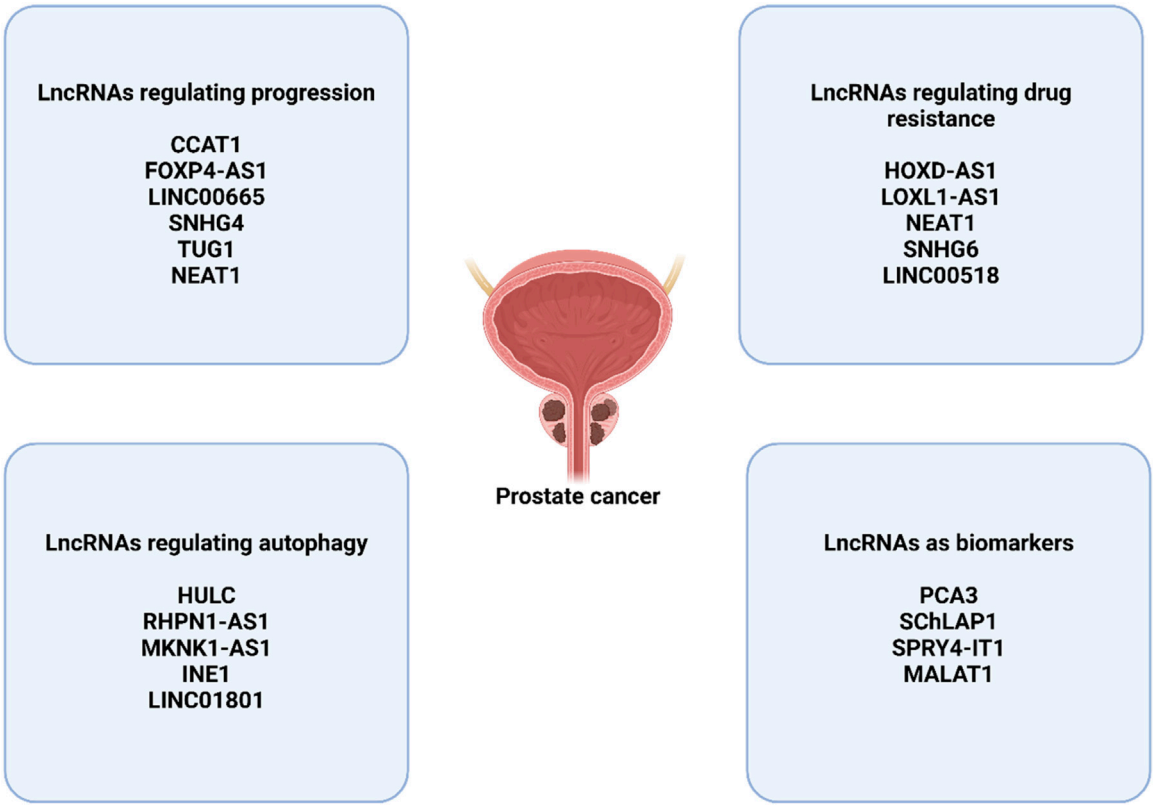

FIGURE 3
The function of lncRNAs in prostate cancer.

RNA is a promising candidate for use as a diagnostic biomarker. MALAT1, which stands for metastasis-associated lung adenocarcinoma transcript 1, is a long noncoding RNA that was initially discovered to may be overexpressed in tissues of non-small-cell lung cancer patients with a high propensity to metastasize? (Ji et al., 2003). Recent research has demonstrated that MALAT1 is also overexpressed in various types of human cancer, such as those that affect the breast, pancreatic, colon, prostate, and liver (Lin et al., 2007; Konishi et al., 2016). MALAT1 overexpression was shown to be related with markers of poor prognosis in prostate cancer, which includes a high Gleason result, advanced stage of tumor node metastasis, and serum PSA levels that were greater than 20 ng/mL. Furthermore, the expression of MALAT1 was considerably higher in hormone-resistant prostate cancer (CRPC) than in cases of prostate cancer that detect hormones (Ren et al., 2013). A study that analyzed MALAT1 expression in prostate cancer patients whose biopsies came back positive and those whose did not found the disease, this lncRNA was shown to be considerably greater in biopsy-positive samples (Wang et al., 2014). This finding suggests as a potential diagnostic biomarker, urine MALAT1 could be useful. By combining EZH2-antibody RNA immunoprecipitation with high-throughput sequencing analysis, it was also determined that MALAT1 binds to EZH2. (Wang et al., 2015). A favorable link between MALAT1 and EZH2 has been shown, and it has been suggested that MALAT1 plays a significant part during the course of CRPC cell line migration and invasion facilitated by EZH2 (Wang et al., 2015; Misawa et al., 2017). Therefore, increasing evidences demonstrate that lncRNAs are potential regulators of tumorigenesis in prostate cancer (Zhang A. et al., 2016; Ramnarine et al., 2019; Ma G. et al., 2016).

4.4 LncRNAs in autophagy regulation in prostate cancer

A few of studies have evaluated the function of lncRNAs in the regulation of autophagy in prostate cancer. The high expression of lncRNA HULC can promote the survival. The HULC silencing can reduce survival rate and enhance apoptosis in prostate cancer. HULC downregulation increases radiosensitivity and stimulates autophagy through Beclin-1 upregulation and mTOR downregulation (Lambert et al., 2018). The lncRNA RHPN1-AS1 downregulation can stimulate apoptosis and autophagy in prostate cancer. LncRNA RHPN1-AS1 sponges miR-7-5p to upregulate EGFR for induction of mTOR to suppress autophagy (Ma X. et al., 2022). On the other hand, the function of REST in the suppression of LINC01801 can transcriptionally stimulate autophagy in enhancing neuroendocrine differentiation of prostate cancer (Chang et al., 2023). Moreover, MKNK1-AS1 and INE1 have been identified as autophagy-related lncRNAs that determine the survival rate of prostate cancer (Li et al., 2021). Figure 3 highlights the function of lncRNAs in prostate cancer.

5 LncRNAs and bladder cancer

5.1 LncRNAs in bladder cancer progression

Different kinds of lncRNAs can be distinguished from one another on the basis of their function, genomic location, and subcellular localization (Cao Y. et al., 2020). There are five different types of lncRNAs that are categorized according to their position in the genome. The long non-coding RNAs can be grouped into several types, such as sense, antisense, bidirectional, intergenic, and intronic. One example of an intergenic long noncoding RNA is H19, another is UCA1, and a third is MALAT1. (Ariel et al., 2000; Xue et al., 2017; Jiao et al., 2018). Intronic lncRNAs includelncRNA-LET, SPRY4-IT1, and BLACAT1 (He et al., 2013; Zhao et al., 2015; Zhuang et al., 2017a). Antisense long noncoding RNAs (lncRNAs) include SNHG16 and GAS5 (Cao et al., 2018; Avgeris et al., 2018), GAS5 transcripts can be either coding RNA or bidirectionally long noncoding RNA. (Wang et al., 2018). On top of that, Two groups are composed of long noncoding RNAs.: nuclear lncRNAs and cytoplasmic lncRNAs, depending on where they are located inside the cell. BLACAT2 and LBCS were shown to be localized in the nucleus of bladder cancer cells, according to the results of investigations involving subcellular fractionation and *in situ* hybridization (ISH) (He W. et al., 2018; Liu P. et al., 2019). Both ARAP1-AS1 and LSINCT5 were shown to be abundant in the cytoplasm of BC cells, as opposed to other proteins (Zhu et al., 2018; Teng et al., 2019). In addition, long noncoding RNAs are categorized into four categories based on the roles that they perform: guide, decoy, signaling, and scaffold lncRNAs. As an illustration, LNMAT1 was responsible for the promotion of lymphatic metastasis of bladder cancer. This was accomplished via enhancing CCL2 promoter recruitment of hnRNPL, which increased the production of CCL2 (Chen et al., 2018). DBCCR1-003 has the potential to bind to DNMT1 and so block the methylation of DBCCR1 in BC that is mediated by DNMT1. Following this, the overexpression of DBCCR1-003 resulted in a considerable reduction in the proliferation of bladder cancer cells as well as the death of these cells (Zhuang J. et al., 2015). Through the process of sponging miR-101-3p, SPRY4-IT1 was able to increase the rate of bladder cancer cell growth and spread (Liu D. et al., 2017). This was accomplished by upregulating zeste homologue 2 (EZH2). In addition, long noncoding RNAs (lncRNAs) are capable of performing their tasks within the transcriptional levels, after the fact, and regulation of epigenetics, independent of the categories that they fall under. The long noncoding RNA (lncRNA) is a regulatory gene that has the potential to exert a significant effect on several biological processes. These activities include cell death, cell proliferation, cell maturation, and cell specialization. For example, Luo et al. reported that an increase in the expression of H19 led to an increase in the proliferation of bladder cancer cells (Luo et al., 2013). When compared with normal tissues, the prevalence of GAPLINC was shown to be considerably higher in bladder cancer tissues. The inhibition of GAPLINC led to the promotion of cell cycle arrest at the G1 phase, as well as the inhibition of a capacity to migrate and invade (Zheng et al., 2018). A similar effect was observed when SNHG16 was knocked down, which led to the halt of the cell cycle at the G1 phase and enhanced apoptosis in bladder cancer cells (Cao et al., 2018). Through its interaction with WDR5, overexpressed BLACAT2 was able to generate intratumoral and peritumoral lymphangiogenesis, which in turn increased the invasiveness of bladder cancer cells (He W. et al., 2018). Furthermore, Not only did MEG3 overexpression inhibit cell invasion and migration, but it also made bladder cancer cells more responsive to cisplatin, a chemotherapeutic agent. (Kim and Tannock, 2005).

5.2 LncRNAs in bladder cancer therapy resistance

In clinical practice, chemotherapy is the first-line treatment for breast cancer, and it is effective in reducing tumor masses in the majority of patients (Zhang et al., 2021). However, after repeated treatment cycles, the majority of patients gradually lose their ability to respond to treatment, and they eventually experience a recurrence of their tumor (Kurtova et al., 2015). The chemotherapeutic response in BCa has been demonstrated to be altered by a number of different long noncoding RNAs. Cisplatin, a fundamental substance used in the initial phase of chemotherapy treatment, has been demonstrated to dramatically enhance the prognosis in patients who are sensitive to the treatment (Herr et al., 2007). Through its role as an oncogene, TUG1 is able to directly sponge miR-194-5p and promote the production of EZH2. There is a correlation when miR-194-5p levels are low and CCND2 expression is high which causes BCa cells to become more resistant to the chemotherapy drug cisplatin (Yu et al., 2019). In addition to this, increasing the sensitivity of BCa cells to adriamycin is achieved by TUG1 knockdown (Sun Z. et al., 2019). A knockdown of LINC00857 makes breast cancer cells more sensitive to cisplatin. This is accomplished via controlling the expression of the LMAN1 gene, which suggests that LINC00857 has the ability to modulate sensitive patient responses to platinum-based chemotherapy (Dudek et al., 2018). A high level of HIF1A-AS2 in cisplatin-resistant breast cancer cells causes an increase in the production of HMGA1, which in turn limits the transcriptional activity of proteins belonging to the p53 family. This, in turn, has an effect on the apoptosis that is caused by cisplatin (Shin et al., 2019). According to the findings of a recent study (Li Y. et al., 2019), When DLEU1 restores the expression of the target gene HS3ST3B1, it improves cisplatin resistance through competitive regulation of miR-99b. It has been demonstrated that the downregulation of MALAT1 increases the susceptibility of BCa cells to cisplatin through the miR-101-3p/VEGFC axis (Liu P. et al., 2019). The susceptibility of breast cancer cells to cisplatin has been discovered to be suppressed by MST1P2, which regulates miR-133b/SIRT1 signaling (Chen J. et al., 2020). It has been demonstrated that UCA1 can reduce the susceptibility of BCa cells to cisplatin by increasing the expression of Wnt6 (Fan et al., 2014a). In addition, long noncoding RNAs have the ability to boost the chemosensitivity of breast cancer cells to cisplatin and suppress treatment resistance. As an illustration, the overexpression of MEG3 may cause BCa cells to become more sensitive to the chemotherapeutic medication cisplatin (Feng et al., 2018).

Another cytotoxic chemotherapeutic drug that is used to treat BCa cells is gemcitabine; nevertheless, the majority of patients, in a manner comparable to those who were treated with cisplatin,

ultimately experience a recurrence of their tumors (Kim and Tannock, 2005). When gemcitabine is used as a treatment, the increase of LET makes it more difficult for BCa to return. It is worth noting that the proinflammatory cytokine TGFβ1 has the ability to directly reduce the levels of LET expression in individuals who are resistant to gemcitabine (Zhuang et al., 2017b). However, FOXD2-AS1 is responsible for the positive regulation of ABCC3 protein through the targeting of miR-143. Evidence suggests that this protein's knockdown suppresses not only the 50% inhibitory concentration of gemcitabine but also invasion, the expression of ABCC3 protein in gemcitabine-resistant BCa cells, and drug resistance-related genes (MDR1, LRP1 MRP2). (An et al., 2018). There is a correlation between high levels of CDKN2B-AS expression and poor gemcitabine sensitivity. Conversely, the Wnt signaling pathway is rendered inactive by decreased levels of the CDKN2B-AS gene, which eventually has an effect on the sensitivity of BCa cells to gemcitabine (Xie et al., 2018). There is a correlation between the high expression of GHET1 and the poor gemcitabine sensitivity in patients with breast cancer, and the knockdown of GHET1 is related with an increase in gemcitabine-induced cytotoxicity (Li B. et al., 2019). In addition, UCA1 is responsible for the activation of the transcription factor CREB by its interaction with its promoter, which ultimately results in the production of miR-196a-5p. Conversely, the inhibition of UCA1 leads to a reduction in chemosensitivity to cisplatin and gemcitabine by reducing the proliferation of BCa cells (Pan et al., 2016). It has been discovered via additional research that lncRNAs also have a significant role in the chemosensitivity of BCa to doxorubicin. Doxorubicin induces cell death, and an increase in GAS5 decreases treatment resistance to doxorubicin. (Shang et al., 2016; Zhang et al., 2017). Increased cell proliferation and decreased doxorubicin chemosensitivity are effects of HOTAIR overexpression., whereas doxorubicin induces cell death. TUG1 role in EMT and radioresistance is mediated via the miR-145/ZEB2 axis, which is responsible for the radioresistance of BCa. Reduced expression of TUG1 enhances radiosensitivity in BCa by repressing the targeting gene The HMGB1 gene (Jiang et al., 2017a; Jiang et al., 2017b).

5.3 LncRNAs as biomarkers in bladder cancer

The expression of thirteen potential long noncoding RNAs was recently assessed by Duan et al. in bladder cancer that was matched to healthy tissue in the surrounding area. They reported a panel of lncRNAs that were expressed differently, and these lncRNAs were then examined using blood samples. There was a discernible difference in the expression of three long noncoding RNAs (MALAT1, SNHG16, and MEG3) in the blood of healthy persons in contrast to serum from both cancerous and noncancerous bladder diseases (Taheri et al., 2018; Duan et al., 2016). It is possible that this panel could aid patients in detecting bladder cancer. There is a statistical correlation between the histological grade and TNM stage of bladder cancer and the expression of several lncRNAs in this malignancy. (Zhuang C. et al., 2015; Zhan et al., 2016a; Zhan et al., 2016b; Chen M. et al., 2016; Li J. et al., 2016; XianGuo et al., 2016). These lncRNAs include HIF1A-AS2, SUMO1P3, PANDAR, CCAT2, PVT1, and NEAT1. Furthermore, according to Chen et al. (Chen et al., 2015), there is a positive correlation between the expression of lncRNA-n336928 and the stage of the bladder tumor, the histological grade, and the patient's survival. There is a correlation between GHET1 overexpression and tumor growth, low survival rates, lymph node status, and the existence of advanced lymph nodes (Li et al., 2014). In bladder cancer, GHET1 expression is more than in surrounding tissues that are unaffected. The presence of lymph node metastases in these individuals is linked to elevated levels of MALAT1 expression, which is also connected with higher grades of histological evaluation and the stage of the tumor (Li et al., 2017). According to other studies (Li et al., 2017; Fan et al., 2014b), the presence of MALAT1 overexpression is a leading indicator of poor survival in these individuals. There is a correlation among patients with muscle-invasive bladder cancer and elevated TUG1 levels in their metastatic tumors (Iliev et al., 2016). TINCR expression levels, on the other hand, have just been established as being related with advanced TNM stage (Chen et al., 2016b). In contrast, a positive correlation was found between low expression of BANCR and MIR31HG and the TNM stage (He et al., 2016a; He et al., 2016b). Moreover, a decrease in the expression of MEG3 is linked to a decrease in the percentage of patients who survive without recurrence (Duan et al., 2016). In bladder cancer, lower GAS5 levels are linked to higher pathological grades and a lower disease-free survival rate. (Zhang et al., 2017).

5.4 LncRNA/ceRNA axis in bladder cancer

Cancer cell stemness, a characteristic of cancer cells that is similar to that of stem cells, has been demonstrated to have a significant role in the development of tumors, the processes of metastasis and recurrence, as well as the development of treatment resistance (Li K. et al., 2023; Tsui and Chan, 2020; Lee et al., 2022). When it comes to human malignancies, particularly bladder cancer, it has been established that lncRNA-mediated ceRNA networks play a role in the creation and maintenance of cancer cell stemness. Zhan et al. (Zhan et al., 2020) discovered bladder cancer was associated with elevated expression of the sex-determining region Y-box2 (SOX2) overlapping transcript (SOX2OT). Furthermore, they found that bladder cancer stem cells were more likely to undergo self-renewal, migration, invasion, and tumorigenicity when SOX2OT expression was up. This was accomplished by means of miR-200c "sponging" and, as a result, increasing SOX2 expression, which is an essential regulator of cancer stemness (Zhu et al., 2021; Mamun et al., 2020). Furthermore, it was shown that through its modulation of the miR-125b/smad2 axis, the oncogenic long noncoding RNA HOXA cluster antisense RNA 2 (HOXA-AS2) enhances the stemness of bladder cancer cells by elevating the expression levels of cancer stem cell markers like OCT4. KLF4, CD44, HMGA2, and ALDH1A1, (Wang F. et al., 2019). Furthermore, it has been reported that a specific type of antisense RNA known as potassium calcium-activated channel subfamily M regulation beta subunit 2 (KCNMB2-AS1) has the ability to improve the stemness of bladder cancer cells. This is accomplished via modulating the miR-3194-3p/smad5 signaling pathway, which in turn increases the expression

of cancer stem cell markers like ALDH1, Oct4, Nanog, CD133, and Nanog. (Chen et al., 2021). Microfilaments, microtubules, and intermediate filaments are the components that make up the eukaryotic cytoskeleton, which is distinguished by its intricate fibrous reticular structure. A growing body of data has proven the cytoskeleton is responsible for signal transduction, cell motility, intercellular transport, and cell division. As a consequence, the cytoskeleton plays a part in the uncontrolled proliferation and migration of cells that occur throughout the evolution of cancer (Eli et al., 2022; Datta et al., 2021). It has been revealed that the lncRNA-mediated ceRNA network is responsible for the rearrangement of the cytoskeleton in the advancement of bladder cancer. For example, Lv et al. (Lv et al., 2017) discovered both human bladder cancer tissues and cell lines exhibit elevated levels of lncRNA H19. Furthermore, they discovered that cytoskeleton reorganization results from overexpression of lncRNA H19. This is accomplished via boosting paxillin and F-actin expression, which are a pair of cytoskeletal proteins involved in cancer cell movement, adhesion, signal transduction, and motor activity (Kim et al., 2009).

Surgical procedures, chemotherapy, and radiation therapy are the conventional therapies for bladder cancer now available. On the other hand, there is a subset of individuals who have bladder cancer who remain refractory to chemotherapy or radiation, and as a result, they have a recurrence of their tumor (Patel et al., 2020; Hensley et al., 2022). In order to achieve improved outcomes for patients with bladder cancer, one of the most significant challenges is to overcome resistance to chemotherapy and radiation. Multiple studies have found that lncRNAs are associated with the ceRNA network and the development of radiation or chemotherapy resistance in bladder cancer. Based on these findings, they discovered networks that target lncRNA-mediated ceRNA might potentially make cancer cells more sensitive to doxorubicin, gemcitabine, and cisplatin. Additionally, along the miR-145/ZEB2 pathway, the lncRNA TUG1, which is significantly expressed at an elevated level in bladder cancer samples and cells, promotes epithelial-mesenchymal transition (EMT) and reduces the susceptibility of cancer cells to ionizing radiation (Tan et al., 2015). By suppressing the production of HMGB1, the promotion of metastasis by a conserved nuclear protein in a variety of malignancies, TUG1 silencing was shown to improve radiosensitivity in a xenograft model, according to the findings of another study (Jiang et al., 2017b; Tripathi et al., 2019). Furthermore, Recent studies that looked at lncRNA signatures in bladder cancer patients who had radiation therapy found that molecular mechanisms related to radiation responses are connected with a 10-lncRNA signature. Furthermore, A small rise in radiosensitivity was observed in bladder cancer cells when one of these lncRNAs was knocked down. (Khan et al., 2021).

5.5 LncRNAs in autophagy regulation in bladder cancer

The lncRNAs are also potential regulators of autophagy in bladder cancer. The lncRNA SNHG1 is able to interact with catalytic subunit PP2A and stimulate autophagy to enhance metastasis of bladder cancer (Xu et al., 2020). The lncRNA ADAMTS9-AS1 stimulates PI3K/Akt/mTOR axis to suppress apoptosis and autophagy in bladder cancer (Yang et al., 2021). In spite of these discussions, more efforts are required regarding understanding the role of lncRNA-mediated autophagy regulation in bladder cancer (Figure 4).

6 LncRNAs and renal cancer

6.1 LncRNAs in renal cancer progression and drug resistance

The lncRNAs have been considered as regulators of drug resistance in kidney cancer (Barth et al., 2020). The sorafenib resistance-associated long noncoding RNA (SRLR) in RCC was firstly tested for functionality by Xu and colleagues. (Xu et al., 2017), who mentioned that SRLR was shown to improve treatment resistance with sorafenib, a multi-kinase inhibitor. Tissue from sorafenib-resistant patients and cells from skin cancer patients both showed an upregulation of SRLR. In terms of the mechanism, SRLR has a direct interaction with the transcription factor NF-KB, which then leads to the stimulation of IL-6 transcription and release of IL-6 by RCC cells in an autocrine manner. The inhibition of receptor tyrosine kinases, such as VEGFR and PDGFR, by sorbafenib is circumvented as a consequence of this, which leads to the activation of the STAT3 pathway. It was demonstrated through experiments that this is true both *in vitro* and *in vivo* (Xu et al., 2017). In a research that looked at SRLR in polycystic ovarian syndrome (Saab et al., 2020), the link between SLRL and IL-6 was only recently verified because it was only just discovered. Higher expression levels of the long noncoding RNA SRLR were found to be associated with a decreased progression-free survival (PFS) in a clinical dataset consisting of 95 patients with recurrent colorectal cancer (RCC) (hazard ratio = 0.407, 95% confidence interval = 0.222–0.744, p = 0.003). Furthermore, this association was also associated with low levels of IL-6 and a lack of benefit from sorafenib treatment. A major influence on resistance to treatment with sunitinib, a multikinase inhibitor, for RCC is exerted by the long noncoding RNA (lncRNA) that is activated in RCC patients who have sunitinib resistance (ARSR) (Qu et al., 2016). Through a mechanism that involves functioning as a competitive endogenous RNA (ceRNA), ARSR is able to sequester miR-34 and miR-449, which in turn leads to a rise in the concentrations of the endpoints AXL and c-MET, which ultimately leads to the promotion of sunitinib resistance. Through sunitinib-resistant cell lines, the ARSR gene is overexpressed, and in turn, By activating FOXO transcriptional factors, AXL enhances the expression of the ARSR gene. This indicates that there is a positive feedback loop between AXL and ARSR in kidney cancer that is resistant to sunitinib. The transfer of sunitinib resistance from cells that are resistant to sunitinib to cells that are sensitive to sunitinib can also occur through the process of exosome-mediated transmission, which is an intriguing phenomenon. *In vivo* and *in vitro* research have demonstrated that targeting ARSR could be considered as a possible treatment option for sunitinib resistance. (Qu et al., 2016). Both of these experiments were conducted. These findings are supported by the fact that pretreatment ARSR levels in the plasma of RCC patients are

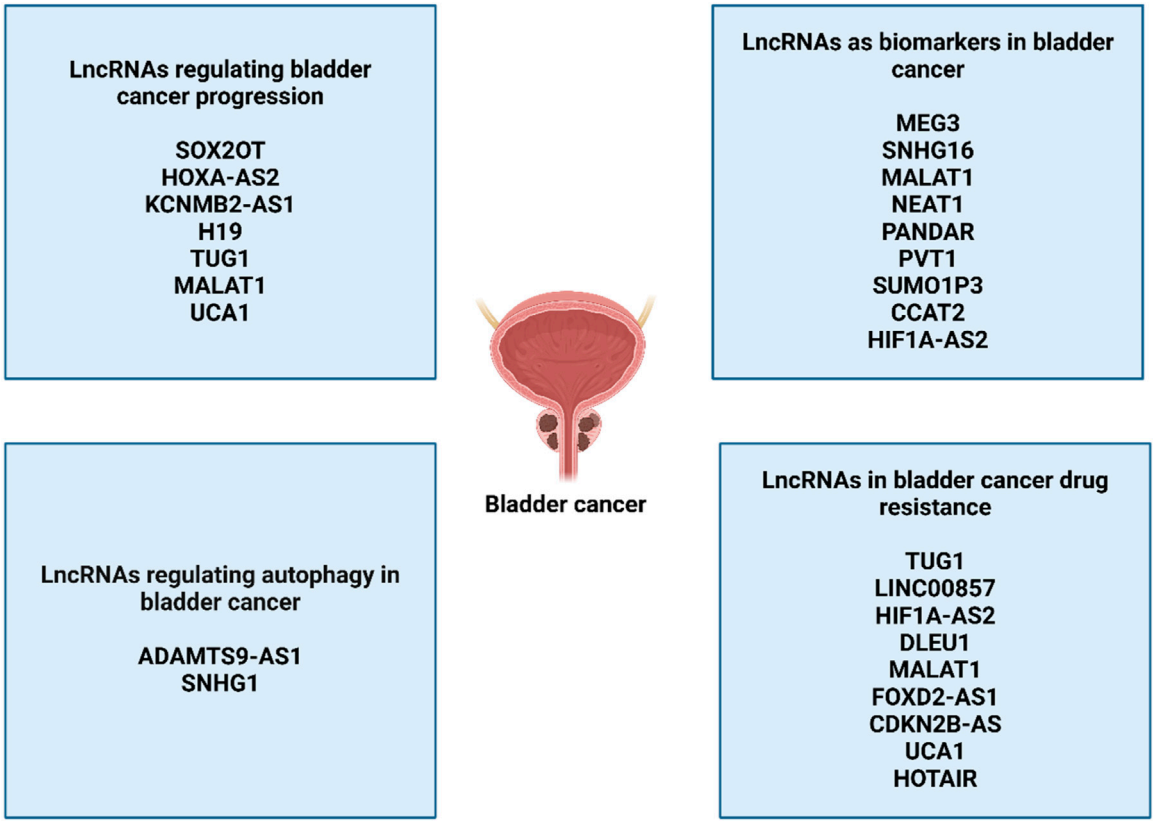

FIGURE 4
The function of lncRNAs in bladder cancer.

substantially connected with poor progression-free survival (PFS) for high vs. low ARSR expression (hazard ratio = 2.9, 95% confidence interval = 1.2–7.1, p = 0.017), respectively (Qu et al., 2016). The ARSR sequence's single nucleotide polymorphisms were also recommended as possible biomarkers for the outcome of RCC in a research that was conducted not too long ago. Numerous investigations have demonstrated which NEAT1—the nuclear paraspeckle assembly transcript and its role as an oncogenic long noncoding RNA have already been thoroughly examined (Klec et al., 2019). There is evidence that NEAT1 contributes to the development of resistance to chemotherapy (Shin et al., 2019; An et al., 2017). Because it acts as a sponge for miR-34a, NEAT1 may be able to block the response to sorafenib therapy in RRC. This is accomplished through the control of the NEAT1/miR-34a/c-MET axis (Liu F. et al., 2017). There have been previous reports that c-MET and miR-34a have an effect on chemoresistance in various types of cancer, such as osteosarcoma and esophageal cancer (Hara et al., 2019; Sun Z-Y. et al., 2019; Pu et al., 2017). Furthermore, NEAT1 has a great deal of expression in RCC cell lines as well as tissues. In addition, there was a correlation between the overexpression of NEAT1 and the change from epithelial to mesenchymal (EMT), as well as a substantial correlation with poor overall survival and progression-free survival in lung cancer. However, the study conducted by Liu et al. did not include any univariate or multivariate analyses, nor did it include any xenograft models (Liu F. et al., 2017).

It has already been established that the long noncoding RNA ADAMTS9 antisense RNA 2 (ADAMTS9-AS2) plays a role in the development of treatment resistance in cancer. Tamoxifen resistance is worsened by ADAMTS9-AS2 downregulation in breast cancer. but its downregulation was related with improved sensitivity to temozolomide in glioblastoma (Yan et al., 2019; Shi et al., 2019). This suggests that its role may vary depending on the kind of cancer being treated. Downregulation of ADAMTS9-AS2 is seen in RCC, and a substantial association is shown between high expression and improved overall survival (Song et al., 2019). Increasing the expression of FOXO1 and restoring chemosensitivity to 5-fluorouracil and cisplatin were both outcomes of overexpressing ADAMTS9-AS2, which was accomplished by the sequestration of miR-27-3p. Nevertheless, there is a lack of evidence carried out in in vivo tests (Song et al., 2019). To this day, chemotherapy is not a viable therapeutic choice for RCC since it has been demonstrated to be unsuccessful; hence, the direct practical significance of the study is restricted (Amato, 2000). Targeting long noncoding RNAs, on the other hand, has the potential to overcome chemoresistance in RCC in the future and open the door for chemotherapy to be considered a viable therapeutic choice for RCC. In a study that was conducted by Liu and colleagues (Liu L. et al., 2019), it was discovered that the long noncoding RNA known as growth arrest specific transcript 1 (GAS5) has an effect on the resistance of RCC to sorafenib. It has already been proven on several occasions (Ma C. et al., 2016) that GAS5 has a tumor suppressive function in the development and

progression of reactive phase carcinoma. In terms of its influence on sorafenib resistance, it was demonstrated that it acts as a sponge for miR-21. Furthermore, it was found that the elevation of GAS5 led to the upregulation of the transcription factor sex determining region Y-box protein 5 (SOX5), which in turn conferred enhanced sensitivity to sorafenib (Ma C. et al., 2016). Multiple models, both *in vitro* and *in vivo*, were used to demonstrate this statement. These findings are supported by the fact that all of the effectors in the GAS5/miR-21/SOX5 pathway, as hypothesized by Liu et al. (Ma C. et al., 2016), have already been found to be effectors in chemoresistance on their own (Gao et al., 2018; Chen Z. et al., 2020; Chen et al., 2019; Dai et al., 2017).

6.2 LncRNAs as diagnostic and prognostic factors in renal cancer

There have been a number of research studies that have focused on lncRNAs with the objective of identifying new biomarkers and gaining a knowledge of the molecular processes that they use to impact the beginning and development of recurrent cardiac tumors (Outeiro-Pinho et al., 2020; Song et al., 2014; Wang et al., 2017; Xue et al., 2019). When compared to their counterparts that code for proteins, lncRNAs are far less expressed. This might be a significant obstacle for their application in clinical practice, since it is extremely difficult to identify them in a reliable manner (Mattick and Rinn, 2015). The investigation of these compounds need to be encouraged, despite the fact that technical advancements might be able to overcome the limits that are currently in place. The most pertinent research that reported lncRNAs as possible diagnostic, prognostic, predictive, and monitoring biomarkers in randomized controlled trials (RCTs) were emphasized in this article. These investigations were conducted on tissue and liquid biopsies. As opposed to sncRNAs, there is a dearth of published information about lncRNAs as diagnostic biomarkers for randomised controlled trials. More than 20 years ago, Thrash–Bingham and colleagues (Thrash-Bingham and Tartof, 1999) made the groundbreaking discovery that the expression of lncRNA varied not only between RCC subtypes but also between subtypes of RCC. It was discovered through the use of semiquantitative PCR that the expression of lncRNA antisense Hypoxia Inducible Factor (aHIF) was significantly higher in ccRCC in comparison to pRCC (Thrash-Bingham and Tartof, 1999). Technology has advanced, and these findings were subsequently verified in 2011, when Bertozzi and colleagues (Bertozzi et al., 2011) discovered a differential expression of lncRNA aHIF between RCC and MNT, as well as between non-pRCC and pRCC tissue samples. This was one of the first times that these findings were validated. In a different research, which included 102 ccRCC and 50 NRT, the lncRNA CYP4A22–2/3 was able to differentiate between ccRCC and NRT with an area under the curve (AUC) of 0.790 (Ellinger et al., 2015). Ren and his colleagues (Ren et al., 2016) conducted an investigation in 2016 to determine the level of expression of the long noncoding RNAs UC009YBY.1 and ENST00000514034 in a collection of 70 ccRCC and 70 MNT cells. These authors observed that the two lncRNAs were able to detect RCC tissue with a sensitivity of 54.29% and a specificity of 82.86% for the former, and with a sensitivity of 60.00% and a specificity of 67.14% for the latter (Ren et al., 2016). Last but not least, a recent research revealed that the lncRNA HOX Transcript Antisense RNA (HOTAIR) might potentially serve as a diagnostic biomarker for colorectal cancer, uncovering an area under the curve (AUC) of 0.9230 (Dasgupta et al., 2018). After doing a search of the relevant literature, we discovered that there were only two publications that were relevant to the evaluation of the potential of lncRNAs as RCC diagnostic biomarkers in liquid biopsies. Using two different sets of ccRCC and AC serum samples, Wu and colleagues (Wu et al., 2016) investigated the expression of five different long non-coding RNAs (lncRNAs): lncRNA–low expression in tumor (LET), Plasmacytoma Variant Translocation 1 (PVT1), Promoter of CDKN1A Antisense DNA Damage Activated RNA (PANDAR), Phosphatase and Tensin Homolog Pseudogene 1 (PTENP1), and long intergenic non-protein RNA 963 (linc00963). These biomarkers, when integrated in a panel, were able to identify malignancy with a sensitivity of 79.2% and a specificity of 88.9% in the training set (consisting of 24 ccRCC and 27 AC), and with a sensitivity of 67.6% and a specificity of 91.4% in the testing set (consisting of 37 ccRCC and 35 AC) (Wu et al., 2016). Following that, the serum expression of the long noncoding RNA GIHCG was evaluated in a total of 46 samples, including 46 ccRCC and 46 AC. The expression of GIHCG was able to differentiate between ccRCC and healthy donors with a sensitivity of 87.0% and a specificity of 84.8%. Particularly remarkable is the fact that it was able to differentiate between early-stage ccRCC and AC (31 stage I ccRCC vs. 46 ACs) with a sensitivity of 80.7% and a specificity of 84.8% (He ZH. et al., 2018).

6.3 LncRNAs in autophagy regulation in renal cancer

The lncRNAs can also regulate autophagy in renal cancer. However, only one experiment has evaluated the function of lncRNAs in the modulation of autophagy in the renal cancer. LncRNA HOTAIR is able to sponge miR-17-5p to induce autophagy through Beclin-1 upregulation in the induction of sunitinib resistance (Li D. et al., 2020). Table 1 summarizes the lncRNAs involved in the regulation of urological cancer progression.

7 Discussion

In the last 10 years, a growing body of research has demonstrated that lncRNAs have a significant role in both the beginning and the advancement of bladder cancer. As of right now, typical biomarkers for bladder cancer are still quite uncommon. This is because they do not possess high sensitivity and specificity, and their use is also rather expensive. There is a need for the development of new biomarkers for the early detection and prognosis of bladder cancer. This is because bladder cancer has a high recurrence rate and a poor prognosis, even after successful transurethral resection and systemic therapy. The purpose of this study is to provide a concise summary of the expression, function, and molecular processes of lncRNAs, as well as the clinical implications of lncRNAs in the diagnosis and prognosis of bladder cancer. There has been research conducted on the molecular processes of lncRNAs in bladder cancer. These mechanisms include lncRNAs interacting with DNA, RNA, and

TABLE 1 The lncRNA-driven regulation of urological cancer progression.

Urological cancer	LncRNA	Remark	References
Prostate cancer	LNC-565686	Increase in the proliferation rate and inhibition of apoptosis via enhancing SND1 stability	Qin et al. (2023)
Prostate cancer	LncRNA TMPO-AS1	Enhancement in the bone metastasis through Wnt upregulation	Wang et al. (2023a)
Prostate cancer	LINC01801	Inhibition of LINC01801 by REST to mediate neuroendocrine differentiation of prostate tumor through autophagy induction	Chang et al. (2023)
Prostate cancer	LncRNA SNHG4	Enhancement in the cell survival and induction of enzalutamide resistance	Dong et al. (2023)
Prostate cancer	LncRNA TYMSOS	Silencing this lncRNA impairs the growth, division and EMT	Xia et al. (2023)
Prostate cancer	TPT1-AS1	Autophagy stimulation to enhance survival	Chen et al. (2024b)
Prostate cancer	CTBP1-AS	Suppressing TP63-induced activation of S100A4	Wu et al. (2024)
Prostate cancer	A1BG-AS1	Transfer by exosomes and reduction in the prostate cancer progression through ZC3H13-induced m6A modification	Yang et al. (2024)
Bladder cancer	LncRNA BCCE4	Increase in the interaction of PD-L1 and PD-1	Zheng et al. (2023)
Bladder cancer	LncRNA AGAP2-AS1	Interaction with IGF2BP2 to enhance tumorigenesis	Zhao et al. (2023)
Bladder cancer	LncRNA-RP11-498C9.13	Antisense lncRNA-RP11-498C9.13 promotes ROS-induced mitophagy to enhance tumorigenesis	Song et al. (2023)
Bladder cancer	LncRNA PVT1	Generating positive feedback loop with STAT5B to increase carcinogenesis	Li et al. (2023b)
Bladder cancer	LncRNA XIST	miR-129-5p/TNFSF10 control to increase cancer progression	Kong et al. (2024)
Bladder cancer	LINC00592	Inducing promoter methylation of WIF1 in carcinogenesis	Wu et al. (2023b)
Bladder cancer	LncRNA MEG	Suppressing EMT through Snail downregulation	Wang et al. (2024b)
Renal cancer	PVT1	Increase in stemness	Wang et al. (2023b)

proteins. Both the urine supernatant and the plasma of patients with bladder cancer can be enriched with circulating long noncoding RNAs, which may offer a more favorable potential for developing novel tests for bladder cancer. There is a strong correlation between the abnormal expression of thirty-six lncRNAs and a number of clinical features that are associated with bladder cancer. For the purpose of acting as diagnostic or prognostic markers for breast cancer, the increased lncRNAs offer advantageous traits because of their low expression and less evolutionarily conserved nature. As a result, we investigated thirty lncRNAs that were upregulated in order to identify possible clinical indicators. UCA1 has reasonably good sensitivity, specificity, and area under the curve (AUC), and it may be regarded the most viable diagnostic biomarker for bladder cancer. This is based on the dissection of fifteen upregulated long noncoding RNAs that are connected with the size of the tumor seen in bladder cancer patients. The need of doing large-scale investigations in cells and clinical specimens prior to the development of new lncRNA biomarkers for clinical diagnosis cannot be overstated. In this context, the diagnostic and therapeutic performance of bladder cancer will be facilitated by large and systematic investigations on lncRNAs. The fact that there is now no lncRNA that can be used to the particular diagnosis, prognosis, and therapy of bladder cancer is something that should be taken into consideration. At the same time that microRNAs, circular RNAs, and exosomes all play significant roles in the development of breast cancer, microRNAs are also involved. According to the information that we currently possess, the combination of mRNAs, microRNAs, and lncRNAs would presumably be more effective in improving the early diagnosis and prognosis of bladder cancer (Liu XS. et al., 2021).

Autophagy is indeed a complex biological process that exerts varying effects in different types of tumors, including those within the genitourinary system. In the context of these cancers, autophagy can play dual roles as both a tumor suppressor and promoter, depending on factors such as the specific type of cancer, its stage, and the presence of particular genetic mutations. For instance, in prostate cancer, autophagy has been shown to support tumor cell survival and therapy resistance, particularly in advanced stages where cells experience hypoxic and nutrient-deprived conditions. Conversely, in the early stages, autophagy can suppress tumorigenesis by preventing the accumulation of damaged organelles and proteins, thus maintaining cellular homeostasis. This dual role underscores the need to understand the specific context in which autophagy operates, as it influences treatment strategies and outcomes. Moreover, the regulatory mechanisms of autophagy in genitourinary cancers are influenced by a variety of pathways and molecular interactions, including those involving lncRNAs. For example, in bladder cancer, lncRNAs such as TUG1 and SNHG1 have been implicated in modulating autophagy and contributing to therapy resistance through interactions with key signaling pathways like PI3K/Akt/mTOR and PP2A catalytic subunit, respectively. The complexity is further compounded by the fact that lncRNAs can act as either oncogenes or tumor suppressors, depending on their expression patterns and the regulatory networks they engage with. This variability necessitates a nuanced understanding of the molecular

and genetic landscape of each cancer type to effectively target autophagy-related pathways in therapeutic settings. Consequently, more comprehensive studies integrating multi-omics approaches are needed to elucidate these intricate mechanisms and optimize therapeutic strategies targeting autophagy in genitourinary cancers.

Without a shadow of a doubt, long noncoding RNAs play a significant part in the development of several forms of cancer, including rheumatoid cancer, in terms of the biology that underlies the disease, the beginning of cancer, and its spread to distant metastases (Seles et al., 2016). Despite all of the promises and recent breakthroughs in research on lncRNAs, the functional role of lncRNAs is still unknown. lncRNAs have the potential to be connected to a wide variety of physiological and pathological roles, as was previously demonstrated. Nevertheless, phenotypic manifestation and the consequences that it has for the person are of the utmost significance in the end. To research phenotypic expression, it is necessary to alter lncRNAs in order to understand the possible implications of these RNAs. This can be accomplished by a variety of methods, including as the deletion of the promoter region or the whole gene, the incorporation of a premature polyadenylation sequence, antisense oligonucleotide blocking, and other methods (Gutschner et al., 2013; Li and Chang, 2014).

A comprehensive understanding of the role of long non-coding RNAs (lncRNAs) in autophagy, particularly in the context of therapy resistance and urological cancers, necessitates the integration of multi-omics data. By leveraging genomics, transcriptomics, and proteomics, researchers can construct a holistic view of the regulatory networks that underpin the function of lncRNAs. Genomics data provide insights into the genetic variants and mutations that may influence lncRNA expression and function. Identifying single nucleotide polymorphisms (SNPs) and copy number variations (CNVs) associated with lncRNA genes can help in understanding their role in cancer susceptibility and progression. For instance, genomic studies can reveal mutations that disrupt the regulatory elements of lncRNAs, thereby affecting their transcription and subsequent impact on autophagy-related pathways. Transcriptomics data, obtained through RNA sequencing (RNA-seq), offer a detailed landscape of lncRNA expression profiles across different tissues and stages of cancer. This data can identify differentially expressed lncRNAs that are implicated in autophagy. Moreover, transcriptomic analyses can elucidate the co-expression networks between lncRNAs and protein-coding genes, highlighting potential regulatory interactions that govern autophagic processes. Proteomics data, derived from mass spectrometry and other techniques, allow for the quantification and identification of proteins that interact with lncRNAs. These protein-lncRNA interactions are crucial for understanding the mechanistic roles of lncRNAs in autophagy. For example, proteomics can uncover how lncRNAs modulate the activity of key autophagy-related proteins such as Beclin-1 and mTOR. Additionally, proteomic analyses can identify post-translational modifications of proteins that are regulated by lncRNAs, further elucidating their functional roles. Integrating these multi-omics data can reveal the complex regulatory networks involving lncRNAs in autophagy. For example, combining transcriptomic and proteomic data can identify lncRNAs that are co-expressed with autophagy-related genes and their corresponding protein products. Genomic data can then be used to pinpoint genetic variants that influence these regulatory networks. This integrated approach can also aid in the identification of potential biomarkers and therapeutic targets for overcoming therapy resistance in urological cancers. By incorporating multi-omics data, researchers can achieve a more comprehensive understanding of how lncRNAs regulate autophagy, thereby providing new avenues for therapeutic intervention and the development of personalized medicine strategies in urological cancers.

The lncRNAs have emerged as crucial regulators in the development of therapy resistance in various cancers, including prostate, bladder, and renal cancers. These lncRNAs can modulate drug resistance through multiple mechanisms, such as interacting with miRNAs, affecting gene expression at the transcriptional and post-transcriptional levels, and altering signaling pathways. For instance, the lncRNA HOXD-AS1 is upregulated in castration-resistant prostate cancer (CRPC) and interacts with WDR5 to promote the expression of genes involved in cell cycle progression and drug resistance, such as UBE2C, FOXM1, CDC25C, AURKA, and PLK1. This interaction enhances chemotherapy resistance and cell proliferation, making HOXD-AS1 a potential target for overcoming drug resistance in prostate cancer. Another example is the lncRNA NEAT1, which is overexpressed in docetaxel-resistant prostate cancer cells. NEAT1 sponges miR-34a-5p and miR-204-5p, leading to increased expression of ACSL4, which contributes to docetaxel resistance. In bladder cancer, lncRNAs also play significant roles in mediating chemotherapy resistance. The lncRNA TUG1, for instance, is implicated in cisplatin resistance by sponging miR-194-5p and promoting EZH2 expression, which in turn affects cell cycle regulation and apoptosis. Another lncRNA, UCA1, enhances cisplatin and gemcitabine resistance by activating the transcription factor CREB and promoting the expression of miR-196a-5p. In renal cancer, the lncRNA SRLR contributes to sorafenib resistance by interacting with NF-κB and promoting IL-6 transcription, which activates the STAT3 pathway. Similarly, the lncRNA ARSR mediates sunitinib resistance by acting as a competitive endogenous RNA for miR-34 and miR-449, leading to increased levels of AXL and c-MET, which are associated with drug resistance. These examples highlight the diverse mechanisms through which lncRNAs regulate therapy resistance, including modulation of miRNA activity, gene expression, and signaling pathways, making them promising targets for developing novel therapeutic strategies to overcome drug resistance in cancer treatment.

The dual role of autophagy as both a tumor suppressor and promoter is indeed complex and context-dependent. Autophagy can act as a tumor suppressor in the early stages of cancer development by maintaining cellular homeostasis and preventing the accumulation of damaged organelles and proteins, which could lead to genomic instability and oncogenic transformation. In this phase, autophagy helps eliminate potentially malignant cells and suppresses tumor initiation. However, in established tumors, cancer cells can hijack the autophagic process to survive under stressful conditions such as hypoxia, nutrient deprivation, and therapeutic interventions. This switch from tumor-suppressive to tumor-promoting roles of autophagy is influenced by various factors,

including the tumor type, stage of cancer, and the cellular microenvironment. Several pathways and mechanisms contribute to this context-dependent switch. For instance, the mTOR pathway, a central regulator of cell growth and metabolism, inhibits autophagy under nutrient-rich conditions, supporting cell growth and proliferation. Conversely, during nutrient starvation, mTOR activity decreases, leading to the induction of autophagy, which can provide metabolic substrates to sustain cancer cell survival and growth. Additionally, hypoxia-inducible factors (HIFs) activated under low oxygen conditions can induce autophagy to adapt to hypoxic stress, thereby promoting tumor progression and resistance to therapy. The involvement of specific lncRNAs in modulating these pathways further underscores the intricate regulation of autophagy in cancer. For example, lncRNA HULC and RHPN1-AS1 have been shown to regulate autophagy and influence therapy resistance in prostate cancer through their interactions with mTOR and EGFR signaling, respectively. Understanding these conditions and mechanisms is crucial for developing targeted therapeutic strategies that can modulate autophagy appropriately depending on the cancer context.

The availability of a number of instances for deletion of lncRNA in cultured cells and animal models, both with and without phenotypic alterations, has recently increased. Neat1, for instance, is a highly abundant long noncoding RNA that is closely related to MALAT1. It is necessary for the development of the mammary glands and the corpus luteum, as well as for the potential of breastfeeding and the creation of pregnancy in mice (Standaert et al., 2014; Nakagawa et al., 2014). On the other hand, knocking out MALAT1 does not appear to have any discernible effects on the pre- and post-natal development of mice (Eißmann et al., 2012; Peters et al., 2016; Zhang et al., 2012; Nakagawa et al., 2012). The deletion of HOTAIR results in surviving mice, but it also causes the spinal vertebrae and metacarpal bones to undergo metamorphosis. On the other hand, the knockout of Fendrr (Foxf1 adjacent non-coding developmental regulatory RNA) leads to embryonic death (Kogure et al., 2013; Sauvageau et al., 2013). Due to the fact that only a small portion of lncRNAs have been studied up until this point, it is not yet feasible to reach a definitive conclusion that explains in full the activities of lncRNAs and their role in physiological and pathological processes. All of the efforts that are being made are ultimately being done with the intention of enhancing the management of cancer in people. To this day, not a single long noncoding RNA has been included into clinical regular practice that is based on urological guidelines (Ljungberg et al., 2015; Babjuk et al., 2013; Hakenberg et al., 2015). However, there are a few candidates that show great promise for treating various forms of cancer (Mouraviev et al., 2016; Chang et al., 2016; Parasramka et al., 2016). In addition, several strategies have been investigated in order to make use of lncRNAs as possible therapeutic agents in the treatment of various forms of cancer. tiny interfering RNAs, ribozymes, aptamers, antisense oligonucleotides, natural antisense transcripts, and tiny compounds are some examples of the methods that fall under this category (Mouraviev et al., 2016; Parasramka et al., 2016). The same may be said for these drugs; they have not yet been included into the standard clinical oncological practice. The use of lncRNAs in RCC is still in its infancy in 2016, with just a few intriguing candidates giving the possibility of application as biomarkers or novel treatment targets. Before the therapeutic use of lncRNAs in patients with RCC becomes a reality, there are still a number of applications and fundamental research investigations that need to be carried out in order to completely understand the underlying processes of their activities.

The role of lncRNAs in regulating autophagy and therapy resistance in urological cancers indeed varies depending on cancer type, stage, and specific genetic mutations. The manuscript discusses how lncRNAs like HULC and RHPN1-AS1 influence autophagy and therapy resistance in prostate cancer by interacting with pathways like mTOR and EGFR signaling. This indicates that lncRNAs can either promote or inhibit autophagy based on their interactions with specific pathways, which can vary depending on the cancer context. For example, HULC promotes survival and resistance to radiotherapy in prostate cancer by upregulating Beclin-1 and downregulating mTOR, while RHPN1-AS1 suppresses autophagy through miR-7-5p sponging and EGFR activation, highlighting the diverse regulatory roles of lncRNAs in autophagy depending on the cellular environment and specific mutations. Additionally, in bladder cancer, lncRNAs like TUG1 and SNHG1 have been shown to modulate autophagy through interactions with signaling pathways such as miR-145/ZEB2 and PP2A catalytic subunit, respectively. The specific impact of these lncRNAs on autophagy and therapy resistance can vary depending on the genetic makeup of the cancer cells and their microenvironment. This context-dependent nature underscores the need for detailed studies to understand the precise conditions under which lncRNAs switch roles from tumor suppression to promotion. Such studies can provide critical insights into how lncRNAs can be targeted for therapeutic interventions, offering a pathway to personalized medicine in treating urological cancers.

The potential of lncRNAs and autophagy-related markers as diagnostic, prognostic, and therapeutic tools in cancer, particularly urological cancers, is promising but indeed requires further validation. As outlined in the manuscript, several lncRNAs, such as HOTAIR, MEG3, and MALAT1, have shown strong correlations with cancer progression, metastasis, and resistance to therapies. For instance, HOTAIR's involvement in modulating chromatin states and influencing gene expression linked to cancer aggressiveness has been extensively documented, suggesting its potential as a biomarker. However, while preclinical studies and initial clinical observations support their utility, large-scale clinical trials and real-world evidence are necessary to establish their efficacy and safety as clinical biomarkers or therapeutic targets. In particular, the use of lncRNAs as therapeutic targets has been mostly explored in preclinical settings, such as *in vitro* studies and animal models, demonstrating the feasibility of targeting these molecules to modulate autophagy and other cancer-related pathways. For example, the suppression of specific lncRNAs like MALAT1 and HOTAIR has shown to inhibit tumor growth and metastasis in animal models. However, translating these findings into effective clinical interventions requires addressing challenges such as ensuring the specificity and delivery of lncRNA-targeted therapies, minimizing off-target effects, and understanding the complex interactions within the tumor microenvironment. The development of reliable methods for detecting and quantifying lncRNAs in clinical samples is also crucial for their application as biomarkers. Therefore, while the potential clinical applications of

lncRNAs and autophagy are compelling, rigorous validation through clinical trials is essential to confirm their utility in improving cancer diagnosis, prognosis, and treatment.

8 Conclusion

In order to effectively treat prostate cancer, it is necessary to tailor treatment plans to each individual patient because the disease process is both lengthy and diverse. The molecular processes that are responsible for the pathogenesis of prostate cancer have been gradually revealed as a result of extensive fundamental medical research that has been carried out over the course of the past few years (Smolle et al., 2017). Patients whose condition is resistant to standard anti-hormonal therapy have seen a significant increase in their life expectancy as a result of the introduction of innovative anti-androgens into clinical practice. In the event that certain biomarkers, such as the AR-V7 splice variation in mCRPC, are identified, the treatment may be modified accordingly. LncRNAs are engaged in each and every one of these phases in the growth of the tumor. They could be able to sustain cellular proliferation and invasion independent of androgens, enhance the progression toward castration-resistant states, or preserve androgen-related pathways in the event that androgens are depleted. Some long noncoding RNAs are already being employed as diagnostic biomarkers, while others may be used in the future. Different patterns of lncRNA expression can be used to make prognostic or predictive statements. As therapeutic targets, lncRNAs have the potential to improve the effectiveness of anti-tumor drugs and contribute to the slowing down of the progression of prostate cancer. The method known as RNAi can be utilized to control the production of lncRNAs. Within the framework of this technique, small double-stranded RNAs, such as siRNA, are utilized to cause a degradation of their target lncRNA through the RNA-induced silencing complex (RISC) (Chen et al., 2016c). It is therefore possible to employ the RNA interference technique to successfully lower the expression levels of long noncoding RNAs that have the potential to cause tumors. Antisense oligonucleotides, also known as ASOs, are comprised of either short single-stranded RNAs or DNAs that are antisense to their target long noncoding RNA (Lin et al., 2011). This is yet another approach that may be utilized. Furthermore, the utilization of small molecules has the potential to, for instance, make it impossible for HOTAIR to interact with LSD1 and PRC2 (Chandra Gupta and Nandan Tripathi, 2017; Tsai et al., 2011). It has already been demonstrated that the therapeutic use of the H19-regulated double-stranded DNA plasmid BC-819 has been evaluated and found to be effective in patients who have bladder cancer (Gofrit et al., 2014). The majority of research that has been conducted on the use of lncRNAs as therapeutic targets has been conducted on cell cultures or animal models, and there have been very few studies that have been conducted on human beings. In addition, the precise role of a great number of long noncoding RNAs is still unclear. This is due to the fact that they do not necessarily share a single target or function inside a cell. Furthermore, depending on the kind of tumor, the same lncRNA may perform a variety of other activities. As a result, the utilization of lncRNAs as therapeutic targets may result in unanticipated side effects or significant adverse responses. In spite of this, the more complete our understanding of the role of lncRNAs becomes, the more effective and extensive their therapeutic applications will be. As a result of current study, more long noncoding RNAs that are implicated in the etiology of prostate cancer, as well as their molecular effects and the possible implications for clinical management, will be discovered.

Author contributions

SW: Conceptualization, Data curation, Investigation, Methodology, Project administration, Resources, Software, Supervision, Validation, Writing–original draft, Writing–review and editing. YB: Conceptualization, Data curation, Formal Analysis, Investigation, Methodology, Project administration, Supervision, Writing–original draft, Writing–review and editing. JM: Conceptualization, Data curation, Investigation, Methodology, Writing–original draft, Writing–review and editing. LQ: Conceptualization, Data curation, Investigation, Methodology, Project administration, Resources, Writing–original draft, Writing–review and editing. MZ: Conceptualization, Data curation, Investigation, Methodology, Project administration, Resources, Software, Supervision, Validation, Visualization, Writing–original draft, Writing–review and editing.

Funding

The author(s) declare that financial support was received for the research, authorship, and/or publication of this article. This work was supported by Wu Jieping Medical Foundation Clinical Research Funding Fund (320.6750.2022-11-48).

Conflict of interest

The authors declare that the research was conducted in the absence of any commercial or financial relationships that could be construed as a potential conflict of interest.

Publisher's note

All claims expressed in this article are solely those of the authors and do not necessarily represent those of their affiliated organizations, or those of the publisher, the editors and the reviewers. Any product that may be evaluated in this article, or claim that may be made by its manufacturer, is not guaranteed or endorsed by the publisher.

References

Adnane, S., Marino, A., and Leucci, E. (2022). LncRNAs in human cancers: signal from noise. *Trends cell Biol.* 32 (7), 565–573. doi:10.1016/j.tcb.2022.01.006

Ahrens, M., Scheich, S., Hartmann, A., Bergmann, L., and Society, I.-NIWGKC. G. C. (2019). Non-clear cell renal cell carcinoma-pathology and treatment options. *Oncol. Res. Treat.* 42 (3), 128–135. doi:10.1159/000495366

Alexandrov, L. B., Nik-Zainal, S., Wedge, D. C., Aparicio, S. A., Behjati, S., Biankin, A. V., et al. (2013). Signatures of mutational processes in human cancer. *Nature* 500 (7463), 415–421. doi:10.1038/nature12477

Alfarouk, K. O., Stock, C.-M., Taylor, S., Walsh, M., Muddathir, A. K., Verduzco, D., et al. (2015). Resistance to cancer chemotherapy: failure in drug response from ADME to P-gp. *Cancer cell Int.* 15 (1), 71–13. doi:10.1186/s12935-015-0221-1

Alharbi, K. S., Almalki, W. H., Makeen, H. A., Albratty, M., Meraya, A. M., Nagraik, R., et al. (2022). Role of Medicinal plant-derived Nutraceuticals as a potential target for the treatment of breast cancer. *J. Food Biochem.* 46 (12), e14387. doi:10.1111/jfbc.14387

Alharthi, N. S., Al-Zahrani, M. H., Hazazi, A., Alhuthali, H. M., Gharib, A. F., alzahrani, S., et al. (2024). Exploring the lncRNA-VEGF axis: implications for cancer detection and therapy. *Pathology - Res. Pract.* 253, 154998. doi:10.1016/j.prp.2023.154998

Allory, Y., Beukers, W., Sagrera, A., Flández, M., Marqués, M., Márquez, M., et al. (2014). Telomerase reverse transcriptase promoter mutations in bladder cancer: high frequency across stages, detection in urine, and lack of association with outcome. *Eur. Urol.* 65 (2), 360–366. doi:10.1016/j.eururo.2013.08.052

Amaral, T. M. S., Macedo, D., Fernandes, I., and Costa, L. (2012). Castration-resistant prostate cancer: mechanisms, targets, and treatment. *Prostate cancer* 2012, 327253. doi:10.1155/2012/327253

Amato, R. J. (2000). Chemotherapy for renal cell carcinoma. *Seminars Oncol.* 27 (2), 177–186.

An, J., Lv, W., and Zhang, Y. (2017). LncRNA NEAT1 contributes to paclitaxel resistance of ovarian cancer cells by regulating ZEB1 expression via miR-194. *OncoTargets Ther.* 10, 5377–5390. doi:10.2147/OTT.S147586

An, Q., Zhou, L., and Xu, N. (2018). Long noncoding RNA FOXD2-AS1 accelerates the gemcitabine-resistance of bladder cancer by sponging miR-143. *Biomed. and Pharmacother. = Biomedecine and Pharmacother.* 103, 415–420. doi:10.1016/j.biopha.2018.03.138

Ang, H. L., Yuan, Y., Lai, X., Tan, T. Z., Wang, L., Huang, B. B., et al. (2021). Putting the BRK on breast cancer: from molecular target to therapeutics. *Theranostics* 11 (3), 1115–1128. doi:10.7150/thno.49716

Ariel, I., Sughayer, M., Fellig, Y., Pizov, G., Ayesh, S., Podeh, D., et al. (2000). The imprinted H19 gene is a marker of early recurrence in human bladder carcinoma. *Mol. Pathol.* 53 (6), 320–323. doi:10.1136/mp.53.6.320

Arriaga-Canon, C., Contreras-Espinosa, L., Aguilar-Villanueva, S., Bargalló-Rocha, E., García-Gordillo, J. A., Cabrera-Galeana, P., et al. (2023). The clinical utility of lncRNAs and their application as molecular biomarkers in breast cancer. *Int. J. Mol. Sci.* 24 (8), 7426. doi:10.3390/ijms24087426

Ashrafizadeh, M., Hushmandi, K., Hashemi, M., Akbari, M. E., Kubatka, P., Raei, M., et al. (2020). Role of microRNA/epithelial-to-mesenchymal transition axis in the metastasis of bladder cancer. *Biomolecules* 10 (8), 1159. doi:10.3390/biom10081159

Ashrafizadeh, M., Rabiee, N., Kumar, A. P., Sethi, G., Zarrabi, A., and Wang, Y. (2022). Long noncoding RNAs (lncRNAs) in pancreatic cancer progression. *Drug Discov. Today* 27 (8), 2181–2198. doi:10.1016/j.drudis.2022.05.012

Avgeris, M., Tsilimantou, A., Levis, P. K., Tokas, T., Sideris, D. C., Stravodimos, K., et al. (2018). Loss of GAS5 tumour suppressor lncRNA: an independent molecular cancer biomarker for short-term relapse and progression in bladder cancer patients. *Br. J. cancer* 119 (12), 1477–1486. doi:10.1038/s41416-018-0320-6

Babjuk, M., Burger, M., Zigeuner, R., Shariat, S. F., van Rhijn, B. W., Compérat, E., et al. (2013). EAU guidelines on non-muscle-invasive urothelial carcinoma of the bladder: update 2013. *Eur. Urol.* 64 (4), 639–653. doi:10.1016/j.eururo.2013.06.003

Bai, T., Liu, Y., and Li, B. (2019). LncRNA LOXL1-AS1/miR-let-7a-5p/EGFR-related pathway regulates the doxorubicin resistance of prostate cancer DU-145 cells. *IUBMB life* 71 (10), 1537–1551. doi:10.1002/iub.2075

Barata, P. C., and Rini, B. I. (2017). Treatment of renal cell carcinoma: current status and future directions. *CA a cancer J. Clin.* 67 (6), 507–524. doi:10.3322/caac.21411

Barth, D. A., Juracek, J., Slaby, O., Pichler, M., and Calin, G. A. (2020). lncRNA and mechanisms of drug resistance in cancers of the genitourinary system. *Cancers* 12 (8), 2148. doi:10.3390/cancers12082148

Begolli, R., Sideris, N., and Giakountis, A. (2019). LncRNAs as chromatin regulators in cancer: from molecular function to clinical potential. *Cancers (Basel)* 11 (10), 1524. doi:10.3390/cancers11101524

Bertozzi, D., Iurlaro, R., Sordet, O., Marinello, J., Zaffaroni, N., and Capranico, G. (2011). Characterization of novel antisense HIF-1α transcripts in human cancers. *Cell cycle* 10 (18), 3189–3197. doi:10.4161/cc.10.18.17183

Bhan, A., Soleimani, M., and Mandal, S. S. (2017). Long noncoding RNA and cancer: a new paradigm. *Cancer Res.* 77 (15), 3965–3981. doi:10.1158/0008-5472.CAN-16-2634

Bhat, A. A., Goyal, A., Thapa, R., Kazmi, I., Alzarea, S. I., Singh, M., et al. (2023). Uncovering the complex role of interferon-gamma in suppressing type 2 immunity to cancer. *Cytokine* 171, 156376. doi:10.1016/j.cyto.2023.156376

Braga, E. A., Fridman, M. V., Moscovtsev, A. A., Filippova, E. A., Dmitriev, A. A., and Kushlinskii, N. E. (2020). LncRNAs in ovarian cancer progression, metastasis, and main pathways: ceRNA and alternative mechanisms. *Int. J. Mol. Sci.* 21 (22), 8855. doi:10.3390/ijms21228855

Brauch, H., Weirich, G., Brieger, J., Glavac, D., Rödl, H., Eichinger, M., et al. (2000). VHL alterations in human clear cell renal cell carcinoma: association with advanced tumor stage and a novel hot spot mutation. *Cancer Res.* 60 (7), 1942–1948.

Bray, F., Ferlay, J., Soerjomataram, I., Siegel, R. L., Torre, L. A., and Jemal, A. (2018). Global cancer statistics 2018: GLOBOCAN estimates of incidence and mortality worldwide for 36 cancers in 185 countries. *CA a cancer J. Clin.* 68 (6), 394–424. doi:10.3322/caac.21492

Bridges, M. C., Daulagala, A. C., and Kourtidis, A. (2021). LNCcation: lncRNA localization and function. *J. cell Biol.* 220 (2), e202009045. doi:10.1083/jcb.202009045

Bussemakers, M. J., van Bokhoven, A., Verhaegh, G. W., Smit, F. P., Karthaus, H. F., Schalken, J. A., et al. (1999). DD3: a new prostate-specific gene, highly overexpressed in prostate cancer. *Cancer Res.* 59 (23), 5975–5979.

Bussolati, B., Bruno, S., Grange, C., Ferrando, U., and Camussi, G. (2008). Identification of a tumor-initiating stem cell population in human renal carcinomas. *FASEB J.* 22 (10), 3696–3705. doi:10.1096/fj.08-102590

Cairns, P. (2011). Renal cell carcinoma. *Cancer biomarkers*. 9 (1-6), 461–473. doi:10.3233/CBM-2011-0176

Cao, C., Sun, G., and Liu, C. (2020a). Long non-coding RNA SNHG6 regulates the sensitivity of prostate cancer cells to paclitaxel by sponging miR-186. *Cancer Cell Int.* 20 (1), 381. doi:10.1186/s12935-020-01462-x

Cao, X., Xu, J., and Yue, D. (2018). LncRNA-SNHG16 predicts poor prognosis and promotes tumor proliferation through epigenetically silencing p21 in bladder cancer. *Cancer gene Ther.* 25 (1-2), 10–17. doi:10.1038/s41417-017-0006-x

Cao, Y., Tian, T., Li, W., Xu, H., Zhan, C., Wu, X., et al. (2020b). Long non-coding RNA in bladder cancer. *Clin. Chim. Acta* 503, 113–121. doi:10.1016/j.cca.2020.01.008

Chakravarty, D., Sboner, A., Nair, S. S., Giannopoulou, E., Li, R., Hennig, S., et al. (2014). The oestrogen receptor alpha-regulated lncRNA NEAT1 is a critical modulator of prostate cancer. *Nat. Commun.* 5 (1), 5383. doi:10.1038/ncomms6383

Chandra Gupta, S., and Nandan Tripathi, Y. (2017). Potential of long non-coding RNAs in cancer patients: from biomarkers to therapeutic targets. *Int. J. Cancer* 140 (9), 1955–1967. doi:10.1002/ijc.30546

Chandrasekar, T., Yang, J. C., Gao, A. C., and Evans, C. P. (2015). Mechanisms of resistance in castration-resistant prostate cancer (CRPC). *Transl. Androl. urology* 4 (3), 365–380. doi:10.3978/j.issn.2223-4683.2015.05.02

Chang, C. H., Cheng, T. Y., Yeh, W. W., Luo, Y. L., Campbell, M., Kuo, T. C., et al. (2023). REST-repressed lncRNA LINC01801 induces neuroendocrine differentiation in prostate cancer via transcriptional activation of autophagy. *Am. J. cancer Res.* 13 (9), 3983–4002.

Chang, L., Wang, G., Jia, T., Zhang, L., Li, Y., Han, Y., et al. (2016). Armored long non-coding RNA MEG3 targeting EGFR based on recombinant MS2 bacteriophage virus-like particles against hepatocellular carcinoma. *Oncotarget* 7, 23988–24004. doi:10.18632/oncotarget.8115

Chen, C., He, W., Huang, J., Wang, B., Li, H., Cai, Q., et al. (2018). LNMAT1 promotes lymphatic metastasis of bladder cancer via CCL2 dependent macrophage recruitment. *Nat. Commun.* 9 (1), 3826. doi:10.1038/s41467-018-06152-x

Chen, D., Wang, R., Yu, C., Cao, F., Zhang, X., Yan, F., et al. (2019). FOX-A1 contributes to acquisition of chemoresistance in human lung adenocarcinoma via transactivation of SOX5. *EBioMedicine* 44, 150–161. doi:10.1016/j.ebiom.2019.05.046

Chen, H., Han, Z., Su, J., Song, X., Ma, Q., Lin, Y., et al. (2024a). Ferroptosis and hepatocellular carcinoma: the emerging role of lncRNAs. *Front. Immunol.* 15, 1424954. doi:10.3389/fimmu.2024.1424954

Chen, J., Li, Y., Li, Z., and Cao, L. (2020b). LncRNA MST1P2/miR-133b axis affects the chemoresistance of bladder cancer to cisplatin-based therapy via Sirt1/p53 signaling. *J. Biochem. Mol. Toxicol.* 34 (4), e22452. doi:10.1002/jbt.22452

Chen, M., Zhuang, C., Liu, Y., Li, J., Dai, F., Xia, M., et al. (2016a). Tetracycline-inducible shRNA targeting antisense long non-coding RNA HIF1A-AS2 represses the malignant phenotypes of bladder cancer. *Cancer Lett.* 376 (1), 155–164. doi:10.1016/j.canlet.2016.03.037

Chen, P. A., Chang, P. C., Yeh, W. W., Hu, T. Y., Hong, Y. C., Wang, Y. C., et al. (2024b). The lncRNA TPT1-AS1 promotes the survival of neuroendocrine prostate cancer cells by facilitating autophagy. *Am. J. cancer Res.* 14 (5), 2103–2123. doi:10.62347/IMBV8599

Chen, S., Zhu, J., Wang, F., Guan, Z., Ge, Y., Yang, X., et al. (2017). LncRNAs and their role in cancer stem cells. *Oncotarget* 8 (66), 110685–110692. doi:10.18632/oncotarget.22161

Chen, T., Xie, W., Xie, L., Sun, Y., Zhang, Y., Shen, Z., et al. (2015). Expression of long noncoding RNA lncRNA-n336928 is correlated with tumor stage and grade and overall survival in bladder cancer. *Biochem. biophysical Res. Commun.* 468 (4), 666–670. doi:10.1016/j.bbrc.2015.11.013

Chen, W., Yu, Z., Huang, W., Yang, Y., Wang, F., and Huang, H. (2020a). LncRNA LINC00665 promotes prostate cancer progression via miR-1224-5p/SND1 Axis. *OncoTargets Ther.* 13, 2527–2535. doi:10.2147/OTT.S241578

Chen, Y.-S., Xu, Y.-P., Liu, W.-H., Li, D.-C., Wang, H., and Li, C.-F. (2021). Long noncoding RNA KCNMB2-AS1 promotes SMAD5 by targeting miR-3194-3p to induce bladder cancer progression. *Front. Oncol.* 11, 649778. doi:10.3389/fonc.2021.649778

Chen, Z., Liu, Y., He, A., Li, J., Chen, M., Zhan, Y., et al. (2016b). Theophylline controllable RNAi-based genetic switches regulate expression of lncRNA TINCR and malignant phenotypes in bladder cancer cells. *Sci. Rep.* 6 (1), 30798. doi:10.1038/srep30798

Chen, Z., Liu, Y., He, A., Li, J., Chen, M., Zhan, Y., et al. (2016c). Theophylline controllable RNAi-based genetic switches regulate expression of lncRNA TINCR and malignant phenotypes in bladder cancer cells. *Sci. Rep.* 6, 30798. doi:10.1038/srep30798

Chen, Z., Pan, T., Jiang, D., Jin, L., Geng, Y., Feng, X., et al. (2020c). The lncRNA-GAS5/miR-221-3p/DKK2 Axis modulates ABCB1-mediated adriamycin resistance of breast cancer via the wnt/β-catenin signaling pathway. *Mol. Therapy-Nucleic Acids* 19, 1434–1448. doi:10.1016/j.omtn.2020.01.030

Cheng, X. B., Zhang, T., Zhu, H. J., Ma, N., Sun, X. D., Wang, S. H., et al. (2021). Knockdown of lncRNA SNHG4 suppresses gastric cancer cell proliferation and metastasis by targeting miR-204-5p. *Neoplasma* 68 (3), 546–556. doi:10.4149/neo_2021_200914n981

Connerty, P., Lock, R. B., and De Bock, C. E. (2020). Long non-coding RNAs: major regulators of cell stress in cancer. *Front. Oncol.* 10, 285. doi:10.3389/fonc.2020.00285

Corro, C., and Moch, H. (2018). Biomarker discovery for renal cancer stem cells. *J. Pathology Clin. Res.* 4 (1), 3–18. doi:10.1002/cjp2.91

Courtney, K. D., and Choueiri, T. K. (2010). Updates on novel therapies for metastatic renal cell carcinoma. *Ther. Adv. Med. Oncol.* 2 (3), 209–219. doi:10.1177/1758834010361470

Cui, Z., Ren, S., Lu, J., Wang, F., Xu, W., Sun, Y., et al. (2013). "The prostate cancer-up-regulated long noncoding RNA PlncRNA-1 modulates apoptosis and proliferation through reciprocal regulation of androgen receptor," in *Urologic oncology: seminars and original investigations* (Elsevier), 1117–1123.

Dai, X., Fang, M., Li, S., Yan, Y., Zhong, Y., and Du, B. (2017). miR-21 is involved in transforming growth factor β1-induced chemoresistance and invasion by targeting PTEN in breast cancer. *Oncol. Lett.* 14 (6), 6929–6936. doi:10.3892/ol.2017.7007

Dasgupta, P., Kulkarni, P., Majid, S., Shahryari, V., Hashimoto, Y., Bhat, N. S., et al. (2018). MicroRNA-203 inhibits long noncoding RNA HOTAIR and regulates tumorigenesis through epithelial-to-mesenchymal transition pathway in renal cell carcinoma. *Mol. cancer Ther.* 17 (5), 1061–1069. doi:10.1158/1535-7163.MCT-17-0925

Datta, A., Deng, S., Gopal, V., Yap, K. C.-H., Halim, C. E., Lye, M. L., et al. (2021). Cytoskeletal dynamics in epithelial-mesenchymal transition: insights into therapeutic targets for cancer metastasis. *Cancers* 13 (8), 1882. doi:10.3390/cancers13081882

Deng, X., Liao, T., Xie, J., Kang, D., He, Y., Sun, Y., et al. (2024). The burgeoning importance of PIWI-interacting RNAs in cancer progression. *Sci. China Life Sci.* 67 (4), 653–662. doi:10.1007/s11427-023-2491-7

Ding, L., Wang, R., Shen, D., Cheng, S., Wang, H., Lu, Z., et al. (2021). Role of noncoding RNA in drug resistance of prostate cancer. *Cell death and Dis.* 12 (6), 590. doi:10.1038/s41419-021-03854-x

Dong, Q., Qiu, H., Piao, C., Li, Z., and Cui, X. (2023). LncRNA SNHG4 promotes prostate cancer cell survival and resistance to enzalutamide through a let-7a/RREB1 positive feedback loop and a ceRNA network. *J. Exp. and Clin. cancer Res. CR* 42 (1), 209. doi:10.1186/s13046-023-02774-2

Du, L., Zhang, L., and Sun, F. (2022). Puerarin inhibits the progression of bladder cancer by regulating circ_0020394/miR-328-3p/NRBP1 axis. *Cancer Biotherapy and Radiopharm.* 37 (6), 435–450. doi:10.1089/cbr.2019.3382

Duan, W., Du, L., Jiang, X., Wang, R., Yan, S., Xie, Y., et al. (2016). Identification of a serum circulating lncRNA panel for the diagnosis and recurrence prediction of bladder cancer. *Oncotarget* 7 (48), 78850–78858. doi:10.18632/oncotarget.12880

Dudek, A. M., van Kampen, J. G. M., Witjes, J. A., Kiemeney, L., and Verhaegh, G. W. (2018). *LINC* expression predicts and mediates the response to platinum-based chemotherapy in muscle-invasive bladder cancer. *Cancer Med.* 7 (7), 3342–3350. doi:10.1002/cam4.1570

Edgar, J. R. (2016). Q&: what are exosomes, exactly? *BMC Biol.* 14, 46–47. doi:10.1186/s12915-016-0268-z

Efstathiou, E., Abrahams, N. A., Tibbs, R. F., Wang, X., Pettaway, C. A., Pisters, L. L., et al. (2010). Morphologic characterization of preoperatively treated prostate cancer: toward a post-therapy histologic classification. *Eur. Urol.* 57 (6), 1030–1038. doi:10.1016/j.eururo.2009.10.020

Efstathiou, E., and Logothetis, C. J. (2010). A new therapy paradigm for prostate cancer founded on clinical observations. *Clin. cancer Res. official J. Am. Assoc. Cancer Res.* 16 (4), 1100–1107. doi:10.1158/1078-0432.CCR-09-1215

Eißmann, M., Gutschner, T., Hämmerle, M., Günther, S., Caudron-Herger, M., Groß, M., et al. (2012). Loss of the abundant nuclear non-coding RNA MALAT1 is compatible with life and development. *RNA Biol.* 9 (8), 1076–1087. doi:10.4161/rna.21089

Eke, I., Bylicky, M. A., Sandfort, V., Chopra, S., Martello, S., Graves, E. E., et al. (2021). The lncRNAs LINC00261 and LINC00665 are upregulated in long-term prostate cancer adaptation after radiotherapy. *Mol. Ther. Nucleic acids* 24, 175–187. doi:10.1016/j.omtn.2021.02.024

Eli, S., Castagna, R., Mapelli, M., and Parisini, E. (2022). Recent approaches to the identification of novel microtubule-targeting agents. *Front. Mol. Biosci.* 9, 841777. doi:10.3389/fmolb.2022.841777

Ellinger, J., Alam, J., Rothenburg, J., Deng, M., Schmidt, D., Syring, I., et al. (2015). The long non-coding RNA lnc-ZNF180-2 is a prognostic biomarker in patients with clear cell renal cell carcinoma. *Am. J. cancer Res.* 5 (9), 2799–2807.

Engreitz, J. M., Haines, J. E., Perez, E. M., Munson, G., Chen, J., Kane, M., et al. (2016). Local regulation of gene expression by lncRNA promoters, transcription and splicing. *Nature* 539 (7629), 452–455. doi:10.1038/nature20149

Entezari, M., Ghanbarirad, M., Taheriazam, A., Sadrkhanloo, M., Zabolian, A., Goharrizi, MASB, et al. (2022). Long non-coding RNAs and exosomal lncRNAs: potential functions in lung cancer progression, drug resistance and tumor microenvironment remodeling. *Biomed. and Pharmacother.* 150, 112963. doi:10.1016/j.biopha.2022.112963

Epstein, J. I., Amin, M. B., Reuter, V. R., Mostofi, F. K., and Committee, B. C. C. (1998). The world health organization/international society of urological pathology consensus classification of urothelial (transitional cell) neoplasms of the urinary bladder. Bladder consensus conference committee. *Am. J. Surg. pathology* 22 (12), 1435–1448. doi:10.1097/00000478-199812000-00001

Fan, Y., Shen, B., Tan, M., Mu, X., Qin, Y., Zhang, F., et al. (2014a). Long non-coding RNA UCA1 increases chemoresistance of bladder cancer cells by regulating Wnt signaling. *Febs J.* 281 (7), 1750–1758. doi:10.1111/febs.12737

Fan, Y., Shen, B., Tan, M., Mu, X., Qin, Y., Zhang, F., et al. (2014b). TGF-β-induced upregulation of malat1 promotes bladder cancer metastasis by associating with suz12. *Clin. cancer Res.* 20 (6), 1531–1541. doi:10.1158/1078-0432.CCR-13-1455

Feng, S. Q., Zhang, X. Y., Fan, H. T., Sun, Q. J., and Zhang, M. (2018). Up-regulation of LncRNA MEG3 inhibits cell migration and invasion and enhances cisplatin chemosensitivity in bladder cancer cells. *Neoplasma* 65 (6), 925–932. doi:10.4149/neo_2018_180125N55

Ferlay, J., Steliarova-Foucher, E., Lortet-Tieulent, J., Rosso, S., Coebergh, J.-W. W., Comber, H., et al. (2013). Cancer incidence and mortality patterns in Europe: estimates for 40 countries in 2012. *Eur. J. cancer* 49 (6), 1374–1403. doi:10.1016/j.ejca.2012.12.027

Fizazi, K., Tran, N., Fein, L., Matsubara, N., Rodriguez-Antolin, A., Alekseev, B. Y., et al. (2017). Abiraterone plus prednisone in metastatic, castration-sensitive prostate cancer. *N. Engl. J. Med.* 377 (4), 352–360. doi:10.1056/NEJMoa1704174

Froberg, J. E., Yang, L., and Lee, J. T. (2013). Guided by RNAs: X-inactivation as a model for lncRNA function. *J. Mol. Biol.* 425 (19), 3698–3706. doi:10.1016/j.jmb.2013.06.031

Gao, Z. Q., Wang, J. F., Chen, D. H., Ma, X. S., Yang, W., Zhe, T., et al. (2018). Long non-coding RNA GAS5 antagonizes the chemoresistance of pancreatic cancer cells through down-regulation of miR-181c-5p. *Biomed. and Pharmacother. = Biomedecine and Pharmacother.* 97, 809–817. doi:10.1016/j.biopha.2017.10.157

Gezer, U., Özgür, E., Cetinkaya, M., Isin, M., and Dalay, N. (2014). Long non-coding RNAs with low expression levels in cells are enriched in secreted exosomes. *Cell Biol. Int.* 38 (9), 1076–1079. doi:10.1002/cbin.10301

Gibb, E. A., Brown, C. J., and Lam, W. L. (2011). The functional role of long non-coding RNA in human carcinomas. *Mol. cancer* 10 (1), 38–17. doi:10.1186/1476-4598-10-38

Gleason, D. F. (1966). Classification of prostatic carcinomas. *Cancer Chemother. Rep.* 50 (3), 125–128.

Gleason, D. F., and Mellinger, G. T. (1974). Prediction of prognosis for prostatic adenocarcinoma by combined histological grading and clinical staging. *J. urology* 111 (1), 58–64. doi:10.1016/s0022-5347(17)59889-4

Gofrit, O. N., Benjamin, S., Halachmi, S., Leibovitch, I., Dotan, Z., Lamm, D. L., et al. (2014). DNA based therapy with diphtheria toxin-A BC-819: a phase 2b marker lesion trial in patients with intermediate risk nonmuscle invasive bladder cancer. *J. urology* 191 (6), 1697–1702. doi:10.1016/j.juro.2013.12.011

Gonzalez, I., Munita, R., Agirre, E., Dittmer, T. A., Gysling, K., Misteli, T., et al. (2015). A lncRNA regulates alternative splicing via establishment of a splicing-specific chromatin signature. *Nat. Struct. and Mol. Biol.* 22 (5), 370–376. doi:10.1038/nsmb.3005

Gramantieri, L., Baglioni, M., Fornari, F., Laginestra, M. A., Ferracin, M., Indio, V., et al. (2018). LncRNAs as novel players in hepatocellular carcinoma recurrence. *Oncotarget* 9 (80), 35085–35099. doi:10.18632/oncotarget.26202

Grange, C., Brossa, A., and Bussolati, B. (2019). Extracellular vesicles and carried miRNAs in the progression of renal cell carcinoma. *Int. J. Mol. Sci.* 20 (8), 1832. doi:10.3390/ijms20081832

Grange, C., Collino, F., Tapparo, M., and Camussi, G. (2014). Oncogenic micro-RNAs and renal cell carcinoma. *Front. Oncol.* 4, 49. doi:10.3389/fonc.2014.00049

Graves, A., Hessamodini, H., Wong, G., and Lim, W. H. (2013). Metastatic renal cell carcinoma: update on epidemiology, genetics, and therapeutic modalities. *ImmunoTargets Ther.* 2, 73–90. doi:10.2147/ITT.S31426

Gravis, G., Fizazi, K., Joly, F., Oudard, S., Priou, F., Esterni, B., et al. (2013). Androgen-deprivation therapy alone or with docetaxel in non-castrate metastatic prostate cancer (GETUG-AFU 15): a randomised, open-label, phase 3 trial. *Lancet Oncol.* 14 (2), 149–158. doi:10.1016/S1470-2045(12)70560-0

Grote, P., Wittler, L., Hendrix, D., Koch, F., Währisch, S., Beisaw, A., et al. (2013). The tissue-specific lncRNA Fendrr is an essential regulator of heart and body wall development in the mouse. *Dev. cell* 24 (2), 206–214. doi:10.1016/j.devcel.2012.12.012

Gu, P., Chen, X., Xie, R., Han, J., Xie, W., Wang, B., et al. (2017). lncRNA HOXD-AS1 regulates proliferation and chemo-resistance of castration-resistant prostate cancer via recruiting WDR5. *Mol. Ther.* 25 (8), 1959–1973. doi:10.1016/j.ymthe.2017.04.016

Guo, C. J., Xu, G., and Chen, L. L. (2020). Mechanisms of long noncoding RNA nuclear retention. *Trends Biochem. Sci.* 45 (11), 947–960. doi:10.1016/j.tibs.2020.07.001

Gupta, R. A., Shah, N., Wang, K. C., Kim, J., Horlings, H. M., Wong, D. J., et al. (2010). Long non-coding RNA HOTAIR reprograms chromatin state to promote cancer metastasis. *nature* 464 (7291), 1071–1076. doi:10.1038/nature08975

Gutschner, T., Hämmerle, M., Eissmann, M., Hsu, J., Kim, Y., Hung, G., et al. (2013). The noncoding RNA MALAT1 is a critical regulator of the metastasis phenotype of lung cancer cells. *Cancer Res.* 73 (3), 1180–1189. doi:10.1158/0008-5472.CAN-12-2850

Haghighi, R., Castillo-Acobo, R. Y., H Amin, A., Ehymayed, H. M., Alhili, F., Mirzaei, M., et al. (2023). A thorough understanding of the role of lncRNA in prostate cancer pathogenesis; Current knowledge and future research directions. *Pathology - Res. Pract.* 248, 154666. doi:10.1016/j.prp.2023.154666

Hakenberg, O. W., Compérat, E. M., Minhas, S., Necchi, A., Protzel, C., and Watkin, N. (2015). EAU guidelines on penile cancer: 2014 update. *Eur. Urol.* 67 (1), 142–150. doi:10.1016/j.eururo.2014.10.017

Han, T.-S., Hur, K., Cho, H.-S., and Ban, H. S. (2020). Epigenetic associations between lncRNA/circRNA and miRNA in hepatocellular carcinoma. *Cancers* 12 (9), 2622. doi:10.3390/cancers12092622

Hanly, D. J., Esteller, M., and Berdasco, M. (2018). Interplay between long non-coding RNAs and epigenetic machinery: emerging targets in cancer? *Philosophical Trans. R. Soc. B Biol. Sci.* 373 (1748), 20170074. doi:10.1098/rstb.2017.0074

Hara, T., Makino, T., Yamasaki, M., Tanaka, K., Miyazaki, Y., Takahashi, T., et al. (2019). Effect of c-Met and CD44v6 expression in resistance to chemotherapy in esophageal squamous cell carcinoma. *Ann. Surg. Oncol.* 26, 899–906. doi:10.1245/s10434-018-07126-5

Harding, C., Heuser, J., and Stahl, P. (1983). Receptor-mediated endocytosis of transferrin and recycling of the transferrin receptor in rat reticulocytes. *J. cell Biol.* 97 (2), 329–339. doi:10.1083/jcb.97.2.329

He, A., Chen, Z., Mei, H., and Liu, Y. (2016a). Decreased expression of LncRNA MIR31HG in human bladder cancer. *Cancer Biomarkers* 17 (2), 231–236. doi:10.3233/CBM-160635

He, A., Liu, Y., Chen, Z., Li, J., Chen, M., Liu, L., et al. (2016b). Over-expression of long noncoding RNA BANCR inhibits malignant phenotypes of human bladder cancer. *J. Exp. and Clin. Cancer Res.* 35, 125–127. doi:10.1186/s13046-016-0397-9

He, J., Sun, M., Geng, H., and Tian, S. (2019). Long non-coding RNA Linc00518 promotes paclitaxel resistance of the human prostate cancer by sequestering miR-216b-5p. *Biol. Cell* 111 (2), 39–50. doi:10.1111/boc.201800054

He, W., Cai, Q., Sun, F., Zhong, G., Wang, P., Liu, H., et al. (2013). linc-UBC1 physically associates with polycomb repressive complex 2 (PRC2) and acts as a negative prognostic factor for lymph node metastasis and survival in bladder cancer. *Biochimica Biophysica Acta (BBA)-Molecular Basis Dis.* 1832 (10), 1528–1537. doi:10.1016/j.bbadis.2013.05.010

He, W., Zhong, G., Jiang, N., Wang, B., Fan, X., Chen, C., et al. (2018a). Long noncoding RNA BLACAT2 promotes bladder cancer–associated lymphangiogenesis and lymphatic metastasis. *J. Clin. investigation* 128 (2), 861–875. doi:10.1172/JCI96218

He, Z. H., Qin, X. H., Zhang, X. L., Yi, J. W., and Han, J. Y. (2018b). Long noncoding RNA GIHCG is a potential diagnostic and prognostic biomarker and therapeutic target for renal cell carcinoma. *Eur. Rev. Med. Pharmacol. Sci.* 22 (1), 46–54. doi:10.26355/eurrev_201801_14099

Hensley, P. J., Panebianco, V., Pietzak, E., Kutikov, A., Vikram, R., Galsky, M. D., et al. (2022). Contemporary staging for muscle-invasive bladder Cancer: accuracy and limitations. *Eur. Urol. Oncol.* 5 (4), 403–411. doi:10.1016/j.euo.2022.04.008

Herr, H. W., Dotan, Z., Donat, S. M., and Bajorin, D. F. (2007). Defining optimal therapy for muscle invasive bladder cancer. *J. urology* 177 (2), 437–443. doi:10.1016/j.juro.2006.09.027

Hirose, T., Virnicchi, G., Tanigawa, A., Naganuma, T., Li, R., Kimura, H., et al. (2014). NEAT1 long noncoding RNA regulates transcription via protein sequestration within subnuclear bodies. *Mol. Biol. cell* 25 (1), 169–183. doi:10.1091/mbc.E13-09-0558

Howard, N., Clementino, M., Kim, D., Wang, L., Verma, A., Shi, X., et al. (2019). New developments in mechanisms of prostate cancer progression. *Seminars Cancer Biol.* 57, 111–116. doi:10.1016/j.semcancer.2018.09.003

Huang, Q., Yan, J., and Agami, R. (2018). Long non-coding RNAs in metastasis. *Cancer metastasis Rev.* 37 (1), 75–81. doi:10.1007/s10555-017-9713-x

Huarte, M. (2015). The emerging role of lncRNAs in cancer. *Nat. Med.* 21 (11), 1253–1261. doi:10.1038/nm.3981

Huggins, C., and Hodges, C. V. (1941). Studies on prostatic cancer. *Cancer Res.* 1 (4), 9–12. doi:10.1097/00005392-200207000-00004

Hussain, M. S., Majami, A. A., Ali, H., Kumar, G., Almalki, W. H., Alzarea, S. I., et al. (2023). The complex role of MEG3: an emerging long non-coding RNA in breast cancer. *Pathology-Research Pract.* 251, 154850. doi:10.1016/j.prp.2023.154850

Iliev, R., Kleinova, R., Juracek, J., Dolezel, J., Ozanova, Z., Fedorko, M., et al. (2016). Overexpression of long non-coding RNA TUG1 predicts poor prognosis and promotes cancer cell proliferation and migration in high-grade muscle-invasive bladder cancer. *Tumor Biol.* 37, 13385–13390. doi:10.1007/s13277-016-5177-9

Jalali, S., Jayaraj, G. G., and Scaria, V. (2012). Integrative transcriptome analysis suggest processing of a subset of long non-coding RNAs to small RNAs. *Biol. direct* 7, 25–13. doi:10.1186/1745-6150-7-25

James, N. D., de Bono, J. S., Spears, M. R., Clarke, N. W., Mason, M. D., Dearnaley, D. P., et al. (2017). Abiraterone for prostate cancer not previously treated with hormone therapy. *N. Engl. J. Med.* 377 (4), 338–351. doi:10.1056/NEJMoa1702900

James, N. D., Sydes, M. R., Clarke, N. W., Mason, M. D., Dearnaley, D. P., Spears, M. R., et al. (2016). Addition of docetaxel, zoledronic acid, or both to first-line long-term hormone therapy in prostate cancer (STAMPEDE): survival results from an adaptive, multiarm, multistage, platform randomised controlled trial. *Lancet* 387 (10024), 1163–1177. doi:10.1016/S0140-6736(15)01037-5

Jarlstad, S. (2021). Kristensen L: circular RNAs as microRNA sponges: evidence and controversies. *Essays Biochem.* 65 (4), 685–696. doi:10.1042/ebc20200060

Ji, P., Diederichs, S., Wang, W., Böing, S., Metzger, R., Schneider, P. M., et al. (2003). MALAT-1, a novel noncoding RNA, and thymosin beta4 predict metastasis and survival in early-stage non-small cell lung cancer. *Oncogene* 22 (39), 8031–8041. doi:10.1038/sj.onc.1206928

Jiang, H., Hu, X., Zhang, H., and Li, W. (2017a). Down-regulation of LncRNA TUG1 enhances radiosensitivity in bladder cancer via suppressing HMGB1 expression. *Radiat. Oncol. Lond. Engl.* 12 (1), 65. doi:10.1186/s13014-017-0802-3

Jiang, H., Hu, X., Zhang, H., and Li, W. (2017b). Down-regulation of LncRNA TUG1 enhances radiosensitivity in bladder cancer via suppressing HMGB1 expression. *Radiat. Oncol.* 12 (1), 65–10. doi:10.1186/s13014-017-0802-3

Jiang, W., Pan, S., Chen, X., Wang, Z.-w., and Zhu, X. (2021). The role of lncRNAs and circRNAs in the PD-1/PD-L1 pathway in cancer immunotherapy. *Mol. cancer* 20 (1), 116–117. doi:10.1186/s12943-021-01406-7

Jiang, X., Guo, S., Zhang, Y., Zhao, Y., Li, X., Jia, Y., et al. (2020). LncRNA NEAT1 promotes docetaxel resistance in prostate cancer by regulating ACSL4 via sponging miR-34a-5p and miR-204-5p. *Cell. Signal.* 65, 109422. doi:10.1016/j.cellsig.2019.109422

Jiao, D., Li, Z., Zhu, M., Wang, Y., Wu, G., and Han, X. (2018). LncRNA MALAT1 promotes tumor growth and metastasis by targeting miR-124/foxq1 in bladder transitional cell carcinoma (BTCC). *Am. J. cancer Res.* 8 (4), 748–760.

Jin, Y., Cui, Z., Li, X., Jin, X., and Peng, J. (2017). Upregulation of long non-coding RNA PlncRNA-1 promotes proliferation and induces epithelial-mesenchymal transition in prostate cancer. *Oncotarget* 8 (16), 26090–26099. doi:10.18632/oncotarget.15318

Khan, M. T., Yang, L., More, E., Irlam-Jones, J. J., Valentine, H. R., Hoskin, P., et al. (2021). Developing tumor radiosensitivity signatures using LncRNAs. *Radiat. Res.* 195 (4), 324–333. doi:10.1667/RADE-20-00157.1

Kim, D. H., Marinov, G. K., Pepke, S., Singer, Z. S., He, P., Williams, B., et al. (2015). Single-cell transcriptome analysis reveals dynamic changes in lncRNA expression during reprogramming. *Cell stem cell* 16 (1), 88–101. doi:10.1016/j.stem.2014.11.005

Kim, H. S., Kim, J. H., Jang, H. J., Han, B., and Zang, D. Y. (2018). Clinicopathologic significance of VHL gene alteration in clear-cell renal cell carcinoma: an updated meta-analysis and review. *Int. J. Mol. Sci.* 19 (9), 2529. doi:10.3390/ijms19092529

Kim, J. J., and Tannock, I. F. (2005). Repopulation of cancer cells during therapy: an important cause of treatment failure. *Nat. Rev. Cancer* 5 (7), 516–525. doi:10.1038/nrc1650

Kim, L. C., Song, L., and Haura, E. B. (2009). Src kinases as therapeutic targets for cancer. *Nat. Rev. Clin. Oncol.* 6 (10), 587–595. doi:10.1038/nrclinonc.2009.129

Kim, T.-K., Hemberg, M., Gray, J. M., Costa, A. M., Bear, D. M., Wu, J., et al. (2010). Widespread transcription at neuronal activity-regulated enhancers. *Nature* 465 (7295), 182–187. doi:10.1038/nature09033

Kirby, M., Hirst, C., and Crawford, E. (2011). Characterising the castration-resistant prostate cancer population: a systematic review. *Int. J. Clin. Pract.* 65 (11), 1180–1192. doi:10.1111/j.1742-1241.2011.02799.x

Klec, C., Prinz, F., and Pichler, M. (2019). Involvement of the long noncoding RNA NEAT1 in carcinogenesis. *Mol. Oncol.* 13 (1), 46–60. doi:10.1002/1878-0261.12404

Kogure, T., Yan, I. K., Lin, W. L., and Patel, T. (2013). Extracellular vesicle-mediated transfer of a novel long noncoding RNA TUC339: a mechanism of intercellular signaling in human hepatocellular cancer. *Genes and cancer* 4 (7-8), 261–272. doi:10.1177/1947601913499020

Kong, Y. L., Wang, H. D., Gao, M., Rong, S. Z., and Li, X. X. (2024). LncRNA XIST promotes bladder cancer progression by modulating miR-129-5p/TNFSF10 axis. *Discov. Oncol.* 15 (1), 65. doi:10.1007/s12672-024-00910-8

Konishi, H., Ichikawa, D., Yamamoto, Y., Arita, T., Shoda, K., Hiramoto, H., et al. (2016). Plasma level of metastasis-associated lung adenocarcinoma transcript 1 is associated with liver damage and predicts development of hepatocellular carcinoma. *Cancer Sci.* 107 (2), 149–154. doi:10.1111/cas.12854

Kurtis, B., Zhuge, J., Ojaimi, C., Ye, F., Cai, D., Zhang, D., et al. (2016). Recurrent TERT promoter mutations in urothelial carcinoma and potential clinical applications. *Ann. diagnostic pathology* 21, 7–11. doi:10.1016/j.anndiagpath.2015.12.002

Kurtova, A. V., Xiao, J., Mo, Q., Pazhanisamy, S., Krasnow, R., Lerner, S. P., et al. (2015). Blocking PGE2-induced tumour repopulation abrogates bladder cancer chemoresistance. *Nature* 517 (7533), 209–213. doi:10.1038/nature14034

Lambert, S. A., Jolma, A., Campitelli, L. F., Das, P. K., Yin, Y., Albu, M., et al. (2018). The human transcription factors. *Cell* 172 (4), 650–665. doi:10.1016/j.cell.2018.01.029

Lavorgna, G., Chiacchiera, F., Briganti, A., Montorsi, F., Pasini, D., and Salonia, A. (2015). Expression-profiling of apoptosis induced by ablation of the long ncRNA TRPM2-AS in prostate cancer cell. *Genomics data* 3, 4–5. doi:10.1016/j.gdata.2014.10.020

Lawrence, M. S., Stojanov, P., Polak, P., Kryukov, G. V., Cibulskis, K., Sivachenko, A., et al. (2013). Mutational heterogeneity in cancer and the search for new cancer-associated genes. *Nature* 499 (7457), 214–218. doi:10.1038/nature12213

Leão, R., Lee, D., Figueiredo, A., Hermanns, T., Wild, P., Komosa, M., et al. (2019). Combined genetic and epigenetic alterations of the TERT promoter affect clinical and biological behavior of bladder cancer. *Int. J. cancer* 144 (7), 1676–1684. doi:10.1002/ijc.31935

Lee, B., Mazar, J., Aftab, M. N., Qi, F., Shelley, J., Li, J. L., et al. (2014). Long noncoding RNAs as putative biomarkers for prostate cancer detection. *J. Mol. diagnostics JMD* 16 (6), 615–626. doi:10.1016/j.jmoldx.2014.06.009

Lee, T. K.-W., Guan, X.-Y., and Ma, S. (2022). Cancer stem cells in hepatocellular carcinoma—from origin to clinical implications. *Nat. Rev. Gastroenterology and Hepatology* 19 (1), 26–44. doi:10.1038/s41575-021-00508-3

Lemos, A. E., Ferreira, L. B., Batoreu, N. M., de Freitas, P. P., Bonamino, M. H., and Gimba, E. R. (2016). PCA3 long noncoding RNA modulates the expression of key cancer-related genes in LNCaP prostate cancer cells. *Tumour Biol. J. Int. Soc. Oncodevelopmental Biol. Med.* 37 (8), 11339–11348. doi:10.1007/s13277-016-5012-3

Li, B., Xie, D., and Zhang, H. (2019b). Long non-coding RNA GHET1 contributes to chemotherapeutic resistance to Gemcitabine in bladder cancer. *Cancer Chemother. Pharmacol.* 84, 187–194. doi:10.1007/s00280-019-03873-8

Li, C., Cui, Y., Liu, L.-F., Ren, W.-B., Li, Q.-Q., Zhou, X., et al. (2017). High expression of long noncoding RNA MALAT1 indicates a poor prognosis and promotes clinical progression and metastasis in bladder cancer. *Clin. Genitourin. cancer* 15 (5), 570–576. doi:10.1016/j.clgc.2017.05.001

Li, D., Li, C., Chen, Y., Teng, L., Cao, Y., Wang, W., et al. (2020c). LncRNA HOTAIR induces sunitinib resistance in renal cancer by acting as a competing endogenous RNA to regulate autophagy of renal cells. *Cancer Cell Int.* 20, 338. doi:10.1186/s12935-020-01419-0

Li, J., Du, H., Chen, W., Qiu, M., He, P., and Ma, Z. (2021). Identification of potential autophagy-associated lncRNA in prostate cancer. *Aging (Albany NY)* 13 (9), 13153–13165. doi:10.18632/aging.202997

Li, J., Zhuang, C., Liu, Y., Chen, M., Zhou, Q., Chen, Z., et al. (2016b). shRNA targeting long non-coding RNA CCAT2 controlled by tetracycline-inducible system inhibits progression of bladder cancer cells. *Oncotarget* 7 (20), 28989–28997. doi:10.18632/oncotarget.8259

Li, K., Yao, T., and Wang, Z. (2023a). lncRNA-mediated ceRNA network in bladder cancer. *Non-coding RNA Res.* 8 (2), 135–145. doi:10.1016/j.ncrna.2022.12.002

Li, L., and Chang, H. Y. (2014). Physiological roles of long noncoding RNAs: insight from knockout mice. *Trends cell Biol.* 24 (10), 594–602. doi:10.1016/j.tcb.2014.06.003

Li, L.-J., Zhu, J.-L., Bao, W.-S., Chen, D.-K., Huang, W.-W., and Weng, Z.-L. (2014). Long noncoding RNA GHET1 promotes the development of bladder cancer. *Int. J. Clin. Exp. pathology* 7 (10), 7196–7205.

Li, W., Notani, D., and Rosenfeld, M. G. (2016a). Enhancers as non-coding RNA transcription units: recent insights and future perspectives. *Nat. Rev. Genet.* 17 (4), 207–223. doi:10.1038/nrg.2016.4

Li, X., Han, X., Wei, P., Yang, J., and Sun, J. (2020b). Knockdown of lncRNA CCAT1 enhances sensitivity of paclitaxel in prostate cancer via regulating miR-24-3p and FSCN1. *Cancer Biol. and Ther.* 21 (5), 452–462. doi:10.1080/15384047.2020.1727700

Li, Y., Qiao, L., Zang, Y., Ni, W., and Xu, Z. (2020a). *Circular RNA FOXO3 suppresses bladder cancer progression and metastasis by regulating MiR-9-5p/TGFBR2.* Cancer Manag. Res., 5049–5056. doi:10.2147/CMAR.S253412

Li, Y., Shi, B., Dong, F., Zhu, X., Liu, B., and Liu, Y. (2019a). Long non-coding RNA DLEU1 promotes cell proliferation, invasion, and confers cisplatin resistance in bladder cancer by regulating the miR-99b/HS3ST3B1 Axis. *Front. Genet.* 10, 280. doi:10.3389/fgene.2019.00280

Li, Z., Fu, H., Liu, J., Song, W., Zeng, M., and Wang, J. (2023b). LncRNA PVT1 promotes bladder cancer progression by forming a positive feedback loop with STAT5B. *Pathology, Res. Pract.* 248, 154635. doi:10.1016/j.prp.2023.154635

Liang, W.-C., Fu, W.-M., Wong, C.-W., Wang, Y., Wang, W.-M., Hu, G.-X., et al. (2015). The lncRNA H19 promotes epithelial to mesenchymal transition by functioning as miRNA sponges in colorectal cancer. *Oncotarget* 6 (26), 22513–22525. doi:10.18632/oncotarget.4154

Lin, H. P., Wang, Z., and Yang, C. (2021). LncRNA DUXAP10 upregulation and the hedgehog pathway activation are critically involved in chronic cadmium exposure-induced cancer stem cell-like property. *Toxicol. Sci. official J. Soc. Toxicol.* 184 (1), 33–45. doi:10.1093/toxsci/kfab099

Lin, R., Maeda, S., Liu, C., Karin, M., and Edgington, T. S. (2007). A large noncoding RNA is a marker for murine hepatocellular carcinomas and a spectrum of human carcinomas. *Oncogene* 26 (6), 851–858. doi:10.1038/sj.onc.1209846

Lin, R., Roychowdhury-Saha, M., Black, C., Watt, A. T., Marcusson, E. G., Freier, S. M., et al. (2011). Control of RNA processing by a large non-coding RNA over-expressed in carcinomas. *FEBS Lett.* 585 (4), 671–676. doi:10.1016/j.febslet.2011.01.030

Ling, H., Spizzo, R., Atlasi, Y., Nicoloso, M., Shimizu, M., Redis, R. S., et al. (2013). CCAT2, a novel noncoding RNA mapping to 8q24, underlies metastatic progression and chromosomal instability in colon cancer. *Genome Res.* 23 (9), 1446–1461. doi:10.1101/gr.152942.112

Liu, B., Xiang, W., Liu, J., Tang, J., Wang, J., Liu, B., et al. (2021a). The regulatory role of antisense lncRNAs in cancer. *Cancer cell Int.* 21 (1), 459–515. doi:10.1186/s12935-021-02168-4

Liu, D., Li, Y., Luo, G., Xiao, X., Tao, D., Wu, X., et al. (2017a). LncRNA SPRY4-IT1 sponges miR-101-3p to promote proliferation and metastasis of bladder cancer cells through up-regulating EZH2. *Cancer Lett.* 388, 281–291. doi:10.1016/j.canlet.2016.12.005

Liu, F., Chen, N., Gong, Y., Xiao, R., Wang, W., and Pan, Z. (2017b). The long non-coding RNA NEAT1 enhances epithelial-to-mesenchymal transition and chemoresistance via the miR-34a/c-Met axis in renal cell carcinoma. *Oncotarget* 8 (38), 62927–62938. doi:10.18632/oncotarget.17757

Liu, L., Pang, X., Shang, W., Xie, H., Feng, Y., and Feng, G. (2019b). RETRACTED ARTICLE: long non-coding RNA GAS5 sensitizes renal cell carcinoma to sorafenib via miR-21/SOX5 pathway. *Cell cycle* 18 (3), 257–263. doi:10.1080/15384101.2018.1475826

Liu, P., Li, X., Cui, Y., Chen, J., Li, C., Li, Q., et al. (2019a). LncRNA-MALAT1 mediates cisplatin resistance via miR-101-3p/VEGF-C pathway in bladder cancer. *Acta biochimica biophysica Sinica* 51 (11), 1148–1157. doi:10.1093/abbs/gmz112

Liu, Q., Zhou, Q., and Zhong, P. (2020). circ_0067934 increases bladder cancer cell proliferation, migration and invasion through suppressing miR-1304 expression and increasing Myc expression levels. *Exp. Ther. Med.* 19 (6), 3751–3759. doi:10.3892/etm.2020.8648

Liu, X. S., Zhou, L. M., Yuan, L. L., Gao, Y., Kui, X. Y., Liu, X. Y., et al. (2021b). NPM1 is a prognostic biomarker involved in immune infiltration of lung adenocarcinoma and associated with m6A modification and glycolysis. *Front. Immunol.* 12, 724741. doi:10.3389/fimmu.2021.724741

Liz, J., and Esteller, M. (2016). lncRNAs and microRNAs with a role in cancer development. *Biochimica Biophysica Acta (BBA)-Gene Regul. Mech.* 1859 (1), 169–176. doi:10.1016/j.bbagrm.2015.06.015

Ljungberg, B., Bensalah, K., Canfield, S., Dabestani, S., Hofmann, F., Hora, M., et al. (2015). EAU guidelines on renal cell carcinoma: 2014 update. *Eur. Urol.* 67 (5), 913–924. doi:10.1016/j.eururo.2015.01.005

Loberg, R. D., Gayed, B. A., Olson, K. B., and Pienta, K. J. (2005). A paradigm for the treatment of prostate cancer bone metastases based on an understanding of tumor cell-microenvironment interactions. *J. Cell. Biochem.* 96 (3), 439–446. doi:10.1002/jcb.20522

Logothetis, C. J., Gallick, G. E., Maity, S. N., Kim, J., Aparicio, A., Efstathiou, E., et al. (2013). Molecular classification of prostate cancer progression: foundation for marker-driven treatment of prostate cancer. *Cancer Discov.* 3 (8), 849–861. doi:10.1158/2159-8290.CD-12-0460

Logothetis, C. J., and Lin, S. H. (2005). Osteoblasts in prostate cancer metastasis to bone. *Nat. Rev. Cancer* 5 (1), 21–28. doi:10.1038/nrc1528

Lu, Q., Lou, J., Cai, R., Han, W., and Pan, H. (2021). Emerging roles of a pivotal lncRNA SBF2-AS1 in cancers. *Cancer Cell Int.* 21, 417–515. doi:10.1186/s12935-021-02123-3

Luo, J., Wang, K., Yeh, S., Sun, Y., Liang, L., Xiao, Y., et al. (2019). LncRNA-p21 alters the antiandrogen enzalutamide-induced prostate cancer neuroendocrine differentiation via modulating the EZH2/STAT3 signaling. *Nat. Commun.* 10 (1), 2571. doi:10.1038/s41467-019-09784-9

Luo, M., Li, Z., Wang, W., Zeng, Y., Liu, Z., and Qiu, J. (2013). Upregulated H19 contributes to bladder cancer cell proliferation by regulating ID2 expression. *FEBS J.* 280 (7), 1709–1716. doi:10.1111/febs.12185

Lv, M., Zhong, Z., Huang, M., Tian, Q., Jiang, R., and Chen, J. (2017). lncRNA H19 regulates epithelial–mesenchymal transition and metastasis of bladder cancer by miR-29b-3p as competing endogenous RNA. *Biochimica Biophysica Acta (BBA)-Molecular Cell Res.* 1864 (10), 1887–1899. doi:10.1016/j.bbamcr.2017.08.001

Ma, C., Shi, X., Zhu, Q., Li, Q., Liu, Y., Yao, Y., et al. (2016b). The growth arrest-specific transcript 5 (GAS5): a pivotal tumor suppressor long noncoding RNA in human cancers. *Tumour Biol. J. Int. Soc. Oncodevelopmental Biol. Med.* 37 (2), 1437–1444. doi:10.1007/s13277-015-4521-9

Ma, G., Tang, M., Wu, Y., Xu, X., Pan, F., and Xu, R. (2016a). LncRNAs and miRNAs: potential biomarkers and therapeutic targets for prostate cancer. *Am. J. Transl. Res.* 8 (12), 5141–5150.

Ma, X., Ren, H., Zhang, Y., Wang, B., and Ma, H. (2022b). LncRNA RHPN1-AS1 inhibition induces autophagy and apoptosis in prostate cancer cells via the miR-7-5p/EGFR/PI3K/AKT/mTOR signaling pathway. *Environ. Toxicol.* 37 (12), 3013–3027. doi:10.1002/tox.23656

Ma, Y., Fan, B., Ren, Z., Liu, B., and Wang, Y. (2019). Long noncoding RNA DANCR contributes to docetaxel resistance in prostate cancer through targeting the miR-34a-5p/JAG1 pathway. *OncoTargets Ther.* 12, 5485–5497. doi:10.2147/OTT.S197009

Ma, Y., Yu, L., Yan, W., Qiu, L., Zhang, J., and Jia, X. (2022a). lncRNA GAS5 sensitizes breast cancer cells to ionizing radiation by inhibiting DNA repair. *BioMed Res. Int.* 2022, 1987519. doi:10.1155/2022/1987519

Majidinia, M., and Yousefi, B. (2016). Long non-coding RNAs in cancer drug resistance development. *DNA repair* 45, 25–33. doi:10.1016/j.dnarep.2016.06.003

Mamun, M. A., Mannoor, K., Cao, J., Qadri, F., and Song, X. (2020). SOX2 in cancer stemness: tumor malignancy and therapeutic potentials. *J. Mol. cell Biol.* 12 (2), 85–98. doi:10.1093/jmcb/mjy080

Martens-Uzunova, E. S., Böttcher, R., Croce, C. M., Jenster, G., Visakorpi, T., and Calin, G. A. (2014). Long noncoding RNA in prostate, bladder, and kidney cancer. *Eur. Urol.* 65 (6), 1140–1151. doi:10.1016/j.eururo.2013.12.003

Mattick, J. S., and Rinn, J. L. (2015). Discovery and annotation of long noncoding RNAs. *Nat. Struct. Mol. Biol.* 22 (1), 5–7. doi:10.1038/nsmb.2942

Maxwell, P. H., Wiesener, M. S., Chang, G.-W., Clifford, S. C., Vaux, E. C., Cockman, M. E., et al. (1999). The tumour suppressor protein VHL targets hypoxia-inducible factors for oxygen-dependent proteolysis. *Nature* 399 (6733), 271–275. doi:10.1038/20459

McKenney, J. K., Simko, J., Bonham, M., True, L. D., Troyer, D., Hawley, S., et al. (2011). The potential impact of reproducibility of Gleason grading in men with early stage prostate cancer managed by active surveillance: a multi-institutional study. *J. urology* 186 (2), 465–469. doi:10.1016/j.juro.2011.03.115

Mehra, R., Shi, Y., Udager, A. M., Prensner, J. R., Sahu, A., Iyer, M. K., et al. (2014). A novel RNA *in situ* hybridization assay for the long noncoding RNA SChLAP1 predicts poor clinical outcome after radical prostatectomy in clinically localized prostate cancer. *Neoplasia (New York, NY)* 16 (12), 1121–1127. doi:10.1016/j.neo.2014.11.006

Mehra, R., Udager, A. M., Ahearn, T. U., Cao, X., Feng, F. Y., Loda, M., et al. (2016). Overexpression of the long non-coding RNA SChLAP1 independently predicts lethal prostate cancer. *Eur. Urol.* 70 (4), 549–552. doi:10.1016/j.eururo.2015.12.003

Milane, L., Singh, A., Mattheolabakis, G., Suresh, M., and Amiji, M. M. (2015). Exosome mediated communication within the tumor microenvironment. *J. Control. release official J. Control. Release Soc.* 219, 278–294. doi:10.1016/j.jconrel.2015.06.029

Millikan, R. E., Wen, S., Pagliaro, L. C., Brown, M. A., Moomey, B., Do, K. A., et al. (2008). Phase III trial of androgen ablation with or without three cycles of systemic chemotherapy for advanced prostate cancer. *J. Clin. Oncol. official J. Am. Soc. Clin. Oncol.* 26 (36), 5936–5942. doi:10.1200/JCO.2007.15.9830

Mirzaei, S., Gholami, M. H., Hushmandi, K., Hashemi, F., Zabolian, A., Canadas, I., et al. (2022a). The long and short non-coding RNAs modulating EZH2 signaling in cancer. *J. Hematol. and Oncol.* 15 (1), 18. doi:10.1186/s13045-022-01235-1

Mirzaei, S., Paskeh, M. D. A., Hashemi, F., Zabolian, A., Hashemi, M., Entezari, M., et al. (2022c). Long non-coding RNAs as new players in bladder cancer: lessons from pre-clinical and clinical studies. *Life Sci.* 288, 119948. doi:10.1016/j.lfs.2021.119948

Mirzaei, S., Paskeh, M. D. A., Okina, E., Gholami, M. H., Hushmandi, K., Hashemi, M., et al. (2022b). Molecular Landscape of LncRNAs in Prostate Cancer: a focus on pathways and therapeutic targets for intervention. *J. Exp. and Clin. Cancer Res.* 41 (1), 214. doi:10.1186/s13046-022-02406-1

Misawa, A., Ki, T., and Inoue, S. (2017). Long non-coding RNAs and prostate cancer. *Cancer Sci.* 108 (11), 2107–2114. doi:10.1111/cas.13352

Misawa, A., Takayama, K.-i., Urano, T., and Inoue, S. (2016). Androgen-induced long noncoding RNA (lncRNA) SOCS2-AS1 promotes cell growth and inhibits apoptosis in prostate cancer cells. *J. Biol. Chem.* 291 (34), 17861–17880. doi:10.1074/jbc.M116.718536

Mitobe, Y., Takayama, K.-i., Horie-Inoue, K., and Inoue, S. (2018). Prostate cancer-associated lncRNAs. *Cancer Lett.* 418, 159–166. doi:10.1016/j.canlet.2018.01.012

Moch, H., Montironi, R., Lopez-Beltran, A., Cheng, L., and Mischo, A. (2015). Oncotargets in different renal cancer subtypes. *Curr. drug targets* 16 (2), 125–135. doi:10.2174/1389450116666150126110632

Mohan, C. D., Bharathkumar, H., Dukanya, R. S., Shanmugam, M. K., Chinnathambi, A., et al. (2018). N-substituted pyrido-1, 4-oxazin-3-ones induce apoptosis of hepatocellular carcinoma cells by targeting NF-κB signaling pathway. *Front. Pharmacol.* 9, 1125. doi:10.3389/fphar.2018.01125

Moran, V. A., Perera, R. J., and Khalil, A. M. (2012). Emerging functional and mechanistic paradigms of mammalian long non-coding RNAs. *Nucleic acids Res.* 40 (14), 6391–6400. doi:10.1093/nar/gks296

Mouraviev, V., Lee, B., Patel, V., Albala, D., Johansen, T. E., Partin, A., et al. (2016). Clinical prospects of long noncoding RNAs as novel biomarkers and therapeutic targets in prostate cancer. *prostate cancer. Prostate cancer prostatic Dis.* 19 (1), 14–20. doi:10.1038/pcan.2015.48

Mytsyk, Y., Dosenko, V., Skrzypczyk, M. A., Borys, Y., Diychuk, Y., Kucher, A., et al. (2018). Potential clinical applications of microRNAs as biomarkers for renal cell carcinoma. *Central Eur. J. Urology* 71 (3), 295–303. doi:10.5173/ceju.2018.1618

Naderi-Meshkin, H., Lai, X., Amirkhah, R., Vera, J., Rasko, J. E., and Schmitz, U. (2019). Exosomal lncRNAs and cancer: connecting the missing links. *Bioinformatics* 35 (2), 352–360. doi:10.1093/bioinformatics/bty527

Nakagawa, S., Ip, J. Y., Shioi, G., Tripathi, V., Zong, X., Hirose, T., et al. (2012). Malat1 is not an essential component of nuclear speckles in mice. *RNA (New York, NY)* 18 (8), 1487–1499. doi:10.1261/rna.033217.112

Nakagawa, S., Shimada, M., Yanaka, K., Mito, M., Arai, T., Takahashi, E., et al. (2014). The lncRNA Neat1 is required for corpus luteum formation and the establishment of pregnancy in a subpopulation of mice. *Dev. Camb. Engl.* 141 (23), 4618–4627. doi:10.1242/dev.110544

Nakazawa, M., Paller, C., and Kyprianou, N. (2017). Mechanisms of therapeutic resistance in prostate cancer. *Curr. Oncol. Rep.* 19, 13–12. doi:10.1007/s11912-017-0568-7

Oehme, F., Krahl, S., Gyorffy, B., Muessle, B., Rao, V., Greif, H., et al. (2019). Low level of exosomal long non-coding RNA HOTTIP is a prognostic biomarker in colorectal cancer. *RNA Biol.* 16 (10), 1339–1345. doi:10.1080/15476286.2019.1637697

Orfanelli, U., Jachetti, E., Chiacchiera, F., Grioni, M., Brambilla, P., Briganti, A., et al. (2015). Antisense transcription at the TRPM2 locus as a novel prognostic marker and therapeutic target in prostate cancer. *Oncogene* 34 (16), 2094–2102. doi:10.1038/onc.2014.144

Orfanelli, U., Wenke, A.-K., Doglioni, C., Russo, V., Bosserhoff, A. K., and Lavorgna, G. (2008). Identification of novel sense and antisense transcription at the TRPM2 locus in cancer. *Cell Res.* 18 (11), 1128–1140. doi:10.1038/cr.2008.296

Ou, X., Tan, Y., Xie, J., Yuan, J., Deng, X., Shao, R., et al. (2024). Methylation of GPRC5A promotes liver metastasis and docetaxel resistance through activating mTOR signaling pathway in triple negative breast cancer. *Drug Resist. Updat. Rev. Comment. Antimicrob. anticancer Chemother.* 73, 101063. doi:10.1016/j.drup.2024.101063

Outeiro-Pinho, G., Barros-Silva, D., Correia, M. P., Henrique, R., and Jerónimo, C. (2020). Renal cell tumors: uncovering the biomarker potential of ncRNAs. *Cancers* 12 (8), 2214. doi:10.3390/cancers12082214

Pan, J., Li, X., Wu, W., Xue, M., Hou, H., Zhai, W., et al. (2016). Long non-coding RNA UCA1 promotes cisplatin/gemcitabine resistance through CREB modulating miR-196a-5p in bladder cancer cells. *Cancer Lett.* 382 (1), 64–76. doi:10.1016/j.canlet.2016.08.015

Parasramka, M. A., Maji, S., Matsuda, A., Yan, I. K., and Patel, T. (2016). Long non-coding RNAs as novel targets for therapy in hepatocellular carcinoma. *Pharmacol. and Ther.* 161, 67–78. doi:10.1016/j.pharmthera.2016.03.004

Parizi, P. K., Yarahmadi, F., Tabar, H. M., Hosseini, Z., Sarli, A., Kia, N., et al. (2020). MicroRNAs and target molecules in bladder cancer. *Med. Oncol.* 37, 118–133. doi:10.1007/s12032-020-01435-0

Paskeh, M. D. A., Entezari, M., Mirzaei, S., Zabolian, A., Saleki, H., Naghdi, M. J., et al. (2022). Emerging role of exosomes in cancer progression and tumor microenvironment remodeling. *J. Hematol. and Oncol.* 15 (1), 83. doi:10.1186/s13045-022-01305-4

Patard, J.-J., Leray, E., Rioux-Leclercq, N., Cindolo, L., Ficarra, V., Zisman, A., et al. (2005). Prognostic value of histologic subtypes in renal cell carcinoma: a multicenter experience. *J. Clin. Oncol.* 23 (12), 2763–2771. doi:10.1200/JCO.2005.07.055

Patel, V. G., Oh, W. K., and Galsky, M. D. (2020). Treatment of muscle-invasive and advanced bladder cancer in 2020. *CA a cancer J. Clin.* 70 (5), 404–423. doi:10.3322/caac.21631

Petejova, N., and Martinek, A. (2016). Renal cell carcinoma: review of etiology, pathophysiology and risk factors. *Biomedical papers of the Medical Faculty of the University Palacky, Olomouc. Biomed. Pap. Med. Fac. Univ. Palacky. Olomouc Czech. Repub.* 160 (2), 183–194. doi:10.5507/bp.2015.050

Peters, T., Hermans-Beijnsberger, S., Beqqali, A., Bitsch, N., Nakagawa, S., Prasanth, K. V., et al. (2016). Long non-coding RNA malat-1 is dispensable during pressure overload-induced cardiac remodeling and failure in mice. *PloS one* 11 (2), e0150236. doi:10.1371/journal.pone.0150236

Portoso, M., Ragazzini, R., Brenčič, Ž., Moiani, A., Michaud, A., Vassilev, I., et al. (2017). PRC 2 is dispensable for HOTAIR-mediated transcriptional repression. *EMBO J.* 36 (8), 981–994. doi:10.15252/embj.201695335

Postepska-Igielska, A., Giwojna, A., Gasri-Plotnitsky, L., Schmitt, N., Dold, A., Ginsberg, D., et al. (2015). LncRNA Khps1 regulates expression of the proto-oncogene SPHK1 via triplex-mediated changes in chromatin structure. *Mol. cell* 60 (4), 626–636. doi:10.1016/j.molcel.2015.10.001

Prensner, J. R., Iyer, M. K., Sahu, A., Asangani, I. A., Cao, Q., Patel, L., et al. (2013). The long noncoding RNA SChLAP1 promotes aggressive prostate cancer and antagonizes the SWI/SNF complex. *Nat. Genet.* 45 (11), 1392–1398. doi:10.1038/ng.2771

Pu, Y., Zhao, F., Li, Y., Cui, M., Wang, H., Meng, X., et al. (2017). The miR-34a-5p promotes the multi-chemoresistance of osteosarcoma via repression of the AGTR1 gene. *BMC cancer* 17, 45–49. doi:10.1186/s12885-016-3002-x

Qin, X., Zhong, J., Wang, L., Chen, Z., and Liu, X. (2023). LncRNA LNC-565686 promotes proliferation of prostate cancer by inhibiting apoptosis through stabilizing SND1. *Biomedicines* 11 (10), 2627. doi:10.3390/biomedicines11102627

Qu, L., Ding, J., Chen, C., Wu, Z.-J., Liu, B., Gao, Y., et al. (2016). Exosome-transmitted lncARSR promotes sunitinib resistance in renal cancer by acting as a competing endogenous RNA. *Cancer cell* 29 (5), 653–668. doi:10.1016/j.ccell.2016.03.004

Quintanal-Villalonga, Á., Chan, J. M., Yu, H. A., Pe'er, D., Sawyers, C. L., Sen, T., et al. (2020). Lineage plasticity in cancer: a shared pathway of therapeutic resistance. *Nat. Rev. Clin. Oncol.* 17 (6), 360–371. doi:10.1038/s41571-020-0340-z

Rachakonda, P. S., Hosen, I., De Verdier, P. J., Fallah, M., Heidenreich, B., Ryk, C., et al. (2013). TERT promoter mutations in bladder cancer affect patient survival and disease recurrence through modification by a common polymorphism. *Proc. Natl. Acad. Sci.* 110 (43), 17426–17431. doi:10.1073/pnas.1310522110

Ramnarine, V. R., Kobelev, M., Gibb, E. A., Nouri, M., Lin, D., Wang, Y., et al. (2019). The evolution of long noncoding RNA acceptance in prostate cancer initiation, progression, and its clinical utility in disease management. *Eur. Urol.* 76 (5), 546–559. doi:10.1016/j.eururo.2019.07.040

Rausch, S., Schollenberger, D., Hennenlotter, J., Stühler, V., Kruck, S., Stenzl, A., et al. (2019). mTOR and mTOR phosphorylation status in primary and metastatic renal cell carcinoma tissue: differential expression and clinical relevance. *J. Cancer Res. Clin. Oncol.* 145 (1), 153–163. doi:10.1007/s00432-018-2775-5

Ren, S., Liu, Y., Xu, W., Sun, Y., Lu, J., Wang, F., et al. (2013). Long noncoding RNA MALAT-1 is a new potential therapeutic target for castration resistant prostate cancer. *J. urology* 190 (6), 2278–2287. doi:10.1016/j.juro.2013.07.001

Ren, X., Lan, T., Chen, Y., Shao, Z., Yang, C., and Peng, J. (2016). lncRNA uc009yby.1 promotes renal cell proliferation and is associated with poor survival in patients with clear cell renal cell carcinomas. *Oncol. Lett.* 12 (3), 1929–1934. doi:10.3892/ol.2016.4856

Rhea, L. P., Mendez-Marti, S., Kim, D., and Aragon-Ching, J. B. (2021). Role of immunotherapy in bladder cancer. *Cancer Treat. Res. Commun.* 26, 100296. doi:10.1016/j.ctarc.2020.100296

Rini, B. I., Campbell, S. C., and Escudier, B. (2009). Renal cell carcinoma. *Lancet* 373 (9669), 1119–1132. doi:10.1016/S0140-6736(09)60229-4

Rinn, J. L., Kertesz, M., Wang, J. K., Squazzo, S. L., Xu, X., Brugmann, S. A., et al. (2007). Functional demarcation of active and silent chromatin domains in human HOX loci by noncoding RNAs. *cell* 129 (7), 1311–1323. doi:10.1016/j.cell.2007.05.022

Ruan, X., Zheng, J., Liu, X., Liu, Y., Liu, L., Ma, J., et al. (2020). lncRNA LINC00665 stabilized by TAF15 impeded the malignant biological behaviors of glioma cells via STAU1-mediated mRNA degradation. *Mol. Ther. Nucleic acids* 20, 823–840. doi:10.1016/j.omtn.2020.05.003

Ryan, C. J., Smith, A., Lal, P., Satagopan, J., Reuter, V., Scardino, P., et al. (2006). Persistent prostate-specific antigen expression after neoadjuvant androgen depletion: an early predictor of relapse or incomplete androgen suppression. *Urology* 68 (4), 834–839. doi:10.1016/j.urology.2006.04.016

Saab, S., Zalzale, H., Rahal, Z., Khalifeh, Y., Sinjab, A., and Kadara, H. (2020). Insights into lung cancer immune-based biology, prevention, and treatment. *Front. Immunol.* 11, 159. doi:10.3389/fimmu.2020.00159

Salameh, A., Lee, A. K., Cardó-Vila, M., Nunes, D. N., Efstathiou, E., Staquicini, F. I., et al. (2015). PRUNE2 is a human prostate cancer suppressor regulated by the intronic long noncoding RNA PCA3. *Proc. Natl. Acad. Sci. U. S. A.* 112 (27), 8403–8408. doi:10.1073/pnas.1507882112

Samata, M., and Akhtar, A. (2018). Dosage compensation of the X chromosome: a complex epigenetic assignment involving chromatin regulators and long noncoding RNAs. *Annu. Rev. Biochem.* 87, 323–350. doi:10.1146/annurev-biochem-062917-011816

Sati, S., Ghosh, S., Jain, V., Scaria, V., and Sengupta, S. (2012). Genome-wide analysis reveals distinct patterns of epigenetic features in long non-coding RNA loci. *Nucleic acids Res.* 40 (20), 10018–10031. doi:10.1093/nar/gks776

Sauvageau, M., Goff, L. A., Lodato, S., Bonev, B., Groff, A. F., Gerhardinger, C., et al. (2013). Multiple knockout mouse models reveal lincRNAs are required for life and brain development. *eLife* 2, e01749. doi:10.7554/eLife.01749

Schmidt, L. S., and Linehan, W. M. (2016). Genetic predisposition to kidney cancer. *Seminars Oncol.* 43 (5), 566–574. doi:10.1053/j.seminoncol.2016.09.001

Seles, M., Hutterer, G. C., Kiesslich, T., Pummer, K., Berindan-Neagoe, I., Perakis, S., et al. (2016). Current insights into long non-coding RNAs in renal cell carcinoma. *Int. J. Mol. Sci.* 17 (4), 573. doi:10.3390/ijms17040573

Sen, R., Ghosal, S., Das, S., Balti, S., and Chakrabarti, J. (2014). Competing endogenous RNA: the key to posttranscriptional regulation. *Sci. World J.* 2014, 896206. doi:10.1155/2014/896206

Shang, A., Wang, W., Gu, C., Chen, W., Lu, W., Sun, Z., et al. (2020). Long non-coding RNA CCAT1 promotes colorectal cancer progression by regulating miR-181a-5p expression. *Aging (Albany NY)* 12 (9), 8301–8320. doi:10.18632/aging.103139

Shang, C., Guo, Y., Zhang, H., and Xue, Y.-x. (2016). Long noncoding RNA HOTAIR is a prognostic biomarker and inhibits chemosensitivity to doxorubicin in bladder transitional cell carcinoma. *Cancer Chemother. Pharmacol.* 77, 507–513. doi:10.1007/s00280-016-2964-3

Shen, C., Wu, Z., Wang, Y., Gao, S., Da, L., Xie, L., et al. (2020). Downregulated hsa_circ_0077837 and hsa_circ_0004826, facilitate bladder cancer progression and predict poor prognosis for bladder cancer patients. *Cancer Med.* 9 (11), 3885–3903. doi:10.1002/cam4.3006

Shi, Y. F., Lu, H., and Wang, H. B. (2019). Downregulated lncRNA ADAMTS9-AS2 in breast cancer enhances tamoxifen resistance by activating microRNA-130a-5p. *Eur. Rev. Med. Pharmacol. Sci.* 23 (4), 1563–1573. doi:10.26355/eurrev_201902_17115

Shin, V. Y., Chen, J., Cheuk, I. W.-Y., Siu, M.-T., Ho, C.-W., Wang, X., et al. (2019). Long non-coding RNA NEAT1 confers oncogenic role in triple-negative breast cancer through modulating chemoresistance and cancer stemness. *Cell death and Dis.* 10 (4), 270. doi:10.1038/s41419-019-1513-5

Shurtleff, M. J., Yao, J., Qin, Y., Nottingham, R. M., Temoche-Diaz, M. M., Schekman, R., et al. (2017). Broad role for YBX1 in defining the small noncoding RNA composition of exosomes. *Proc. Natl. Acad. Sci. U. S. A.* 114 (43), E8987-E8995–e8995. doi:10.1073/pnas.1712108114

Si, Z., Yu, L., Jing, H., Wu, L., and Wang, X. (2021). Oncogenic lncRNA ZNF561-AS1 is essential for colorectal cancer proliferation and survival through regulation of miR-26a-3p/miR-128-5p-SRSF6 axis. *J. Exp. and Clin. cancer Res. CR* 40 (1), 78. doi:10.1186/s13046-021-01882-1

Siegel, R. L., Miller, K. D., and Jemal, A. (2018). Cancer statistics. *CA a cancer J. Clin.* 68 (1), 7–30. doi:10.3322/caac.21442

Sim, W. J., Iyengar, P. V., Lama, D., Lui, S. K. L., Ng, H. C., Haviv-Shapira, L., et al. (2019). c-Met activation leads to the establishment of a TGFβ-receptor regulatory network in bladder cancer progression. *Nat. Commun.* 10 (1), 4349. doi:10.1038/s41467-019-12241-2

Smolle, M. A., Bauernhofer, T., Pummer, K., Calin, G. A., and Pichler, M. (2017). Current insights into long non-coding RNAs (LncRNAs) in prostate cancer. *Int. J. Mol. Sci.* 18 (2), 473. doi:10.3390/ijms18020473

Song, E.-l., Xing, L., Wang, L., Song, W.-t., Li, D.-b., Wang, Y., et al. (2019). LncRNA ADAMTS9-AS2 inhibits cell proliferation and decreases chemoresistance in clear cell renal cell carcinoma via the miR-27a-3p/FOXO1 axis. *Aging (Albany NY)* 11 (15), 5705–5725. doi:10.18632/aging.102154

Song, H., Xu, Y., Shi, L., Xu, T., Fan, R., Cao, M., et al. (2018). LncRNA THOR increases the stemness of gastric cancer cells via enhancing SOX9 mRNA stability. *Biomed. and Pharmacother.* 108, 338–346. doi:10.1016/j.biopha.2018.09.057

Song, S., Wu, Z., Wang, C., Liu, B., Ye, X., Chen, J., et al. (2014). RCCRT1 is correlated with prognosis and promotes cell migration and invasion in renal cell carcinoma. *Urology* 84 (3), 730. e731–e7. doi:10.1016/j.urology.2014.05.033

Song, W., Li, Z., Yang, K., Gao, Z., Zhou, Q., and Li, P. (2023). Antisense lncRNA-RP11-498C9.13 promotes bladder cancer progression by enhancing reactive oxygen species-induced mitophagy. *J. gene Med.* 25 (9), e3527. doi:10.1002/jgm.3527

Standaert, L., Adriaens, C., Radaelli, E., Van Keymeulen, A., Blanpain, C., Hirose, T., et al. (2014). The long noncoding RNA Neat1 is required for mammary gland development and lactation. *RNA (New York, NY)* 20 (12), 1844–1849. doi:10.1261/rna.047332.114

Sun, Z., Huang, G., and Cheng, H. (2019a). Transcription factor Nrf2 induces the up-regulation of lncRNA TUG1 to promote progression and adriamycin resistance in urothelial carcinoma of the bladder. *Cancer Manag. Res.* 11, 6079–6090. doi:10.2147/CMAR.S200998

Sun, Z.-Y., Jian, Y.-K., Zhu, H.-Y., and Li, B. (2019b). lncRNAPVT1 targets miR-152 to enhance chemoresistance of osteosarcoma to gemcitabine through activating c-MET/PI3K/AKT pathway. *Pathology-Research Pract.* 215 (3), 555–563. doi:10.1016/j.prp.2018.12.013

Sweeney, C. J., Chen, Y.-H., Carducci, M., Liu, G., Jarrard, D. F., Eisenberger, M., et al. (2015). Chemohormonal therapy in metastatic hormone-sensitive prostate cancer. *N. Engl. J. Med.* 373 (8), 737–746. doi:10.1056/nejmoa1503747

Taheri, M., Omrani, M. D., and Ghafouri-Fard, S. (2018). Long non-coding RNA expression in bladder cancer. *Biophys. Rev.* 10 (4), 1205–1213. doi:10.1007/s12551-017-0379-y

Tan, J., Qiu, K., Li, M., and Liang, Y. (2015). Double-negative feedback loop between long non-coding RNA TUG1 and miR-145 promotes epithelial to mesenchymal transition and radioresistance in human bladder cancer cells. *FEBS Lett.* 589 (20), 3175–3181. doi:10.1016/j.febslet.2015.08.020

Tan, Y. T., Lin, J. F., Li, T., Li, J. J., Xu, R. H., and Ju, H. Q. (2021). LncRNA-mediated posttranslational modifications and reprogramming of energy metabolism in cancer. *Cancer Commun. Lond. Engl.* 41 (2), 109–120. doi:10.1002/cac2.12108

Taneja, K., and Williamson, S. R. (2018). Updates in pathologic staging and histologic grading of renal cell carcinoma. *Surg. Pathol. Clin.* 11 (4), 797–812. doi:10.1016/j.path.2018.07.004

Tang, Y., Tian, W., Zheng, S., Zou, Y., Xie, J., Zhang, J., et al. (2023). Dissection of FOXO1-induced LYPLAL1-DT impeding triple-negative breast cancer progression via mediating hnRNPK/β-Catenin complex. *Res. Wash. DC* 6, 0289. doi:10.34133/research.0289

Teng, J., Ai, X., Jia, Z., Wang, K., Guan, Y., and Guo, Y. (2019). Long non-coding RNA ARAP1-AS1 promotes the progression of bladder cancer by regulating miR-4735-3p/NOTCH2 axis. *Cancer Biol. and Ther.* 20 (4), 552–561. doi:10.1080/15384047.2018.1538613

Thomson, D. W., and Dinger, M. E. (2016). Endogenous microRNA sponges: evidence and controversy. *Nat. Rev. Genet.* 17 (5), 272–283. doi:10.1038/nrg.2016.20

Thrash-Bingham, C. A., and Tartof, K. D. (1999). aHIF: a natural antisense transcript overexpressed in human renal cancer and during hypoxia. *J. Natl. Cancer Inst.* 91 (2), 143–151. doi:10.1093/jnci/91.2.143

Tran, L., Xiao, J.-F., Agarwal, N., Duex, J. E., and Theodorescu, D. (2021). Advances in bladder cancer biology and therapy. *Nat. Rev. Cancer* 21 (2), 104–121. doi:10.1038/s41568-020-00313-1

Treeck, O., Skrzypczak, M., Schüler-Toprak, S., Weber, F., and Ortmann, O. (2020). Long non-coding RNA CCAT1 is overexpressed in endometrial cancer and regulates growth and transcriptome of endometrial adenocarcinoma cells. *Int. J. Biochem. and cell Biol.* 122, 105740. doi:10.1016/j.biocel.2020.105740

Tripathi, A., Shrinet, K., and Kumar, A. (2019). HMGB1 protein as a novel target for cancer. *Toxicol. Rep.* 6, 253–261. doi:10.1016/j.toxrep.2019.03.002

Tsai, M. C., Spitale, R. C., and Chang, H. Y. (2011). Long intergenic noncoding RNAs: new links in cancer progression. *Cancer Res.* 71 (1), 3–7. doi:10.1158/0008-5472.CAN-10-2483

Tsui, Y.-M., and Chan, L.-K. (2020). Ng IO-L: cancer stemness in hepatocellular carcinoma: mechanisms and translational potential. *Br. J. cancer* 122 (10), 1428–1440. doi:10.1038/s41416-020-0823-9

Wang, D., Ding, L., Wang, L., Zhao, Y., Sun, Z., Karnes, R. J., et al. (2015). LncRNA MALAT1 enhances oncogenic activities of EZH2 in castration-resistant prostate cancer. *Oncotarget* 6 (38), 41045–41055. doi:10.18632/oncotarget.5728

Wang, F., Ren, S., Chen, R., Lu, J., Shi, X., Zhu, Y., et al. (2014). Development and prospective multicenter evaluation of the long noncoding RNA MALAT-1 as a diagnostic urinary biomarker for prostate cancer. *Oncotarget* 5 (22), 11091–11102. doi:10.18632/oncotarget.2691

Wang, F., Wu, D., Chen, J., Chen, S., He, F., Fu, H., et al. (2019b). Long non-coding RNA HOXA-AS2 promotes the migration, invasion and stemness of bladder cancer via regulating miR-125b/Smad2 axis. *Exp. cell Res.* 375 (1), 1–10. doi:10.1016/j.yexcr.2018.11.005

Wang, F. W., Cao, C. H., Han, K., Zhao, Y. X., Cai, M. Y., Xiang, Z. C., et al. (2019a). APC-activated long noncoding RNA inhibits colorectal carcinoma pathogenesis through reduction of exosome production. *J. Clin. Invest* 129 (2), 727–743. doi:10.1172/JCI122478

Wang, K. C., Yang, Y. W., Liu, B., Sanyal, A., Corces-Zimmerman, R., Chen, Y., et al. (2011). A long noncoding RNA maintains active chromatin to coordinate homeotic gene expression. *Nature* 472 (7341), 120–124. doi:10.1038/nature09819

Wang, L., Wang, P., Liu, B., Zhang, H., Wei, C. C., Xiong, M., et al. (2024b). LncRNA MEG3 inhibits the epithelial-mesenchymal transition of bladder cancer cells through the snail/E-cadherin Axis. *Curr. Med. Sci.* 44, 726–734. doi:10.1007/s11596-024-2895-x

Wang, L., Yang, G., Guo, P., Lv, Y., Fu, B., Bai, Y., et al. (2023b). LncRNA PVT1 promotes strong stemness and endothelial progenitor cell characteristics in renal carcinoma stem cells. *FASEB J.* 37 (9), e23118. *official publication of the Federation of American Societies for Experimental Biology*. doi:10.1096/fj.202201880R

Wang, M., Guo, C., Wang, L., Luo, G., Huang, C., Li, Y., et al. (2018). Long noncoding RNA GAS5 promotes bladder cancer cells apoptosis through inhibiting EZH2 transcription. *Cell death and Dis.* 9 (2), 238. doi:10.1038/s41419-018-0264-z

Wang, M., Yin, C., Wu, Z., Wang, X., Lin, Q., Jiang, X., et al. (2023a). The long transcript of lncRNA TMPO-AS1 promotes bone metastases of prostate cancer by regulating the CSNK2A1/DDX3X complex in Wnt/β-catenin signaling. *Cell Death Discov.* 9 (1), 287. doi:10.1038/s41420-023-01585-w

Wang, S., Zhu, W., Qiu, J., and Chen, F. (2021). lncRNA SNHG4 promotes cell proliferation, migration, invasion and the epithelial-mesenchymal transition process via sponging miR-204-5p in gastric cancer. *Mol. Med. Rep.* 23 (1), 85–91. doi:10.3892/mmr.2020.11724

Wang, Y., Chen, L., Yu, M., Fang, Y., Qian, K., Wang, G., et al. (2020a). Immune-related signature predicts the prognosis and immunotherapy benefit in bladder cancer. *Cancer Med.* 9 (20), 7729–7741. doi:10.1002/cam4.3400

Wang, Y., Huang, X., Luo, G., Xu, Y., Deng, X., Lin, Y., et al. (2024a). The aging lung: microenvironment, mechanisms, and diseases. *Front. Immunol.* 15, 1383503. doi:10.3389/fimmu.2024.1383503

Wang, Y., Liu, J., Bai, H., Dang, Y., Lv, P., and Wu, S. (2017). Long intergenic non-coding RNA 00152 promotes renal cell carcinoma progression by epigenetically suppressing P16 and negatively regulates miR-205. *Am. J. cancer Res.* 7 (2), 312–322.

Wang, Z. Y., Duan, Y., and Wang, P. (2020b). SP1-mediated upregulation of lncRNA SNHG4 functions as a ceRNA for miR-377 to facilitate prostate cancer progression through regulation of ZIC5. *J. Cell. physiology* 235 (4), 3916–3927. doi:10.1002/jcp.29285

Williamson, S. R., Taneja, K., and Cheng, L. (2019). Renal cell carcinoma staging: pitfalls, challenges, and updates. *Histopathology* 74 (1), 18–30. doi:10.1111/his.13743

Wu, G., Dong, Z., Dong, Y., Chen, Y., Zhu, H., Ding, D., et al. (2024). LncRNA CTBP1-AS inhibits TP63-mediated activation of S100A14 during prostate cancer progression. *Cancer Sci.* 115 (5), 1492–1504. doi:10.1111/cas.16138

Wu, S., Deng, H., He, H., Xu, R., Wang, Y., Zhu, X., et al. (2020). The circ_0004463/miR-380-3p/FOXO1 axis modulates mitochondrial respiration and bladder cancer cell apoptosis. *Cell Cycle* 19 (24), 3563–3580. doi:10.1080/15384101.2020.1852746

Wu, T., Li, N., Wu, X., Du, Y., and Tang, Z. (2023b). LncRNA LINC00592 mediates the promoter methylation of WIF1 to promote the development of bladder cancer. *Open Med. Wars. Pol.* 18 (1), 20230788. doi:10.1515/med-2023-0788

Wu, X., Xiao, Y., Zhou, Y., Zhou, Z., and Yan, W. (2019). lncRNA SNHG20 promotes prostate cancer migration and invasion via targeting the miR-6516-5p/SCGB2A1 axis. *Am. J. Transl. Res.* 11 (8), 5162–5169.

Wu, Y., Mou, J., Liu, Y., and Zheng, W. (2023a). Association of LncRNA PCBP1-AS1 with cancer occurrence and development: a review. *Medicine* 102 (43), e35631. doi:10.1097/MD.0000000000035631

Wu, Y., Wang, Y. Q., Weng, W. W., Zhang, Q. Y., Yang, X. Q., Gan, H. L., et al. (2016). A serum-circulating long noncoding RNA signature can discriminate between patients with clear cell renal cell carcinoma and healthy controls. *Oncogenesis* 5 (2), e192. doi:10.1038/oncsis.2015.48

Xia, Z., Wu, J., Li, Y., Yuan, X., Sun, J., Lv, C., et al. (2023). LncRNA TYMSOS is a novel prognostic biomarker associated with immune infiltration in prostate cancer. *Am. J. cancer Res.* 13 (10), 4531–4546.

Xiang, J.-F., Yin, Q.-F., Chen, T., Zhang, Y., Zhang, X.-O., Wu, Z., et al. (2014). Human colorectal cancer-specific CCAT1-L lncRNA regulates long-range chromatin interactions at the MYC locus. *Cell Res.* 24 (5), 513–531. doi:10.1038/cr.2014.35

XianGuo, C., ZongYao, H., Jun, Z., Song, F., GuangYue, L., LiGang, Z., et al. (2016). Promoting progression and clinicopathological significance of NEAT1 over-expression in bladder cancer. *Oncotarget* 5. doi:10.18632/oncotarget.10084

Xiao, L., Wu, J., Wang, J. Y., Chung, H. K., Kalakonda, S., Rao, J. N., et al. (2018). Long noncoding RNA uc.173 promotes renewal of the intestinal mucosa by inducing degradation of MicroRNA 195. *Gastroenterology* 154 (3), 599–611. doi:10.1053/j.gastro.2017.10.009

Xie, D., Zhang, H., and Shang, C. (2018). Long non-coding RNA CDKN2B antisense RNA 1 gene inhibits Gemcitabine sensitivity in bladder urothelial carcinoma. *J. Cancer* 9 (12), 2160–2166. doi:10.7150/jca.25236

Xie, J., Ye, F., Deng, X., Tang, Y., Liang, J. Y., Huang, X., et al. (2023). Circular RNA: a promising new star of vaccine. *J. Transl. Intern. Med.* 11 (4), 372–381. doi:10.2478/jtim-2023-0122

Xing, C., Sun, S. G., Yue, Z. Q., and Bai, F. (2021). Role of lncRNA LUCAT1 in cancer. *Biomed. and Pharmacother. = Biomedecine and Pharmacother.* 134, 111158. doi:10.1016/j.biopha.2020.111158

Xiu, D., Liu, L., Cheng, M., Sun, X., and Ma, X. (2020). Knockdown of lncRNA TUG1 enhances radiosensitivity of prostate cancer via the TUG1/miR-139-5p/smc1a Axis. *OncoTargets Ther.* 13, 2319–2331. doi:10.2147/OTT.S236860

Xu, J., Yang, R., Hua, X., Huang, M., Tian, Z., Li, J., et al. (2020). lncRNA SNHG1 promotes basal bladder cancer invasion via interaction with PP2A catalytic subunit and induction of autophagy. *Mol. Ther. Nucleic acids* 21, 354–366. doi:10.1016/j.omtn.2020.06.010

Xu, R., Rai, A., Chen, M., Suwakulsiri, W., Greening, D. W., and Simpson, R. J. (2018). Extracellular vesicles in cancer—implications for future improvements in cancer care. *Nat. Rev. Clin. Oncol.* 15 (10), 617–638. doi:10.1038/s41571-018-0036-9

Xu, Z., Yang, F., Wei, D., Liu, B., Chen, C., Bao, Y., et al. (2017). Long noncoding RNA-SRLR elicits intrinsic sorafenib resistance via evoking IL-6/STAT3 axis in renal cell carcinoma. *Oncogene* 36 (14), 1965–1977. doi:10.1038/onc.2016.356

Xue, D., Wang, H., Chen, Y., Shen, D., Lu, J., Wang, M., et al. (2019). Circ-AKT3 inhibits clear cell renal cell carcinoma metastasis via altering miR-296-3p/E-cadherin signals. *Mol. cancer* 18, 151–213. doi:10.1186/s12943-019-1072-5

Xue, M., Chen, W., Xiang, A., Wang, R., Chen, H., Pan, J., et al. (2017). Hypoxic exosomes facilitate bladder tumor growth and development through transferring long non-coding RNA-UCA1. *Mol. cancer* 16, 143–213. doi:10.1186/s12943-017-0714-8

Yan, Y., Xu, Z., Chen, X., Wang, X., Zeng, S., Zhao, Z., et al. (2019). Novel function of lncRNA ADAMTS9-AS2 in promoting temozolomide resistance in glioblastoma via upregulating the FUS/MDM2 ubiquitination Axis. *Front. cell Dev. Biol.* 7, 217. doi:10.3389/fcell.2019.00217

Yang, F., Xue, X., Bi, J., Zheng, L., Zhi, K., Gu, Y., et al. (2013). Long noncoding RNA CCAT1, which could be activated by c-Myc, promotes the progression of gastric carcinoma. *J. cancer Res. Clin. Oncol.* 139, 437–445. doi:10.1007/s00432-012-1324-x

Yang, F., Xue, X., Zheng, L., Bi, J., Zhou, Y., Zhi, K., et al. (2014). Long non-coding RNA GHET1 promotes gastric carcinoma cell proliferation by increasing c-Myc mRNA stability. *FEBS J.* 281 (3), 802–813. doi:10.1111/febs.12625

Yang, G., Li, Z., Dong, L., and Zhou, F. (2021). lncRNA ADAMTS9-AS1 promotes bladder cancer cell invasion, migration, and inhibits apoptosis and autophagy through PI3K/AKT/mTOR signaling pathway. *Int. J. Biochem. and cell Biol.* 140, 106069. doi:10.1016/j.biocel.2021.106069

Yang, Z., Luo, Y., Zhang, F., and Ma, L. (2024). Exosome-derived lncRNA A1BG-AS1 attenuates the progression of prostate cancer depending on ZC3H13-mediated m6A modification. *Cell Div.* 19 (1), 5. doi:10.1186/s13008-024-00110-4

You, Z., Liu, C., Wang, C., Ling, Z., Wang, Y., Wang, Y., et al. (2019). LncRNA CCAT1 promotes prostate cancer cell proliferation by interacting with DDX5 and MIR-28-5P. *Mol. cancer Ther.* 18 (12), 2469–2479. doi:10.1158/1535-7163.MCT-19-0095

Yu, G., Zhou, H., Yao, W., Meng, L., and Lang, B. (2019). lncRNA TUG1 promotes cisplatin resistance by regulating CCND2 via epigenetically silencing miR-194-5p in bladder cancer. *Mol. Ther. Nucleic acids* 16, 257–271. doi:10.1016/j.omtn.2019.02.017

Yu, J., Han, J., Zhang, J., Li, G., Liu, H., Cui, X., et al. (2016). The long noncoding RNAs PVT1 and uc002mbe. 2 in sera provide a new supplementary method for hepatocellular carcinoma diagnosis. *Medicine* 95 (31), e4436. doi:10.1097/MD.0000000000004436

Yu, X., Li, Z., Zheng, H., Chan, M. T., and Wu, W. K. K. (2017). NEAT 1: a novel cancer-related long non-coding RNA. *Cell Prolif.* 50 (2), e12329. doi:10.1111/cpr.12329

Zhan, Y., Chen, Z., He, S., Gong, Y., He, A., Li, Y., et al. (2020). Long non-coding RNA SOX2OT promotes the stemness phenotype of bladder cancer cells by modulating SOX2. *Mol. Cancer* 19 (1), 25–13. doi:10.1186/s12943-020-1143-7

Zhan, Y., Lin, J., Liu, Y., Chen, M., Chen, X., Zhuang, C., et al. (2016a). Up-regulation of long non-coding RNA PANDAR is associated with poor prognosis and promotes tumorigenesis in bladder cancer. *J. Exp. and Clin. cancer Res.* 35 (1), 83–10. doi:10.1186/s13046-016-0354-7

Zhan, Y., Liu, Y., Wang, C., Lin, J., Chen, M., Chen, X., et al. (2016b). Increased expression of SUMO1P3 predicts poor prognosis and promotes tumor growth and metastasis in bladder cancer. *Oncotarget* 7 (13), 16038–16048. doi:10.18632/oncotarget.6946

Zhang, A., Zhang, J., Kaipainen, A., Lucas, J. M., and Yang, H. (2016b). Long non-coding RNA: a newly deciphered "code" in prostate cancer. *Cancer Lett.* 375 (2), 323–330. doi:10.1016/j.canlet.2016.03.003

Zhang, A., Zhao, J. C., Kim, J., Fong, K.-w., Yang, Y. A., Chakravarti, D., et al. (2015). LncRNA HOTAIR enhances the androgen-receptor-mediated transcriptional program and drives castration-resistant prostate cancer. *Cell Rep.* 13 (1), 209–221. doi:10.1016/j.celrep.2015.08.069

Zhang, B., Arun, G., Mao, Y. S., Lazar, Z., Hung, G., Bhattacharjee, G., et al. (2012). The lncRNA Malat1 is dispensable for mouse development but its transcription plays a cis-regulatory role in the adult. *Cell Rep.* 2 (1), 111–123. doi:10.1016/j.celrep.2012.06.003

Zhang, H., Guo, Y., Song, Y., and Shang, C. (2017). Long noncoding RNA GAS5 inhibits malignant proliferation and chemotherapy resistance to doxorubicin in bladder transitional cell carcinoma. *Cancer Chemother. Pharmacol.* 79, 49–55. doi:10.1007/s00280-016-3194-4

Zhang, J., Liu, S. C., Luo, X. H., Tao, G. X., Guan, M., Yuan, H., et al. (2016a). Exosomal Long noncoding RNA s are differentially expressed in the Cervicovaginal lavage samples of cervical cancer patients. *J. Clin. laboratory analysis* 30 (6), 1116–1121. doi:10.1002/jcla.21990

Zhang, Y., Chen, X., Lin, J., and Jin, X. (2021). Biological functions and clinical significance of long noncoding RNAs in bladder cancer. *Cell Death Discov.* 7 (1), 278. doi:10.1038/s41420-021-00665-z

Zhang, Y., Huang, W., Yuan, Y., Li, J., Wu, J., Yu, J., et al. (2020). Long non-coding RNA H19 promotes colorectal cancer metastasis via binding to hnRNPA2B1. *J. Exp. and Clin. cancer Res. CR* 39 (1), 141. doi:10.1186/s13046-020-01619-6

Zhang, Y., and Tang, L. (2018). The application of lncRNAs in cancer treatment and diagnosis. *Recent Pat. anti-cancer drug Discov.* 13 (3), 292–301. doi:10.2174/1574892813666180226121819

Zhao, X., Chen, J., Zhang, C., Xie, G., Othmane, B., Kuang, X., et al. (2023). LncRNA AGAP2-AS1 interacts with IGF2BP2 to promote bladder cancer progression via regulating LRG1 mRNA stability. *Cell. Signal.* 111, 110839. doi:10.1016/j.cellsig.2023.110839

Zhao, X.-L., Zhao, Z.-H., Xu, W.-C., Hou, J.-Q., and Du, X.-Y. (2015). Increased expression of SPRY4-IT1 predicts poor prognosis and promotes tumor growth and metastasis in bladder cancer. *Int. J. Clin. Exp. pathology* 8 (2), 1954–1960.

Zheng, Q. X., Wang, J., Gu, X. Y., Huang, C. H., Chen, C., Hong, M., et al. (2021). TTN-AS1 as a potential diagnostic and prognostic biomarker for multiple cancers. *Biomed. and Pharmacother. = Biomedecine and Pharmacother.* 135, 111169. doi:10.1016/j.biopha.2020.111169

Zheng, R., Gao, F., Mao, Z., Xiao, Y., Yuan, L., Huang, Z., et al. (2023). LncRNA BCCE4 genetically enhances the PD-L1/PD-1 interaction in smoking-related bladder cancer by modulating miR-328-3p-USP18 signaling. *Adv. Sci. Weinheim, Baden-Wurttemberg, Ger.* 10 (30), e2303473. doi:10.1002/advs.202303473

Zheng, Z., Zhu, D., Zhao, F., Han, J., Chen, H., Cai, Y., et al. (2018). Upregulated GAPLINC predicts a poor prognosis in bladder cancer patients and promotes tumor proliferation and invasion. *Oncol. Lett.* 15 (5), 6770–6776. doi:10.3892/ol.2018.8158

Zhong, Y., Li, H., Li, P., Chen, Y., Zhang, M., Yuan, Z., et al. (2021). Exosomes: a new pathway for cancer drug resistance. *Front. Oncol.* 11, 743556. doi:10.3389/fonc.2021.743556

Zhou, N., Chen, Y., Yang, L., Xu, T., Wang, F., Chen, L., et al. (2021). LncRNA SNHG4 promotes malignant biological behaviors and immune escape of colorectal cancer cells by regulating the miR-144-3p/MET axis. *Am. J. Transl. Res.* 13 (10), 11144–11161.

Zhu, X., Li, Y., Zhao, S., and Zhao, S. (2018). LSINCT5 activates Wnt/β-catenin signaling by interacting with NCYM to promote bladder cancer progression. *Biochem. biophysical Res. Commun.* 502 (3), 299–306. doi:10.1016/j.bbrc.2018.05.076

Zhu, Y., Huang, S., Chen, S., Chen, J., Wang, Z., Wang, Y., et al. (2021). SOX2 promotes chemoresistance, cancer stem cells properties, and epithelial–mesenchymal transition by β-catenin and Beclin1/autophagy signaling in colorectal cancer. *Cell death and Dis.* 12 (5), 449. doi:10.1038/s41419-021-03733-5

Zhuang, C., Li, J., Liu, Y., Chen, M., Yuan, J., Fu, X., et al. (2015b). Tetracycline-inducible shRNA targeting long non-coding RNA PVT1 inhibits cell growth and induces apoptosis in bladder cancer cells. *Oncotarget* 6 (38), 41194–41203. doi:10.18632/oncotarget.5880

Zhuang, J., Lu, Q., Shen, B., Huang, X., Shen, L., Zheng, X., et al. (2015a). TGFβ1 secreted by cancer-associated fibroblasts induces epithelial-mesenchymal transition of bladder cancer cells through lncRNA-ZEB2NAT. *Sci. Rep.* 5 (1), 11924. doi:10.1038/srep11924

Zhuang, J., Shen, L., Yang, L., Huang, X., Lu, Q., Cui, Y., et al. (2017a). TGFβ1 promotes gemcitabine resistance through regulating the LncRNA-LET/NF90/miR-145 signaling Axis in bladder cancer. *Theranostics* 7 (12), 3053–3067. doi:10.7150/thno.19542

Zhuang, J., Shen, L., Yang, L., Huang, X., Lu, Q., Cui, Y., et al. (2017b). TGFβ1 promotes gemcitabine resistance through regulating the LncRNA-LET/NF90/miR-145 signaling Axis in bladder cancer. *Theranostics* 7 (12), 3053–3067. doi:10.7150/thno.19542

Znaor, A., Lortet-Tieulent, J., Laversanne, M., Jemal, A., and Bray, F. (2015). International variations and trends in renal cell carcinoma incidence and mortality. *Eur. Urol.* 67 (3), 519–530. doi:10.1016/j.eururo.2014.10.002

Glossary

ncRNAs	Non-Coding RNAs
lncRNAs	Long Non-Coding RNAs
mRNAs	Messenger RNAs
miRNAs	MicroRNAs
MVBs	Multivesicular Bodies
CRPC	Castration-Resistant Prostate Cancer
HIFs	Hypoxia-Inducible Factors
EZH2	Enhancer of Zeste Homolog 2
AR	Androgen Receptor
EGFR	Epidermal Growth Factor Receptor
EMT	Epithelial-Mesenchymal Transition
TGFβ1	Transforming Growth Factor Beta 1
mTOR	Mechanistic Target of Rapamycin
PTEN	Phosphatase and Tensin Homolog
VHL	Von Hippel-Lindau
VEGF	Vascular Endothelial Growth Factor
PDGF	Platelet-Derived Growth Factor
HOTAIR	HOX Transcript Antisense RNA
GAS5	Growth Arrest-Specific 5
FOXM1	Forkhead Box M1
SOX2	SRY-Box Transcription Factor 2
HMGA1	High Mobility Group AT-Hook 1
NF-κB	Nuclear Factor Kappa B
AXL	AXL Receptor Tyrosine Kinase
c-MET	Mesenchymal-Epithelial Transition Factor
IL-6	Interleukin 6
STAT3	Signal Transducer and Activator of Transcription 3
UCA1	Urothelial Cancer Associated 1
PCA3	Prostate Cancer Antigen 3
TMPRSS2-ERG	Transmembrane Protease Serine 2 - Erythroblast Transformation-Specific Related Gene
SChLAP1	Second Chromosomal Locus Associated with Prostate Cancer 1
PVT1	Plasmacytoma Variant Translocation 1
MALAT1	Metastasis-Associated Lung Adenocarcinoma Transcript 1
HOXD-AS1	HOXD Antisense Growth-Associated Long Non-Coding RNA 1
NEAT1	Nuclear Enriched Abundant Transcript 1
SOX5	SRY-Box Transcription Factor 5
PRC2	Polycomb Repressive Complex 2
MDM2	Mouse Double Minute 2 Homolog
SND1	Staphylococcal Nuclease and Tudor Domain Containing 1
PTX	Paclitaxel
RCC	Renal Cell Carcinoma
ccRCC	Clear Cell Renal Cell Carcinoma
MNT	Metanephric Tumor
TUG1	Taurine Upregulated Gene 1
CYP4A22	Cytochrome P450 Family 4 Subfamily A Member 22
GHET1	Gastric Carcinoma High Expressed Transcript 1
BLACAT2	Bladder Cancer Associated Transcript 2
SPRY4-IT1	Sprouty 4 Intronic Transcript 1
LINC00857	Long Intergenic Non-Protein Coding RNA 857
TINCR	Terminal Differentiation-Induced Non-Coding RNA

frontiers | Frontiers in Pharmacology

TYPE Original Research
PUBLISHED 01 November 2024
DOI 10.3389/fphar.2024.1500731

Check for updates

OPEN ACCESS

EDITED BY
Hailin Tang,
Sun Yat-sen University Cancer Center (SYSUCC), China

REVIEWED BY
Yong Zhang,
The Second Affiliated Hospital of Xi'an Jiaotong University, China
Yanfeng Liu,
Shandong University, China
Xiaofang Guo,
University of South Florida, United States

*CORRESPONDENCE
Ziyang Cao,
mccaozy@scut.edu.cn
Jie Cao,
eycaojie@scut.edu.cn

†These authors share first authorship

RECEIVED 23 September 2024
ACCEPTED 15 October 2024
PUBLISHED 01 November 2024

CITATION
Shen F, Zheng Y-S, Dong L, Cao Z and Cao J (2024) Enhanced tumor suppression in colorectal cancer via berberine-loaded PEG-PLGA nanoparticles.
Front. Pharmacol. 15:1500731.
doi: 10.3389/fphar.2024.1500731

COPYRIGHT
© 2024 Shen, Zheng, Dong, Cao and Cao. This is an open-access article distributed under the terms of the Creative Commons Attribution License (CC BY). The use, distribution or reproduction in other forums is permitted, provided the original author(s) and the copyright owner(s) are credited and that the original publication in this journal is cited, in accordance with accepted academic practice. No use, distribution or reproduction is permitted which does not comply with these terms.

Enhanced tumor suppression in colorectal cancer via berberine-loaded PEG-PLGA nanoparticles

Fei Shen[1,2†], Yun-Sheng Zheng[2†], Lan Dong[2], Ziyang Cao[2]* and Jie Cao[1,2]*

[1]Department of General Surgery, The First Affiliated Hospital, Jinan University, Guangzhou, China, [2]Department of General Surgery, Guangzhou Digestive Disease Center, The Second Affiliated Hospital, School of Medicine, South China University of Technology, Guangzhou, China

Colorectal cancer (CRC) stands as the third most widespread cancer globally with poor prognosis. Berberine (Ber), as one herbal phytochemical, showed promise in CRC therapy, but its exact mechanism is unclear. Small molecule traditional drugs face challenges in quick metabolism and low bio-availability after systemic administration. Nanodrug deliver system, with their unique properties, has the advantages of protecting drugs, improving drug bio-availability, and reducing toxic and side effects, which exhibited huge drug delivery potential. Herein, the PEG-PLGA nanocarrier was used for encapsulated Ber according to nanoprecipitation and obtained nanomedicine, denoted as NPBer. *In vitro*, the flow cytometry test and CCK8 assays indicated that NPBer was more easily taken up by HCT116 CRC cells, and had stronger inhibition on cell proliferation with the increase of drug concentration. In addition, RNA-Seq was employed to explore the alterations in the transcriptomes of cancer cells subsequent to treatment with Free Ber or NPBer.The sequencing results indicate that Free Ber could activate cellular aging mechanisms, intensified the iron death pathway, optimized oxidative phosphorylation efficiency, exacerbated apoptosis, accelerated programmed cell death, and negatively modulated key signaling pathways in CRC cells including Wnt, TGF-beta, Hippo, and mTOR signaling pathways. Based on PEG-PLGA nanocarriers, NPBer can improve the *in vivo* delivery efficiency of Ber, thereby enhancing its antitumor efficacy *in vivo*, enhancing apoptosis by enhancing the mitochondrial autophagy and autophagy activities of CRC cells, negatively regulating the inflammatory mediator to regulate TRP channels, and inhibiting the activation of Notch signaling pathway. *In vivo*, NPBer can significantly improve its accumulation and durable drug targeting in tumor site, resulting in induce maximum cell apoptosis and effectively inhibit the proliferation of HCT116 tumor. This strategy provided a promising antitumor therapeutic strategy using Ber-based drugs.

KEYWORDS

colorectal cancer, berberine, RNA-seq, nanocarrier, signaling pathways

1 Introduction

Colorectal cancer (CRC) is classified as a malignant tumor of the digestive system and ranks third in the estimated number of new cases among both men and women in the United States (Siegel et al., 2024), also seriously endangering the health of the Chinese people (Ju et al., 2023). Surgical treatment, chemotherapy, radiotherapy, and

immunotherapy are currently the main treatments for CRC (Shinji et al., 2022; Riesco-Martinez et al., 2022; Modest et al., 2019; Sanuki et al., 2022; Zhao et al., 2022). Among these treatments, chemotherapy plays a crucial role as both a primary and adjuvant therapy for CRC. Current research focuses on optimizing the efficacy of chemotherapeutic agents, while addressing challenges related to drug toxicity, side effects, and the development of resistance (Gottesman et al., 2023; Yang et al., 2024). Most diseases are caused by abnormal gene expression, and identifying drugs that can specifically target these genes is crucial for disease prevention and treatment (Singh et al., 2018; Tao et al., 2024). It is worth noting that traditional Chinese medicine (TCM) has seen increasingly widespread application in tumor treatment (Xiang et al., 2019; Liu Y. et al., 2024). Numerous studies have consistently demonstrated that TCM not only has the potential to alleviate cancer-related symptoms, such as fatigue, loss of appetite, cachexia, and persistent pain, thereby improving patients' quality of life, but it also effectively reduces the adverse reactions and complications commonly associated with chemotherapy, radiotherapy, and targeted therapies (Zhou and Jiang, 2019; Zhang et al., 2021; Huang et al., 2019; Liu K. et al., 2024; Wang et al., 2022). However, the poor water solubility and low bio-availability of many TCM compounds, along with their short circulation times in the body, result in reduced drug efficacy and limited accumulation in tumor tissues. Thus, enhancing the therapeutic potency of chemotherapeutic agents and improving their tumor accumulation and retention is a key. Recently, nanocarriers have emerged as important tools in drug delivery, regarded as ideal vehicles for transporting a wide range of drugs due to their excellent storage stability, inherent biocompatibility, biodegradability, and ease of surface modification (Sun et al., 2022; Wei et al., 2022; Kang et al., 2023). Furthermore, novel strategies employing nanocarriers have shown promise in overcoming drug resistance in cancer (Hu et al., 2022; Benko et al., 2021).

In this study, we utilized a FDA-proved nanomaterial, PEG-PLGA (Zhang et al., 2014), consist of covalent connected polyethylene glycol (PEG) and PLGA, to encapsulate Berberine (Ber) according to nanoprecipitation and obtained a berberine-loaded nanomedicine (denoted as NPBer). Flow cytometry and confocal microscopy revealed that NPBer is effectively internalized by HCT116 tumor cells, leading to significant inhibition of HCT116 CRC cell proliferation. Furthermore, to assess its *in vivo* antitumor efficacy, the HCT116 nude mouse xenograft model was used to study the systemic administration of NPBer. The results demonstrated that NPBer could effectively accumulate and remains in the tumor site, ultimately achieving notable anti-tumor effects. These findings provided a novel nanocarrier-based delivery strategy for Ber drug therapy in CRC.

2 Materials and methods

2.1 Cell lines and animals

The HCT116 CRC cancer cell lines were sourced from the American Type Culture Collection and then propagated in Dulbecco's Modified Eagle Medium (DMEM) that was fortified with 10% fetal bovine serum (FBS) and 1% penicillin-streptomycin, maintained at 37°C in an incubator, which was adjusted to a 5% CO_2 environment.

The male BALB/c nude mice (aged 6 weeks) were procured from Charles River, Beijing, China. The experimental procedures received approval from the Animal Care and Use Committee of the South China University of Technology.

2.2 Preparation of NPBer

PEG-PLGA nanoparticles and Berberine (Ber, Sigma-Aldrich, Germany) were fabricated according to the nanoprecipitation method (Almoustafa et al., 2017). After uniformly mixing 10 mg of polyethylene glycol-poly lactic acid-co-glycolic acid (PEG-PLGA) (1 mL DMSO) with 1 mg of Ber (200 μL DMSO), the mixture was added dropwise to 1 mL of deionized water and stirred for 2 h. Free drugs and DMSO were removed by dialysis. The particles were concentrated using a rotary evaporator, and the drug concentration was quantified using a microplate reader (UV absorption peak at 340 nm) to prepare the nanoparticle Ber (NPBer). Therefore, the drug loading capacity (DLC) of Ber within NPBer was quantified by applying the subsequent equation: $DLC\% = (M_{Ber}/M_{nanocarrier}) \times 100\%$.

2.3 *In Vitro* cytotoxicity evaluation using CCK-8 assay

To examine the effect of PEG-PLGA nanomaterials on cell proliferation *in vitro*, the CCK-8 reagent (supplied by Biosharp, Hefei, China) was employed. The experimental protocol commenced by seeding HCT116 CRC cells onto 96-well plates at a density of 6×10^3 cells per well. These plates were then incubated at 37°C to allow for cellular attachment and growth.The culture medium was exchanged with complete medium, which contained PEG-PLGA at varying concentrations. The CCK-8 reagent was administered to each group according to the manufacturer's instructions. The absorbance was then measured using an appropriate spectrophotometer to quantify the viability of HCT116 CRC cells.

Further, in order to verify whether Ber can be rapidly absorbed by cells and continue to act after being coated with nanomaterials. Subsequently, after cell adhesion, the culture medium was exchanged with complete medium, which contained different concentrations of Free Ber, or NPBer for 4 h, replaced the complete medium, and continued to incubate for 20 h, and then carried out CCK-8 detection.

To assess the ongoing cytotoxic effects of Free Ber or NPBer on HCT116 CRC cells, after cell adhesion, the culture medium was exchanged with complete medium, which contained either Free Ber, or NPBer, each at varying concentrations, and carried out CCK-8 detection after a 36-h incubation period.

2.4 *In Vitro* cellular uptake

To evaluate the cellular internalization of the nanoparticles, both confocal laser scanning microscopy (CLSM) and flow cytometry techniques were utilized.

In the flow cytometry experiment, the initiation of the experimental protocol involved seeding HCT116 CRC cells onto 6-well plates, ensuring a density of 1×10^5 cells per well, and then subsequent to the incubation with PBS, Free Ber or NPBer for 2 h or 4 h. The resulting cell suspension was then analyzed using a flow cytometer to quantify the uptake of the nanoparticles.

In the CLSM protocol, HCT116 CRC cells were plated onto 12-well plates equipped with cell-adherent slides. Once the cells adhered, the culture medium was exchanged with a serum-free medium containing Free Ber or NPBer. Following a 4-h incubation period, the cells underwent a rinsing process with phosphate-buffered saline (PBS), followed by fixation with 4% paraformaldehyde (PFA). Subsequently, the cells were counterstained with Hoechst 33,342 living cell staining solution (Beyotime, China) to visualize their nuclei, and subsequently observed under a confocal laser scanning microscope.

2.5 Transcriptomic analysis for uncovering anticancer mechanisms of NPBer

To elucidate the underlying anticancer biological mechanisms of NPBer, we conducted a comprehensive transcriptomic analysis on cancer cells utilizing RNA sequencing technology.

2.6 Biodistribution and targeting capacity of NPBer *In Vivo*

HCT116 CRC tumor-bearing mice were intravenously injected with Free Ber or NPBer (Ber = 1.0 mg/kg, n = 3). 24 h after drug injection, the mice were humanely euthanized, and subsequently, their tumor tissues and primary organs were harvested, and the Xenogen IVIS Lumina system (Caliper Life Sciences) was utilized to capture images of the Mean Fluorescence Intensity (MFI) for further imaging analysis.

2.7 *In Vivo* antitumor activity of NPBer

A total of 15 Tumor-bearing Balb/c mice were randomly allocated into groups of five mice each, and underwent treatment via tail vein injection. The treatments included PBS, Free Ber and NPBer (at a concentration of 1.0 mg/kg). Throughout the experiment, the tumor volume and body weight of the mice were carefully monitored and recorded.

Following a period of 15 days, the mice underwent euthanasia procedures. Subsequently, their tumors were carefully excised and then precisely weighed. Additionally, the vital organs including the heart, liver, spleen, lungs, and kidneys were harvested and subjected to H&E staining for histological examination. Blood samples were also collected for serum biochemical analysis. Alanine aminotransferase (ALT/GPT) test kit, creatinine (Cr) test kit, urea nitrogen (BUN) test kit, uric acid (UA) test kit, albumin test kit, aspartate aminotransferase (AST/GOT) test kit were purchased from Nanjing Jianguo Bioengineering Research Institute Co., LTD., and detected by ELISA method according to instructions in the manual.

For the tumor tissues collected from the euthanized mice, formalin fixation was carried out to prepare paraffin-embedded slides, which were subsequently subjected to TUNEL assay (#G1504, Servicebio, China) for detecting cell apoptosis and Ki67 (#GB111141, Servicebio, China) immunohistochemistry staining for the assessment of proliferation.

2.8 Statistical analysis

All data are expressed as mean ± standard deviation. SPSS 18.0 software was used for statistical analysis. The measurement data were analyzed using one-way ANOVA, and LSD test and Mann-Whitney U test were used to compare the mean values between groups. A P-value <0.05 was considered statistically significant.

3 Result

3.1 Preparation and characterization of NPBer nanomedicine

First, we assessed the impact of PEG-PLGA nanomaterials on cell viability by testing a concentration range from 0 to 1.6 mg/mL. The results indicated that PEG-PLGA nanomaterials did not affect cell viability (Figure 1A). PEG-PLGA nanoparticles and Ber were synthesized using the nanoprecipitation method. Dynamic light scattering (DLS) analysis revealed that the size of the bare NPBer was approximately 102.3 ± 1.9 nm (Figure 1B). Additionally, UV-Vis spectroscopy demonstrated that NPBer exhibited absorption peaks similar to those of free Berberine (Figure 1C). The entrapment efficiency (EE) of NPBer was found to be 48.9% ± 1.1%, and the drug loading capacity (DLC) of Berberine within NPBer was 4.9% ± 0.1% (Figure 1D).

3.2 Cellular uptake and cellur proliferation of NPBer *in vitro*

To investigate the effect of drug-encapsulating nanomaterials on cellular uptake, flow cytometry (FCM) was employed to measure the fluorescence intensity of drug internalization. Compared to Free Ber, NPBer demonstrated significantly higher cellular uptake in HCT116 CRC cells at various time points, indicating that nanomaterial encapsulation enhances Ber's internalization (Figure 1E). Confocal laser scanning microscopy (CLSM) further confirmed that HCT116 CRC cells incubated with NPBer exhibited superior uptake efficiency compared to cells treated with Free Ber (Figure 1F).

To ascertain whether Ber, when encapsulated with nanomaterials, retains its ability to be swiftly absorbed by cells and sustain its activity, we conducted an experiment. We first incubated various concentrations of Free Ber or NPBer for 4 h. Subsequently, we replaced the medium with fresh complete medium and extended the incubation period for an additional 20 h. Following this, we employed the CCK-8 assay to evaluate the cellular response. The results showed that compared with the

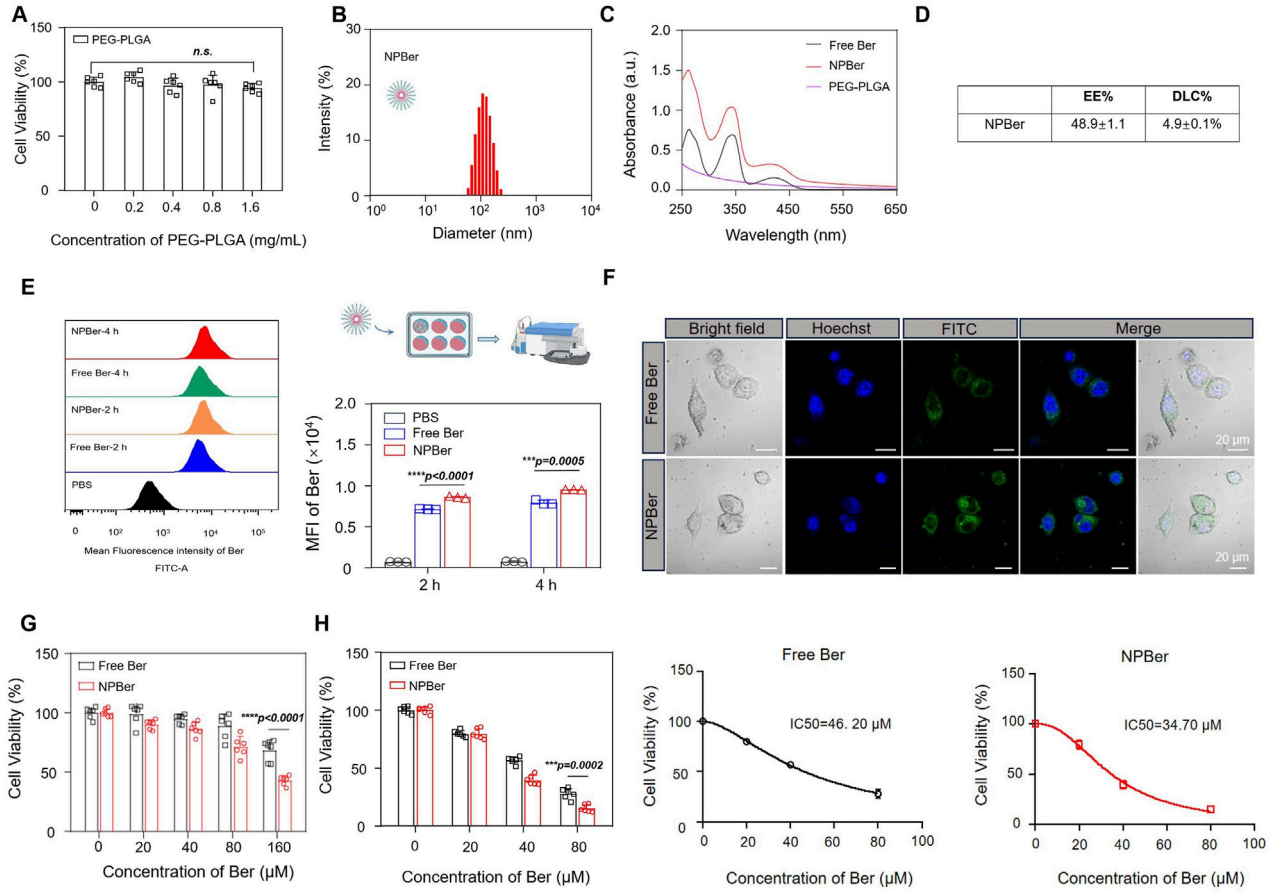

FIGURE 1
Preparation, Characterization and the intracellular uptake of NPBer, and *In vitro* experiments affect the proliferation of tumor cells. **(A)** Effect of PEG-PLGA on cell activity of HCT116 CRC cells. **(B)** The hydrodynamic size of the NPBer. **(C)** UV–vis spectra of Free Ber, NPBer, and PEG-PLGA. **(D)** The entrapment efficiency (EE) and the drug loading capacity (DLC)of NPBer. **(E)** Flow cytometry analysis of HCT116 CRC cells co-incubated with Free Ber, NPBer, or PBS. **(F)** CLSM images of HCT116 CRC cells internalization of Free Ber or NPBer. Blue: Hoechst 33,342, green: Ber. Scale bar: 20 μm. **(G)** Viability of HCT116 CRC cells were co-cultured with Free Ber and NPBer at different concentrations for 4 h. **(H)**Viability of HCT116 CRC cells were co-cultured with Free Ber and NPBer at different concentrations for 36 h.

Free Ber group, the cell proliferation inhibition ability of the NPBer group was stronger with the increase of drug concentration during early incubation (Figure 1G). These results indicated that NPBer could exhibit stronger antitumor activity, which was consistent with the previous cell uptake experimental results, mainly due to the easier uptake of NPBer by HCT116 CRC cells.

Subsequently, we evaluated the ongoing effect of Free Ber or NPBer on cell proliferation. HCT116 CRC cells were co-cultured with Free Ber or NPBer at different concentrations. The CCK-8 assay results, presented in Figure 1H, revealed that cell viability in the NPBer group was significantly lower than in the Free Ber group. The IC50 values for Free Ber and NPBer were 46.20 μM and 34.70 μM, respectively (Figure 1H).

3.3 RNA-seq analysis

To elucidate the mechanism of NPBer, we performed RNA-Seq analysis on HCT116 CRC cells exposed to PBS, Free Ber, or NPBer. Our initial analysis focused on the transcriptional profiles of 6,163 genes (Figure 2A). As shown in Figure 2B, we identified a distinct set of 1,331 genes that were exclusively transcribed in cells treated with Free Ber compared to the PBS-treated control group. Conversely, 1,053 genes were specifically transcribed in cells treated with NPBer relative to the PBS group. Additionally, 126 genes were uniquely transcribed in NPBer-treated cells compared to those treated with Free Ber.

Figure 2B also illustrates that, compared to the PBS control, Free Ber treatment led to the upregulation of 1,825 genes and downregulation of 3,029 genes. Similarly, NPBer treatment resulted in the upregulation of 1,784 genes and downregulation of 2,769 genes. Notably, NPBer treatment induced differential gene expression compared to Free Ber, with an upregulation of 361 genes and a downregulation of 157 genes.

To visualize these changes, we compared the top 60 differentially expressed genes (DEGs) from each sample and generated a heatmap (Figure 2C). We utilized the Kyoto Encyclopedia of Genes and Genomes (KEGG) database (http://www.genome.jp/) for bio-pathway enrichment analysis to identify significantly enriched pathways among DEGs from the various samples. Figure 2D

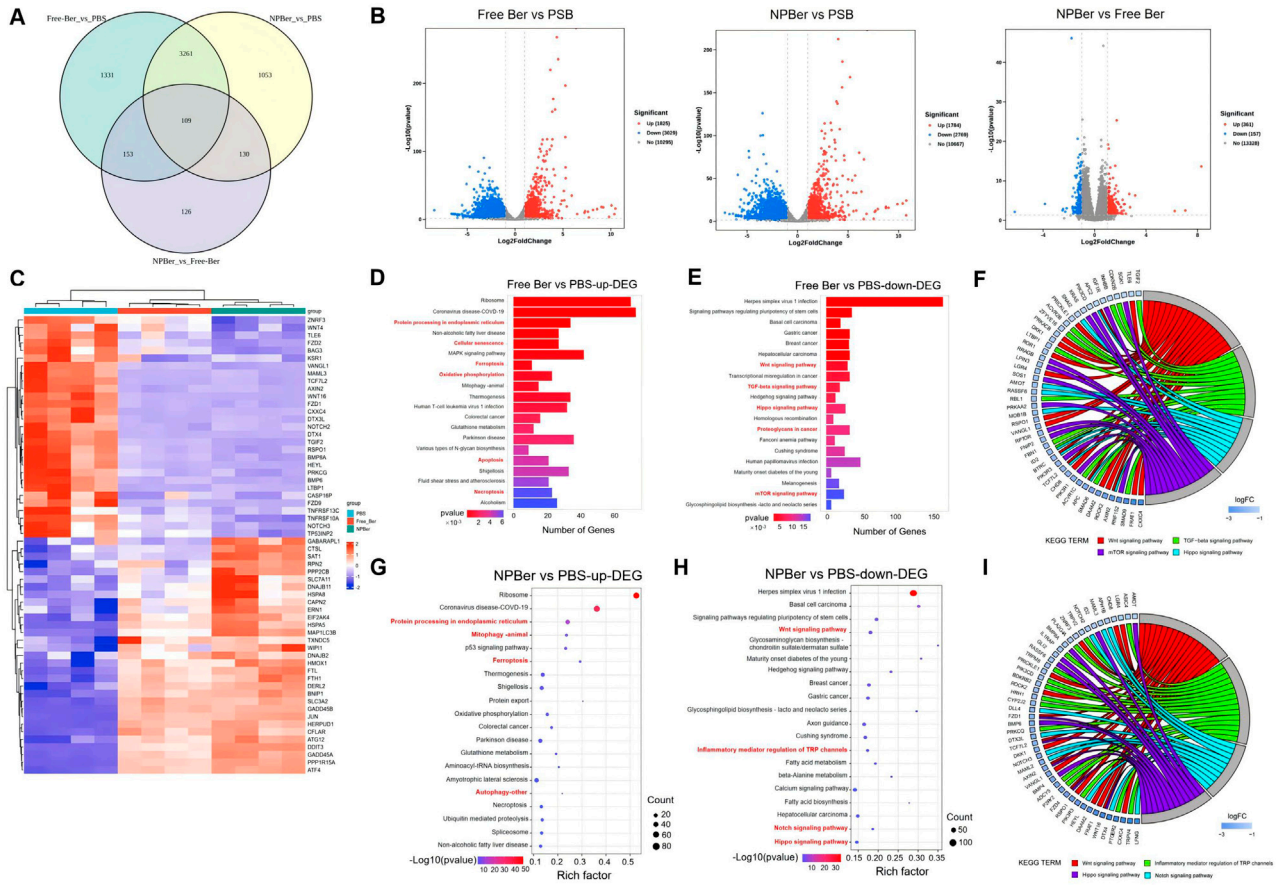

FIGURE 2
RNA-seq analysis of HCT116 CRC cells treated with PBS, Free Ber and NPBer. **(A)** Venn diagram revealed the number of genes transcribed in each treatment group. **(B)** Volcano plots displayed the differentially expressed genes. **(C)** Heat-map of gene expressions in cells treated with PBS, Free Ber, and NPBer. KEGG analysis of **(D)** upregulated and downregulated **(E)** differentially expressed genes between cells treated with PBS and those treated with Free Ber. **(F)** The chord diagram displays specific molecules/genes enriched in pathways between cells treated with PBS and those treated with Free Ber in KEGG. KEGG analysis of **(G)** upregulated and downregulated **(H)** differentially expressed genes between cells treated with PBS and those treated with NPBer. **(I)** The chord diagram displays specific molecules/genes enriched in pathways between cells treated with PBS and those treated with NPBer in KEGG.

presents the enrichment analysis results for upregulated genes following Free Ber treatment, highlighting key biological pathways such as protein processing in the endoplasmic reticulum, activation of cellular senescence mechanisms, enhancement of ferroptosis pathways, improved oxidative phosphorylation efficiency, increased apoptosis, and facilitated necroptosis.

Figure 2E shows the enrichment analysis results for downregulated genes after Free Ber treatment, revealing significant downregulation of pathways including Wnt signaling, TGF-beta signaling, Hippo signaling, and mTOR signaling—all of which are closely related to CRC development. Additionally, proteoglycans incancer were found to be downregulated. Figure 2F displays a chord diagram illustrating specific molecules/genes that impact the main enriched pathways in KEGG. These findings collectively reveal the multifaceted effects of Free Ber on the biological processes of CRC cells.

NPBer treatment significantly enhanced the expression levels of specific biological pathways, similar to those observed with Free Ber treatment. This included increased protein processing within the endoplasmic reticulum and augmentation of ferroptosis pathways, along with additional improvements in mitophagy and autophagy (Figure 2G). Conversely, Figure 2H illustrates that NPBer treatment induced downregulation of pathways akin to Free Ber treatment, notably suppressing the Wnt and Hippo signaling pathways while promoting ferroptosis. Additionally, NPBer treatment downregulated the regulatory role of inflammatory mediators on TRP channels and inhibited the Notch signaling pathway. The key molecules and genes involved in these pathways are further detailed in the chord diagram (Figure 2I). These findings highlight the potential of drug encapsulated in nanomaterials to modulate cellular signal transduction and inflammatory responses effectively.

3.4 Biodistribution, targeting capacity, antitumor performance and biosafety of NPBer *In Vivo*

HCT116 CRC xenograft tumor-bearing mice were established with three mice per group to investigate the *in vivo* biodistribution and targeting capacity of NPBer. Mice received tail vein injections of either Free Ber or NPBer (n = 3 each group), and the fluorescence

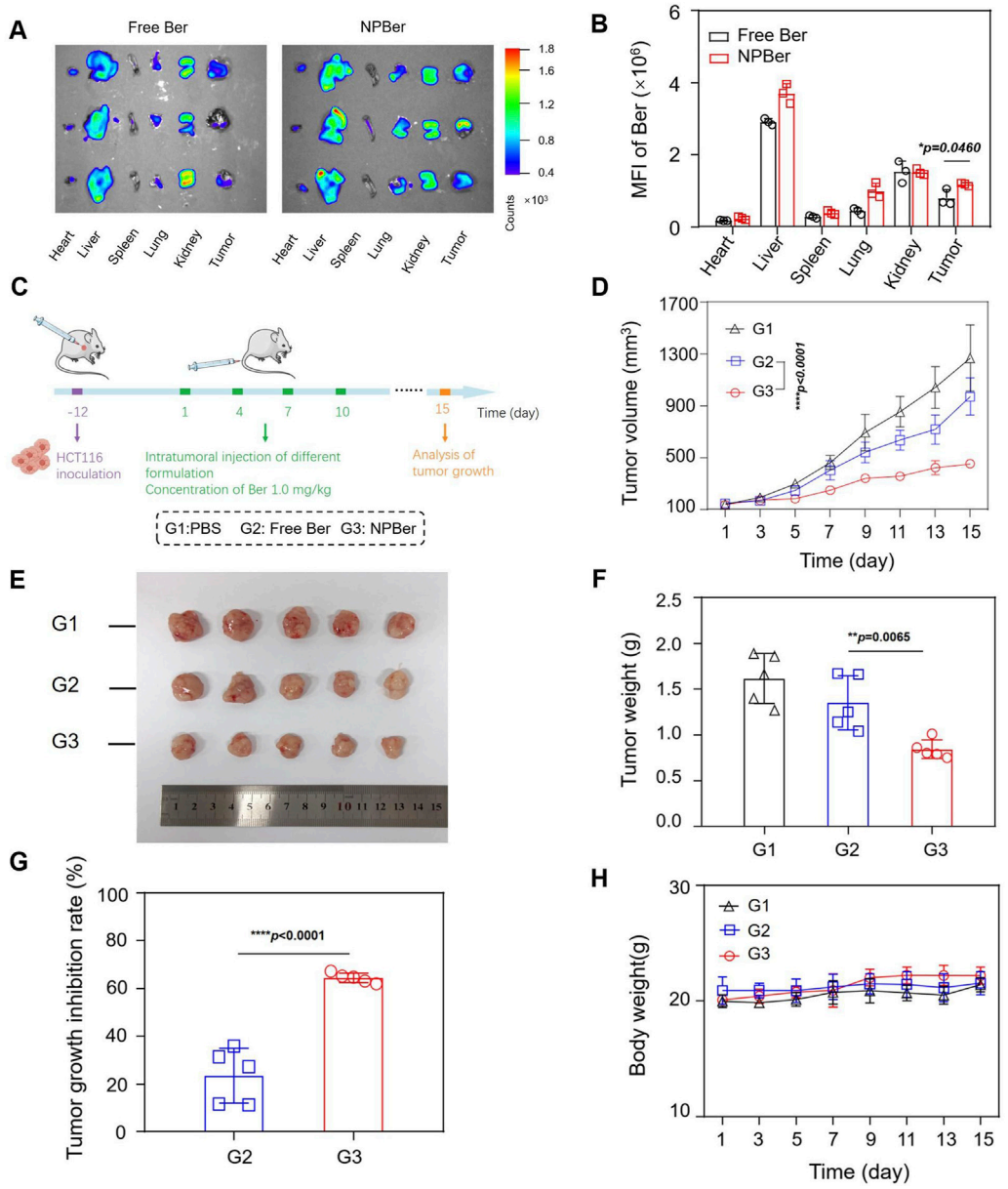

FIGURE 3
Biodistribution, Targeting Capacity and Antitumor Performance of NPBer *In Vivo*. **(A)** Fluorescence images and **(B)** mean fluorescence intensity of *ex vivo* tumor tissues and major organs. **(C)** Schematic treatment schedule. Arrows show the time points of intravenous injection of different drugs (n = 5). **(D)** HCT116 CRC tumor average growth curve after different treatments. **(E)** Images, weights **(F)** and growth inhibition rate **(G)** of extracted tumor tissues after various treatments. **(H)** The change curve of Mice body weight in various treatment groups.

signals were monitored using an *In Vivo* Imaging System (IVIS). After 24 h, the mice were sacrificed, and ex*vivo* biodistribution of NPBer was analyzed. Figure 3A and B reveal that NPBer treatment resulted in significantly stronger fluorescence at the tumor site compared to Free Ber treatment. In major organs, the fluorescence intensity was most pronounced in the liver, with lower intensity observed in other organs such as the heart, spleen, lungs, and kidneys.

To evaluate the antitumor efficacy of NPBer, HCT116 CRC xenograft tumor-bearing mice were intravenously injected with PBS, Free Ber, or NPBer (at a total dose of 1 mg Ber/kg, n = 5 each group) via the tail vein on days 1, 4, 7, and 10 (Figure 3C). On day 15, blood samples, as well as major tissues and organs, were collected from the treated mice for comprehensive analysis. Figure 3D shows that NPBer treatment led to the most significant suppression of HCT116 tumor growth, compared to Free Ber, which exhibited a moderate inhibitory effect on tumor progression. Assessment of tumor tissue images, post-treatment weight, and tumor growth inhibition rates demonstrated that NPBer was the most effective in terms of anti-tumor efficacy (Figures 3E–G). There were no significant changes in body weight among the mice in any treatment group throughout the study period (Figure 3H).

TUNEL assay results, which are depicted in Figure 4, revealed DNA double-strand breaks. Nuclei were stained blue with 4′,6-

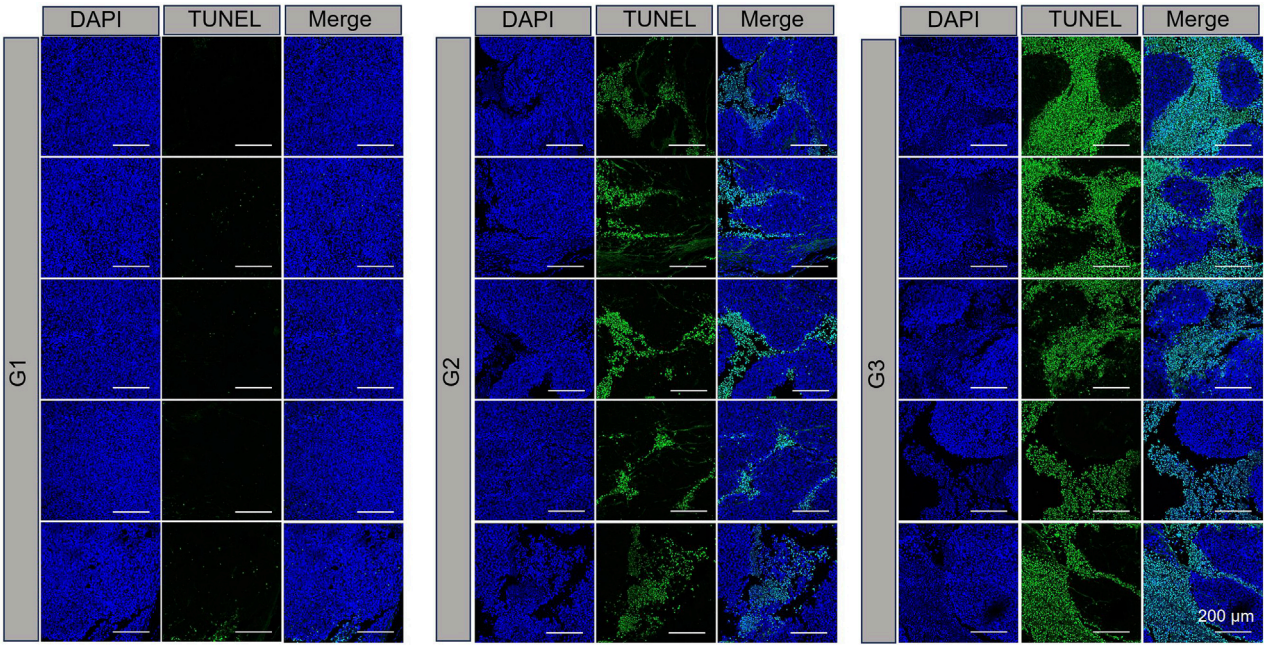

FIGURE 4
TUNEL staining of tumor tissues. G1: treatment with PBS; G2: treatment with Free Ber; G3: treatment with NPBer.

diamidino-2-phenylindole (DAPI), while nuclear damage was indicated by green fluorescence. The proportion of TUNEL-positive cells with green fluorescence was notably higher in the NPBer group, followed by the Free Ber group, compared to the control tissues. Immunohistochemical staining further confirmed that NPBer treatment was the most effective in inhibiting tumor cell proliferation, as evidenced by the significant reduction in brown-stained Ki67-positive cells (Figure 5). These results indicate that NPBer demonstrated superior performance in targeting tumors.

Next, the bio-safety of NPBer was evaluated *in vivo*. Figure 3H illustrated that there were no significant changes in body weight among mice in any treatment group throughout the treatment period. Furthermore, histological examination using hematoxylin and eosin (H&E) staining of major organs revealed no discernible morphological changes in mice treated with Free Ber or NPBer, compared to those treated with PBS (Figure 6A). Additionally, an extensive analysis of blood physiological and biochemical markers showed that levels of albumin (ALB), alanine aminotransferase (ALT), aspartate aminotransferase (AST), blood urea nitrogen (BUN), serum creatinine (Cre), and uric acid (UA) in mice treated with Free Ber or NPBer remained statistically similar to those of the PBS-treated group (Figures 6B–G). Collectively, these findings underscore the minimal toxicity and robust safety profile of NPBer *in vivo*.

4 Discussion

In recent years, colorectal cancer (CRC) has emerged as the third most prevalent cause of cancer-related mortality worldwide. This increase is attributed to factors such as an aging population, modern dietary habits, insufficient physical activity, smoking, obesity, and other risk factors. In the United States, CRC is the third leading cause of both new cancer cases and cancer-related deaths among men and women (Siegel et al., 2023). In recent years, significant progress has been made in the third-line treatment options for advanced CRC, with a notable expansion in therapeutic drugs. Notably, the 2020 Chinese Society of Clinical Oncology (CSCO) Guidelines for Diagnosis and Treatment of CRC introduced Trifluridine/Tipiracil (TAS-102), further broadening the therapeutic options. In 2021, the combination therapy of TAS-102 and Bevacizumab gained recognition, offering patients even more diverse treatment choices. However, the challenge remains in achieving specific targeting of antitumor drugs to cancer cells, enhancing the ability of chemotherapy drugs to be taken up by cancer cells, thereby boosting anti-tumor efficacy and mitigating side effects of chemotherapy. In the realm of pharmacotherapy, there is a need to design novel anticancer drugs that can augment therapeutic efficacy, providing CRC patients with both effective treatment modalities and rational therapeutic regimens. Investigating the molecular mechanisms driving CRC initiation and progression, identifying pertinent biomarkers for diagnosis and treatment, and developing innovative therapeutic strategies are essential for improving clinical outcomes, enhancing patients' quality of life, and extending survival rates. Tumorigenesis and cancer development are typically multifactorial and not attributable to a single gene mutation alone. Consequently, the multi-target properties of active compounds in traditional Chinese medicine (TCM) have increasingly attracted attention as potential anti-tumor agents or adjunctive therapies to conventional chemotherapy (Zhang et al., 2021; Yan et al., 2017).

Berberine (Ber), an isoquinoline alkaloid extracted from Coptis chinensis, has gained considerable attention for its diverse biological activities, including anti-inflammatory, anti-cancer, anti-ulcer,

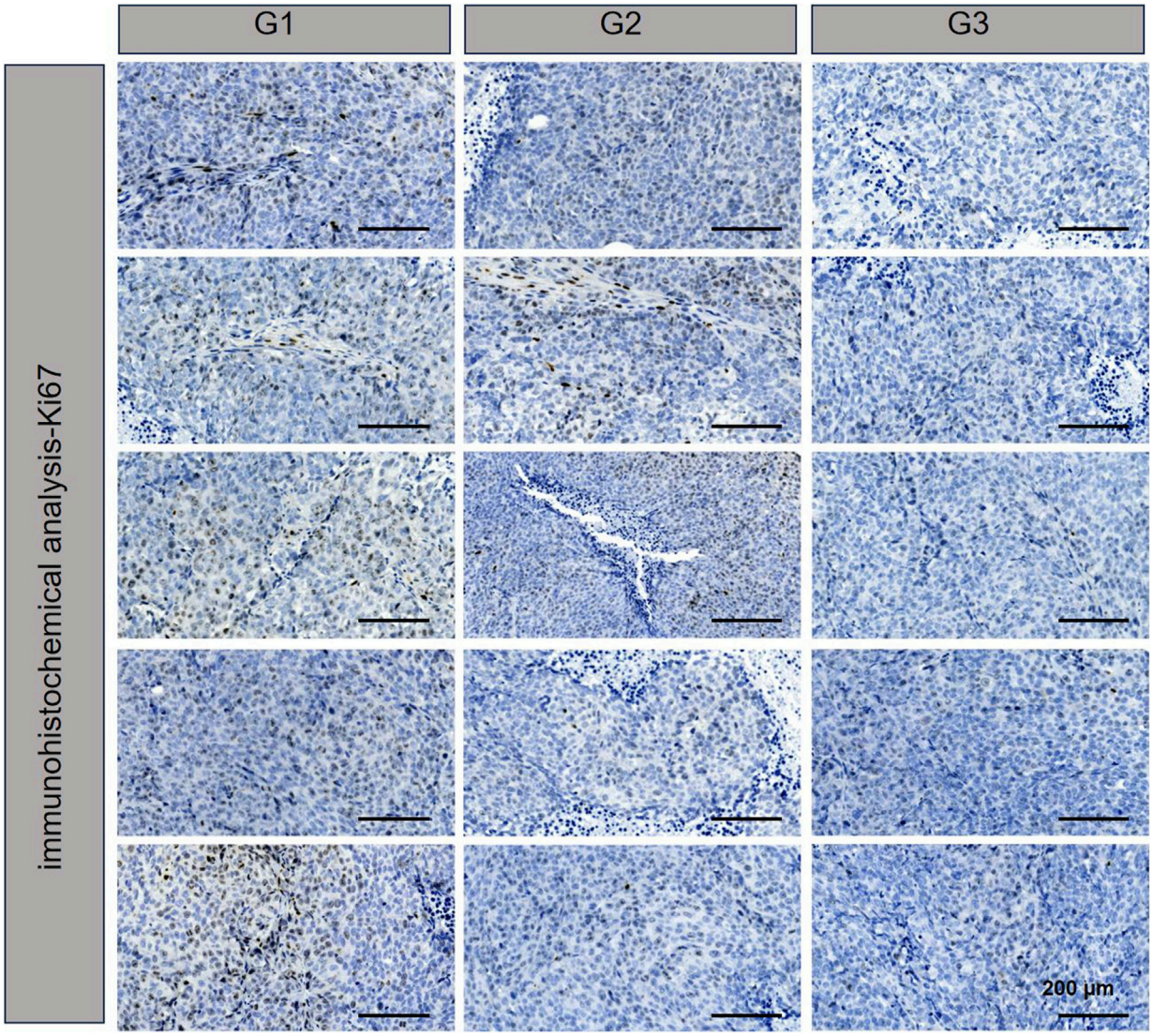

FIGURE 5
Ki67 of tumor tissues.G1: treatment with PBS; G2: treatment with Free Ber; G3: treatment with NPBer.

antibacterial, and immune-enhancing effects. These activities are attributed to its pharmacological properties. In the treatment of neurodegenerative diseases, Ber, through its activation of 5′-AMP-activated protein kinase (AMPK), has been shown to counteract common neurodegenerative events (Qin et al., 2020). Recent research, encompassing basic, translational, and clinical studies, has unveiled numerous novel molecular targets of Ber, highlighting its promising potential in treating cardiovascular diseases (Feng et al., 2019). Furthermore, Ber's anti-tumor properties have recently attracted significant interest. For instance, Xu et al. demonstrated that Ber inhibits gastric cancer development by downregulating IL-6 expression via the JAK2/STAT3 signaling pathway (Xu et al., 2022). Similarly, Gu et al. (2022) proposed that Ber may modulate Protein Arginine Deiminase 4 (PAD4)-associated macrophage functions to prevent lung cancer. Despite these promising findings, the clinical application of Ber is limited by its poor intestinal absorption and rapid metabolism, leading to low oral bio-availability and a short half-life (Wang et al., 2017).

To address these limitations, encapsulating Ber within nanomedicine delivery systems such as PEG-PLGA nanoparticles (NPs) has been explored. Menconi et al. (2021) encapsulated 3PAuCl into biocompatible PLGA-PEG NPs, which preserved the drug's free characteristics while enhancing apoptosis and mediating autophagy in CRC cells, thereby demonstrating greater cytotoxic effects.Therefore, encapsulating these active substances within the shell of nanomedicine delivery systems such as PEG-PLGA NPs can significantly enhance their performance and effectiveness. These nanoparticles, a recent innovation, exhibit exceptional biocompatibility and lack immunogenicity, thereby boosting the solubility, safety, stability, and targeted delivery of chemotherapeutic agents (Lee et al., 2022; Lu et al., 2024). Research by Paudel et al. found that loading Ber with nanomaterials can enhance its anti-proliferative and anti-metastatic activities against lung cancer cells (Paudel et al., 2022). In these study, due to the enhanced retention and permeation effect, NPs can remain within the tumor tissue-rich blood vessels and the extensive vascular surface. Phytochemicals and

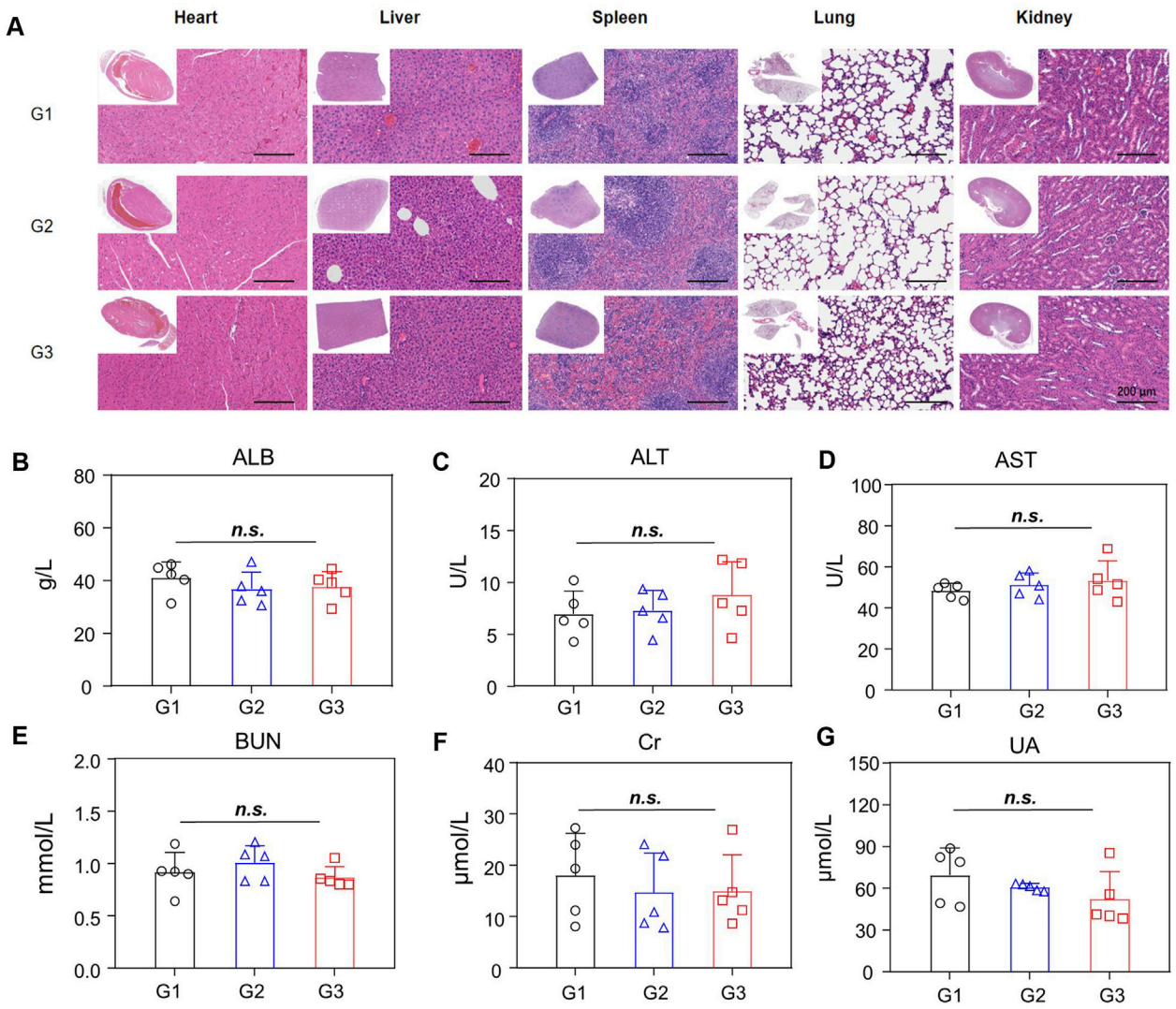

FIGURE 6
Biosafety of NPBer *In Vivo*. **(A)** The assessment of main organs by H&E staining. **(B–G)** Biochemical analysis of the serum of mice with various treatments (n = 5): **(B)** ALB; **(C)** ALT/GPT; **(D)** AST/GOT; **(E)** BUN; **(F)** Cre; **(G)** UA. G1: treatment with PBS; G2: treatment with Free Ber; G3: treatment with NPBer.

their derivatives are swiftly gaining recognition as potential adjunctive treatments for cancer, owing to their ability to modulate signaling cascades that govern cell cycle progression or to directly impact cell cycle regulatory molecules. However, pure phytochemicals have poor bioavailability and short half-lives, making them unsuitable as anticancer drugs. In a related study, Hassani et al. (2022) utilized PLGA-PEG NPs co-loaded with artemisinin and metformin. The results showed that these NPs significantly downregulated hTERT, Bcl-2, cyclin D1, and survivin, while upregulating caspase-3, caspase-7, and Bax in breast cancer cells, thereby enhancing the antitumor therapeutic effect. These findings underscore the potential of combining traditional Chinese medicine (TCM) bioactive components with nanomedicine delivery systems, such as PEG-PLGA NPs, to improve cancer treatment strategies and overcome drug resistance.

Based on the results presented, we hypothesize that encapsulating Ber within nano-drug delivery systems could yield more effective therapeutic outcomes. To investigate this, we first conducted *in vitro* cell viability assays to confirm that pure PEG-PLGA nanomaterials did not affect the viability of CRC cells, thereby demonstrating the biological safety of these materials *in vitro*. Following this, we utilized the PEG-PLGA nano-drug delivery system to encapsulate Ber, resulting in the formation of Berberine nanoparticles (NPBer). Dynamic light scattering (DLS) analysis revealed that NPBer had a size distribution of 102.3 ± 1.9 nm. Ultraviolet-visible (UV-Vis) spectrophotometry was employed to measure the absorption spectra of Free Ber, NPBer, and PEG-PLGA, which indicated that NPBer exhibited the same characteristic UV absorption peak as Free Ber, confirming the successful encapsulation of Ber within the nanoparticles. The encapsulation efficiency of NPBer was determined to be 48.9% ± 1.1%. Additionally, drug loading (4.9% ± 0.1%) was quantified by measuring the absorbance at 340 nm using a multi-function.

To further assess the effect of nano-encapsulated drugs on the uptake capacity of CRC cells, we initially employed flow cytometry

to measure fluorescent intensity (MFI). The results indicated that the MFI in the NPBer group was significantly higher compared to the Free Ber group, both at 2 and 4 h post-treatment, with an observable increase in fluorescence over time. Additionally, we performed a confocal laser scanning microscopy (CLSM) experiment. HCT116 CRC cells incubated with NPBer displayed a markedly enhanced intensity of green fluorescence in the cytoplasm compared to the control group. This finding indicates that the nano-encapsulation of Ber notably improves cellular uptake, which is consistent with the flow cytometry results. Further cell proliferation experiments also confirmed that the drug could continue to act on cells after being pretreated for 4 h. Further research on the effect of continuous drug administration (36 h) on cell proliferation showed that compared with the Free Ber group, the cell proliferation in the NPBer group showed a more significant inhibitory effect when the concentration was gradually increased.

Next, we conducted RNA-seq to further explore the mechanisms of how Free Ber and NPBer inhibit CRC tumor progression. After treatment with Free Ber, CRC cells exhibited upregulation of 1,825 genes and downregulation of 3,029 genes. After treatment with NPBer, the expression levels of 1,784 genes were upregulated, while 2,769 genes were downregulated. Gene Ontology analysis of differentially expressed genes revealed that both Free Ber and NPBer significantly impacted the translation process in the cytoplasm, as well as the structural components of cytoplasmic ribosomes and ribosomes. NPBer further enhanced the nuclear transcription mRNA catabolic process and affected intracellular structural composition, particularly the formation and function of ribonucleoprotein complexes, strengthening regulatory capabilities for ubiquitin ligase inhibitor activity and tRNA binding at the molecular function level. Bioinformatic pathway enrichment analysis using the KEGG database showed that Free Ber treatment activated cell senescence mechanisms, enhanced ferroptosis pathways, improved oxidative phosphorylation efficiency, intensified tumor cell apoptosis, and promoted programmed death. Enrichment analysis of downregulated genes after Free Ber treatment identified CRC-related signaling pathways, including Wnt, TGF-beta, Hippo, and mTOR signaling pathways. The Wnt signaling pathway is a complex network of protein interactions, most commonly observed in tissue embryonic development and cancer but also involved in normal adult physiological processes. Multiple reports have elucidated that the classical Wnt signaling pathway is a recognized driver of colon cancer and holds significant therapeutic significance (Wan et al., 2021). Tanton et al. investigated clinical target therapies for Wnt/β-catenin signaling, exploring a novel β-catenin/BCL9 complex inhibitor that can block oncogenic Wnt signaling and disrupt cholesterol homeostasis in colorectal cancer (Tanton et al., 2022). The TGF-beta signaling pathway plays a crucial role in CRC through four primary mechanisms: promoting epithelial-mesenchymal transition (EMT) by activating downstream signaling pathways (such as Smad-dependent and non-Smad-dependent pathways), enhancing angiogenesis by up-regulating angiogenesis-related factors (e.g., VEGF, MMPs, and Ang-2), inhibiting immune cell activation and function to create an immunosuppressive microenvironment, and regulating stem cell properties in CRC by modulating related signaling pathways such as Wnt/β-catenin and Notch (Li et al., 2022). Modifications and disruptions within crucial elements of the Hippo pathway can trigger cancer development, increase malignancy, foster invasion, promote migration, stimulate metastasis, and induce resistance to therapeutic interventions (Mohajan et al., 2021). The mTOR signaling pathway promotes tumor cell survival, proliferation, and cell cycle progression (Silva et al., 2021). KEGG results show that NPBer treatment also enhances the ferroptosis pathway in CRC cells, additionally boosting mitochondrial autophagy and autophagy functions in tumor cells. NPBer treatment also downregulates the regulatory effects of inflammatory mediators on TRP channels and inhibits the Notch signaling pathway. Ion channels hold crucial positions in a variety of biological processes, like cell cycle regulation and the progression of cancer. Specifically, the TRP family of channels has emerged as potential therapeutic targets (Marini et al., 2023). The Notch signaling pathway has been reported to play a key role in the development of CRC, with at least 86% of CRC and 56% of adenoma patients exhibiting gene over-expression in the Notch signaling pathway (Shaik et al., 2020). Our previous research also indicates that mutations in the Notch signaling pathway are related to the enhancement of anti-tumor immunity in CRC (Wang et al., 2020).

To further investigate the therapeutic potential of Ber encapsulated in nanomaterials, we utilized a nude mouse model implanted with CRC cells. Initially, we examined the biodistribution of NPBer *in vivo*. The fluorescence intensity within the tumor region of the NPBer-treated mice was notably higher, confirming that nanoencapsulation improves the drug's targeting ability. To assess the therapeutic impact, we compared the inhibitory effects of NPBer on CRC tumors with those of Free Ber and PBS. Tumor volumes in both the Free Ber and NPBer groups were significantly reduced compared to the PBS group. Importantly, the NPBer group exhibited significantly smaller tumor volumes compared to the Free Ber group, providing *in vivo* evidence that nano-encapsulation enhances Ber's efficacy in inhibiting tumor growth. Additionally, TUNEL and Ki67 assays of tumor tissues from each group indicated that NPBer induced maximal tumor cell apoptosis and effectively inhibited cell proliferation. These findings underscore the superior therapeutic potential of Ber when encapsulated in nanomaterials.

To further evaluate the *in vivo* bio-safety of the nano-drug delivery system, we monitored the body weights of nude mice throughout the study and conducted histological and biochemical analyses at the study's conclusion. The results including Body Weight Analysis: No significant changes in body weight were observed across all treatment groups, indicating no adverse effects on general health. Histological Examination: Hematoxylin and eosin (HE) staining of major organs—including the liver, spleen, heart, lungs, and kidneys—revealed normal cellular morphology. No abnormalities were detected in the nuclei or intracellular structures of these organs. Serum Biochemical Analysis: Serum biochemical parameters did not show any significant deviations among the different groups, suggesting that the nano-drug delivery system did not induce any detectable systemic toxicity. These findings confirm the excellent biosafety profile of the nano-drug delivery materials used in this study.

5 Conclusion

This research focused on the synthesis of a novel nanoparticle-encapsulated berberine (NPBer) and evaluated its therapeutic

potential. The NPBer nanoparticles demonstrated exceptional stability and durable drug targeting *in vivo*. They were rapidly internalized by tumor cells and effectively inhibited tumor cell proliferation. The activation of Free Ber in CRC cells triggered a cascade of cellular mechanisms, including enhanced ferroptosis, improved oxidative phosphorylation efficiency, and intensified apoptosis, while modulating critical signaling pathways such as Wnt, TGF-beta, Hippo, and mTOR. Furthermore, NPBer facilitated increased mitochondrial and overall autophagy activity, fine-tuned the inflammatory environment by regulating TRP channels, and suppressed the Notch signaling pathway. Collectively, these findings underscore NPBer's potential as a promising therapeutic approach for CRC and suggest its broader applicability in the treatment of various cancers.

Data availability statement

The datasets presented in this study can be found in online repositories. The names of the repository/repositories and accession number(s) can be found below: https://www.ncbi.nlm.nih.gov, PRJNA1166403.

Ethics statement

The animal study was approved by the Animal Care and Use Committee of the South China University of Technology. The study was conducted in accordance with the local legislation and institutional requirements.

Author contributions

FS: Writing–review and editing, Writing–original draft, Investigation, Data curation. Y-SZ: Writing–review and editing, Data curation. LD: Writing–review and editing, Data curation. ZC: Writing–review and editing, Conceptualization. JC: Writing–review and editing, Conceptualization.

Funding

The author(s) declare that financial support was received for the research, authorship, and/or publication of this article. Guangzhou Science and Technology Planning Project (202206080008).

Conflict of interest

The authors declare that the research was conducted in the absence of any commercial or financial relationships that could be construed as a potential conflict of interest.

Publisher's note

All claims expressed in this article are solely those of the authors and do not necessarily represent those of their affiliated organizations, or those of the publisher, the editors and the reviewers. Any product that may be evaluated in this article, or claim that may be made by its manufacturer, is not guaranteed or endorsed by the publisher.

References

Almoustafa, H. A., Alshawsh, M. A., and Chik, Z. (2017). Technical aspects of preparing PEG-PLGA nanoparticles as carrier for chemotherapeutic agents by nanoprecipitation method. *Int. J. Pharm.* 533 (1), 275–284. doi:10.1016/j.ijpharm.2017.09.054

Benko, A., Medina-Cruz, D., Vernet-Crua, A., O'Connell, C. P., Świętek, M., Barabadi, H., et al. (2021). Nanocarrier drug resistant tumor interactions: novel approaches to fight drug resistance in cancer. *Cancer drug Resist. Alhambra, Calif.* 4 (2), 264–297. doi:10.20517/cdr.2020.81

Feng, X., Sureda, A., Jafari, S., Memariani, Z., Tewari, D., Annunziata, G., et al. (2019). Berberine in cardiovascular and metabolic diseases: from mechanisms to therapeutics. *Theranostics* 9 (7), 1923–1951. doi:10.7150/thno.30787

Gottesman, M. M., Robey, R. W., and Ambudkar, S. V. (2023). New mechanisms of multidrug resistance: an introduction to the Cancer Drug Resistance special collection. *Cancer drug Resist. Alhambra, Calif.* 6 (3), 590–595. doi:10.20517/cdr.2023.86

Gu, W., Zhang, M., Gao, F., Niu, Y., Sun, L., Xia, H., et al. (2022). Berberine regulates PADI4-related macrophage function to prevent lung cancer. *Int. Immunopharmacol.* 110, 108965. doi:10.1016/j.intimp.2022.108965

Hassani, N., Jafari-Gharabaghlou, D., Dadashpour, M., and Zarghami, N. (2022). The effect of dual bioactive compounds artemisinin and metformin Co-loaded in PLGA-PEG nano-particles on breast cancer cell lines: potential apoptotic and anti-proliferative action. *Appl. Biochem. Biotechnol.* 194 (10), 4930–4945. doi:10.1007/s12010-022-04000-9

Hu, T., Gong, H., Xu, J., Huang, Y., Wu, F., and He, Z. (2022). Nanomedicines for overcoming cancer drug resistance. *Pharmaceutics* 14 (8), 1606. doi:10.3390/pharmaceutics14081606

Huang, S., Peng, W., Mao, D., Zhang, S., Xu, P., Yi, P., et al. (2019). Kangai injection, a traditional Chinese medicine, improves efficacy and reduces toxicity of chemotherapy in advanced colorectal cancer patients: a systematic review and meta-analysis. *Evidence-based complementary Altern. Med. eCAM* 2019, 8423037. doi:10.1155/2019/8423037

Ju, W., Zheng, R., Zhang, S., Zeng, H., Sun, K., Wang, S., et al. (2023). Cancer statistics in Chinese older people, 2022: current burden, time trends, and comparisons with the US, Japan, and the Republic of Korea. *Sci. China Life Sci.* 66 (5), 1079–1091. doi:10.1007/s11427-022-2218-x

Kang, C., Wang, J., Li, R., Gong, J., Wang, K., Wang, Y., et al. (2023). Smart targeted delivery systems for enhancing antitumor therapy of active ingredients in traditional Chinese medicine. *Mol. Basel, Switz.* 28 (16), 5955. doi:10.3390/molecules28165955

Lee, C. K., Atibalentja, D. F., Yao, L. E., Park, J., Kuruvilla, S., and Felsher, D. W. (2022). Anti-PD-L1 F(ab) conjugated PEG-PLGA nanoparticle enhances immune checkpoint therapy. *Nanotheranostics* 6 (3), 243–255. doi:10.7150/ntno.65544

Li, X., Wu, Y., and Tian, T. (2022). TGF-B signaling in metastatic colorectal cancer (mCRC): from underlying mechanism to potential applications in clinical development. *Int. J. Mol. Sci.* 23 (22), 14436. doi:10.3390/ijms232214436

Liu, K., Li, Q., Lu, X., Fan, X., Yang, Y., Xie, W., et al. (2024b). Seven oral traditional Chinese medicine combined with chemotherapy for the treatment of non-small cell lung cancer: a network meta-analysis. *Pharm. Biol.* 62 (1), 404–422. doi:10.1080/13880209.2024.2351940

Liu, Y., Fang, C., Luo, J., Gong, C., Wang, L., and Zhu, S. (2024a). Traditional Chinese medicine for cancer treatment. *Am. J. Chin. Med.* 52 (3), 583–604. doi:10.1142/s0192415x24500253

Lu, X., Chen, X., Lin, C., Yi, Y., Zhao, S., Zhu, B., et al. (2024). Elesclomol loaded copper oxide nanoplatform triggers cuproptosis to enhance antitumor immunotherapy. *Adv. Sci. Weinheim, Baden-Wurttemberg, Ger.* 11 (18), e2309984. doi:10.1002/advs.202309984

Marini, M., Titiz, M., Souza Monteiro de Araújo, D., Geppetti, P., Nassini, R., and De Logu, F. (2023). TRP channels in cancer: signaling mechanisms and translational approaches. *Biomolecules* 13 (10), 1557. doi:10.3390/biom13101557

Menconi, A., Marzo, T., Massai, L., Pratesi, A., Severi, M., Petroni, G., et al. (2021). Anticancer effects against colorectal cancer models of chloro(triethylphosphine)gold(I) encapsulated in PLGA-PEG nanoparticles. *Biometals Int. J. role metal ions Biol. Biochem. Med.* 34 (4), 867–879. doi:10.1007/s10534-021-00313-0

Modest, D. P., Pant, S., and Sartore-Bianchi, A. (2019). Treatment sequencing in metastatic colorectal cancer. *Eur. J. cancer Oxf. Engl.* 109, 70–83. doi:10.1016/j.ejca.2018.12.019

Mohajan, S., Jaiswal, P. K., Vatanmakarian, M., Yousefi, H., Sankaralingam, S., Alahari, S. K., et al. (2021). Hippo pathway: regulation, deregulation and potential therapeutic targets in cancer. *Cancer Lett.* 507, 112–123. doi:10.1016/j.canlet.2021.03.006

Paudel, K. R., Mehta, M., Yin, G. H. S., Yen, L. L., Malyla, V., Patel, V. K., et al. (2022). Berberine-loaded liquid crystalline nanoparticles inhibit non-small cell lung cancer proliferation and migration *in vitro*. *Environ. Sci. Pollut. Res. Int.* 29 (31), 46830–46847. doi:10.1007/s11356-022-19158-2

Qin, S., Tang, H., Li, W., Gong, Y., Li, S., Huang, J., et al. (2020). AMPK and its activator berberine in the treatment of neurodegenerative diseases. *Curr. Pharm. Des.* 26 (39), 5054–5066. doi:10.2174/1381612826666200523172334

Riesco-Martinez, M. C., Modrego, A., Espinosa-Olarte, P., La Salvia, A., and Garcia-Carbonero, R. (2022). Perioperative chemotherapy for liver metastasis of colorectal cancer: lessons learned and future perspectives. *Curr. Treat. options Oncol.* 23 (9), 1320–1337. doi:10.1007/s11864-022-01008-5

Sanuki, N., Takeda, A., Tsurugai, Y., and Eriguchi, T. (2022). Role of stereotactic body radiotherapy in multidisciplinary management of liver metastases in patients with colorectal cancer. *Jpn. J. radiology* 40 (10), 1009–1016. doi:10.1007/s11604-022-01307-9

Shaik, J. P., Alanazi, I. O., Pathan, A. A. K., Parine, N. R., Almadi, M. A., Azzam, N. A., et al. (2020). Frequent activation of notch signaling pathway in colorectal cancers and its implication in patient survival outcome. *J. Oncol.* 2020, 6768942. doi:10.1155/2020/6768942

Shinji, S., Yamada, T., Matsuda, A., Sonoda, H., Ohta, R., Iwai, T., et al. (2022). Recent advances in the treatment of colorectal cancer: a review. *J. Nippon Med. Sch. = Nippon Ika Daigaku zasshi* 89 (3), 246–254. doi:10.1272/jnms.JNMS.2022_89-310

Siegel, R. L., Giaquinto, A. N., and Jemal, A. (2024). Cancer statistics. *CA a cancer J. Clin.* 74 (1), 12–49. doi:10.3322/caac.21820

Siegel, R. L., Miller, K. D., Wagle, N. S., and Jemal, A. (2023). Cancer statistics. *CA a cancer J. Clin.* 73 (1), 17–30. doi:10.3322/caac.21332

Silva, V. R., Santos, L. S., Dias, R. B., Quadros, C. A., and Bezerra, D. P. (2021). Emerging agents that target signaling pathways to eradicate colorectal cancer stem cells. *Cancer Commun. Lond. Engl.* 41 (12), 1275–1313. doi:10.1002/cac2.12235

Singh, A. J., Ramsey, S. A., Filtz, T. M., and Kioussi, C. (2018). Differential gene regulatory networks in development and disease. *Cell. Mol. life Sci. CMLS* 75 (6), 1013–1025. doi:10.1007/s00018-017-2679-6

Sun, R., Dai, J., Ling, M., Yu, L., Yu, Z., and Tang, L. (2022). Delivery of triptolide: a combination of traditional Chinese medicine and nanomedicine. *J. nanobiotechnology* 20 (1), 194. doi:10.1186/s12951-022-01389-7

Tanton, H., Sewastianik, T., Seo, H. S., Remillard, D., Pierre, R. S., Bala, P., et al. (2022). A novel β-catenin/BCL9 complex inhibitor blocks oncogenic Wnt signaling and disrupts cholesterol homeostasis in colorectal cancer. *Sci. Adv.* 8 (17), eabm3108. doi:10.1126/sciadv.abm3108

Tao, Y., Zhang, Q., Wang, H., Yang, X., and Mu, H. (2024). Alternative splicing and related RNA binding proteins in human health and disease. *Signal Transduct. Target. Ther.* 9 (1), 26. doi:10.1038/s41392-024-01734-2

Wan, C., Mahara, S., Sun, C., Doan, A., Chua, H. K., Xu, D., et al. (2021). Genome-scale CRISPR-Cas9 screen of Wnt/β-catenin signaling identifies therapeutic targets for colorectal cancer. *Sci. Adv.* 7 (21), eabf2567. doi:10.1126/sciadv.abf2567

Wang, F., Long, J., Li, L., Zhao, Z. B., Wei, F., Yao, Y., et al. (2020). Mutations in the notch signalling pathway are associated with enhanced anti-tumour immunity in colorectal cancer. *J. Cell. Mol. Med.* 24 (20), 12176–12187. doi:10.1111/jcmm.15867

Wang, K., Feng, X., Chai, L., Cao, S., and Qiu, F. (2017). The metabolism of berberine and its contribution to the pharmacological effects. *Drug metab. Rev.* 49 (2), 139–157. doi:10.1080/03602532.2017.1306544

Wang, K. L., Yu, Y. C., Chen, H. Y., Chiang, Y. F., Ali, M., Shieh, T. M., et al. (2022). Recent advances in Glycyrrhiza glabra (Licorice)-Containing herbs alleviating radiotherapy- and chemotherapy-induced adverse reactions in cancer treatment. *Metabolites* 12 (6), 535. doi:10.3390/metabo12060535

Wei, D., Yang, H., Zhang, Y., Zhang, X., Wang, J., Wu, X., et al. (2022). Nano-traditional Chinese medicine: a promising strategy and its recent advances. *J. Mater. Chem. B* 10 (16), 2973–2994. doi:10.1039/d2tb00225f

Xiang, Y., Guo, Z., Zhu, P., Chen, J., and Huang, Y. (2019). Traditional Chinese medicine as a cancer treatment: modern perspectives of ancient but advanced science. *Cancer Med.* 8 (5), 1958–1975. doi:10.1002/cam4.2108

Xu, M., Ren, L., Fan, J., Huang, L., Zhou, L., Li, X., et al. (2022). Berberine inhibits gastric cancer development and progression by regulating the JAK2/STAT3 pathway and downregulating IL-6. *Life Sci.* 290, 120266. doi:10.1016/j.lfs.2021.120266

Yan, Z., Lai, Z., Lin, J., and Anticancer Properties of Traditional Chinese Medicine (2017). Anticancer properties of traditional Chinese medicine. *Comb. Chem. High. Throughput Screen.* 20 (5), 423–429. doi:10.2174/1386207320666170116141818

Yang, L., Yang, J., Kleppe, A., Danielsen, H. E., and Kerr, D. J. (2024). Personalizing adjuvant therapy for patients with colorectal cancer. *Nat. Rev. Clin. Oncol.* 21 (1), 67–79. doi:10.1038/s41571-023-00834-2

Zhang, K., Tang, X., Zhang, J., Lu, W., Lin, X., Zhang, Y., et al. (2014). PEG-PLGA copolymers: their structure and structure-influenced drug delivery applications. *J. Control. release official J. Control. Release Soc.* 183, 77–86. doi:10.1016/j.jconrel.2014.03.026

Zhang, X., Qiu, H., Li, C., Cai, P., and Qi, F. (2021). The positive role of traditional Chinese medicine as an adjunctive therapy for cancer. *Biosci. trends* 15 (5), 283–298. doi:10.5582/bst.2021.01318

Zhao, W., Jin, L., Chen, P., Li, D., Gao, W., and Dong, G. (2022). Colorectal cancer immunotherapy-Recent progress and future directions. *Cancer Lett.* 545, 215816. doi:10.1016/j.canlet.2022.215816

Zhou, S. S., and Jiang, J. G. (2019). Anti-fatigue effects of active ingredients from traditional Chinese medicine: a review. *Curr. Med. Chem.* 26 (10), 1833–1848. doi:10.2174/0929867324666170414164607

frontiers | Frontiers in Pharmacology

TYPE Original Research
PUBLISHED 01 November 2024
DOI 10.3389/fphar.2024.1494131

Check for updates

OPEN ACCESS

EDITED BY
Zhi Tian,
University of South Florida, United States

REVIEWED BY
Chenwei Wang,
Baylor College of Medicine, United States
Wankun Deng,
University of Texas Health Science Center at Houston, United States

*CORRESPONDENCE
Yongqiang Zheng,
zhengyq@sysucc.org.cn
Minggang Cheng,
cmg70@163.com

RECEIVED 10 September 2024
ACCEPTED 14 October 2024
PUBLISHED 01 November 2024

CITATION
Wu J, Lu J, Chen Q, Chen H, Zheng Y and Cheng M (2024) Pan-cancer analysis of CLDN18.2 shed new insights on the targeted therapy of upper gastrointestinal tract cancers. *Front. Pharmacol.* 15:1494131.
doi: 10.3389/fphar.2024.1494131

COPYRIGHT
© 2024 Wu, Lu, Chen, Chen, Zheng and Cheng. This is an open-access article distributed under the terms of the Creative Commons Attribution License (CC BY). The use, distribution or reproduction in other forums is permitted, provided the original author(s) and the copyright owner(s) are credited and that the original publication in this journal is cited, in accordance with accepted academic practice. No use, distribution or reproduction is permitted which does not comply with these terms.

Pan-cancer analysis of CLDN18.2 shed new insights on the targeted therapy of upper gastrointestinal tract cancers

Jun Wu[1,2], Jinghua Lu[1], Qiuyue Chen[1], Haojie Chen[2], Yongqiang Zheng[2]* and Minggang Cheng[1]*

[1]Department of Clinical Laboratory, People's Hospital of Bao'an District, Shenzhen Baoan Clinical Medical College of Guangdong Medical University, Shenzhen, China, [2]State Key Laboratory of Oncology in South China, Guangdong Provincial Clinical Research Center for Cancer, Sun Yat-sen University Cancer Center, Guangzhou, China

Background: CLDN18.2 is a widely researched drug target. However, previous research has primarily been based on immunohistochemistry results and focused on gastric cancer.

Methods: To analyze the potential cancer-targeting effect of CLDN18.2 from a multi-omics perspective, this study quantified CLDN18.2 expression in The Cancer Genome Atlas (TCGA) pan-cancer cohort. Thus, the relationships between CLDN18.2 expression and genomic alterations, immune infiltration, and prognosis were analyzed. Additionally, we performed analyses of the differentially expressed genes and enriched pathways between the high- and low-CLDN18.2 expression groups, as well as the corresponding drug sensitivity analyses.

Results: The results indicated that CLDN18.2 was highly expressed in pancreatic adenocarcinoma (PAAD), stomach adenocarcinoma (STAD), colorectal cancer (CRC), and esophageal carcinoma (ESCA). Moreover, the high- and low-CLDN18.2 expression groups presented significant differences in terms of genomic alterations and immune infiltration, such as the levels of methylation and $CD4^+$ T cell infiltration. Furthermore, high CLDN18.2 expression was significantly associated with poor prognosis in bladder urothelial carcinoma (BLCA), ESCA, and PAAD. In upper gastrointestinal tract cancers (STAD, ESCA, and PAAD), downregulated gene-enriched pathways were associated with cell signaling, whereas upregulated gene-enriched pathways were associated with angiogenesis. Finally, we identified drugs associated with CLDN18.2 expression to which samples with different levels of expression were differentially sensitive.

Conclusion: CLDN18.2 was highly expressed in upper gastrointestinal tract cancers, and its expression had a significant effect on genomic alterations and the tumor microenvironment. Additionally, low CLDN18.2 expression was linked to favorable prognosis. Our study reveals the potential value of CLDN18.2 for tumor prognosis and targeted therapy in various cancers, especially upper gastrointestinal tract cancers.

KEYWORDS

CLDN18.2, alternative splicing events, upper gastrointestinal tract cancers, prognosis, drug sensitivity

1 Introduction

In terms of current global disease trends, cancer remains one of the leading causes of death among non-communicable diseases and poses an enormous burden on social development and healthcare resources (Vollset et al., 2024). According to a statistical analysis of data from the International Agency for Research on Cancer (IARC) in 2022, lung, breast, colorectal, prostate, and gastric cancers are at the forefront of morbidity and mortality, which cause irreversible physical and financial losses to a large number of patients and their families (Bray et al., 2024; Jokhadze et al., 2024). Currently, seven primary treatments are available for tumors, namely, surgery (Are et al., 2023), radiotherapy (Schaue and McBride, 2015), chemotherapy (Anand et al., 2023), immunotherapy (Carlino et al., 2021), targeted therapy (Zhong et al., 2021), hormone therapy (Yung and Davidson, 2021) and stem cell transplantation (Chu et al., 2020). Among them, targeted therapy is a type of specific therapy that inhibits specific molecular targets of cancer cells to hinder their growth and proliferation, which has already played an important role in the treatment of multiple cancers, such as lung (Niu et al., 2022), breast (Esteva et al., 2019), and gastric (Zhu et al., 2021) cancers.

The claudin18 gene (CLDN18) is a coding gene belonging to the claudin family that is often expressed in epithelial cells, where it plays an important role in intercellular junctions and maintenance of cell polarity (Günzel and Yu, 2013). The human CLDN18 gene is located on chromosome 3 (3q22.3) and contains six exons and five introns, as well as two alternate promoters (APs). The two promoters mediate different transcription start sites, which in turn affect different downstream exons (1a and 1b), resulting in two isoforms, CLDN18.1 and CLDN18.2 (Niimi et al., 2001). The structures of the two isoforms are very similar, with four hydrophobic transmembrane structural domains and two extracellular loops, and they differ in only a few amino acids at the N-terminal first extracellular loop, which leads to differences in their functions and expression specificity (Türeci et al., 2011). CLDN18.1 is expressed primarily in the lungs, whereas CLDN18.2 is expressed predominantly in the stomach (Niimi et al., 2001). In gastric cancer, CLDN18.2 is predominantly located in the apical tight junctions of epithelial cells in normal tissues, whereas it is exposed in tumor cells due to alterations in the junctions and polarity between epithelial cells as a result of epithelial mesenchymal transition (EMT) and is also ectopically activated in tumor tissues from various other cancers (Sahin et al., 2008).

Therefore, CLDN18.2 has the potential to be a cancer therapeutic target (Nakayama et al., 2024). Currently, CLDN18.2 is a widely researched target for cancer therapy, and a series of therapeutic agents have been developed. Zolbetuximab, the first monoclonal antibody to target CLDN18.2, can activate immune cells through the antibody-dependent cellular cytotoxicity (ADCC) mechanism and activate the complement system through the complement-dependent cytotoxicity (CDC) mechanism, both of which synergistically achieve therapeutic effects in cells that specifically express CLDN18.2 (Mitnacht-Kraus et al., 2017). In addition to monoclonal antibodies, other targeted therapies based on CLDN18.2, such as chimeric antigen receptor T cells (CAR T cells), bispecific antibodies, and antibody-drug conjugates (ADCs), have been developed. These therapies have made notable progress in the targeted treatment of cancers such as gastric, esophageal, and pancreatic cancers (Jiang et al., 2019; Shah et al., 2023; Shitara et al., 2023; Xu R.-h. et al., 2023; Xu Y. et al., 2023).

Moreover, several studies have analyzed the pathological characteristics and prognosis of CLDN18.2-positive patients. Wang et al. found that gastric cancer tumor tissues exhibited lower levels of CLDN18.2 expression compared to normal tissues. Furthermore, the combination of low CLDN18.2 expression and increased infiltration of $CD4^+$ or $CD8^+$ T cells was associated with a better prognosis (Wang et al., 2023). Kwak et al. analyzed the association between CLDN18.2 and several biomarkers in gastric cancer. This study demonstrated that the positive rate of CLDN18.2 was higher in patients with EBV-positive or PD-L1-positive gastric cancer, whereas it was lower in HER2-positive patients (Kwak et al., 2024). However, related research primarily uses immunohistochemistry to determine CLDN18.2 expression, focusing primarily on gastric cancer and lacking a multi-omics landscape of CLDN18.2 across various cancers. Additionally, current transcript sequencing technologies have focused on quantifying the expression of each gene rather than each isoform (Garber et al., 2011; Stark et al., 2019), and the data from numerous bioinformatics databases rarely involve specific isoforms, which makes analyzing the biological properties of CLDN18.2 from a multi-omics perspective difficult. The TCGASpliceSeq database (https://bioinformatics.mdanderson.org/TCGASpliceSeq) utilizes the data associated with The Cancer Genome Atlas (TCGA) project to provide a comprehensive and detailed interpretation of the alternative splicing patterns of these samples and quantify the corresponding percent spliced in (PSI) values for splice events (Ryan et al., 2016). This pioneering work presents possibilities for us to quantify and subsequently analyze CLDN18.2 at the transcriptome level.

Therefore, this study analyzed CLDN18.2 expression across cancers and the associations of CLDN18.2 expression with genomic alterations, immune infiltration, and prognosis from a multi-omics perspective. In upper gastrointestinal tract cancers with high CLDN18.2 expression, we further analyzed the differences in gene expression, enriched pathways, and drug sensitivity between the high- and low-expression groups. The workflow of this study was shown in Figure 1. Taken together, our findings expand the current state of research on CLDN18.2 across various cancers, especially upper gastrointestinal tract cancers, and provide new insights for subsequent CLDN18.2-based targeted therapy.

2 Materials and methods

2.1 Data collection and preprocessing

Alternative splicing data for CLDN18 were obtained from the TCGASpliceSeq database, and all cancer data containing PSI values for CLDN18 were downloaded (26 cancers). Multi-omics data of the pan-cancer cohort in TCGA, including RNA-seq data, clinical information, methylation data, and copy number variant (CNV) data, were downloaded from the UCSC Xena (Goldman et al., 2020) database (https://xenabrowser.net/datapages/). Tumor mutation

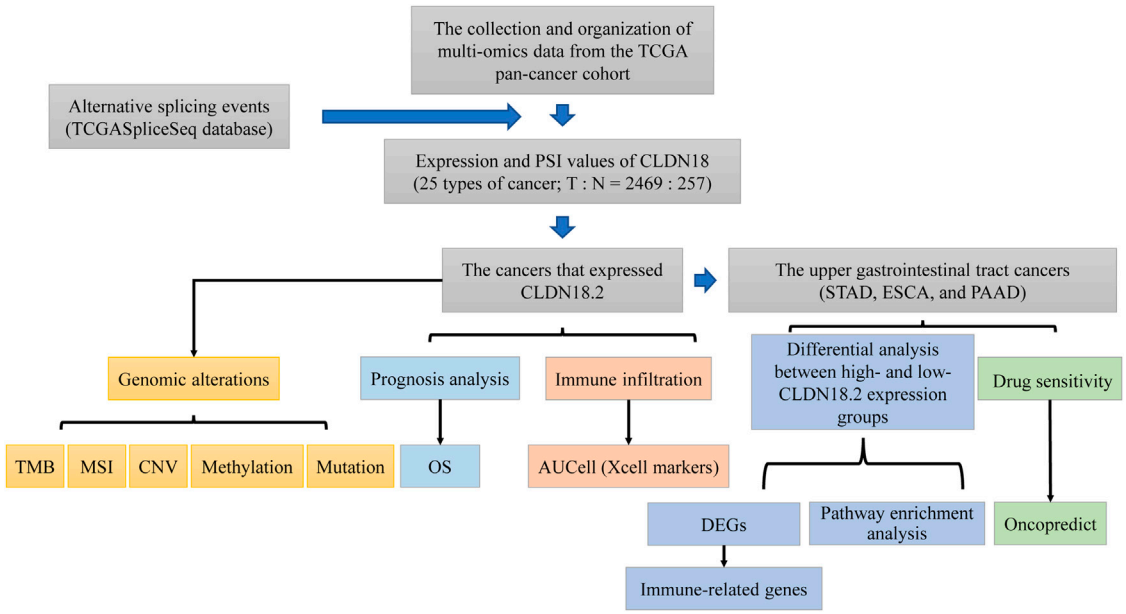

FIGURE 1
The workflow of this study.

burden (TMB) and microsatellite instability (MSI) data were obtained from the cBioPortal (Cerami et al., 2012) database (https://www.cbioportal.org/), whereas tumor neoantigen data was sourced from the Supplementary Material in the literature on the pan-cancer immune landscape of TCGA (Thorsson et al., 2018). Moreover, we downloaded the mutation data via the "TCGAMutations" (v0.4.0) R package. The above data were filtered to retain only those samples that included both the PSI values of CLDN18 and its expression profiles. In addition, samples from colon adenocarcinoma (COAD) and rectum adenocarcinoma (READ) were mixed together and defined as colorectal cancer (CRC).

2.2 Expression of CLDN18.2 and CLDN18.1

For RNA-seq data, fragments per kilobase million (FPKM) values were converted to transcripts per million (TPM) values, and then the "clusterProfiler" (v4.10.1) R package (Wu et al., 2021) was used to convert Ensembl IDs to gene symbols while filtering out unmatched records. Building upon this, we partitioned CLDN18 expression into CLDN18.2 and CLDN18.1 based on the proportion of AP, where AP1 corresponds to CLDN18.2 and AP2 corresponds to CLDN18.1, totaling 1 (Supplementary Table S1). The samples from each cancer type were categorized into high- and low-expression groups according to the median expression value of CLDN18.2.

We demonstrated the expression of CLDN18, CLDN18.1, and CLDN18.2 among cancers and between tumor samples and normal samples. Additionally, PSI values were presented for each type of cancer and for comparisons between tumor samples and normal samples. We visualized the information about cancer samples based on the sorting of PSI values for CLDN18.2. Differences between the above data were analyzed with the Kruskal–Wallis test and the Wilcoxon rank sum test and visualized by the "ggplot2" (v3.5.1) and "complexHeatmap" (v2.18.0) R packages.

2.3 Genomic alterations

In our study, ten cancers expressed CLDN18.2, namely, bladder urothelial carcinoma (BLCA), cholangiocarcinoma (CHOL), CRC, esophageal carcinoma (ESCA), liver hepatocellular carcinoma (LIHC), lung adenocarcinoma (LUAD), lung squamous cell carcinoma (LUSC), pancreatic adenocarcinoma (PAAD), stomach adenocarcinoma (STAD), and testicular germ cell tumors (TGCT). Thus, we analyzed the correlation between CLDN18.2 expression and TMB or MSI in these cancers. Moreover, differences in the levels of methylation and CNV between the high- and low-CLDN18.2 expression groups across these cancers were analyzed via the Wilcoxon rank sum test. In four cancers with high CLDN18.2 expression (STAD, CRC, ESCA, and PAAD), we explored the differences in mutated genes between the high- and low-CLDN18.2 expression groups using the "maftools" (v2.18.0) R package.

2.4 Immune infiltration analysis

For the cancers that expressed CLDN18.2, we calculated the level of immune cell infiltration in each sample using the "AUCell" (v1.24.0) (Aibar et al., 2017) R package, which is based on Xcell (Aran, 2020) markers. We subsequently assessed the correlation between CLDN18.2 expression and the infiltration level of each immune cell type using the "cor.test" R function and visualized it using the "complexHeatmap" R package. For the four cancers with high CLDN18.2 expression, the immune cell infiltration levels of the high- and low-CLDN18.2 expression groups were compared, and

the differences between the two groups were analyzed with the Wilcoxon rank sum test.

2.5 Prognosis analysis

For the cancers that expressed CLDN18.2, after the optimal cutoff point was determined by the "surv_cutpoint" function of the "survminer" (v0.4.9) R package, we analyzed the relationship between CLDN18.2 expression and overall survival (OS) across these cancers using the "survival" (v3.6-4) R package and visualized them with Kaplan–Meier plots. Furthermore, the corresponding log-rank P values and hazard ratios (HRs) with 95% confidence intervals were visualized by the "forestplot" (v3.1.3) R package. In addition, as patients' HER2 status is a crucial consideration in gastric cancer treatment, we identified HER2-amplified samples in STAD using CNV data, where a CNV score of 1 indicates amplification. We then analyzed the correlation between CLDN18.2 expression and ERBB2 expression in STAD, as well as the association between CLDN18.2 expression and OS in HER2-amplified samples.

2.6 Differential gene expression and enrichment analysis between the high- and low-CLDN18.2 expression groups

In this study, CLDN18.2 was highly expressed in four cancers (STAD, CRC, ESCA, and PAAD), but high CLDN18.2 expression may improve the prognosis of patients with CRC, which was different from the results of the other three cancers. Therefore, subsequent analysis focused on the remaining three cancers. Because the pancreas and upper gastrointestinal tract are anatomically proximate, we classified pancreatic cancer as upper gastrointestinal tract cancer for follow-up analysis.

In upper gastrointestinal tract cancers (STAD, ESCA, and PAAD), we explored the differentially expressed genes (DEGs) between the high- and low-CLDN18.2 expression groups using the "DESeq2" (v1.42.1) R package, where genes with the false discovery rate (FDR) < 0.05 and a |fold change| > 2 were considered significant.

The overlaps of differential gene results for the three cancers were calculated and visualized by the "ggvenn" (v0.1.10) R package. Moreover, we performed Kyoto Encyclopedia of Genes and Genomes (KEGG) pathway and hallmark pathway enrichment analyses on the overlapping differential gene sets from the three cancers and visualized them using the "clusterProfiler" R package. Additionally, we used the "ggplot2" and "complexHeatmap" R packages to visualize the expression of immune-related genes between the high- and low-CLDN18.2 expression groups and their correlation with CLDN18.2 expression.

2.7 Drug sensitivity analysis

The Cancer Therapeutics Response Portal (CTRP) database (https://portals.broadinstitute.org/ctrp.v2.1/) collects a large amount of data on interactions between cell lines and related compounds. And it is designed to assist in identifying drugs beneficial to patients by correlating the cellular characteristics (genetic, lineage, etc.) of cancer cell lines with their sensitivity to small molecules (Rees et al., 2016). Oncopredict (v1.2) is an R package designed to be used for drug response prediction and drug–gene association prediction based on data from the CTRP database, which predicts the drug sensitivity of samples to 545 drugs (Maeser et al., 2021). We utilized this package to predict the sensitivity of samples from the upper gastrointestinal tract cancers to 545 drugs. We then visualized the results of the sensitivity score ranking and several drugs with the highest correlation with CLDN18.2 expression using the "ggplot2" R package. To explore the differences in drug sensitivity scores between the high- and low-CLDN18.2 expression groups, we selected the top 100 drugs with the lowest scores in each cancer and calculated their correlation with CLDN18.2 expression. Drugs with correlations greater than 0.4 and significant differences between the high- and low-CLDN18.2 expression groups were then displayed.

2.8 Statistical analysis

In this study, we compared differences between two groups and between multiple groups using the Wilcoxon rank sum test and the Kruskal–Wallis test, respectively. The data correlation was calculated via Pearson's correlation. All the above methods were performed with R (v4.3.1) software.

3 Results

3.1 Expression of CLDN18, CLDN18.2 and CLDN18.1 across cancers

In the TCGA pan-cancer cohort, PAAD, CRC, STAD, and LUAD expressed higher levels of CLDN18, whereas lower grade glioma (LGG), prostate adenocarcinoma (PRAD), glioblastoma multiforme (GBM), and ovarian serous cystadenocarcinoma (OV) had lower levels of CLDN18 expression (Figure 2A). Further comparison between tumor samples and normal samples revealed significant differences in CRC, STAD, LUAD, LUSC, ESCA, and kidney renal papillary cell carcinoma (KIRP), and the CLDN18 expression levels in the remaining four cancers were significantly higher in normal samples than in tumor samples, except for CRC and KIRP (Figure 2B).

Sorting the PSI values of CLDN18 revealed that the distribution of cancer types in samples with higher PSI values of CLDN18.2 was more diverse, but the distribution of cancer types in samples with higher PSI values of CLDN18.1 was more concentrated and included breast invasive carcinoma (BRCA), kidney renal clear cell carcinoma (KIRC), KIRP, LUAD, LUSC, and sarcoma (SARC) (Figure 2C). We compared the PSI values of CLDN18.2 and CLDN18.1, and the results showed no significant difference only in BLCA and LIHC (Figure 2D). In addition, there were no significant differences in the PSI values of two isoforms between tumor samples and normal samples across other cancers except for CRC (Supplementary Figure S1).

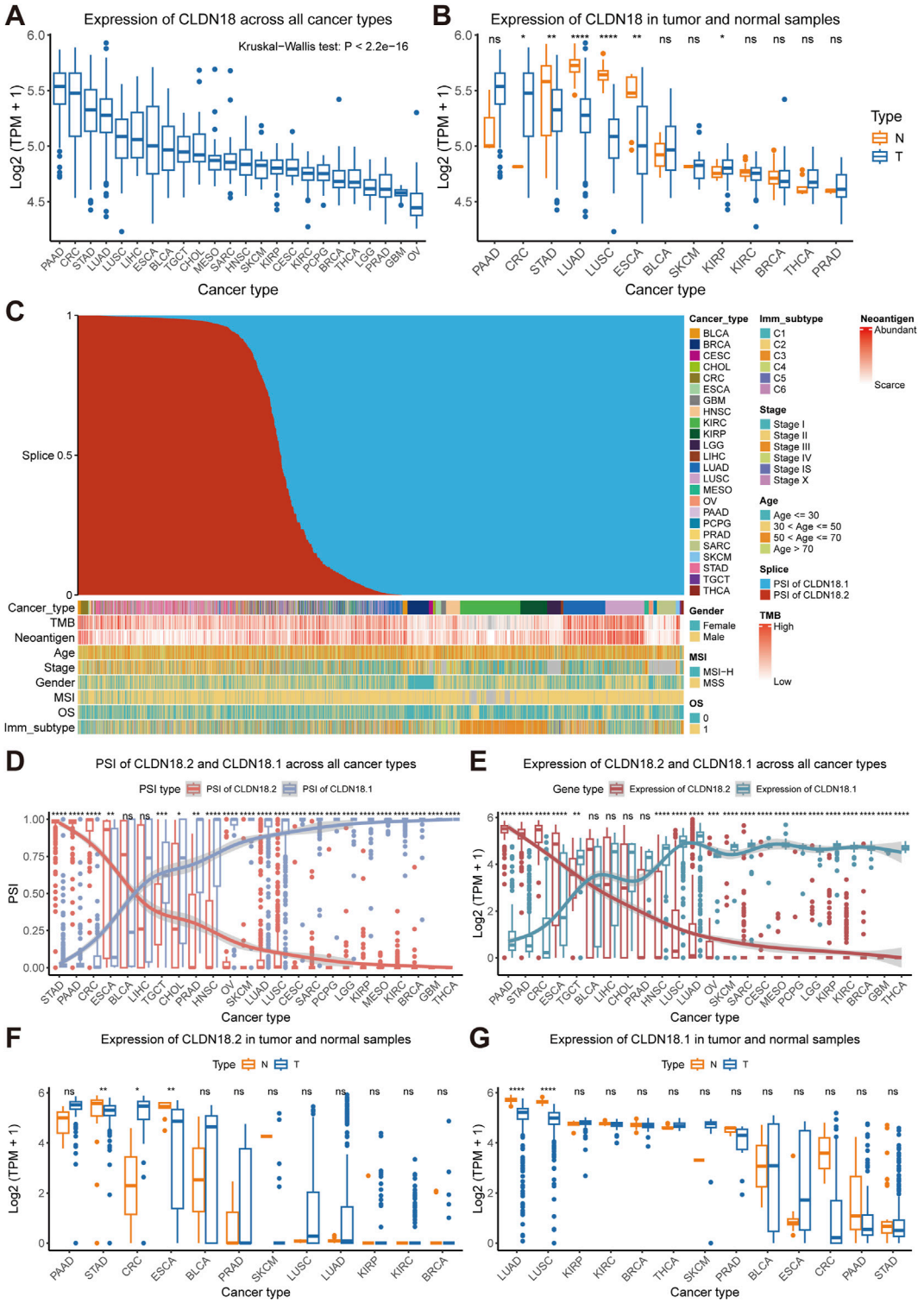

FIGURE 2
Expression and alternative splicing events of CLDN18, CLDN18.2, and CLDN18.1. **(A)** CLDN18 expression across various cancers. **(B)** CLDN18 expression in tumor and normal samples across various cancers. **(C)** Details of cancer samples after sorting by PSI values. **(D)** PSI values of CLDN18.2 and CLDN18.1 across various cancers. **(E)** Expression of CLDN18.2 and CLDN18.1 across various cancers. The expression of CLDN18.2 **(F)** and CLDN18.1 **(G)** in tumor and normal samples across various cancers. *, P < 0.05; **, P < 0.01; ***, P < 0.001; ****, P < 0.0001; ns, not statistically significant. Note: BLCA, Bladder urothelial carcinoma; BRCA, Breast invasive carcinoma; CESC, Cervical squamous cell carcinoma and endocervical adenocarcinoma; CHOL, Cholangiocarcinoma; CRC, Colorectal cancer; ESCA, Esophageal carcinoma; GBM, Glioblastoma multiforme; HNSC, Head and neck squamous cell carcinoma; KICH, Kidney chromophobe; KIRC, Kidney renal clear cell carcinoma; KIRP, Kidney renal papillary cell carcinoma; LGG, Lower grade glioma; LIHC, Liver hepatocellular carcinoma; LUAD, Lung adenocarcinoma; LUSC, Lung squamous cell carcinoma; MESO, Mesothelioma;
(*Continued*)

FIGURE 2 (Continued)
OV, Ovarian serous cystadenocarcinoma; PAAD, Pancreatic adenocarcinoma; PCPG, Pheochromocytoma and paraganglioma; PRAD, Prostate adenocarcinoma; SARC, Sarcoma; SKCM, Skin cutaneous melanoma; STAD, Stomach adenocarcinoma; TGCT, Testicular germ cell tumors; THCA, Thyroid carcinoma.

Further analysis of the differences in expression between CLDN18.2 and CLDN18.1 revealed significant differences in results for all cancer types except for BLCA, LIHC, CHOL, and PRAD (Figure 2E). Moreover, CLDN18.2 expression significantly differed between tumor samples and normal samples in patients with STAD, CRC, and ESCA (Figure 2F). Correspondingly, CLDN18.1 expression between tumor samples and normal samples was significantly different only in LUAD and LUSC (Figure 2G). These results indicate highly specific expression levels of CLDN18.2 and CLDN18.1 across different cancers, with higher CLDN18.2 expression in PAAD, STAD, CRC, and ESCA and higher CLDN18.1 expression in LUAD and LUSC.

3.2 Genomic alterations in cancers that expressed CLDN18.2

We calculated the correlation of TMB and MSI with CLDN18.2 expression in ten cancers that expressed CLDN18.2 separately (BLCA, CHOL, CRC, ESCA, LIHC, LUAD, LUSC, PAAD, STAD, and TGCT). Although significant positive correlations were observed in BLCA ($P = 0.042$) and ESCA ($P = 0.016$), TMB and CLDN18.2 expression did not significantly correlate in other cancers (Figure 3A). For MSI, only CRC ($P = 0.008$) showed a significant positive correlation (Figure 3B). Moreover, the differences in methylation and CNV levels between the high- and low-CLDN18.2 expression groups were compared in each cancer type. The results indicated that methylation levels significantly differed between the high- and low-CLDN18.2 expression groups in all cancers (Figure 3C), whereas CNV levels did not significantly differ between two groups in LUSC and TGCT (Figure 3D).

For the four cancers (PAAD, STAD, CRC, and ESCA) with higher CLDN18.2 expression levels than the other cancers shown in Figure 2E, we analyzed the mutation profiles of the high- and low-CLDN18.2 expression groups. In STAD, the mutated gene types and frequencies differed between the high- and low-CLDN18.2 expression groups and were dominated by missense mutations and multiple mutations (Figures 3E, F). A comparison of the top 20 mutated genes (excluding several large genes) revealed DNAH5, PIK3CA, ZFHX4, SACS, KMT2D, PCDH15, LRRK2, and LAMA1 as the differently mutated genes between the high- and low-CLDN18.2 expression groups (Figures 3E, F). We further compared the mutations in TP53 and ARID1A and observed that the mutation rate of TP53 in the high-CLDN18.2 expression group was lower than that in the low-CLDN18.2 expression group, but the opposite was true for ARID1A (Figures 3G, H).

In the high-CLDN18.2 expression group of CRC, TP53 was not among the top-ranked mutated genes, and the APC gene mutation rate in the low-CLDN18.2 expression group was much higher than that in the high-CLDN18.2 expression group (Supplementary Figures S2A, B). The mutation profile of TP53 in ESCA was similar to that in STAD, which also indicated a higher mutation rate of TP53 in the low-CLDN18.2 expression group. In addition, among the genes with the highest mutation rate in ESCA, the overall mutation rate of the top-ranked mutated genes in the high-CLDN18.2 expression group was higher than that in the low-CLDN18.2 expression group (Supplementary Figures S2C, D). For the high- and low-CLDN18.2 expression groups of PAAD, the mutation rates of the other genes except for KRAS, TP53, SMAD4, and CDKN2A were lower. The mutation rates of KRAS and TP53 were higher in the high-CLDN18.2 expression group than in the low-CLDN18.2 expression group (Supplementary Figures S2E, F).

CLDN18 had few mutations in the four cancers, with only a small number of mutations in STAD and CRC, which predominantly consisted of missense mutations and nonsense mutations (Supplementary Figures S2G, H). Overall, the types of genomic alterations differ between the high- and low-CLDN18.2 expression groups across these cancers, especially the patterns of mutated genes.

3.3 Relationships between CLDN18.2 expression and immune infiltration

Tumor immune cells play a bidirectional role in cancer development, either inhibiting tumor growth by eliminating tumor cells or promoting tumor progression via immune escape mechanisms. To investigate the relationship between CLDN18.2 expression and the level of immune cell infiltration, we calculated the correlation between CLDN18.2 expression and infiltrations of various immune cells in each cancer that expressed CLDN18.2. Overall, the infiltration levels of $CD4^+$ Tcm cells, $CD4^+$ T cells, and NK cells and neutrophils were negatively correlated with CLDN18.2 expression in most cancers, whereas the results for other immune cells were cancer-specific (Figure 4A).

In the four cancers that expressed more CLDN18.2 than other cancers, CLDN18.2 expression was negatively correlated with $CD8^+$ T cells, myocytes, chondrocytes, and fibroblasts, but this negative correlation was not significant in CRC. In STAD, CLDN18.2 expression was significantly positively correlated with M2 macrophages, eosinophils, and NKT cells and significantly negatively correlated with $CD4^+$ memory T cells, $CD8^+$ T cells, and Th2 cells. In PAAD, the analysis revealed a strong positive correlation between CLDN18.2 expression and both B cells and Tregs, which was not observed in the other cancers. In ESCA, CLDN18.2 expression significantly and negatively correlated with the infiltration levels of sebocytes and keratinocytes (Figure 4A).

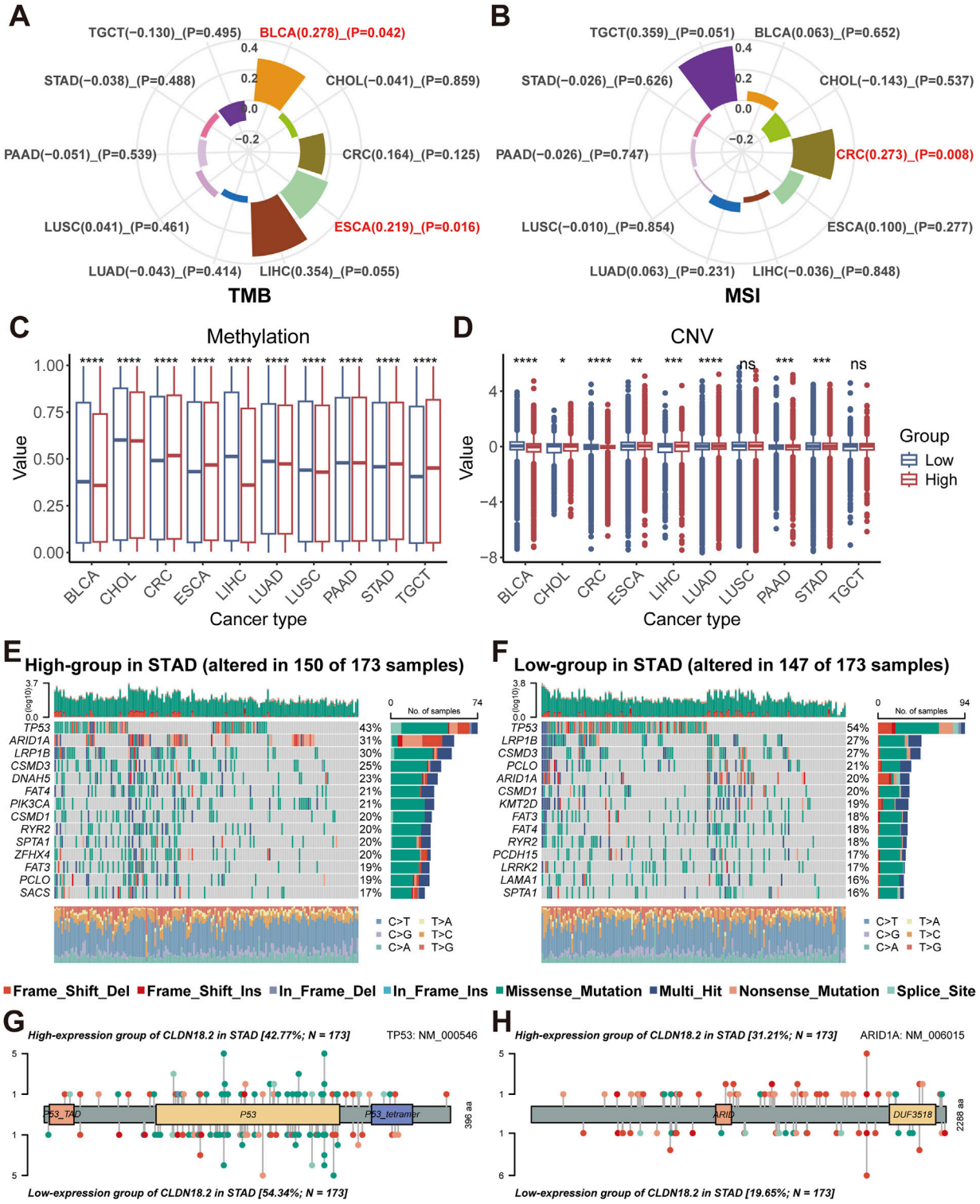

FIGURE 3
Relationships between CLDN18.2 expression and genomic alterations across ten cancers. Correlations of TMB **(A)** and MSI **(B)** with CLDN18.2 expression across ten cancers. Differences in levels of methylation **(C)** and CNV **(D)** between high- and low-CLDN18.2 expression groups. Mutation profiles between the high- **(E)** and low-CLDN18.2 **(F)** expression groups in STAD. Protein mutation lollipop plots for TP53 **(G)** and ARID1A **(H)** between high- and low-CLDN18.2 expression groups in STAD. *, P < 0.05; **, P < 0.01; ***, P < 0.001; ****, P < 0.0001; ns, not statistically significant.

Moreover, we analyzed the differences in the levels of immune cell infiltration between the high- and low-CLDN18.2 expression groups in patients with STAD, which identified significant differences in various immune cells, such as $CD8^+$ T cells, $CD4^+$ memory T cells, $CD4^+$ naive T cells, $CD4^+$ T cells, and $CD4^+$ Tcm cells. Additionally, the high-CLDN18.2 expression group exhibited a

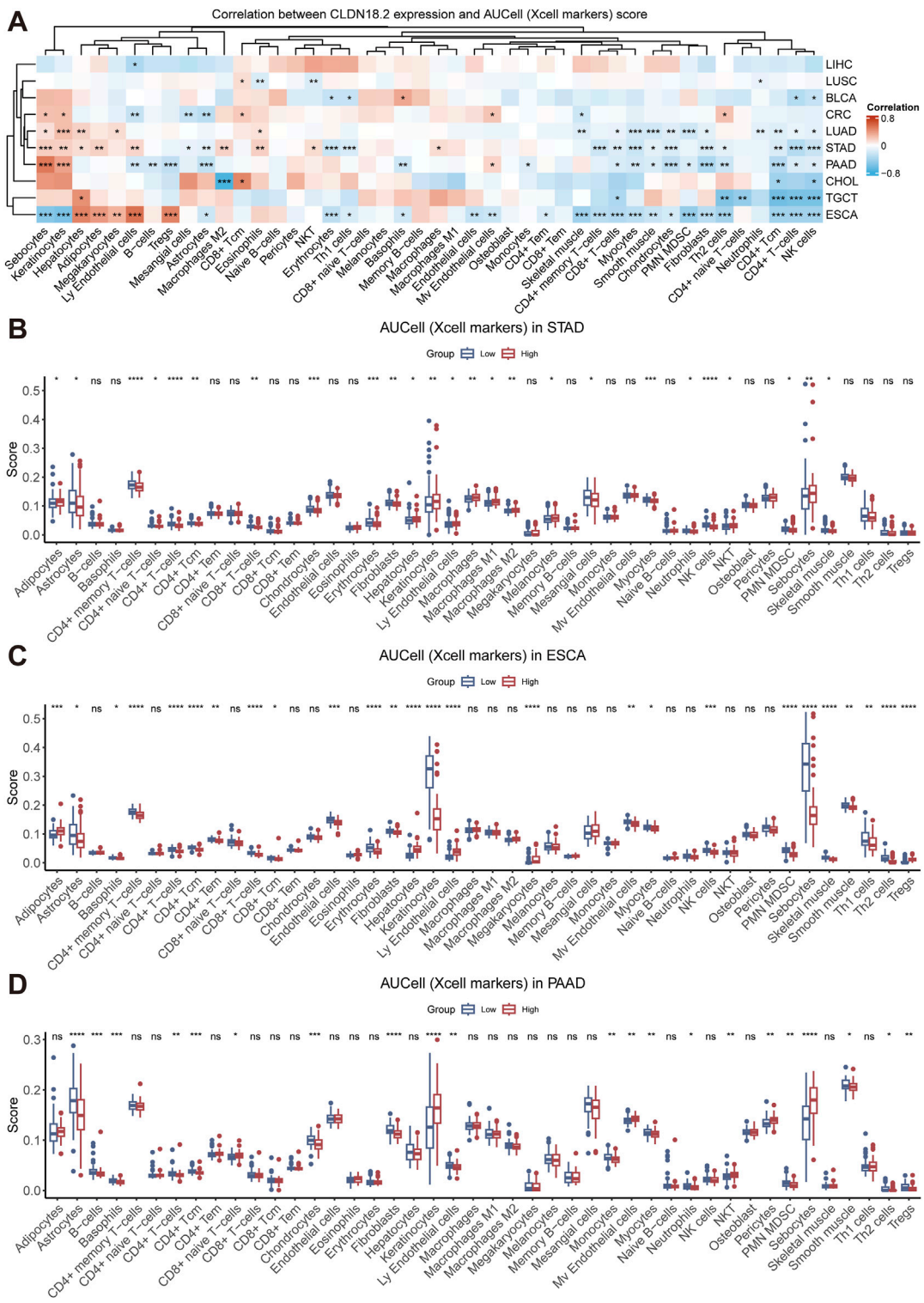

FIGURE 4
Immune infiltration analyses across ten cancers. **(A)** The correlations between CLDN18.2 expression and immune infiltration across ten cancers. **(B–D)** The levels of immune cell infiltration between high- and low-CLDN18.2 expression groups in STAD, ESCA, and PAAD. *, P < 0.05; **, P < 0.01; ***, P < 0.001; ****, P < 0.0001; ns, not statistically significant.

higher level of immune infiltration in M2 macrophages compared to the low-CLDN18.2 expression group, whereas the level of NK cells infiltration was lower in the high-CLDN18.2 expression group (Figure 4B). Further combining the results of ESCA and PAAD revealed that the infiltration patterns of the $CD4^+$ T cell subsets were similar between the high- and low-CLDN18.2 expression groups across the three cancers, as were those of $CD8^+$ T cell subsets. However, there were significant differences in infiltration levels of

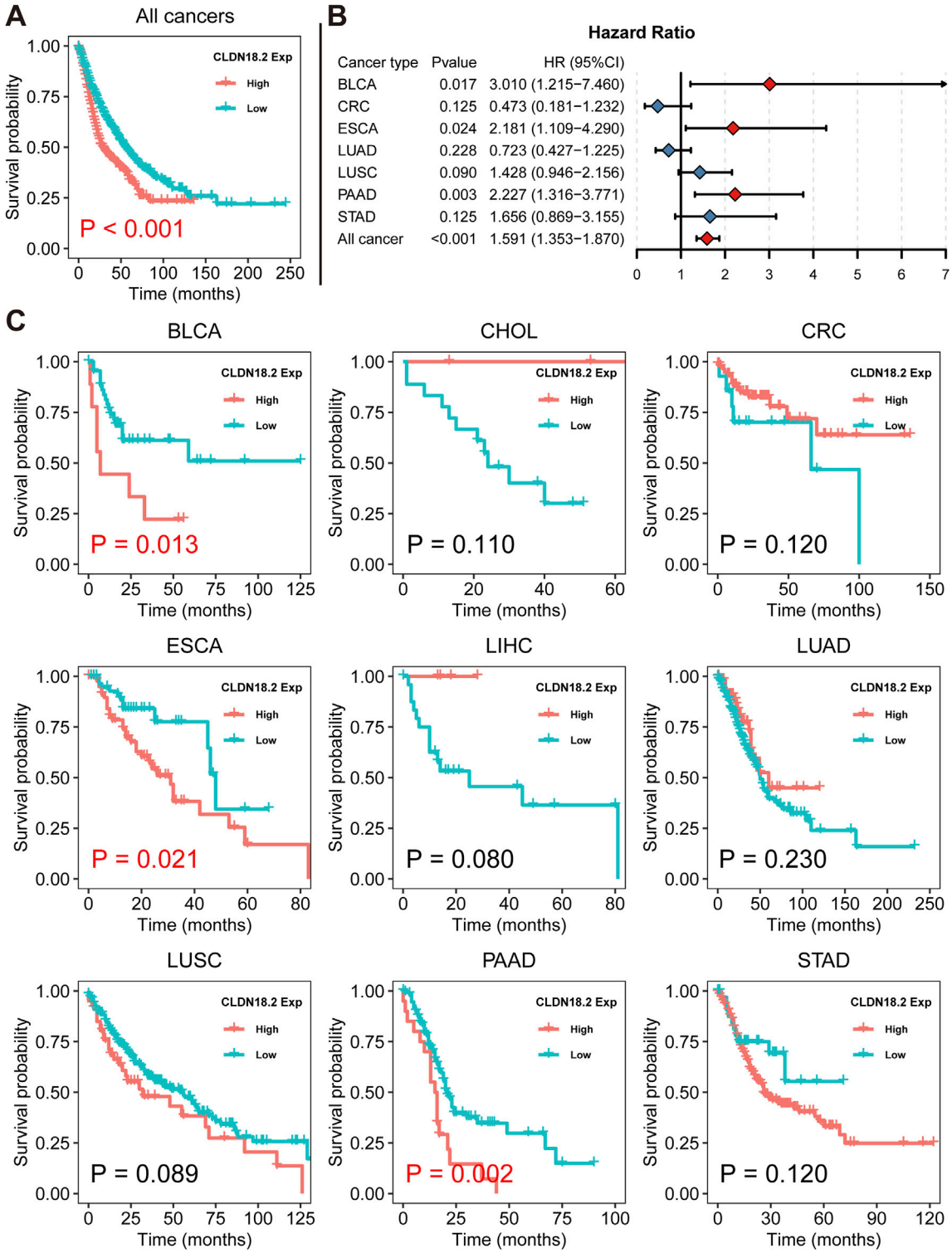

FIGURE 5
Relationships between CLDN18.2 expression and overall survival across ten cancers. **(A)** Kaplan–Meier analysis of the relationship between CLDN18.2 expression and OS across ten cancers. **(B)** Forest plot of the relationships between CLDN18.2 expression and OS across ten cancers. **(C)** Kaplan–Meier analyses of the relationship between CLDN18.2 expression and OS for individual cancers. Note: The analyses of CHOL and LIHC were not presented due to HR being very close to 0 and P values being approaching 1. And the analysis of TCGT was not presented because all samples had reached the OS endpoint.

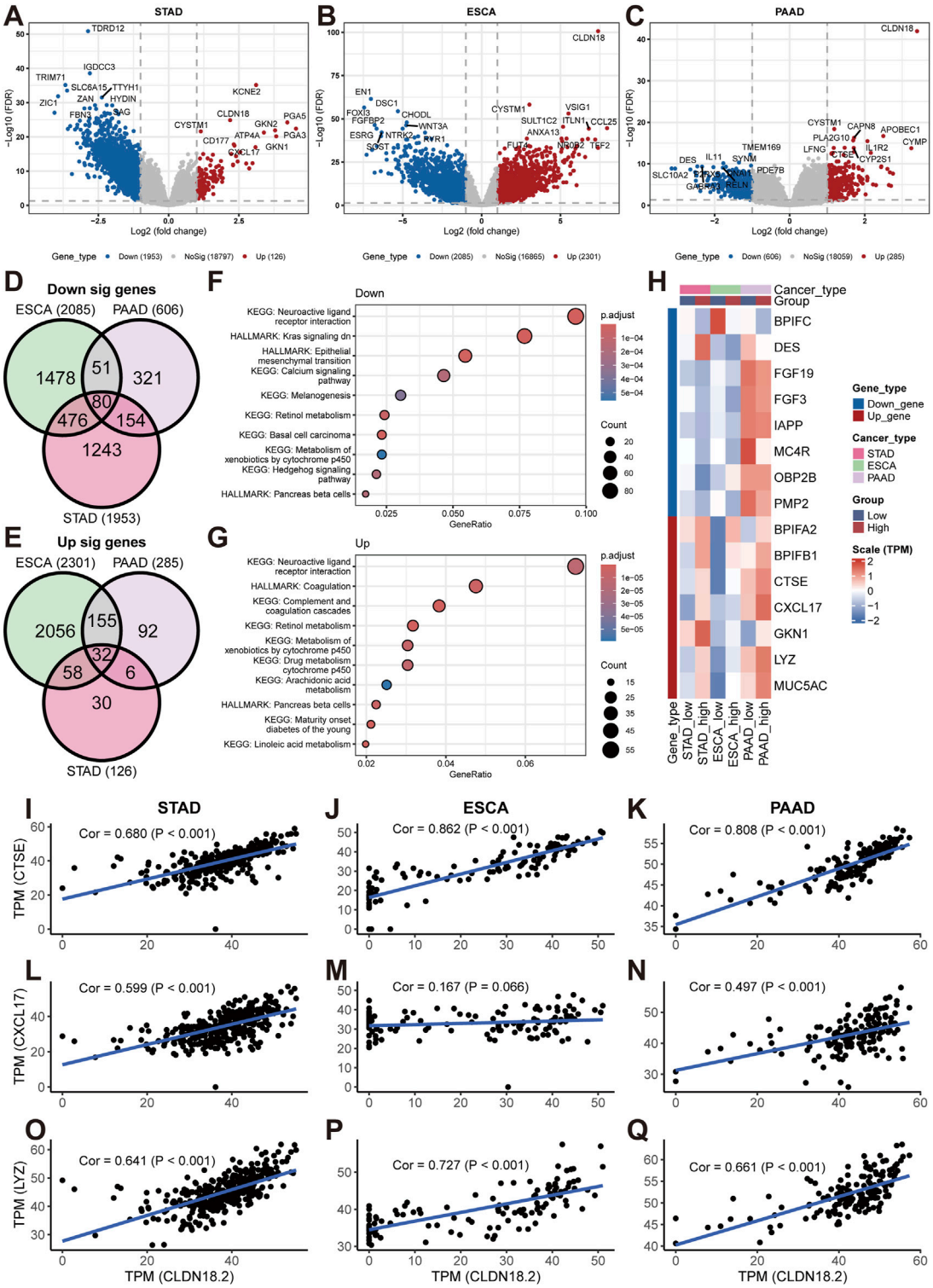

FIGURE 6
Differential analyses between high- and low-CLDN18.2 expression groups in STAD, ESCA, and PAAD. Volcano plots between high- and low-CLDN18.2 expression groups in STAD **(A)**, ESCA **(B)**, and PAAD **(C)**. Venn diagrams of upregulated genes **(D)** and downregulated **(E)** genes across three cancers. **(F, G)** KEGG and hallmark pathway enrichment plots across three cancers. **(H)** Correlations between CLDN18.2 expression and immune-related genes between high- and low-CLDN18.2 expression groups across three cancers. **(I–Q)** Scatter plots of the correlations between CLDN18.2 expression and three immune-related genes (CTSE, CXCL17, and LYZ) in three cancers.

macrophage subsets between the two groups in STAD, which were not observed in ESCA or PAAD (Figures 4C, D). Additionally, the infiltration level of most immune cells did not differ between the two groups in CRC (Supplementary Figure S3). These findings indicate that the effect of CLDN18.2 expression on the infiltration levels of immune cells is highly cancer-specific, and high and low CLDN18.2 expression may have differential effects.

3.4 Relationships between CLDN18.2 expression and OS

We revealed the association between overall CLDN18.2 expression and OS across ten cancers via Kaplan–Meier analysis. Overall, low CLDN18.2 expression was associated with longer OS (P = 0.001) (Figure 5A). A Cox proportional hazards regression model showed that CLDN18.2 expression was a significant low-risk factor in BLCA patients (P = 0.017), ESCA patients (P = 0.024), PAAD patients (P = 0.003), and overall patients (P = 0.001) (Figure 5B). Moreover, Kaplan–Meier analysis of these cancers individually revealed that high CLDN18.2 expression was a poor prognostic factor in BLCA (P = 0.013), ESCA (P = 0.021) and PAAD (P = 0.002) (Figure 5C). These results indicate that CLDN18.2 expression has a guiding significance for the prognosis of several cancers, notably upper gastrointestinal tract cancers.

Through a more detailed analysis of the association between CLDN18.2 and HER2 in STAD, we found that CLDN18.2 expression was significantly positively correlated with ERBB2 expression (P = 0.023) (Supplementary Figure S4A). Furthermore, we observed that low CLDN18.2 expression was significantly associated with longer OS in HER2-amplified samples (Supplementary Figure S4B).

3.5 Analyses of DEGs and pathway enrichment between the high- and low-CLDN18.2 expression groups

For upper gastrointestinal tract cancers (STAD, ESCA, and PAAD), we performed differential analysis on the high- and low-CLDN18.2 expression groups to identify genes that were differentially expressed between the two groups. The results of the volcano plot showed a large number of downregulated genes in both STAD and ESCA, but fewer genes were downregulated in PAAD. Within the upregulated fraction, only ESCA exhibited a greater number of upregulated genes, whereas STAD and PAAD demonstrated fewer upregulated genes (Figures 6A–C). Further analysis revealed that 80 of the downregulated genes overlapped and that 32 of the upregulated genes overlapped in the three cancers (Figures 6D, E). The pathway enrichment results revealed that the downregulated genes were enriched in pathways such as the downregulation of the KRAS signaling pathway, the EMT pathway, and the calcium signaling pathway (Figure 6F). The pathways enriched among the upregulated genes included the arachidonic acid metabolism pathway, the coagulation pathway, and the retinol metabolism pathway (Figure 6G).

Furthermore, various immune-related genes were identified among the downregulated and upregulated overlapping genes, and their expression profiles were analyzed between the high- and low-CLDN18.2 expression groups. The results revealed large differences in the expression of most immune-related genes between the high- and low-CLDN18.2 groups of the three cancers (Figure 6H). This finding reflects a relationship between these genes and CLDN18.2 expression in these three cancers. Moreover, for CTSE, CXCL17, and LYZ, we explored the correlation between their expression and CLDN18.2 expression in three cancers (Figures 6I–Q). The results exhibited that, with the exception of ESCA, where CXCL17 expression was less strongly correlated with CLDN18.2 expression (Figure 6M), the remaining analyses revealed strong and significant correlation. The above results indicate that in upper gastrointestinal tract cancers, high or low CLDN18.2 expression is associated with different physiological activities, particularly the activity of cancer-related pathways and the expression of immune-related genes.

3.6 Relationships between CLDN18.2 expression and drug sensitivity

Because drug sensitivity analysis is important for cancer research, in upper gastrointestinal tract cancers, we predicted the sensitivity scores for 545 drugs and analyzed the correlation between the scores and CLDN18.2 expression (Supplementary Table S2). A higher drug sensitivity score indicated a potentially worse effect of the drug. The ranking of the drug sensitivity scores revealed that in STAD, LBH-589, leptomycin B, and quabain all had lower sensitivity scores between the high- and low-CLDN18.2 expression groups, but BRD-K09344309 had higher sensitivity scores (Figures 7A, B). Furthermore, we observed that the drug sensitivity scores of SGX-523, GSK2636771, and GSK4112 had a strongly significant and negative correlation with CLDN18.2 expression (Figures 7C–E). Conversely, the drug sensitivity scores of niclosamide, pazopanib, and TW-37 were strongly and positively correlated with CLDN18.2 expression (Figures 7F–H). We selected the top 100 drugs with the lowest drug sensitivity scores in STAD and identified six drugs that were significantly different between the high- and low-CLDN18.2 expression groups and had a correlation with CLDN18.2 expression greater than 0.4. With the exception of navitoclax:gemcitabine, the remaining five drugs were likely to have worse efficacy in the high-CLDN18.2 expression group (Figure 7I).

Moreover, we counted the overlap of drugs significantly associated with CLDN18.2 expression in the three cancers and identified 148 overlapping drugs (Figure 7J). For ESCA and PAAD, the ranking results of certain drugs, such as LBH-589, were similar to those of STAD (Supplementary Figures S5A–D). In ESCA, CLDN18.2 expression was significantly negatively correlated with the drug sensitivity scores of brefeldin A and selumetinib:MK-2206, whereas it was significantly positively correlated with the scores of PI-103 and MST-312 (Supplementary Figures S5E–H). In PAAD, the ML258 and MI-1 scores were significantly positively correlated with CLDN18.2 expression, but the effects of niclosamide and piperlongumine:MST-312 were reversed (Supplementary Figures S5I–L). Additionally, we compared the drug sensitivity scores between the high- and low-CLDN18.2 expression groups in

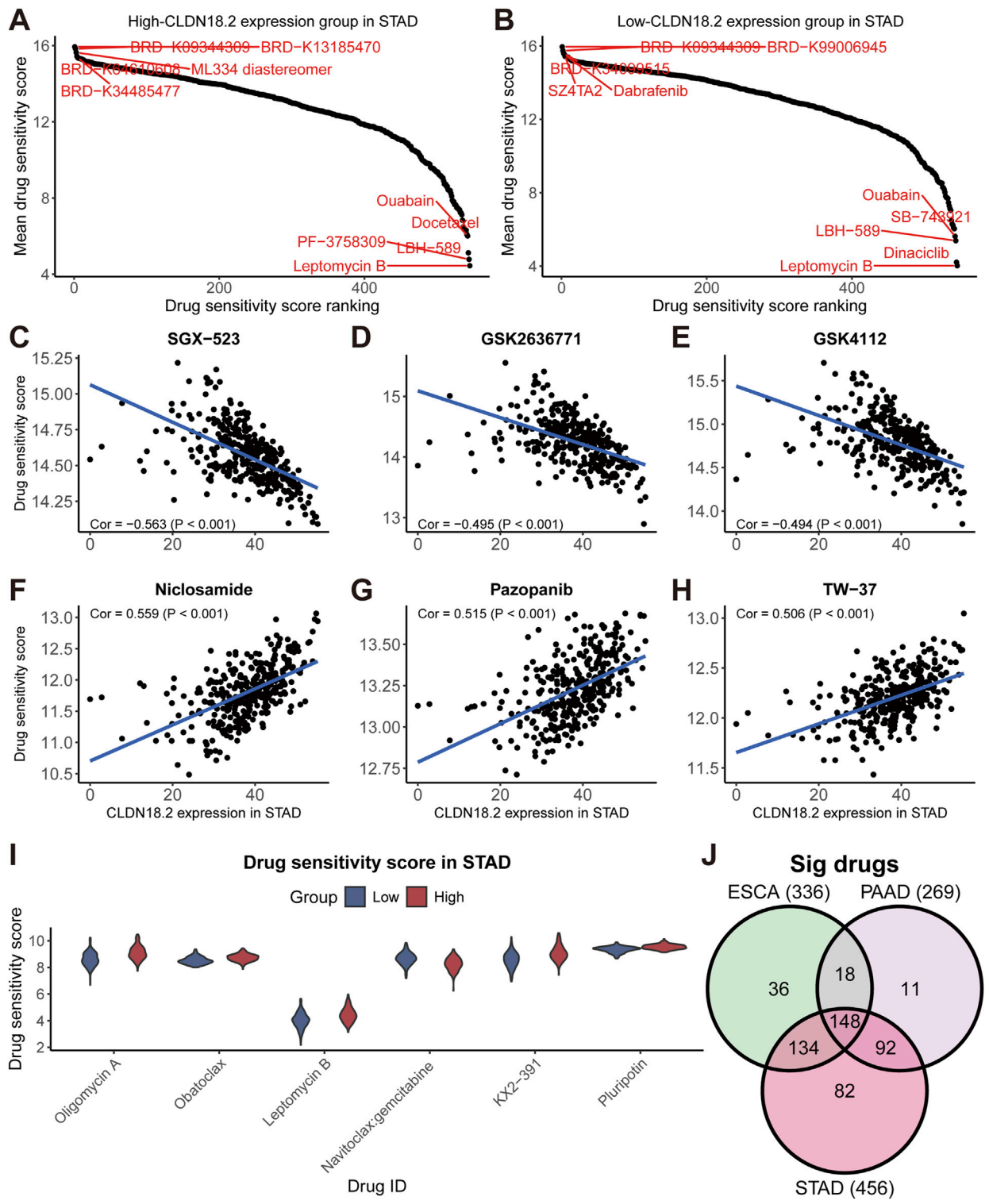

FIGURE 7
Drug sensitivity analyses in STAD. **(A, B)** Drug sensitivity score ranking diagram of high- and low-CLDN18.2 expression groups in STAD. **(C–H)** Scatter plots of the correlations between CLDN18.2 expression and the drug sensitivity score of six drugs in STAD. **(I)** Drug sensitivity scores between high- and low-CLDN18.2 expression groups in STAD. **(J)** Venn diagram of drugs with significant correlation between CLDN18.2 expression and drug sensitivity score in three cancers.

ESCA and PAAD. The results indicated that there were more drugs with significant differences in ESCA, and selumetinib:GDC-0941 had similar effects on both cancers (Supplementary Figures S5M, N). Overall, the results of the drug sensitivity analysis reveal that several drugs may specifically treat CLDN18.2-positive tumors among these three cancers.

4 Discussion

This study provides a comprehensive analysis of CLDN18.2 expression and genomic alterations across multiple cancers, especially upper gastrointestinal tract cancers, and its associations with immune infiltration, prognosis, DEGs, and drug sensitivity. The results revealed that CLDN18 is expressed to some extent in various cancers, which may be related to the prevalent expression of claudin family genes in epithelial cells (Günzel and Yu, 2013). In addition, differences in CLDN18 expression between tumor samples and normal samples were present in only certain cancers, indicating that the development of other cancers may not lead to significant differences in CLDN18 expression. Further analysis of the expression of CLDN18.2 and CLDN18.1 revealed that both had strong cancer specificity and that their expression varied greatly among different cancers. CLDN18.2 is usually expressed predominantly in the stomach, but this study also revealed high CLDN18.2 expression in PAAD, CRC, ESCA, and LUAD, indicating that CLDN18.2 is ectopically expressed in these cancers. The presence of CLDN18.2 was immunohistochemically demonstrated in studies related to these several cancers, and this expression corresponded to the transcriptomic results of this study (Micke et al., 2014; Wöll et al., 2014; Moentenich et al., 2020; Iwaya et al., 2021). Additionally, unlike previous studies in which CLDN18.1 was predominantly highly expressed in lung-related cancers (Niimi et al., 2001), this study also revealed high CLDN18.1 expression in cancers such as SARC, KIRC, and KIRP. This finding shows that CLDN18.1 may also act in other tissues of the human body, which extends the research related to CLDN18.1. Interestingly, CLDN18.2 expression in cancer samples was lower than that in normal samples in STAD, which may be related to the early proliferation and invasion of gastric cancer (Nakayama et al., 2024).

In this study, the associations between CLDN18.2 expression and TMB, MSI, methylation, and CNV were investigated in ten cancers that expressed CLDN18.2. The results revealed limited associations between CLDN18.2 expression and TMB and MSI, with a positive correlation observed only in certain cancers. However, the levels of methylation and CNV differed between the high- and low-CLDN18.2 expression groups among most cancers. Moreover, analyses of the mutation profiles of STAD, CRC, ESCA, and PAAD revealed significant differences between the high- and low-CLDN18.2 groups. Among the differentially mutated genes between the two groups in STAD, certain genes have been reported to be related to gastric cancer. For example, PIK3CA mutation is associated with EBV-positive gastric adenocarcinoma (Network, 2014), and KMT2D may promote the proliferation of gastric cancer cells (Li et al., 2021). The remaining genes have been studied in other cancers (Yan et al., 2022; Song et al., 2023). These results indicate that CLDN18.2 expression is linked to genomic alterations, and the impact of genomic alterations in patients should be considered when studying CLDN18.2 in cancer.

CLDN18.2 expression was also related to the tumor microenvironment and had strong cancer specificity. For example, in STAD and ESCA, the infiltration level of NK cells was significantly lower in the high-CLDN18.2 expression group than in the low-CLDN18.2 expression group, but this difference was not observed in PAAD. This phenomenon has also been reported in a previous study related to gastric cancer (Lenz et al., 2022). Moreover, the two groups exhibited greater differences in the $CD4^+$ T cell subset infiltration levels in these cancers, with smaller differences observed in the $CD8^+$ T cell subsets. These results differ from those reported by Wang et al., whose study demonstrated a higher number of $CD4^+$ and $CD8^+$ T cells in CLDN18.2-positive gastric cancer tumors (Wang et al., 2023). Jia et al. performed a comprehensive analysis of the tumor immune microenvironment in CLDN18.2-positive gastric cancer patients. Their findings revealed no significant difference in macrophage infiltration between CLDN18.2-positive and CLDN18.2-negative groups (Jia et al., 2022). However, our study revealed a significant difference in the infiltration levels of macrophage subsets between the high- and low-CLDN18.2 expression groups in STAD, whereas no similar phenomenon was observed in ESCA, PAAD, and CRC. These results deserve further exploration.

The prognostic analysis of CLDN18.2 expression revealed that high CLDN18.2 expression was a significant risk factor in an integrated analysis of ten cancers. Specifically, in individual cancers, low CLDN18.2 expression was more conducive to prognosis in BLCA, ESAC, and PAAD. Among these cancers, CLDN18.2 appeared less common in research related to BLCA. Combined with the expression levels shown in Figure 2 for CLDN18.2 and CLDN18.1, these findings indicate that CLDN18.2 may have significance for the development of BLCA, which may expand the research in this area. Furthermore, although low CLDN18.2 expression in STAD patients predicted a better prognosis, the results were not significant. Similar situations have also been reported in several previous prognostic analyses of samples with high CLDN18.2 expression based on immunohistochemical results (Arnold et al., 2020; Kayikcioglu et al., 2023); that is, the prognosis of CLDN18.2-positive patients was similar to that of CLDN18.2-negative patients. Taken together, these findings will advance in-depth research on CLDN18.2 in the fields of immune infiltration and prognosis.

By analyzing the differences between the high- and low-CLDN18.2 expression groups in the three cancers, relevant DEGs were identified and enriched in the corresponding pathways. The downregulated pathways included several, such as the KRAS signaling pathway, the EMT pathway, and the calcium signaling pathway, all of which are strongly associated with cancer progression (Monteith et al., 2017; Oshi et al., 2024; Singhal et al., 2024). These findings indicate that high CLDN18.2 expression may affect disease progression through the disruption of intercellular signaling. The upregulated pathways included several, such as the arachidonic acid metabolism pathway, coagulation pathway, and retinol metabolism pathway, all of which are related to angiogenesis (Falanga et al., 2013; Li et al., 2017; Wang et al., 2021). This finding may indicate a connection between the upregulation of CLDN18.2 expression and the mechanism of angiogenesis in the occurrence and development of cancer. In subsequent analyses, three immune-related genes that were highly correlated with CLDN18.2 expression were identified. Among them, CTSE has been shown to synergize with docetaxel in gastric cancer research to facilitate treatment (Li et al., 2022). CXCL17 is a chemokine involved in angiogenesis and has anti-inflammatory effects (Lee et al., 2013). And LYZ is considered a

potential biomarker and target for hepatocellular carcinoma (Gu et al., 2023). These findings indicate that these genes may serve as potential biomarkers to drive relevant therapies in the treatment of cancers with high CLDN18.2 expression.

Drug sensitivity analysis revealed that the effects of niclosamide were reduced in three cancers as CLDN18.2 expression increased. In addition, drugs such as dinaciclib (a cyclin-dependent kinase inhibitor), LBH-589 (a histone deacetylase inhibitor), leptomycin B (an antibiotic that inhibits the activity of nucleoplasmic transfer proteins), and quabain (a cardiac glycoside compound that inhibits the sodium–potassium pump) had sensitivity scores that were very low, indicating that they may be applicable in the treatment of multiple cancers. At present, several research advances in these drugs have been reported (Saqub et al., 2020; Shen et al., 2020; Zhu et al., 2020; Lee et al., 2021). In addition to these versatile drugs, certain specific drugs may exist for each cancer. For example, PF-3758309, also known as pictilisib, is a phosphoinositide 3-kinase inhibitor that inhibits the intracellular phosphoinositide 3-kinase pathway, which in turn inhibits the growth and spread of cancer cells. The drug is currently being used in research in combination with clofarabine for the treatment of gastric cancer (Khalafi et al., 2022). In the STAD results of our study, PF-3758309 had a low drug sensitivity score in the high-CLDN18.2 expression group, which may imply that it plays a role in the treatment of CLDN18.2-positive patients and can be further studied. Thus, our findings will likely promote relevant drug research based on CLDN18.2.

5 Conclusion

In summary, this study revealed CLDN18.2 expression across various cancers and its potential associations with genomic alterations, immune infiltration, and prognosis. CLDN18.2 was highly expressed in upper gastrointestinal tract cancers (STAD, ESCA, and PAAD), but high CLDN18.2 expression may be associated with poor prognosis. Combining the pathway enrichment results of these three cancers, we found that low CLDN18.2 expression was closely associated with cell signaling, whereas high CLDN18.2 expression may promote disease progression through angiogenesis mechanisms. Additionally, the immune microenvironment and the drug efficacy differed between the high- and low-CLDN18.2 expression groups, which may imply different therapeutic strategies. From a multi-omics perspective, these results indicate that CLDN18.2 has potential as a biomarker or therapeutic target in multiple cancers, especially upper gastrointestinal tract cancers.

Data availability statement

The datasets presented in this study can be found in online repositories. The names of the repository/repositories and accession number(s) can be found in the article/Supplementary Material.

Author contributions

JW: Data curation, Formal Analysis, Visualization, Writing–original draft. JL: Writing–review and editing, Data curation. QC: Writing–review and editing, Data curation. HC: Writing–review and editing, Data curation. YZ: Data curation, Methodology, Writing–original draft. MC: Conceptualization, Project administration, Supervision, Writing-review and editing.

Funding

The author(s) declare that financial support was received for the research, authorship, and/or publication of this article. This study was supported by the Chih Kuang Scholarship for Outstanding Young Physician-Scientists of Sun Yat-sen University Cancer Center (CKS-SYSUCC-2024009) and the Postdoctoral Fellowship Program of CPSF (GZB20240907).

Conflict of interest

The authors declare that the research was conducted in the absence of any commercial or financial relationships that could be construed as a potential conflict of interest.

Publisher's note

All claims expressed in this article are solely those of the authors and do not necessarily represent those of their affiliated organizations, or those of the publisher, the editors and the reviewers. Any product that may be evaluated in this article, or claim that may be made by its manufacturer, is not guaranteed or endorsed by the publisher.

Supplementary material

The Supplementary Material for this article can be found online at: https://www.frontiersin.org/articles/10.3389/fphar.2024.1494131/full#supplementary-material

References

Aibar, S., González-Blas, C. B., Moerman, T., Huynh-Thu, V. A., Imrichova, H., Hulselmans, G., et al. (2017). SCENIC: single-cell regulatory network inference and clustering. *Nat. Methods* 14 (11), 1083–1086. doi:10.1038/nmeth.4463

Anand, U., Dey, A., Chandel, A. K. S., Sanyal, R., Mishra, A., Pandey, D. K., et al. (2023). Cancer chemotherapy and beyond: current status, drug candidates, associated risks and progress in targeted therapeutics. *Genes Dis.* 10 (4), 1367–1401. doi:10.1016/j.gendis.2022.02.007

Aran, D. (2020). Cell-type enrichment analysis of bulk transcriptomes using xCell. *Methods Mol. Biol.* 2120, 263–276. doi:10.1007/978-1-0716-0327-7_19

Are, C., Murthy, S. S., Sullivan, R., Schissel, M., Chowdhury, S., Alatise, O., et al. (2023). Global Cancer Surgery: pragmatic solutions to improve cancer surgery outcomes worldwide. *Lancet Oncol.* 24 (12), e472–e518. doi:10.1016/s1470-2045(23)00412-6

Arnold, A., Daum, S., von Winterfeld, M., Berg, E., Hummel, M., Rau, B., et al. (2020). Prognostic impact of Claudin 18.2 in gastric and esophageal adenocarcinomas. *Clin. Transl. Oncol.* 22 (12), 2357–2363. doi:10.1007/s12094-020-02380-0

Bray, F., Laversanne, M., Sung, H., Ferlay, J., Siegel, R. L., Soerjomataram, I., et al. (2024). Global cancer statistics 2022: GLOBOCAN estimates of incidence and mortality worldwide for 36 cancers in 185 countries. *CA Cancer J. Clin.* 74 (3), 229–263. doi:10.3322/caac.21834

Carlino, M. S., Larkin, J., and Long, G. V. (2021). Immune checkpoint inhibitors in melanoma. *Lancet* 398 (10304), 1002–1014. doi:10.1016/s0140-6736(21)01206-x

Cerami, E., Gao, J., Dogrusoz, U., Gross, B. E., Sumer, S. O., Aksoy, B. A., et al. (2012). The cBio cancer genomics portal: an open platform for exploring multidimensional cancer genomics data. *Cancer Discov.* 2 (5), 401–404. doi:10.1158/2159-8290.Cd-12-0095

Chu, D. T., Nguyen, T. T., Tien, N. L. B., Tran, D. K., Jeong, J. H., Anh, P. G., et al. (2020). Recent progress of stem cell therapy in cancer treatment: molecular mechanisms and potential applications. *Cells* 9 (3), 563. doi:10.3390/cells9030563

Esteva, F. J., Hubbard-Lucey, V. M., Tang, J., and Pusztai, L. (2019). Immunotherapy and targeted therapy combinations in metastatic breast cancer. *Lancet Oncol.* 20 (3), e175–e186. doi:10.1016/s1470-2045(19)30026-9

Falanga, A., Marchetti, M., and Vignoli, A. (2013). Coagulation and cancer: biological and clinical aspects. *J. Thromb. Haemost.* 11 (2), 223–233. doi:10.1111/jth.12075

Garber, M., Grabherr, M. G., Guttman, M., and Trapnell, C. (2011). Computational methods for transcriptome annotation and quantification using RNA-seq. *Nat. Methods* 8 (6), 469–477. doi:10.1038/nmeth.1613

Goldman, M. J., Craft, B., Hastie, M., Repečka, K., McDade, F., Kamath, A., et al. (2020). Visualizing and interpreting cancer genomics data via the Xena platform. *Nat. Biotechnol.* 38 (6), 675–678. doi:10.1038/s41587-020-0546-8

Gu, Z., Wang, L., Dong, Q., Xu, K., Ye, J., Shao, X., et al. (2023). Aberrant LYZ expression in tumor cells serves as the potential biomarker and target for HCC and promotes tumor progression via csGRP78. *Proc. Natl. Acad. Sci. U. S. A.* 120 (29), e2215744120. doi:10.1073/pnas.2215744120

Günzel, D., and Yu, A. S. (2013). Claudins and the modulation of tight junction permeability. *Physiol. Rev.* 93 (2), 525–569. doi:10.1152/physrev.00019.2012

Iwaya, M., Hayashi, H., Nakajima, T., Matsuda, K., Kinugawa, Y., Tobe, Y., et al. (2021). Colitis-associated colorectal adenocarcinomas frequently express claudin 18 isoform 2: implications for claudin 18.2 monoclonal antibody therapy. *Histopathology* 79 (2), 227–237. doi:10.1111/his.14358

Jia, K., Chen, Y., Sun, Y., Hu, Y., Jiao, L., Ma, J., et al. (2022). Multiplex immunohistochemistry defines the tumor immune microenvironment and immunotherapeutic outcome in CLDN18.2-positive gastric cancer. *BMC Med.* 20 (1), 223. doi:10.1186/s12916-022-02421-1

Jiang, H., Shi, Z., Wang, P., Wang, C., Yang, L., Du, G., et al. (2019). Claudin18.2-Specific chimeric antigen receptor engineered T cells for the treatment of gastric cancer. *J. Natl. Cancer Inst.* 111 (4), 409–418. doi:10.1093/jnci/djy134

Jokhadze, N., Das, A., and Dizon, D. S. (2024). Global cancer statistics: a healthy population relies on population health. *CA Cancer J. Clin.* 74 (3), 224–226. doi:10.3322/caac.21838

Kayikcioglu, E., Yüceer, R. O., Cetin, B., Yüceer, K., and Karahan, N. (2023). Prognostic value of claudin 18.2 expression in gastric adenocarcinoma. *World J. Gastrointest. Oncol.* 15 (2), 343–351. doi:10.4251/wjgo.v15.i2.343

Khalafi, S., Zhu, S., Khurana, R., Lohse, I., Giordano, S., Corso, S., et al. (2022). A novel strategy for combination of clofarabine and pictilisib is synergistic in gastric cancer. *Transl. Oncol.* 15 (1), 101260. doi:10.1016/j.tranon.2021.101260

Kwak, Y., Kim, T. Y., Nam, S. K., Hwang, H. J., Han, D., Oh, H. J., et al. (2024). Clinicopathologic and molecular characterization of stages II-IV gastric cancer with Claudin 18.2 expression. *Oncologist*, oyae238. doi:10.1093/oncolo/oyae238

Lee, N. R., Kim, D. Y., Jin, H., Meng, R., Chae, O. H., Kim, S. H., et al. (2021). Inactivation of the akt/FOXM1 signaling pathway by panobinostat suppresses the proliferation and metastasis of gastric cancer cells. *Int. J. Mol. Sci.* 22 (11), 5955. doi:10.3390/ijms22115955

Lee, W. Y., Wang, C. J., Lin, T. Y., Hsiao, C. L., and Luo, C. W. (2013). CXCL17, an orphan chemokine, acts as a novel angiogenic and anti-inflammatory factor. *Am. J. Physiol. Endocrinol. Metab.* 304 (1), E32–E40. doi:10.1152/ajpendo.00083.2012

Lenz, A., Zeng, J., Xiu, J., Algaze, S., Jayachandran, P., Soni, S., et al. (2022). Claudin 18 (CLDN18) gene expression and related molecular profile in gastric cancer (GC). *J. Clin. Oncol.* 40 (16_Suppl. l), 4048. doi:10.1200/JCO.2022.40.16_suppl.4048

Li, N., Lu, Y., Li, D., Zheng, X., Lian, J., Li, S., et al. (2017). All-trans retinoic acid suppresses the angiopoietin-Tie2 pathway and inhibits angiogenesis and metastasis in esophageal squamous cell carcinoma. *PLoS One* 12 (4), e0174555. doi:10.1371/journal.pone.0174555

Li, Q., Wu, R., Wu, F., and Chen, Q. (2021). KMT2D promotes proliferation of gastric cancer cells: evidence from ctDNA sequencing. *J. Clin. Lab. Anal.* 35 (4), e23721. doi:10.1002/jcla.23721

Li, Y., Xu, C., Wang, B., Xu, F., Ma, F., Qu, Y., et al. (2022). Proteomic characterization of gastric cancer response to chemotherapy and targeted therapy reveals potential therapeutic strategies. *Nat. Commun.* 13 (1), 5723. doi:10.1038/s41467-022-33282-0

Maeser, D., Gruener, R. F., and Huang, R. S. (2021). oncoPredict: an R package for predicting *in vivo* or cancer patient drug response and biomarkers from cell line screening data. *Brief. Bioinform* 22 (6), bbab260. doi:10.1093/bib/bbab260

Micke, P., Mattsson, J. S., Edlund, K., Lohr, M., Jirström, K., Berglund, A., et al. (2014). Aberrantly activated claudin 6 and 18.2 as potential therapy targets in non-small-cell lung cancer. *Int. J. Cancer* 135 (9), 2206–2214. doi:10.1002/ijc.28857

Mitnacht-Kraus, R., Kreuzberg, M., Utsch, M., Sahin, U., and Türeci, Ö. (2017). Preclinical characterization of IMAB362 for the treatment of gastric carcinoma. *Ann. Oncol.* 28, v126. doi:10.1093/annonc/mdx367.012

Moentenich, V., Gebauer, F., Comut, E., Tuchscherer, A., Bruns, C., Schroeder, W., et al. (2020). Claudin 18.2 expression in esophageal adenocarcinoma and its potential impact on future treatment strategies. *Oncol. Lett.* 19 (6), 3665–3670. doi:10.3892/ol.2020.11520

Monteith, G. R., Prevarskaya, N., and Roberts-Thomson, S. J. (2017). The calcium-cancer signalling nexus. *Nat. Rev. Cancer* 17 (6), 367–380. doi:10.1038/nrc.2017.18

Nakayama, I., Qi, C., Chen, Y., Nakamura, Y., Shen, L., and Shitara, K. (2024). Claudin 18.2 as a novel therapeutic target. *Nat. Rev. Clin. Oncol.* 21 (5), 354–369. doi:10.1038/s41571-024-00874-2

Network, C. G. A. R. (2014). Comprehensive molecular characterization of gastric adenocarcinoma. *Nature* 513 (7517), 202–209. doi:10.1038/nature13480

Niimi, T., Nagashima, K., Ward, J. M., Minoo, P., Zimonjic, D. B., Popescu, N. C., et al. (2001). claudin-18, a novel downstream target gene for the T/EBP/NKX2.1 homeodomain transcription factor, encodes lung- and stomach-specific isoforms through alternative splicing. *Mol. Cell Biol.* 21 (21), 7380–7390. doi:10.1128/mcb.21.21.7380-7390.2001

Niu, Z., Jin, R., Zhang, Y., and Li, H. (2022). Signaling pathways and targeted therapies in lung squamous cell carcinoma: mechanisms and clinical trials. *Signal Transduct. Target Ther.* 7 (1), 353. doi:10.1038/s41392-022-01200-x

Oshi, M., Roy, A. M., Yan, L., Kinoshita, S., Tamura, Y., Kosaka, T., et al. (2024). Enhanced epithelial-mesenchymal transition signatures are linked with adverse tumor microenvironment, angiogenesis and worse survival in gastric cancer. *Cancer Gene Ther.* 31 (5), 746–754. doi:10.1038/s41417-024-00756-w

Rees, M. G., Seashore-Ludlow, B., Cheah, J. H., Adams, D. J., Price, E. V., Gill, S., et al. (2016). Correlating chemical sensitivity and basal gene expression reveals mechanism of action. *Nat. Chem. Biol.* 12 (2), 109–116. doi:10.1038/nchembio.1986

Ryan, M., Wong, W. C., Brown, R., Akbani, R., Su, X., Broom, B., et al. (2016). TCGASpliceSeq a compendium of alternative mRNA splicing in cancer. *Nucleic Acids Res.* 44 (D1), D1018–D1022. doi:10.1093/nar/gkv1288

Sahin, U., Koslowski, M., Dhaene, K., Usener, D., Brandenburg, G., Seitz, G., et al. (2008). Claudin-18 splice variant 2 is a pan-cancer target suitable for therapeutic antibody development. *Clin. Cancer Res.* 14 (23), 7624–7634. doi:10.1158/1078-0432.Ccr-08-1547

Saqub, H., Proetsch-Gugerbauer, H., Bezrookove, V., Nosrati, M., Vaquero, E. M., de Semir, D., et al. (2020). Dinaciclib, a cyclin-dependent kinase inhibitor, suppresses cholangiocarcinoma growth by targeting CDK2/5/9. *Sci. Rep.* 10 (1), 18489. doi:10.1038/s41598-020-75578-5

Schaue, D., and McBride, W. H. (2015). Opportunities and challenges of radiotherapy for treating cancer. *Nat. Rev. Clin. Oncol.* 12 (9), 527–540. doi:10.1038/nrclinonc.2015.120

Shah, M. A., Shitara, K., Ajani, J. A., Bang, Y. J., Enzinger, P., Ilson, D., et al. (2023). Zolbetuximab plus CAPOX in CLDN18.2-positive gastric or gastroesophageal junction adenocarcinoma: the randomized, phase 3 GLOW trial. *Nat. Med.* 29 (8), 2133–2141. doi:10.1038/s41591-023-02465-7

Shen, J. J., Zhan, Y. C., Li, H. Y., and Wang, Z. (2020). Ouabain impairs cancer metabolism and activates AMPK-Src signaling pathway in human cancer cell lines. *Acta Pharmacol. Sin.* 41 (1), 110–118. doi:10.1038/s41401-019-0290-0

Shitara, K., Lordick, F., Bang, Y. J., Enzinger, P., Ilson, D., Shah, M. A., et al. (2023). Zolbetuximab plus mFOLFOX6 in patients with CLDN18.2-positive, HER2-negative, untreated, locally advanced unresectable or metastatic gastric or gastro-oesophageal junction adenocarcinoma (SPOTLIGHT): a multicentre, randomised, double-blind, phase 3 trial. *Lancet* 401 (10389), 1655–1668. doi:10.1016/s0140-6736(23)00620-7

Singhal, A., Li, B. T., and O'Reilly, E. M. (2024). Targeting KRAS in cancer. *Nat. Med.* 30 (4), 969–983. doi:10.1038/s41591-024-02903-0

Song, Z., Song, X., Li, H., Cheng, Z., Mo, Z., and Yang, X. (2023). Identification and validation of a prognostic-related mutant gene DNAH5 for hepatocellular carcinoma. *Front. Immunol.* 14, 1236995. doi:10.3389/fimmu.2023.1236995

Stark, R., Grzelak, M., and Hadfield, J. (2019). RNA sequencing: the teenage years. *Nat. Rev. Genet.* 20 (11), 631–656. doi:10.1038/s41576-019-0150-2

Thorsson, V., Gibbs, D. L., Brown, S. D., Wolf, D., Bortone, D. S., Ou Yang, T. H., et al. (2018). The immune landscape of cancer. *Immunity* 48 (4), 812–830.e14. doi:10.1016/j.immuni.2018.03.023

Türeci, O., Koslowski, M., Helftenbein, G., Castle, J., Rohde, C., Dhaene, K., et al. (2011). Claudin-18 gene structure, regulation, and expression is evolutionary conserved in mammals. *Gene* 481 (2), 83–92. doi:10.1016/j.gene.2011.04.007

Vollset, S. E., Ababneh, H. S., Abate, Y. H., Abbafati, C., Abbasgholizadeh, R., Abbasian, M., et al. (2024). Burden of disease scenarios for 204 countries and territories, 2022-2050: a forecasting analysis for the Global Burden of Disease Study 2021. *Lancet* 403 (10440), 2204–2256. doi:10.1016/S0140-6736(24)00685-8

Wang, B., Wu, L., Chen, J., Dong, L., Chen, C., Wen, Z., et al. (2021). Metabolism pathways of arachidonic acids: mechanisms and potential therapeutic targets. *Signal Transduct. Target Ther.* 6 (1), 94. doi:10.1038/s41392-020-00443-w

Wang, C., Wang, Y., Chen, J., Wang, Y., Pang, C., Liang, C., et al. (2023). CLDN18.2 expression and its impact on prognosis and the immune microenvironment in gastric cancer. *BMC Gastroenterol.* 23 (1), 283. doi:10.1186/s12876-023-02924-y

Wöll, S., Schlitter, A. M., Dhaene, K., Roller, M., Esposito, I., Sahin, U., et al. (2014). Claudin 18.2 is a target for IMAB362 antibody in pancreatic neoplasms. *Int. J. Cancer* 134 (3), 731–739. doi:10.1002/ijc.28400

Wu, T., Hu, E., Xu, S., Chen, M., Guo, P., Dai, Z., et al. (2021). clusterProfiler 4.0: a universal enrichment tool for interpreting omics data. *Innov. (Camb)* 2 (3), 100141. doi:10.1016/j.xinn.2021.100141

Xu, R.-h., Wei, X., Zhang, D., Qiu, M., Zhang, Y., Zhao, H., et al. (2023a). A phase 1a dose-escalation, multicenter trial of anti-claudin 18.2 antibody drug conjugate CMG901 in patients with resistant/refractory solid tumors. *J. Clin. Oncol.* 41 (4_Suppl. l), 352. doi:10.1200/JCO.2023.41.4_suppl.352

Xu, Y., Fu, J., Henderson, M., Lee, F., Jurcak, N., Henn, A., et al. (2023b). CLDN18.2 BiTE engages effector and regulatory T cells for antitumor immune response in preclinical models of pancreatic cancer. *Gastroenterology* 165 (5), 1219–1232. doi:10.1053/j.gastro.2023.06.037

Yan, J., Zhao, W., Yu, W., Cheng, H., and Zhu, B. (2022). LRRK2 correlates with macrophage infiltration in pan-cancer. *Genomics* 114 (1), 316–327. doi:10.1016/j.ygeno.2021.11.037

Yung, R. L., and Davidson, N. E. (2021). Optimal adjuvant endocrine therapy for breast cancer. *Lancet Oncol.* 22 (10), 1357–1358. doi:10.1016/s1470-2045(21)00420-4

Zhong, L., Li, Y., Xiong, L., Wang, W., Wu, M., Yuan, T., et al. (2021). Small molecules in targeted cancer therapy: advances, challenges, and future perspectives. *Signal Transduct. Target Ther.* 6 (1), 201. doi:10.1038/s41392-021-00572-w

Zhu, H., Yang, Y., Wang, L., Xu, X., Wang, T., and Qian, H. (2020). Leptomycin B inhibits the proliferation, migration, and invasion of cultured gastric carcinoma cells. *Biosci. Biotechnol. Biochem.* 84 (2), 290–296. doi:10.1080/09168451.2019.1673148

Zhu, Y., Zhu, X., Wei, X., Tang, C., and Zhang, W. (2021). HER2-targeted therapies in gastric cancer. *Biochim. Biophys. Acta Rev. Cancer* 1876 (1), 188549. doi:10.1016/j.bbcan.2021.188549

Frontiers in Pharmacology

Explores the interactions between chemicals and living beings

The most cited journal in its field, which advances access to pharmacological discoveries to prevent and treat human disease.

Discover the latest Research Topics

See more →

Frontiers

Avenue du Tribunal-Fédéral 34
1005 Lausanne, Switzerland
frontiersin.org

Contact us

+41 (0)21 510 17 00
frontiersin.org/about/contact